Passivity Approach to Pneumatic Actuated Human Interactive Robots

A DISSERTATION
SUBMITTED TO THE FACULTY OF THE GRADUATE SCHOOL
OF THE UNIVERSITY OF MINNESOTA
BY

Venkat Phaneender Durbha

IN PARTIAL FULFILLMENT OF THE REQUIREMENTS
FOR THE DEGREE OF
Doctor of Philosophy

Perry Y. Li

November, 2014

Acknowledgements

First and foremost, I would like to thank Dr. Perry Li for his advise and guidance. His keen insight and technical prowess were instrumental in helping me solve quite a few key technical challenges in my research.

The work presented in this thesis was funded by NSF through their funding for Center for Compact and Efficient and Fluid Power (CCEFP) under the grant EEC-0540834. I am indebted to CCEFP (and NSF) for their financial support. Special thanks to the CCEFP member companies, FESTO and Enfield Technologies for generously contributing hardware for my experimental work.

The experimental work on the robotic crawler was done at the Intelligent Machine Dynamics Lab (IMDL) at Georgia Tech. During my many visits to Georgia Tech, Dr. Wayne Book was an extremely gracious host. My sincere thanks for his hospitality. J.D. Huggins was a great help with any hardware issues that cropped up with the robot. Many thanks to Hannes Daep, Brian Post, and Michael Valente for their help in conducting the experiments. A big thanks to my friend Raghuram Rajan for allowing me to crash at his place for free during a three month stay in Atlanta.

Many thanks to all the current and former colleagues of the Mechatronics and Intelligent Machines Lab for their help during the course of my research work. A majority of my graduate school was spent in the company of Haink, Nicole, Raghuram, Teck Ping, Mike, Rachael, Jicheng, Jon and Stephen. I learned to enjoy and appreciate Minneapolis in their company. They were like a family, providing support and company during both the highs and the lows of the graduate school. I could not have gone through graduate school without their friendship and support. Thanks also to all the friends I have made in Minneapolis over the years for some wonderful memories.

Finally, I would like to thank my parents, my brother and my extended family

for their immeasurable patience during this period in my life. Without their love and support it would have been near impossible to focus on research.

Dedication

To my parents

Abstract

The high power density of fluid-powered actuators can facilitate design of compact and powerful devices. Pneumatic actuators in particular are preferred in human interactive devices due to their properties such as inherent compliance, backdrivability and benign consequences of leakage. A drawback of pneumatic actuators is that the current sources of compressed air are bulky and not suitable for mobile human-centered applications. To address these concerns, research is underway on advanced gas based actuation devices such as chemo-fluidic actuators, dry ice actuators, and mini-HCCI engines. These actuators are ideal for development of powerful and mobile devices for human scale applications. The operation of these devices typically requires direct human interaction between the pneumatic (or gas) actuated system and the human operator. Therefore safety of operation is imperative. One way of investigating interaction stability (and hence safe operation) between multiple systems is by using the framework of *Passivity* analysis from systems theory.

The objective of the research presented in this dissertation is investigation of passivity characteristics of pneumatic actuators. This passivity analysis is a preliminary step in understanding the feasibility of using gas based actuators in human interactive applications. Passivity analysis requires definition of a storage function to quantify the effect of inputs and outputs on the system dynamics. The nonlinear dynamics of air compression and expansion in a pneumatic actuator are affected by the heat transfer across the walls of the actuator. In this thesis, physics based energy functions are developed and defined to be the storage function for three specific models of heat transfer *viz* adiabatic, isothermal, and finite heat transfer. For reversible thermodynamic process (adiabatic or isothermal), the storage function is defined as the work that can be extracted from the actuator. The storage function for actuator with finite heat transfer is defined as the maximum work that can be extracted from the pneumatic actuator. It is shown that the solution to this optimization problem provides a storage function similar to exergy of the air in the actuator. The supply rate based on these storage functions corresponds to physically meaningful power interaction between different subsystems, such as the actuator and the inertia load. Both adiabatic and isothermal actuators have

two ports for power interaction : mechanical port corresponding to interaction with an inertial load, and fluid port corresponding to interaction with source/sink of compressed air. The adiabatic/isothermal actuator behaves as a two-port nonlinear spring with an active flow input at the fluid port of the actuator. Pneumatic actuator with finite heat transfer to the ambient has an additional port corresponding to the thermal interaction with the ambient. The supply rate to the pneumatic actuator with finite heat transfer illustrates that irrespective of chamber air temperature, heat transfer reduces the ability of the actuator to do work, thus contributing to passive behavior of the actuator.

Energetically passive controller design for pneumatic actuated human power amplifier and tele-operated human scale devices is presented in this thesis. A framework for controlling the active flow variable at the fluid port of the pneumatic actuator to provide passive operation of a pneumatically actuated human power amplifier is presented by assuming the heat transfer model in the actuator to be either adiabatic or isothermal. This framework is then extended to define the framework for achieving co-ordinated tele-operation of multiple pneumatic actuated devices, while again amplifying input human power. The control problem is suitably defined within the proposed framework and a two-stage back-stepping controller is used to achieve the control objective. The Lyapunov function for the actuator controller design is defined based on the energy functions developed for adiabatic and isothermal actuators. The designed controllers are implemented on single-DOF systems and a multi-DOF robotic rescue crawler with pneumatic actuators. Experimental results confirming the efficacy of the proposed controller are provided.

Finally, independent metering of each actuator chamber to improve the operational efficiency of the pneumatic actuators is investigated. In independent metering, two servo valves are used to control the air flow rate to the two chambers of the actuator. The valves are controlled to maintain a low operating pressure in both the chambers, while providing the desired actuator force. This mitigates the losses associated with discharge of high pressure air to atmosphere. Effectiveness of independent metering is evaluated in a single-DOF human power amplifier by assuming the heat transfer model in the actuator to be isothermal. Experimental results show 70% improvement in operation time.

Contents

List of Tables

List of Figures

Chapter 1

Introduction

1.1 Motivation

An emerging frontier in robotics is their application in human-centered tasks. Electro-mechanical actuators are commonly used in robotic applications due to their simpler dynamics and ease of controllability. A drawback of the existing electro-mechanical actuators is that due to their poor power density, significantly larger actuator will be required for human-scale systems. The robotic system will have to be designed to accommodate the higher weight of these actuators. The high power density of fluid-powered actuators makes them an attractive alternative to electro-mechanical actuators. The hydraulic rescue tool shown in Fig. (1.1) is an example of a human scale fluid-powered devices currently in use. Traditionally, fluid-powered actuators have been very popular in systems requiring high power output such as, excavators and mining equipment. However, the recent surge of activity in human scale robots has brought more attention to the potential benefits of using fluid-powered actuators at lower power levels. In tools such as the jaws of life shown in Fig. (1.1), a preferable characteristic of these devices is amplification of input human power. This feature will enable intuitive operation of such rescue devices, as the system output power would be proportional to the input human power. Other potential applications that will benefit with the ability to amplify input human power include powered hand tools, prosthetic/orthotic devices and industrial exo-skeletons.

Human power amplification and co-ordinated tele-operation of multiple pneumatic

Figure 1.1: Jaws of life : A hydraulic rescue tool being used to cut through a car. *Courtesy : http://www.publicsafetyoutfitters.com/training.htm*

actuated systems to assist a human operator will be useful in tasks that require moving unwieldy loads such as sheetrock. Tele-operation can also be used to move inertial loads in a remote, inaccessible and/or inhospitable location. Figure (1.2) depicts the multi-DOF tele-operated system used as an experimental test bed in this study. In this tele-operator, the master system is a PHANToM(TM[1]) haptic device, while the slave system to be operated in a remote environment takes the form of a crawling robot with pneumatic actuators. The intended application of this tele-operated system is to aid in rescue operations. In mobile, untethered applications of fluid power, pneumatic actuators are preferable over hydraulic actuators as they can be designed to be lighter. In addition, the ubiquitous nature of air available for compression, and the benign nature of any leakage in the system, makes pneumatic actuators more amenable for both indoor and outdoor mobile applications. Characteristics of pneumatic actuators such as inherent compliance of air, backdrivability, and ability to provide continuously variable transmission and variable impedance makes them very attractive for human interactive applications with contact tasks.

Effectiveness of human interactive devices can be greatly enhanced through suitable

[1] PHANToM is a trademarked product of Sensable Technologies, MA

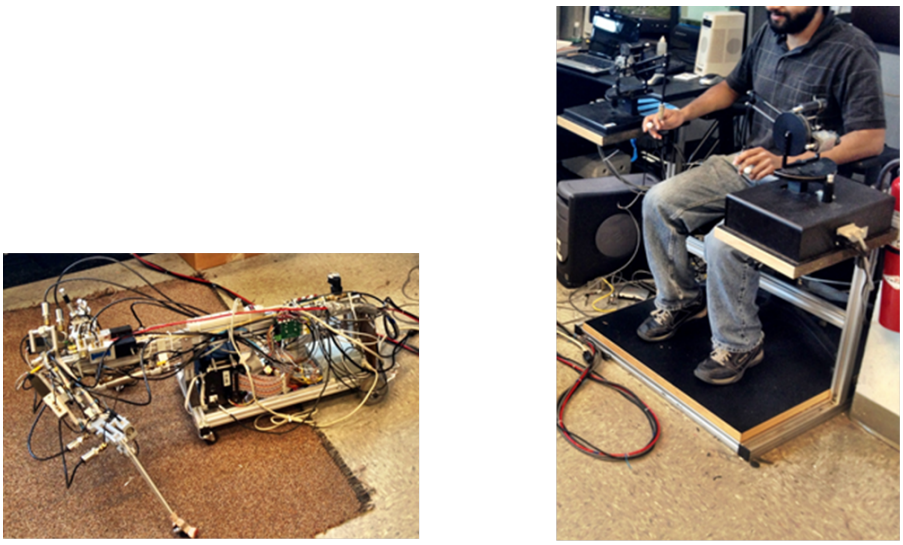

Figure 1.2: The rescue crawler robot and the PHANToM[1] interface used in the experimental study.

haptic feedback. In this thesis, the interaction forces between the crawler and its environment are fed back to the human operator. This haptic feedback provides the human operator with a 'feel' for the crawlers' work environment, thus enabling the operator to navigate the crawler in the absence of suitable visual information. Presence of human operator in the decision making loop enables robust performance in navigating unknown terrain. Such a feedback also ensures that the operation of the tele-operator is bilateral. Due to the difference in the operating power range of the PHANToM(TM[1]) device and the crawler, the interaction forces between the crawler and its environment are appropriately scaled before being imposed on the PHANToM(TM[1]). A useful feature on the rescue crawler is the ability to amplify input human power. This feature can be used by people on-site to move heavy loads and aid in the rescue mission. For the experiments reported in this study, an interface with a force sensor is provided on the right leg of the crawler. Power input at this interface is amplified by the actuators on the crawler leg.

Due to the higher power density of pneumatic actuators it is very important to guarantee stable interaction with different environments during the tasks performed by the human operator. It is in fact desirable that these devices using pneumatic actuators behave as a common passive mechanical tool that interacts simultaneously with multiple mechanical input from sources such as a local and/or remotely located human operator, and the physical environment, and provides work output due to power interaction at these ports only. As interaction between two stable systems is not always guaranteed to be stable, one approach to investigating stable interaction with unknown environments is by using the concept of "passivity" from systems theory [2]. A passive device is energetically neutral or dissipative in nature. A good example of a passive device is a bicycle: it remains stationary when provided with no external input and only moves when sufficient torque is provided on the pedals. It has been shown in [3] that closed loop interaction between a passive system and a strictly passive system is always guaranteed to be passive and stable. Most external environments are passive in nature. Earlier studies on human interactive systems [4] had shown that the human muscular dynamics can be approximated to be passive. Therefore, interaction stability while operating pneumatic powered actuators can be guaranteed if the pneumatic actuator behaves as a passive device. Pneumatic (and fluid-powered) actuators are however not passive devices as they can draw energy from the compressor to do work on the system without any input from a human operator.

Passive behavior can be enforced through either integration of dissipative elements in the actuator [5], or through active feedback [6]. In the current work, active feedback is used to make the pneumatic actuator behave as a passive system. In [7], a pseudo-bond graph model is used to design passive controller for force tracking with a pneumatic actuator. While such a controller can provide stable operation, defining supply rate in terms of physical power flow is more useful as it enables intuitive analysis of multi-domain systems. Systems that are passive with respect to supply rates that correspond to physics based power flow in the system are referred to as energetically passive. This approach is similar to investigation of human interaction stability through bond graph based modeling and analysis presented in [8], [9], [10].

To realize a physically meaningful supply rate for energetic passivity, a suitable storage function corresponding to the energy available in the pneumatic actuator has

to be defined. Energy in the pneumatic actuator depends on the heat transfer model associated with the compression and the expansion of air. Therefore, in this dissertation, energy functions for three different heat transfer models in pneumatic actuator *viz* isothermal, adiabatic, and finite heat transfer processes are developed. Energetically passive operation of human interactive applications (human power amplifier, tele-operation with human power amplification) is achieved by designing appropriate controllers for the flow variable at the fluid port of the pneumatic actuator.

Inefficiency of operation is also a big drawback for fluid-powered actuators. This can greatly affect the duration of operation in mobile applications. In pneumatic actuators, discharge of high pressure air to atmosphere is a source of inefficiency [11]. In this dissertation, a feedback based approach through independent metering of air flow to individual actuator chambers is investigated for improving the efficiency of operation of human power amplifier.

A concern with using pneumatic actuator for mobile applications is that the energy density offered by these actuators is lower than batteries and servomotors. Recent research efforts to address this issue have led to development of other gas-based actuation devices such as chemo-fluidic actuators [12], dry ice based actuators [13], free piston compression engine [14] and the miniature HCCI engines [15]. These actuators retain the advantages of power density offered by gas-based (pneumatic) actuators, while providing better energy density than pneumatic actuators. It has been shown in [12] that the energy density of chemo-fluidic actuators is an order of magnitude higher than that of a typical battery or servomotors. The actuation mechanism in these gas-based devices is similar to pneumatic actuators. Energetic passivity analysis of pneumatic actuators provided in this thesis is the first step in understanding the feasibility of using these new gas-based actuators in human interactive applications.

1.2 Research goals

The goal of this project are to

1. Develop physics based energy function for a pneumatic actuator. Such an energy function will provide insight into the characteristics of the pneumatic actuator and also facilitate development of energetically passive controllers. These controllers

are required to guarantee safe operation of pneumatic actuators in human centered robotic applications.

2. Provide a framework for energetically passive control of pneumatic actuators. With this framework controllers for two specific human centered applications *viz.* human power amplification, and co-ordinated tele-operation of multiple human scale pneumatic actuated systems, will be developed.

3. Investigate independent metering of air flow rate as a means to improve operational efficiency of the pneumatic actuators.

In the following section, the contributions of this work are enumerated.

1.3 Contributions

The contributions of this work include the following,

1. *A formal definition of storage function for pneumatic actuators:* For pneumatic actuators with reversible thermodynamics (isothermal and adiabatic actuators), the storage function is obtained as the work available from the actuator. For pneumatic actuators that have finite heat transfer, the storage function is obtained by maximizing the available energy in the actuator. It is shown that the resulting energy function for actuator with finite heat transfer is similar to exergy of the pneumatic actuator. From these storage functions, physics based supply rate can be defined for the pneumatic actuators for monitoring their interaction with external inputs.

2. *A framework for passive operation of adiabatic/isothermal pneumatic actuator for application in human power amplifier and co-ordinated operation of multiple pneumatic actuators:* Due to the active flow input at fluid port of the pneumatic actuator, it is not immediately suitable for human interactive applications. A framework for achieving energetically passive operation of human power amplifier with adiabatic/isothermal pneumatic actuator by suitably designing the active fluid port flow input is reported in this thesis. The control problem for achieving human power amplification is then defined within this framework. It

is also shown that the proposed framework for human power amplification can be easily extended to achieve co-ordinated tele-operation between multiple adiabatic/isothermal pneumatic actuators. In this framework for multi-actuator co-ordination, individual actuators can be either pneumatic or hydraulic (with reversible thermodynamic process). The proposed framework also lends itself well to co-ordinated tele-operation of multiple fluid power actuated systems with one electro-mechanically actuated system.

3. *Independent metering of pneumatic actuators:* To enhance the operation time of mobile systems with pneumatic actuators, independent metering of air flow to the actuator chambers is investigated. The additional degree of control freedom afforded by independent metering is used to maintain the working pressure low, thus minimizing energy loss associated with discharge of high pressure air to atmosphere.

1.4 Outline

The rest of the document is structured as follows,

- Chapter 2 provides a survey of the existing work on passive control of human interactive robots. The available literature on passive control of fluid-powered actuators is listed and the existing gaps are brought to attention.

- In chapter 3, the dynamics of the pneumatic actuator are presented, and the underlying assumptions are explained. Energy based storage functions for isothermal and adiabatic model are also derived. Based on this energy function, an energy function for the error dynamics of pneumatic actuator is also derived in this section.

- In chapter 4, a storage function for pneumatic actuator with finite heat transfer is developed. Passivity of the actuator with respect to the storage function is demonstrated.

- In chapter 5, a framework for energetically passive operation of pneumatic actuated human power amplifiers is presented. Controller design for a single-DOF

power amplifier is also derived in this chapter. Experimental results verifying the controller performance are also presented.

- In chapter 6, a framework for co-ordination of multiple fluid-powered actuators is presented. In this proposed framework for multiple systems, one single system can also be electro-mechanically actuated. Controller design for achieving the desired position and velocity co-ordination is developed within the proposed passivity framework. Experimental results demonstrating efficacy of the controller are presented for a system consisting of two single-DOF pneumatic actuated systems.

- Bilateral tele-operation of a multi-DOF rescue crawler is presented in chapter 7. The framework for bilateral tele-operation also includes a feature where in the multi-DOF crawler leg behaves as human power amplifier. This feature can help with on-site rescue operation. The co-ordination controller that provides both bilateral tele-operation and on-site human power amplification is designed. Results from implementing this controller on the experimental test bed are also reported.

- In chapter 8, independent metering of air flow to each chamber in a two-chambered pneumatic actuator is developed as a potential solution for improving operational efficiency of pneumatic actuators in mobile applications. Efficiency improvements in the performance of a pneumatic actuator through independent metering are demonstrated for the human power amplifier.

- Concluding remarks and future research directions are presented in chapter 9.

Chapter 2

Literature Survey

In this chapter, a brief overview of the modeling and control strategies for pneumatic actuators is presented. Passivity based controllers have been extensively investigated for tele-operation and human power amplification with electro-mechanical actuators. Relevant literature on passivity based controllers is also briefly reviewed.

2.1 Pneumatic systems modeling and control: Background

Due to the compressibility of air, pneumatic actuator dynamics has strong nonlinearities. Earlier controller schemes for pneumatic actuators were however based on actuator models linearized about the mod-stroke position [16],[17]. While these linear controllers were simple to analyze and implement, they can only guarantee good performance in the neighborhood of the nominal position. A linear time varying model was proposed in [18] to provide a better approximation to the nonlinear actuator dynamics. This model was used to design controllers for position tracking. Adaptive control strategies were used in [19], [20], to achieve position and force tracking. While these methods improved the performance of linear controllers, their bandwidth of operation is still limited. Much of the early work on pneumatic actuators also ignores the nonlinearities induced by the flow of the compressible air across a valve. A simple linear mapping is used to characterize the relationship between the command input to the valve and the air flow across the valve. In [21], a complete nonlinear model of a pneumatic actuator was proposed. In addition to the compressibility of air in both the cylinder and the valve, the authors considered

the dynamics of the valve and the transmission loss associated with the hoses, and. A sliding mode controller to track a desired force was proposed in an accompanying paper [22]. It is shown in [22] that the valve dynamics and the transmission losses can be ignored for operations below 20Hz frequency. The applications involving direct human interaction usually operate at lower frequencies. Therefore, in this thesis, the valve dynamics are ignored in the actuator model.

Traditional industrial application of pneumatic actuators has been largely limited to position control systems. The high power to weight ratio and the clean working environment provided by pneumatic actuators has recently made them a popular choice for actuation in human centered robots. This is especially true in therapy robots [23],[24], where the power density of the pneumatic actuators is used to help in rehabilitation of people with muscle disabilities. Due to the nature of interaction, safety of operation is extremely important. In [23], multiple measure to ensure a safe operation of an upper body rehabilitation device are outlined. The device has hard stops much within the range of motion of human operator. This is to prevent the arm from being forced into unnatural configurations. Additional valves are provided to discharge the actuator quickly in case of emergencies. Multiple fault checks are also included in the software to monitor the actuator performance. While this leads to design of simpler controllers, the system requires a lot of redundancy for safe operation. In addition, the robots used in rehabilitation interact with a known set of environments. Therefore the controller can be tuned to respond in a safe manner while interacting with these environments. However, for human interactive applications such as the human power amplifier or the rescue robot, the system will need to interact with unknown and un-modeled environments. Passivity is a concept from systems theory that can guarantee safety when interacting with unknown environments. In the following section, the notion of passivity is briefly explained and the relevant literature is reviewed.

2.2 Passivity based control : Background

Passive systems do not generate any energy internally, and require external energy input to perform any task. In general, for any system with input $u \in R^m$ and output $y \in R^m$,

the external energy supply rate $s(u, y)$ is defined as,

$$s(u, y) \equiv u^T y \tag{2.1}$$

The system is said to be passive with respect to the external supply rate $s(u, y)$ if,

$$\int_0^t s(u, y)\ d\tau \geq -c_o^2 \tag{2.2}$$

where c_o^2 is some positive quantity. The input-output pair (u, y) associated with the supply rate are usually referred to as effort and flow variables. The flow variable represents the flow of matter, while the effort variable represents the effort required for/imposed by the flow of matter. The product of the effort and the flow variables corresponds to the power interaction with the system. For a given system, the input u can be either an effort or a flow variable, and the output y would correspondingly represent either the flow or the effort variable. For example, in a typical electrical system, voltage (effort) and current (flow) correspond to the input-output pair. In mechanical systems, the force (effort) provided by actuator is usually the input, while the velocity (flow) of the inertia is one of the outputs. The supply rate for many mechanical and electrical systems corresponds to physically meaningful power input/extracted from the system. Therefore, the integral inequality in Eq. (2.2) states that the amount of energy that can be extracted from the system to do a particular task is finite, with c_o^2 representing the lower bound on the available energy. As will be shown in later chapters, c_o^2 is usually a function of the initial available energy in the system. Systems with supply rate corresponding to physically meaningful power flow and satisfying the inequality in Eq. (2.2) are said to be energetically passive. Stabilizing controllers satisfying the passivity condition in Eq. (2.2) can also be designed for an arbitrary input and output pair [25]. Such systems are passive with respect to pseudo power variables. Energetic passivity enables simple controller design by taking advantage of passive properties inherent in the system dynamics. The primary objective of our study is to make the pneumatic actuated system behave as a passive mechanical tool (such as a plier or a wrench) to the human operator and the physical environment, that is capable of doing work only when external power from a human operator is provided to the system and remain at rest in the absence of such power input. The desired supply rate is thus defined to be suitable mechanical power extracted from the system.

The main advantage of passivity framework is that it facilitates an intuitive and stable interconnection between systems. As shown by the passivity theorems in [26], closed loop interaction between a passive system and a strictly passive system (strict inequality in Eq. (2.2)) is always passive and hence stable. As shown in the seminal work by Willems [3], with appropriate choice of supply rate, systems operating in multiple domains can be interconnected.

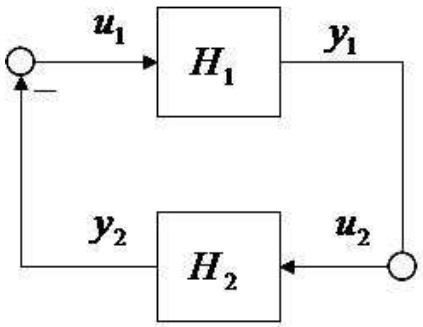

Figure 2.1: Two interconnected passive systems.

Lemma 2.1. *Consider a feedback interconnection between two passive systems as shown in Fig. (2.1). The interconnection is asymptotically stable if one of the systems is strictly passive.*

Proof. The input-output pair for the two systems is defined as,

$$u_2 = y_1, \qquad u_1 = -y_2 \tag{2.3}$$

Assume that the system H_1 is passive and the H_2 is strictly passive. For $V_1 \in \Re^+$ and $V_2 \in \Re^+$, the input-output pair to H_1 and H_2 therefore satisfy the following inequalities,

$$\dot{V}_1 \leq u_1^T y_1, \qquad \dot{V}_2 \leq u_2^T y_2 - \beta(t) \tag{2.4}$$

where $\beta(t) \geq 0$ is a positive function. Define the following Lyapunov function for the combined system,

$$V = V_1 + V_2 \tag{2.5}$$

On differentiating the above Lyapunov function and using the conditions in Eq. (2.3) and Eq. (2.4), we get,

$$\dot{V} \leq -\beta \tag{2.6}$$

Assuming that a series interconnection of the systems satisfy the required observability conditions, the inequality in Eq. (2.6) proves that the interconnected system is asymptotically stable.

□

Typical examples of passive componemts include the damper, the friction brakes, and the spring. These components are energetically dissipative or neutral, and are thus intrinsically passive. Using a combination of these elements, an energetically passive device can be constructed. Examples of such devices include Passive Trajectory Enhancement Robots (PTER) [27], and Cobots [28]. As explained in [27], PTER is built using brakes and clutches as controlling elements and simple trajectory tracking controllers are designed. The driving force is provided externally, either by a human operator or any other power source. As the actuators (brakes and clutches) are energetically dissipative, the forces generated by the PTER are lower and difficult to control [29]. On the other hand, Cobots are built with energetically neutral components and are designed to collaborate with a human operator. They use a computer controlled continuously variable transmission (CVT) to drive the robot along the desired trajectory, while the human operator provides the necessary forces to move the robot. The control input to CVT is the velocity of an internal link. By using amplified human force to control the velocity of this link, desired amplification of human effort can be achieved. In general, while the construction of Cobots makes them passive, their design is usually complicated. Enforcing passive behavior through feedback control provides a convenient way to operate the existing components and devices in a safe manner.

2.2.1 Passivity based control of mechanical systems

A significant focus of earlier work on passive control was on systems with electromechanical actuators ([30] and the references therein). The skew-symmetry property of the inertia dynamics enables design of energetically passive controllers for Euler-Lagrangian systems [31]. However, the applicability of this approach is limited due

to certain assumptions on inverse dynamics [32]. Port-Controlled Hamiltonian (PCH) models of physical systems provide an alternate way to design energetically passive controllers [32]. In this approach, physical power flow variables for individual subsystems are identified to understand the underlying interconnection. This network model utilizes any inherent passive properties of the system in defining the controller. A similar approach is pursued in this thesis. The PCH based controller design as presented in [9], [32] are suitable for regulation of state dynamics to zero and not trajectory tracking. Therefore, these methods are not useful in human interactive applications that usually involves tracking a time varying trajectory generated by the human operator. The major impediment to passivity analysis in such applications is the active energy associated with feed-forward terms in the control input. The feed-forward terms are however required to achieve the desired control objective. In [33], the PCH framework is extended to trajectory tracking problems. However, the passivity analysis shown in [33] is with respect to a modified control input that includes the feed-forward terms. In this thesis, using the approach presented in [34] the total energy demanded by the feed-forward terms is extracted from a fictitious flywheel. The energy of the flywheel is monitored, and if the energy of the flywheel falls below a threshold value, the control input is modified with additional damping to put energy back into the flywheel. This method of monitoring the energy demanded by the controller is similar to the passivity observer proposed in [35].

2.2.2 Passive control of fluid powered devices

Passivity based control for fluid powered systems is a fairly recent research area. The nonlinear actuator dynamics and the inherently non-passive nature of the components [36] presents unique challenges for passive control of fluid powered systems. As shown in [36], a hydraulic valve is not passive. It is shown that passification of the valve can be achieved either through re-design of valve or through active feedback. In [6], the feedback based passification scheme for hydraulic valves was used to achieve passive bilateral tele-operation of a backhoe. In [37], a passivity based control for regulation of hydraulic actuator is presented. A PCH model for hydraulic systems is presented in [38]. By assuming constant bulk modulus, an energy function for hydraulic systems was developed in [38] from first principles. A nonlinear controller for position regulation

was then developed based on this energy function. In [39] the states of the hydraulic system are transformed to define a new energy function. A stabilization controller is defined based on this new energy function. A simplified model of hydraulic system is analyzed in [40] for PCH based controller design. In [41], an energetic formulation for hydraulic actuators with pressure dependent bulk modulus is reported. A Lyapunov function based on the energy function is used to design controller for desired trajectory tracking. As clearly evident, there has been some recent effort towards energy based control of hydraulic systems. On the other hand, very little work has been done on development of such schemes for pneumatic actuators.

In [7], a passive control for force tracking with a pneumatic actuator is designed by defining a pseudo energy function in terms of the actuator force output. The operation is shown to be passive for a supply rate defined as the product of force and the input command to the valve. This choice of supply rate is only for convenience of controller design and does not correspond to the actual energy being input or extracted from the system. Energetically passive controller design requires an appropriate definition of the actuator energy function. The proper choice of energy function for a pneumatic actuator varies with the assumed thermodynamic process in the actuator. In [42], sum of change in internal energy in each chamber of a two-chambered pneumatic actuator defined with respect to ambient conditions is used as an energy function. This energy function is shown to be similar to that of a linear spring, with the mid-stroke position of the actuator corresponding to the fixed equilibrium point. The energy function is used to design controllers for position tracking in a hopping robot. But, as shown in [43], the stiffness of the actuator is a nonlinear function of the piston position, with a maximum value in the mid-stroke position and minimum value towards the ends . In this thesis, energy function for the pneumatic actuator is developed by considering the nonlinear dynamics of the actuator. Energy based storage functions for isothermal, adiabatic and finite heat transfer models are presented. The energy function for adiabatic model is similar to the one presented in [42], but is defined with respect to the adiabatic equilibrium pressure and temperature. The energy function for pneumatic actuator with finite heat transfer is defined as the maximum work available from the actuator. The solution to the maximization problem is shown to be similar to the exergy of air in the cylinder chambers. Using exergy as the measure of work potential from compressed

air, an instrument for measuring the exergy of air is developed in [44] and is used to evaluate efficiency of operation in industrial pneumatic systems. Exergy as a definition of work potential in systems with multiple domains is discussed in [45]. For mechanical systems, exergy corresponds to mechanical energy in the system. In [45], this definition of exergy is used as a Lyapunov function to develop a stabilizing controller for an aircraft. It should be mentioned that our conclusion regarding exergy as an appropriate definition for work potential was attained prior to our knowledge of the work presented in [44] or [45]. In the following subsection, relevant prior work in the area of human-machine interaction is reviewed.

2.2.3 Human-machine interaction

The human-machine interactive applications of interest in this study are a human power amplifier and a bilateral tele-operator. Kazerooni and his collaborators have done significant work on hydraulic human power amplifiers ([46], [47] and the references therein), which they refer to as *human extenders*. The controllers in these applications were however not developed to achieve passive operation and thus cannot guarantee interaction stability with any unknown or un-modeled environments. Passive operation through feedback has been extensively investigated for systems with human machine interactions (e.g. [48], [34], [49],[50], [35] and the references therein). In ([48],[34],[49] and [50]), an energy dependent velocity field is used to passively guide a robot along a prescribed trajectory in the robot workspace. Labeled as Passive Velocity Field Control (PVFC), this method provides a safe way for performing repetitive tasks while requiring minimum supervision from the human operator.

In applications with human-machine interaction, it is desired that the machine respond as a common passive mechanical tool. In applications requiring tele-operation, the system consisting of both the master and the slave should behave as a passive mechanical tool with ports for mechanical power interaction with human operators at both the master and the slave systems, and physical environments at both the master and the slave locations. The operation of a common passive mechanical tool feels as if it were a simple extension of human limb providing the operator with extended physiological proprioception (EPP) [51], [52]. In [53], this property is imposed while achieving scaled tele-manipulation with electromechanical actuators. A passive controller, to track the

desired dynamics of a virtual rigid mechanical tool, is obtained by canceling out the nonlinear dynamics. However, passivity is only shown for the linearized dynamics. Thus, robustness may become an issue in the absence of complete information about the system dynamics. In [30], a passive controller for nonlinear bilateral tele-operation between two systems with electromechanical actuators is presented. The co-ordinated system is controlled to follow the dynamics of a desired rigid mechanical tool. However, unlike in [53], the nonlinear dynamics are not canceled out. A major advantage of this approach is that passivity can be enforced robustly, even with inadequate information about the environment forces. In [54], [55], energetically passive controllers were developed by using bond graphs for bilateral tele-operation of hydraulic systems. The co-ordinated tele-operator is again controlled to behave as a rigid mechanical tool with desired dynamics.

In tele-operators, passivity based controllers are used to guarantee safety and stability when interacting with unknown and un-modeled environments. While some prior work has been done on tele-operation with hydraulic actuators ([54],[6], [55] and the references therein), not much work has been published on tele-operation with pneumatic actuators. In [56], an impedance control scheme is proposed for tele-operation of a four d.o.f. master-slave system that is used in laparoscopic surgery. The master system is actuated by electro-mechanical actuators, while the slave system is pneumatically actuated. While the authors do not describe the actuator model, the control schematic indicates that a linear model of the pneumatic actuator is used in the controller design. In [57], a 4-channel scheme is used to achieve tele-operation between two single DOF pneumatic actuators. Solenoid valves are used to meter the air flow to the actuators. While the results show position co-ordination, passive operation is not investigated. In [58], a linear PID control scheme was used to tele-operate a rescue robot. In the current dissertation, a new framework for rendering passive mechanical tool characteristics to pneumatic actuated systems is presented.

In [59], a novel method for energetically passive human power amplification with hydraulic actuators was presented. The compressible actuator is modeled as a combination of an ideal actuator (velocity source) with no compressibility and a nonlinear spring for modeling the compressibility effects. By controlling the ideal velocity as velocity of a virtual inertia, an energetically passive structure is obtained. In [60], a

general framework of this approach for both hydraulic and pneumatic actuators, using the energy function as a storage function, was presented. In [61], contour following using the PVFC based control from [34] was implemented on a two-DOF hydraulic human power amplifiers. In addition to contour following, the control implemented in [61] also provided obstacle avoidance. The energy function in [60] and [61] was however derived by assuming that the fluid-powered actuator behaves a linear spring. In this dissertation, the nonlinear characteristics of the pneumatic actuator are considered in deriving a physics based energy function for the pneumatic actuator. This energy function is used to define a framework for achieving energetically passive operation of pneumatic actuated human power amplifier and co-ordinated tele-operation of multiple fluid powered systems. Lyapunov function based on the physics based energy function is used to design the controllers for achieving the control objective.

2.3 Independent metering

In mobile applications with limited supply of pressurized air, improvements in operational efficiency can greatly enhance the total operation time. When using a single valve to meter the air flow to the two-chambered pneumatic actuator, a source of loss is the discharge of high pressure air to the atmosphere. One of the ways to mitigate this loss is to scavenge the discharged high pressure air for additional mechanical work. In [62], high pressure air on the discharge side is rerouted to the charging side through an accumulator. In [63], a two-way valve is used to achieve cross flow from the discharging side to the charging side. Efficiency can also be enhanced by operating the system at a lower pressure, thus minimizing the loss associated with discharge of high pressure air. In this dissertation, independent metering of air to the two chambers of the pneumatic actuator is used to lower the maximum pressure required to perform a task.

In a proportional servo-valve, the flow areas metering the flow in and out of the actuator are mechanically coupled. As a result, it is impossible to control the pressure in both chambers of the actuator independently. Independent metering ([11],[64]) is an approach that can be used to overcome the coupling between the two flow areas. A schematic of the pneumatic actuator with independent metering is shown in Fig. (2.3). By having two independent valves, the desired task from the actuator can be performed

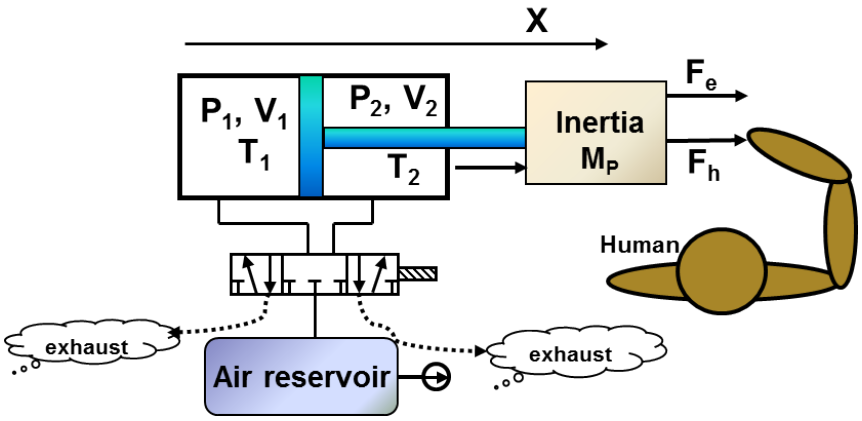

Figure 2.2: A typical application of a pneumatic actuator to move inertial loads. A single 5-port, 3-way proportional valve is used to meter air flow to the actuator

while controlling the operating pressure of the system. In [11], an optimization method is proposed for a pneumatic actuator to minimize the operating pressure to the atmospheric pressure, while tracking a sinusoidal trajectory. While this method is suitable for trajectory tracking, it is not amenable for force tracking. As the desired force changes, higher pressure might be required in one of the chambers, which negates the objective of maintaining average pressure at atmospheric pressure. In [64], the operating pressure is lowered by regulating the pressure on the discharging side to a lower value. While this is similar to our proposed method for energy saving, our method provides an explicit way to exponentially regulate the pressure on the discharging side. In this thesis, the advantage offered by independent metering through improved efficiency of operation is evaluated on a single-DOF penumatic human power amplifier.

2.4 Summary

Passivity is a useful control strategy for ensuring safety in human-machine interaction. While extensive research has been done towards passive control of electro-mechanical actuators, such controllers for pneumatic actuators is an open research problem. The preliminary published ideas on passivity based control of pneumatic actuators are limited by their underlying assumptions. In the current work, physics based energy functions

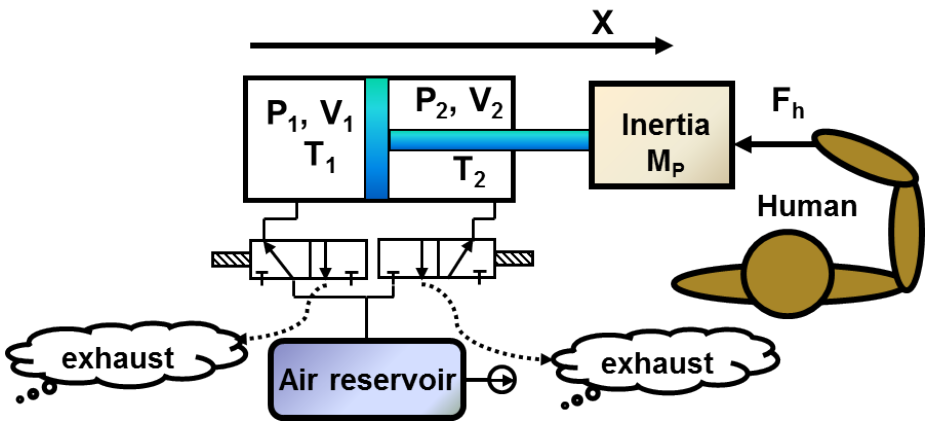

Figure 2.3: Operation of pneumatic actuator with two independent, 3-port 2-way proportional valves

for three different thermodynamic models (adiabatic, isothermal and finite heat transfer) of the pneumatic actuator are developed by considering the nonlinear dynamics of the actuator. These energy functions are used to design energetically passive controllers for the pneumatic actuator. In the following chapter, the pneumatic actuator model used in this study is presented. Storage functions for isothermal and adiabatic models of the actuator are also derived in chapter 3. Storage function for pneumatic actuator with finite heat transfer is derived in chapter 4. Energetically passive controllers for human power amplification and co-ordinated tele-operation of multiple actuators is presented in chapter 5 and chapter 6 respectively. Independent metering of an isothermal pneumatic actuator used in a human power amplifier is presented in chapter 8.

Chapter 3

Pneumatic Actuator : Dynamics and Energy

In this chapter, lumped-parameter model of a pneumatic actuator is presented. A two-chambered pneumatic actuator as shown in Fig. (3.1) is used to provide the required force in this study. For a two-chambered actuator, it is common practice to designate the air volume on the piston cap side as chamber 1, while the air volume on the piston rod side is referred to as chamber 2. The force F_a generated by the actuator depends on the air pressures P_1 and P_2 in chambers 1 and 2 of the actuator respectively, and is given by,

$$F_a(P_1, P_2) = P_1(t)A_1 - P_2(t)A_2 - P_oA_p \tag{3.1}$$

where P_o represents the atmospheric pressure, A_1 is the cap-side cross-sectional area of the piston, A_p is the rod cross-sectional area and $A_2 \triangleq (A_1 - A_p)$ is the rod-side cross-sectional area of the piston. The pressure in each actuator chamber is varied to achieve the desired output force from the actuator. The pneumatic valve in Fig. (3.1) is used as the control element for changing the pressure dynamics in each chamber of the actuator.

A two-chambered pneumatic actuator can be interpreted as two single chamber actuators mechanically coupled by the actuator piston. For clarity of presentation, dynamics and energy function for single-chamber actuator are first developed in section 3.1. As shown in Fig. (3.1), a control volume can be defined for each chamber of the

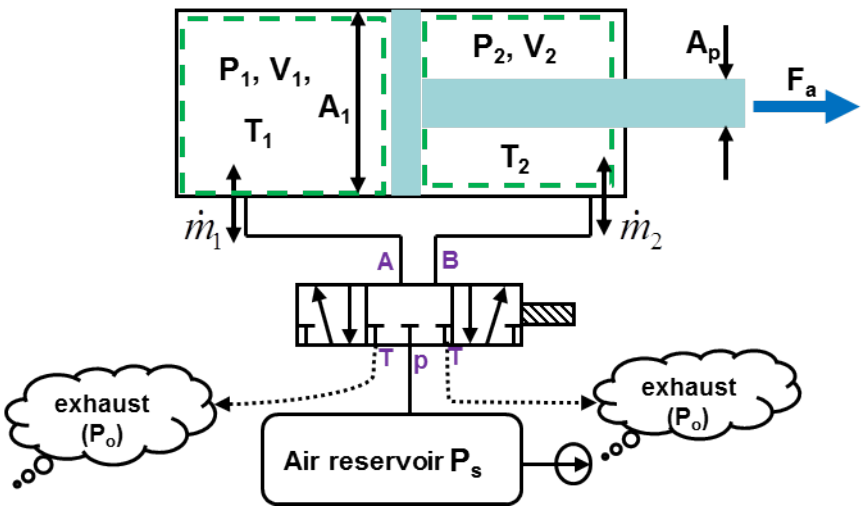

Figure 3.1: Schematic illustrating the control volume (CV) in each actuator chamber of a two-chambered pneumatic actuator. The dashed green line in the schematic represents the boundary of the control volume in each chamber.

actuator. The actuator dynamics is developed for a generic heat transfer model by applying first law of thermodynamics to the control volume. Temperature and pressure dynamics in a control volume(CV) representing a single chamber actuator chamber with a generic heat transfer model are reported in section 3.1.1. Dynamics corresponding to isothermal and adiabatic actuators are then identified from this general model. In section 3.1.3, the energy function for the air in the control volume is derived. By defining this energy function as a storage function, the supply rate for energetically passive interaction with the single-chamber pneumatic actuator is identified in section 3.1.4. The port variables for establishing this energetically passive interconnection between the corresponding pneumatic actuator and other physical subsystems are also highlighted. By treating the two-chambered actuator as two interacting single chamber actuators, the corresponding dynamics, energy function and supply rate are developed in section 3.2. In section 3.2.1, the dynamics of two-chambered adiabatic and isothermal actuators is presented. The energy function corresponding these actuators is presented in section 3.2.3. The actuator supply rate for achieving energetically passive operation of two-chambered isothermal and adiabatic actuators is presented in section 3.2.4. In section

3.3, the energy function for the two-chambered actuator from section 3.2 is used to define the energy function corresponding to actuator error dynamics. Concluding remarks for the chapter are presented in section 3.4

3.1 Single chambered actuator

In this section, pressure and temperature dynamics of a single chamber pneumatic actuator are developed for a generic model of heat transfer between the chamber air and the environment. Two specific thermodynamic models *viz*, isothermal and adiabatic models are explored further. Energy function corresponding to these reversible thermodynamic models is also developed in this section. By defining the energy function to be the storage function of the actuator, the supply rate for achieving energetically passive operation of single-chamber pneumatic actuator is also presented in this section.

3.1.1 Actuator dynamics

Consider a control volume as shown in Fig. (3.2). This control volume can also be interpreted as a single chamber actuator. It is assumed that the pressure and temperature are uniformly distributed in the control volume and can therefore be represented by a differential equation. The temperature dynamics in the control volume is obtained by applying the first law of thermodynamics. The pressure dynamics in the control volume is obtained by assuming that air behaves as an ideal gas.

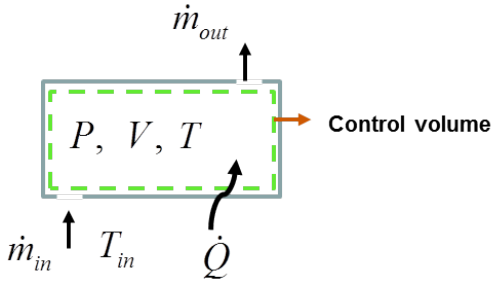

Figure 3.2: Schematic of an open system with both ingress and egress of matter from the control volume (CV)

Let P, V, m, T respectively correspond to the pressure, volume, mass, and temperature of air in the control volume. From ideal gas law [65], they are related as,

$$PV = mRT \tag{3.2}$$

where R is the universal gas constant. Let $\dot{m}_{in}$ and $\dot{m}_{out}$ correspond to the mass flow rate of air entering and leaving the control volume respectively. From conservation of mass, the rate of change of mass in the control volume is given by,

$$\dot{m} = \dot{m}_{in} - \dot{m}_{out} \tag{3.3}$$

As air is assumed to behave as an ideal gas, the specific heat at constant pressure C_p, and the specific heat at constant volume C_v, are constant over the operating regime of the actuator and are related to the universal gas constant R as,

$$C_p = \frac{R\gamma}{\gamma - 1}, \qquad C_v = \frac{R}{\gamma - 1} \tag{3.4}$$

where $\gamma \triangleq C_p/C_v$ is the ratio of specific heats and has a value of 1.4 for air. Let T_{in} be the temperature of the air entering the control volume. The internal energy U of the air in the control volume, the specific enthalpy h_{in} of the air entering the control volume, and the specific enthalpy h_{out} of the air exiting the control volume are given by,

$$U \triangleq mC_vT, \quad h_{in} \triangleq C_pT_{in}, \quad h_{out} \triangleq C_pT \tag{3.5}$$

By defining the heat transfer rate $\dot{Q}$ to be positive when heat is supplied to the control volume from ambient, and defining the boundary work $P\dot{V}$ done by the control volume to be positive, the rate of change of internal energy in the control volume is obtained from the first law of thermodynamics [65] as,

$$\dot{U} = \dot{Q} - P\dot{V} + \dot{m}_{in}h_{in} - \dot{m}_{out}h_{out} \tag{3.6}$$

Using the definition of the internal energy and the specific enthalpies from Eq. (3.5), and from the definition of mass continuity in Eq. (3.3), the air temperature dynamics in the control volume is obtained from the first law statement in Eq. (3.6) as,

$$mC_v\dot{T} = -(\dot{m}_{in} - \dot{m}_{out})C_vT + \dot{Q} - P\dot{V} + \dot{m}_{in}C_pT_{in} - \dot{m}_{out}C_pT \tag{3.7}$$

By using Eq. (3.4) to express C_p in terms of C_v and R, the temperature dynamics in Eq. (3.7) can be written as,

$$mC_v\dot{T} = \dot{m}_{in}C_v(\gamma-1)T - \dot{m}_{out}C_v(\gamma-1)T - P\dot{V} + \dot{Q} + \dot{m}_{in}C_p(T_{in}-T) \tag{3.8}$$

Assuming there are no leakage paths, the mass of air in the control volume can be changed only through the pneumatic valve. In typical applications with pneumatic actuators, a single valve as shown in Fig. (3.1) is used to meter the air flow to/from the actuator. As a result, at any given time, air is either entering the control volume ($\dot{m}_{out} = 0$), or exiting from the control volume to the ambient ($\dot{m}_{in} = 0$). Therefore the temperature dynamics in the actuator chamber varies with the direction of air mass flow rate. Using the ideal gas law from Eq. (3.2) to expresses the chamber pressure P in terms of the chamber temperature T, the temperature dynamics in Eq. (3.8) can be expressed as,

$$\frac{\dot{T}}{T} = \begin{cases} (\gamma-1)\left(\frac{\dot{m}}{m} - \frac{\dot{V}}{V} + \frac{\dot{Q}}{mRT}\right) + \gamma\frac{\dot{m}}{m}\left(\frac{T_{in}}{T} - 1\right) & \text{if } \dot{m} \geq 0 \text{ charging} \\ (\gamma-1)\left(\frac{\dot{m}}{m} - \frac{\dot{V}}{V} + \frac{\dot{Q}}{mRT}\right) & \text{if } \dot{m} < 0 \text{ discharging} \end{cases} \tag{3.9}$$

On differentiating the ideal gas law in Eq. (3.2), and using the temperature dynamics from Eq. (3.9), the pressure dynamics in an actuator chamber are obtained as,

$$\frac{\dot{P}}{P} = \begin{cases} \gamma\left(\frac{\dot{m}}{m} - \frac{\dot{V}}{V}\right) + (\gamma-1)\frac{\dot{Q}}{PV} + \gamma\frac{\dot{m}}{m}\left(\frac{T_{in}}{T} - 1\right) & \text{if } \dot{m} \geq 0 \text{ charging} \\ \gamma\left(\frac{\dot{m}}{m} - \frac{\dot{V}}{V}\right) + (\gamma-1)\frac{\dot{Q}}{PV} & \text{if } \dot{m} < 0 \text{ discharging} \end{cases} \tag{3.10}$$

The heat transfer rate $\dot{Q}$, and the inlet air temperature T_{in}, are external factors effecting the pressure dynamics. The rate of change of volume $\dot{V}$, is determined by the forces acting on the actuator piston. The air mass flow rate $\dot{m}$ is the control input available for achieving the desired pressure while compensating the effect of these factors on the actuator pressure dynamics.

The commonly studied thermodynamic process in the actuator are the adiabatic process ($\dot{Q} = 0$) and the isothermal process ($\dot{T} = 0$). Both these processes are reversible and their dynamics are amenable for analysis and controller design. For both the isothermal and the adiabatic processes, it is common to assume that the inlet air temperature is the same as the chamber air temperature ($T_{in} = T$ in Eq. (3.9)). This

assumption is reasonable, as T_{in} corresponds to the temperature of the air in the dead volume just outside the control volume. If the inlet air temperature T_{in} is different from the ambient temperature T, entropy is generated during mixing of the inlet air with the chamber air. Therefore, the thermodynamics of the actuator will not be reversible. The effect of this irreversibility is investigated for an actuator with finite heat transfer model in the next chapter. In the following section, dynamics corresponding to the adiabatic process are presented.

Adiabatic process

The schematic for a single chamber actuator with a servo valve for controlling the air flow to the chamber is as shown in Fig. (3.3). In an actuator with adiabatic process, there is no thermal interaction between the actuator and the environment ($\dot{Q} = 0$ in Eq. (3.6)). Such an actuator can be realized by providing thermal insulation between the actuator chamber and the ambient.

Let $\rho = m/V$ be the density of air in the actuator chamber. For an ideal gas, the density ρ is obtained in terms of chamber P and temperature T by using the ideal gas law from Eq. (3.2) as,

$$\rho(P,T) = \frac{m}{V} = \frac{P}{RT} \tag{3.11}$$

From Eq. (3.9) and Eq. (3.10), the temperature and pressure dynamics in an adiabatic actuator chamber can be expressed in terms of density ρ as,

$$\frac{\dot{T}}{T} = (\gamma - 1)\left(\frac{\dot{m}}{m} - \frac{\dot{V}}{V}\right) = (\gamma - 1)\frac{\dot{\rho}}{\rho} \tag{3.12}$$

$$\frac{\dot{P}}{P} = \gamma\left(\frac{\dot{m}}{m} - \frac{\dot{V}}{V}\right) = \gamma\frac{\dot{\rho}}{\rho} \tag{3.13}$$

For ease of presentation, it is assumed that when the temperature corresponds to ambient temperature T_o, the chamber pressure P corresponds to the ambient pressure P_o. Integrating the pressure dynamics in the above equation, the chamber pressure P and the air density ρ are related as,

$$\frac{P}{\rho^\gamma} = k_{a\rho} = \frac{(RT_o)^\gamma}{P_o^{\gamma-1}} \tag{3.14}$$

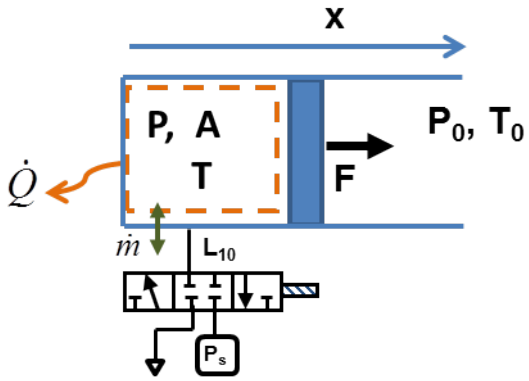

Figure 3.3: Schematic of a single chamber actuator with a 3-position, 2-way pneumatic valve for controlling air flow to the actuator.

where the integration constant $k_{a\rho}$ is determined from the initial condition that at $P = P_o$, the air temperature is given by $T = T_o$ and the air density is given by $\rho(P_o, T_o) = P_o/RT_o$. For given initial conditions (P_o, T_o), the air density $\rho(P, T)$ for an adiabatic actuator can be expressed as a function of the chamber pressure P only, and is obtained from Eq. (3.14) as,

$$\rho(P,T) = \left(\frac{P}{k_{a\rho}}\right)^{1/\gamma} = \frac{P}{RT_o}\left(\frac{P_o}{P}\right)^{\frac{\gamma-1}{\gamma}} \tag{3.15}$$

An example trajectory generated by the adiabatic characteristic curve in Eq. (3.14) is as shown in Fig. (3.4).

From the temperature dynamics in Eq. (3.12) and the pressure dynamics in Eq. (3.13), the temperature and the pressure dynamics in the adiabatic actuator are related as,

$$\frac{\dot{T}}{T} = \frac{\gamma - 1}{\gamma}\frac{\dot{P}}{P} \tag{3.16}$$

Integrating the above equation, and using the condition that at ambient temperature T_o, the chamber pressure P corresponds to ambient pressure P_o, temperature and pressure in an adiabatic actuator are related as,

$$TP^{(1-\gamma)/\gamma} = k_{tp} = T_o P_o^{(1-\gamma)/\gamma} \tag{3.17}$$

where the integration constant k_{tp} is calculated from P_o and T_o. From the above equation, the chamber air temperature T can be determined from the chamber air pressure P as,

$$T = k_{tp} P^{(\gamma-1)/\gamma} = T_o \left(\frac{P}{P_o} \right)^{(\gamma-1)/\gamma} \tag{3.18}$$

Note that the expression for density $\rho(P,T)$ in Eq. (3.15) for adiabatic actuator is also obtained by using the temperature-pressure relationship from Eq. (3.18) in the expression for ideal gas density in Eq. (3.11).

Dynamics of single chambered isothermal actuator are presented in the next section.

Isothermal process

The other reversible process that is commonly studied is the isothermal thermodynamic process. By definition, the air temperature in the chamber of an isothermal actuator is constant. For achieving a constant temperature ($\dot{T} = 0$ in Eq. (3.9)) in the actuator chamber along with the assumption that the inlet air temperature T_{in} is the same as the chamber air temperature T, the required heat transfer rate $\dot{Q}$ between the chamber air and the ambient is obtained from Eq. (3.9) as,

$$\dot{Q} = -mRT \left(\frac{\dot{m}}{m} - \frac{\dot{V}}{V} \right) \tag{3.19}$$

Using the above expression for $\dot{Q}$, the pressure dynamics for the isothermal thermodynamic process is obtained from Eq. (3.10) as,

$$\frac{\dot{P}}{P} = \frac{\dot{m}}{m} - \frac{\dot{V}}{V} = \frac{\dot{\rho}}{\rho} \tag{3.20}$$

Typically, it is assumed that the chamber temperature in the isothermal actuator is the same as the ambient air temperature T_o ($T_{in} = T = T_o$). This can be realized if the actuator dynamics are very slow providing sufficient time for thermal equilibrium between the chamber air and the ambient. Isothermal process can also be realized if the thermal transmittance of the actuator surface is high enough to guarantee instantaneous equilibrium with the ambient temperature T_o.

Integrating the pressure dynamics in Eq. (3.20) and using the condition that at $P = P_o$, the air density is given by $\rho(P_o, T_o) = P_o/RT_o$, the characteristic equation for

an isothermal process is obtained as,

$$\frac{P}{\rho} = k_{c\rho} = RT_o \tag{3.21}$$

From the above equation, the air density for the isothermal actuator is obtained as $\rho(P, T_o) = P/RT_o$ and thus depends only on the chamber pressure P. An example trajectory generated by the isothermal characteristic curve in Eq. (3.21) is as shown in Fig. (3.4).

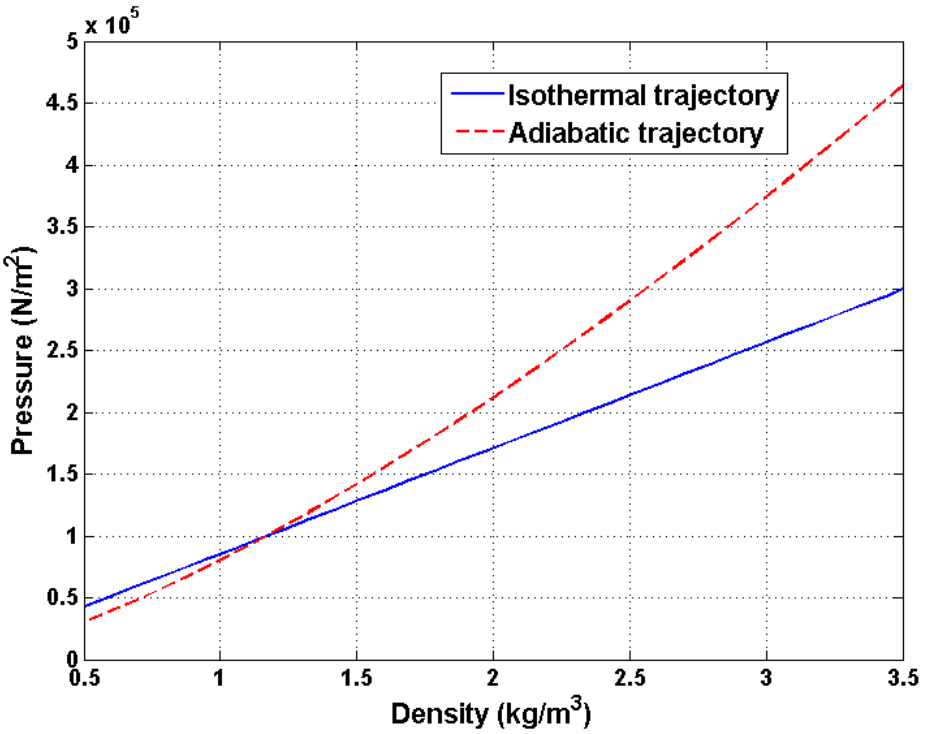

Figure 3.4: Schematic of example characteristic curves for adiabatic and isothermal processes generated from Eq. (3.32) and Eq. (3.42) respectively.

3.1.2 Mass flow rate

In this study a proportional servo-valve is used to modulate the air flow rate to/from the actuator chamber. The position of the valve spool determines if the chamber is

connected to the supply pressure P_s or the ambient pressure P_o. The magnitude and direction of air flow rate $\dot{m}$ across the valve depends on the pressure at the inlet and the outlet of the valve, and the effective orifice area available in the valve. In a proportional servo-valve, the effective orifice area available can be varied by adjusting the spool position. To achieve the desired air flow rate, the spool position is varied by providing a current or a voltage command to the valve solenoid. As the spool dynamics are much faster than the pressure dynamics in the actuator, it is reasonable to assume that the spool reaches the commanded position instantaneously [21]. Therefore, the effective orifice area is selected to be the command input u to the pneumatic actuator. For a positive value of the command input u, the spool is positioned such that the actuator chamber is connected to the supply pressure P_s, while a negative command input u to the spool connects the chamber volume to the ambient pressure P_o.

Prior to defining the mass flow rate as a function of the input command u and the pressures P_s, P_o and P, a function $Sg(.)$ is defined as follows,

$$Sg(x) = \begin{cases} 1 & \text{if } x > 0 \\ 0 & \text{if } x \leq 0 \end{cases} \tag{3.22}$$

The air flows from the high pressure side (upstream side) to the low pressure side (downstream side). For a given supply pressure P_s and ambient pressure P_o, the air pressure $P_u(P,u)$ upstream of the valve and pressure $P_d(P,u)$ downstream of the valve are obtained in terms of the command input u and the chamber pressure P as,

$$\begin{aligned} P_u(P,u) = {} & (P_s Sg(P_s - P) + P Sg(P - P_s))Sg(u) \\ & + (P Sg(P - P_o) + P_o Sg(P_o - P))Sg(-u) \end{aligned} \tag{3.23}$$

$$\begin{aligned} P_d(P,u) = {} & (P_s Sg(P - P_s) + P Sg(P_s - P))Sg(u) \\ & + (P Sg(P_o - P) + P_o Sg(P - P_o))Sg(-u) \end{aligned} \tag{3.24}$$

where $Sg(.)$ is as defined in Eq. (3.22). For a given inlet air temperature T_{in} to the actuator chamber, the air temperature $T_u(T,u)$ upstream of the valve is defined as,

$$T_u(T,u) = (T_{in} Sg(P_s - P) + T Sg(P - P_s))Sg(u) + (T Sg(P - P_o) + T_{in} Sg(P_o - P))Sg(-u) \tag{3.25}$$

It is common to assume that the air flow through the valve is analogous to isentropic compression and expansion of air in a converging-diverging nozzle [21]. Thus, for a constant supply pressure P_s and ambient pressure P_o, the magnitude of the air mass flow rate to the actuator chamber is determined by the chamber pressure P, the air temperature T upstream of the valve and the valve orifice area determined by the input command u to the actuator valve and is defined as [21],

$$\dot{m} = \Psi(P, T, u)u \tag{3.26}$$

where the nonlinear function $\Psi(P, T_u, u)$ depends on the upstream pressure $P_u(P, u)$ in Eq. (3.23), the downstream pressure $P_d(P, u)$ in Eq. (3.24) and the upstream temperature $T_u(T, u)$ in Eq. (3.25) as,

$$\Psi(P,T,u) = \begin{cases} C_1 \frac{P_u(P,u)}{\sqrt{RT_u(T,u)}} & \text{if } \frac{P_d(P,u)}{P_s(P,u)} \leq P_{cr} \text{ (choked flow)} \\ C_2 \frac{P_u(P,u)}{\sqrt{RT_u(T,u)}} \left(\frac{P_d(P,u)}{P_u(P,u)}\right)^{\frac{1}{\gamma}} \sqrt{1 - \left(\frac{P_d(P,u)}{P_u(P,u)}\right)^{\frac{\gamma-1}{\gamma}}} & \frac{P_d(P,u)}{P_u(P,u)} > P_{cr} \text{ (unchoked flow)} \end{cases} \tag{3.27}$$

In the above equation, the units corresponding to the input u are m^2 and the units corresponding to the nonlinear function $\Psi(P, T_u, u)$ are $kg/m^2/s$. The dimensionless parameters C_1, C_2 and the critical pressure ratio P_{cr} are given by,

$$C_1 = \sqrt{\gamma \left(\frac{2}{\gamma+1}\right)^{\gamma+1/\gamma-1}}, \quad C_2 = \sqrt{\frac{2\gamma}{\gamma-1}}, \quad P_{cr} = \left(\frac{2}{\gamma+1}\right)^{\gamma/\gamma-1} \tag{3.28}$$

As stated in the earlier section, the air temperature T_{in} at the valve outlet ($i.e$ the chamber dead volume) is assumed to be the same as the chamber temperature T for isothermal and adiabatic actuators. As a consequence, the upstream temperature will be the same as chamber temperature ($T_u(T, u) = T$).

In this study, the command input u to the actuator, is to be designed for achieving energetically passive operation of the pneumatic actuator. Therefore, it is important to define a suitable energy function for the pneumatic actuator. By defining the energy function to be the storage function, the supply rate for achieving energetically passive operation of pneumatic actuator is derived. In the following subsection, energy function for a single chamber pneumatic actuator is developed.

3.1.3 Single chamber actuator energy function

In this section, energy functions are developed for adiabatic and isothermal processes in the single chamber actuator. For ease of presentation it is assumed that the piston area exposed to both the chamber pressure P and ambient pressure P_o is the same. The force exerted by the single chamber actuator then is given by,

$$F(P) = (P - P_o)A \tag{3.29}$$

where A is the piston cross-sectional area. The ambient air pressure P_o therefore determines the equilibrium state in a single chamber actuator. The initial state of the actuator corresponds to mechanical equilibrium ($P = P_o$) and thermal equilibrium ($T = T_o$) with the ambient. As additional air mass is added to the actuator chamber for extracting work output, the pressure-volume($P - V$) and temperature-volume ($T - V$) curves in the actuator chamber will move along a trajectory that passes through (P_o, T_o).

As both isothermal and adiabatic processes are reversible, the energy in the actuator for these processes is the boundary work available from the actuator with respect to the equilibrium state corresponding to zero actuator force $F(P) = 0$. From ideal gas law in Eq. (3.2), the chamber volume at the equilibrium state $\bar{V}$ is obtained in terms of the air mass m in the actuator chamber as,

$$\bar{V}(m) = \frac{mRT_o}{P_o} \tag{3.30}$$

For a chamber pressure p and a chamber volume υ, the energy available in the single chambered actuator with a reversible thermodynamic process is then given by,

$$W_{act}(m, P, P_o) = \int_{V(m,P)}^{\bar{V}(m)} (p - P_o)\, d\upsilon \tag{3.31}$$

The relationship between the pressure p, and the volume υ is determined by the underlying thermodynamic process in the actuator. In the next two subsections, energy available in the single chambered actuator for adiabatic and isothermal thermodynamic process are derived.

Adiabatic process

On integrating the pressure dynamics in Eq. (3.13), and using the boundary condition that for chamber pressure $p = P_o$, the chamber volume υ is given by the equilibrium

volume $\bar{V}(m)$ in Eq. (3.30), the pressure-volume characteristic equation for adiabatic actuator is obtained as,

$$p\upsilon^{\gamma} = k_a(m) = \frac{(mRT_o)^{\gamma}}{P_o^{\gamma-1}} = m^{\gamma}k_{a\rho} \tag{3.32}$$

where $k_{a\rho}$ is a positive constant and $k_a(m)$ is a constant for a fixed mass of air m in the actuator chamber.

For a fixed mass of air m, using Eq. (3.32), a differential change $d\upsilon$ in the chamber volume υ of the adiabatic actuator can be expressed in terms of corresponding chamber pressure p and differential change in pressure dp as,

$$d\upsilon = -\frac{\upsilon}{\gamma p}dp = -\frac{mk_{a\rho}^{1/\gamma}}{\gamma p^{(\gamma+1)/\gamma}}dp \tag{3.33}$$

Using the above equation, the energy function for a single chambered adiabatic actuator is obtained from Eq. (3.31) as,

$$W_{act}^{adb}(m,P,P_o) = \int_{V(m,P)}^{\bar{V}(m)} (p-P_o)\, d\upsilon = \frac{mk_{a\rho}^{1/\gamma}}{\gamma}\int_{P_o}^{P} (p-P_o)\,\frac{dp}{p^{(\gamma+1)/\gamma}} \tag{3.34}$$

On integrating the above equation, the energy in an adiabatic actuator is obtained as,

$$W_{act}^{adb}(m,P,P_o) = mk_{a\rho}^{1/\gamma}\left(\frac{1}{\gamma-1}\left(P^{(\gamma-1)/\gamma} - P_o^{(\gamma-1)/\gamma}\right) + P_o\left(\frac{1}{P^{1/\gamma}} - \frac{1}{P_o^{1/\gamma}}\right)\right) \tag{3.35}$$

Using the relationship $mk_{a\rho}^{1/\gamma}p^{-1/\gamma} = \upsilon$ between the pressure p and the volume υ for the pressure volume pairs (P,V) and $(P_o,\bar{V}(m))$ from Eq. (3.32), and using the ideal gas law ($PV = mRT$) from Eq. (3.2), the actuator energy function in Eq. (3.35) can be expressed as,

$$W_{act}^{adb}(m,P,P_o) = mC_v(T-T_o) - P_o(\bar{V}(m) - V) \tag{3.36}$$

where the temperature T and the volume V are related to pressure P and mass m as given in Eq. (3.18) and Eq. (3.32) respectively. From the above equation it can be seen that the energy function for the adiabatic actuator is the sum of change in the chamber internal energy and the work done against ambient pressure P_o before reaching

the equilibrium state. From Eq. (3.35) the gravimetric energy density of the actuator is obtained as,

$$\begin{aligned} W_m^{adb}(P,P_o) &= \frac{W_{act}^{adb}(m,P,P_o)}{m} \\ &= k_{a\rho}^{1/\gamma}\left(\frac{1}{\gamma-1}\left(P^{(\gamma-1)/\gamma}-P_o^{(\gamma-1)/\gamma}\right)+P_o\left(\frac{1}{P^{1/\gamma}}-\frac{1}{P_o^{1/\gamma}}\right)\right) \end{aligned} \tag{3.37}$$

For an adiabatic actuator, the air density $\rho = m/V$ can be defined in terms of the chamber pressure P by using the ideal gas law from Eq. (3.2), and the temperature-pressure relationship from Eq. (3.18) as,

$$\rho(P,T) = \frac{m}{V} = \frac{P}{RT} = \frac{P_o}{RT_o}\left(\frac{P}{P_o}\right)^{\gamma} \tag{3.38}$$

Using the definition of the density $\rho(P,T)$ from the above equation, the gravimetric energy density of a single chamber adiabatic actuator is obtained from Eq. (3.36) as,

$$W_m^{adb}(P,P_o) = C_v(T-T_o) - P_o\left(\frac{1}{\rho(P_o,T_o)}-\frac{1}{\rho(P,T)}\right) \tag{3.39}$$

To establish that the gravimetric energy density $W_m^{adb}(P,P_o)$ of a single chamber adiabatic actuator is non-negative, the following lemma is proposed.

Lemma 3.1. *For $\alpha \in \Re^+$ and $n \neq 0$, the following conditions are always true,*

1. $\mathcal{F}(\alpha,n) := (\alpha^n - 1) - n(\alpha-1) > 0, \ \forall \quad |n| > 1$
2. $\mathcal{F}(\alpha,n) := (\alpha^n - 1) - n(\alpha-1) < 0, \ \forall \quad |n| < 1$
3. $\mathcal{F}(\alpha,n) := (\alpha^n - 1) - n(\alpha-1) = 0$, *if and only if* $\alpha = 1$

Proof. For a given magnitude of $n \neq 0$, the maximum and/or minimum value of $\mathcal{F}(\alpha,n)$ can be evaluated by looking at the solution to the first and the second order optimality conditions. On differentiating $\mathcal{F}(\alpha,n)$ with respect to α, these conditions are obtained as,

$$\text{First order optimality condition : } \frac{d\mathcal{F}(\alpha,n)}{d\alpha} = n(\alpha^{n-1}-1) = 0 \text{ iff } \alpha = 1 \ \forall \ n \neq 0$$

$$\text{Second order optimality condition : } \left.\frac{d^2\mathcal{F}(\alpha,n)}{d\alpha^2}\right|_{\alpha=1} = n(n-1) = \begin{cases} > 0, & \text{if } |n| > 1 \\ < 0, & \text{if } |n| < 1 \end{cases}$$

At the extremum point ($\alpha = 1$), the value of the function is obtained as $\mathcal{F}(1, n) = 0$ for all n. Therefore, for $|n| > 1$, $\mathcal{F}(\alpha, n)$ has a minimum value of 0 at $\alpha = 1$, and is positive everywhere else, and for $|n| < 1$, $\mathcal{F}(\alpha, n)$ has a maximum value of 0 at $\alpha = 1$, and is negative for all other α.

□

Theorem 3.1. *The gravimetric energy density $W_m^{adb}(P, P_o)$ of a single chambered adiabatic actuator defined in Eq. (3.39) is non-negative for all $(P, P_o) \in \Re^+$, and is identically zero if only if $P = P_o$.*

Proof. Using the definition of density $\rho(P, T) = P/RT$ from Eq. (3.11), the gravimetric energy density $W_m^{adb}(P, P_o)$ in Eq. (3.39) can be expressed as,

$$\begin{aligned} W_m^{adb}(P, P_o) &= C_v(T - T_o) + R(T - T_o) - P_o\left(\frac{1}{\rho(P_o, T_o)} - \frac{1}{\rho(P, T)}\right) - R(T - T_o) \\ &= C_pT\left(1 - \frac{T_o}{T}\right) - RT\left(1 - \frac{P_o}{P}\right) \end{aligned} \tag{3.40}$$

where the temperature T is related to the pressure P as given in Eq. (3.18), while $C_p \triangleq (C_v + R)$ for an ideal gas. Using the definition of C_p from Eq. (3.4) and the temperature-pressure relation from Eq. (3.18), the gravimetric energy density in the above equation can be expressed as,

$$W_m^{adb}(P, P_o) = -C_pT\left(\left(\left(\frac{P_o}{P}\right)^{(\gamma-1)/\gamma} - 1\right) - \frac{\gamma - 1}{\gamma}\left(\frac{P_o}{P} - 1\right)\right) \tag{3.41}$$

On defining $n = (\gamma - 1)/\gamma$ and $\alpha = P_o/P$ in the above equation, and using the results from lemma 3.1, the result follows.

□

The energy function for a single chamber actuator with isothermal thermodynamic process is presented in the next subsection.

Isothermal process

The equilibrium volume $\bar{V}(m)$ of the single chamber isothermal actuator for a given mass of air m is again as defined in Eq. (3.30). The characteristic equation of the isothermal

actuator relating the chamber air pressure p and the corresponding volume υ with the equilibrium pressure P_o and equilibrium volume $\bar{V}(m)$ is obtained from integrating the pressure dynamics in Eq. (3.20) as,

$$p\upsilon = mRT_o = P_o\bar{V}(m) \tag{3.42}$$

For a given mass of air m in the actuator chamber, the pressure-volume $(P-V)$ trajectory in the isothermal actuator is therefore determined by m. A differential change $d\upsilon$ in the chamber volume υ can be expressed in terms of the differential change dp in the corresponding chamber pressure p as,

$$d\upsilon = -\frac{\upsilon}{p}dp = -\frac{mRT_o}{p^2}dp \tag{3.43}$$

Using the above equation in Eq. (3.31), the energy function for a single chamber isothermal actuator is obtained as,

$$W_{act}^{iso}(m,P,P_o) = \int_{V(m,P)}^{\bar{V}(m)} (p-P_o)\, d\upsilon = mRT_o \int_{P_o}^{P} (p-P_o)\, \frac{dp}{p^2} \tag{3.44}$$

Integrating the $r.h.s$ of the above equation the energy available in a single chamber isothermal chamber with respect to the ambient pressure P_o is obtained as,

$$W_{act}^{iso}(m,P,P_o) = mRT_o \log\left(\frac{P}{P_o}\right) - P_o\left(\bar{V}(m) - V\right) \tag{3.45}$$

where the chamber volume V and pressure P are related by the isothermal characteristic curve in Eq. (3.42). For a pressure P in the actuator chamber, and an ambient pressure of P_o, the change in specific entropy of air in the isothermal actuator chamber with respect to ambient conditions is given by [65],

$$\sigma_{iso}(P,P_o) = R\log\left(\frac{P}{P_o}\right) \tag{3.46}$$

Therefore the actuator energy function in Eq. (3.45) can be interpreted as the sum of the work due to change in the chamber entropy with respect to ambient conditions $(mT_o\sigma(P,P_o))$, and the work done against the ambient pressure P_o, as the actuator is traversing to the equilibrium state (P_o,T_o).

From Eq. (3.45), the gravimetric energy density of the isothermal actuator with respect to the ambient pressure P_o is defined as,

$$W_m^{iso}(P,P_o) = \frac{W_{act}^{iso}(m,P,P_o)}{m} = RT_o\log\left(\frac{P}{P_o}\right) - P_o\left(\frac{\bar{V}(m)}{m} - \frac{V}{m}\right) \tag{3.47}$$

Using the definition of the equilibrium volume $\bar{V}(m) = mRT_o/P_o$ from Eq. (3.30), and using the ideal gas law from Eq. (3.2), the gravimetric energy density in the above equation can be expressed as,

$$W_m^{iso}(P, P_o) = RT_o \log\left(\frac{P}{P_o}\right) - P_o\left(\frac{1}{\rho(P_o, T_o)} - \frac{1}{\rho(P, T_o)}\right) \tag{3.48}$$

where $\rho(P, T_o)$ corresponds to the density of air for the isothermal actuator and is obtained from Eq. (3.11) as $\rho(P, T_o) = \frac{P}{RT_o}$.

Theorem 3.2. *The gravimetric energy density $W_m^{iso}(P, P_o)$ for a single-chambered isothermal pneumatic actuator as defined in Eq. (3.48) is non-negative for any pair of $(P, P_o) \in \Re^+$, and is identically zero only when $P = P_o$.*

Proof. Using the definition of $\rho(P, T_o) = P/RT_o$, the gravimetric energy density in Eq. (3.48) can be expressed as,

$$W_m^{iso}(P, P_o) = RT_o \log\left(\frac{P}{P_o}\right) - RT_o\left(1 - \frac{P_o}{P}\right) \tag{3.49}$$

The above equation can be re-written as,

$$W_m^{iso}(P, P_o) = RT_o\left(\left(\frac{P_o}{P} - 1\right) - \log\left(\frac{P_o}{P}\right)\right) \tag{3.50}$$

Define $\alpha = P_o/P_1$. As P_o and P_1 are always positive, using the following property,

$$\alpha - \log(1 + \alpha) = \begin{cases} > 0 & \text{if } \alpha > -1 \\ 0 & \text{if } \alpha = 1 \end{cases} \tag{3.51}$$

it can be seen that the gravimetric energy density for the isothermal actuator chamber is positive for any positive pair of (P, P_o), and is identically zero, only if $P = P_o$.

□

Variation in the gravimetric energy density of the adiabatic actuator ($W_m^{adb}(P, P_o)$) and the isothermal actuator ($W_m^{iso}(P, P_o)$) with different operating pressures P is shown in Fig. (3.5). As seen in the figure, the gravimetric energy density for both the adiabatic and the isothermal single chamber actuators is a non-negative function of the operating pressure P, with a minimum value at $P = P_o$. In addition, it can be seen that for

$P/P_o > 1$, the gravimetric energy density of the isothermal actuator is greater than the adiabatic actuator. When the chamber pressure P is less than the ambient pressure P_o, the gravimetric energy density of the adiabatic actuator is greater than the isothermal actuator.

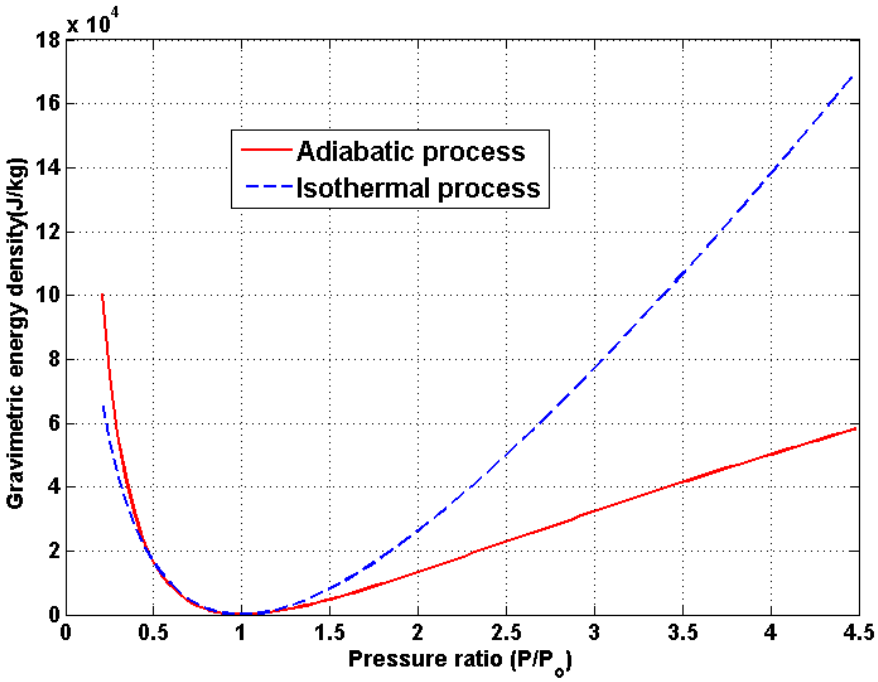

Figure 3.5: Gravimetric energy density of adiabatic and isothermal single chambered actuators

By changing the energy available from the actuator, the chamber pressure and consequently the actuator force output can be varied. To achieve passive operation of the pneumatic actuator, appropriate supply rate to the pneumatic actutor has to be identified. In the following section supply rate for the single chamber adiabatic and isothermal actuators is derived. The port power variables available for providing this supply rate are also identified.

3.1.4 Passivity property of single chambered actuator

Passivity is an input-output property a system. For an input vector $\boldsymbol{u}$ and an output vector $\boldsymbol{y}$ the external supply rate $s(\boldsymbol{u}, \boldsymbol{y})$ is defined as,

$$s(\boldsymbol{u}, \boldsymbol{y}) = \boldsymbol{u}^T \boldsymbol{y} \tag{3.52}$$

For a system to be passive the supply rate $s(\boldsymbol{u}, \boldsymbol{y})$ in the above equation has to satisfy the following condition [2],

$$\int_0^t s(\boldsymbol{u}, \boldsymbol{y})\, d\tau \geq -c_o^2 \tag{3.53}$$

where c_o^2 is a positive constant. If the input-output pair $(\boldsymbol{u}, \boldsymbol{y})$ corresponds to power variables, then the supply rate $s(\boldsymbol{u}, \boldsymbol{y})$ in Eq. (3.52) corresponds to physically meaningful power input to the system. The system satisfying the passivity condition in Eq. (3.53) for such input-output pair is said to be energetically passive.

Equation 3.53 can then be interpreted as minimum energy input required for the system to do work. The negative sign on the lower bound indicates that an initial energy corresponding to c_o^2 is available for the system to do work, in the absence of any external energy input. On multiplying both sides of Eq. (3.53) by the negative sign ('-'), the upper bound c_o^2 on the resulting inequality corresponds to the maximum available energy in the system to do work. In the absence of power input to the system, the maximum available energy in the system corresponds to the initial energy represented by c_o^2.

The supply rate $s(\boldsymbol{u}, \boldsymbol{y})$ for a single chamber adiabatic and isothermal actuators are derived in this section by defining the actuator energy function as the storage function. As the actuator energy function for reversible thermodynamic process defined in Eq. (3.31) corresponds to be the boundary work extracted from the actuator, the pneumatic actuator will be passive with respect to the mechanical supply rate. The port variables corresponding to the input vector $\boldsymbol{u}$ and the output vector $\boldsymbol{y}$ are also identified in this section. To facilitate extension to the two-chambered actuator, some of the preliminary analysis presented in this section assumes that the ambient pressure P_o is a variable. The supply rate for the single chambered actuator presented in this section is however for an actuator interacting with an ambient at a constant pressure. Supply rate for the adiabatic actuator is presented in the following subsection.

Adiabatic process

For a mass of air m in the actuator chamber, using the definition of the gravimetric energy density $W_m^{adb}(P, P_o)$ from Eq. (3.39), the energy in a single chamber pneumatic actuator with adiabatic thermodynamic process can be expressed as,

$$W_{act}^{adb}(m, P, P_o) = mW_m^{adb}(P, P_o) \tag{3.54}$$

The derivative of the above energy function is given by,

$$\dot{W}_{act}^{adb}(m, P, P_o) = \dot{m}W_m^{adb}(P, P_o) + m\frac{\partial W_m^{adb}(P, P_o)}{\partial P}\bigg|_{P_o}\dot{P} + m\frac{\partial W_m^{adb}(P, P_o)}{\partial P_o}\bigg|_{P}\dot{P}_o \tag{3.55}$$

Using the relationship $(k_{a\rho}/P)^(1/\gamma) = 1/\rho(P, T)$ from Eq. (3.14), the partial derivatives of the chamber gravimetric energy density $W_m^{adb}(P, P_o)$ in Eq. (3.37) with respect to the chamber pressure P and with respect to ambient pressure P_o are obtained as,

$$\begin{aligned}\frac{\partial W_m^{adb}(P, P_o)}{\partial P}\bigg|_{P_o} &= \left(\frac{P - P_o}{\rho(P, T)}\right)\frac{1}{\gamma P} \\ \frac{\partial W_m^{adb}(P, P_o)}{\partial P_o}\bigg|_{P} &= -\left(\frac{1}{\rho(P_o, T_o)} - \frac{1}{\rho(P, T)}\right)\end{aligned} \tag{3.56}$$

Using the pressure dynamics for the adiabatic process from Eq. (3.13) and the expressions for the partial derivative of gravimetric energy density from Eq. (3.56), the derivative of the actuator energy function in Eq. (3.55) is obtained as,

$$\dot{W}_{act}^{adb}(m, P, P_o) = \dot{m}\left(W_m^{adb}(P, P_o) + \frac{(P - P_o)}{\rho(P, T)}\right) - (P - P_o)\dot{V} - \dot{P}_o\left(V(\bar{x}) - V(x)\right) \tag{3.57}$$

In the above equation, if the air mass flow rate $\dot{m}$ is designated as the flow variable at the fluid port, then the corresponding effort variable is the sum of the gravimetric energy density, and the specific flow work. From Eq. (3.18) the chamber temperature T and pressure P are related as $T = T_o(P/P_o)^{(\gamma-1)/\gamma}$. Therefore, the effort variable $\Phi_{adb}(P, P_o)$ at the fluid port of the single chamber adiabatic actuator is defined as,

$$\Phi_{adb}(P, P_o) := W_m^{adb}(P, P_o) + \frac{(P - P_o)}{\rho(P, T)} \tag{3.58}$$

Theorem 3.3. *For a constant ambient pressure P_o, the single chamber adiabatic actuator is passive with respect to the following supply rate,*

$$s_{adb}((\dot{m}, \dot{x}), (\Phi_{adb}(P, P_o), F(P))) := \dot{m}\Phi_{adb}(P, P_o) - F(P)\dot{x} \tag{3.59}$$

where $\dot{m}$ is the flow variable at the fluid port of the single chamber adiabatic actuator, $\Phi_{adb}(P, P_o)$ is the corresponding effort variable at the fluid port of the actuator and is as defined in Eq. (3.58), the piston velocity $\dot{x}$ is the flow variable at the mechanical port of the actuator, and the actuator force $F(P) = (P - P_o)A$ is the effort variable at the mechanical port of the actuator.

Proof. Define the adiabatic actuator energy function $W_{act}^{adb}(m, P, P_o)$ in Eq. (3.54) to be the actuator storage function. The time derivative of the actuator energy function $\dot{W}_{act}^{adb}(m, P, P_o)$, is as given in Eq. (3.57). At constant ambient pressure ($\dot{P}_o = 0$), using the definition of the fluid port effort variable $\Phi_{adb}(P, P_o)$ from Eq. (3.58), the definition of the actuator force $F(P)$ for the single chambered actuator from Eq. (3.29) and the relationship between the actuator volume $V(x)$ and the piston position x from Eq. (3.73) the derivative of the energy function in Eq. (3.57) can be expressed in terms of the supply rate $s_{adb}(.)$ in Eq. (3.59) as,

$$\dot{W}_{act}^{adb}(m, P, P_o) = \dot{m}\Phi_{adb}(P, P_o) - F(P)\dot{x} = s_{adb}((\dot{m}, \dot{x}), (\Phi_{adb}(P, P_o), F(P))) \quad (3.60)$$

On the integrating the above equation, and using the result from theorem 3.1 that the gravimetric energy density $W_m^{adb}(P, P_o)$ (and hence the actuator energy function $W_{act}^{adb}(m, P, P_o)$) is a non-negative function, it can be shown that the single chamber adiabatic actuator supply rate $s_{adb}(.)$ satisfies the following passivity condition,

$$\int_0^t s_{adb}((\dot{m}, \dot{x}), (\Phi_{adb}(P, P_o), F(P)))\, d\tau \geq -W_{act}^{adb}(m, P, P_o)\Big|_{t=0} \quad (3.61)$$

where $W_{act}^{adb}(m, P, P_o)\Big|_{t=0} \geq 0$ corresponds to initial energy in the single chamber adiabatic actuator. □

In the following section, the supply rate for a single chamber isothermal actuator is presented. The port variables corresponding to this supply rate are also identified.

Isothermal process

Using the definition of the gravimetric energy density $W_m^{iso}(P, P_o)$ from Eq. (3.48), the energy available in a single chamber isothermal actuator can be written as,

$$W_{act}^{iso}(m, P, P_o) = mW_m^{iso}(P, P_o) \quad (3.62)$$

where m corresponds to the mass of air in chamber volume. The time derivative of the above energy function is given by,

$$\dot{W}_{act}^{iso}(m,P,P_o) = \dot{m}W_m^{iso}(P,P_o) + m\frac{\partial W_m^{iso}(P,P_o)}{\partial P}\bigg|_{P_o}\dot{P} + m\frac{\partial W_m^{iso}(P,P_o)}{\partial P_o}\bigg|_{P}\dot{P}_o \quad (3.63)$$

The partial derivative of chamber gravimetric energy density $W_m^{iso}(P,P_o)$ in Eq. (3.48) with respect to the chamber pressure P and the ambient pressure P_o is obtained as,

$$\begin{aligned}\frac{\partial W_m^{iso}(P,P_o)}{\partial P}\bigg|_{P_o} &= \frac{RT_o}{P} - \frac{P_o}{\rho^2(P,T_o)}\frac{\partial\rho(P,T_o)}{\partial P}\\ \frac{\partial W_m^{iso}(P,P_o)}{\partial P_o}\bigg|_{P} &= -\frac{RT_o}{P_o} + \frac{1}{\rho(P,T)}\end{aligned} \quad (3.64)$$

Using the definition of air density $\rho(P,T_o) = P/RT_o$ from Eq. (3.11), the partial derivatives of the gravimetric energy density $W_m^{iso}(P,P_o)$ in the above equation can be simplified as,

$$\begin{aligned}\frac{\partial W_m^{iso}(P,P_o)}{\partial P}\bigg|_{P_o} &= \frac{(P-P_o)}{P\rho(P,T_o)}\\ \frac{\partial W_m^{iso}(P,P_o)}{\partial P_o}\bigg|_{P} &= -\left(\frac{1}{\rho(P_o,T_o)} - \frac{1}{\rho(P,T)}\right)\end{aligned} \quad (3.65)$$

Using the pressure dynamics for isothermal process from Eq. (3.20) and the expression for the partial derivative of gravimetric energy density $W_m^{iso}(P,P_o)$ from Eq. (3.65), the derivative of the actuator energy function in Eq. (3.63) can be expressed as,

$$\dot{W}_{act}^{iso}(m,P,P_o) = \dot{m}\left(W_m^{iso}(P,P_o) + \frac{(P-P_o)}{\rho(P,T_o)}\right) - (P-P_o)\dot{V} - \dot{P}_o\left(V(\bar{x}) - V(x)\right) \quad (3.66)$$

In the above equation, if the air mass flow rate $\dot{m}$ is designated as the flow variable at the fluid port, then the corresponding effort variable is the sum of the gravimetric energy density, and the specific flow work. As seen from Eq. (3.57), this structure for the effort variable at the port interacting with the fluid source is similar to the single chamber adiabatic actuator. Let this effort variable be represented by $\Phi_{iso}(P,P_o)$ as,

$$\Phi_{iso}(P,P_o) := W_m^{iso}(P,P_o) + \frac{(P-P_o)}{\rho(P,T_o)} \quad (3.67)$$

Theorem 3.4. *For a constant ambient pressure P_o, the single chamber isothermal actuator is passive with respect to the following supply rate,*

$$s_{iso}((\dot{m},\dot{x}),(\Phi_{iso}(P,P_o),F(P))) := \dot{m}\Phi_{iso}(P,P_o) - F(P)\dot{x} \tag{3.68}$$

where the air mass flow rate $\dot{m}$ is designated to be the flow variable at the fluid port of the actuator, $\Phi_{iso}(P,P_o)$ is the corresponding effort variable at the fluid port of the actuator and is as defined in Eq. (3.67), the piston velocity $\dot{x}$ is the flow variable at the mechanical port of the actuator, and the actuator force $F(P) = (P - P_o)A$ is the effort variable at the mechanical port of the actuator.

Proof. Define the isothermal actuator energy function $W_{act}^{iso}(m,P,P_o)$ from Eq. (3.62) to be the storage function. The time derivative of this energy function $\dot{W}_{act}^{iso}(m,P,P_o)$ is as given in Eq. (3.66). For constant ambient pressure ($\dot{P}_o = 0$), using the definition of the fluid port effort variable $\Phi_{iso}(P,P_o)$ from Eq. (3.67), the definition of the actuator force $F(P)$ from Eq. (3.29), and the relationship between the actuator volume $V(x)$ and the piston position x in Eq. (3.73), the derivative of the energy function in Eq. (3.66) is written in terms of the supply rate $s_{iso}(.)$ defined in Eq. (3.68) as,

$$\dot{W}_{act}^{iso}(m,P,P_o) = \dot{m}\Phi_{iso}(P,P_o) - F(P)\dot{x} = s_{iso}((\dot{m},\dot{x}),(\Phi_{iso}(P,P_o),F(P))) \tag{3.69}$$

Integrating the above equation, and using the result from theorem 3.2 that the gravimetric energy density $W_m^{iso}(P,P_o)$ (and hence the actuator energy function $W_{act}^{iso}(m,P,P_o)$) is a non-negative function, it can be seen that the supply rate for the single chambered isothermal actuator $s_{iso}(.)$ in Eq. (3.68) satisfies the following passivity condition,

$$\int_0^t s_{iso}((\dot{m},\dot{x}),(\Phi_{iso}(P,P_o),F(P)))\,d\tau \geq -W_{act}^{iso}(m,P,P_o)\Big|_{t=0} \tag{3.70}$$

where $W_{act}^{iso}(m,P,P_o)\Big|_{t=0} \geq 0$ corresponds to the initial energy in the single chambered isothermal actuator. □

Some properties of the supply rates for the single chamber adiabatic and isothermal pneumatic actuators, given in Eq. (3.59) and Eq.(3.68) respectively, are listed in the following remark.

Remark 3.1. *The supply rate $s_{adb}((\dot{m},\dot{x}),(\Phi_{adb}(P,P_o),F(P)))$ for the single chamber adiabatic actuator defined in Eq. (3.59) and the supply rate $s_{iso}(\dot{m},\Phi_{iso}(P,P_o),F(P),\dot{x})$ for the single chamber isothermal actuator defined in Eq. (3.68) have the following characteristics:*

1. *The supply rates $s_{(adb)}(\dot{m},\Phi_{(adb,adb)}(P,P_o),F(P),\dot{x})$ in Eq. (3.59) for the single chamber adiabatic actuator, and $s_{(iso)}(\dot{m},\Phi_{(adb,adb)}(P,P_o),F(P),\dot{x})$ in Eq. (3.68) for the single chamber isothermal actuator, have two ports for power interaction. One port corresponds to interaction with the fluid source with the corresponding power interaction being $\dot{m}\Phi_{(adb,iso)}(P,P_o)$. The other port corresponds to mechanical interaction, the corresponding power interaction being $-F(P)\dot{x}$. The negative sign for the power interaction at the mechanical port implies that the power is being extracted from this port of the actuator.*

2. *From the definition of the gravimetric energy density $W_m^{adb}(P,P_o)$ in Eq. (3.39) and using the definition of air density from Eq. (3.11), the fluid port effort variable $\Phi_{adb}(P,P_o)$ in Eq. (3.58) can be expressed as the change in specific enthalpy of the chamber air as the actuator traverses to equilibrium position and is given by,*

$$\Phi_{adb}(P,P_o) := W_m^{adb}(P,P_o) + \frac{(P-P_o)}{\rho(P,T)} = C_p(T-T_o) \tag{3.71}$$

where $C_p = (C_v + R)$ is the specific heat of air at constant pressure and is as defined in Eq. (3.4).

3. *From the definition of the gravimetric energy density $W_m^{iso}(P,P_o)$ in the above equation and the definition of density $\rho(P,T_o) = P/RT_o$, the fluid port effort variable $\Phi_{iso}(P,P_o)$ for the single chamber isothermal actuator in Eq. (3.67) can be expressed in terms of the the specific work extracted due to change in specific entropy $\sigma_{iso}(P,P_o)$ as,*

$$\Phi_{iso}(P,P_o) := W_m^{iso}(P,P_o) + \frac{(P-P_o)}{\rho(P,T_o)} = T_o\sigma_{iso}(P,P_o) \tag{3.72}$$

where $\sigma_{iso}(P,P_o) = RT_o \log\left(\frac{P}{P_o}\right)$ is as defined in Eq. (3.46).

The pneumatic actuators available for the experimental work in this study are all two-chambered. A two-chambered pneumatic actuator can be considered as two interacting single chamber pneumatic actuators. The actuator dynamics, the energy function and the supply developed in this section for a single chamber pneumatic actuator are extended to a two-chambered pneumatic actuator in the following section.

3.2 Two-chambered pneumatic actuator

In this section, actuator dynamics, energy function, and supply rate for passive operation of a two-chambered pneumatic actuator are reported. Schematic of a two-chambered pneumatic actuator is as shown in Fig. (3.6). The air chamber on the piston cap side is referred to as chamber 1, and the air chamber on the piston rod side is referred to as chamber 2. The two chambers of the actuator are mechanically coupled through the actuator piston. For a piston position x, the volume of chamber 1 ($V_1(x)$) and the volume of chamber 2 ($V_2(x)$) are given by,

$$V_1(x) \triangleq A_1(L_{1o} + x), \qquad V_2(x) \triangleq A_2(L'_{2o} + L - x) = A_2(L_{2o} - x) \tag{3.73}$$

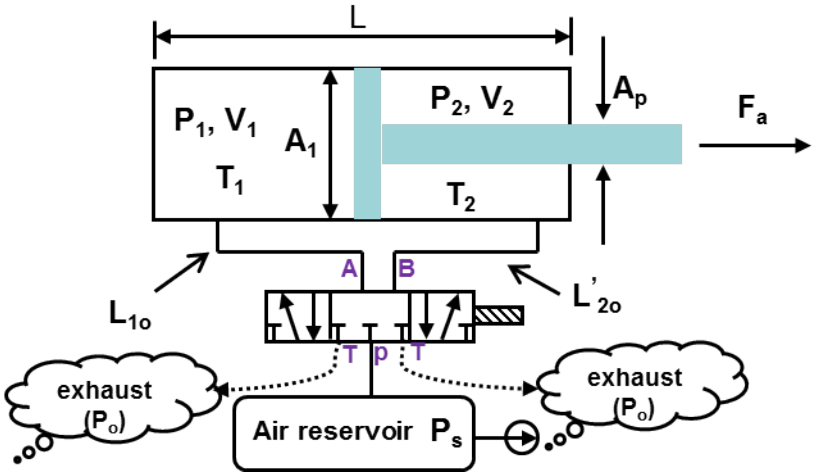

Figure 3.6: Schematic of a two-chambered pneumatic actuator

where A_1 and A_2 refer to the piston cross-sectional area in chamber 1 and chamber 2

respectively, while $A_1 L_{1o}$ and $A_2 L'_{2o}$ correspond to the dead volume in chambers 1 and 2 respectively, and L corresponds to the actuator stroke length.

Let T_1 and T_2 be the air temperatures in chambers 1 and 2 of the actuator respectively. It is assumed that air in each actuator chamber behaves as an ideal gas. For a given mass of air m_1 and m_2 in chambers 1 and 2 of the actuator, the corresponding chamber air pressures P_1 and P_2 are obtained from the ideal gas law as

$$P_1 = \frac{m_1 R T_1}{V_1(x)}, \qquad P_2 = \frac{m_2 R T_2}{V_2(x)} \tag{3.74}$$

The temperature and pressure dynamics for the two-chambered actuator are presented in the next section.

3.2.1 Actuator dynamics

As adiabatic and isothermal processes are of interest in this chapter, the pressure and temperature dynamics corresponding to these models only is reported in this section.

Adiabatic actuator

Similar to the single chambered actuator it is assumed that the adiabatic trajectory in each chamber of the two-chambered actuator passes through (P_o, T_o), where P_o is the ambient pressure while T_o is the ambient temperature. As shown in Eq. (3.30), the volume of each chamber at ambient pressure P_o and ambient temperature T_o depends on the mass of air in each chamber. For an air mass of m_1 in chamber 1 and m_2 in chamber 2, the chamber volumes $V_{1o}(m_1)$ and $V_{2o}(m_2)$ corresponding to a chamber pressure P_o and chamber temperature of T_o is obtained from ideal gas law as,

$$V_{1o}(m_1) = \frac{m_1 R T_o}{P_o}, \qquad V_{2o}(m_2) = \frac{m_2 R T_o}{P_o} \tag{3.75}$$

The temperature and pressure dynamics in each chamber of the two-chambered adiabatic actuator are obtained from Eq. (3.12) and Eq. (3.13) as,

$$\frac{\dot{T}_i}{T_i} = (\gamma - 1)\left(\frac{\dot{m}_i}{m_i} - \frac{\dot{V}_i}{V_i}\right) \tag{3.76}$$

$$\frac{\dot{P}_i}{P_i} = \gamma\left(\frac{\dot{m}_i}{m_i} - \frac{\dot{V}_i}{V_i}\right) \tag{3.77}$$

where $i \in (1,2)$ is the index for representing the two actuator chambers. Integrating the above equations for a fixed mass of air m_1 and m_2 in chambers 1 and 2 respectively, the temperature-volume $(T-V)$ and the pressure-volume $(P-V)$ relationships for each chamber of an adiabatic actuator are obtained as,

$$\begin{aligned} T_1 V_1(x)^{\gamma-1} = k_{t_1}(m_1) = T_o V_{1o}^{\gamma-1}(m_1), \quad T_2 V_2(x)^{\gamma-1} = k_{t_2}(m_2) = T_o V_{2o}^{\gamma-1}(m_2) \\ P_1 V_1^{\gamma}(x) = k_{p_1}(m_1) = P_o V_{1o}^{\gamma}(m_1), \quad P_2 V_2^{\gamma}(x) = k_{p_2}(m_2) = P_o V_{2o}^{\gamma}(m_2) \end{aligned} \tag{3.78}$$

where $k_{t_{(1)}}(m_1)$ and $k_{t_{(2)}}(m_2)$ are integration constants for chamber 1 and chamber 2 temperature dynamics respectively in Eq. (3.76), while $k_{p_{(1)}}(m_1)$ and $k_{p_{(2)}}(m_2)$ are the integration constant for chamber 1 and chamber 2 pressure dynamics respectively in Eq. (3.77). These integration constants are determined from the assumed initial pressure P_o and temperature T_o in each chamber of the actuator. For these initial conditions, trajectories of the temperature-volume and the pressure-volume curves is determined by the the mass of air in each actuator chamber.

For the initial pressure P_o and temperature T_o, the pressure P_i and the temperature T_i in each chamber of the actuator are related as shown in Eq. (3.18) for a single-chambered adiabatic actuator and this relationship is given by,

$$T_1 = T_o \left(\frac{P_1}{P_o}\right)^{\frac{\gamma-1}{\gamma}}, \qquad T_2 = T_o \left(\frac{P_2}{P_o}\right)^{\frac{\gamma-1}{\gamma}} \tag{3.79}$$

Note that the relationship between the pressure P_i and the temperature T_i in the above equation depends only on the initial conditions (P_o, T_o) and is independent of the air mass. Dynamic characteristics of an isothermal actuator are presented in the next section.

Isothermal actuator

For the isothermal actuator, the temperature in both chambers of the actuators is assumed to be at ambient temperature T_o. Using Eq. (3.20), the temperature and pressure dynamics in each chamber of the two-chambered isothermal actuator are given by,

$$T_i = T_o \tag{3.80}$$

$$\frac{\dot{P}_i}{P_i} = \left(\frac{\dot{m}_i}{m_i} - \frac{\dot{V}_i}{V_i}\right) \tag{3.81}$$

where again $i \in (1, 2)$ is the index for representing the two actuator chambers. On integrating the pressure dynamics in the above equation and then applying the ideal gas law from Eq. (3.2), the chamber pressure and volume are related as,

$$P_1 V_1(x) = k_{c_1}(m_1) = m_1 R T_o, \qquad P_2 V_2(x) = k_{c_2}(m_2) = m_2 R T_o \tag{3.82}$$

where $k_{c_1}(m_1)$ and $k_{c_2}(m_2)$ are constant for fixed mass of air m_1 and m_2 in chamber 1 and 2 respectively of the isothermal actuator. Therefore the characteristics of the curve traversed in each chamber of the isothermal actuator depends only on the mass of air in each chamber. The expression for mass flow rate to each chamber of the two-chambered actuator is presented in the following section.

3.2.2 Mass flow rate

In this study it is assumed that there is no air leakage between the two chambers. Therefore the mass flow rates $\dot{m}_1$ and $\dot{m}_2$ to the chambers 1 and 2 of the actuator respectively, is determined by the pneumatic valve only. The mass flow rate to each actuator chamber is determined from Eq. (3.26). As shown in Fig. (3.6), if a single valve is used to meter the air flow, then the pressure port connections to the two chambers are mechanically coupled through the valve spool position. If the spool is positioned such that chamber 1 is connected to the supply pressure P_s, then chamber 2 would be connected to the ambient pressure P_o, and vice-versa. The convention for valve operation is that a positive command input u to the valve corresponds to a positive valve command input u_1 to chamber 1 and a negative valve command input u_2 to chamber 2. As a result chamber 1 is connected to the supply pressure P_s and chamber 2 is connected to the ambient pressure P_o. When the command input u is negative, the spool is position such that chamber 1 is now connected to ambient pressure ($u_1 < 0$), while chamber 2 is connected to the supply pressure ($u_2 \geq 0$). Assuming that the orifice area available for air flow to both the chambers is the same, the input commands u_1 and u_2 are related to the single valve input command u as,

$$u = u_1 = -u_2 \tag{3.83}$$

In addition to the orifice area, the mass flow rate $\dot{m}_i$ to each chamber depends on the chamber pressure P_i, air temperature upstream to the valve orifice T_{u_i}, and the

external pressure port connected to the chamber (either the supply pressure P_s or the ambient pressure P_o). Similar to the single chambered actuator, the air temperature T_{u_i} at the upstream of the valve is assumed to be the same as chamber temperature for both the isothermal and adiabatic actuators (*i.e* $T_{u_1} = T_1$ and $T_{u_2} = T_2$). From Eq. (3.26), the mass flow rates $\dot{m}_1$ and $\dot{m}_2$ thus obtained as,

$$\dot{m}_1 = \Psi(P_1, T_1, u)u, \qquad \dot{m}_2 = -\Psi(P_2, T_2, -u)u \tag{3.84}$$

where the nonlinear function $\Psi_{P_i,T_i,u}$ is as defined in Eq. (3.27). Energy function for the two-chambered isothermal and adiabatic actuators is presented in the following section.

3.2.3 Two-chambered actuator energy function

For ease of presentation, let $\boldsymbol{m} = (m_1, m_2)$ be the vector of air mass m_1 and m_2 from chambers 1 and 2 of the actuator, while $\boldsymbol{P} = (P_1, P_2)$ represent the vector of chamber pressures.

Similar to the single chamber actuator, the energy function for the two-chambered actuator is defined as the work that can be extracted from the actuator, as it traverses to the equilibrium state ($F_a(\boldsymbol{P}) = 0$ in Eq. (3.1)). For known initial conditions (P_o, T_o), trajectory of the pressure-volume curve for the adiabatic actuator and the isothermal actuator, in Eq. (3.78) and Eq. (3.82) respectively, is determined by the air mass $\boldsymbol{m}$ in the actuator.

For a piston position of x, the chamber volumes are obtained from Eq. (3.73) as, $V_1(x) = A_1(L_{1o} + x)$ and $V_2(x) = A_2(L_{2o} - x)$. For a given air mass $\boldsymbol{m}$, the pressure P_1, determined from Eq. (3.78) and Eq. (3.82) for adiabatic and isothermal actuators respectively, decreases monotonically with the piston position x, while the pressure P_2 increases monotonically with x. Therefore, for a given thermodynamic process, there will be a unique position $\bar{x}(\boldsymbol{m})$ of the actuator, where the chamber pressures $\bar{P}_1(\boldsymbol{m})$ and $\bar{P}_2(\boldsymbol{m})$ (determined from Eq. (3.78) or Eq. (3.82) depending on the thermodynamic process) satisfy the following equilibrium condition,

$$F_a(\bar{P}_1, \bar{P}_2) = \bar{P}_1(\boldsymbol{m})A_1 - \bar{P}_2(\boldsymbol{m})A_2 - P_oA_p = 0 \tag{3.85}$$

where $A_p = (A_1 - A_2)$ is the rod cross-sectional area exposed to the ambient pressure

P_o. From Eq. (3.85), the actuator force in Eq. (3.1) can be expressed as,

$$F_a(\boldsymbol{P}) = (P_1 - \bar{P}_1(\boldsymbol{m}))A_1 - (P_2 - \bar{P}_2(\boldsymbol{m}))A_2 \tag{3.86}$$

The volume of each chamber at equilibrium state is obtained from the volume-position relationship in Eq. (3.73) as,

$$V_1(\bar{x}(\boldsymbol{m})) = A_1(L_{1o} + \bar{x}(\boldsymbol{m})), \qquad V_2(\bar{x}(\boldsymbol{m})) = A_2(L_{2o} - \bar{x}(\boldsymbol{m})) \tag{3.87}$$

For air pressure of p_1 and p_2 in chambers 1 and 2 of the actuator for an actuator position of χ, the energy that can be extracted from the actuator as it traverses from an initial position of x to the equilibrium position $\bar{x}(\boldsymbol{m})$ is given by,

$$W_{act}(\boldsymbol{m}, \boldsymbol{P}) = \int_x^{\bar{x}(\boldsymbol{m})} ((p_1 - \bar{P}_1(\boldsymbol{m}))A_1 - (p_2 - \bar{P}_2(\boldsymbol{m}))A_2)\, d\chi \tag{3.88}$$

Using the relationship between the actuator position x and the chamber volumes $V_1(x)$ and $V_2(x)$ from Eq. (3.73), the actuator energy function in the above equation can be expressed as,

$$W_{act}(\boldsymbol{m}, \boldsymbol{P}) = \int_{V_1(x)}^{V_1(\bar{x}(\boldsymbol{m}))} (p_1 - \bar{P}_1(\boldsymbol{m}))\, d\upsilon_1 + \int_{V_2(x)}^{V_2(\bar{x}(\boldsymbol{m}))} (p_2 - \bar{P}_2(\boldsymbol{m}))\, d\upsilon_2 \tag{3.89}$$

where $\upsilon_{(1,2)}(\chi)$ corresponds to volume of chambers 1 and 2 of the actuator for a piston position of χ and are as defined in Eq. (3.73). Comparing Eq. (3.89) with the definition of energy function for a single chamber actuator in Eq. (3.31), the available energy in the two-chambered actuator with a reversible thermodynamic process is therefore the sum of the work that can be extracted from individual actuator chambers as the actuator traverses to the equilibrium position $\bar{x}(\boldsymbol{m})$. In the following sections, the equilibrium thermodynamic states for the two-chambered isothermal and the adiabatic actuators is identified and their corresponding energy function is presented.

Adiabatic actuator

The temperature-volume ($T-V$) and pressure-volume ($P-V$) characteristic curves for the adiabatic actuator are as given in Eq. (3.78). Using the definition of the chamber volumes $V_1(\bar{x}(\boldsymbol{m}))$ and $V_2(\bar{x}(\boldsymbol{m}))$ from Eq. (3.87) in the pressure-volume characteristic

equation given by Eq. (3.78), the equilibrium pressures $\bar{P}_1(\boldsymbol{m})$, $\bar{P}_2(\boldsymbol{m})$ can be expressed in terms of the equilibrium position $\bar{x}(\boldsymbol{m})$ as,

$$\bar{P}_1(\boldsymbol{m}) = \frac{k_{p_1}(m_1)}{A_1^{\gamma}(L_{1o} + \bar{x}(\boldsymbol{m}))^{\gamma}}, \quad \bar{P}_2(\boldsymbol{m}) = \frac{k_{p_2}(m_2)}{A_2^{\gamma}(L_{2o} - \bar{x}(\boldsymbol{m}))^{\gamma}} \tag{3.90}$$

where A_1 and A_2 are the piston cross-sectional areas in chambers 1 and 2 respectively and are constant for an actuator. Using the definition of equilibrium pressures from above equation in the equilibrium pressure relationship given by Eq. (3.85), the equilibrium position $\bar{x}(\boldsymbol{m})$ is obtained as the solution of the following equation,

$$\frac{k_{p_1}(m_1)}{A_1^{\gamma-1}(L_{1o} + \bar{x}(\boldsymbol{m}))^{\gamma}} - \frac{k_{p_2}(m_2)}{A_2^{\gamma-1}(L_{2o} - \bar{x}(\boldsymbol{m}))^{\gamma}} - P_o A_p = 0 \tag{3.91}$$

After obtaining the equilibrium position from the above equation, the equilibrium pressures $\bar{P}_1(\boldsymbol{m})$ and $\bar{P}_2(\boldsymbol{m})$ in actuator chambers 1 and 2 respectively, are determined from Eq. (3.90). Due to change in the air mass $\boldsymbol{m}$, the equilibrium pressure $\bar{P}_1(\boldsymbol{m})$ and $\bar{P}_2(\boldsymbol{m})$ do not necessarily correspond to the assumed initial pressure of P_o in each chamber. Therefore, from Eq. (3.79), the equilibrium temperatures $\bar{T}_1(\boldsymbol{m})$ and $\bar{T}_2(\boldsymbol{m})$ in chambers 1 and 2 respectively also do not correspond to initial temperature T_o. The equilibrium temperatures $\bar{T}_1(\boldsymbol{m})$ and $\bar{T}_2(\boldsymbol{m})$ are determined from Eq. (3.78) as,

$$\bar{T}_1(\boldsymbol{m}) = \frac{k_{t_1}(m_1)}{V_1^{\gamma-1}(\bar{x}(\boldsymbol{m}))}, \quad \bar{T}_2(\boldsymbol{m}) = \frac{k_{t_2}(m_2)}{V_2^{\gamma-1}(\bar{x}(\boldsymbol{m}))} \tag{3.92}$$

Proposition 3.1. *For a given mass of air m_1 and m_2 in chambers 1 and 2 of the actuator, and for corresponding chamber pressures of P_1 and P_2, the energy function for the two-chambered adiabatic actuator is given by,*

$$W_{act}^{adb}(\boldsymbol{m}, \boldsymbol{P}) = m_1 W_m^{adb}(P_1, \bar{P}_1(\boldsymbol{m})) + m_2 W_m^{adb}(P_2, \bar{P}_2(\boldsymbol{m})) \tag{3.93}$$

$$= m_1 C_v(T_1 - \bar{T}_1(\boldsymbol{m})) + m_2 C_v(T_2 - \bar{T}_2(\boldsymbol{m})) - P_o A_p(\bar{x}(\boldsymbol{m}) - x) \tag{3.94}$$

where $W_m^{adb}(.)$ represents the gravimetric energy density of the air in an adiabatic actuator chamber and is as defined in Eq. (3.39), $\bar{P}_1(\boldsymbol{m})$ and $\bar{P}_2(\boldsymbol{m})$ correspond to the equilibrium pressures in chamber 1 and 2 of the actuator, while $\bar{T}_1(\boldsymbol{m})$ and $\bar{T}_2(\boldsymbol{m})$ correspond to air temperature in chamber 1 and 2 of the adiabatic actuator at the equilibrium position $\bar{x}(\boldsymbol{m})$ and are as defined in Eq. (3.92). Moreover, the actuator energy function as defined in Eq. (3.93) is a positive definite function of air mass in each chamber (m_1, m_2), and the chamber pressures (P_1, P_2).

Proof. On comparing Eq. (3.89) with Eq. (3.34) the energy available from each actuator chamber of the two-chambered actuator has a form similar to the energy function of a single chamber adiabatic actuator in Eq. (3.89). Therefore, using the definition of the gravimetric energy density $W_m^{adb}(P, \bar{P})$ for a single chamber adiabatic actuator from Eq. (3.39), the energy function for the two-chambered adiabatic actuator is obtained from Eq. (3.89) as,

$$\begin{aligned} W_{act}^{adb}(\boldsymbol{m}, \boldsymbol{P}) &= m_1 W_m^{adb}(P_1, \bar{P}_1(\boldsymbol{m})) + m_2 W_m^{adb}(P_2, \bar{P}_2(\boldsymbol{m})) \\ &= m_1 C_v(T_1 - \bar{T}_1(\boldsymbol{m})) + m_2 C_v(T_2 - \bar{T}_2(\boldsymbol{m})) - \bar{P}_1(\boldsymbol{m})\,(V_1(\bar{x}) - V_1(x)) \\ &\qquad - \bar{P}_2(\boldsymbol{m})\,(V_1(\bar{x}) - V_1(x)) \end{aligned} \tag{3.95}$$

Using the relationship between the chamber volumes $V_1(x)$, $V_2(x)$ and the actuator position x from Eq. (3.73), and from the relationship between equilibrium pressures $\bar{P}_1(\boldsymbol{m})$, $\bar{P}_2(\boldsymbol{m})$ in Eq. (3.85), the energy function $W_{act}^{adb}(\boldsymbol{m}, \boldsymbol{P})$ in the above equation can be simplified as,

$$W_{act}^{adb}(\boldsymbol{m}, \boldsymbol{P}) = m_1 C_v(T_1 - \bar{T}_1(\boldsymbol{m})) + m_2 C_v(T_2 - \bar{T}_2(\boldsymbol{m})) - P_o A_p\,(\bar{x}(\boldsymbol{m}) - x) \tag{3.96}$$

As stated in the remark 3.1, the gravimetric energy density $W_m^{adb}(P, \bar{P})$ of the adiabatic actuator is positive definitive for all $(P, \bar{P}) \in \Re^+$. Therefore the energy function for the two-chambered adiabatic actuator in Eq. (3.93) is also a positive definite function for all feasible elements of the chamber mass (m_1, m_2), and chamber pressure (P_1, P_2). □

Remark 3.2. *The energy function for a two-chambered adiabatic actuator is the sum of change in internal energy in each actuator chamber and the work done against ambient pressure P_o, as the actuator traverses to the equilibrium position $\bar{x}(\boldsymbol{m})$.*

The energy function for the two-chambered isothermal actuator is presented in the following section.

Isothermal actuator

The pressure-volume $(P - V)$ curve in each chamber of the two-chambered isothermal actuator is as given in Eq. (3.82). The air temperature in both chambers of isothermal actuator is assumed to be constant and same as the ambient temperature ($T_1 = T_o$ and $T_2 = T_o$ for all t). Therefore the air temperature in chambers 1 and 2 of the actuator

at the equilibrium state are the same as ambient temperature ($\bar{T}_1 = T_o$ and $\bar{T}_2 = T_o$). For a given mass of air m_1 and m_2 in the actuator chambers 1 and 2 respectively, the equilibrium pressures $\bar{P}_1(\boldsymbol{m})$ and $\bar{P}_2(\boldsymbol{m})$ in the actuator chambers 1 and 2 can be expressed in terms of the equilibrium position $\bar{x}(\boldsymbol{m})$ by using the ideal gas law from Eq. (3.2) as,

$$\bar{P}_1(\boldsymbol{m}) = \frac{m_1 R T_o}{V_1(\bar{x}(\boldsymbol{m}))} = \frac{m_1 R T_o}{A_1(L_{1o} + \bar{x}(\boldsymbol{m}))}, \quad \bar{P}_2(\boldsymbol{m}) = \frac{m_2 R T_o}{V_2(\bar{x}(\boldsymbol{m}))} = \frac{m_2 R T_o}{A_2(L_{2o} - \bar{x}(\boldsymbol{m}))} \tag{3.97}$$

Using the definition of the equilibrium pressures from the above equation in the equilibrium pressure relationship given in Eq. (3.85), the equilibrium position $\bar{x}(\boldsymbol{m})$ is obtained as solution of the following equation,

$$\frac{m_1 R T_o}{L_{1o} + \bar{x}(\boldsymbol{m})} - \frac{m_2 R T_o}{L_{2o} - \bar{x}(\boldsymbol{m})} - P_o A_p = 0 \tag{3.98}$$

Proposition 3.2. *For a given mass of air m_1 and m_2 in chamber 1 and 2 of the actuator respectively, and for the corresponding chamber pressures of P_1 and P_2, the energy function for the two-chambered isothermal actuator is given by,*

$$W_{act}^{iso}(\boldsymbol{m}, \boldsymbol{P}) = m_1 W_m^{iso}(P_1, \bar{P}_1(\boldsymbol{m})) + m_2 W_m^{iso}(P_2, \bar{P}_2(\boldsymbol{m})) \tag{3.99}$$

$$= m_1 R T_o \log\left(\frac{P_1}{\bar{P}_1(\boldsymbol{m})}\right) + m_2 R T_o \log\left(\frac{P_2}{\bar{P}_2(\boldsymbol{m})}\right) - P_o A_p \left(\bar{x}(\boldsymbol{m}) - x\right) \tag{3.100}$$

where $W_m^{iso}(.)$ represents the gravimetric energy density of the air in a single chambered isothermal actuator and is as defined in Eq. (3.47), $\bar{P}_1(\boldsymbol{m})$ and $\bar{P}_2(\boldsymbol{m})$ represent the equilibrium pressure in chambers 1 and 2 of the actuator respectively, while $\boldsymbol{x}(m)$ is the equilibrium position of the actuator. Also, the actuator energy function as defined in Eq. (3.99) is a positive definite function of mass (m_1, m_2) and pressures (P_1, P_2) in each actuator chamber.

Proof. On comparing Eq. (3.89) with Eq. (3.44) the energy available from each actuator chamber of the two-chambered actuator has a form similar to the energy available from a single chamber isothermal actuator in Eq. (3.89). Therefore, using the definition of the gravimetric energy density $W_m^{iso}(P, \bar{P})$ for a single chamber isothermal actuator from Eq. (3.47), the energy function for the two-chambered isothermal actuator is obtained

from Eq. (3.89) as,

$$\begin{aligned} W_{act}^{iso}(\boldsymbol{m},\boldsymbol{P}) &= m_1 W_m^{iso}(P_1,\bar{P}_1(\boldsymbol{m})) + m_2 W_m^{iso}(P_2,\bar{P}_2(\boldsymbol{m})) \\ &= m_1 R T_o \log\left(\frac{P_1}{\bar{P}_1(\boldsymbol{m})}\right) + m_2 R T_o \log\left(\frac{P_2}{\bar{P}_2(\boldsymbol{m})}\right) - \bar{P}_1(\boldsymbol{m})\left(V_1(\bar{x}) - V_1(x)\right) \\ &\quad - \bar{P}_2(\boldsymbol{m})\left(V_2(\bar{x}) - V_2(x)\right) \end{aligned} \tag{3.101}$$

From the definition of $V_1(x)$ and $V_2(x)$ in Eq. (3.73), and using the relationship between equilibrium pressures $\bar{P}_1(\boldsymbol{m})$ and $\bar{P}_2(\boldsymbol{m})$ in Eq. (3.85), the energy function in the above equation can be simplified as,

$$W_{act}^{iso}(\boldsymbol{m},\boldsymbol{P}) = m_1 R T_o \log\left(\frac{P_1}{\bar{P}_1(\boldsymbol{m})}\right) + m_2 R T_o \log\left(\frac{P_2}{\bar{P}_2(\boldsymbol{m})}\right) - P_o A_p\left(\bar{x}(\boldsymbol{m}) - x\right) \tag{3.102}$$

As stated in remark 3.2, the gravimetric energy density $W_m^{iso}(P,\bar{P})$ of the isothermal actuator is positive definitive for all $(P,\bar{P}) \in \Re^+$. Therefore the energy function for the two-chambered isothermal actuator in Eq. (3.99) is also a positive definite function. □

Remark 3.3. *The energy function for a two-chambered isothermal actuator can be expressed as the sum of work done due to change in entropy in each actuator chamber ($\sigma_{iso}(P_{(1,2)},\bar{P}_{(1,2)}(\boldsymbol{m}))$ in Eq. (3.46)) and the work done against ambient pressure P_o, as the actuator traverses to the equilibrium position $\bar{x}(\boldsymbol{m})$.*

Unlike in the single chamber actuator, the equilibrium pressures $\bar{P}_1(\boldsymbol{m})$ and $\bar{P}_2(\boldsymbol{m})$ in chamber 1 and 2 respectively, of a two-chambered actuator can be different from the ambient pressure P_o. They are only required to satisfy the equilibrium condition in Eq. (3.85). Let $j \in (iso, adb)$ be the index to represent the thermodynamic process in the pneumatic actuator. The available energy $W_{act}^{j}(\boldsymbol{m},\boldsymbol{P})$ from the adiabatic actuator given in Eq. (3.94) and from the isothermal actuator given in Eq. (3.100) satisfy the following lemma.

Lemma 3.2. *For a given mass of air m_1 and m_2 in chamber 1 and 2 of the actuator respectively, the gravimetric energy density $W_m^j(P,P_o)$ as defined in Eq. (3.39) and Eq. (3.48) for the adiabatic actuator ($j = adb$) and the isothermal actuator ($j = iso$)*

respectively, the energy $W^j_{act}(\boldsymbol{m}, \boldsymbol{P})$ *available from the two-chambered actuator can be expressed as,*

$$\begin{aligned} W^j_{act}(\boldsymbol{m}, \boldsymbol{P}) = (m_1 W^j_m(P_1, P_o) + m_2 W^j_m(P_2, P_o)) \\ - (m_1 W^j_m(\bar{P}_1(\boldsymbol{m}), P_o) + m_2 W^j_m(\bar{P}_2(\boldsymbol{m}), P_o)) \end{aligned} \tag{3.103}$$

Proof. Using the definition of the gravimetric energy density $W^j_m(P, P_o)$ from Eq. (3.48) for the isothermal actuator ($j = iso$) and from Eq. (3.39) for adiabatic actuator ($j = adb$), the gravimetric energy density $W^j_m(P_i, \bar{P}_i(\boldsymbol{m}))$ in the $i^{th} \in (1, 2)$ chamber of the actuator corresponding to the equilibrium pressure $\bar{P}_i(\boldsymbol{m})$ can be expressed as,

$$\begin{aligned} W^j_m(P_i, \bar{P}_i(\boldsymbol{m})) = (W^j_m(P_i, P_o) - W^j_m(\bar{P}_i(\boldsymbol{m}), P_o)) \\ + (\bar{P}_i(\boldsymbol{m}) - P_o) \left(\frac{1}{\rho(\bar{P}_i(\boldsymbol{m}), \bar{T}_i(\boldsymbol{m}))} - \frac{1}{\rho(P_i, T_i)} \right) \end{aligned} \tag{3.104}$$

where $\bar{T}_i(\boldsymbol{m})$ is the air temperature in the i^{th} chamber at equilibrium pressure $\bar{P}_i(\boldsymbol{m})$. For the two-chambered adiabatic actuator, the air temperature $\bar{T}_i(\boldsymbol{m})$ at equilibrium state is as defined in Eq. (3.92), while for the isothermal actuator, the chamber temperatures always correspond to the ambient temperature T_o.

Using the expression for the gravimetric density $W^j_m(P_i, \bar{P}_i(\boldsymbol{m}))$ from Eq. (3.104), the energy $W^j_{act}(\boldsymbol{m}, \boldsymbol{P})$ available from a two-chambered adiabatic and isothermal actuators, presented in Eq. (3.94) and Eq. (3.100) respectively, can be expressed as,

$$\begin{aligned} W^j_{act}(\boldsymbol{m}, \boldsymbol{P}) &= m_1 W^j_m(P_1, \bar{P}_1(\boldsymbol{m})) + m_2 W^j_m(P_2, \bar{P}_2(\boldsymbol{m})) \\ &= m_1 (W_m(P_1, P_o) - W_m(\bar{P}_1(\boldsymbol{m}), P_o)) + m_2 (W_m(P_2, P_o) - W_m(\bar{P}_2(\boldsymbol{m}), P_o)) \\ &\quad + (\bar{P}_1(\boldsymbol{m}) - P_o)(\bar{V}_1(\bar{x}(\boldsymbol{m})) - V_1(x)) + (\bar{P}_2(\boldsymbol{m}) - P_o)(\bar{V}_2(\bar{x}(\boldsymbol{m})) - V_2(x)) \end{aligned} \tag{3.105}$$

Using the definition for the chamber volume $V_i(x)$ from Eq. (3.73), and the relationship ($(\bar{P}_1(\boldsymbol{m}) - P_o)A_1 = (\bar{P}_2(\boldsymbol{m}) - P_o)A_2$) between the equilibrium pressures $\bar{P}_1(\boldsymbol{m})$, $\bar{P}_2(\boldsymbol{m})$ and the ambient pressure P_o from Eq. (3.85), the expression in Eq. (3.103) for the energy $W^j_{act}(\boldsymbol{m}, \boldsymbol{P})$ available from the two-chambered adiabatic actuator follows. □

Remark 3.4. *The energy extracted from the two-chambered pneumatic actuator is less than or equal to the sum of the maximum energy that can be extracted from each chamber of the two-chambered actuator.*

Proof. Let m_1 and m_2 be the mass of air in chamber 1 and 2 of the actuator, while P_1 and P_2 be the pressure in each chamber. Let $j \in (iso, adb)$ represent the thermodynamic process in the actuator. For the given initial conditions, the energy $W^j_{act_s}(m_i, P, P_o)$ available from the i^{th} chamber of the actuator with respect to the ambient pressure P_o is obtained from the definition of the gravimetric energy density $W^j_m(P_i, P_o)$ in Eq. (3.39) and Eq. (3.47) for adiabatic and isothermal actuators respectively as,

$$W^j_{act_s}(m_i, P_i, P_o) = m_i W^j_m(P_i, P_o) \tag{3.106}$$

The sum of the maximum available work from each chamber of the actuator, represented by $W^j_{act_t}(\boldsymbol{m}, \boldsymbol{P}, P_o)$, is given by,

$$W^j_{act_t}(\boldsymbol{m}, \boldsymbol{P}, P_o) = m_1 W^j_m(P_1, P_o) + m_2 W^j_m(P_2, P_o) \tag{3.107}$$

From theorems 3.1 and 3.2, the gravimetric energy density $W^j_m(P_i, P_o)$ is non-negative for any pair $(P_i, P_o) \in \Re^+$. Using this property in the expression for the available energy $W^j_{act}(\boldsymbol{m}, \boldsymbol{P})$ in Eq. (3.103), proof follows.

□

In the following section, supply rate for the two-chambered isothermal/adiabatic actuators is derived by defining the actuator energy function as the storage function. The port variables required for energetic interconnection with the actuator are also identified in the following section.

3.2.4 Passivity property of two-chambered actuator

As presented in section 3.1.4, a system with an input vector $\boldsymbol{u}$ and an output vector $\boldsymbol{y}$ is passive if the external supply rate $s(\boldsymbol{u}, \boldsymbol{y})$ as defined in Eq. (3.52) satisfies the following condition [2],

$$\int_0^t s(\boldsymbol{u}, \boldsymbol{y})\, d\tau \geq -c_o^2 \tag{3.108}$$

where c_o^2 is a positive constant. If the supply rate $s(\boldsymbol{u}, \boldsymbol{y})$ in the above inequality corresponds to physically meaningful power input, then the system is said to be energetically passive. A supply rate required for energetically passive operation of the two-chambered actuator is derived in this section first for the isothermal case and then for the adiabatic case.

Isothermal process

Given an air mass of m_1 and m_2 in chambers 1 and 2 of the actuator, as shown in Eq. (3.99), the energy function for the two-chambered isothermal actuator is the sum of the energy available from each chamber of the actuator with respect to the equilibrium pressures $\bar{P}_1(\boldsymbol{m})$, $\bar{P}_2(\boldsymbol{m})$ and is given by,

$$W_{act}^{iso}(\boldsymbol{m}, \boldsymbol{P}) = m_1 W_m^{iso}(P_1, \bar{P}_1(\boldsymbol{m})) + m_2 W_m^{iso}(P_2, \bar{P}_2(\boldsymbol{m})) \tag{3.109}$$

where P_1 and P_2 correspond to the air pressure in chamber 1 and 2 respectively.

From the expression for the time derivative of the single chamber actuator energy function in Eq. (3.66), the time derivative of the energy function for the two-chambered isothermal actuator is obtained as,

$$\begin{aligned}\dot{W}_{act}^{iso}(\boldsymbol{m}, \boldsymbol{P}) = \dot{m}_1 &\left(W_m^{iso}(P_1, \bar{P}_1(\boldsymbol{m})) + \frac{P_1 - \bar{P}_1(\boldsymbol{m})}{\rho(P_1, T_o)} \right) - (P_1 - \bar{P}_1(\boldsymbol{m}))\dot{V}_1(x) \\ &+ \dot{m}_2 \left(W_m^{iso}(P_2, \bar{P}_2(\boldsymbol{m})) + \frac{P_2 - \bar{P}_2(\boldsymbol{m})}{\rho(P_2, T_o)} \right) - (P_2 - \bar{P}_2(\boldsymbol{m}))\dot{V}_2(x) \\ &- \dot{\bar{P}}_1(\boldsymbol{m})(\bar{V}_1(\bar{x}(\boldsymbol{m})) - V_1(x)) - \dot{\bar{P}}_2(\boldsymbol{m})(\bar{V}_2(\bar{x}(\boldsymbol{m})) - V_2(x))\end{aligned} \tag{3.110}$$

On differentiation of the equilibrium pressure relationship in Eq. (3.85), the equilibrium pressure derivatives $\dot{\bar{P}}_1(\boldsymbol{m})$ and $\dot{\bar{P}}_2(\boldsymbol{m})$ are related as,

$$\dot{\bar{P}}_1(\boldsymbol{m})A_1 = \dot{\bar{P}}_2(\boldsymbol{m})A_2 \tag{3.111}$$

Using the relationship between the chamber volumes $V_1(x)$, $V_2(x)$ and the piston position x from Eq. (3.73), and the relationship between the equilibrium pressure derivatives in Eq. (3.111), the time derivative of the energy function $W_{act}^{iso}(\boldsymbol{m}, \boldsymbol{P})$ in Eq. (3.110) simplifies to,

$$\begin{aligned}\dot{W}_{act}^{iso}(\boldsymbol{m}, \boldsymbol{P}) = \dot{m}_1 &\left(W_m^{iso}(P_1, \bar{P}_1(\boldsymbol{m})) + \frac{P_1 - \bar{P}_1(\boldsymbol{m})}{\rho(P_1, T_o)} \right) - (P_1 - \bar{P}_1(\boldsymbol{m}))A_1\dot{x} - \\ &+ \dot{m}_2 \left(W_m^{iso}(P_2, \bar{P}_2(\boldsymbol{m})) + \frac{P_2 - \bar{P}_2(\boldsymbol{m})}{\rho(P_2, T_o)} \right) - (P_2 - \bar{P}_2(\boldsymbol{m}))A_2\dot{x}\end{aligned} \tag{3.112}$$

Theorem 3.5. *The two-chambered isothermal actuator is passive with respect to the following supply rate,*

$$\begin{aligned}&s_{iso_{2m}}((\dot{m}_1, \dot{m}_2, \dot{x}), (\Phi_{iso}(P_1, \bar{P}_1(\boldsymbol{m})), \Phi_{iso}(P_2, \bar{P}_2(\boldsymbol{m})), F_a(\boldsymbol{P}))) \\ &\qquad := \dot{m}_1 \Phi_{iso}(P_1, \bar{P}_1(\boldsymbol{m})) + \dot{m}_2 \Phi_{iso}(P_2, \bar{P}_2(\boldsymbol{m})) - F_a(\boldsymbol{P})\dot{x}\end{aligned} \tag{3.113}$$

where the mass flow rates $\dot{m}_1$ and $\dot{m}_2$ are the flow variables at the fluid ports of chamber 1 and 2 respectively of two-chambered actuator, $\Phi_{iso}(.)$ is the effort variable at the corresponding fluid port of the actuator chamber and from Eq. (3.67) is given by,

$$\Phi_{iso}(P_i, \bar{P}_i) = W_m^{iso}(P_i, \bar{P}_i(\boldsymbol{m})) + \frac{P_i - \bar{P}_i(\boldsymbol{m})}{\rho(P_i, T_o)} = RT_o \log\left(\frac{P_i}{\bar{P}_i(\boldsymbol{m})}\right) \tag{3.114}$$

while piston velocity $\dot{x}$ is the flow variable at the mechanical port of the actuator with the actuator force $F_a(\boldsymbol{P})$ being the corresponding effort variable.

Proof. Let the actuator energy function $W_{act}^{iso}(\boldsymbol{m}, \boldsymbol{P})$ in Eq. (3.109) to be the storage function for the two-chambered isothermal actuator. The time derivative of the actuator energy function ($\dot{W}_{act}^{iso}(\boldsymbol{m}, \boldsymbol{P})$) is as given in Eq. (3.112). From the definition of the fluid port effort variable $\Phi_{iso}(.)$ in Eq. (3.67) and the actuator force $F_a(\boldsymbol{P})$ in Eq. (3.86), the derivative of the energy function in Eq. (3.112) can be expressed in terms of the supply rate $s_{iso_{2m}}(.)$ in Eq. (3.113) as,

$$\begin{aligned} \dot{W}_{act}^{iso}(\boldsymbol{m}, \boldsymbol{P}) &= \dot{m}_1 \Phi_{iso}(P_1, \bar{P}_1(\boldsymbol{m})) + \dot{m}_2 \Phi_{iso}(P_2, \bar{P}_2(\boldsymbol{m})) - F_a(\boldsymbol{P})\dot{x} \\ &= s_{iso_{2m}}((\dot{m}_1, \dot{m}_2, \dot{x}), (\Phi_{iso}(P_1, \bar{P}_1(\boldsymbol{m})), \Phi_{iso}(P_2, \bar{P}_2(\boldsymbol{m})), F_a(\boldsymbol{P}))) \end{aligned} \tag{3.115}$$

Integrating the above equation and using the condition from proposition 3.2 that the two-chambered actuator energy function $W_{act}^{iso}(\boldsymbol{m}, \boldsymbol{P})$ is always positive, the supply rate $s_{iso_{2m}}(.)$ in Eq. (3.113) can be shown to satisfy the following passivity condition,

$$\begin{aligned} &\int_0^t s_{iso_{2m}}((\dot{m}_1, \dot{m}_2, \dot{x}), (\Phi_{iso}(P_1, \bar{P}_1(\boldsymbol{m})), \Phi_{iso}(P_2, \bar{P}_2(\boldsymbol{m})), F_a(\boldsymbol{P})))\, d\tau \\ &\quad \geq -W_{act}^{iso}(\boldsymbol{m}, \boldsymbol{P})\Big|_{t=0} \end{aligned} \tag{3.116}$$

where $W_{act}^{iso}(\boldsymbol{m}, \boldsymbol{P})\Big|_{t=0} \geq 0$ represents initial energy in the two-chambered isothermal actuator. □

Single valve metering two-chambered isothermal actuator:

As given in Eq. (3.84), the mass flow rates $\dot{m}_1$ and $\dot{m}_2$ to the two chambers of the isothermal actuator and the valve command input u are related as,

$$\dot{m}_1 = \Psi(P_1, T_o, u)u, \quad \dot{m}_2 = -\Psi(P_2, T_o, -u)u \tag{3.117}$$

where the nonlinear function $\Psi_{P_i,T_i,u}$ is as defined in Eq. (3.27). From the definition of the mass flow rate in the above equation, the energy function derivative in Eq.(3.115) for the isothermal actuator can be expressed as,

$$\dot{W}^{iso}_{act}(\boldsymbol{m},\boldsymbol{P}) = Z^{iso}_{\gamma}(\boldsymbol{m},\boldsymbol{P},u)u - F_a(\boldsymbol{P})\dot{x} \tag{3.118}$$

where $Z^{iso}_{\gamma}(\boldsymbol{m},\boldsymbol{P},u)$ is given by,

$$Z^{iso}_{\gamma}(\boldsymbol{m},\boldsymbol{P},u) = \Psi(P_1,T_o,u)RT_o\log\left(\frac{P_1}{\bar{P}_1(\boldsymbol{m})}\right) - \Psi(P_2,T_o,-u)RT_o\log\left(\frac{P_2}{\bar{P}_2(\boldsymbol{m})}\right) \tag{3.119}$$

Proposition 3.3. *For a flow variable corresponding to the valve command input u, the effort variable at the fluid interaction port of an isothermal actuator, designated by $Z^{iso}_{\gamma}(\boldsymbol{m},\boldsymbol{P},u)$ in Eq. (3.119), varies monotonically with the actuator force $F_a(\boldsymbol{P})$, and is identically zero at $F_a(\boldsymbol{P}) = 0$. Also, the nonlinear gain $\gamma^{iso}_1(\boldsymbol{m},\boldsymbol{P},u)$ mapping the actuator force $F_a(\boldsymbol{P})$ to the effort variable $Z^{iso}_{\gamma}(\boldsymbol{m},\boldsymbol{P},u)$ is given by,*

$$\begin{aligned}\gamma^{iso}_1(\boldsymbol{m},\boldsymbol{P},u) &= \frac{Z^{iso}_{\gamma}(\boldsymbol{m},\boldsymbol{P},u)}{F_a(\boldsymbol{P})} \\ &= \frac{RT_o}{F_a(\boldsymbol{P})}\left(\Psi(P_1,T_o,u)\log\left(\frac{P_1}{\bar{P}_1(\boldsymbol{m})}\right) - \Psi(P_2,T_o,-u)\log\left(\frac{P_2}{\bar{P}_2(\boldsymbol{m})}\right)\right)\end{aligned} \tag{3.120}$$

and is well defined for all feasible values of air mass m_1, m_2, air pressure P_1, P_2 in chambers 1 and 2 of the isothermal actuator, and input command u to the single pneumatic valve.

Proof. Proof as shown in appendix A.1.1. □

The power variables at the fluid port as given in Eq. (3.118) are transformed such that the new effort variable at the fluid port corresponds to actuator force $F_a(\boldsymbol{P})$, and the corresponding new flow variable is given by $\gamma^{iso}_1(\boldsymbol{m},\boldsymbol{P},u)u$. To define a plausible power interaction, $\gamma^{iso}_1(\boldsymbol{m},\boldsymbol{P},u)u$ must represent a velocity variable. Therefore, the measurement units for $\gamma^{iso}_1(\boldsymbol{m},\boldsymbol{P},u)$ defined in Eq. (3.120) are $m^{-1}s^{-1}$.

Theorem 3.6. *The two-chambered isothermal pneumatic actuator, with a single pneumatic valve for metering the air flow, is passive with respect to the following supply*

rate,

$$s_{iso_{2u}}((\gamma_1^{iso}(.)u, \dot{x}), (F_a(\boldsymbol{P}), F_a(\boldsymbol{P}))) = \gamma_1^{iso}(\boldsymbol{m}, \boldsymbol{P}, u)F_a(\boldsymbol{P})u - F_a(\boldsymbol{P})\dot{x} \tag{3.121}$$

where u is the command input to the pneumatic valve, the nonlinear gain $\gamma_1^{iso}(\boldsymbol{m}, \boldsymbol{P}, u)$ is as defined in Eq. (3.120) and $\gamma_1^{iso}(\boldsymbol{m}, \boldsymbol{P}, u)u$ represents the flow variable at the fluid port of the actuator. The piston velocity $\dot{x}$ corresponds to the flow variable at the mechanical port of the actuator, while the actuator force $F_a(\boldsymbol{P})$ is the effort variable at both the fluid port and the mechanical port of the actuator.

Proof. Let the actuator energy function $W_{act}^{iso}(\boldsymbol{m}, \boldsymbol{P})$ defined in Eq. (3.109) be the storage function for the two-chambered isothermal actuator. When using a single valve for metering the air flow to the actuator, the time derivative of actuator energy function $\dot{W}_{act}^{iso}(\boldsymbol{m}, \boldsymbol{P})$ can be expressed as in Eq. (3.118). Using the transformation of the fluid port effort variable $Z_{\gamma}^{iso}(\boldsymbol{m}, \boldsymbol{P}, u)$ from Eq. (3.120), the energy function derivative $\dot{W}_{act}^{iso}(\boldsymbol{m}, \boldsymbol{P})$ in Eq. (3.118) can be expressed in terms of the supply rate $s_{iso_{2u}}(.)$ from Eq. (3.121) as,

$$\dot{W}_{act}^{iso}(\boldsymbol{m}, \boldsymbol{P}) = \gamma_1^{iso}(\boldsymbol{m}, \boldsymbol{P}, u)F_a(\boldsymbol{P})u - F_a(\boldsymbol{P})\dot{x} = s_{iso_{2u}}((\gamma_1^{iso}(.)u, \dot{x}), (F_a, F_a)) \tag{3.122}$$

On integrating both side of the above equation, and using the condition that the energy function $W_{act}^{iso}(\boldsymbol{m}, \boldsymbol{P})$ is always positive it can be seen that the supply rate $s_{iso_{2u}}(.)$ in Eq. (3.121) satisfies the following passivity condition,

$$\int_0^t s_{iso_{2u}}((\gamma_1^{iso}(.)u, \dot{x}), (F_a(\boldsymbol{P}), F_a(\boldsymbol{P}))) \, d\tau \geq -W_{act}^{iso}(\boldsymbol{m}, \boldsymbol{P})\Big|_{t=0} \tag{3.123}$$

where $W_{act}^{iso}(\boldsymbol{m}, \boldsymbol{P})\Big|_{t=0} \geq 0$ corresponds to the initial energy in the two-chambered isothermal actuator. □

As the isothermal process is reversible (and hence lossless), the isothermal actuator can therefore be interpreted as a two-port nonlinear spring as shown in Fig. (3.7). The flow variable $\gamma_1^{iso}(\boldsymbol{m}, \boldsymbol{P}, u)u$ at the fluid port of the actuator represents active velocity commanded at one port of the spring which can be modulated to achieve the desired actuator force output.

The port variables and the supply rate for a two-chambered actuator with adiabatic thermodynamic process are developed in the following subsection.

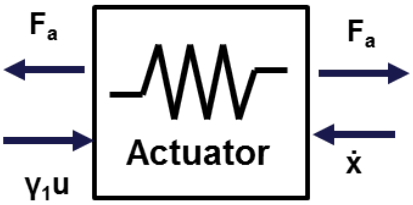

Figure 3.7: Representation of a pneumatic actuator with reversible thermal dynamics as a two-port nonlinear spring

Adiabatic process

The energy function for the two-chambered adiabatic actuator $W_{act}^{adb}(\boldsymbol{m}, \boldsymbol{P})$ in Eq. (3.93) is the sum of the energy function for each actuator chamber with respect to the equilibrium position $\bar{x}(\boldsymbol{m})$ obtained from Eq. (3.91). Therefore, for a given air mass of m_1 and m_2 in chambers 1 and 2 of the actuator, the energy function $W_{act}^{adb}(\boldsymbol{m}, \boldsymbol{P})$ for the two-chambered actuator can be expressed in terms of the gravimetric energy density of an adiabatic actuator chamber $W_m^{adb}(.)$ from Eq. (3.39) as,

$$W_{act}^{adb}(\boldsymbol{m}, \boldsymbol{P}) = m_1 W_m^{adb}(P_1, \bar{P}_1(\boldsymbol{m})) + m_2 W_m^{adb}(P_2, \bar{P}_2(\boldsymbol{m})) \tag{3.124}$$

Using the expression for derivative of the single chamber energy function in Eq. (3.57), the time derivative of the energy function $W_{act}^{adb}(\boldsymbol{m}, \boldsymbol{P})$ of a two-chambered adiabatic actuator defined in Eq. (3.124) is obtained as,

$$\begin{aligned}\dot{W}_{act}^{adb}(\boldsymbol{m}, \boldsymbol{P}) = \dot{m}_1 &\left(W_m^{adb}(P_1, \bar{P}_1(\boldsymbol{m})) + \frac{P_1 - \bar{P}_1(\boldsymbol{m})}{\rho(P_1, T_1)} \right) - (P_1 - \bar{P}_1(\boldsymbol{m}))\dot{V}_1(x) \\ &+ \dot{m}_2 \left(W_m^{iso}(P_2, \bar{P}_2(\boldsymbol{m})) + \frac{P_2 - \bar{P}_2(\boldsymbol{m})}{\rho(P_2, T_2)} \right) - (P_2 - \bar{P}_2(\boldsymbol{m}))\dot{V}_2(x) \\ &- \dot{\bar{P}}_1(\boldsymbol{m})(\bar{V}_1(\bar{x}(\boldsymbol{m})) - V_1(x)) - \dot{\bar{P}}_2(\boldsymbol{m})(\bar{V}_2(\bar{x}(\boldsymbol{m})) - V_2(x))\end{aligned} \tag{3.125}$$

From the relationship between the chamber volumes $V_1(x)$, $V_2(x)$ and the piston position x in Eq. (3.73), and using the relationship between the derivatives of the equilibrium pressures $\dot{\bar{P}}_1(\boldsymbol{m})$ and $\dot{\bar{P}}_2(\boldsymbol{m})$ from Eq. (3.111), the above equation can be

simplified as,

$$\dot{W}_{act}^{adb}(\boldsymbol{m},\boldsymbol{P}) = \dot{m}_1\left(W_m^{adb}(P_1,\bar{P}_1(\boldsymbol{m})) + \frac{P_1-\bar{P}_1(\boldsymbol{m})}{\rho(P_1,T_1)}\right) - (P_1-\bar{P}_1(\boldsymbol{m}))A_1\dot{x} + \dot{m}_2\left(W_m^{iso}(P_2,\bar{P}_2(\boldsymbol{m})) + \frac{P_2-\bar{P}_2(\boldsymbol{m})}{\rho(P_2,T_2)}\right) - (P_2-\bar{P}_2(\boldsymbol{m}))A_2\dot{x} \tag{3.126}$$

Theorem 3.7. *The two-chambered adiabatic actuator is passive with respect to the following supply rate,*

$$\begin{aligned} &s_{adb_{2m}}((\dot{m}_1,\dot{m}_2,\dot{x}),(\Phi_{adb}(P_1,\bar{P}_1(\boldsymbol{m})),\Phi_{adb}(P_2,\bar{P}_2(\boldsymbol{m})),F_a(\boldsymbol{P}))) \\ &\qquad := \dot{m}_1\Phi_{adb}(P_1,\bar{P}_1(\boldsymbol{m})) + \dot{m}_2\Phi_{adb}(P_2,\bar{P}_2(\boldsymbol{m})) - F_a(\boldsymbol{P})\dot{x} \end{aligned} \tag{3.127}$$

where the air flow rates $\dot{m}_1$ and $\dot{m}_2$ are designated to be flow variables at the fluid ports of chamber 1 and 2 respectively of the two-chambered adiabatic actuator, $\Phi_{adb}(.)$ represents the effort variable at the corresponding fluid ports of the actuator chamber and is obtained from Eq. (3.58) as,

$$\Phi_{adb}(P_i,\bar{P}_i) = W_m^{adb}(P_i,\bar{P}_i(\boldsymbol{m})) + \frac{P_i-\bar{P}_i(\boldsymbol{m})}{\rho(P_i,T_i)} = C_p(T_1-\bar{T}_i(\boldsymbol{m})) \tag{3.128}$$

while the piston velocity $\dot{x}$ is the flow variable at the mechanical port of the actuator with the actuator force $F_a(\boldsymbol{P})$ being the corresponding effort variable.

Proof. Let the actuator energy function $W_{act}^{adb}(\boldsymbol{m},\boldsymbol{P})$ from Eq. (3.124) be the storage function for the two-chambered adiabatic actuator. The time derivative of the storage function $\dot{W}_{act}^{adb}(\boldsymbol{m},\boldsymbol{P})$ is as given in Eq. (3.126). From the definition of the fluid port effort variable $\Phi_{adb}(.)$ in Eq. (3.128) and the actuator force $F_a(\boldsymbol{P})$ in Eq. (3.86), the derivative of the energy function in Eq. (3.126) can be expressed in terms of the supply rate $s_{adb_{2m}}(.)$ in Eq. (3.127) as,

$$\begin{aligned} \dot{W}_{act}^{adb}(\boldsymbol{m},\boldsymbol{P}) &= \dot{m}_1\Phi_{adb}(P_1,\bar{P}_1(\boldsymbol{m})) + \dot{m}_2\Phi_{adb}(P_2,\bar{P}_2(\boldsymbol{m})) - F_a(\boldsymbol{P})\dot{x} \\ &= s_{adb_{2m}}((\dot{m}_1,\dot{m}_2,\dot{x}),(\Phi_{adb}(P_1,\bar{P}_1(\boldsymbol{m})),\Phi_{adb}(P_2,\bar{P}_2(\boldsymbol{m})),F_a(\boldsymbol{P}))) \end{aligned} \tag{3.129}$$

On integrating the above equation and using the condition from proposition 3.1 that the two-chambered actuator energy function $W_{act}^{adb}(\boldsymbol{m},\boldsymbol{P})$ is always positive, the supply

rate $s_{adb_{2m}}(.)$ in Eq. (3.127) can be shown to satisfy the following passivity condition,

$$\int_0^t s_{adb_{2m}}((\dot{m}_1, \dot{m}_2, \dot{x}), (\Phi_{adb}(P_1, \bar{P}_1(\boldsymbol{m})), \Phi_{adb}(P_2, \bar{P}_2(\boldsymbol{m})), F_a(\boldsymbol{P})))\, d\tau$$
$$\geq -W_{act}^{adb}(\boldsymbol{m}, \boldsymbol{P})\Big|_{t=0} \tag{3.130}$$

where $W_{act}^{adb}(\boldsymbol{m}, \boldsymbol{P})\Big|_{t=0} \geq 0$ represents initial energy in the two-chambered adiabatic actuator.

□

Single valve metering the two-chambered adiabatic actuator:

As given in Eq. (3.84), the mass flow rates $\dot{m}_1$ and $\dot{m}_2$ to the two chambers of the adiabatic actuator are related to the valve command input u as,

$$\dot{m}_1 = -\Psi(P_1, T_1, u)u, \quad \dot{m}_2 = -\Psi(P_2, T_2, -u)u \tag{3.131}$$

From the definition of the mass flow rate in the above equation, the energy function derivative $\dot{W}_{act}^{adb}(\boldsymbol{m}, \boldsymbol{P})$ in Eq. (3.129) for the adiabatic actuator is written as,

$$\dot{W}_{act}^{adb}(\boldsymbol{m}, \boldsymbol{P}) = Z_\gamma^{adb}(\boldsymbol{m}, \boldsymbol{P}, u)u - F_a(\boldsymbol{P})\dot{x} \tag{3.132}$$

where $Z_\gamma^{adb}(\boldsymbol{m}, \boldsymbol{P}, u)$ is the effort variable at the fluid port of the actuator when the valve command input u is designated to be the flow variable and is given by,

$$Z_\gamma^{adb}(\boldsymbol{m}, \boldsymbol{P}, u) = C_p \left(\Psi(P_1, T_1, u)(T_1 - \bar{T}_1(\boldsymbol{m})) - \Psi(P_2, T_2, -u)(T_2 - \bar{T}_2(\boldsymbol{m}))\right) \tag{3.133}$$

Proposition 3.4. *For a flow variable corresponding to the valve command input u, the effort variable $Z_\gamma^{adb}(\boldsymbol{m}, \boldsymbol{P}, u)$ at the fluid interaction port of an adiabatic actuator in Eq. (3.133), varies monotonically with the actuator force $F_a(\boldsymbol{P})$, and is identically zero at the equilibrium state defined by $F_a(\boldsymbol{P}) = 0$. Also, the nonlinear gain $\gamma_1^{adb}(\boldsymbol{m}, \boldsymbol{P}, u)$ mapping the actuator force $F_a(\boldsymbol{P})$ to the effort variable $Z_\gamma^{adb}(\boldsymbol{m}, \boldsymbol{P}, u)$ is given by,*

$$\gamma_1^{adb}(\boldsymbol{m}, \boldsymbol{P}, u) = \frac{C_p}{F_a(\boldsymbol{P})} \left(\Psi(P_1, T_1, u)\left(T_1 - \bar{T}_1(\boldsymbol{m})\right) - \Psi(P_2, T_2, -u)\left(T_2 - \bar{T}_2(\boldsymbol{m})\right)\right) \tag{3.134}$$

and is well defined for all feasible elements of air mass vector $\boldsymbol{m} \triangleq (m_1, m_2)$, chamber pressure vector $\boldsymbol{P} \triangleq (\boldsymbol{P})$, and valve input command u to the pneumatic valve.

Proof. Proof as shown in appendix A.2.1. □

The measurement units for the nonlinear gain $\gamma_1^{adb}(\boldsymbol{m}, \boldsymbol{P}, u)$ are $m^{-1}s^{-1}$. Similar to the isothermal actuator, the power variables at the fluid port of an adiabatic actuator, as given in Eq. (3.132), are transformed such that the new effort variable at the fluid port corresponds to actuator force $F_a(\boldsymbol{P})$. The new flow variable at the fluid port $\gamma_1^{adb}(\boldsymbol{m}, \boldsymbol{P}, u)u$ must therefore represent a velocity variable.

Theorem 3.8. *The two-chambered adiabatic actuator, with a single pneumatic valve for metering the air flow to the actuator, is passive with respect to the following supply rate,*

$$s_{adb_{2u}}((\gamma_1^{adb}u, \dot{x}), (F_a(\boldsymbol{P}), F_a(\boldsymbol{P}))) := \gamma_1^{adb}(\boldsymbol{m}, \boldsymbol{P}, u)F_a(\boldsymbol{P})u - F_a(\boldsymbol{P})\dot{x} \tag{3.135}$$

where u is the command input to the pneumatic valve, the nonlinear gain $\gamma_1^{adb}(\boldsymbol{m}, \boldsymbol{P}, u)$ is as defined in Eq. (3.134), with $\gamma_1^{adb}(\boldsymbol{m}, \boldsymbol{P}, u)u$ representing the velocity variable at the fluid port of the actuator. The piston velocity $\dot{x}$ is the flow variable at the mechanical port of the actuator. The actuator force $F_a(\boldsymbol{P})$ is the effort variable at both the fluid port and the mechanical port of the actuator.

Proof. Let the actuator energy function $W_{act}^{adb}(\boldsymbol{m}, \boldsymbol{P})$ in Eq. (3.124) be the storage function for the two-chambered adiabatic actuator. When using a single valve for metering the air flow to the actuator, the time derivative of actuator energy function $\dot{W}_{act}^{adb}(\boldsymbol{m}, \boldsymbol{P})$ is obtained as given in Eq. (3.132). Using the transformation of the fluid port effort variable $Z_\gamma^{adb}(\boldsymbol{m}, \boldsymbol{P}, u)$ from Eq. (3.134), the energy function derivative in Eq. (3.132) can be expressed in terms of the supply rate $s_{adb_{2u}}(.)$ in Eq. (3.135) as,

$$\dot{W}_{act}^{adb}(\boldsymbol{m}, \boldsymbol{P}) = \gamma_1^{adb}(\boldsymbol{m}, \boldsymbol{P}, u)F_a(\boldsymbol{P})u - F_a(\boldsymbol{P})\dot{x} = s_{adb_{2u}}((\gamma_1^{adb}u, \dot{x}), (F_a(\boldsymbol{P}), F_a(\boldsymbol{P}))) \tag{3.136}$$

On integrating the above equation, and using the condition that the energy function $W_{act}^{adb}(\boldsymbol{m}, \boldsymbol{P})$ is always positive it can be seen that the supply rate $s_{adb_{2u}}(.)$ satisfies the following passivity condition,

$$\int_0^t s_{adb_{2u}}((\gamma_1^{adb}u, \dot{x}), (F_a(\boldsymbol{P}), F_a(\boldsymbol{P}))) \, d\tau \geq -W_{act}^{adb}(\boldsymbol{m}, \boldsymbol{P})\Big|_{t=0} \tag{3.137}$$

where $W_{act}^{adb}(\boldsymbol{m}, \boldsymbol{P})\Big|_{t=0} \geq 0$ corresponds to the initial energy in the two-chambered adiabatic actuator. □

From the definition of the supply rate to the adiabatic actuator in Eq. (3.135), the two-chambered adiabatic actuator can thus be interpreted as a two-port nonlinear spring, with an active velocity input (due to u) at the port corresponding to interaction with the fluid source.

By appropriately selecting the valve input command u, the supply rate for the isothermal actuator in Eq. (3.121) and the adiabatic actuator in Eq. (3.135) can be changed such that the corresponding energy functions in Eq. (3.100) and Eq. (3.94) respectively follow a desired profile. As the pneumatic actuator is used to provide actuation force, the desired energy profile of the actuator is determined by the desired force from the actuator. In the following section, an energy function corresponding to the error between the current state of the actuator and the state of the actuator providing the desired force, is derived. This error state energy function is used in later chapters as a Lyapunov function for designing the valve command input u to the actuator.

3.3 Energy function for actuator error dynamics

Pneumatic actuators are used to provide the force required for performing mechanical work. The desired force $F_a^d(t)$ required from the actuator for doing the mechanical is obtained by designing suitable valve input command u. Let $P_1^d(t)$ and $P_2^d(t)$ correspond to the desired pressure in chambers 1 and 2 of the actuator. These pressures are related to the desired actuator force $F_a^d(t)$ as,

$$F_a^d(t) := P_1^d(t)A_1 - P_2^d(t)A_2 - P_oA_p \tag{3.138}$$

where again A_1 and A_2 are the cross-sectional areas at the cap side and the rod side of the actuator, while the rod area is given by, $A_p = A_1 - A_2$. The error $\tilde{F}$ between the available force from the actuator and the required force from the actuator is defined as,

$$\tilde{F} = F_a - F_a^d(t) \tag{3.139}$$

In this section, energy function for the pneumatic actuator corresponding to the force error $\tilde{F}$ is defined. This energy function is used to identify the supply rate to the actuator error dynamics. The command input can then be defined such that this supply rate is decreasing for non-zero error and is identically zero when the error converges to

zero. In the following subsection the actuator states corresponding to the desired force profile $F_a^d(t)$ are presented.

3.3.1 Actuator states corresponding to desired force profile $F_a^d(t)$

For a given mass of air m_1 and m_2 in chambers 1 and 2 of a two-chambered actuator, let $x_d(t)$ be position of the actuator where the desired force $F_a^d(t)$ is achieved. From the definition of the pressure-volume curves for isothermal and adiabatic process in Eq. (3.82) and Eq. (3.78) respectively, the desired pressures $P_1^d(t)$ and $P_2^d(t)$ in chambers 1 and 2 of the actuator are related to the desired actuator piston position $x_d(t)$ as,

$$\begin{aligned} \textbf{Isothermal:} \quad & P_1^d(t) = \frac{k_{c_1}(m_1)}{A_1(L_{1o} + x_d(t))}, \quad P_2^d(t) = \frac{k_{c_2}(m_2)}{A_2(L_{2o} - x_d(t))} \\ \textbf{Adiabatic:} \quad & P_1^d(t) = \frac{k_{p_1}(m_1)}{A_1^\gamma(L_{1o} + x_d(t))^\gamma}, \quad P_2^d(t) = \frac{k_{p_2}(m_2)}{A_2^\gamma(L_{2o} - x_d(t))^\gamma} \end{aligned} \tag{3.140}$$

where the mass dependent parameters $k_{c_1}(m_1) = m_1 RT_o$ and $k_{c_2}(m_2) = m_2 RT_o$ for the isothermal process are as defined in Eq. (3.82), while the parameters $k_{p_1}(m_1)$ and $k_{p_2}(m_2)$ for the adiabatic process are as defined in Eq. (3.78). From Eq. (3.140) it can be seen that for both the isothermal and adiabatic actuators, the pressure in chamber 1 decreases monotonically with the piston position x, while the pressure in chamber 2 increases monotonically with piston position x. Therefore, for a given mass of air in each actuator chamber, there is a unique position of the actuator $x_d(t)$ providing the desired actuator force $F_a^d(t)$.

Using the relationship between the desired chamber pressures $P_1^d(t)$, $P_2^d(t)$ and the corresponding actuator position $x_d(t)$ from Eq. (3.140) in the definition of the desired actuator force $F_a^d(t)$ in Eq. (3.138), the desired actuator position $x_d(t)$ is obtained as the solution of the following equation,

$$\begin{aligned} \textbf{Isothermal :} \quad & \frac{k_{c_1}(m_1)}{L_{1o} + x_d(t)} - \frac{k_{c_2}(m_2)}{L_{2o} - x_d(t)} - (P_o A_p - F_a^d(t)) = 0 \\ \textbf{Adiabatic :} \quad & \frac{k_{p_1}(m_1)}{A_1^{\gamma-1}(L_{1o} + x_d(t))^\gamma} - \frac{k_{p_2}(m_2)}{A_2^{\gamma-1}(L_{2o} - x_d(t))^\gamma} - (P_o A_p - F_a^d(t)) = 0 \end{aligned} \tag{3.141}$$

After solving for $x_d(t)$ from the above equation, the desired chamber pressures $P_1^d(t)$ and $P_2^d(t)$ are obtained from Eq. (3.140). In section 3.2.4 it has been shown that the

pneumatic actuator with reversible thermodynamics (adiabatic or isothermal) can be represented as a two-port nonlinear spring. In the following remark it is shown that the actuator force error $\tilde{F}$ and the position error $(x_d(t) - x)$ also have a monotonic relationship.

Remark 3.5. *The relationship between the actuator force error $\tilde{F}$ and the position error $(x_d(t) - x)$ has the following properties,*

1. *For both the isothermal and the adiabatic actuators, the actuator force error $\tilde{F}$ as defined in Eq. (3.139), varies monotonically with the error between the desired position $x_d(t)$ as defined in Eq. (3.141) and the current actuator position x. In addition, the actuator force error $\tilde{F}$ is zero only if the position error $(x_d(t) - x)$ is also identically zero.*

2. *The position error $(x_d(t) - x)$ can be mapped to the actuator force error $\tilde{F}$ through a nonlinear gain, designated by $K^d_{iso}(\boldsymbol{m}, x, x_d)$ for the isothermal actuator and by $K^d_{adb}(\boldsymbol{m}, x, x_d)$ for the adiabatic actuator. By defining the actuator force F_a and the desired force F^d_a in terms of the mass in each chamber (m_1, m_2), position of the actuator x and the desired position of the actuator $x_d(t)$, these gains are obtained as,*

$$\begin{aligned} \textbf{Isothermal :} \quad & K^d_{iso}(\boldsymbol{m}, x, x_d) = \frac{m_1 R T_o}{(L_{1o} + x)(L_{1o} + x_d)} + \frac{m_2 R T_o}{(L_{2o} - x)(L_{2o} - x_d(t))} \\ \textbf{Adiabatic :} \quad & K^d_{adb}(\boldsymbol{m}, x, x_d) = \frac{F_a(\boldsymbol{m}, \boldsymbol{T}, x) - F^d_a(\boldsymbol{m}, \boldsymbol{T}, x_d)}{(x_d(t) - x)} \end{aligned} \tag{3.142}$$

The nonlinear functions $K^d_{iso}(\boldsymbol{m}, x, x_d)$ and $K^d_{adb}(\boldsymbol{m}, x, x_d)$ are also well defined for all values of m_1, m_2, x and $x_d(t)$.

Proof. Proof is as shown in appendix A.2.2.

□

The properties of the relationship between the force error $\tilde{F}$ and the position error $(x_d(t) - x)$ stated in the above remark will be used in the passivity analysis of the actuator error energy function in the subsequent section. Let $\boldsymbol{P} \triangleq (P_1, P_2)$, be the

vector of pressure, and $\boldsymbol{P^d} \triangleq (P_1^d, P_2^d)$ be the vector of desired pressures in chambers 1 and 2 of the actuator respectively. By considering the desired pressure vector $\boldsymbol{P^d}$ to be the new equilibrium pressure, the energy function for the actuator force error is defined as the available energy from the actuator when traversing from the current pressure vector $\boldsymbol{P}$ to the desired pressure vector $\boldsymbol{P^d}$. The energy function corresponding to the actuator force output error $\tilde{F}$ is presented in the following section.

3.3.2 Energy function for actuator force error dynamics

Let $\boldsymbol{m} \triangleq (m_1, m_2)$ be the vector of known air mass in chamber 1 and 2 respectively, and let $j \in (iso, adb)$ be the index to represent the thermodynamic process in the actuator. The gravimetric energy density of air $W_m^j(P_i, P_i^d)$ in $i^{th} \in (1, 2)$ chamber of the actuator, as the chamber pressure P_i is regulated to the desired chamber pressure P_i^d is as given in Eq. (3.39) and Eq. (3.47) for adiabatic and isothermal actuators respectively. For given air mass $\boldsymbol{m}$, the energy available $W_L^j(\boldsymbol{m}, \boldsymbol{P}, \boldsymbol{P^d})$ from the actuator, as the pressure vector $\boldsymbol{P}$ is regulated to desired pressure vector $\boldsymbol{P^d}$, is the sum of available energy from both chambers of the actuator and is defined as,

$$W_L^j(\boldsymbol{m}, \boldsymbol{P}, \boldsymbol{P^d}) = m_1 W_m^j(P_1, P_1^d) + m_2 W_m^j(P_2, P_2^d) \tag{3.143}$$

where adiabatic chamber gravimetric energy density $W_m^{adb}(P_i, P_i^d)$ and the isothermal chamber gravimetric energy density $W_m^{iso}(P_i, P_i^d)$ are defined as,

$$\text{Adiabatic: } W_m^{adb}(P_i, P_i^d) = -C_p T_i \left(\left(\left(\frac{P_i^d}{P_i} \right)^{\gamma - 1/\gamma} - 1 \right) - \frac{\gamma - 1}{\gamma} \left(\frac{P_i^d}{P_i} - 1 \right) \right) \tag{3.144}$$

$$\text{Isothermal: } W_m^{iso}(P_i, P_i^d) = RT_o \left(\left(\frac{P_i^d}{P_i} - 1 \right) - \log \left(\frac{P_i^d}{P_i} \right) \right) \tag{3.145}$$

Lemma 3.3. *For a desired actuator force $F_a^d(t)$, the energy function $W_L^j(\boldsymbol{m}, \boldsymbol{P}, \boldsymbol{P^d})$ defined in Eq. (3.143) is a non-negative function of the actuator force output error $\tilde{F} = (F_a - F_a^d(t))$.*

Proof. The actuator force error $\tilde{F} := ((P_1 - P_1^d)A_1 - (P_2 - P_2^d)A_2)$ varies with the chamber pressure vector $\boldsymbol{P} := (P_1, P_2)$ and the desired chamber pressure vector $\boldsymbol{P^d} :=$

(P_1^d, P_2^d). As shown in Theorem 3.1 and Theorem 3.2, the gravimetric energy densities $W_m^{adb}(P_i, P_i^d)$ and $W_m^{iso}(P_i, P_i^d)$ for the adiabatic and the isothermal actuator chambers respectively, is a non-negative function of any pair (P_i, P_i^d) of pressure inputs. Therefore, for any force error $\tilde{F}$ due to difference between the chamber pressure vector $\boldsymbol{P}$ and the desired pressure vector $\boldsymbol{P^d}$, the available energy $W_L^j(\boldsymbol{m}, \boldsymbol{P}, \boldsymbol{P^d})$ from the actuator as defined in Eq. (3.143) is a non-negative function of the force error $\tilde{F}$.

□

In the following section, the supply rate to the actuator error dynamics is presented.

3.3.3 Supply rate to the actuator error energy function

The supply rate to the error dynamics is obtained by defining the energy function for the error dynamics $W_L^j(\boldsymbol{m}, \boldsymbol{P}, \boldsymbol{P^d})$ from Eq. (3.143) as the storage function. Using the derivative of the energy function for a single chamber isothermal and adiabatic actuators in Eq. (3.66) and Eq. (3.57) respectively, the derivative of the actuator error energy function $W_L^j(\boldsymbol{m}, \boldsymbol{P}, \boldsymbol{P^d})$ in Eq. (3.143) is obtained as,

$$\dot{W}_L^j(\boldsymbol{m}, \boldsymbol{P}, \boldsymbol{P^d}) = \sum_{i=1}^{2} \dot{m}_i \left(W_{m_i}(P_i, P_i^d) + \frac{P_i - P_i^d}{\rho(P_i, T_i)} \right) - (P_i - P_i^d)\dot{V}_i(x) - \dot{P}_i^d(V_i(x_d) - V_i(x)) \tag{3.146}$$

where again $j \in (iso, adb)$ is the index to represent the thermodynamic process in the actuator and $V_i(x)$ is the volume of i^{th} actuator chamber at piston position corresponding to x. The derivative of the actuator Lyapunov function in the above equation is similar in form to the derivative of the energy function of two-chambered isothermal actuator as shown in Eq. (3.110) and a two-chambered adiabatic actuator as shown in Eq. (3.125). From the definition of the air mass flow rate in Eq. (3.26), and using the definition of gravimetric energy density $W_m(P_i, P_i^d)$ from Eqs. (3.145 and 3.144), the actuator Lyapunov function derivative $\dot{W}_L^j(\boldsymbol{m}, \boldsymbol{P}, \boldsymbol{P^d})$ in the above equation can be expressed as,

$$\dot{W}_L^j(\boldsymbol{m}, \boldsymbol{P}, \boldsymbol{P^d}) = Z_\gamma^j(\boldsymbol{m}, \boldsymbol{P}, \boldsymbol{P^d}, u)u - \tilde{F}\dot{x} + \dot{F}_a^d(x - x_d) \tag{3.147}$$

where the nonlinear function $Z_\gamma^j(\boldsymbol{m}, \boldsymbol{P}, \boldsymbol{P^d}, u)$ depends on the thermodynamic process in the actuator and is defined for the isothermal and the adiabatic actuators as,

$$Z_\gamma^{iso}(\boldsymbol{m}, \boldsymbol{P}, \boldsymbol{P^d}, u) = \Psi(P_1, T_o, u) RT_o \log\left(\frac{P_1}{P_1^d}\right) - \Psi(P_2, T_o, -u) RT_o \log\left(\frac{P_2}{P_2^d}\right) \tag{3.148}$$

$$\begin{aligned} Z_\gamma^{adb}(\boldsymbol{m}, \boldsymbol{P}, \boldsymbol{P^d}, u) = {} & \Psi(P_1, T_1, u) C_p T_1 \left(1 - \left(\frac{P_1^d}{P_1}\right)^{\gamma - 1/\gamma}\right) \\ & - \Psi(P_2, T_2, -u) C_p T_2 \left(1 - \left(\frac{P_2^d}{P_2}\right)^{\gamma - 1/\gamma}\right) \end{aligned} \tag{3.149}$$

The nonlinear function $Z_\gamma^j(\boldsymbol{m}, \boldsymbol{P}, \boldsymbol{P^d}, u)$ in the above equations is transformed using the monotonic relationship between the actuator force error $\tilde{F}$ and the position error $(x_d(t) - x)$. This transformation is presented in the following remark.

Remark 3.6. *The function $Z_\gamma^j(\boldsymbol{m}, \boldsymbol{P}, \boldsymbol{P^d}, u)$ in Eq. (3.147), varies monotonically with the actuator force error $\tilde{F}$, and is identically zero only if the $\tilde{F}$ is also zero. The nonlinear gain $\gamma_3^j(\boldsymbol{m}, \boldsymbol{P}, \boldsymbol{P^d}, u)$ to map the force error $\tilde{F}$ to the effort variable $Z_\gamma^j(\boldsymbol{m}, \boldsymbol{P}, \boldsymbol{P^d}, u)$ is positive and well defined, for all elements of the vector $(\boldsymbol{m}, \boldsymbol{P}, \boldsymbol{P^d}, u)$.*

Proof. Proof of this remark is presented in appendix C. □

As a consequence of above remark, $Z_\gamma^j(\boldsymbol{m}, \boldsymbol{P}, \boldsymbol{P^d}, u)$ for isothermal and adiabatic actuators in Eq. (3.148) and Eq. (3.149) respectively can be expressed as,

$$Z_\gamma^j(\boldsymbol{m}, \boldsymbol{P}, \boldsymbol{P^d}, u) = \gamma_3^j(\boldsymbol{m}, \boldsymbol{P}, \boldsymbol{P^d}, u)\tilde{F} \tag{3.150}$$

where again $j \in (iso, adb)$ represents the index for isothermal or adiabatic actuator. Using the transformation of the effort variable $Z_\gamma^j(\boldsymbol{m}, \boldsymbol{P}, \boldsymbol{P^d}, u)$ from the above equation, and the monotonic relationship between position error $(x_d(t) - x)$ and the force error $\tilde{F}$ from Eq. (3.142), the derivative of the actuator Lyapunov function in Eq. (3.147) can be expressed as,

$$\dot{W}_L^j(\boldsymbol{m}, \boldsymbol{P}, \boldsymbol{P^d}) = \gamma_3^j(\boldsymbol{m}, \boldsymbol{P}, \boldsymbol{P^d}, u)\tilde{F}u - \tilde{F}\dot{x} - \dot{F}_a^d(t)\frac{\tilde{F}}{K_j^d(\boldsymbol{m}, x, x_d)} \tag{3.151}$$

Let the valve command input u be defined as,

$$u = \tilde{u} + \frac{\dot{F}_a^d(t)}{K_j^d(\boldsymbol{m}, x, x_d)} \tag{3.152}$$

where $\tilde{u}$ is the feedback part of the valve command input. Passivity property of the control Lyapunov function is presented in the following theorem.

Theorem 3.9. *Given a desired actuator force of $F_a^d(t)$, for an input command u as defined in Eq. (3.152), the pneumatic actuator error dynamics is passive with respect to the following supply rate,*

$$s_{ctrl}((\gamma_3^j(.)\tilde{u}, \dot{x}), (\tilde{F}, \tilde{F})) := \gamma_3^j(\boldsymbol{m}, \boldsymbol{P}, \boldsymbol{P^d}, u)\tilde{F}\tilde{u} - \tilde{F}\dot{x} \tag{3.153}$$

where $\gamma_3^j(\boldsymbol{m}, \boldsymbol{P}, \boldsymbol{P^d}, u)\tilde{u}$ represents the flow variable at the fluid port of the control Lyapunov function, the piston velocity $\dot{x}$ is the flow variable at the mechanical port of the control Lyapunov function, while the force error $\tilde{F}$ is the effort variable at both the fluid port and the mechanical port of the actuator.

Proof. Consider the energy function $W_L^j(\boldsymbol{m}, \boldsymbol{P}, \boldsymbol{P^d})$ as defined in Eq. (3.143) as the storage function for the pneumatic actuator controller. As shown in theorems 3.1, and 3.2 for adiabatic and isothermal actuators respectively, $W_L^j(\boldsymbol{m}, \boldsymbol{P}, \boldsymbol{P^d}) \in \Re^+$ for all physically acceptable values of $(\boldsymbol{m}, \boldsymbol{P}, \boldsymbol{P^d})$. The time derivative $\dot{W}_L^j(\boldsymbol{m}, \boldsymbol{P}, \boldsymbol{P^d})$ of this storage function is as given in Eq. (3.151). Using the definition of the valve command input u from Eq. (3.152) in the expression for $\dot{W}_L^j(\boldsymbol{m}, \boldsymbol{P}, \boldsymbol{P^d})$ in Eq. (3.151), the storage function derivative is obtained as,

$$\begin{aligned} \dot{W}_L^j(\boldsymbol{m}, \boldsymbol{P}, \boldsymbol{P^d}) &= \gamma_3^j(\boldsymbol{m}, \boldsymbol{P}, \boldsymbol{P^d}, u)\tilde{F}\tilde{u} - \tilde{F}\dot{x} \\ &= s_{ctrl}((\gamma_3^j(.)\tilde{u}, \tilde{F}), (\dot{x}, \tilde{F})) \end{aligned} \tag{3.154}$$

On integrating both side of the above equation, it can be shown that the controller supply rate $s_{ctrl}((\gamma_3^j(.)\tilde{u}, \tilde{F}), (\dot{x}, \tilde{F}))$ satisfies the following passivity condition for all time t,

$$\int_0^t s_{ctrl}((\gamma_3^j(.)\tilde{u}, \tilde{F}), (\dot{x}, \tilde{F}))\ d\tau \geq -W_L^j(\boldsymbol{m}, \boldsymbol{P}, \boldsymbol{P^d})\Big|_{t=0} \tag{3.155}$$

where $W_L^j(\boldsymbol{m}, \boldsymbol{P}, \boldsymbol{P^d})\Big|_{t=0} \in \Re^+$ corresponds to the initial value of the controller Lyapunov function. □

The supply rate for the actuator error function presented in Eq. (3.153) will be used in the subsequent chapters to design appropriate controllers for passive operation of the pneumatic actuator while providing desired force output.

3.4 Summary

In this chapter, dynamics for a lumped-parameter model of a pneumatic actuator with generic thermodynamic process have been presented. Two specific thermodynamics process *viz* isothermal process and adiabatic process were further investigated. Energy function for both the isothermal and adiabatic actuators has been developed to facilitate energetic passivity analysis. For clarity of presentation, the dynamics and energy of the pneumatic actuator were first reported for a single chamber actuator and were then extended to the two-chambered actuator. It is shown that for a two-chambered isothermal actuator the energy function corresponds to sum of work done due to change in the entropy of each actuator chamber and the work done against the ambient pressure. For the adiabatic actuator, the energy function is obtained as the sum of change in the internal energy in each chamber and the work done against the ambient pressure. These energy functions were defined as storage functions to determine the supply rate for energetically passive operation of the actuator. The supply rate for a single chamber actuator shows that the pneumatic actuator is a two-port system, with one port corresponding to interaction with the source of compressed air, and the other port corresponding to mechanical power delivered by the actuator. The definition of the energy function as the storage function enables lossless interconnection between the pneumatic actuator and mechanical systems. For both the isothermal and the adiabatic actuators, the effort variable at the fluid port is obtained as the sum of gravimetric energy density and the specific flow work. As reported in [66], this structure for the fluid port effort variable is analogous to hydraulic systems.

When using a single valve for metering the air flow to the two-chambered actuator, the effort variable at the fluid port of the isothermal/adiabatic actuator is shown to be a monotonic function of actuator force $F_a(\boldsymbol{P})$. The corresponding flow variable at the fluid port represents a velocity input that is the function of the valve command input u. Consequently, the pneumatic actuator with reversible thermodynamics behaves as

a two-port nonlinear spring with an active velocity variable at one of the ports. This active velocity variable can be modulated to achieve the desired behavior from the pneumatic actuator. By defining the actuator energy function as the storage function, the supply rates for achieving energetically passive operation with isothermal/adiabatic actuators has also been presented in this chapter. For closed loop operation requiring a desired force output from the actuator, the energy associated with the actuator error dynamics has been derived. This energy function will be used as a Lyapunov function in subsequent chapters for defining suitable control input for regulating the actuator error dynamics to zero.

In this chapter reversible thermodynamic process (adiabatic and isothermal) have been studied. The thermodynamic process in most pneumatic applications is however not reversible. Finite heat interaction is bound to happen between the air in an actuator chamber and its environment. From second law of thermodynamics it is known that heat transfer generates entropy and leads to loss of work potential. The energy functions reported in this chapter do not lend themselves well to analyze the effect of heat transfer on the passive characteristics of pneumatic actuator. Energy based storage function, suitable for passivity analysis of pneumatic actuators that have finite heat interaction with ambient is reported in chapter 4.

In chapter 5, the energy functions developed in this chapter are used to design passive controllers for human power amplifier. A framework for bilateral tele-operation with fluid powered actuators is presented in chapter 6. Passive controllers based on prescribed energy functions are derived to achieve position and velocity co-ordination.

Chapter 4

Passivity Analysis of Pneumatic Actuator with Heat Transfer

In the previous chapter, work potential of pneumatic actuator was defined by assuming the thermodynamic process to be either isothermal or adiabatic. However these ideal processes are physically not easy to realize. The temperature change due to compression and expansion of gas in pneumatic systems results in finite heat interaction with the ambient. Due to the higher operating temperature in new actuation technologies such as chemo-fluidic actuators [12] and HCCI engines [15], heat transfer will have significant effect on system dynamics. A polytropic model is not accurate for modeling the thermodynamic process with finite heat transfer, as it does not capture the energy change due to hysteresis [67]. In [68], it was shown that heat transfer to the ambient during a cyclical process of compression and expansion of air results in loss of work potential. As presented in later chapters the applications of interest for this study are not necessarily cyclical in nature.

In [69], various empirical models for pressure and temperature dynamics in a pneumatic actuator are provided. In [21], the authors use a mixed model for pressure dynamics, adiabatic during charging and isothermal during discharging. To evaluate the feasibility of energetically passive operation, external supply rate to the actuator has to be identified. An adiabatic or isothermal process model fails to capture energetic interactions in a real actuator due to heat transfer from the ambient. In this chapter,

an energy based storage function is first developed for a pneumatic actuator with finite heat transfer, and then the supply rate for the actuator is derived by using the energy function as a storage function.

In [3], [70], the storage function for a system is defined as the *Supremum* of the work that can be extracted from the system over all feasible trajectories. Using this definition, the storage function for the pneumatic actuator with finite heat transfer is defined as the maximum work that can be extracted from the mechanical port of the actuator over all feasible values of heat transfer coefficient and piston velocity, for a given thermodynamic state of air in the actuator chamber. An optimization problem is formulated for identifying the maximum available work from the actuator, with the piston velocity and the heat transfer coefficients designated as the inputs available for generation of the optimal trajectory for maximum work output. The optimality conditions demonstrate that maximum work output is achieved if the thermodynamic process in the actuator is a combination of adiabatic and isothermal trajectories. In reality, the thermodynamic process in the pneumatic actuator is not reversible. Hence the maximum work output identified through optimization represents an upper bound (*supremum*) on the available work from the actuator.

Along the optimal trajectory, the maximum work potential of pneumatic actuator is derived to be similar to exergy of the actuator for the given thermodynamic state of air in the actuator chambers. Exergy as the measure of a system's work potential has been studied in a few other papers. In [44], the authors propose exergy as a measure of work potential for compressed air. This measure is used to identify efficiency of compressed air usage in industrial applications. In [45], exergy is investigated as a generalized measure of work for mechanical, electrical or thermal systems. Mechanical energy is shown to be a subset of generalized exergy and is used to investigate stability of a Vanderpol oscillator. Exergy has however not been used to investigate passivity of pneumatic actuators.

Similar to the presentation in chapter 3, the storage function is first developed for a single-chambered pneumatic actuator in section 4.1. Relevant dynamics of a single-chambered actuator presented in section 3.1 are repeated in section 4.1.1 for completeness. The optimization problem for extracting maximum work from the actuator is presented in section 4.1.2. The optimization problem is solved and the corresponding

optimal trajectory is identified in section 4.1.3. Maximum available work along the optimal trajectory is also identified in this section. Using the maximum available work as the storage function, the supply rate for energetically passive interconnection with a single-chambered actuator with finite heat interaction with ambient is derived in section 4.1.4. It is shown that irrespective of the direction of heat transfer, thermal interaction with the ambient results in loss of actuator's work potential. Results from the analysis of a single-chambered actuator with finite heat transfer are extended to the two-chambered actuator in section 4.2. Dynamics of the two-chambered actuator with finite heat interaction with the ambient is presented in section 4.2.1. In section 4.2.2, maximum available work from a two-chambered actuator is obtained to be the sum of the exergy of individual actuator chambers. By using the maximum available work as a storage function, it is shown in section 4.2.3 that for the two-chambered actuator, finite heat transfer again reduces the actuator's ability to do work. The two-chambered actuator is shown to be passive with respect to a supply rate that has a structure similar to actuators with isothermal/adiabatic thermodynamics.

4.1 Single-chambered pneumatic actuator

The storage function for a single-chambered actuator is developed for a given mass of air in the actuator chamber. It is assumed that air in the actuator chamber follows ideal gas law, and that the air temperature and pressure are uniformly distributed in the chamber volume. In this section, the relevant dynamics affecting the work output of a single-chambered pneumatic actuator are first presented. The equilibrium position for the single-chambered actuator corresponding to the thermodynamic dead state is then identified. The storage function is then defined as the maximum work that can be extracted from the actuator by changing the heat transfer coefficient and the actuator velocity, as the actuator is traversing to the equilibrium state. The path followed by the actuator, while providing work output, is subject to the constraints imposed by the actuator dynamics.

4.1.1 Actuator dynamics

The schematic for a single-chambered actuator is as shown in Fig. (4.1). For convenience of analysis, it is assumed that the cross sectional areas of the piston exposed to chamber pressure P and the ambient pressure P_o are the same, and are represented by A. Let m represent the air mass in the chamber, T be the chamber air temperature and $V(x)$ be the chamber volume at piston position x. The chamber volume $V(x)$ is related to the piston position x as,

$$V(x) = A(L_{1o} + x) \tag{4.1}$$

where AL_{1o} represents a constant dead volume. The air entering the control volume of the actuator chamber in Fig. (4.1) is assumed at a temperature T_u. A difference between an adiabatic or an isothermal actuator studied in chapter 3, and the general actuator with heat transfer being studied in this chapter is the effect of upstream air temperature T_u on the temperature and pressure dynamics. To achieve adiabatic thermodynamic process in the actuator, T_u in Eq. (3.9) was assumed to be same as the chamber temperature T. For the thermodynamic process in the actuator to be isothermal, T_u was assumed to be the ambient temperature T_o. For the actuator with finite heat transfer studied in this chapter, no such assumptions are imposed on T_u. From the first law of thermodynamics applied to a single-chambered actuator in Eq. (3.8), T_u depends on whether the chamber is being charged or discharged. As given in Eq. (3.25), if the actuator chamber is being charged, then T_u corresponds to the air temperature T_{in} at the chamber inlet (which usually corresponds to the ambient temperature T_o). If the chamber is being discharged, then by definition $T_u = T$.

In this study, it is assumed that heat transfer Q occurs between the chamber air and the ambient atmosphere only. Therefore, the heat transfer rate $\dot{Q}$ is defined as,

$$\dot{Q} = h^2(t)(T_o - T) \tag{4.2}$$

where T_o is the ambient temperature, and $h^2(t) \in \Re^+$ is possibly a time varying heat transfer coefficient. Various heat transfer models can be captured for different forms of the heat transfer coefficient $h^2(t)$. In this work, $h(t)$ is assumed to be largely unknown and the worst case scenario for heat transfer is considered.

Using the first law of thermodynamics, the lumped-parameter model of the single-chambered pneumatic actuator for a generic heat transfer model has been presented in

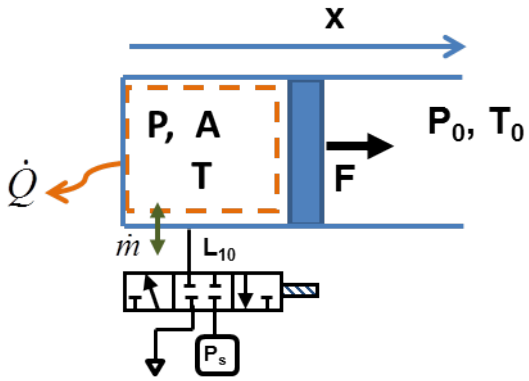

Figure 4.1: Schematic of a single-chambered actuator with a 3-position, 2-way pneumatic valve for controlling air flow to the actuator.

section 3.1.1. For a closed volume of gas with fixed air mass of m, piston velocity of $\dot{x}$ and using the definition of heat transfer rate $\dot{Q}$ from Eq. (4.2), the dynamics of the actuator volume $V(x)$ and temperature T are obtained as,

$$\begin{aligned} \dot{V} &= A\dot{x}(t) \\ \dot{T} &= (\gamma - 1)\left(-\frac{TA\dot{x}(t)}{V(x)} + \frac{h^2(t)(T_o - T)}{mR}\right) \end{aligned} \tag{4.3}$$

In the above equation, the external independent factors affecting the actuator volume $V(x)$ and temperature T are the piston velocity $\dot{x}(t)$, and the heat transfer coefficient $h^2(t)$. Therefore, $\dot{x}(t)$ and $h(t)$ are designated as the inputs to the state dynamics in Eq. (4.3). For a given mass of air m, the chamber pressure P is determined from the volume $V(x)$ and temperature T by using the ideal gas law in Eq. (3.2) as,

$$P = \frac{mRT}{V(x)} \tag{4.4}$$

The actuator force $F(P)$ depends on the actuator volume $V(x)$ and temperature T as,

$$F(P) = (P - P_o)A = \left(\frac{mRT}{V(x)} - P_o\right)A \tag{4.5}$$

By judicially selecting the velocity $\dot{x}(t)$ and the heat transfer coefficient $h^2(t)$, maximum work can be extracted from the actuator. The heat transfer coefficient $h^2(t)$

depends on the thermal conductivity of the material used in making the pneumatic actuator, and the surface area available for heat transfer. Therefore, $h^2(t)$ required for extracting maximum work from the actuator may not be physically realizable. In such a case, the maximum available work from the actuator represents the *Supremum* of work that can be extracted from the actuator. In the following section, the optimization problem for extracting maximum available work for a given thermodynamic state in the single-chambered actuator is presented.

4.1.2 Available storage as maximum extractable work

In this study, the storage function for the single-chambered actuator is defined as the maximum work that can be extracted over all possible trajectories that are constrained to satisfy the state dynamics in Eq. (4.3). Such a storage function will be passive with respect to any mechanical supply rate to the actuator for given actuator states.

A single-chambered actuator reaches equilibrium state when the chamber air temperature T is the same as the ambient temperature T_o, and the chamber pressure P is the same as ambient pressure P_o. Using the ideal gas law from Eq. (3.2), and relationship between chamber volume $V(x)$ and piston position x from Eq. (4.1), the piston position $\bar{x}(m)$ at equilibrium state is obtained in terms of the chamber air mass m from the following equation,

$$V(\bar{x}(m)) = A(L_{1o} + \bar{x}(m)) = \frac{mRT_o}{P_o} \tag{4.6}$$

Therefore, the mass of air m in the actuator chamber determines the equilibrium position $\bar{x}(m)$. As shown in Eq. (4.5), for a given air mass m, the actuator force $F(P)$ depends on the chamber volume $V(x)$ and the chamber air temperature T. The force output can be varied by selecting the inputs $h(t)$ and $\dot{x}(t)$ in Eq. (4.3) such that the actuator states $V(x)$ and T follow a trajectory that provides maximum work output. Therefore, the actuator storage function $W_{act}(m, P, T, P_o, T_o)$ is defined as the solution of the following optimization problem,

$$\begin{aligned} W_{act}(m, P, T, P_o, T_o) \triangleq \sup_{h(.),\dot{x}(.)} \quad & \int_0^\infty \left(\frac{mRT(\tau)}{V(x(\tau))} - P_o \right) A\dot{x}(\tau)\ d\tau \\ \text{subject to Eq. (4.3)} \end{aligned} \tag{4.7}$$

With the available mechanical work as storage function, the pneumatic actuator will be passive with respect to mechanical supply rate ($F(P)\dot{x}$). Note that in the above optimization problem, the inputs $h(t)$ and $\dot{x}(t)$ are not constrained. In reality however, it might not be possible to change the inputs $h(t)$ and $\dot{x}(t)$ as identified from the optimization problem. The piston velocity $\dot{x}(t)$ is limited by available supply pressure and the response time of the servo-valve metering the flow to the actuator. The heat transfer coefficient is $h^2(t)$ is usually unknown and is limited by the material properties of the actuator walls. Therefore, the worst case scenario is considered by maximizing the available energy from the actuator. The available storage identified from the optimization statement in Eq. (4.7) will represent the upper bound on the work that can be extracted from the actuator over all feasible trajectories of the actuator states $V(x)$ and T. Solution to the optimization problem in Eq. (4.7) determining the inputs $h(t)$ and $\dot{x}(t)$ for extracting the maximum work from the actuator is presented in the next section.

4.1.3 Optimal trajectories

To solve the state constrained optimization problem in Eq. (4.7) as an unconstrained optimization problem, the cost function $W_{act}(m, P, T, P_o, T_o)$ is augmented with the state dynamics in Eq. (4.3) by using Lagrange multiplier $\lambda_T(t)$ and $\lambda_V(t)$ as,

$$W_{act}(m,P,T,P_o,T_o) \triangleq \sup_{h(.),\dot{x}(.)} \int_0^\infty \left(\left(\frac{mRT(\tau)}{V(x)} - P_o \right) A\dot{x}(\tau) + \lambda_V(\tau) \left(A\dot{x}(\tau) - \dot{V} \right) \right.$$
$$\left. + \lambda_T(\tau) \left((\gamma - 1) \left(-\frac{T(\tau)A}{V(x)}\dot{x}(\tau) + \frac{h^2(\tau)(T_o - T(\tau))}{mR} \right) - \dot{T}(\tau) \right) \right) \, d\tau \tag{4.8}$$

For ease of analysis, the following Hamiltonian function $H(T, V, h, \dot{x})$ is defined,

$$H(T,V,h,\dot{x}) = \left(\frac{mRT}{V(x)} - P_o \right) A\dot{x}(t) + \lambda_T(t)(\gamma - 1) \left(-\frac{TA}{V(x)}\dot{x} + \frac{h^2(t)(T_o - T)}{mR} \right)$$
$$+ \lambda_V(t) A\dot{x}(t) \tag{4.9}$$

On integrating $\lambda_T(\tau)\dot{T}(\tau)$ and $\lambda_V(\tau)\dot{V}(x)$ by parts, and using the definition of the Hamiltonian $H(T, V, h(t), \dot{x})$ from the above equation, the cost function in Eq. (4.8)

can be expressed as,

$$W_{act}(m,P,T,P_o,T_o) \triangleq \max_{h(.),\dot{x}(.)} \Bigg(-(\lambda_T(t)T(t)+\lambda_V(t)V(x(t)))\Big|_{t=0}^{t=\infty} + \int_0^{\infty} \Big(H(T(\tau),V(x),h(\tau),\dot{x}) + \dot{\lambda}_T(\tau)T(\tau) + \dot{\lambda}_V(\tau)V(x) \Big)\ d\tau \Bigg) \tag{4.10}$$

The first order and second order variations in $W_{act}(m,P,T,P_o,T_o)$ due to variation in control inputs $h(t)$ and $\dot{x}(t)$ are obtained as,

$$\begin{aligned} \delta W_{act}(m,P,T,P_o,T_o) &= \int_{t=0}^{t=\infty} \Bigg(\frac{\partial H(T,V,h,\dot{x})}{\partial h}\delta h(\tau) + \frac{\partial H(T,V,h,\dot{x})}{\partial \dot{x}}\delta\dot{x}(\tau) \\ &+ \left(\frac{\partial H(T,V,h,\dot{x})}{\partial V} + \dot{\lambda}_V \right)\delta V(x) + \left(\frac{\partial H(T,V,h,\dot{x})}{\partial T} + \dot{\lambda}_T \right)\delta T(\tau) \Bigg)\ d\tau \\ &- (\lambda_T(t)\delta T(t) + \lambda_V(t)\delta V(x))\Big|_{t=0}^{t=\infty} \end{aligned} \tag{4.11}$$

$$\delta^2 W_{act}(m,P,T,P_o,T_o) = \int_{t=0}^{t=\infty} \left(\begin{pmatrix} \delta T(\tau) \\ \delta V(x) \\ \delta\dot{x}(\tau) \\ \delta h(\tau) \end{pmatrix}^T \boldsymbol{\mathcal{H}} \begin{pmatrix} \delta T(\tau) \\ \delta V(x) \\ \delta\dot{x}(\tau) \\ \delta h(\tau) \end{pmatrix} \right) d\tau \tag{4.12}$$

where

$$\boldsymbol{\mathcal{H}} = \begin{pmatrix} \frac{\partial^2 H(T,V,h,\dot{x})}{\partial T^2} & \frac{\partial^2 H(T,V,h,\dot{x})}{\partial T \partial V} & \frac{\partial^2 H(T,V,h,\dot{x})}{\partial T \partial h} & \frac{\partial^2 H(T,V,h,\dot{x})}{\partial T \partial \dot{x}} \\ \frac{\partial^2 H(T,V,h,\dot{x})}{\partial V \partial T} & \frac{\partial^2 H(T,V,h,\dot{x})}{\partial V^2} & \frac{\partial^2 H(T,V,h,\dot{x})}{\partial V \partial h} & \frac{\partial^2 H(T,V,h,\dot{x})}{\partial V \partial \dot{x}} \\ \frac{\partial^2 H(T,V,h,\dot{x})}{\partial h \partial T} & \frac{\partial^2 H(T,V,h,\dot{x})}{\partial h \partial V} & \frac{\partial^2 H(T,V,h,\dot{x})}{\partial h^2} & \frac{\partial^2 H(T,V,h,\dot{x})}{\partial h \partial \dot{x}} \\ \frac{\partial^2 H(T,V,h,\dot{x})}{\partial \dot{x} \partial T} & \frac{\partial^2 H(T,V,h,\dot{x})}{\partial \dot{x} \partial V} & \frac{\partial^2 H(T,V,h,\dot{x})}{\partial \dot{x} \partial h} & \frac{\partial^2 H(T,V,h,\dot{x})}{\partial^2 \dot{x}} \end{pmatrix}$$

At maximum condition, for all possible values of the inputs $h(.)$ and $\dot{x}(.)$, the first order variation $\delta W_{act}(.)$ and the second order variation $\delta^2 W_{act}(.)$ of the cost function must satisfy the following conditions [71],

$$\delta W_{act}(m,P,T,P_o,T_o) = 0, \qquad \delta^2 W_{act}(m,P,T,P_o,T_o) \leq 0 \tag{4.13}$$

For known initial conditions ($\delta T(0) = 0$ and $\delta V(x)\Big|_{t=0} = 0$), the necessary conditions

for determining the optimal inputs are obtained from the above equation as [71],

$$\frac{\partial H(T,V,h,\dot{x})}{\partial h} = 0, \qquad \frac{\partial H(T,V,h,\dot{x})}{\partial \dot{x}} = 0 \tag{4.14}$$

$$\dot{\lambda}_T = -\frac{\partial H(T,V,h,\dot{x})}{\partial T} = -(\gamma-1)\left(\frac{mC_v - \lambda_T(t)}{V(x)}\right) A\dot{x} + \frac{\lambda_T}{mC_v}h^2(t) \tag{4.15}$$

$$\dot{\lambda}_V = -\frac{\partial H(T,V,h,\dot{x})}{\partial V} = (\gamma-1)\left(\frac{mC_v - \lambda_T(t)}{V^2(x)}\right) TA\dot{x} \tag{4.16}$$

$$\lim_{t\to\infty} \lambda_T(t) = 0, \qquad \lim_{t\to\infty} \lambda_V(t) = 0 \tag{4.17}$$

$$\begin{bmatrix} \frac{\partial^2 H(T,V,h,\dot{x})}{\partial h^2} & \frac{\partial^2 H(T,V,h,\dot{x})}{\partial h \partial \dot{x}} \\ \frac{\partial^2 H(T,V,h,\dot{x})}{\partial \dot{x} \partial h} & \frac{\partial^2 H(T,V,h,\dot{x})}{\partial \dot{x}^2} \end{bmatrix} \leq 0 \tag{4.18}$$

The optimal values of the heat transfer coefficient $h(t)$ and the piston velocity $\dot{x}(t)$ are determined as the solution of the first order optimality conditions in Eq. (4.14). From the definition of the Hamiltonian $H(T,V,h,\dot{x})$ in Eq. (4.9), the partial differential equations in Eq. (4.14) can be expressed as,

$$\lambda_T(t)h(t)(T_o - T) = 0 \tag{4.19}$$

$$\left(\frac{mRT}{V(x)} - P_o\right) A - (\gamma-1)\lambda_T(t)A\frac{T}{V(x)} + \lambda_V(t)A = 0 \tag{4.20}$$

From Eq. (4.9) it can be seen that $\partial^2 H(.)/\partial h \partial \dot{x}$, $\partial^2 H(.)/\partial \dot{x} \partial h$ and $\partial^2 H(.)/\partial \dot{x}^2$ are all identically equal to zero. Therefore, from the second order optimality condition in Eq. (4.18), maximum work output is achieved if the following condition is satisfied along the optimal solutions identified from Eqs. (4.19, 4.20),

$$\frac{\partial^2 H(T,V,h,\dot{x})}{\partial h^2} = \lambda_T(t)(T_o - T) < 0 \tag{4.21}$$

Solution for $\lambda_T(t)$ and $\lambda_V(t)$

The optimality condition in Eq. (4.20) can be expressed as,

$$(\gamma-1)\left(\frac{(mC_v - \lambda_T(t))T}{V(x)} - P_o\right) A + \lambda_V(t)A = 0 \tag{4.22}$$

Using the above equation, and the definition of chamber volume $V(x)$ from Eq. (4.1), the dynamics of $\lambda_V(t)$ in Eq. (4.16) are obtained as,

$$\dot{\lambda}_V(t) = -(\lambda_V(t) - P_o)\frac{\dot{x}}{L_{1o} + x(t)} \tag{4.23}$$

On integrating both sides of the above equation and using the boundary conditions $\lambda_V(t)|_{t\to\infty} = 0$ and $x(t)|_{t\to\infty} = \bar{x}(m)$, the expression for $\lambda_V(t)$ is obtained as,

$$\lambda_V(t) = P_o \left(1 - \frac{L_{1o} + \bar{x}(m)}{L_{1o} + x(t)}\right) \tag{4.24}$$

Substituting the expression for $\lambda_V(t)$ from the above equation in Eq. (4.22) and using the relationship $P_o A(L_{1o} + \bar{x}(m)) = mRT_o$ from Eq. (4.6), the expression for $\lambda_T(t)$ is obtained as,

$$\lambda_T(t) = mC_v \left(1 - \frac{T_o}{T}\right) \tag{4.25}$$

Remark 4.1. *For a single-chambered pneumatic actuator with gas temperature of T, the definition of $\lambda_T(t)$ in Eq. (4.25) ensures that the second order optimality condition in Eq. (4.21) is satisfied for all $T \neq T_o$.*

From Eq. (4.19), at any time t, the optimal solution has to satisfy one of the following three conditions,

$$\lambda_T(t) = 0, \quad T(t) = T_o, \quad h(t) = 0 \tag{4.26}$$

For given initial conditions, as the optimal trajectory is a combination of the segments listed in Eq. (4.26), relevant properties these segments are now analyzed.

Segment $\lambda_T(t) = 0$

Over a finite time interval $[t_1, t_2]$, if the optimal solution $\lambda_T(t) = 0$ is imposed, it is also required that $\dot{\lambda}_T(t) = 0$. Using this condition in Eq. (4.15), for a given air mass m and finite actuator position x, the following stationary condition on the piston velocity $\dot{x}(t)$ is obtained,

$$\dot{x}(t) = 0 \tag{4.27}$$

From the definition of available work in Eq. (4.7), the stationarity condition Eq. (4.27) implies that mechanical work cannot be extracted from the actuator. In addition, from Eq. (4.25), $\lambda_T(t) = 0$ is satisfied only at thermal equilibrium condition $T(t) = T_o$. Therefore, with no energetic mechanical or thermal interaction with its surroundings, $\lambda_T = 0$ corresponds to a stationary state of the single-chambered actuator with no change in the available energy of the actuator.

Isothermal segment ($T = T_o$)

When the chamber temperature is T_o, an isothermal process ($T(t) = T_o$) also satisfies the first order optimality condition in Eq. (4.26). When the chamber temperature T corresponds to T_o, and the chamber pressure P is not at P_o, a direct optimal path to the equilibrium state (P_o, T_o) is along the isothermal trajectory. Due to the conservative nature of the isothermal process, any work put into the system can be completely recovered. Therefore, different trajectories along the isothermal process, each with multiple cycles but all ending at the equilibrium state (P_o, T_o) are all optimal paths. For a fixed mass of air m at temperature $T(t) = T_o$, the piston velocity $\dot{x}(t)$ required along the isothermal trajectory ($\dot{T} = 0$) is obtained from the temperature dynamics in Eq. (4.3) to be zero. In practice however, an infinitesimally slow velocity will be able to provide the required isothermal trajectory.

Adiabatic segment ($h^2(t) = 0$)

For the optimal solution $h^2(t) = 0$ there will be no heat transfer between the chamber air and the ambient. Thus, the thermodynamic process in the actuator chamber is adiabatic. The adiabatic segment can reach the equilibrium state (P_o, T_o) directly, if the intial temperature T and the initial pressure P satisfy the following adiabatic relationship,

$$T = T_o \left(\frac{P}{P_o} \right)^{\frac{(\gamma-1)}{\gamma}} \tag{4.28}$$

The adiabatic process is also reversible and thus any work put into the actuator along the adiabatic segment can be completely recovered. For an initial pressure P and temperature T, the net work output along any cyclical path following the adiabatic process will be zero. If the initial temperature and pressure satisfy the relationship in Eq. (4.28), then there are different trajectories with multiple cycles, each ending at the equilibrium state (P_o, T_o) with the same work output, and would thus be optimal. The trajectory for reaching the equilibrium point is therefore non-unique. For a given mass of air m in the actuator chamber, from the temperature dynamics in Eq. (4.3), the piston velocity input $\dot{x}(t)$ along the adiabatic trajectory ($h^2(t) = 0$) can be any of value. The sign of the velocity will however determine the direction of change in the chamber air temperature.

Characteristics of optimal trajectory obtained from the first order optimality conditions in Eq. (4.26) are stated in the following proposition.

Proposition 4.1. *The optimal trajectory for extracting maximum work from the actuator consists of a combination of the following segments,*

1. *Segments along the isothermal trajectory wherein the chamber temperature is the same as ambient temperature ($T = T_o$).*

2. *Segments along the adiabatic trajectory with the heat transfer coefficient given by $h^2(t) = 0$.*

Proof. Each solution in Eq. (4.26) represents a segment of the trajectory for optimal work interaction with the actuator. From Eq. (4.25), $\lambda_T(t) = 0$ is satisfied only when $T(t) = T_o$. Therefore, the optimal trajectory for extracting maximum work from the actuator will be a combination of isothermal segments ($T(t) = T_o$) and adiabatic segments ($h^2(t) = 0$). □

In the following theorem, a trajectory for extracting maximum work from the actuator is presented and the total available work along this trajectory is derived.

Theorem 4.1. *For a given air mass of m at temperature T and pressure P in a single-chambered actuator, the heat transfer coefficient $h^2(t)$ and the piston velocity $\dot{x}(t)$ along one trajectory for extracting maximum work from the actuator are given by,*

1. Adiabatic expansion/compression: *If the chamber air temperature T is greater than the ambient temperature T_o, the optimal heat transfer coefficient is given by $h^2(.) = 0$, and the piston velocity $\dot{x}(.)$ is selected to be positive until the chamber temperature at some time $t = t_1$ is the same as the ambient temperature ($T(t_1) = T_o$). If the chamber air temperature $T(.)$ is less than the ambient temperature T_o, the optimal heat transfer coefficient is again given by $h^2(.) = 0$, and the piston velocity $\dot{x}(.)$ is selected to be negative until the chamber temperature at some time $t = t_2$ is the same as the ambient temperature ($T(t_2) = T_o$). At $T(t_{1,2}) = T_o$, the chamber air pressure P_a is obtained from the adiabatic relationship in Eq. (3.18) as,*

$$P_a = P\left(\frac{T_o}{T}\right)^{\frac{\gamma}{\gamma-1}} \tag{4.29}$$

2. Isothermal expansion/compression : *When the chamber air temperature $T(.)$ is the same as the ambient temperature T_o, and the chamber pressure P_a is different from ambient pressure P_o, then the optimal segment is selected to be isothermal process. From the temperature dynamics in Eq. (4.3), the piston velocity $\dot{x}(.)$ is determined to be an infinitesimally small positive quantity if the piston position x is less than the equilibrium position $\bar{x}(m)$ defined in Eq. (4.6). The velocity $\dot{x}(.)$ is an infinitesimally small negative quantity if the current actuator position x is greater than the equilibrium position $\bar{x}(m)$. The corresponding heat transfer coefficient along the isothermal segment is given by $h^2(.) >>> 1$.*

The available work along the proposed trajectory to the equilibrium pressure P_o and the equilibrium temperature T_o is obtained as,

$$W_{act}(m,P,T,P_o,T_o) = mC_v(T-T_o) - mT_o\left(C_p\log\left(\frac{T}{T_o}\right) - R\log\left(\frac{P}{P_o}\right)\right) - mP_o\left(\frac{1}{\rho(P_o,T_o)} - \frac{1}{\rho(P,T)}\right) \tag{4.30}$$

Proof. In this proof, optimality of the proposed trajectory is first established. Work available along this trajectory is then evaluated. **Optimality of the trajectory :** The segments for defining the optimal trajectory corresponding to maximum available work are as listed in Eq. (4.26). When the chamber temperature T is different from the ambient temperature T_o, then $\lambda_T(t)$ in Eq. (4.25) is non zero. Therefore, when $T(t) \neq T_o$, the adiabatic trajectory ($h(t) = 0$) is the optimal solution. Along this adiabatic trajectory, if the chamber temperature is greater than the ambient temperature ($T > T_o$), then from Eq. (4.3) expansion ($\dot{x}(t) \geq 0$) of the chamber volume will reduce the chamber air temperature ($\dot{T} < 0$). The change in chamber volume and pressure due to this expansion process is illustrated by the red trace in Fig. (4.2). In this figure, V_a represents the chamber volume at $T(t) = T_o$. If the volume V_a does not correspond to equilibrium volume $\bar{V}(m)$, then isothermal trajectory is the only available path to the equilibrium volume. In Fig. (4.2), the isothermal trajectory is illustrated by the blue line.

When the chamber air temperature T is less than ambient temperature T_o, adiabatic trajectory is again the optimal solution from Eq. (4.26). For $T(t) < T_o$, compression

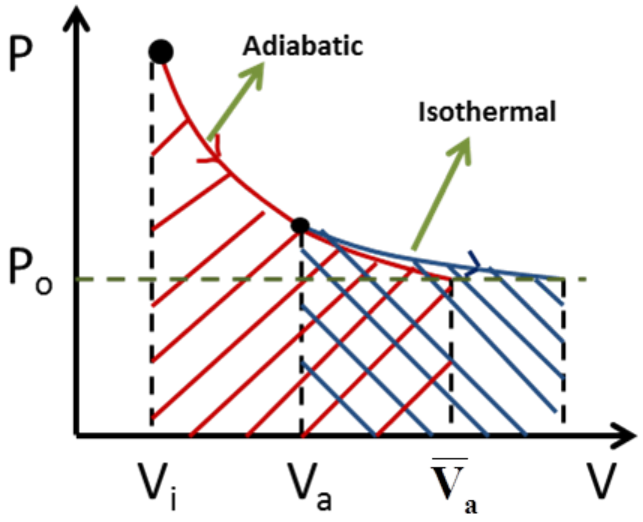

Figure 4.2: Schematic showing work done when chamber temperature is greater than ambient temperature. Volume of chamber is plotted along the x-axis and pressure is plotted along the y-axis.

($\dot{x}(t) < 0$) will increase the chamber temperature T. At $T(t) = T_o$ along the adiabatic trajectory, if the chamber volume V_a does not correspond to equilibrium volume $\bar{V}(m)$, then from Eq. (4.26), isothermal trajectory is the only feasible solution to reach the equilibrium volume. In Fig. (4.3), the proposed combination of adiabatic (red curve) and isothermal (blue curve) trajectories, is illustrated for $T(t) < T_o$. Note that when $T < T_o$, the process for extracting maximum work requires work input (compression) along an adiabatic trajectory, and then expansion along isothermal trajectory (at $T = T_o$). However, the adiabatic process is reversible and any work put into the system can be completely recovered.

Therefore the proposed combination of adiabatic (when $T(t) \neq T_o$) and isothermal (when $T = T_o$) trajectories satisfies the necessary optimality conditions in Eq. (4.26). As the equilibrium state corresponds to zero energy state, the maximum available work is evaluated with respect to the equilibrium position $\bar{x}(m)$ defined in Eq. (4.60).

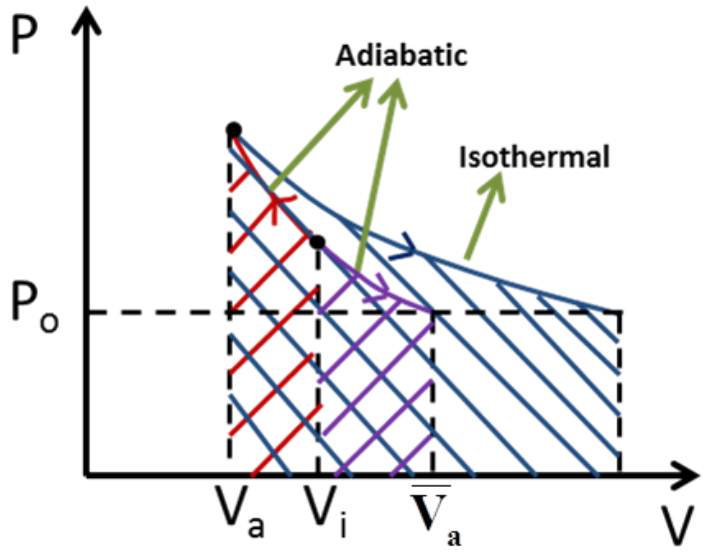

Figure 4.3: Schematic showing work done when chamber temperature is less than ambient temperature. In this scenario, trajectory for maximum work extraction requires compression (work input) along adiabatic path and then work extraction along isothermal path. Volume of chamber is plotted along the x-axis and pressure is plotted along the y-axis.

Work extracted along the proposed optimal trajectory : Along the adiabatic segment ($T \neq T_o$), for a known initial chamber pressure of P, let P_a be the air pressure at $T(t) = T_o$. Using the temperature-pressure relationship curve for adiabatic trajectory from Eq. (3.18), the pressure P_a is expressed in terms of the chamber pressure P, and temperature T as shown in Eq. (4.29).

For a given air mass m, the available work along the adiabatic trajectory is obtained by integrating the adiabatic characteristic curve in Eq. (3.34) as,

$$W_{act_a}(m, P, T, P_a, T_o) = mC_v(T - T_o) - mP_o\left(\frac{1}{\rho(P_a, T_o)} - \frac{1}{\rho(P, T)}\right) \tag{4.31}$$

where $\rho(P, T) := P/RT$ is the density of air in the adiabatic chamber. At $T(t) = T_o$, the proposed trajectory is along the isothermal process to the equilibrium state (P_o, T_o).

From the definition of the gravimetric energy density $W_m^{iso}(.)$ for the isothermal actuator in Eq. (3.48), and using the definition of P_a from Eq. (4.29), available work along the isothermal trajectory is obtained as,

$$\begin{aligned} W_{act_b}(m, P_a, T_o, P_o, T_o) &= mRT_o \log\left(\frac{P_a}{P_o}\right) - mP_o\left(\frac{1}{\rho(P_o, T_o)} - \frac{1}{\rho(P_a, T_o)}\right) \\ &= mT_o\left(R\log\left(\frac{P}{P_o}\right) - C_p\log\left(\frac{T}{T_o}\right)\right) - mP_o\left(\frac{1}{\rho(P_o, T_o)} - \frac{1}{\rho(P_a, T_o)}\right) \end{aligned} \tag{4.32}$$

where $C_p = R\gamma/(\gamma - 1)$ is the specific heat at constant pressure. The total available work along the proposed optimal trajectory is the sum of the available work along the adiabatic segment $W_{act_a}(m, P, T, P_a, T_o)$ from Eq. (4.31), and the available work along the isothermal segment $W_{act_b}(m, P_a, T_o, P_o, T_o)$ from Eq. (4.32) and is given by,

$$W_{act}(m, P, T, P_o, T_o) = W_{act_a}(m, P, T, P_a, T_o) + W_{act_b}(m, P_a, T_o, P_o, T_o) \tag{4.33}$$

Using the expression for $W_{act_a}(m, P, T, P_a, T_o)$ and $W_{act_b}(m, P_a, T_o, P_o, T_o)$ from Eq. (4.31) and Eq. (4.32) respectively in the above equation, the available work as defined in Eq. (4.30) is obtained.

□

For the optimal trajectory presented in the above theorem, the piston velocity input $\dot{x}(t)$ along the adiabatic segment can be of any magnitude as long as the sign of velocity corresponds with the desired direction of temperature change. Along the isothermal segment of the proposed trajectory, the piston velocity is required to be infinitesimally small with the sign of velocity determined the position x of the actuator relative to the equilibrium position $\bar{x}(\boldsymbol{m})$.

Remark 4.2. *For a given air mass m, pressure P and temperature T, the process for extracting maximum work $W_{act}(m, P, T, P_o, T_o)$ from the actuator in Eq. (4.30) is not unique.*

Proof. The temperature-actuator position phase plot of the proposed optimal trajectories in Theorem 4.1 are shown in Fig. (4.4). Non-uniqueness of the proposed trajectory is due to the following conditions :

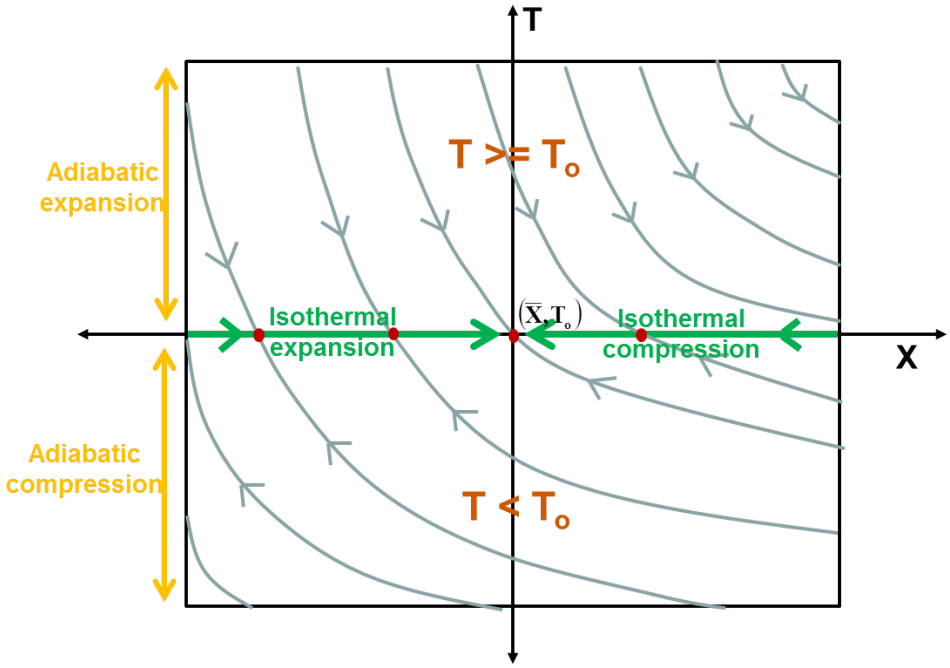

Figure 4.4: Phase plot of the optimal trajectories for extracting maximum work at different thermodynamic states of the actuator. The red dots in the figure correspond to the segment $\lambda_T = 0$.

1. The net work interaction along a cyclic path with a reversible thermodynamic process (isothermal/adiabatic) is always identically zero. Each segment of the trajectory for maximum work extraction as defined in Theorem 4.1 is along a reversible thermodynamic process. Thus the available work from any process that requires cyclical operation along any of these reversible segments, for indefinite cycles, before traversing to equilibrium position $\bar{x}(m)$ along the trajectory proposed in Theorem 4.1, will also be given by Eq. (4.30). For a given initial state (x, T) on a level set in the phase plot in Fig. (4.4), the actuator thermodynamic state can be taken to any other level set before reaching the equilibrium state $(\bar{x}(m), T_o)$ without changing the net available energy from the actuator.

2. When the chamber temperature T corresponds to ambient temperature T_o (along the x-axis in Fig. (4.4)), the optimal segment $\lambda_T = 0$ can be realized for zero

piston velocity ($\dot{x}(t) = 0$). Along this segment (red dots along the x-axis in Fig. (4.4)), the actuator is completely isolated with no energetic interactions with its environment. Thus, this segment can be interspersed with the isothermal segment multiple times (imagine arbitrary number of red dots along the x-axis on the way to equilibrium position), and each time for an arbitrary time interval, without any change to the available energy from the actuator.

□

For a gas at pressure P and temperature T, the entropy change as it traverses to equilibrium pressure and temperature of (P_o, T_o) along a reversible path is given by [65],

$$\sigma(P,T) - \sigma(P_o,T_o) = C_p \log\left(\frac{T}{T_o}\right) - R\log\left(\frac{P}{P_o}\right) \tag{4.34}$$

Therefore, the maximum available work in Eq. (4.30) can be expressed as,

$$\begin{aligned} W_{act}(m,P,T,P_o,T_o) = mC_v(T-T_o) &- mT_o(\sigma(P,T)-\sigma(P_o,T_o)) \\ &- mP_o\left(\frac{1}{\rho(P_o,T_o)} - \frac{1}{\rho(P,T)}\right) \end{aligned} \tag{4.35}$$

Remark 4.3. *The maximum available work from a single-chambered actuator in Eq. (4.35) has the following properties,*

1. *The maximum available work from a single-chambered pneumatic actuator as given in Eq. (4.35) corresponds to the sum of change in internal energy, change in available work due to change in entropy, and work done against ambient pressure P_o, and is thus analogous to exergy [65] of air with respect to P_o and ambient temperature T_o.*

2. *When the chamber temperature T corresponds to ambient temperature T_o, then the maximum available work corresponds to work available along isothermal trajectory.*

3. *If the initial temperature T and pressure P are related as $T = T_o(P/P_o)^{(\gamma-1)/\gamma}$ in Eq. (4.28), then the entropy change in Eq. (4.34) satisfies $\sigma(P,T)-\sigma(P_o,T_o) = 0$. The equilibrium position (P_o, T_o) can then be reached by traversing along the adiabatic trajectory only (isothermal segment not required) and the maximum available work in Eq. (4.35) corresponds to work available along adiabatic trajectory.*

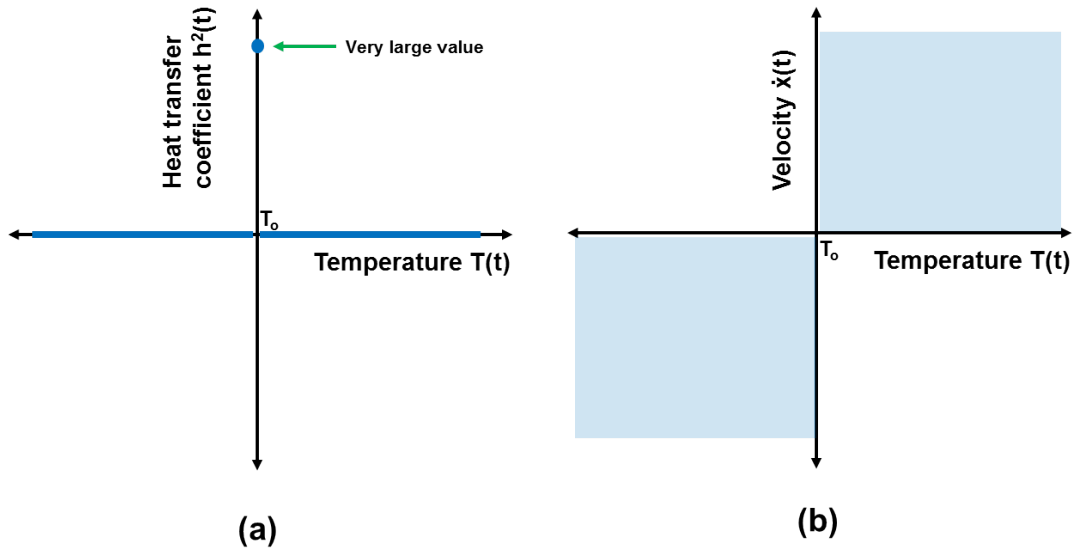

Figure 4.5: Heat transfer coefficient $h^2(t)$ and piston velocity $\dot{x}(t)$ required to realize the maximum available work from the actuator in Eq. (4.35)

The optimal heat transfer coefficient $h^2(t)$ and the optimal velocity $\dot{x}(t)$ required for obtaining the maximum work output from a single-chambered actuator in Eq. (4.35) is as shown in Fig. (4.5). The heat transfer coefficient $h^2(t)$ is zero for $T \neq T_o$ (adiabatic segment) as represented by the blue line in Fig. (4.5a). At $T = T_o$ (isothermal segment), the heat transfer coefficient $h^2(t)$ is required to switch instantaneously to a very large value. Adiabatic process can possibly be achieved in the actuator by using a poor conducting material for the pneumatic actuator surface. For $T \neq T_o$, the actuator velocity $\dot{x}(t)$ should lie in the shaded region in Fig. (4.5b). As there is no constraint on the actual magnitude of the piston speed, the actuator speed $\dot{x}(t)$ can also be selected to be very high to provide very little time for heat transfer across the actuator walls, thus simulating adiabatic process. Isothermal thermodynamics can be achieved by using a material with very high thermal conductance $h^2(t) >>> 1$ as illustrated in Fig. (4.5a), or selecting infinitesimally small velocity ($\dot{x}(t) <<< 1$) to provide long enough time for achieving thermal equilibrium.

However, there are no known materials that can provide perfect insulation at $T \neq T_o$,

and then instantaneously switch to very high thermal conductance ($h^2(t) >>> 1$) at $T = T_o$. In addition, in human interactive applications, the velocity of the actuator is determined by the comfort of the human operator. Therefore, in real life applications, the maximum energy available from the actuator in Eq. (4.35) can not be typically realized and represents the upper bound of the energy that can be extracted from the actuator.

From the definition of maximum available work $W_{act}(m, P, T, P_o, T_o)$ in Eq. (4.35), the gravimetric energy density of the single-chambered actuator is obtained as,

$$\begin{aligned} W_m(P, T, P_o, T_o) &= \frac{W_{act}(m, P, T, P_o, T_o)}{m} \\ &= C_v(T - T_o) - T_o(\sigma(P, T) - \sigma(P_o, T_o)) - P_o\left(\frac{1}{\rho(P_o, T_o)} - \frac{1}{\rho(P, T)}\right) \end{aligned} \tag{4.36}$$

Remark 4.4. *The gravimetric energy density $W_m(P, T, P_o, T_o)$ in Eq. (4.36) is zero at the equilibrium state (P_o, T_o), and is positive at all other feasible values of pressure P and temperature T.*

Proof. Proof is as shown in appendix B.1 □

A contour plot of the gravimetric energy density $W_m(P, T, P_o, T_o)$ for different values of pressure ratio P/P_o and temperature ratio T/T_o is as shown in Fig. (4.6). From the value of the contour lines in the figure it can be seen that the gravimetric energy density is positive for all pressures (P, P_o) and temperatures (T, T_o). The magnitude of the contour also decreases as the pressure ratio P/P_o and temperature ratio T/T_o tends to 1, thus confirming that (P_o, T_o) corresponds to a zero energy state. In the Fig. (4.6), the optimal trajectory for an initial chamber pressure P greater than ambient pressure P_o, and initial chamber temperature T greater than ambient temperature T_o is illustrated by the red lines. The change in the slope of the red line represents the switching point from adiabatic trajectory to isothermal trajectory.

In the next section, the maximum available work in Eq. (4.30) is used as the storage function to identify the external supply rate to the single-chambered actuator with finite heat transfer. This supply rate is used to define the condition for passive operation of the single-chambered actuator.

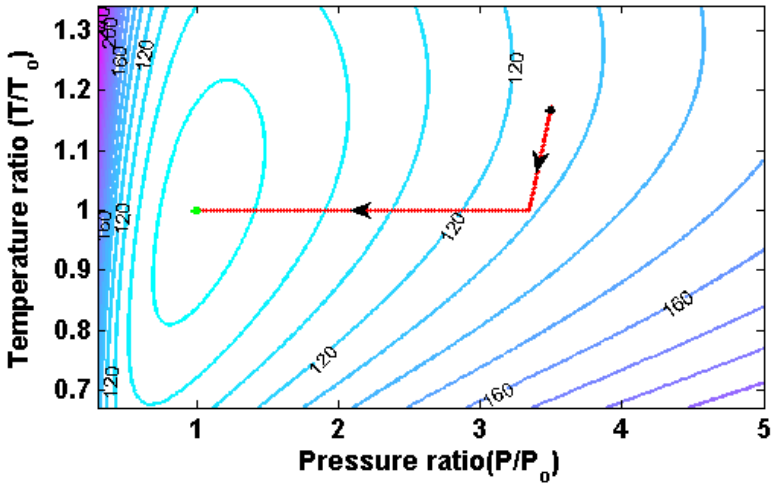

Figure 4.6: Contour plot of the gravimetric energy density $W_m(P, P_o, T, T_o)$ for different pressure ratios P/P_o and temperature ratios T/T_o. The red trace in the plot corresponds to optimal trajectory for a given set of initial conditions. The arrows indicate the direction in which the trajectory is traversed.

4.1.4 Passivity property of single-chambered actuator

In this section, supply rate to the pneumatic actuator is derived by defining the maximum available energy in Eq. (4.30) as the storage function. For a single-chambered pneumatic actuator, the storage function $W_{act}(m, P, T, P_o, T_o)$ from Eq. (4.30) can be expressed as,

$$W_{act}(m, P, T, P_o, T_o) = mW_m(P, T, P_o, T_o) \tag{4.37}$$

where $W_m(P, T, P_o, T_o)$ represents the gravimetric energy density of the actuator and is as defined in Eq. (4.36). For a constant ambient temperature T_o, the time derivative of the energy function $\dot{W}_{act}(m, P, T, P_o, T_o)$ is obtained as,

$$\begin{aligned}\dot{W}_{act}(m, P, T, P_o, T_o) = \dot{m}W_m(P, T, P_o, T_o) + m\frac{\partial W_m(P, T, P_o, T_o)}{\partial T}\dot{T} \\ + m\frac{\partial W_m(P, T, P_o, T_o)}{\partial P}\dot{P} + m\frac{\partial W_m(P, T, P_o, T_o)}{\partial P_o}\dot{P}_o\end{aligned} \tag{4.38}$$

The partial derivative of gravimetric energy density $W_m(P, T, P_o, T_o)$ with respect

to temperature T, pressure P and ambient pressure P_o is given by,

$$\begin{aligned}
\left.\frac{\partial W_m(P,T,P_o,T_o)}{\partial T}\right|_{(P,P_o)} &= C_v - C_p\frac{T_o}{T} - \frac{P_o}{\rho^2(P,T)}\frac{\partial \rho(P,T)}{\partial T} \\
\left.\frac{\partial W_m(P,T,P_o,T_o)}{\partial P}\right|_{(T,P_o)} &= \frac{RT_o}{P} - \frac{P_o}{\rho^2(P,T)}\frac{\partial \rho(P,T)}{\partial P} \\
\left.\frac{\partial W_m(P,T,P_o,T_o)}{\partial P_o}\right|_{(P,T)} &= -\left(\frac{RT_o}{P_o} + \frac{P_o}{\rho^2(P,T)}\frac{\partial \rho(P,T)}{\partial P}\right)
\end{aligned} \tag{4.39}$$

Using the definition $\rho(P,T) := P/RT$ of air density from Eq. (3.38), and after some algebraic manipulations, the partial derivatives in the above equation can be simplified as,

$$\begin{aligned}
\left.\frac{\partial W_m(P,T,P_o,T_o)}{\partial T}\right|_{(P,P_o)} &= \frac{1}{T}\left(C_p(T-T_o) - \frac{P-P_o}{\rho(P,T)}\right) \\
\left.\frac{\partial W_m(P,T,P_o,T_o)}{\partial P}\right|_{(P,P_o)} &= \frac{1}{P}\left(-R(T-T_o) + \frac{P-P_o}{\rho(P,T)}\right) \\
\left.\frac{\partial W_m(P,T,P_o,T_o)}{\partial P_o}\right|_{(P,P_o)} &= -\left(\frac{1}{\rho(P_o,T_o)} - \frac{1}{\rho(P,T)}\right)
\end{aligned} \tag{4.40}$$

Using the partial derivatives from the above equation, the derivative of the actuator energy function $\dot{W}_{act}(m,P,T,P_o,T_o)$ in Eq. (4.38) can be expressed as,

$$\begin{aligned}
\dot{W}_{act}(m,P,T,P_o,T_o) = \dot{m}W_m(P,T,P_o,T_o) + m(T-T_o)\left(C_p\frac{\dot{T}}{T} - R\frac{\dot{P}}{P}\right) \\
+ m\left(\frac{P-P_o}{\rho(P,T)}\right)\left(\frac{\dot{P}}{P} - \frac{\dot{T}}{T}\right) - \dot{P}_o\left(\frac{m}{\rho(P_o,T_o)} - \frac{m}{\rho(P,T)}\right)
\end{aligned} \tag{4.41}$$

The temperature and pressure dynamics in the single-chambered actuator are as given in Eq. (3.9) and Eq. (3.10) respectively. Note that when charging the actuator with finite heat transfer, the upstream air temperature T_u is not assumed to be the same as the chamber air temperature T. As presented in Eq. (3.25), depending on the valve position and direction of air flow, the upstream temperature T_u is depends on the inlet temperature T_u (usually assumed to be T_o) or the chamber temperature T.

Using the temperature and pressure dynamics from Eq. (3.9) and Eq. (3.10) respectively, and assuming a constant ambient pressure ($\dot{P}_o = 0$), the derivative of the energy

function in Eq. (4.41) can then be simplified as,

$$\dot{W}_{act}(m,P,T,P_o,T_o) = \dot{m}\left(\left(W_m(P,T,P_o,T_o) + \frac{P-P_o}{\rho(P,T)}\right) + C_p(T-T_o)\left(\frac{T_u}{T}-1\right)\right) - (P-P_o)\dot{V} + \dot{Q}\left(1-\frac{T_o}{T}\right) \tag{4.42}$$

where $T_u = T_o$ if $\dot{m} \geq 0$, and $T_u = T$ if $\dot{m} < 0$. In Eq. (4.42), the first term on the *r.h.s* represents the power interaction at the fluid port. The second term, $-(P-P_o)\dot{V}$, corresponds to the mechanical power interaction of the pneumatic actuator. The negative sign implies that the power is being extracted from the actuator at the mechanical port. The third term on the *r.h.s* of Eq. (4.42) represents power interaction at the thermal port of the actuator. Therefore, the single-chambered pneumatic actuator with finite heat transfer model is a three port system.

For ease of presentation, let $\Phi_{ht}(P,T,P_o,T_o)$ be defined as,

$$\Phi_{ht}(P,T,P_o,T_o) := W_m(P,T,P_o,T_o) + \frac{P-P_o}{\rho(P,T)} \tag{4.43}$$

After some algebraic manipulations, the derivative $\dot{W}_{act}(m,P,T,P_o,T_o)$ of the storage function in Eq. (4.42) can be expressed as,

$$\dot{W}_{act}(m,P,T,P_o,T_o) = \dot{m}\Phi_{ht}(P,T_u,P_o,T_o) - \dot{m}C_pT_o\underbrace{\left(\left(\frac{T_u}{T}-1\right) - \log\left(\frac{T_u}{T}\right)\right)}_{\geq 0} - (P-P_o)\dot{V} + \dot{Q}\left(1-\frac{T_o}{T}\right) \tag{4.44}$$

For any $\alpha > 0$, the condition $(\alpha-1)-\log(\alpha) > 0$ is always true. Defining $\alpha := T_u/T$, and given that $T_u = T$ only when the chamber is discharging ($\dot{m} < 0$), the second term on the *r.h.s* of the above equation has a dissipative effect on the available storage of the actuator. This loss in power is a consequence of entropy generated due to mixing of air at two different temperatures (T_u and T). Therefore, the derivative of the energy function $\dot{W}_{act}(m,P,T,P_o,T_o)$ in the above equation satisfies the following inequality,

$$\dot{W}_{act}(m,P,T,P_o,T_o) \leq \dot{m}\Phi_{ht}(P,T_u,P_o,T_o) - (P-P_o)\dot{V} + \dot{Q}\left(1-\frac{T_o}{T}\right) \tag{4.45}$$

Theorem 4.2. *For a constant ambient pressure P_o, ambient temperature T_o, upstream air temperature of T_u at the fluid port of the actuator as defined in Eq. (3.25) and the heat transfer rate $\dot{Q}$ for an arbitrary heat transfer coefficient $h^2(t)$ given by,*

$$\dot{Q} = h^2(t)(T_o - T) \tag{4.46}$$

a single-chambered pneumatic actuator with air pressure P and air mass m is passive with respect to the supply rate $s_{ht}((\dot{m}, \Phi_{ht}(P, T_u, P_o, T_o)), (F(P), \dot{x}))$ defined as,

$$s_{ht}((\dot{m}, \Phi_{ht}(P, T_u, P_o, T_o)), (F(P), \dot{x})) := \dot{m}\Phi_{ht}(P, T_u, P_o, T_o) - F(P)\dot{x} \tag{4.47}$$

where the air mass flow rate $\dot{m}$ is the flow variable at the fluid port, $\Phi_{ht}(P, T_u, P_o, T_o)$ is the effort variable at the fluid port, the actuator velocity $\dot{x}$ is the flow variable at the mechanical port of the actuator, and the actuator force $F(P)$ is the effort variable at the mechanical port of the actuator.

Proof. Let $W_{act}(m, P, T, P_o, T_o)$ as given in Eq. (4.37) be the storage function for the single-chambered actuator. As shown in the remark 4.4, the gravimetric energy density $W_m(P, T, P_o, To)$ of single-chambered actuator is always positive, and hence the storage function $W_{act}(m, P, T, P_o, T_o)$ in Eq. (4.37) is also always positive. The time derivative of this storage function $\dot{W}_{act}(m, P, T, P_o, T_o)$ is as given in Eq. (4.45).

From the definition of the heat transfer rate $\dot{Q}$ in Eq. (4.46), the power interaction at the thermal port of the actuator satisfies the following dissipative condition,

$$\dot{Q}\left(1 - \frac{T_o}{T}\right) = h^2(t)(T_o - T)\left(\frac{T - T_o}{T}\right) \leq 0 \tag{4.48}$$

Therefore, the interaction at the thermal port reduces the ability of the actuator to provide work output, irrespective of the direction of heat transfer to the actuator chamber. Using the definition of the actuator force $F(P)$ from Eq. (3.29), the relationship between actuator volume $V(x)$ and the piston position x from Eq. (3.73) and due to the dissipative nature of thermal interaction from Eq. (4.48), the derivative of the energy function $\dot{W}_{act}(m, P, T, P_o, T_o)$ in Eq. (4.45) can be expressed in terms of the supply rate $s_{ht}(.)$ in Eq. (4.47) as,

$$\begin{aligned} \dot{W}_{act}(m, P, T, P_o, T_o) \leq & \dot{m}\Phi_{ht}(P, T_u, P_o, T_o) - F(P)\dot{x} \\ & = s_{ht}((\dot{m}, \Phi_{ht}(P, T_u, P_o, T_o)), (F(P), \dot{x})) \end{aligned} \tag{4.49}$$

Integrating both sides of the above equation, and using the condition that the energy function $W_{act}(m, P, T, P_o, T_o)$ is always positive, it can be shown that the the actuator supply in Eq. (4.47) satisfies the following passivity condition,

$$\int_0^t s_{ht}((\dot{m}, \Phi_{ht}(P, T_u, P_o, T_o)), (F(P), \dot{x}))\ d\tau \geq -W_{act}(m, P, T, P_o, T_o)\Big|_{t=0} \tag{4.50}$$

where $W_{act}(m, P, T, P_o, T_o)\Big|_{t=0} > 0$ corresponds to maximum initial available work in the single-chambered actuator with finite heat transfer. □

The supply rate $s_{ht}((\dot{m}, \Phi_{ht}(P, T_u, P_o, T_o)), (F(P), \dot{x}))$ in Eq. (4.47) for the single-chambered actuator with heat transfer consists of a port for mechanical power interaction and a port for fluid port power interaction whose effort variable $\Phi(.)$ is the sum of the gravimetric energy density $W_m(.)$ and the flow work. This structure is similar to the supply rates for adiabatic and isothermal actuators given in Eq. (3.59) and Eq. (3.68) respectively.

In the next section, energy function for the two-chambered actuator is developed by using the results presented for the single-chambered actuator. The supply rate for the two-chambered actuator is also presented in the following section.

4.2 Two-chambered pneumatic actuator

Commonly used pneumatic actuators have two air chambers. In this section, two-chambered pneumatic actuator with finite heat interaction with the ambient is studied. Dynamics of the two-chambered actuator are obtained by treating it as two interacting single-chambered actuators. Similar to the single-chambered actuator, the storage function is defined as the maximum work that can be extracted from the actuator, as the actuator traverses to the equilibrium position. This storage function is used to define the supply rate for achieving energetically passive operation with the two-chambered pneumatic actuator. The actuator dynamics are presented in the following section.

4.2.1 Actuator dynamics

The schematic for a two-chambered actuator is as shown in Fig. 4.7. The two-chambered pneumatic actuator can be interpreted as two interacting single-chambered pneumatic

actuators. The two chambers of the actuator are mechanically coupled through the actuator piston. For a piston position x, the chamber volumes $V_1(x)$, $V_2(x)$ are obtained as,

$$V_1(x) = A_1(L_{1o} + x), \qquad V_2(x) = A_2(L'_{2o} + L - x) = A_2(L_{2o} - x) \tag{4.51}$$

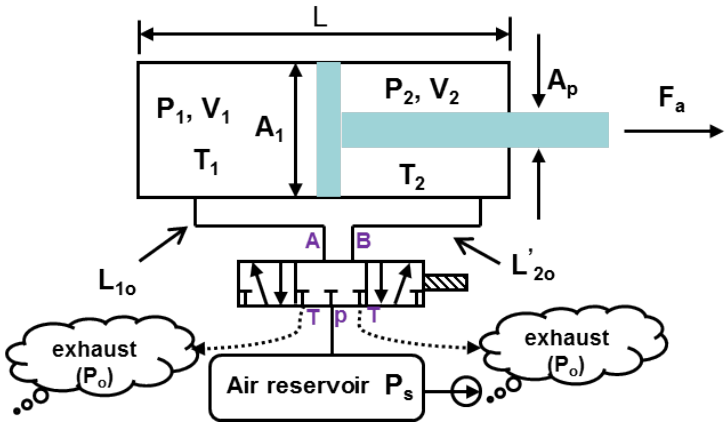

Figure 4.7: Schematic of a two-chambered actuator with a pneumatic servo valve for controlling air flow to the actuator.

where A_1 and A_2 refer to the piston cross-sectional area in chamber 1 and chamber 2 respectively, while A_1L_{1o} and $A_2L'_{2o}$ correspond to the dead volume in chambers 1 and 2 respectively, and L corresponds to the actuator stroke length. Both $V_1(x)$ and $V_2(x)$ are well defined by the actuator position x. Therefore, the actuator position is defined to be an actuator state.

It is assumed that the heat transfer rates $\dot{Q}_1$ and $\dot{Q}_2$ in the two actuator chambers are only due to thermal interaction between the chamber air and the the ambient at temperature T_o. It is assumed that there is no heat transfer between the two actuator chambers themselves. Therefore, $\dot{Q}_1$ and $\dot{Q}_2$ are defined as,

$$\dot{Q}_1 = h_1^2(t)(T_o - T_1), \qquad \dot{Q}_2 = h_2^2(t)(T_o - T_2) \tag{4.52}$$

where the heat transfer coefficients $h_1^2(t)$ and $h_2^2(t)$ are positive for all t and can be varied to simulate different heat transfer models in each actuator chamber.

The dynamics of temperature T_1 in chamber 1 and temperature T_2 in chamber 2 are obtained from the first law of thermodynamics and are as given in Eq. (3.9). Let T_{u_1} and T_{u_2} be the air temperature upstream of the control volume in chambers 1 and 2 respectively. Again, the difference in the temperature dynamics for adiabatic/isothermal actuators and the actuator with finite heat transfer is the assumption on the upstream air temperature T_{u_i} in Eq. (3.25). For adiabatic/isothermal actuators, T_{u_i} is assumed to be the same as the chamber temperature T_i. In this chapter, T_{u_i} is determined from the direction of air flow. Assuming that the air temperature immediately outside the control volume in Fig. (4.7) to be the same as ambient temperature T_o, the upstream air temperatures T_{u_1} and T_{u_2} for chamber 1 and chamber 2 are defined as,

$$T_{u_1} = \begin{cases} T_o \text{ if } \dot{m}_1 \geq 0 \\ T_1 \text{ if } \dot{m}_1 < 0 \end{cases}, \qquad T_{u_2} = \begin{cases} T_o \text{ if } \dot{m}_2 \geq 0 \\ T_2 \text{ if } \dot{m}_2 < 0 \end{cases} \tag{4.53}$$

For a fixed mass of air m_1 and m_2 in chambers 1 and 2 respectively, and from the definition of heat transfer rates $\dot{Q}_1$, $\dot{Q}_2$ in Eq. (4.52), the dynamics of the actuator states (x, T_1, T_2) depend on the piston velocity $\dot{x}$ and the heat transfer coefficients $h_1^2(t)$ and $h_2^2(t)$ as,

$$\begin{aligned} \dot{x} &= \dot{x} \\ \frac{\dot{T}_1}{T_1} &= (\gamma - 1)\left(-\frac{A_1\dot{x}}{V_1(x)} + \frac{h_1^2(t)(T_o - T_1)}{m_1 R T_1}\right) \\ \frac{\dot{T}_2}{T_2} &= (\gamma - 1)\left(\frac{A_2\dot{x}}{V_2(x)} + \frac{h_2^2(t)(T_o - T_1)}{m_2 R T_2}\right) \end{aligned} \tag{4.54}$$

The pressures P_1 and P_2 in chamber 1 and 2 of the actuator respectively are obtained from the actuator states (x, T_1, T_2) by using the ideal gas law as,

$$P_1 = \frac{m_1 R T_1}{A_1(L_{1o} + x)}, \qquad P_2 = \frac{m_2 R T_2}{A_2(L_{2o} - x)} \tag{4.55}$$

For convenience of representation, consider the following vector definitions for chamber pressures, temperatures and air mass,

$$\boldsymbol{P} = (P_1, P_2), \quad \boldsymbol{T} = (T_1, T_2), \quad \boldsymbol{m} = (m_1, m_2) \tag{4.56}$$

Using the definition of chamber pressures in Eq. (4.55), the actuator force $F_a(\boldsymbol{P})$ from Eq. (3.1) can be expressed in terms of ($\boldsymbol{m}$, $\boldsymbol{T}$, x) as,

$$F_a(\boldsymbol{P}) = \frac{m_1 R T_1}{(L_{1o} + x)} - \frac{m_2 R T_2}{(L_{2o} - x)} - P_o A_p \tag{4.57}$$

where $A_p = (A_1 - A_2)$ is the piston rod cross sectional area exposed to the ambient pressure P_o. In the two-chambered actuator, the actuator force output $F_a(\boldsymbol{P})$ can be varied by changing the actuator states (x, T_1, T_2) with appropriate selection of the inputs $(\dot{x}(t), h_1(t), h_2(t))$. In the following section, optimization problem for identifying the maximum available energy from the two-chambered actuator is presented. The inputs required to extract this maximum energy are identified, and the expression for maximum available energy is derived.

4.2.2 Maximum available energy from a two-chambered actuator

At the equilibrium state, the two-chambered actuator is both in mechanical equilibrium with the ambient ($F_a(\boldsymbol{P}) = 0$), and in thermal equilibrium with the ambient ($T_1 = T_o$ and $T_2 = T_o$). The equilibrium position of the actuator with finite heat interaction thus corresponds to that of an isothermal actuator. Note that in contrast, the equilibrium temperature of the adiabatic actuator is determined by the chamber pressures along the adiabatic trajectory that satisfy the equilibrium condition $F_a(\boldsymbol{P}) = 0$. The corresponding chamber temperatures in the adiabatic actuator chamber need not correspond to ambient temperature T_o. As shown in section 3.2.3, the equilibrium position of the isothermal actuator is a function of only the mass m_1 and m_2 in chambers 1 and 2 of the actuator. Let $\bar{x}(\boldsymbol{m})$ represent the to be determined equilibrium position of the actuator. The individual chamber pressures $\bar{P}_1(\boldsymbol{m})$ and $\bar{P}_2(\boldsymbol{m})$ at equilibrium are obtained from Eq. (4.55) as,

$$\bar{P}_1(\boldsymbol{m}) = \frac{m_1 R T_o}{A_1(L_{1o} + \bar{x}(\boldsymbol{m}))}, \qquad \bar{P}_2(\boldsymbol{m}) = \frac{m_2 R T_o}{A_2(L_{2o} - \bar{x}(\boldsymbol{m}))} \tag{4.58}$$

Note that unlike a single-chambered actuator, it is not necessary that the individual chamber equilibrium pressures correspond to the ambient pressure P_o. As shown in Eq. (3.85), the pressures $\bar{P}_1(\boldsymbol{m})$ and $\bar{P}_2(\boldsymbol{m})$ are related as,

$$F_a(\bar{\boldsymbol{P}}) = \bar{P}_1(\boldsymbol{m})A_1 - \bar{P}_2(\boldsymbol{m})A_2 - P_o A_p = 0 \tag{4.59}$$

where $\bar{\boldsymbol{P}} := (\bar{P}_1(\boldsymbol{m}), \bar{P}_2(\boldsymbol{m}))$. Using the definition of $\bar{P}_1(\boldsymbol{m})$ and $\bar{P}_2(\boldsymbol{m})$ from Eq. (4.58) in the above equation, the equilibrium position $\bar{x}(\boldsymbol{m})$ is determined as the solution of the following equation,

$$\frac{m_1 R T_o}{L_{1o} + \bar{x}(\boldsymbol{m})} - \frac{m_2 R T_o}{L_{2o} - \bar{x}(\boldsymbol{m})} - P_o A_p = 0 \tag{4.60}$$

Using the property of the equilibrium state from Eq. (4.60), the actuator force $F_a(\boldsymbol{P})$ in Eq. (4.57) can be expressed as,

$$F_a(\boldsymbol{P}) = \left(\frac{m_1 R T_1}{A_1(L_{1o}+x)} - \bar{P}_1(\boldsymbol{m})\right) A_1 - \left(\frac{m_2 R T_2}{A_2(L_{2o}-x)} - \bar{P}_2(\boldsymbol{m})\right) A_2 \tag{4.61}$$

Due to heat interaction with the ambient, the thermodynamic process in the actuator is not reversible. Therefore the work extracted from the actuator, as it traverses to equilibrium state, is path dependent. By using the definition of the actuator force $F_a(\boldsymbol{P})$ from Eq. (4.61) in terms of $(\boldsymbol{m}, \boldsymbol{T}, x)$, the work available $W_{act}(\boldsymbol{m}, \boldsymbol{P}, \boldsymbol{T}, \dot{x})$ from the two-chambered actuator is defined as,

$$\begin{aligned} W_{act}(\boldsymbol{m}, \boldsymbol{P}, \boldsymbol{T}, \dot{x}) &= \int_0^\infty F_a(\boldsymbol{P})\dot{x}(\tau)\ d\tau \\ &= \int_0^\infty \left(\left(\frac{m_1 R T_1(\tau)}{A_1(L_{1o}+x(\tau))} - \bar{P}_1(\boldsymbol{m})\right) A_1 - \left(\frac{m_2 R T_2(\tau)}{A_2(L_{2o}-x(\tau))} - \bar{P}_2(\boldsymbol{m})\right) A_2\right)\dot{x}(\tau)\ d\tau \end{aligned} \tag{4.62}$$

To show passive operation for all feasible mechanical power interaction, the storage function for the two-chambered actuator is defined to be maximum mechanical work that can be extracted from the actuator for a fixed mass of air in each chamber. This is similar to definition of the storage function for the single-chambered actuator.

For a given air mass $\boldsymbol{m}$, the work available from the actuator can be varied by defining the vector of inputs $\boldsymbol{u}(t) \triangleq (h_1(t), h_2(t), \dot{x}(t))$ to vary the actuator states (x, T_1, T_2) and consequently the actuator force $F_a(\boldsymbol{P})$. The actuator states (x, T_1, T_2) are however constrained to follow the dynamics in Eq. (4.54). The optimization problem to determine the storage function for the two-chambered actuator is thus defined as,

$$\begin{aligned} \bar{W}_{act}(\boldsymbol{m}, \boldsymbol{P}, \boldsymbol{T}) = \sup_{\boldsymbol{u}(.)} \quad & \int_0^\infty F_a(\boldsymbol{P})\dot{x}(\tau)\ d\tau \\ \text{subject to Eq. (4.54)} & \end{aligned} \tag{4.63}$$

In the following subsection, the optimality conditions required to determine the input vector $\boldsymbol{u}(t)$ for extracting maximum available work are presented.

Necessary optimality conditions

Similar to the single-chambered actuator in section 4.1.3, the cost function in Eq. (4.63) can be augmented with the dynamic constraints in Eq. (4.54) by using Lagrange multipliers $\lambda_{T_1}(t)$, $\lambda_{T_2}(t)$ and $\lambda_x(t)$. As a result, the constrained optimization problem in

Eq. (4.63) can be reposed as an unconstrained optimization problem. In Eq. (4.10) the unconstrained problem for the single-chambered actuator is expressed in terms of a Hamiltonian function. As shown in Eq. (4.14) and Eq. (4.18), both the first and second order conditions for optimal solution are then obtained in terms of the Hamiltonian function. To identify the solution to the optimization problem for the two-chambered actuator in Eq. (4.63), a similar Hamiltonian function $\bar{H}(x, \boldsymbol{T}, \boldsymbol{u})$ is defined,

$$\begin{aligned}\bar{H}(x, \boldsymbol{T}, \boldsymbol{u}) = &\left(\frac{m_1 R T_1}{L_{1o} + x} - \frac{m_2 R T_2}{L_{2o} - x} - P_o A_p\right) \dot{x}(t) + \lambda_x(t)\dot{x}(t) + \lambda_{T_1}(t)(\gamma - 1)\left(-\frac{T_1 A_1}{V_1(x)}\dot{x}(t)\right. \\ &\left. + \frac{h_1^2(t)(T_o - T_1)}{m_1 C_v}\right) + \lambda_{T_2}(t)(\gamma - 1)\left(-\frac{T_2 A_2}{V_2(x)}\dot{x}(t) + \frac{h_2^2(t)(T_o - T_2)}{m_2 C_v}\right)\end{aligned} \tag{4.64}$$

The necessary optimality conditions for the optimization problem in Eq. (4.63) are then given by,

$$\frac{\partial \bar{H}(x, \boldsymbol{T}, \boldsymbol{u})}{\partial h_1} = 0, \quad \frac{\partial \bar{H}(x, \boldsymbol{T}, \boldsymbol{u})}{\partial h_2} = 0, \quad \frac{\partial \bar{H}(x, \boldsymbol{T}, \boldsymbol{u})}{\partial \dot{x}} = 0 \tag{4.65}$$

$$\dot{\lambda}_{T_1}(t) = -\frac{\partial \bar{H}(x, \boldsymbol{T}, \boldsymbol{u})}{\partial T_1} = -(\gamma - 1)\left(\frac{m_1 C_v - \lambda_{T_1}}{L_{1o} + x}\right)\dot{x}(t) + \frac{\lambda_{T_1}(t)}{m_1 C_v} h_1^2(t) \tag{4.66}$$

$$\dot{\lambda}_{T_2}(t) = -\frac{\partial \bar{H}(x, \boldsymbol{T}, \boldsymbol{u})}{\partial T_2} = (\gamma - 1)\left(\frac{m_2 C_v - \lambda_{T_2}}{L_{2o} - x}\right)\dot{x}(t) + \frac{\lambda_{T_2}(t)}{m_2 R} h_2^2(t) \tag{4.67}$$

$$\dot{\lambda}_x(t) = -\frac{\partial \bar{H}(x, \boldsymbol{T}, \boldsymbol{u})}{\partial x} = (\gamma - 1)\left(\frac{(m_1 C_v - \lambda_{T_1})T_1}{(L_{1o} + x)^2} - \frac{(m_2 C_v - \lambda_{T_2})T_2}{(L_{2o} - x)^2}\right)\dot{x}(t) \tag{4.68}$$

$$\lim_{t\to\infty} \lambda_{T_1}(t) = 0, \qquad \lim_{t\to\infty} \lambda_{T_2}(t) = 0 \lim_{t\to\infty} \lambda_x(t) = 0 \tag{4.69}$$

$$\left[\begin{array}{ccc} \frac{\partial^2 \bar{H}(x,\boldsymbol{T},\boldsymbol{u})}{\partial h_1^2} & \frac{\partial^2 \bar{H}(x,\boldsymbol{T},\boldsymbol{u})}{\partial h_1 \partial h_2} & \frac{\partial^2 \bar{H}(x,\boldsymbol{T},\boldsymbol{u})}{\partial h_1 \partial \dot{x}} \\ \frac{\partial^2 \bar{H}(x,\boldsymbol{T},\boldsymbol{u})}{\partial \partial h_2 \partial h_1} & \frac{\partial^2 \bar{H}(x,\boldsymbol{T},\boldsymbol{u})}{\partial h_2^2} & \frac{\partial^2 \bar{H}(x,\boldsymbol{T},\boldsymbol{u})}{\partial h_2 \partial \dot{x}} \\ \frac{\partial^2 \bar{H}(x,\boldsymbol{T},\boldsymbol{u})}{\partial \partial \dot{x} \partial h_1} & \frac{\partial^2 \bar{H}(x,\boldsymbol{T},\boldsymbol{u})}{\partial \dot{x} \partial h_2} & \frac{\partial^2 \bar{H}(x,\boldsymbol{T},\boldsymbol{u})}{\partial \dot{x}^2} \end{array}\right]\Bigg|_{\boldsymbol{u}(.)=\boldsymbol{u}^*} \leq 0 \tag{4.70}$$

where $\boldsymbol{u}^*$ is the solution of the first order optimality conditions in Eq. (4.65). The algebraic equations corresponding to the first order optimality condition in Eq. (4.65) are obtained as,

$$\begin{aligned} &\lambda_{T_1}(t) h_1(t)(T_o - T_1) = 0 \\ &\lambda_{T_2}(t) h_2(t)(T_o - T_2) = 0 \\ &(\gamma - 1)\left(\frac{(m_1 C_v - \lambda_{T_1}(t))T_1}{(L_{1o} + x)} - \frac{(m_2 C_v - \lambda_{T_2}(t))T_2}{(L_{2o} - x)}\right) - P_o A_p + \lambda_x(t) = 0 \end{aligned} \tag{4.71}$$

Similar to the single-chambered actuator in Eq. (4.26), the optimal trajectory for each chamber is obtained from the above equation as a combination of the following segments,

$$\begin{aligned} &\textbf{Chamber 1 :}\ \lambda_{T_1}(t) = 0, \quad h_1(t) = 0, \quad T_1 = T_o \\ &\textbf{Chamber 2 :}\ \lambda_{T_2}(t) = 0, \quad h_2(t) = 0, \quad T_2 = T_o \end{aligned} \tag{4.72}$$

Each of the three possible segments for chamber 1 can be combined with any of the three possible segments for chamber 2, providing a total of nine possible segments for the optimal trajectory of a two-chambered actuator.

Solution for $\lambda_{T_1}(t)$, $\lambda_{T_2}(t)$ and $\lambda_x(t)$

The dynamics of Lagrange multipliers $\lambda_{T_1}(t)$ and $\lambda_{T_2}(t)$ in Eq. (4.66) and Eq. (4.67) respectively are the same as the dynamics of the single-chambered Lagrange multiplier $\lambda_T(t)$ in Eq. (4.15). Therefore, from the definition of $\lambda_T(t)$ from Eq. (4.25), the following definition of $\lambda_{T_1}(t)$ and $\lambda_{T_2}(t)$ will satisfy Eq. (4.66) and Eq. (4.67) respectively,

$$\lambda_{T_1}(t) = m_1 C_v \left(1 - \frac{T_o}{T_1}\right), \quad \lambda_{T_2}(t) = m_2 C_v \left(1 - \frac{T_o}{T_2}\right) \tag{4.73}$$

Using the definition of λ_{T_1} and λ_{T_2} from the above equation in the optimality condition in Eq. (4.71), $\lambda_x(t)$ is obtained as,

$$\lambda_x(t) = -\left(\frac{m_1 R T_o}{L_{1o} + x} - \frac{m_2 R T_o}{L_{2o} - x} - P_o A_p\right) \tag{4.74}$$

It is easy to verify that the expressions for $\lambda_{T_1}(t)$, $\lambda_{T_2}(t)$ and $\lambda_x(t)$ from Eq. (4.73) and Eq. (4.74) respectively, satisfy the dynamic equation for $\lambda_x(t)$ in Eq. (4.68).

In the next section it is shown that the maximum available energy $\bar{W}_{act}(\boldsymbol{m}, \boldsymbol{P}, \boldsymbol{T})$ from the two-chambered actuator is bounded from above by the sum of maximum available energy from each chamber of the two-chambered actuator.

Upper bound on the available work from two-chambered actuator

Using the expression for actuator force $F_a(\boldsymbol{P})$ from Eq. (4.61), the optimization problem in Eq. (4.63) can be written as,

$$\bar{W}_{act}(\boldsymbol{m},\boldsymbol{P},\boldsymbol{T}) = \sup_{\boldsymbol{u}(.)} \left(\int_0^{\infty} \left(\left(\frac{m_1 R T_1}{L_{1o}+x} - \bar{P}_1(\boldsymbol{m}) A_1 \right) - \left(\frac{m_2 R T_2}{L_{2o}-x} - \bar{P}_2(\boldsymbol{m}) A_2 \right) \right) \dot{x}\, d\tau \right)$$
$$\text{subject to Eq. (4.54)} \tag{4.75}$$

Using the relationship between the chamber volume $V_i(x)$ and the piston position x, and from triangle inequality, maximum available energy $\bar{W}_{act}(\boldsymbol{m},\boldsymbol{P},\boldsymbol{T})$ in the above equation can be expressed as,

$$\begin{aligned} \bar{W}_{act}(\boldsymbol{m},\boldsymbol{P},\boldsymbol{T}) \leq & \sup_{(h_1(.),\dot{x}(.))} \left(\int_0^{\infty} \frac{m_1 R T_1}{V_1(x)} - \bar{P}_1(\boldsymbol{m}) \right) A_1 \dot{x}\ d\tau \\ & + \sup_{(h_2(.),\dot{x}(.))} - \left(\int_0^{\infty} \frac{m_2 R T_2}{V_2(x)} - \bar{P}_2(\boldsymbol{m}) \right) A_2 \dot{x}\ d\tau \end{aligned} \tag{4.76}$$
$$\text{subject to Eq. (4.54)}$$

Define a change of variable $(L_{2o} - x) := (L_{2o}^{'} + y)$, where y represents a new position variable, and $L_{2o}^{'}$ corresponds to the dead volume in chamber 2. The volume of chamber 2 is defined in terms of y as $V_2^{'}(y) = A_2(L_{2o}^{'} + y)$. The optimization problem defined in Eq. (4.76) can then be reformulated as,

$$\begin{aligned} \bar{W}_{act}(\boldsymbol{m},\boldsymbol{P},\boldsymbol{T}) \leq & \sup_{(h_1(.),\dot{x}(.))} \left(\int_0^{\infty} \frac{m_1 R T_1}{V_1(x)} - \bar{P}_1(\boldsymbol{m}) \right) A_1 \dot{x}\ d\tau \\ & + \sup_{(h_2(.),\dot{y}(.))} \left(\int_0^{\infty} \frac{m_2 R T_2}{V_2^{'}(y)} - \bar{P}_2(\boldsymbol{m}) \right) A_2 \dot{y}\ d\tau \end{aligned} \tag{4.77}$$
$$\text{subject to Eq. (4.54)}$$

The first term on the *r.h.s* of the above equation represents the maximum work that can be extracted from chamber 1, with $\bar{P}_1(\boldsymbol{m})$ being the equilibrium pressure in chamber 1. The second term on the *r.h.s* of the above equation represents the maximum work that can be extracted from chamber 2 with $\bar{P}_2(\boldsymbol{m})$ being the equilibrium pressure in chamber 2. For a given equilibrium pressure of P_o and equilibrium temperature of T_o, the maximum extractable work from a single-chambered actuator is as presented in

Eq. (4.35). By using the appropriate equilibrium pressure ($\bar{P}_1(\boldsymbol{m})$ or $\bar{P}_2(\boldsymbol{m})$) in Eq. (4.35), the *r.h.s* of Eq. (4.77) is then obtained as,

$$\begin{aligned}\bar{W}_{act}(\boldsymbol{m},\boldsymbol{P},\boldsymbol{T}) \leq\ & m_1C_v(T_1-T_o) - m_1T_o(\sigma(P_1,T_1)-\sigma(\bar{P}_1(\boldsymbol{m}),T_o)) \\ & + m_2C_v(T_2-T_o) - m_2T_o(\sigma(P_2,T_2)-\sigma(\bar{P}_2(\boldsymbol{m}),T_o)) \\ & - \bar{P}_1(\boldsymbol{m})\left(V_1(\bar{x}(\boldsymbol{m}))-V_1(x)\right) - \bar{P}_2\boldsymbol{m}\left(V_2^{'}(\bar{y}(\boldsymbol{m}))-V_2^{'}(y)\right)\end{aligned} \tag{4.78}$$

where $\bar{y}(\boldsymbol{m}) := (L_{2o}-\bar{x}(\boldsymbol{m})-L_{2o}^{'})$. Using the volume definitions $V_1(x) := A_1(L_{1o}+x)$, $V_2^{'}(y) := A_2(L_{2o}^{'}+y) = A_2(L_{2o}-x)$, and from the relationship between equilibrium pressures $\bar{P}_1(\boldsymbol{m})$, $\bar{P}_2(\boldsymbol{m})$ in Eq. (4.59), the upper bound on the maximum available energy in Eq. (4.78) can be simplified as,

$$\begin{aligned}\bar{W}_{act}(\boldsymbol{m},\boldsymbol{P},\boldsymbol{T}) \leq\ & m_1C_v(T_1-T_o) - m_1T_o(\sigma(P_1,T_1)-\sigma(\bar{P}_1(\boldsymbol{m}),T_o)) \\ & + m_2C_v(T_2-T_o) - m_2T_o(\sigma(P_2,T_2)-\sigma(\bar{P}_2(\boldsymbol{m}),T_o)) \\ & - P_oA_p(\bar{x}-x)\end{aligned} \tag{4.79}$$

In the following subsection, available work along a particular combination of the segments satisfying the optimality conditions in Eq. (4.72) is evaluated. The work extracted along this trajectory is shown to be the same as the upper bound on the maximum available energy in Eq. (4.79) as the actuator traverses to the equilibrium position $\bar{x}(\boldsymbol{m})$ defined in Eq. (4.60).

Optimal trajectory candidate

For the two-chambered actuator, let the air temperatures T_1 and T_2 in chambers 1 and 2 of the actuator be different from the ambient temperature T_o. Consider a trajectory consisting of the following three sequence of segments for extracting work from the actuator,

1. Adiabatic expansion (or compression) of chamber 1 ($h_1(t) = 0$ in Eq. (4.72)) to ambient temperature T_o and adiabatic compression (or expansion) of chamber 2 ($h_2(t) = 0$ in Eq. (4.72))

2. Isothermal compression (or expansion) of chamber 1 ($T_1 = T_o$ in Eq. (4.72)) and adiabatic expansion (or compression) of chamber 2 to ambient temperature T_o ($h_2(t) = 0$ in Eq. (4.72))

3. Isothermal process ($T_1 = T_o$ and $T_2 = T_o$) to the equilibrium position $\bar{x}(m)$ defined as the solution of Eq. (4.60)

Note that along each segment enumerated above, the first order optimality conditions in Eq. (4.71) are satisfied in each chamber of the actuator. Work extracted along each of these three segments is now evaluated.

Adiabatic trajectory in both chambers ($h_1(t) = 0$ ***and*** $h_2(t) = 0$***):*** Let P_1 and P_2 be the initial pressure in chamber 1 and 2 of the actuator. Let x_a be the position of the actuator piston where the temperature of air in chamber 1 corresponds to the ambient temperature T_o. Let P_{1_a} and $V_1(x_a)$ be the pressure and volume in chamber 1 at the piston position x_a. At this position of the actuator, let P_{2_a} and $V_2(x_a)$ be the pressure and volume of chamber 2 of the actuator. Also, let T_{2_a} be the air temperature in chamber 2 at the end of first segment. From Eq. (3.78) and Eq. (3.17), the pressure-volume ($P - V$) and the pressure-temperature ($P - T$) characteristic curves along the adiabatic segment are respectively given by,

$$\begin{aligned} &\textbf{Chamber 1:} \quad P_1 V_1^{\gamma_1}(x) = P_{1_a} V_1^{\gamma}(x_a), \qquad \frac{T_1}{P_1^{(\gamma-1)/\gamma}} = \frac{T_o}{P_{1_a}^{(\gamma-1)/\gamma}} \\ &\textbf{Chamber 2:} \quad P_2 V_2^{\gamma_2}(x) = P_{2_a} V^{\gamma_2}(x_a), \qquad \frac{T_2}{P_2^{(\gamma-1)/\gamma}} = \frac{T_{2_a}}{P_{2_a}^{(\gamma-1)/\gamma}} \end{aligned} \tag{4.80}$$

At position x_a of the actuator, let $\boldsymbol{P}_a := (P_{1_a}, P_{2_a})$ and $\boldsymbol{T}_a := (T_o, T_{2_a})$ be the vector of pressures and temperatures in chambers 1 and 2 of the actuator respectively. The work $W_{act_a}(\boldsymbol{m}, \boldsymbol{P}, \boldsymbol{T}, P_{2_a})$ extracted from two-chambered actuator while following the adiabatic trajectory in both chambers is obtained from Eq. (3.34) as,

$$\begin{aligned} W_{act_a}(\boldsymbol{m}, \boldsymbol{P}, \boldsymbol{T}, \boldsymbol{P}_a, \boldsymbol{T}_a) = &\frac{P_1 V_1(x)}{\gamma - 1} \left(1 - \left(\frac{P_{1_a}}{P_1}\right)^{\frac{(\gamma-1)}{\gamma}}\right) + \bar{P}_1(\boldsymbol{m}) V_1(x) \left(1 - \left(\frac{P_1}{P_{1_a}}\right)^{1/\gamma}\right) \\ &+ \frac{P_2 V_2(x)}{\gamma - 1} \left(1 - \left(\frac{P_{2_a}}{P_2}\right)^{(\gamma-1)/\gamma}\right) + \bar{P}_2(\boldsymbol{m}) V_2(x) \left(1 - \left(\frac{P_2}{P_{2_a}}\right)^{1/\gamma}\right) \end{aligned} \tag{4.81}$$

where $\bar{P}_1(\boldsymbol{m})$ and $\bar{P}_2(\boldsymbol{m})$ correspond to the pressures in chamber 1 and 2 of the actuator at the equilibrium state and are as related in Eq. (4.59). From Eq. (4.80) note that P_{1_a} can be expressed in terms of P_1, T_1 and T_o. Therefore, the available energy

$W_{act_a}(\boldsymbol{m}, \boldsymbol{P}, \boldsymbol{T}, P_{2_a})$ does not explicitly depend on P_{1_a}. Using the ideal gas law from Eq. (3.2), and the pressure-volume and pressure-temperature relationships for adiabatic process from Eq. (4.80), the work extracted along the adiabatic trajectory in Eq. (4.81) can be written as,

$$W_{act_a}(\boldsymbol{m}, \boldsymbol{P}, \boldsymbol{T}, \boldsymbol{P}_a, \boldsymbol{T}_a) = m_1 C_v(T_1 - T_o) + \bar{P}_1(\boldsymbol{m})\left(V_1(x) - V_1(x_a)\right) + m_2 C_v(T_2 - T_{2_a}) + \bar{P}_2(\boldsymbol{m})\left(V_2(x) - V_2(x_a)\right) \tag{4.82}$$

Isothermal trajectory in chamber 1 ***($T_1 = T_o$) and adiabatic trajectory in chamber*** 2 ***($h_2(t) = 0$):*** Along this segment of the trajectory, chamber 1 traverses along an isothermal curve, while chamber 2 traverses along an adiabatic curve. Let x_b be the actuator piston position at the end of this segment. Let P_{1_b}, and $V_1(x_b)$ be the pressure and volume in chamber 1 at the position x_b. At this position of the actuator, let the corresponding pressure and volume in chamber 2 be P_{2_b} and $V_2(x_b)$. The temperature and pressure characteristics in both chambers of the actuator are given by,

$$\begin{aligned} &\textbf{Chamber 1:} \quad P_{1_b} V_1(x_b) = P_{1_a} V_1(x_a), \qquad T_1 = T_o \\ &\textbf{Chamber 2:} \quad P_{2_b} V_2^{\gamma}(x_b) = P_{2_a} V_2^{\gamma}(x_a), \qquad \frac{T_o}{P_{2_b}^{(\gamma-1)/\gamma}} = \frac{T_{2_a}}{P_{2_a}^{(\gamma-1)/\gamma}} \end{aligned} \tag{4.83}$$

At position x_b of the actuator, let $\boldsymbol{P}_b := (P_{1_b}, P_{2_b})$ and $\boldsymbol{T}_b := (T_o, T_o)$ be the vector of pressures and temperatures in chambers 1 and 2 of the actuator respectively. Using the definition of available work from single-chambered isothermal actuator in Eq. (3.44), and single-chambered adiabatic actuator in Eq. (3.34), along with the definition of the characteristic curves from Eq. (4.83), the work $W_{act_b}(\boldsymbol{m}, \boldsymbol{P}, \boldsymbol{T}, \boldsymbol{P}_b, \boldsymbol{T}_b)$ extracted from the two-chambered actuator in the second segment of the proposed trajectory is obtained as,

$$\begin{aligned} W_{act_b}(\boldsymbol{m}, \boldsymbol{P}_a, \boldsymbol{T}_a, \boldsymbol{P}_b, \boldsymbol{T}_b) =& m_1 R T_o \log\left(\frac{P_{1_b}}{P_{1_a}}\right) + \bar{P}_1(\boldsymbol{m})(V_1(x_a) - V_1(x_b)) \\ &+ m_2 C_v(T_{2_a} - T_o) + \bar{P}_2(\boldsymbol{m})(V_2(x_a) - V_2(x_b)) \end{aligned} \tag{4.84}$$

Isothermal trajectory in both chambers ($T_1 = T_o$, $T_2 = T_o$): If the actuator position at the end of the second segment does not correspond to the equilibrium position $\bar{x}(\boldsymbol{m})$, then in the third segment of the proposed trajectory, the two-chambered actuator is traversed along an isothermal curve in both chambers of the actuator to the

equilibrium position $\bar{x}(\boldsymbol{m})$. Define $\bar{\boldsymbol{P}} := (\bar{P}_1(\boldsymbol{m}), \bar{P}_2(\boldsymbol{m}))$ to be the vector of chamber pressures at equilibrium position. Using the definition of isothermal work from Eq. (3.101), work $W_{act_c}(\boldsymbol{m}, \boldsymbol{P}_b, \boldsymbol{T}_b, \bar{\boldsymbol{P}}, T_o)$ available along this segment of the proposed trajectory is obtained as,

$$\begin{aligned} W_{act_c}(\boldsymbol{m}, \boldsymbol{P}_b, \boldsymbol{T}_b, \bar{\boldsymbol{P}}, T_o) = m_1 R T_o \log\left(\frac{\bar{P}_1(\boldsymbol{m})}{P_{1_b}}\right) + \bar{P}_1(\boldsymbol{m})(V_1(x_b) - V_1(\bar{x}(\boldsymbol{m}))) \\ + m_2 R T_o \log\left(\frac{P_2(\boldsymbol{m})}{P_{2_b}}\right) + \bar{P}_2(\boldsymbol{m})(V_2(x_b) - V_2(\bar{x}(\boldsymbol{m}))) \end{aligned} \tag{4.85}$$

Theorem 4.3. *For a fixed mass of air m_1 and m_2 in chambers 1 and 2 respectively of the two-chambered actuator with the corresponding air temperatures $T_1 \neq T_o$ and $T_2 \neq T_o$, a trajectory consisting of the following sequence of segments satisfies the optimality conditions in Eq. (4.71) as the actuator traverses to the equilibrium position $\bar{x}(\boldsymbol{m})$,*

1. *Adiabatic expansion or compression of chamber 1 ($h_1(t) = 0$) to ambient temperature T_o, while simultaneous adiabatic compression or expansion of chamber 2 ($h_2(t) = 0$)*
2. *Isothermal compression or expansion of chamber 1 ($T_1 = T_o$) while simulataneous adiabatic expansion or compression of chamber 2 to ambient temperature T_o ($h_2(t) = 0$)*
3. *Isothermal trajectory in both the actuator chambers ($T_1 = T_o$, $T_2 = T_o$) until the actuator position corresponds to the equilibrium position $\bar{x}(m)$ defined as the solution of Eq. (4.60)*

The proposed trajectory is optimal as the available work ($\bar{W}_{act}(\boldsymbol{m}, \boldsymbol{P}, \boldsymbol{T}) \geq 0$) along this trajectory corresponds to the maximum available work from the two-chambered actuator (in Eq. (4.79)) and is given by,

$$\begin{aligned} \bar{W}_{act}(\boldsymbol{m}, \boldsymbol{P}, \boldsymbol{T}) = m_1 C_v(T_1 - T_o) - m_1 T_o(\sigma(P_1, T_1) - \sigma(\bar{P}_1(\boldsymbol{m}), T_o)) + m_2 C_v(T_2 - T_o) \\ - m_2 T_o(\sigma(P_2, T_2) - \sigma(\bar{P}_2(\boldsymbol{m}), T_o)) - P_o A_p(\bar{x}(\boldsymbol{m}) - x) \end{aligned} \tag{4.86}$$

where $\bar{P}_1(\boldsymbol{m})$ and $\bar{P}_2(\boldsymbol{m})$ correspond to equilibrium pressures in each chamber 1 and 2 of the actuator, while $(\sigma(P_i, T_i) - \sigma(\bar{P}_i(\boldsymbol{m}), T_o))$ as defined in Eq. (4.34) represents the

specific entropy change in the i^{th} chamber of the actuator with respect to equilibrium state and is given by,

$$\sigma(P_i, T_i) - \sigma(\bar{P}_i(\boldsymbol{m}), T_o) = C_p \log\left(\frac{T_i}{T_o}\right) - R\log\left(\frac{P_i}{\bar{P}_i(\boldsymbol{m})}\right) \tag{4.87}$$

Proof. In the proof, the available work along each segment of the proposed trajectory is determined and their sum is shown to correspond to the upper bound on the available work in Eq. (4.79). The proposed trajectory will consequently be an optimal path for extracting maximum work from the two-chambered actuator.

The work available along each segment of the proposed trajectory is as given in Eq. (4.82), Eq. (4.84) and Eq. (4.85) respectively. The total work $\bar{W}_{act}(\boldsymbol{m}, \boldsymbol{P}, \boldsymbol{T})$ extracted from the two-chambered actuator along the proposed trajectory is obtained as,

$$\begin{aligned}
\bar{W}_{act}(\boldsymbol{m}, \boldsymbol{P}, \boldsymbol{T}) &= W_{act_a}(\boldsymbol{m}, \boldsymbol{P}, \boldsymbol{T}, \boldsymbol{P}_a, \boldsymbol{T}_a) + W_{act_b}(\boldsymbol{m}, \boldsymbol{P}_a, \boldsymbol{T}_a, \boldsymbol{P}_b, \boldsymbol{T}_b) \\
&\qquad + W_{act_c}(\boldsymbol{m}, \boldsymbol{P}_b, \boldsymbol{T}_b, \bar{\boldsymbol{P}}, T_o) \\
&= m_1 C_v(T_1 - T_o) + m_1 R T_o \log\left(\frac{\bar{P}_1(\boldsymbol{m})}{P_{1_a}}\right) + \bar{P}_1(\boldsymbol{m})\left(V_1(x) - V_1(\bar{x}(\boldsymbol{m}))\right) \\
&\quad + m_2 C_v(T_2 - T_o) + m_2 R T_o \log\left(\frac{\bar{P}_2(\boldsymbol{m})}{P_{2_b}}\right) + \bar{P}_2(\boldsymbol{m})\left(V_2(x) - V_2(\bar{x}(\boldsymbol{m}))\right)
\end{aligned} \tag{4.88}$$

Using the pressure-temperature relationship from Eq. (4.80) to express P_{1_a} in terms of P_1, and similarly using the pressure-temperature relationship from Eq. (4.80) and Eq. (4.83) to express P_{2_b} in terms of P_2, the work $\bar{W}_{act}(\boldsymbol{m}, \boldsymbol{P}, \boldsymbol{T})$ extracted along the proposed trajectory for the two-chambered actuator is obtained as,

$$\begin{aligned}
\bar{W}_{act}(\boldsymbol{m}, \boldsymbol{P}, \boldsymbol{T}) &= m_1 C_v(T_1 - T_o) + m_1 T_o\left(R\log\left(\frac{\bar{P}_1(\boldsymbol{m})}{P_1}\right) + C_p\log\left(\frac{T_o}{T_1}\right)\right) \\
&\quad + m_2 C_v(T_2 - T_o) + m_2 T_o\left(R\log\left(\frac{\bar{P}_2(\boldsymbol{m})}{P_2}\right) + C_p\log\left(\frac{T_o}{T_2}\right)\right) \\
&\quad + \bar{P}_1(\boldsymbol{m})\left(V_1(x) - V_1(\bar{x}(\boldsymbol{m}))\right) + \bar{P}_2(\boldsymbol{m})\left(V_2(x) - V_2(\bar{x}(\boldsymbol{m}))\right)
\end{aligned} \tag{4.89}$$

On using the relationship between the chamber volumes $V_i(x)$ and the piston position x from Eq. (4.51), the definition of entropy change ($\sigma(P_i, T_i) - \sigma(\bar{P}_i(\boldsymbol{m}), T_o)$) from Eq. (4.87) and the relationship between the equilibrium pressures $\bar{P}_1(\boldsymbol{m})$ and $\bar{P}_2(\boldsymbol{m})$ from

Eq. (4.59), the available work $\bar{W}_{act}(\boldsymbol{m}, \boldsymbol{P}, \boldsymbol{T})$ in the above equation can be simplified to the desired form in Eq. (4.86) as,

$$\begin{aligned}\bar{W}_{act}(\boldsymbol{m}, \boldsymbol{P}, \boldsymbol{T}) = {} & m_1 C_v (T_1 - T_o) - m_1 T_o (\sigma(P_1, T_1) - \sigma(\bar{P}_1(\boldsymbol{m}), T_o)) \\ & + m_2 C_v (T_2 - T_o) - m_2 T_o (\sigma(P_2, T_2) - \sigma(\bar{P}_2(\boldsymbol{m}), T_o)) \\ & - P_o A_p (\bar{x}(\boldsymbol{m}) - x)\end{aligned} \tag{4.90}$$

Using the definition of density of air $\rho(P, T) := P/RT = m/V(x)$, and from the definition of gravimetric energy density $W_m(.)$ for a single-chambered actuator in Eq. (4.36), the available work from the two-chambered actuator can be expressed as,

$$\bar{W}_{act}(\boldsymbol{m}, \boldsymbol{P}, \boldsymbol{T}) = m_1 W_m(P_1, T_1, \bar{P}_1(\boldsymbol{m}), T_o) + m_2 W_m(P_2, T_2, \bar{P}_2(\boldsymbol{m}), T_o) \tag{4.91}$$

As shown in remark 4.4, the gravimetric energy density $W_m(P, T, P_o, T_o)$ for a single-chambered actuator is a positive definite function for any pair of pressures $(P, P_o) \in \Re^+$ and temperatures $(T, T_o) \in \Re^+$, and is identically equal to zero only at the equilibrium state ($P = P_o$ and $T = T_o$). As the air mass is always positive, the storage function as defined in Eq. (4.91) is the sum of two positive functions, and hence is always positive for feasible air mass $\boldsymbol{m}$, pressure $\boldsymbol{P}$ and temperature $\boldsymbol{T}$ in each actuator chamber. The storage function is also identically zero at the equilibrium state of the two-chambered actuator which is characterized by, $P_1 = \bar{P}_1(\boldsymbol{m})$, $T_1 = T_o$, $P_2 = \bar{P}_2(\boldsymbol{m})$ and $T_2 = T_o$.

□

Remark 4.5. *The trajectory for extracting maximum available energy from the actuator in Theorem 4.3 is not unique. Similar to the single-chambered actuator, each chamber of the two-chambered actuator can cycle indefinitely along an adiabatic or an isothermal segment of the proposed trajectory before reaching the equilibrium position $\bar{x}(\boldsymbol{m})$. As the net work done in a cyclic path is always zero, maximum available energy along all such class of trajectories will be same and is as given in Eq. (4.86).*

Remark 4.6. *The maximum available energy from the two-chambered actuator in Eq. (4.86) is less than the sum total of maximum energy that can be extracted from the decoupled single chambers of the actuator.*

Proof. Let m_1, m_2 be the air mass, P_1, P_2 be the air pressure, and T_1, T_2 be the air temperature in chamber 1 and 2 respectively of the two-chambered actuator. The maximum available energy for the two-chambered actuator is as given in Eq. (4.91).

For ambient pressure P_o and ambient temperature T_o, using the definition of gravimetric energy density $W_m(P, T, P_o, T_o)$ for a single-chambered actuator from Eq. (4.36), the sum of the maximum energy that can be extracted from each decoupled chamber is given by,

$$W_t(\boldsymbol{m}, \boldsymbol{P}, \boldsymbol{T}) = m_1 W_m(P_1, T_1, P_o, T_o) + m_2 W_m(P_2, T_2, P_o, T_o) \tag{4.92}$$

The sum $W_t(\boldsymbol{m}, \boldsymbol{P}, \boldsymbol{T})$ in the above equation can be expressed in terms of the equilibrium pressures, $\bar{P}_1(\boldsymbol{m})$ and $\bar{P}_2(\boldsymbol{m})$ as,

$$\begin{aligned} W_t(\boldsymbol{m}, \boldsymbol{P}, \boldsymbol{T}) &= m_1(W_m(P_1, T_1, \bar{P}_1(\boldsymbol{m}), T_o) + W_m(\bar{P}_1(\boldsymbol{m}), T_o, P_o, T_o)) \\ &\quad + m_2(W_m(P_2, T_2, \bar{P}_2(\boldsymbol{m}), T_o) + W_m(\bar{P}_2(\boldsymbol{m}), T_o, P_o, T_o)) \\ &= \bar{W}_{act}(\boldsymbol{m}, \boldsymbol{P}, \boldsymbol{T}) + m_1 W_m^{iso}(\bar{P}_1(\boldsymbol{m}), P_o) + m_2 W_m^{iso}(\bar{(}P_2\boldsymbol{m}), P_o) \end{aligned} \tag{4.93}$$

where $W_m^{iso}(P, P_o)$ is the gravimetric energy density along an isothermal trajectory and as shown in theorem 3.2 is a non-negative function for all $(P, P_o) \in \Re^+$. Therefore, the sum of the maximum available energy from each chamber of the decoupled two-chambered actuator $W_t(\boldsymbol{m}, \boldsymbol{P}, \boldsymbol{T})$ is related to the maximum available energy from the two-chambered actuator as,

$$W_t(\boldsymbol{m}, \boldsymbol{P}, \boldsymbol{T}) \geq \bar{W}_{act}(\boldsymbol{m}, \boldsymbol{P}, \boldsymbol{T}) \tag{4.94}$$

□

As stated for the single-chambered actuator, the maximum available energy from the two-chambered actuator in Eq. (4.86) represent the upper bound of the energy available from the actuator and cannot be realized in typical real life applications. In the following section, supply rate for achieving energetically passive interaction with the two-chambered pneumatic actuator is presented.

4.2.3 Passivity property of two-chambered actuator

The air temperature T_{u_i} upstream of the direction air flow to each chamber is as defined in Eq. (4.53). As defined in Eq. (4.43), let $\Phi_{ht}(P_i, T_{u_i}, \bar{P}_i(\boldsymbol{m}), T_o)$ be the sum of the gravimetric energy density $W_m(P_i, T_{u_i}, \bar{P}_i(\boldsymbol{m}), T_o)$ and the flow work $(P_i -$

$\bar{P}_i(\boldsymbol{m}))/\rho(P_i, T_{u_i})$ for the i^{th} chamber as,

$$\Phi_{ht}(P_i, T_{u_i}, \bar{P}_i(\boldsymbol{m}), T_o) := \left(W_m(P_i, T_{u_i}, \bar{P}_i(\boldsymbol{m}), T_o) + \frac{P_i - \bar{P}_i(\boldsymbol{m})}{\rho(P_i, T_{u_i})} \right) \tag{4.95}$$

From the definition of the time derivative of the available energy from a single-chambered actuator in Eq. (4.41), the time derivative $\dot{\bar{W}}_{act}(\boldsymbol{m}, \boldsymbol{P}, \boldsymbol{T})$ of available energy from the two-chambered actuator is obtained as,

$$\begin{aligned} \dot{\bar{W}}_{act}(\boldsymbol{m}, \boldsymbol{P}, \boldsymbol{T}) = \sum_{i=1}^{2} \Bigg(\dot{m}_i \left(\Phi_{ht}(P_i, T_{u_i}, \bar{P}_i(\boldsymbol{m}), T_o) + C_p(T_i - T_o) \left(\frac{T_{u_i}}{T_i} - 1 \right) \right) \\ -(P_i - \bar{P}_i(\boldsymbol{m}))\dot{V}_i - \dot{\bar{P}}_i(\boldsymbol{m}) \left(V_i(\bar{x}(\boldsymbol{m})) - V_i(x) \right) + \dot{Q}_i \left(1 - \frac{T_o}{T_i} \right) \Bigg) \end{aligned} \tag{4.96}$$

where from Eq. (4.53), $T_{u_i} = T_o$ if $\dot{m}_i \geq 0$, and $T_{u_i} = T_i$ if $\dot{m}_i < 0$. In the following section, passivity property of a two-chambered actuator with two independent ports for fluid interaction is presented.

Two-chambered actuator with two independent fluid ports

Theorem 4.4. *For a given air mass m_1, m_2, pressure P_1, P_2, temperature T_1, T_2, and heat transfer coefficients of the cylinder walls $h_1^2(t)$, $h_2^2(t)$ in chamber 1 and 2 of the two-chambered actuator respectively, assuming that there is no thermal interaction between each chamber and that the heat transfer rates $\dot{Q}_1$ and $\dot{Q}_2$ between chamber 1 and the ambient, and chamber 2 and the ambient respectively are given by,*

$$\dot{Q}_1 = h_1^2(t)(T_o - T_1), \qquad \dot{Q}_2 = h_2^2(t)(T_o - T_2) \tag{4.97}$$

and for an upstream air temperature of T_{u_1} and T_{u_2} for chambers 1 and 2 respectively as defined in Eq. (4.53), the two-chambered actuator is passive with respect to the following supply rate,

$$\begin{aligned} s_{ht_{2m}}((\dot{m}_1, \Phi_{ht}(P_1, T_{u_1}, \bar{P}_1(\boldsymbol{m}), T_o)), (\dot{m}_2, \Phi_{ht}(P_2, T_{u_2}, \bar{P}_2(\boldsymbol{m}), T_o)), (F_a(\boldsymbol{P}), \dot{x})) \\ = \dot{m}_1 \Phi_{ht}(P_1, T_{u_1}, \bar{P}_1(\boldsymbol{m}), T_o) + \dot{m}_2 \Phi_{ht}(P_2, T_{u_2}, \bar{P}_2(\boldsymbol{m}), T_o) - F_a(\boldsymbol{P})\dot{x} \end{aligned} \tag{4.98}$$

where $\Phi_{ht}(P_i, T_{u_i}, \bar{P}_i(\boldsymbol{m}), T_o)$ is as defined in Eq. (4.95) and represents the effort variable at the fluid port of the $i^{th} \in (1, 2)$ chamber of the two-chambered actuator, with the corresponding flow variable being $\dot{m}_i$. The actuator force $F_a(\boldsymbol{P})$ is the effort variable at

the mechanical port of the actuator with the piston velocity $\dot{x}$ being the corresponding flow variable.

Proof. Let the maximum available energy $\bar{W}_{act}(\boldsymbol{m}, \boldsymbol{P}, \boldsymbol{T})$ in Eq. (4.91) be the storage function for the two-chambered actuator. As shown in theorem 4.3, the maximum available energy is a positive definite function of the states $(\boldsymbol{m}, \boldsymbol{P}, \boldsymbol{T})$. The time derivative of this storage function $\dot{\bar{W}}_{act}(\boldsymbol{m}, \boldsymbol{P}, \boldsymbol{T})$ is obtained as given in Eq. (4.96).

Due to entropy generated from mixing of air at two different temperatures (T_{u_i} and T_i), as shown in Eq. (4.45), the derivative of the energy function $\dot{\bar{W}}_{act}(\boldsymbol{m}, \boldsymbol{P}, \boldsymbol{T})$ satisfies the following inequality,

$$\begin{aligned}\dot{\bar{W}}_{act}(\boldsymbol{m}, \boldsymbol{P}, \boldsymbol{T}) \leq \sum_{i=1}^{2} \Big(& \dot{m}_i \Phi_{ht}(P_i, T_{u_i}, \bar{P}_i(\boldsymbol{m}), T_o) - \dot{\bar{P}}_i(\boldsymbol{m}) \left(V_i(\bar{x}) - V_i(x)\right) \\ & -(P_i - \bar{P}_i(\boldsymbol{m}))\dot{V}_i + \dot{Q}_i \left(1 - \frac{T_o}{T_i}\right)\Big)\end{aligned} \tag{4.99}$$

From the definition of the heat transfer rates $\dot{Q}_1$ and $\dot{Q}_2$ in Eq. (4.97), the power interaction at the thermal port of the actuator satisfies the following dissipativity condition,

$$\dot{Q}_1 \left(1 - \frac{T_o}{T_1}\right) \leq 0, \qquad \dot{Q}_2 \left(1 - \frac{T_o}{T_2}\right) \leq 0 \tag{4.100}$$

From the relationship between the equilibrium pressures $\bar{P}_1(\boldsymbol{m})$, $\bar{P}_2(\boldsymbol{m})$ in Eq. (4.59), the pressure derivatives $\dot{\bar{P}}_1(\boldsymbol{m})$ and $\dot{\bar{P}}_2(\boldsymbol{m})$ are related as,

$$\dot{\bar{P}}_1(\boldsymbol{m}) A_1 = \dot{\bar{P}}_2(\boldsymbol{m}) A_2 \tag{4.101}$$

Using the dissipativity condition from Eq. (4.100), the relationship between $\dot{\bar{P}}_1(\boldsymbol{m})$ and $\dot{\bar{P}}_2(\boldsymbol{m})$ from the above equation, the relationship between $V_i(x)$ and the actuator position x from Eq. (4.51), and the definition of the actuator force $F_a(\boldsymbol{P})$ from Eq. (4.57), the derivative of the storage function $\dot{\bar{W}}_{act}(\boldsymbol{m}, \boldsymbol{P}, \boldsymbol{T})$ in Eq. (4.99) can be expressed in terms of the supply rate $s_{ht_{2m}}(.)$ in Eq. (4.98) as,

$$\begin{aligned}&\dot{\bar{W}}_{act}(\boldsymbol{m}, \boldsymbol{P}, \boldsymbol{T}) \leq \dot{m}_1 \Phi_{ht}(P_1, T_{u_1}, \bar{P}_1(\boldsymbol{m}), T_o) + \dot{m}_2 \Phi_{ht}(P_2, T_{u_2}, \bar{P}_2(\boldsymbol{m}), T_o) - F_a(\boldsymbol{P})\dot{x} \\ &= s_{ht_{2m}}((\dot{m}_1, \Phi_{ht}(P_1, T_{u_1}, \bar{P}_1(\boldsymbol{m}), T_o)), (\dot{m}_2, \Phi_{ht}(P_2, T_{u_2}, \bar{P}_2(\boldsymbol{m}), T_o)), (F_a(\boldsymbol{P}), \dot{x}))\end{aligned} \tag{4.102}$$

Integrating both sides of the above equation, and using the condition that the storage function $\bar{W}_{act}(\boldsymbol{m}, \boldsymbol{P}, \boldsymbol{T})$ is positive for all time t, the supply rate in Eq. (4.98) is shown to satisfy the following passivity condition,

$$\int_0^t s_{ht_{2m}}((\dot{m}_1, \Phi_{ht}(P_1, T_{u_1}, \bar{P}_1(\boldsymbol{m}), T_o)), (\dot{m}_2, \Phi_{ht}(P_2, T_{u_2}, \bar{P}_2(\boldsymbol{m}), T_o)), (F_a, \dot{x}))\ d\tau \geq -\bar{W}_{act}(\boldsymbol{m}, \boldsymbol{P}, \boldsymbol{T})\Big|_{t=0} \tag{4.103}$$

where $\bar{W}_{act}(\boldsymbol{m}, \boldsymbol{P}, \boldsymbol{T})\Big|_{t=0} > 0$ represents the value of the storage function $\bar{W}_{act}(\boldsymbol{m}, \boldsymbol{P}, \boldsymbol{T})$ at time $t = 0$. □

Passivity properties of a two-chambered actuator with a single valve for metering the air flow to the actuator chambers is presented in the following section.

Two-chambered actuator with the two fluid ports coupled by a single valve

When using a single valve for metering the air flow to the actuator, as given in Eq. (3.84), the mass flow rates $\dot{m}_1$ and $\dot{m}_2$ are related to the valve input command u as,

$$\dot{m}_1 = \Psi(P_1, T_{u_1}, u)u, \qquad \dot{m}_2 = -\Psi(P_2, T_{u_2}, -u)u \tag{4.104}$$

The time derivative of the storage function $\dot{\bar{W}}_{act}(\boldsymbol{m}, \boldsymbol{P}, \boldsymbol{T})$ in Eq. (4.102) can be expressed in terms of the valve input command u as,

$$\begin{aligned}\dot{\bar{W}}_{act}(\boldsymbol{m}, \boldsymbol{P}, \boldsymbol{T}) \leq \big(&\Psi(P_1, T_{u_1}, u)\Phi_{ht}(P_1, T_{u_1}, \bar{P}_1(\boldsymbol{m}), T_o) \\ &-\Psi(P_2, T_{u_2}, -u)\Phi_{ht}(P_2, T_{u_2}, \bar{P}_2(\boldsymbol{m}), T_o)\big)\, u - F_a(\boldsymbol{P})\dot{x}\end{aligned} \tag{4.105}$$

The effort variable $Z_\gamma^{ht}(\boldsymbol{m}, \boldsymbol{P}, \boldsymbol{T}, u)$ corresponding to the valve command input u on the *r.h.s* of the above equation is defined as,

$$\begin{aligned}Z_\gamma^{ht}(\boldsymbol{m}, \boldsymbol{P}, \boldsymbol{T}, u) = &\Psi(P_1, T_{u_1}, u)\Phi_{ht}(P_1, T_{u_1}, \bar{P}_1(\boldsymbol{m}), T_o) \\ &- \Psi(P_2, T_{u_2}, -u)\Phi_{ht}(P_2, T_{u_2}, \bar{P}_2(\boldsymbol{m}), T_o)\end{aligned} \tag{4.106}$$

Theorem 4.5. *The two-chambered pneumatic actuator with a single valve for metering air flow to the actuator is passive with respective to the following supply rate,*

$$s_{ht_{2u}}((u, Z_\gamma^{ht}(\boldsymbol{m}, \boldsymbol{P}, \boldsymbol{T}, u), (F_a(\boldsymbol{P}), \dot{x})) = Z_\gamma^{ht}(\boldsymbol{m}, \boldsymbol{P}, \boldsymbol{T}, T_o, u)u - F_a(\boldsymbol{P})\dot{x} \tag{4.107}$$

where $Z_\gamma^{ht}(\boldsymbol{m}, \boldsymbol{P}, \boldsymbol{T}, T_o, u)$ as defined in Eq. (4.106) is the effort variable at the actuator fluid port, with the valve command input u being the flow variable at the fluid port. The actuator force $F_a(\boldsymbol{P})$ is as defined in Eq. (4.57) and corresponds to the effort variable at the mechanical port of the actuator, while $\dot{x}$ is the corresponding flow variable.

Proof. Let the maximum available energy $\bar{W}_{act}(\boldsymbol{m}, \boldsymbol{P}, \boldsymbol{T})$ from the two-chambered actuator in Eq. (4.91) be defined as the storage function. From the definition of $Z_\gamma^{ht}(.)$ in Eq. (4.106), the derivative of the storage function $\dot{\bar{W}}_{act}(\boldsymbol{m}, \boldsymbol{P}, \boldsymbol{T})$ as given in Eq. (4.105) is related to the supply rate $s_{ht_{2u}}(.)$ in Eq. (4.107) as,

$$\begin{aligned} \dot{\bar{W}}_{act}(\boldsymbol{m}, \boldsymbol{P}, \boldsymbol{T}) &\leq Z_\gamma^{ht}(\boldsymbol{m}, \boldsymbol{P}, \boldsymbol{T}, T_o, u)u - F_a(\boldsymbol{P})\dot{x} \\ &= s_{ht_{2u}}((u, Z_\gamma^{ht}(\boldsymbol{m}, \boldsymbol{P}, \boldsymbol{T}, u), (F_a(\boldsymbol{P}), \dot{x})) \end{aligned} \tag{4.108}$$

Integrating both sides of the above equation and using the condition from theorem 4.3 that the storage function $\bar{W}_{act}(\boldsymbol{m}, \boldsymbol{P}, \boldsymbol{T})$ is always positive, the supply rate $s_{ht_{2u}}(.)$ in Eq. (4.107) satisfies the following passivity condition,

$$\int_0^t s_{ht_{2u}}((u, Z_\gamma^{ht}(\boldsymbol{m}, \boldsymbol{P}, \boldsymbol{T}, u), (F_a(\boldsymbol{P}), \dot{x}))\ d\tau \geq -\bar{W}_{act}(\boldsymbol{m}, \boldsymbol{P}, \boldsymbol{T})\Big|_{t=0} \tag{4.109}$$

where $\bar{W}_{act}(\boldsymbol{m}, \boldsymbol{P}, \boldsymbol{T})\Big|_{t=0} \in \Re^+$ corresponds to the value of the storage function at time $t = 0$. □

Similar to the supply rate for adiabatic and isothermal actuators in Eq. (3.132) and Eq. (3.118) respectively, the supply rate $s_{ht_{2u}}((u, Z_\gamma^{ht}(\boldsymbol{m}, \boldsymbol{P}, \boldsymbol{T}, u), (F_a(\boldsymbol{P}), \dot{x}))$ to the two-chambered actuator in Eq. (4.107) has two ports, one port corresponding to the power interaction at the fluid port $(Z_\gamma^{ht}(\boldsymbol{m}, \boldsymbol{P}, \boldsymbol{T}, T_o, u)u)$, while the other port corresponding to mechanical power interaction $(-F_a(\boldsymbol{P})\dot{x})$.

For the isothermal and the adiabatic actuators, it is shown in propositions 3.3 and 3.4 respectively that the fluid port effort variable $Z_\gamma^{iso,adb}(.)$ is a monotonic function of the actuator force $F_a(\boldsymbol{P})$. In establishing this monotonic mapping, relationship between the chamber pressure P and the chamber temperature T along the isothermal $(T = T_o)$ or adiabatic (Eq. (3.32)) trajectories is used to express the fluid port effort variable as a function of the chamber pressures P_1 and P_2 only. However, for the actuator with finite

heat transfer, the chamber temperature depends on both the chamber pressure and the heat transfer across the actuator walls. As a result, there will be a combination of chamber pressures P_1, P_2 for chamber temperatures $T_1 \neq T_o$ and $T_2 \neq T_o$ corresponding to a zero actuator force $F_a(\boldsymbol{P})$ but a non-zero value of effort variable $Z_\gamma^{ht}(.)$ in Eq. (4.106). Thus, the fluid port effort variable $Z_\gamma^{ht}(.)$ cannot be expressed as a monotonic function of the actuator force $F_a(\boldsymbol{P})$. In addition, due to the irreversible nature of heat transfer, pneumatic actuator with finite heat transfer cannot be interpreted as a two-port nonlinear spring. Consequently, it is difficult to a supply rate for the error dynamics of a two-chambered actuator with heat transfer in a fashion similar to the adiabatic and the isothermal actuators presented in section 3.3.

4.3 Summary

In this chapter, storage function for a pneumatic actuator with finite heat interaction with the ambient is reported. As a preliminary step, storage function for a single-chambered actuator is provided. The storage function is defined as the maximum available work in the actuator and the optimal trajectory for extracting maximum work from the actuator are identified. The work extracted along this optimal trajectory is determined to be similar to exergy of air in the single-chambered pneumatic actuator. For the two-chambered pneumatic actuator, the storage function is defined to be the sum of maximum work available from each actuator chamber, as the actuator traverses to the equilibrium position $\bar{x}(\boldsymbol{m})$. The heat transfer coefficient $h^2(t)$ and the piston velocity $\dot{x}(t)$ required to extract the maximum available energy from the actuator are however difficult to realize in real physical applications. Therefore, the maximum available actuator energy derived in this chapter corresponds to the upper bound of the energy that can be extracted from the actuator. The storage functions for both the single-chambered and the two-chambered actuator are used to define the appropriate supply rate for energetically passive interaction with the respective actuators. The external supply rate shows that there are three ports for energetic interaction with a pneumatic actuator with finite heat transfer : the mechanical port, the fluid port and the thermal port. The port power variable obtained from the storage function demonstrate that the actuators can have a lossless connection at the mechanical port of the actuator. At

the fluid port of the actuator it is noticed that if the upstream air temperature at the chamber inlet T_u is different from the chamber temperature T, then mixing of air at these two different temperatures has a dissipative effect on the available storage of the actuator. This loss in work potential is due to entropy generated by mixing of air at two different temperatures. In addition, unlike the isothermal and the adiabatic actuators, the effort variable at fluid port of the actuator with finite heat transfer cannot be expressed as a monotonic function of the actuator force. At the thermal port of the actuator, it is observed that irrespective of the chamber temperature, heat transfer between the actuator and the ambient will always lead to loss in the ability of the actuator to do work. Therefore heat transfer has a dissipative effect on the actuator supply rate.

In the following chapters, the energy functions developed for the two-chambered pneumatic actuators in chapter 3 are used to define energetically passive controller for human interactive applications.

Chapter 5

Single-DOF Human Power Amplifier Control

In this chapter, control of a two-chambered pneumatic actuator in a single DOF human power amplifier is investigated. The human power amplifier is intended to be a directly operable device for amplifying input power from an interacting human operator. Typical applications of a human power amplifier include, but not limited to, enabling humans to move heavy loads in a warehouse, or help people with muscular disabilities perform simple tasks requiring force input. In these applications, the power amplifier could take the form of an exo-skeleton directly attached to the operator. Most tasks executed by the operator through the power amplifier are typically in the immediate vicinity of the operator.

The power density of pneumatic actuators enables compact design of human power amplifier, while providing the required power output. The high force often associated with such applications, and the nature of these applications requiring direct human interaction necessitates design of features that guarantee safe and intuitive interaction. As shown in previous studies [3], interaction between passive systems is always guaranteed to be stable. Most environments exhibit passive behavior, and as shown in [4], human muscle dynamics can be approximated to be passive. If the pneumatic actuator also behaves as a passive system, then safe interaction between the operator, the actuator and the environment can be guaranteed.

The earliest work on human power amplifiers with fluid powered actuators was reported in [46]. The authors in [46] refer to the human power amplifier as *human extenders*. These human extenders used hydraulic actuators to provide the actuation force. Linearized system dynamics were assumed in [46] to design controllers for human power amplification. Passivity of operation was however not enforced on the power amplifier.

A novel method for energetically passive operation of human power amplification with hydraulic actuators was reported in [59]. The hydraulic actuator is modeled as a combination of an ideal actuator (velocity source) with no compressibility and a spring for modeling the compressibility effect of the actuating fluid. By formulating the ideal velocity as the velocity of a virtual inertia, an energetically passive structure is obtained. In [60], a general framework of this approach using a storage function method was presented for both hydraulic and pneumatic actuators. The storage function reported for hydraulic and pneumatic actuators in [60] was however designed by assuming the actuator to be a linear spring. In [66] a physics based energy function was developed for hydraulic actuators. Passive controllers for position tracking with the hydraulic actuator by using the energy function as the Lyapunov function were also presented in [66].

In the current chapter, the energy functions developed in chapter 3 for adiabatic and isothermal actuators is used to define passive controllers for achieving human power amplification with pneumatic actuators. As shown in chapter 3, both isothermal and adiabatic actuators can be modeled as a two-port nonlinear spring, with one port available for lossless interconnection with mechanical systems. The other port of the actuator corresponds to interaction with the fluid source. The flow variable at the fluid port represents a pseudo-velocity input to the nonlinear spring and includes the command input to the actuator flow control valve. This two-port representation of the pneumatic actuator is analogous to the port representation of hydraulic system in [66].

The mass flow rate to the pneumatic actuator is typically provided from compressed air sources with very high energy content. In open loop operation, for a finite value of the input command, a large amount of energy can be transferred from the source of compressed air to the pneumatic actuator. In such state of operation, the two-chambered pneumatic actuator will not satisfy the passivity condition in Eq. (3.137).

Passive behavior can however be imposed on the actuator by appropriately controlling the pseudo-velocity input at the actuator fluid port and thus regulating the energy transfer between actuator and the source of compressed air. Following the approach presented in [59], the flow variable at the fluid port is defined to be the sum of the inertial velocity of a virtual mass and a feedback control input. In this chapter, the feedback control input design for the specific application of human power amplification is reported. To evaluate the effect of thermodynamics on the actuator performance, independent controllers are developed for both isothermal and adiabatic models of the actuator.

Inertial dynamics of the human power amplifier, and the problem of human power amplification are presented in section 5.1. As only isothermal and adiabatic actuators are considered in this chapter, a brief overview of the actuator dynamics is presented in 5.2. For detailed description of the actuator dynamics please refer of chapter 3. Controller design for achieving human power amplification is provided in section 5.3. Modifications to the proposed controller for preserving passive operation are presented in section 5.4. Implementation results validating efficacy of the controllers for both isothermal and adiabatic actuators are provided in section 5.5.

5.1 Problem statement

Figure (5.1) illustrates a potential application of human power amplifier in a warehouse, wherein the task involves repetitively moving heavy loads. The force $F_h(t)$ exerted by the human operator must overcome the external force $F_e(t)$ due to gravity, friction and any other unknown/un-modeled forces. Additional power input from the pneumatic actuator can aid the human operator in moving the loads more effectively. An interface with a sensor for measuring the input force is provided for the human operator to directly interact with the power amplifier. The power input at this interface by the operator, when amplified by the pneumatic actuator, enables the operator to intuitively move heavy loads with much ease.

The dynamics of the inertial mass M_p being moved in Fig. (5.1) is given by,

$$M_p\ddot{x} = F_h(t) + F_e(t) + F_a \tag{5.1}$$

where x corresponds to position of the inertia and F_a is the force exerted by the actuator.

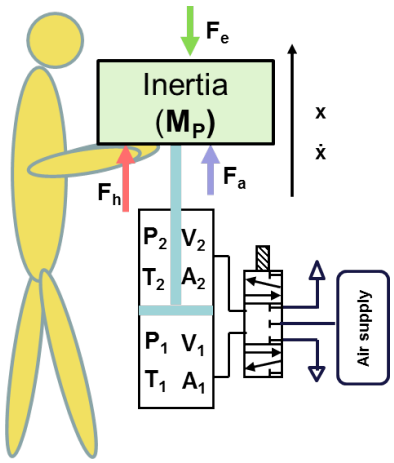

Figure 5.1: Schematic of an application requiring human power amplification. The user is trying to lift a heavy load. The force input is being amplified through the pneumatic actuator and is aiding to comfortably move the load.

A pneumatic actuator with an inbuilt piston position sensor is used in this study. This sensor is used to determine the position of the inertia relative to the actuator. Velocity of the inertia is estimated from the position measurement. By defining the inertia velocity $\dot{x}$ as the relevant output measurement of the amplifier and for a power scaling factor of $\rho \in \Re^{+}$, the desired external supply rate for the human power amplifier is defined by,

$$s(F_h, F_e, \dot{x}) := (\rho + 1)F_h(t)\dot{x} + F_e(t)\dot{x} \tag{5.2}$$

To achieve energetically passive operation of the power amplifier, the system should satisfy the following passivity condition for all time t [3] with respect to the supply rate $s(F_h, F_e, \dot{x})$ in Eq. (5.2),

$$\int_0^t s(F_h, F_e, \dot{x})\ d\tau \geq -c^2 \tag{5.3}$$

where c^2 represents a positive constant. The above inequality implies that the power amplifier requires energy input from external agents to do any work on the object to be moved. The constant c^2 in the above inequality typically corresponds to the initial available energy that can be used to do limited work in the absence of external power input. Once this energy is expended, and with no additional input power, a passive power amplifier will remain at a dead state, and would thus be stable.

As both the power amplifier and the operator's hand move with the same velocity $\dot{x}$, power amplification can be achieved through force amplification as,

$$F_a = \rho F_h(t) \tag{5.4}$$

If the actuator is able to provide the force F_a as desired in the above equation, the dynamics of the inertia in Eq. (5.1) would become,

$$M_p\ddot{x} = (\rho + 1)F_h(t) + F_e(t) \tag{5.5}$$

The forces on the *r.h.s* of the above equation correspond to the desired external forces on the inertia. Note that the passivity condition in Eq. (5.3) is naturally satisfied for the desired inertia dynamics in Eq. (5.5), with the constant c^2 corresponding to amplified initial kinetic energy of the inertia.

The actuator force F_a depends on the pressures P_1 and P_2 in chambers 1 and 2 of the two-chambered actuator and as presented in Eq. (3.1) is given by,

$$F_a = P_1A_1 - P_2A_2 - P_oA_p \tag{5.6}$$

where A_1 is the piston cross-sectional area in chamber 1, A_2 is the piston cross-sectional area in chamber 2, while $A_p = (A_1 - A_2)$ is the rod area exposed to ambient pressure P_o. The pressures P_1 and P_2 are measured by using pressure sensors attached at the inlet of each actuator chamber. The actuator force output can be varied as desired by varying the pressure in the actuator chambers. Pressure dynamics for isothermal and adiabatic actuators and the control inputs available in these actuators for varying the chamber pressures are briefly revisited in the next section.

5.2 Isothermal and adiabatic actuator dynamics

In this section, pressure dynamics of both isothermal and adiabatic actuators derived in section 3.2.1 are briefly presented for completeness.

For a piston position of x, the volume $V_1(x)$ of chamber 1 and $V_2(x)$ of chamber 2 of the actuator are obtained from Eq. (3.73) as,

$$V_1 = A_1(L_{1o} + x), \quad V_2 = A_2(L_{2o} - x) \tag{5.7}$$

Let m_1 and m_2 be the mass of air in chambers 1 and 2 of the actuator respectively. Assuming that air in both chambers of the two-chambered actuator behaves as an ideal gas, and that the inlet air temperature T_{in_i} for the $i^{th} \in (1, 2)$ chamber is the same as the chamber air temperature T_i, the dynamics of pressure P_i in the i^{th} chamber of an isothermal and adiabatic actuator chamber are obtained from Eq. (3.81) and Eq. (3.77) respectively as,

$$\begin{aligned} \textbf{Isothermal actuator:} \quad & \frac{\dot{P}_i}{P_i} = \left(\frac{\dot{m}_i}{m_i} - \frac{\dot{V}_i}{V_i} \right) \\ \textbf{Adiabatic actuator:} \quad & \frac{\dot{P}_i}{P_i} = \gamma \left(\frac{\dot{m}_i}{m_i} - \frac{\dot{V}_i}{V_i} \right) \end{aligned} \tag{5.8}$$

where γ is the ratio of specific heat and has a value of 1.4 for air. The pressure dynamics in the i^{th} chamber can thus be varied by changing the corresponding mass flow rate $\dot{m}_i$.

When using a single valve for metering the air flow, as is the case in this study, the mass flow rates $\dot{m}_1$ and $\dot{m}_2$ to each actuator chamber are related to the valve input command u as,

$$\dot{m}_1 = \Psi(P_1, T_1, u)u, \qquad \dot{m}_2 = \Psi(P_2, T_2, -u)u \tag{5.9}$$

where the nonlinear function $\Psi(.)$ is as defined in Eq. (3.27).

The control objective in the human power amplification problem is to design the input command u to the actuator valve such that the actuator force corresponds to desired amplified human force, with the power amplifier dynamics satisfying the desired passivity condition in Eq. (5.3). Controller design for achieving human power amplification is presented in the next section.

5.3 Controller design

In this section, control input to the pneumatic actuated human power amplifier for achieving the desired supply rate in Eq. (5.2) is derived. As stated earlier, a possible way to achieve the desired supply rate is by formulating a force tracking problem that regulates the force error $(F_a - \rho F_h)$ to zero. However, as shown in a previous study [72] with hydraulic actuator, this approach requires positive feedback of the actuator velocity, causing unstable operation in the presence of uncertainty in the velocity measurement, especially during unconstrained motion. This drawback of the controller is

summarized in the next section. In section 5.3.2, a control design framework for human power amplification with hydraulic actuators as presented in [59] is extended to pneumatic actuators. The controller for the pneumatic actuator is then derived in subsequent sections.

5.3.1 Drawback of force tracking controller

From the equation for the pressure dynamics in both isothermal and adiabatic actuators given in Eq. (5.8) it can be noticed that to achieve the desired pressure (and correspondingly the desired actuator force F_a from Eq. (5.6)), feed-forward compensation of change in chamber volume due to the piston velocity $\dot{x}$ is required. During controller implementation however, accurate compensation of the velocity is not feasible as the velocity of actuator would have changed before the calculated velocity compensation can be applied through the controller. As shown in [72], the positive feedback due to inaccurate compensation of the actuator velocity leads to instabilities in operation of hydraulic actuators in the free space. When interacting with a hard surface, the velocity of the actuator is nearly zero, and therefore the power amplification controller proposed in [72] is effective in providing the desired human power amplification when interacting with a hard surface.

In [59], desired force from the hydraulic actuators is achieved by reformulating the force tracking problem as a velocity co-ordination problem between the inertia being moved and a virtual mechanical inertia. As the nature of operation of pneumatic actuators is similar to hydraulic actuators, the approach proposed in [59] can be adopted for pneumatic systems as well. In the next section, this new frame work for achieving power amplification through velocity co-ordination is presented for actuators with isothermal and adiabatic thermodynamic processes.

5.3.2 Velocity co-ordination controller framework

As shown in chapter 3, isothermal and adiabatic pneumatic actuators can be represented as a two-port system. The power flow variables at different interacting ports of the human power amplifier are as shown in Fig. (5.2). In a typical pneumatic system, the air compressor along with the flow control valves, acts as the flow source in the

schematic. Following the procedure in [59] for hydraulic human power amplification, the flow source in Fig. (5.2) is replaced by a virtual inertia of mass M_v and acted upon by the amplified human force ρF_h and the current actuator force F_a. The schematic for this modified system interconnection is as shown in Fig. (5.3). The inertia mass M_v is referred to as virtual inertia because it is a construct devised for controller design only, and does not represent a real physical inertia.

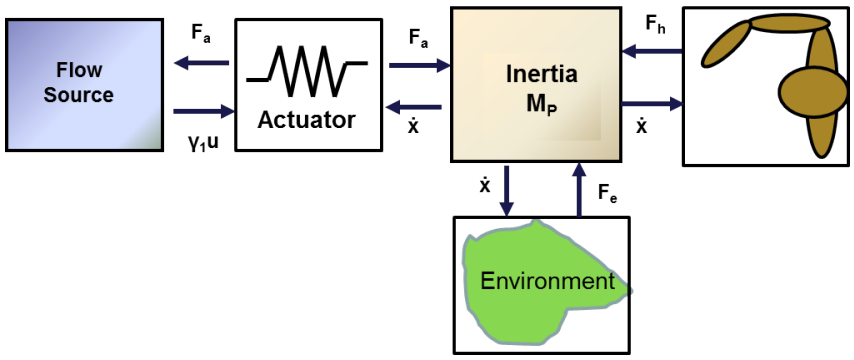

Figure 5.2: Schematic showing the power signal flow and interconnection for a typical isothermal or adiabatic actuator

From Fig. (5.3), inertial dynamics of the virtual mass is obtained as,

$$M_v \ddot{x}_v = (\rho F_h(t) - u_d) - F_a \tag{5.10}$$

where u_d is an additional force input on the virtual mass for shaping the target dynamics of the human power amplifier. The input u_d can for example be used to guide the power amplifier along a certain trajectory.

If the velocities of the inertial elements M_p and M_v are co-ordinated ($i.e\ \dot{x} = \dot{x}_v$), then the dynamics of the co-ordinated system in Fig. (5.3) is given by,

$$(M_p + M_v)\ddot{x} = (\rho + 1)F_h(t) + F_e(t) - u_d \tag{5.11}$$

From the above equation it can be noticed that the inertial dynamics of the combined system are affected by the desired amplified human force and other external forces ($F_e(t)$, u_d) acting on the inertias M_p and M_v. The perceived inertia ($M_p + M_v$) of the dynamics in Eq. (5.11) is higher than the inertia M_p of the desired dynamics in Eq.

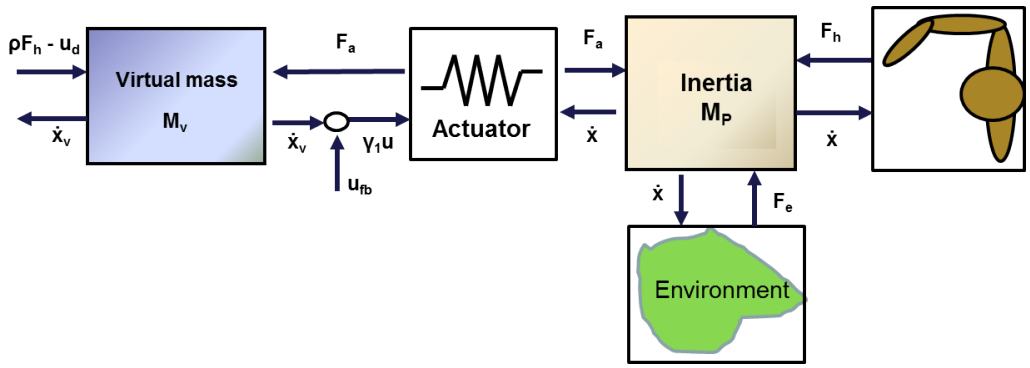

Figure 5.3: Schematic illustrating modification to the actuator input for achieving passive human power amplification. The input u_d is included to preserve passive behavior in closed loop operation.

(5.5). This increase in perceived inertia can be tuned by changing M_v for improving the feel factor, while lending additional stability to the response of the power amplifier. Another difference between the inertial dynamics in Eq. (5.5) and the desired dynamics in Eq. (5.11) is the presence of additional force input u_d. In this study, u_d is used to enforce passive operation of human power amplifier. As will be shown in section 5.4 and section 5.5, u_d is not required during the entire time of operation and the magnitude of the input u_d is fairly small when used for enforcing passivity only. By appropriately selecting the virtual inertia M_v, and due to the small magnitude of u_d, the desired supply rate in Eq. (5.2) is achieved through velocity co-ordination.

The new control objective is therefore to achieve the following velocity co-ordination,

$$V_E \triangleq \dot{x} - \dot{x}_v \to 0 \tag{5.12}$$

while satisfying the passivity condition in Eq. (5.3).

Controller design for velocity co-ordination is typically formulated in the velocity error space. In [30], a passive decomposition is presented to transform the dynamics of individual systems in a tele-operator into two decoupled systems. Decomposition scheme for an n-dof mechanical system with co-ordination requirements is presented in [73]. One of the two decoupled systems, referred to as *Shape system*, represents the dynamics of co-ordination error. The other decoupled system, referred to as *Locked*

system, represents center of mass dynamics of a system consisting of the actual inertia and the virtual inertia. In this study, the passive decomposition proposed in [30] is used to transform the velocity vector space $(\dot{x}, \dot{x}_v)$ of the power amplifier to a space consisting of velocity (V_L) of the system center of mass and the co-ordination velocity error V_E. The decomposition scheme, and the the Locked and the Shape system dynamics in the decomposed space are presented in the next section. Controller design for regulating the velocity error V_E to 0 is presented in subsequent sections.

5.3.3 Passive decomposition

The inertia dynamics of interest for velocity co-ordination control are,

$$\begin{pmatrix} M_p & 0 \\ 0 & M_v \end{pmatrix} \begin{pmatrix} \ddot{x} \\ \ddot{x}_v \end{pmatrix} = \begin{pmatrix} F_h(t) + F_e(t) \\ \rho F_h(t) - u_d \end{pmatrix} + \begin{pmatrix} 1 \\ -1 \end{pmatrix} F_a \tag{5.13}$$

To obtain the matrix for decomposing the velocity space $[\dot{x}, \dot{x}_v]$, define the quantity ϕ as,

$$\phi := \frac{M_v}{M_p + M_v} \tag{5.14}$$

From [30], decomposition of the velocity space is then defined as,

$$\begin{pmatrix} V_L \\ V_E \end{pmatrix} = \underbrace{\begin{pmatrix} 1-\phi & \phi \\ 1 & -1 \end{pmatrix}}_{\boldsymbol{S}} \begin{pmatrix} \dot{x} \\ \dot{x}_v \end{pmatrix} \tag{5.15}$$

where $\boldsymbol{S}$ is the transformation matrix, V_L corresponds to the velocity of the Locked system and V_E represents velocity of the Shape system. The inertial matrix $\boldsymbol{M}_T \in \boldsymbol{R}^{2\times 2}$ of the Locked and the Shape systems is obtained as,

$$\boldsymbol{M}_T = \boldsymbol{S}^{-T} \begin{pmatrix} M_p & 0 \\ 0 & M_v \end{pmatrix} \boldsymbol{S} = \begin{pmatrix} M_L & 0 \\ 0 & M_E \end{pmatrix} \tag{5.16}$$

where M_L and M_E correspond to the inertia of the Locked and the Shape systems respectively and are obtained as,

$$M_L := M_p + M_v, \quad M_E := \frac{M_v M_p}{(M_p + M_v)} \tag{5.17}$$

Decoupling of the Locked and the Shape system inertia in Eq. (5.16) is facilitated by selection of the factor ϕ in Eq. (5.15). The definition of the inertial matrix $\boldsymbol{M_T}$ in Eq. (5.16) satisfies conservation of kinetic energy,

$$\frac{1}{2}\begin{pmatrix} V_L & V_E \end{pmatrix}\boldsymbol{M}_T\begin{pmatrix} V_L \\ V_E \end{pmatrix} = \frac{1}{2}M_p\dot{x}^2 + \frac{1}{2}M_v\dot{x}_v^2 \tag{5.18}$$

Imposing the transformation of inertial matrices presented in Eq. (5.16) on the system dynamics in Eq. (5.13), the decoupled inertia dynamics in the transformed state space are obtained as,

$$M_L\dot{V}_L = (\rho+1)F_h(t) + F_e(t) - u_d \tag{5.19}$$

$$M_E\dot{V}_E = F_a - \rho F_h(t) + \phi((\rho+1)F_h(t) + F_e(t)) + (1-\phi)u_d \tag{5.20}$$

Due to the decoupled dynamics of the Locked and the Shape systems, they can be analyzed as two independent mechanical systems. Comparing the Locked system dynamics in Eq. (5.19) with the desired dynamics in Eq. (5.11), it can be seen that after co-ordination ($\dot{x} = \dot{x}_v = V_L$), the Locked system dynamics represents the desired dynamics of the human power amplifier. By defining the storage function to be the kinetic energy of the Locked system, the desired energetic passivity condition in Eq. (5.2) can be demonstrated after velocity co-ordination is achieved. To this end, the input u_d must be appropriately selected to enforce energetically passive operation. Dynamics of the velocity co-ordination error are given by the Shape system dynamics in Eq. (5.20). Velocity co-ordination is achieved by regulating the Shape system dynamics to zero. Controller design for regulation of Shape system dynamics is presented in the next section.

5.3.4 Velocity co-ordination controller

For ease of analysis, the Shape system dynamics in Eq. (5.20) are expressed as,

$$M_E\dot{V}_E = F_a - F_{ex}(t) \tag{5.21}$$

where $F_{ex}(t)$ is given by,

$$F_{ex}(t) = \rho F_h(t) - \phi((\rho+1)F_h(t) + F_e(t)) - (1-\phi)u_d \tag{5.22}$$

As shown in Eq. (5.6), the actuator force F_a depends on the pressures P_1 and P_2 in chambers 1 and 2 of the actuator, and is independent of the Shape system velocity. Due to this cascaded structure between the inertia dynamics and the actuator dynamics, the controller design for Shape system regulation is achieved in two stages. In the first stage, the required actuator force for regulation of the Shape system dynamics in Eq. (5.21) is identified. In the second stage, command input to the pneumatic actuator valve is designed for providing the desired actuator force identified in the first stage of controller design. This multi-stage approach to controller design is commonly referred to as back-stepping controller design [2]. Design of the required actuator force for regulation of Shape system dynamics is presented in the following section.

First stage controller design

In this section, the desired actuator force for regulation of Shape system velocity is first presented for the situation when perfect information about the force $F_{ex}(t)$ in Eq. (5.22) is available. A controller is then presented if $F_{ex}(t)$ is not perfectly known and has to be estimated by designing an observer.

Perfect information of $F_{ex}(t)$: The system dynamics of interest in the first stage of controller design correspond to the inertial dynamics of the Shape system. Therefore, kinetic energy of the Shape system is the appropriate energy based Lyapunov function candidate for determining the required actuator force for velocity regulation. The Lyapunov function for the first stage of controller design is thus defined as,

$$V_1 = \frac{1}{2} M_E V_E^2 \tag{5.23}$$

As the Lyapunov function in the above equation is a positive definite function of V_E, the Shape system velocity can be regulated by driving the Lyapunov function to zero. Using the Shape system dynamics from Eq. (5.21), the derivative of the above Lyapunov function is obtained as,

$$\dot{V}_1 = V_E(F_a - F_{ex}(t)) \tag{5.24}$$

where $F_{ex}(t)$ is as defined in Eq. (5.22). Suppose that the actuator force F_a can be directly controlled, and let F_a^d represent the actuator force required for regulating of

the Shape system velocity. If the actuator is able to provide the following force,

$$F_a^d = F_{ex}(t) - K_v V_E \tag{5.25}$$

where K_v is a positive constant, then using Eq. (5.23), the derivative of the Lyapunov function can be expressed as,

$$\dot{V}_1 = -K_v V_E^2 = -\frac{2K_v}{M_E} V_1 \tag{5.26}$$

Integrating both side of the above equation, it can be seen that the Lyapunov function exponentially converges to zero. As the Lyapunov function is a positive definite function of V_E, the Shape system velocity also converges exponentially to zero.

Unknown/un-modeled $F_{ex}(t)$: It may be infeasible or expensive to integrate force sensors for measuring all the external forces acting on the system. Forces such as friction are also difficult to model accurately for exact compensation. Therefore, an observer is used to provide an estimate of the force $F_{ex}(t)$ for controller implementation. Let $\hat{F}_{ex}(t)$ represent an estimate of $F_{ex}(t)$. The desired actuator force in Eq. (5.25) is then expressed in terms of the force estimate $\hat{F}_{ex}(t)$ as,

$$F_a^d = \hat{F}_{ex}(t) - K_v V_E \tag{5.27}$$

Using the desired actuator force from the above equation in Eq. (5.21), the Shape system dynamics are obtained as,

$$M_E \dot{V}_E = \hat{F}_{ex}(t) - F_{ex} - K_v V_E = -\tilde{F}_{ex}(t) - K_v V_E \tag{5.28}$$

where $\tilde{F}_{ex} \triangleq (F_{ex} - \hat{F}_{ex})$ is the error in estimating the force $F_{ex}(t)$. From the above equation it can be noticed that the information about the magnitude of error in estimating the force $F_{ex}(t)$ will be embedded in Shape system velocity V_E. Assuming that the Shape system velocity measurement is available, a full-order Luenberger observer dynamics is used to estimate the force $F_{ex}(t)$. For the sake of convenience $F_{ex}(t)$ is assumed to be a constant or slowly varying function, and the observer dynamics are defined as,

$$\begin{aligned} M_E \dot{\hat{V}}_E &= F_a - \hat{F}_{ex} + L_1(V_E - \hat{V}_E) \\ \dot{\hat{F}}_{ex} &= -L_2(V_E - \hat{V}_E) \end{aligned} \tag{5.29}$$

where $\hat{V}_E$ corresponds to the estimate of the Shape system velocity, while L_1 and L_2 are positive constants representing the observer gains. Let $\tilde{V}_E \triangleq (V_E - \hat{V}_E)$ represent the error in estimating the Shape system velocity. The estimation error dynamics in Eq. (5.29) can then be expressed as,

$$\begin{pmatrix} \dot{\tilde{V}}_E \\ \dot{\tilde{F}}_{ex} \end{pmatrix} = \underbrace{\begin{pmatrix} -L_1/M_E & -1/M_E \\ L_2 & 0 \end{pmatrix}}_{\boldsymbol{\mathcal{A}}_o} \begin{pmatrix} \tilde{V}_E \\ \tilde{F}_{ex} \end{pmatrix} \tag{5.30}$$

In the above equation $\boldsymbol{\mathcal{A}}_o$ is a *Hurwitz* matrix. Therefore, the estimation error dynamics in the above equation has exponential convergence. Also, as $\boldsymbol{\mathcal{A}}_o \in \boldsymbol{R}^{2\times 2}$ is *Hurwitz*, for any given positive definite matrix $\boldsymbol{Q}_o \in \boldsymbol{R}^{2\times 2}$, there exists a positive definite matrix $\boldsymbol{P}_o \in \boldsymbol{R}^{2\times 2}$ that satisfies the following Lyapunov equation,

$$\boldsymbol{P}_o \boldsymbol{\mathcal{A}}_o + \boldsymbol{\mathcal{A}}_o^T \boldsymbol{P}_o = -\boldsymbol{Q}_o \tag{5.31}$$

For Shape system with unknown external force $F_{ex}(t)$, consider the following Lyapunov function for designing the desired actuator force F_a^d,

$$V_1(V_E, \tilde{V}_E, \tilde{F}_{ex}) = \frac{1}{2} \begin{pmatrix} V_E \\ \tilde{V}_E \\ \tilde{F}_{ex} \end{pmatrix}^T \underbrace{\begin{pmatrix} M_E & \mathbf{0}_{1\times 2} \\ \mathbf{0}_{2\times 1} & \boldsymbol{P}_o \end{pmatrix}}_{\boldsymbol{\mathcal{Q}}_1} \begin{pmatrix} V_E \\ \tilde{V}_E \\ \tilde{F}_{ex} \end{pmatrix} \tag{5.32}$$

The Lyapunov function $V_1(V_E, \tilde{V}_E, \tilde{F}_{ex})$ in the above equation can be bounded as,

$$\sigma_{min}(\boldsymbol{\mathcal{Q}}_1) \left\| \begin{pmatrix} V_E \\ \tilde{V}_E \\ \tilde{F}_{ex} \end{pmatrix} \right\|_2^2 \leq V_1(V_E, \tilde{V}_E, \tilde{F}_{ex}) \leq \sigma_{max}(\boldsymbol{\mathcal{Q}}_1) \left\| \begin{pmatrix} V_E \\ \tilde{V}_E \\ \tilde{F}_E \end{pmatrix} \right\|_2^2 \tag{5.33}$$

where $\sigma_{min}(.)$ and $\sigma_{max}(.)$ represent the operators for obtaining the minimum and the maximum singular values. The Lyapunov function $V_1(V_E, \tilde{V}_E, \tilde{F}_{ex})$ in Eq. (5.32) is a positive definite function of Shape system velocity V_E, velocity estimation error $\tilde{V}_E$ and the external force estimation error $\tilde{F}_{ex}$. Therefore, if the Lyapunov function has a value of zero, then V_E, $\tilde{V}_E$ and $\tilde{F}_{ex}$ are all identically zero. The desired actuator force is thus designed such that the Lyapunov function converges to zero.

Using the Shape system dynamics from Eq. (5.21), and the Shape system velocity estimation error dynamics from Eq. (5.30), the time-derivative $\dot{V}_1$ of the Lyapunov function in Eq. (5.32) is obtained as,

$$\dot{V}_1(V_E, \tilde{V}_E, \tilde{F}_{ex}) = (F_a - (\hat{F}_{ex} + \tilde{F}_{ex}))V_E + \frac{1}{2}\begin{pmatrix} \tilde{V}_E \\ \tilde{F}_{ex} \end{pmatrix}^T \left(\boldsymbol{P}_o\boldsymbol{\mathcal{A}}_o + \boldsymbol{\mathcal{A}}_o^T\boldsymbol{P}_o\right)\begin{pmatrix} \tilde{V}_E \\ \tilde{F}_{ex} \end{pmatrix} \tag{5.34}$$

If the actuator force F_a corresponds to the desired actuator force F_a^d in Eq. (5.27), and from the Lyapunov equation in Eq. (5.31), the derivative $\dot{V}_1(V_E, \tilde{V}_E, \tilde{F}_{ex})$ in the above equation can be expressed as,

$$\dot{V}_1(V_E, \tilde{V}_E, \tilde{F}_{ex}) = -K_v V_E^2 - \tilde{F}_{ex}V_E - \frac{1}{2}\begin{pmatrix} \tilde{V}_E \\ \tilde{F}_{ex} \end{pmatrix}^T \boldsymbol{Q}_o \begin{pmatrix} \tilde{V}_E \\ \tilde{F}_{ex} \end{pmatrix} \tag{5.35}$$

where $\boldsymbol{Q}_o$ is a positive definite matrix. The required actuator force F_a^d for regulating $V_1(V_E, \tilde{V}_E, \tilde{F}_{ex})$ and consequently V_E to zero is presented in the following theorem.

Theorem 5.1. *If perfect information about the environmental forces $F_{ex}(t)$ in Eq. (5.22) is available, then the Shape system inertial dynamics in Eq. (5.21) will have exponential convergence to zero if the actuator force F_a corresponds to the desired actuator force F_a^d in Eq. (5.25),* i.e. $F_a = F_{ex}(t) - K_v V_E$.

For a constant but unknown external force F_{ex} in Eq. (5.22), exponential convergence of the Shape system velocity V_E to 0 *is achieved if the actuator force F_a corresponds to the desired force F_a^d in Eq. (5.27),* i.e $F_a = \hat{F}_{ex}(t) - K_v V_E$*, where the estimate $\hat{F}_{ex}(t)$ of the force F_{ex} is obtained from the following observer dynamics,*

$$M_E\dot{\hat{V}}_E = F_a - \hat{F}_{ex}(t) + L_1(V_E - \hat{V}_E(t)) \tag{5.36}$$

$$\dot{\hat{F}}_{ex} = -L_2(V_E - \hat{V}_E) \tag{5.37}$$

where $L_1 \in \Re^+$ and $L_2 \in \Re^+$ are the observer gains.

Proof. If the external force $F_{ex}(t)$ is perfectly known, then as given in Eq. (5.23), the Lyapunov function $V_1(V_E)$ can be defined to be a positive definite function of V_E only. From the definition of the desired actuator force $F_a^d(t)$ in Eq. (5.25), the derivative of this Lyapunov function $\dot{V}_1(V_E)$ is obtained as given in Eq. (5.26). On integrating

Eq. (5.26) exponential convergence of the Lyapunov function $V_1(V_E)$ to zero follows. Consequently the Shape system velocity V_E also converges to zero exponentially.

On the other hand, if the external force F_{ex} is constant (or slowly varying), consider the Lyapunov function $V_1(V_E, \tilde{V}_E, \tilde{F}_{ex})$ as defined in Eq. (5.32). If the actuator force F_a corresponds to the desired force $F_a^d(t)$ in Eq. (5.27), then for $\boldsymbol{Q}_o \triangleq \begin{pmatrix} q_o^{11} & q_o^{12} \\ q_o^{21} & q_o^{22} \end{pmatrix}$ derivative of the Lyapunov function $\dot{V}_1(V_E, \tilde{V}_E, \tilde{F}_{ex})$ as given in Eq. (5.35) can be expressed as,

$$\dot{V}_1(V_E, \tilde{V}_E, \tilde{F}_{ex}) = -K_v V_E^2 - \tilde{F}_{ex} V_E - \frac{1}{2} \begin{pmatrix} \tilde{V}_E \\ \tilde{F}_E \end{pmatrix}^T \boldsymbol{Q}_o \begin{pmatrix} \tilde{V}_E \\ \tilde{F}_{ex} \end{pmatrix} \tag{5.38}$$

$$= - \begin{pmatrix} V_E \\ \tilde{V}_E \\ \tilde{F}_{ex} \end{pmatrix}^T \underbrace{\begin{pmatrix} K_v & 0 & 0.5 \\ 0 & q_o^{11} & q_o^{12} \\ 0.5 & q_o^{21} & q_o^{22} \end{pmatrix}}_{\boldsymbol{\mathcal{Q}}_2} \begin{pmatrix} V_E \\ \tilde{V}_E \\ \tilde{F}_{ex} \end{pmatrix} \tag{5.39}$$

For suitably high values of the controller gain K_v and the elements of matrix $\boldsymbol{Q}_o$ the Lyapunov function derivative $\dot{V}_1(V_E, \tilde{V}_E, \tilde{F}_{ex})$ is negative definite. Using the bounds on the Lyapunov function $V_1(V_E, \tilde{V}_E, \tilde{F}_{ex})$ from Eq. (5.33), the Lyapunov function derivative $\dot{V}_1(V_E, \tilde{V}_E, \tilde{F}_{ex})$ in the above equation can be expressed as,

$$\dot{V}_1(V_E, \tilde{V}_E, \tilde{F}_{ex}) \leq -\sigma_{min}(\boldsymbol{\mathcal{Q}}_2) \left\| \begin{pmatrix} V_E \\ \tilde{V}_E \\ \tilde{F}_{ex} \end{pmatrix} \right\|_2^2 \leq -\frac{2\sigma_{min}(\boldsymbol{\mathcal{Q}}_2)}{\sigma_{max}(\boldsymbol{\mathcal{Q}}_1)} V_1(V_E, \tilde{V}_E, \tilde{F}_{ex}) \tag{5.40}$$

On integrating both sides of the above equation, exponentially convergence of the Lyapunov function $V_1(V_E, \tilde{V}_E, \tilde{F}_{ex})$ to zero follows. From Eq. (5.33) the $2-$norm of $(V_E, \tilde{V}_E, \tilde{F}_{ex})$ can be expressed as,

$$\left\| \begin{pmatrix} V_E \\ \tilde{V}_E \\ \tilde{F}_{ex} \end{pmatrix} \right\|_2 \leq \left(\frac{V_1(V_E, \tilde{V}_E, \tilde{F}_{ex})}{\sigma_{min}(\boldsymbol{\mathcal{Q}}_1)} \right)^{1/2} \tag{5.41}$$

Thus exponential convergence of V_E, $\tilde{V}_E$ and $\tilde{F}_{ex}$ follows.

□

Remark 5.1. *If the external force $F_{ex}(t)$ is time varying signal with a bounded first order time derivative ($\|\dot{F}_{ex}(t)\|_\infty < D_{max}$ for some $D_{max} \geq 0$), then the error in estimating $F_{ex}(t)$ by using the observer dynamics in Eq. (5.37) exponentially reduces to a region around origin. The size of this region is determined by magnitude of D_{max}. Another consequence of time-varying nature of $F_{ex}(t)$ is that the Shape system velocity V_E also converges exponentially only to a region around origin.*

***Effect of the actuator force error* :** Due to the dynamics of the pneumatic actuator, the actuator force F_a is not directly controllable. Let $\tilde{F}$ represent the error between the current actuator force F_a and the desired actuator force F_a^d defined in Eq. (5.25) or Eq. (5.27). This error is defined as,

$$\tilde{F} = F_a - F_a^d \tag{5.42}$$

For a non-zero force error ($\tilde{F} \neq 0$), the derivative of the Lyapunov function in Eq. (5.32) is obtained as,

$$\dot{V}_1(V_E, \tilde{V}_E, \tilde{F}_{ex}) = -\begin{pmatrix} V_E \\ \tilde{V}_E \\ \tilde{F}_{ex} \end{pmatrix}^T \boldsymbol{\mathcal{Q}}_2 \begin{pmatrix} V_E \\ \tilde{V}_E \\ \tilde{F}_{ex} \end{pmatrix} + \tilde{F} V_E \tag{5.43}$$

In the above equation, as $\tilde{F}V_E$ is sign indefinite, regulation of Shape system velocity V_E to zero can only be achieved by regulating the actuator force error $\tilde{F}$ to zero. Control input for regulating the actuator force error $\tilde{F}$ to zero is presented in the following section.

Second stage Lyapunov analysis

In this section, the input command u to the actuator valve in Eq. (5.9) required to achieve regulation of the actuator force error $\tilde{F}$ is derived. Let $P_1^d(t)$ and $P_2^d(t)$ be the desired pressure in each chamber of the actuator corresponding to the desired actuator force $F_a^d(t)$. From Eq. (5.6), $P_1^d(t)$ and $P_2^d(t)$ are related to $F_a^d(t)$ as,

$$F_a^d(t) = P_1^d(t)A_1 - P_2^d(t)A_2 - P_o A_p \tag{5.44}$$

where A_1 and A_2 represent the piston cross-sectional area in chamber 1 and 2 respectively, while $A_p \triangleq (A_1 - A_2)$ represents the rod cross-sectional area exposed to

atmospheric pressure. Let $\boldsymbol{P} \triangleq (P_1, P_2)$ be the vector of current chamber pressures, $\boldsymbol{P^d} \triangleq (P_1^d, P_2^d)$ be the vector of desired chamber pressures and let x_d be the position of the actuator when providing the desired actuator force $F_a^d(t)$. Let $j \in (adb, iso)$ be the index to represent the thermodynamic process in the actuator chambers. As shown in remark 3.5, the actuator force error $\tilde{F} := (F_a - F_a^d)$ varies monotonically with the actuator position error $(x_d - x)$. The actuator force error $\tilde{F}$ and the position error $(x_d - x)$ are related as,

$$\tilde{F} = K_j^d(\boldsymbol{m}, x, x_d)(x_d - x) \tag{5.45}$$

where the nonlinear function $K_j^d(\boldsymbol{m}, x, x_d)$ mapping the position error $(x_d - x)$ to the force error $\tilde{F}$ is as given in Eq. (3.142). In the following lemma, an energy based Lyapunov function for designing the valve command input u to regulate the force error $\tilde{F}$ is presented.

Lemma 5.1. *Given the desired actuator force $F_a^d(t)$, and for the gravimetric energy density $W_m^j(.)$ for adiabatic ($j = adb$) and isothermal ($j = iso$) actuators as given in Eq. (3.144) and Eq. (3.145) respectively, the Lyapunov function candidate for designing the valve command input u required for regulating the actuator force error $\tilde{F}$ to zero is defined to be the error energy function $W_L^j(\boldsymbol{m}, \boldsymbol{P}, \boldsymbol{P^d})$ presented in Eq. (3.143),*

$$W_L^j(\boldsymbol{m}, \boldsymbol{P}, \boldsymbol{P^d}) = m_1 W_m^j(P_1, P_1^d) + m_2 W_m^j(P_2, P_2^d) \tag{5.46}$$

as it satisfies the following three properties,

1. $W_L^j(\boldsymbol{m}, \boldsymbol{P}, \boldsymbol{P^d}) \geq 0 \ \forall \ \boldsymbol{m}, \ \boldsymbol{P}, \ \boldsymbol{P^d}$
2. $W_L^j(\boldsymbol{m}, \boldsymbol{P}, \boldsymbol{P^d}) = 0$ *if and only if,* $P_1 = P_1^d$, $P_2 = P_2^d$ i.e. $F_a = F_a^d(t)$
3. $W_L^j(\boldsymbol{m}, \boldsymbol{P}, \boldsymbol{P^d})$ *is a radially unbounded function of the pressure error* $(\boldsymbol{P} - \boldsymbol{P^d})$

Proof. Proof of this lemma is provided in the appendix C.1. □

To demonstrate exponential convergence of the actuator Lyapunov function candidate $W_L^j(\boldsymbol{m}, \boldsymbol{P}, \boldsymbol{P^d})$ in Eq. (5.46), the following remark is presented.

Remark 5.2. *For both isothermal and adiabatic actuators, there exists positive constants $Q_{min}(\boldsymbol{m})$ and $Q_{max}(\boldsymbol{m})$ such that the radially unbounded actuator Lyapunov function candidate $W_L^j(\boldsymbol{m}, \boldsymbol{P}, \boldsymbol{P^d})$ in Eq. (5.46) satisfies the following inequality,*

$$\frac{1}{2}Q_{min}(\boldsymbol{m})\tilde{F}(\boldsymbol{m}, \boldsymbol{P}, \boldsymbol{P^d})^2 \leq W_L^j(\boldsymbol{m}, \boldsymbol{P}, \boldsymbol{P^d}) \leq \frac{1}{2}Q_{max}(\boldsymbol{m})\tilde{F}(\boldsymbol{m}, \boldsymbol{P}, \boldsymbol{P^d})^2 \tag{5.47}$$

Proof. Proof as shown in appendix C.2 □

For a Shape system with unknown force $F_{ex}(t)$, consider the following Lyapunov function for the composite dynamics of the Shape system inertia and the pneumatic actuator,

$$\begin{aligned} V_2(V_E, \tilde{V}_E, \tilde{F}_{ex}, \boldsymbol{m}, \boldsymbol{P}, \boldsymbol{P^d}) &= V_1(V_E, \tilde{V}_E, \tilde{F}_{ex}) + W_L^j(\boldsymbol{m}, \boldsymbol{P}, \boldsymbol{P^d}) \\ &= \frac{1}{2}\begin{pmatrix} V_E \\ \tilde{V}_E \\ \tilde{F}_E \end{pmatrix}^T \boldsymbol{\mathcal{Q}}_1 \begin{pmatrix} V_E \\ \tilde{V}_E \\ \tilde{F}_{ex} \end{pmatrix} + W_L^j(\boldsymbol{m}, \boldsymbol{P}, \boldsymbol{P^d}) \end{aligned} \tag{5.48}$$

where $V_1(V_E, \tilde{V}_E, \tilde{F}_{ex})$ is the Lyapunov function for the first stage of the controller design and is defined in Eq. (5.32). From the definition of the bounds on the actuator Lyapunov function $W_L^j(\boldsymbol{m}, \boldsymbol{P}, \boldsymbol{P^d})$ in Eq. (5.47), the Lyapunov function $V_2(.)$ in the above equation can be bounded as,

$$\begin{aligned} V_2(V_E, \tilde{V}_E, \tilde{F}_{ex}, \boldsymbol{m}, \boldsymbol{P}, \boldsymbol{P^d}) &< \frac{1}{2}\begin{pmatrix} V_E \\ \tilde{V}_E \\ \tilde{F}_{ex} \\ \tilde{F} \end{pmatrix}^T \underbrace{\begin{pmatrix} \boldsymbol{\mathcal{P}}_2 & \mathbf{0}_{1\times 3} \\ \mathbf{0}_{3\times 1} & Q_{max}(\boldsymbol{m}) \end{pmatrix}}_{\boldsymbol{\mathcal{P}}_3} \begin{pmatrix} V_E \\ \tilde{V}_E \\ \tilde{F}_{ex} \\ \tilde{F} \end{pmatrix} \\ &< \frac{1}{2}\sigma_{max}(\boldsymbol{\mathcal{P}}_3)\left\| \begin{pmatrix} V_E \\ \tilde{V}_E \\ \tilde{F}_{ex} \\ \tilde{F} \end{pmatrix} \right\|_2^2 \end{aligned} \tag{5.49}$$

In Eq. (5.48), $V_1(.)$ is a non-negative function of Shape system velocity V_E, velocity estimation error $\tilde{V}_E$ and the force estimation error $\tilde{F}_{ex}$, while the actuator Lyapunov function $W_L^j(\boldsymbol{m}, \boldsymbol{P}, \boldsymbol{P^d})$ is a non-negative function of air mass $\boldsymbol{m}$, chamber pressure $\boldsymbol{P}$ and desired chamber pressure $\boldsymbol{P^d}$. By regulating the Lyapunov function $V_2(.)$ to zero,

the desired velocity regulation ($V_E \to 0$) and force regulation ($\tilde{F} \to 0$) can be achieved. Using the time derivative $\dot{V}_1(.)$ from Eq. (5.43), and the derivative of the actuator Lyapunov function $\dot{W}_L^j(.)$ from Eq. (3.151), the time derivative $\dot{V}_2(.)$ of the Lyapunov function in Eq. (5.48) is obtained as,

$$\dot{V}_2(V_E, \tilde{V}_E, \tilde{F}_{ex}, \boldsymbol{m}, \boldsymbol{P}, \boldsymbol{P^d}) = -\begin{pmatrix} V_E \\ \tilde{V}_E \\ \tilde{F}_{ex} \end{pmatrix}^T \boldsymbol{\mathcal{Q}}_2 \begin{pmatrix} V_E \\ \tilde{V}_E \\ \tilde{F}_{ex} \end{pmatrix} - \tilde{F}\dot{x}_v + \gamma_3^j(\boldsymbol{m}, \boldsymbol{P}, \boldsymbol{P^d}, u)\tilde{F}u - \dot{F}_a^d \frac{\tilde{F}}{K_j^d(\boldsymbol{m}, x, x_d)} \tag{5.50}$$

where the nonlinear gain $\gamma_3^j(\boldsymbol{m}, \boldsymbol{P}, \boldsymbol{P^d}, u)$ is as defined in Eq. (3.150) and represents the mapping from the actuator force error $\tilde{F}$ to the effort variable $Z_\gamma^j(\boldsymbol{m}, \boldsymbol{P}, \boldsymbol{P^d}, u)$ at the fluid port of the actuator Lyapunov function derivative.

The valve command input u for regulating the actuator force error $\tilde{F}$ (and consequently the Shape system velocity V_E) to zero, is presented in the following theorem.

Theorem 5.2. *For the pneumatic actuator pressure dynamics and mass flow rate as given in Eq. (5.8) and Eq. (5.9) respectively, if perfect information about all the external forces in $F_{ex}(t)$ in Eq. (5.22) is available, exponentially regulation of the Shape system velocity V_E and the actuator force error $\tilde{F} := (F_a - F_a^d)$ to zero can be achieved for the desired actuator force $F_a^d := F_{ex} - K_v V_E$ as given in Eq. (5.25) and for the following definition of valve command input u,*

$$u = \frac{1}{\gamma_3^j((\boldsymbol{m}, \boldsymbol{P}, \boldsymbol{P^d}, u))} \left(\dot{x}_v + \frac{\dot{F}_a^d}{K_j^d(\boldsymbol{m}, x, x_d)} - K_F(F_a - F_a^d) \right) \tag{5.51}$$

where K_F is a positive constant, $j \in (iso, adb)$ is the index for representing the thermodynamic process in the actuator, the nonlinear function $K_j^d(\boldsymbol{m}, x, x_d)$ is as defined in Eq. (3.142) and the nonlinear gain $\gamma_3^j((\boldsymbol{m}, \boldsymbol{P}, \boldsymbol{P^d}, u))$ is as defined in Eq. (3.150).

For a constant but un-known force $F_{ex}(t)$ in Eq. (5.22) acting on the Shape system dynamics, exponential regulation of $\tilde{F}$ and V_E to zero is achieved with the control input u from Eq. (5.51) and for the desired actuator force $F_a^d := \hat{F}_{ex} - K_v V_E$ as given Eq. (5.27), where $\hat{F}_{ex}$ represents an estimate of the force $F_{ex}(t)$, and is obtained from Eq. (5.37).

Proof. When $F_{ex}(t)$ in Eq. (5.22) is completely known, consider the following definition of the system Lyapunov function,

$$\bar{V}_2(V_E, \boldsymbol{m}, \boldsymbol{P}, \boldsymbol{P^d}) = \frac{1}{2} M_E V_E^2 + W_L^j(\boldsymbol{m}, \boldsymbol{P}, \boldsymbol{P^d}) \tag{5.52}$$

Using bounds on the actuator Lyapunov function $W_L^j(\boldsymbol{m}, \boldsymbol{P}, \boldsymbol{P^d})$ from Eq. (5.47), the Lyapunov function $\bar{V}_2(V_E, \boldsymbol{m}, \boldsymbol{P}, \boldsymbol{P^d})$ can be bounded as,

$$\begin{aligned} \bar{V}_2(V_E, \boldsymbol{m}, \boldsymbol{P}, \boldsymbol{P^d}) &< \frac{1}{2} \begin{pmatrix} V_E & \tilde{F} \end{pmatrix} \begin{pmatrix} M_E & 0 \\ 0 & Q_{max}(\boldsymbol{m}) \end{pmatrix} \begin{pmatrix} V_E \\ \tilde{F} \end{pmatrix} \\ &< \frac{1}{2} \sigma_{max}(\mathcal{P}) \left\| \begin{pmatrix} V_E \\ \tilde{F} \end{pmatrix} \right\|_2^2 \end{aligned} \tag{5.53}$$

where $\mathcal{P} \triangleq diag(M_E, Q_{max}(\boldsymbol{m}))$, and $\sigma_{max}(\mathcal{P})$ represents the maximum singular value of $\mathcal{P}$. Using the Shape system dynamics from Eq. (5.21), and the time-derivative $\dot{W}_L^j(\boldsymbol{m}, \boldsymbol{P}, \boldsymbol{P^d})$ of error energy function from Eq. (3.151), the derivative $\dot{\bar{V}}_2$ of the Lyapunov function in Eq. (5.52) is obtained as,

$$\begin{aligned} \dot{\bar{V}}_2(V_E, \boldsymbol{m}, \boldsymbol{P}, \boldsymbol{P^d}) = (F_a - F_{ex}(t)) V_E + \gamma_3^j(\boldsymbol{m}, \boldsymbol{P}, \boldsymbol{P^d}, u) \tilde{F} u - \tilde{F} \dot{x}_v \\ - \dot{F}_a^d \frac{\tilde{F}}{K_j^d(\boldsymbol{m}, x, x_d)} \end{aligned} \tag{5.54}$$

For known $F_{ex}(t)$, using the expression for desired actuator force F_a^d from Eq. (5.25) and the valve command input u from Eq. (5.51) in the above equation, the derivative $\dot{\bar{V}}_2(V_E, \boldsymbol{m}, \boldsymbol{P}, \boldsymbol{P^d})$ of the Lyapunov function can be expressed as,

$$\dot{\bar{V}}_2(V_E, \boldsymbol{m}, \boldsymbol{P}, \boldsymbol{P^d}) = - \begin{pmatrix} V_E & \tilde{F} \end{pmatrix} \underbrace{\begin{pmatrix} K_v & 0 \\ 0 & K_F \end{pmatrix}}_{\mathcal{Q}} \begin{pmatrix} V_E \\ \tilde{F} \end{pmatrix} \leq -\sigma_{min}(\mathcal{Q}) \left\| \begin{pmatrix} V_E \\ \tilde{F} \end{pmatrix} \right\|_2^2 \tag{5.55}$$

where $\sigma_{min}(\mathcal{Q})$ gives the minimum singular value of $\mathcal{Q}$. Using the upper bound on $\bar{V}_2(V_E, \boldsymbol{m}, \boldsymbol{P}, \boldsymbol{P^d})$ from Eq. (5.53), the derivative $\dot{\bar{V}}_2(V_E, \boldsymbol{m}, \boldsymbol{P}, \boldsymbol{P^d})$ in the above equation can be expressed as,

$$\dot{\bar{V}}_2(V_E, \boldsymbol{m}, \boldsymbol{P}, \boldsymbol{P^d}) \leq - \left(\frac{2\sigma_{min}(\mathcal{Q})}{\sigma_{max}(\mathcal{P})} \right) \bar{V}_2(V_E, \boldsymbol{m}, \boldsymbol{P}, \boldsymbol{P^d}) \tag{5.56}$$

On integrating both sides of the above equation exponential convergence of the Lyapunov function $\bar{V}_2(V_E, \boldsymbol{m}, \boldsymbol{P}, \boldsymbol{P^d})$ follows. As $\bar{V}_2(V_E, \boldsymbol{m}, \boldsymbol{P}, \boldsymbol{P^d})$ is a positive definite function of V_E and $\tilde{F}$, exponential convergence of Shape system velocity V_E and the actuator force error $\tilde{F}$ is also achieved.

If the external forces contributing to $F_{ex}(t)$ are constant but unknown, consider $V_2(.)$ defined in Eq. (5.48) as the system Lyapunov function candidate. The time derivative $\dot{V}_2(.)$ of the Lyapunov function is as given in Eq. (5.50). Using the definition of the valve command input u from Eq. (5.51), the Lyapunov function derivative $\dot{V}_2(.)$ in Eq. (5.50) can be expressed as,

$$\dot{V}_2(V_E, \tilde{V}_E, \tilde{F}_{ex}, \boldsymbol{m}, \boldsymbol{P}, \boldsymbol{P^d}) = -\begin{pmatrix} V_E \\ \tilde{V}_E \\ \tilde{F}_{ex} \\ \tilde{F} \end{pmatrix}^T \underbrace{\begin{pmatrix} \boldsymbol{\mathcal{Q}}_2 & 0 \\ \boldsymbol{0_{3\times 1}} & K_F \end{pmatrix}}_{\boldsymbol{\mathcal{Q}}_3} \begin{pmatrix} V_E \\ \tilde{V}_E \\ \tilde{F}_{ex} \\ \tilde{F} \end{pmatrix} \tag{5.57}$$

Using the definition of the bounds on the Lyapunov function $V_2(.)$ from Eq. (5.49), the Lyapunov function derivative $\dot{V}_2(.)$ in Eq. (5.57) can be expressed as,

$$\dot{V}_2(V_E, \tilde{V}_E, \tilde{F}_{ex}, \boldsymbol{m}, \boldsymbol{P}, \boldsymbol{P^d}) \leq -\sigma_{min}(\boldsymbol{\mathcal{Q}}_3) \left\| \begin{pmatrix} V_E \\ \tilde{V}_E \\ \tilde{F}_{ex} \\ \tilde{F} \end{pmatrix} \right\|_2^2 \leq -\frac{2\sigma_{min}(\boldsymbol{\mathcal{Q}}_3)}{\sigma_{max}(\boldsymbol{\mathcal{P}}_3)} V_2(V_E, \tilde{V}_E, \tilde{F}_{ex}, \tilde{F}) \tag{5.58}$$

where $\boldsymbol{\mathcal{P}}_3$ is as defined in Eq. (5.49). On integrating both sides of the above equation exponential convergence of $V_2(.)$ follows. As $V_2(.)$ is a positive definite function of the Shape system velocity V_E and the actuator force error $\tilde{F}$, thay also converge exponentially to zero.

□

While the above theorem assumes that $F_{ex}(t)$ is a constant, the dynamics in Eq. (5.37) can be used to estimate slowly varying signals with reasonable accuracy by increasing the observer gains. For fast varying unknown force signal, the error in estimating $F_{ex}(t)$ from Eq. (5.37) is bounded by the magnitude of the time derivative $\dot{F}_{ex}(t)$. Due to the resulting error in estimating $F_{ex}(t)$, the Shape system velocity V_E

can only converge exponentially to a bounded region around origin. The actuator force F_a however converges exponentially to the desired force $F_a^d(t)$ in Eq. (5.27).

In the next section, passivity analysis of the closed loop system for the proposed valve command input u in Eq. (5.51) is investigated.

5.4 Closed loop passivity analysis

In this section, the controller is appropriately modified to satisfy the desired passivity condition in Eq.(5.3), while providing the desired regulation of Shape system velocity ($V_E = 0$). The valve command input from Eq. (5.51) is defined as,

$$u = \frac{1}{\gamma_3^j(\boldsymbol{m}, \boldsymbol{P}, \boldsymbol{P^d}, u)} \left(\dot{x}_v + \frac{\dot{F}_a^d}{K_j^d(\boldsymbol{m}, x, x_d)} + u_{fb} \right) \tag{5.59}$$

where u_{fb} is the feedback component of the controller and is given by,

$$u_{fb} = -K_F \tilde{F} \tag{5.60}$$

The valve command input in Eq. (5.59) guarantees exponential regulation of the Shape system dynamics in Eq. (5.21). After velocity co-ordination, the combined dynamics of the actual inertia and the virtual inertia are obtained from Eq. (5.19) as,

$$M_L \ddot{x} = (\rho + 1) F_h + F_e(t) - u_d \tag{5.61}$$

The locked system dynamics in the above equation has the desired external supply rate in Eq. (5.2) if the input u_d to the virtual inertia is defined to have dissipative characteristics. In the following section, supply rate to the closed loop system is identified by defining an appropriate storage function. The input force u_d on the virtual inertia is then defined such that u_d has a dissipative effect on the closed loop system dynamics. As shown in the next section, feed-forward components of the control input consisting of $\dot{x}_v$ and $\dot{F}_a^d$, and the velocity and the force tracking errors V_E, $\tilde{F}$ respectively also have energetic interaction with the closed loop system. This interaction is monitored to ensure that the effective external supply rate to the human power amplifier corresponds to the desired supply rate in Eq. (5.2) and satisfies the desired passivity condition in Eq. (5.3).

5.4.1 Storage function and supply rate for pneumatic power amplifier

As the supply rate in Eq. (5.2) corresponds to physically meaningful power interaction, a storage function corresponding to the cumulative energy in different elements of the human power amplifier is appropriate. Consider the following definition of the storage function consisting of the kinetic energy of the virtual inertia M_v, kinetic energy of the inertia M_p, and the actuator potential energy $W^j_{act}(\boldsymbol{m}, \boldsymbol{P})$,

$$W_s(\dot{x}, \dot{x}_v, \boldsymbol{m}, \boldsymbol{P}) = \frac{1}{2} M_v \dot{x}_v^2 + W^j_{act}(\boldsymbol{m}, \boldsymbol{P}) + \frac{1}{2} M_p \dot{x}^2 \tag{5.62}$$

where $j \in (iso, adb)$ is the index to represent the appropriate thermodynamic process assumed in the actuator. The available energy in the adiabatic actuator ($W^{adb}_{act}(\boldsymbol{m}, \boldsymbol{P})$) and the isothermal actuator ($W^{iso}_{act}(\boldsymbol{m}, \boldsymbol{P})$) is as given in Eq. (3.94) and Eq. (3.100) respectively. From the dynamics of inertia M_p in Eq. (5.1), the virtual mass dynamics in Eq. (5.10) and by using the actuator supply rate for isothermal and adiabatic actuators from Eq. (3.122) and Eq. (3.136) respectively, derivative of the storage function in Eq. (5.62) is obtained as,

$$\dot{W}_s(\dot{x}, \dot{x}_v, \boldsymbol{m}, \boldsymbol{P}) = ((\rho + 1)F_h + F_e)\dot{x} - \rho F_h V_E - (F_a + u_d)\dot{x}_v + F_a \gamma^j_1(\boldsymbol{m}, \boldsymbol{P}, u)u \tag{5.63}$$

Using the definition of the command input from Eq. (5.59), the time derivative of the storage function $\dot{W}_s(.)$ in the above equation can be expressed as,

$$\begin{aligned}\dot{W}_s(\dot{x}, \dot{x}_v, \boldsymbol{m}, \boldsymbol{P}) &= ((\rho + 1)F_h(t) + F_e(t))\dot{x} - \rho F_h V_E \\ &+ \left(\left(\frac{\gamma^j_1(\boldsymbol{m}, \boldsymbol{P}, u)}{\gamma^j_3(\boldsymbol{m}, \boldsymbol{P}, \boldsymbol{P^d}, u)} - 1 \right) F_a - u_d \right) \dot{x}_v + F_a \frac{\gamma^j_1(\boldsymbol{m}, \boldsymbol{P}, u)}{\gamma^j_3(\boldsymbol{m}, \boldsymbol{P}, \boldsymbol{P^d}, u)} \left(u_{fb} + \frac{\dot{F}^d_a}{K^d_j(\boldsymbol{m}, x, x_d)} \right)\end{aligned} \tag{5.64}$$

The first term on the *r.h.s* of the above equation represents the desired external supply rate to the human power amplifier from Eq. (5.2). The other terms on the *r.h.s* of the above equation represent the effects due to co-ordination error (V_E and $\tilde{F}$), and other exogenous signals ($\dot{F}^d_a$). The energetic interaction (time integral of supply rate) due to the co-ordination error and the exogenous signal must have a finite upper bound to achieve the desired passivity condition in Eq. (5.3). To this end, the force input u_d

on the virtual inertia as,

$$u_d = \begin{cases} \left(\frac{\gamma_1^j(\boldsymbol{m},\boldsymbol{P},u)}{\gamma_3^j(\boldsymbol{m},\boldsymbol{P},\boldsymbol{P^d},u)} - 1 \right) F_a, & \text{if } \left(\frac{\gamma_1^j(\boldsymbol{m},\boldsymbol{P},u)}{\gamma_3^j(\boldsymbol{m},\boldsymbol{P},\boldsymbol{P^d},u)} - 1 \right) F_a \dot{x}_v > 0 \\ 0 & \text{if } \left(\frac{\gamma_1^j(\boldsymbol{m},\boldsymbol{P},u)}{\gamma_3^j(\boldsymbol{m},\boldsymbol{P},\boldsymbol{P^d},u)} - 1 \right) F_a \dot{x}_v \leq 0 \end{cases} \tag{5.65}$$

Consequently, the third term on the *r.h.s* of Eq. (5.64) satisfies the following dissipative condition,

$$\left(\left(\frac{\gamma_1^j(\boldsymbol{m},\boldsymbol{P},u)}{\gamma_3^j(\boldsymbol{m},\boldsymbol{P},\boldsymbol{P^d},u)} - 1 \right) F_a - u_d \right) \dot{x}_v \leq 0 \tag{5.66}$$

Due to the above dissipative property the storage function derivative $\dot{W}_s(\dot{x},\dot{x}_v,\boldsymbol{m},\boldsymbol{P})$ in Eq. (5.64) satisfies the following condition,

$$\begin{aligned} \dot{W}_s(\dot{x},\dot{x}_v,\boldsymbol{m},\boldsymbol{P}) \leq ((\rho+1)F_h(t) + F_e(t))\dot{x} - \rho F_h V_E \\ + F_a \frac{\gamma_1^j(\boldsymbol{m},\boldsymbol{P},u)}{\gamma_3^j(\boldsymbol{m},\boldsymbol{P},\boldsymbol{P^d},u)} \left(u_{fb} + \frac{\dot{F}_a^d}{K_j^d(\boldsymbol{m},x,x_d)} \right) \end{aligned} \tag{5.67}$$

In the above equation, the exogenous input corresponding to $\dot{F}_a^d$ is typically a non-zero external signal. As the control input u in Eq. (5.51) is required to actively compensate for the actions of $\dot{F}_a^d$, this exogenous input represents an energy source/sink. For a time-varying $F_{ex}(t)$, the control input u in Eq. (5.51) also guarantees exponential convergence of V_E and $\tilde{F}$ only to a neighborhood around origin. Therefore, the actuator on the human power amplifier can also require active energy input to compensate for the Shape system velocity V_E and provide feedback input u_{fb}. In [30], passive operation of mechanical systems was preserved by defining a fictitious flywheel element to monitor the total energy supplied by the controller to the actuator. In the following section this method is applied to operation of pneumatic human power amplifier.

5.4.2 Augmented system with fictitious flywheel dynamics

Operation principle

The flywheel is a fictitious element defined to monitor the energy demanded by the pneumatic actuator due to the controller requirements. The dynamics of the flywheel

is defined as,

$$M_f \ddot{x}_f = T_f \tag{5.68}$$

where M_f is the flywheel inertia, x_f is the flywheel position and T_f corresponds to the torque acting on the flywheel.

By defining the flywheel torque such that the energy transfer to or from the pneumatic actuator due to controller requirements correspond to change in the kinetic energy of the flywheel, energy supplied to the actuator can be determined by monitoring the kinetic energy of the flywheel. This proposed approach for actively monitoring the power interaction between the controller and the actuator is similar to the passivity observer scheme reported in [35].

When the kinetic energy of the flywheel is above a threshold value ($\dot{x}_f > f_o$), the power amplifier is referred to be in normal mode of operation. If the kinetic energy of the flywheel falls below a threshold value ($\dot{x}_f < f_o$) due to significant transfer of energy to the pneumatic actuator, the operation of the power amplifier is switched to emergency mode. In this mode, the input u_d on the virtual mass dynamics in Eq. (5.10) is augmented with an additional damping force $-b\dot{x}_v$. The dynamics of the virtual inertia in Eq. (5.10) are thus modified as,

$$M_v \ddot{x}_v = \rho F_h(t) - F_a - u_d - b\dot{x}_v \tag{5.69}$$

where $b \geq 0$ is the damping coefficient, and the input force u_d is as defined in Eq. (5.65). By suitably defining the flywheel torque T_f in Eq. (5.68), the energy dissipated by the amplifier due to the damping $-b\dot{x}_v$ is transferred to the flywheel. The resulting increase in the kinetic energy of the flywheel will transition the power amplifier operation to normal mode. As the total energy available to the pneumatic actuator is bounded by the finite initial energy of the flywheel, passive operation of the power amplifier is guaranteed.

Note that the additional damping force is only applied in emergency mode to avoid unrequited effort from the operator in normal mode of operation. By augmenting the system storage function with the kinetic energy of the flywheel, the flywheel torque T_f required for maintaining passive operation is determined in the following section.

Passivity property of the flywheel augmented system

By considering the energy available from the flywheel, the storage function for the human power amplifier is now defined as,

$$W_{tot}(\dot{x}, \dot{x}_v, \boldsymbol{m}, \boldsymbol{P}, \dot{x}_f) = \frac{1}{2} M_v \dot{x}_v^2 + W_{act}^j(\boldsymbol{m}, \boldsymbol{P}) + \frac{1}{2} M_p \dot{x}^2 + \frac{1}{2} M_f \dot{x}_f^2 \tag{5.70}$$

Differentiating the above storage function and using the virtual inertia dynamics from Eq. (5.69), the time derivative $\dot{W}_{tot}(.)$ is obtained as,

$$\begin{aligned} \dot{W}_{tot}(\dot{x}, \dot{x}_v, \boldsymbol{m}, \boldsymbol{P}, \dot{x}_f) = ((\rho+1)F_h + F_e)\dot{x} - F_d V_E + \gamma_1^j(\boldsymbol{m}, \boldsymbol{P}, u) F_a u \\ - u_d \dot{x}_v - b\dot{x}_v^2 + T_f \dot{x}_f \end{aligned} \tag{5.71}$$

Design of the valve command input u, the input torque T_f on the flywheel and the damping coefficient b required for achieving the desired passive operation is presented in the following theorem.

Theorem 5.3. *For the inertial dynamics given in Eq. (5.1), when actuated by an adiabatic or an isothermal pneumatic actuator with pressure dynamics as given in Eq. (5.8) and air mass flow rate as defined in Eq. (5.9), with the command input u to the servo-proportional valve metering flow to the actuator given by,*

$$u = \frac{1}{\gamma_3^j(\boldsymbol{m}, \boldsymbol{P}, \boldsymbol{P^d}, u)} \left(\dot{x}_v + \frac{\dot{F}_a^d}{K_j^d(\boldsymbol{m}, x, x_d)} + \hat{u}_{fb} \right) \tag{5.72}$$

where the velocity $\dot{x}_v$ of the virtual inertia interacting at the fluid port of the actuator is obtained from Eq. (5.69), the nonlinear functions $\gamma_3^j(\boldsymbol{m}, \boldsymbol{P}, \boldsymbol{P^d}, u) \in \Re^+$ and $K_j^d(\boldsymbol{m}, x, x_d) \in \Re^+$ are as defined in Eq. (3.150), and Eq. (3.142) for adiabatic and isothermal actuators respectively, while the control input $\hat{u}_{fb}$ in Eq. (5.72) and the flywheel torque T_f in Eq. (5.68) are defined to have the following skew-symmetric relationship,

$$\begin{aligned} \begin{pmatrix} \hat{u}_{fb} \\ T_f \end{pmatrix} = \begin{pmatrix} 0 & g(\dot{x}_f) u_{fb} \\ -g(\dot{x}_f) u_{fb} & 0 \end{pmatrix} \begin{pmatrix} \frac{\gamma_1^j(\boldsymbol{m}, \boldsymbol{P}, u)}{\gamma_3^j(\boldsymbol{m}, \boldsymbol{P}, \boldsymbol{P}^d, u)} F_a \\ \dot{x}_f \end{pmatrix} + \\ \begin{pmatrix} 0 \\ \frac{1}{\dot{x}_f} \left(\rho F_h V_E - \left(\left(\frac{\gamma_1^j(\boldsymbol{m}, \boldsymbol{P}, u)}{\gamma_3^j(\boldsymbol{m}, \boldsymbol{P}, \boldsymbol{P^d}, u)} - 1 \right) F_a - u_d \right) \dot{x}_v + b\dot{x}_v^2 \\ + \frac{\gamma_1^j(\boldsymbol{m}, \boldsymbol{P}, u)}{\gamma_3^j(\boldsymbol{m}, \boldsymbol{P}, \boldsymbol{P^d}, u)} \frac{\dot{F}_a^d}{K_j^d(\boldsymbol{m}, x, x_d)} \end{pmatrix} \end{pmatrix} \end{aligned} \tag{5.73}$$

where u_{fb} is as defined in Eq. (5.60), while $g(\dot{x}_f)$ and the damping coefficient b depend on the flywheel velocity $\dot{x}_f$ and are defined as,

$$\textit{Regular mode} : \begin{pmatrix} g(\dot{x}_f) = \frac{1}{|\dot{x}_f|} \\ b = 0 \end{pmatrix} \quad \textit{if } |\dot{x}_f| \geq f_o \tag{5.74}$$

$$\textit{Emergency mode} : \begin{pmatrix} g(\dot{x}_f) = \frac{1}{f_o} \\ b \in \Re^+ \end{pmatrix} \quad \textit{if } |\dot{x}_f| < f_o \tag{5.75}$$

where f_o is a pre-defined threshold velocity of the flywheel for operating in safe mode, the desired condition from Eq. (5.3) for passive human power amplification is satisfied,

$$\int_0^t ((\rho+1)F_h + F_e)\dot{x}\ d\tau \geq -c_o^2 \tag{5.76}$$

Proof. The augmented storage function $W_{tot}(\dot{x}, \dot{x}_v, \boldsymbol{m}, \boldsymbol{P}, \dot{x}_f)$ for the human power amplifier is as defined in Eq. (5.70). From the definition of valve command input u in Eq. (5.72), the time derivative $\dot{W}_{tot}(\dot{x}, \dot{x}_v, \boldsymbol{m}, \boldsymbol{P}, \dot{x}_f)$ of this storage function in Eq. (5.71) can be expressed as,

$$\begin{aligned}\dot{W}_{tot}(\dot{x}, \dot{x}_v, \boldsymbol{m}, \boldsymbol{P}, \dot{x}_f) &= ((\rho+1)F_h + F_e)\dot{x} - \rho F_h V_E - b\dot{x}_v^2 + T_f \dot{x}_f \\ &+ \left(\left(\frac{\gamma_1^j(\boldsymbol{m}, \boldsymbol{P}, u)}{\gamma_3^j(\boldsymbol{m}, \boldsymbol{P}, \boldsymbol{P^d}, u)} - 1 \right) F_a - u_d \right) \dot{x}_v + F_a \frac{\gamma_1^j(\boldsymbol{m}, \boldsymbol{P}, u)}{\gamma_3^j(\boldsymbol{m}, \boldsymbol{P}, \boldsymbol{P^d}, u)} \left(\hat{u}_{fb} + \frac{\dot{F}_a^d}{K_j^d(\boldsymbol{m}, x, x_d)} \right)\end{aligned} \tag{5.77}$$

Using the definition of the flywheel torque from Eq. (5.73) and integrating both sides of Eq. (5.77) the following passivity condition is achieved,

$$\int_0^t ((\rho+1)F_h(t) + F_e(t))\dot{x}\ \ d\tau \geq -W_{tot}(\dot{x}, \dot{x}_v, \boldsymbol{m}, \boldsymbol{P}, \dot{x}_f)\Big|_{t=0} = -c_o^2 \tag{5.78}$$

where $W_{tot}(\dot{x}, \dot{x}_v, \boldsymbol{m}, \boldsymbol{P}, \dot{x}_f)\Big|_{t=0} \in \Re^+$ is the total initial energy of the composite system. The above equation satisfies the required energetic passivity condition in Eq. (5.76). Note that from Eq. (5.73), in regular mode of operation, the damping force $(-b\dot{x}_v)$ on the virtual inertia is identically zero. In emergency mode of operation, the damping coefficient b is selected to be sufficiently large to result in net energy input to the flywheel.

□

The energy dissipated by the pneumatic actuator due to the damping force $-b\dot{x}_v$ increases the velocity $\dot{x}_f$ of the flywheel. As the flywheel velocity is increasing, it is usually advisable to remain in emergency mode until $\dot{x}_f$ is greater than f_1, where $f_1 > f_o$ represents velocity of the flywheel required to switch back to regular mode of operation. This is required to prevent any high frequency switching at the boundary between emergency mode and regular mode of operation.

The control algorithm for human power amplification with a pneumatic actuator is tested on an experimental setup with a single-DOF actuator.

5.5 Experimental results

The experimental setup, as shown in Fig. (5.5), consists of a vertically mounted, two-chambered, single-DOF pneumatic actuator with position feedback. The maximum supply air pressure P_s available in the supply line is $6.89e5Pa$ $(100psi)$, and all the experiments are conducted at this supply pressure. The atmosphere pressure P_o is assumed to be $1.01e5Pa$ $(14.7psi)$. The cap side has an internal diameter of $0.0508m$ (2 inches), while the stroke length of the actuator is $0.3048m$ (12 inches). The diameter of the piston rod is $0.0254m$ (1 inch). A MLP-50 force sensor from Transducer Techniques, used to measure the input human force, is attached on the actuator as shown in Fig. (5.5). A pair of SDET-22T-D16 pressure sensors from FESTO are used to measure the pressure in the two actuator chambers. A MPYE-5-LF010 proportional servo valve from FESTO is used to meter the air flow to the actuator. The input voltage range for the valve is 0 volts to 10 volts, with the spool positioned at the center of the valve body for an input of 5 volts. Open loop experiments were performed to determine the rate of change of air mass in the actuator for different voltage command inputs to the flow control valve solenoid. Using the measured pressure data and an estimate of the mass flow rate $\dot{m}$ from this experiment in Eq. (3.27), the relationship between the desired valve open area u and the required voltage command to the valve V_o is determined as,

$$V_o = \begin{cases} 4.59 - 6.847e5u + 1.732e11u^2 - 5.971e16u^3 & \text{if } u \geq 0 \\ 5.37 - 1.089e6u - 4.383e11u^2 - 1.048e17u^3 & \text{if } u < 0 \end{cases} \tag{5.79}$$

The polynomial correlation in the above equation is defined such that for a positive value of u (connecting chamber 1 to supply pressure P_s) the voltage command to the

valve is less than 5 volts, and a negative value of u (connecting chamber 2 to supply pressure) corresponds to a voltage command of greater than 5 volts to the valve. This relationship is as illustrated in Fig. (5.4), with the maximum valve effective area of $4.2e-6m^2$ corresponding to an input of either 0 or 10.

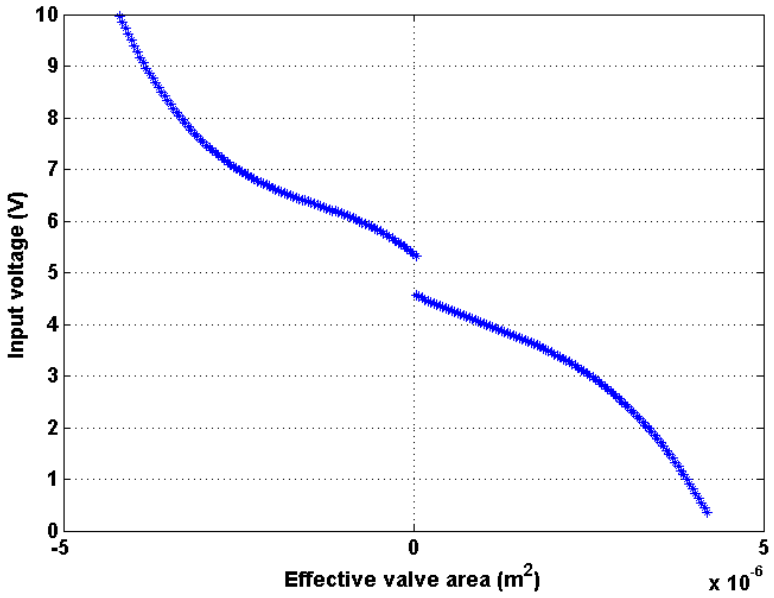

Figure 5.4: Figure illustrating the relationship between the effective valve area u and the voltage command V_o to the valve required to achieve this area.

In this study, controllers developed for both the isothermal and the adiabatic actuators are experimentally evaluated to understand the appropriate thermodynamic model for the actuator. The controller gains K_v and K_F, the observer gain L_1 and λ_1, the control λ_2 used in the definition of the Lyapunov function V_2 in Eq. (5.48), the mass M_v of the virtual inertia and the amplification factor ρ are all listed in table 5.1. These parameters are relevant for both the isothermal and the adiabatic thermodynamic models of the actuator. The inertial load M_p on the actuator in Fig. (5.5) is $3.4kgs$. High gains are used on the observer dynamics in Eq. (5.37) to achieve fast estimation of the external forces. The velocity gain K_v used to define the desired actuator force in Eq. (5.27) is selected to be high enough for quick regulation of Shape system velocity V_E

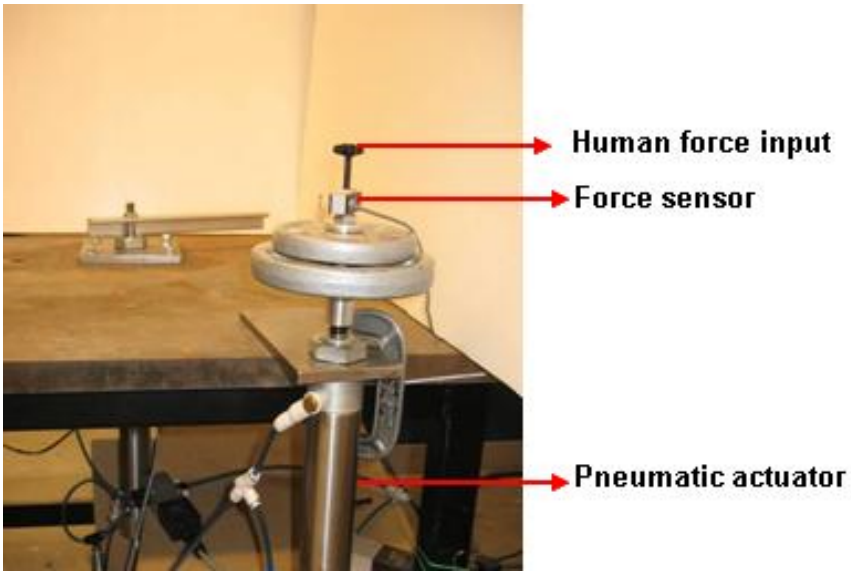

Figure 5.5: Experimental setup for testing controller schemes for human power amplification. The inertial load on the actuator is 3.4 kgs.

to zero. The gain on the force error K_F used in Eq. (5.51) for defining the actuator valve command input u is not required to be very high, as the feed-forward input of virtual velocity $\dot{x}_v$ is typically sufficient to achieve the desired velocity tracking. The amplification factor ρ on the input human force is selected to be 7.

Quick estimation of the actuator velocity is essential for appropriate feedback input. Design of observers for velocity estimation is still an active area of research [74]. In this study the piston velocity estimate $\dot{\hat{x}}$ is obtained from the position signal x by assuming constant velocity and using a high gain observer. The full-order observer dynamics are given by,

$$\begin{pmatrix} \dot{\hat{x}} \\ \ddot{\hat{x}} \end{pmatrix} = \begin{pmatrix} 0 & 1 \\ 0 & 0 \end{pmatrix} \begin{pmatrix} \hat{x} \\ \dot{\hat{x}} \end{pmatrix} + \begin{pmatrix} k_1 \\ k_2 \end{pmatrix} (x - \hat{x}) \tag{5.80}$$

where the observer gains k_1 and k_2 are as listed in table 5.1. The velocity observer in the above equation is has the form of a low-pass filter. The accuracy of the velocity estimate provided by this observer is verified by comparing it with the slope of the variation of position data with time.

Performance of the human power amplifier for the control input u in Eq. (5.72) is

Table 5.1: Parameters used in the implementation of power amplification controller for the isothermal and the adiabatic models of the actuator

Parameter	Magnitude (Isothermal)	Magnitude (Adiabatic)
K_v	750	1250
K_F	0.002	0.004
L_1	2.03e3	2.03e3
L_2	5.22e7	13.05e7
$\boldsymbol{Q_o}$	$1.74e5 \begin{pmatrix} 2e3 & 150 \\ 150 & 2e3 \end{pmatrix}$	$1.74e5 \begin{pmatrix} 2e3 & 375 \\ 375 & 2e3 \end{pmatrix}$
M_v	8.5 kgs	8.5 kgs
ρ	7	7
k_1	44	44
k_2	1000	1000

evaluated when operating in free space and during interaction with a hard surface. A metal rod clamped at both ends is placed in the path of the actuator as an obstacle with a hard surface.

Velocity tracking achieved when assuming that the thermodynamic process in the actuator is isothermal is as shown in Fig. (5.6). The figure illustrates good tracking characteristics in free space for an arbitrary velocity profile. When suddenly interacting with a hard surface (at about $t = 59.5s$ and $t = 65.5s$), there is a small overshoot in the velocity in the virtual inertia due to sudden change in momentum. However, the velocity of both actual inertia $\dot{x}$ and the virtual inertia $\dot{x}_v$ drop to zero very quickly and remain at zero for the duration ($59.5s < t < 61.7s$ and $65.5s < t < 67.5s$) of the interaction with hard surface. During this time the velocity plots indicate that no contact instability is induced due to sudden interaction with a hard surface. For the isothermal actuator, comparison of the actuator force output F_a with the amplified human force ρF_h is as shown in Fig. (5.7). The figure shows that the actuator force corresponds well with the amplified human force when traversing an arbitrary trajectory in free space. When interacting with the hard surface, at the moment of contact there is

a force spike due to sudden change in momentum, but the actuator force quickly settles down and provides the desired force response. The lack of oscillation in the velocity in Fig. (5.6) for the contact force shown in Fig. (5.7) confirms stability of interaction. As the actuator force corresponds to the amplified human force ($F_a = \rho F_h$), and velocity of the actual inertia $\dot{x}$ corresponds to the velocity of the virtual inertia $\dot{x}_v$, the supply rate to the power amplifier corresponds to the desired external supply rate in Eq. (5.2).

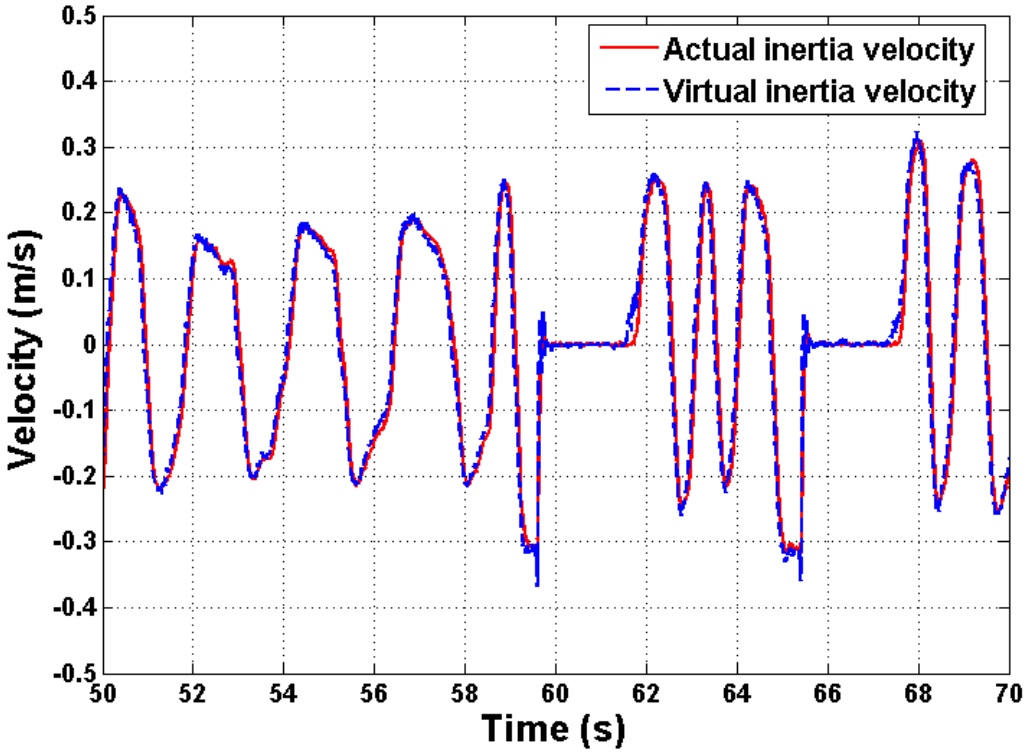

Figure 5.6: Comparison of the virtual inertia velocity $\dot{x}_v$ with the actual inertia velocity $\dot{x}$ during motion in free space and when interacting with a hard surface. The thermodynamic process in the actuator is assumed to be isothermal.

Velocity and force tracking results when the thermodynamic process in the actuator is assumed to be adiabatic are provided in Figs. (5.8 and 5.9) respectively. These plots again illustrate good tracking characteristics when moving the actuator along an

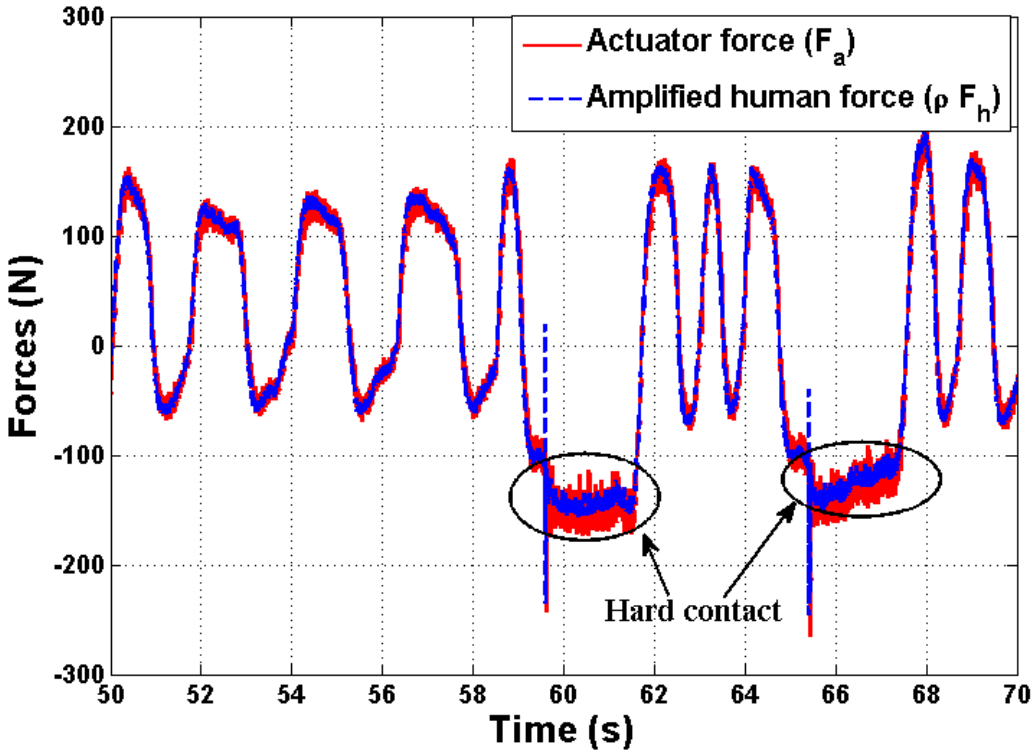

Figure 5.7: Comparison of the actuator force F_a with the amplified human force ρF_h. The thermodynamic process in the actuator is assumed to be isothermal.

arbitrary trajectory in free space. During interaction with hard surface ($21s < t < 23s$ and $26s < t < 28s$) the velocity plot in Fig. (5.8) and the force plot in Fig. (5.9) indicate an initial spike due to sudden change in momentum. However, the velocity of the inertia $\dot{x}$ and the velocity of virtual inertia $\dot{x}_v$ quickly settle down to zero. Again, even with high contact force exerted by the actuator, no contact instabilities are noticed. The velocity and the force co-ordination shown in Fig. (5.8) and Fig. (5.9) demonstrate that the desired external supply rate in Eq. (5.2) is achieved.

For demonstrating the desired passivity condition in Eq. (5.3), the input u_d to the virtual inertia dynamics in Eq. (5.10) is defined as given in Eq. (5.65). As seen from the Locked system dynamics in Eq. (5.19), this input on the virtual inertia input

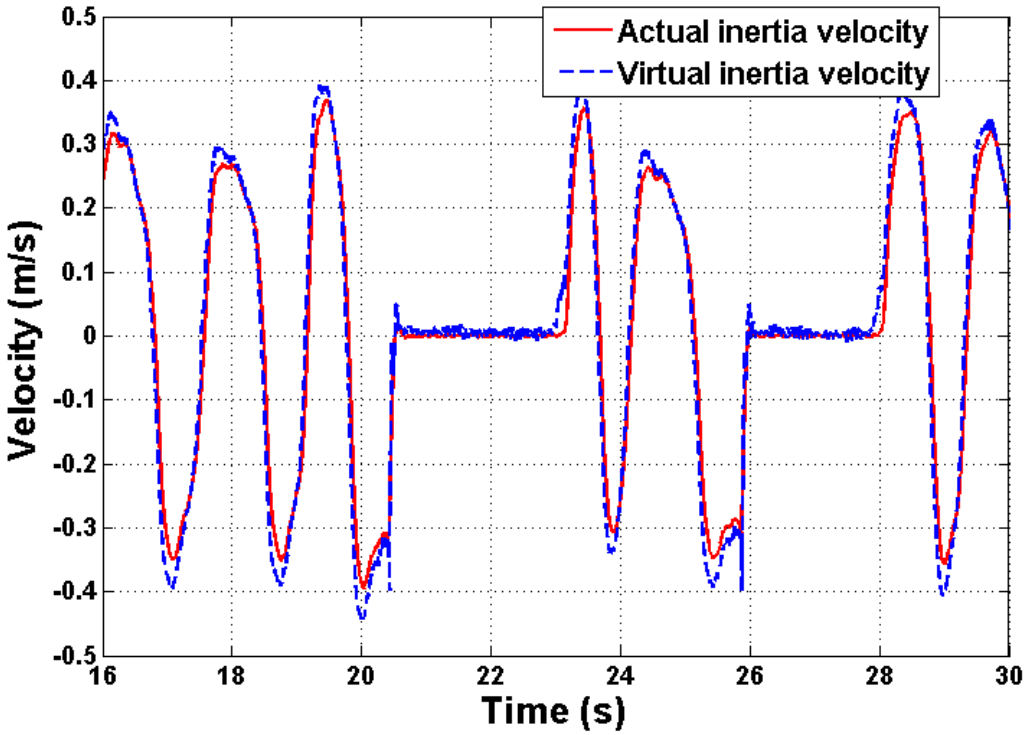

Figure 5.8: Comparison of the virtual inertia velocity $\dot{x}_v$ with the actual inertia velocity $\dot{x}$ during motion in free space and when interacting with a hard surface. The thermodynamic process in the actuator is assumed to be adiabatic.

will influence the response of the human power amplifier. To understand the effect of u_d on the "'feel"' factor experienced by the human operator, the magnitude of the ratio of nonlinear functions $\gamma_1^{iso,adb}(\boldsymbol{m}, \boldsymbol{P}, u)$ to $\gamma_3^{iso,adb}(\boldsymbol{m}, \boldsymbol{P}, \boldsymbol{P^d}, u)$ is investigated. For the isothermal and the adiabatic actuators, the magnitude of this ratio is as shown in Fig. (5.10) and Fig. (5.11) respectively. From these plots, it can be seen that during free motion, magnitude of the ratio of $\gamma_1^{iso,adb}(\boldsymbol{m}, \boldsymbol{P}, u)$ to $\gamma_3^{iso,adb}(\boldsymbol{m}, \boldsymbol{P}, \boldsymbol{P^d}, u)$ varies between 0.97 and 1.03. In these plots, the actuator position varies across its entire operation range, while tracking an arbitrary force profile. Therefore, these plots are a good representation of the expected magnitude of the ratio along most trajectories

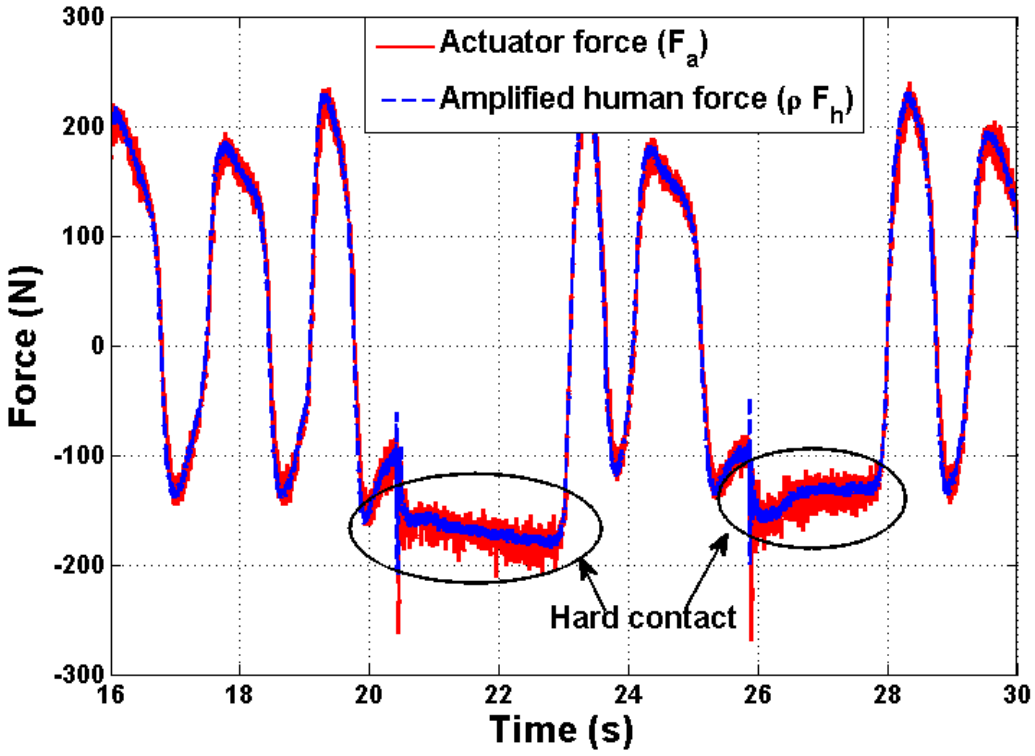

Figure 5.9: Comparison of the actuator force F_a with the amplified human force ρF_h. The thermodynamic process in the actuator is assumed to be adiabatic.

anticipated during operations of the power amplifier. On using the magnitude of this ratio in Eq. (5.65), the magnitude of input u_d is very small compared to other forces (such as F_a) acting on the Locked system. During interaction with a hard contact, the power amplifier is at rest ($\dot{x} = \dot{x}_v = 0$). For zero velocity of the amplifier, the input u_d is identically zero due to its definition. As observed in the reported experiments, the additional input u_d on the virtual mass M_v will therefore have negligible effect on the "'feel"' factor for the human operator while interacting with the power amplifier.

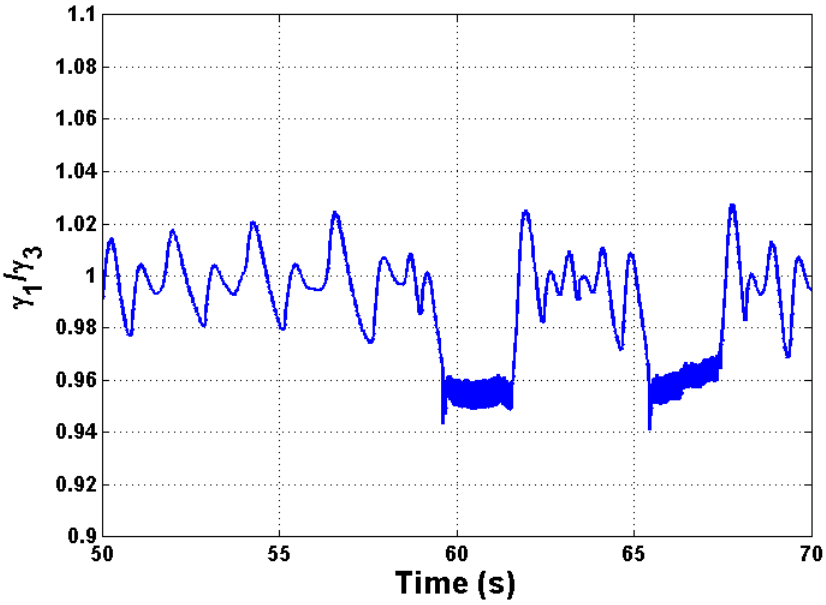

Figure 5.10: Magnitude of the ratio $\gamma_1^{iso}(\boldsymbol{m}, \boldsymbol{P}, u)/\gamma_3^{iso}(\boldsymbol{m}, \boldsymbol{P}, \boldsymbol{P^d}, u)$ used in the definition of u_d in Eq. (5.65) when the thermodynamic process is assumed to be isothermal.

5.6 Summary

In this chapter, passive controller for a two-chambered pneumatic actuator for providing the actuation force in human power amplifier has been presented. By modeling the fluid port flow variable of the reversible pneumatic system as a combination of a velocity source $\dot{x}_v$ (virtual inertia) under the influence of the amplified human force ρF_h and a feedback input u_{fb}, the problem of human power amplification is reformulated as a velocity co-ordination problem. Regulation of velocity co-ordination error $\dot{q}_E := (\dot{x} - \dot{x}_v)$ is achieved by using a standard back-stepping controller to determine the feedback input u_{fb} at the fluid port of the pneumatic actuator. Controllers for both adiabatic and isothermal actuator models were developed. These controllers were tested on a vertically mounted single DOF pneumatic actuator. The experimental results demonstrated efficacy of the controllers in achieving the desired velocity co-ordination and the associated human power amplification. Stable interaction with a hard metal surface was also

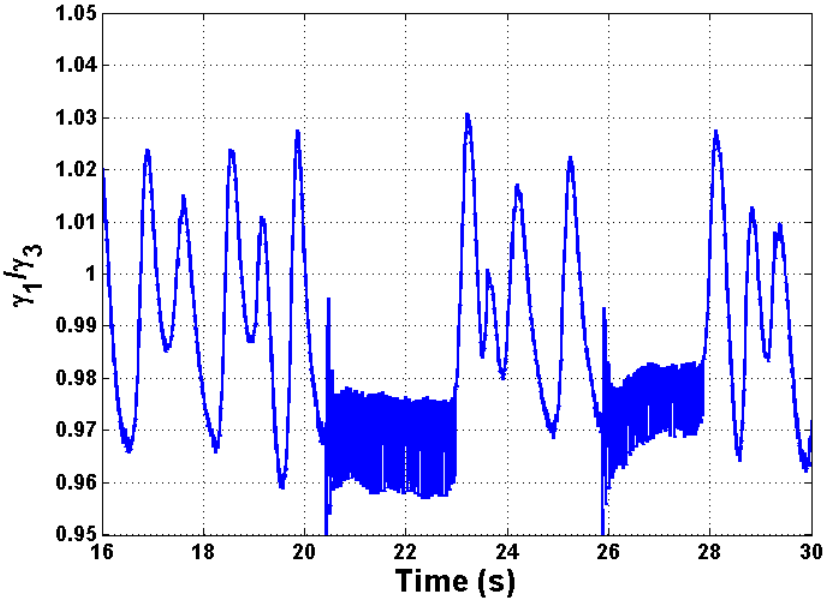

Figure 5.11: Magnitude of the ratio $\gamma_1^{adb}(\boldsymbol{m}, \boldsymbol{P}, u)/\gamma_3^{adb}(\boldsymbol{m}, \boldsymbol{P}, \boldsymbol{P^d}, u)$ used in the definition of u_d in Eq. (5.65), when the thermodynamic process is assumed to be adiabatic.

demonstrated in the experiments. Controllers designed under the assumption of both isothermal and adiabatic actuators have good velocity co-ordination and interaction stability, with no significant difference in their performance characteristics.

In the following chapter the proposed framework for human power amplification is extended to formulate a framework for tele-operation between multiple single-DOF pneumatic actuators. In chapter 7, the control methodology developed in this chapter and in chapter 6 are extended to a multi-DOF system and implemented on two legs of a pneumatically actuated rescue robot.

Chapter 6

Multilateral Tele-operation and Human Power Amplification with Single DOF Pneumatic Actuators

Tele-operation is typically used to extend the range of human influence to places that are remote to access. A tele-operation set-up typically consists of independent and physically separated systems that are expected to move in a co-ordinated fashion. Examples of operations with such characteristics include underwater exploration, tele-surgery, space exploration, or a nuclear reactor clean-up. In a tele-operation setting, one of the systems is accessible for direct human interaction and manipulation. This system is referred to as the *Master*. Other systems are typically expected to operate in regions that are normally inaccessible to humans and are expected to follow the position and velocity commands at the master. These systems are referred to as the *Slave* systems. By establishing a virtual interconnection between the master and each of the slave systems, the slaves are remotely operated by manipulating the master system. Thus, unlike a human power amplifier, the task accomplished by a tele-operator are not in the immediate vicinity of the human operator.

For intuitive tele-operation, it is preferable to provide haptic feedback about the interaction between the slave systems and the environment around them, to the human operator interacting with the master. This is achieved by formulating tele-operation in

a multilateral operation framework wherein the interaction force between a slave system and its surrounding environment is transmitted to the master system and the other slave systems. This force feedback at the master will inform the operator about the nature of environment interacting with the slave system, thus aiding the human operator to effectively navigate the slave systems remotely. Note that in some applications, external input at a slave system could be provided by another human operator, with the master and other slave systems expected to follow these command inputs. In this context, the master and the slave systems have equal status in our proposed framework for multilateral operation with multiple actuators. In applications such as remote under water exploration, or tele-surgery, the master and the slave systems are typically at different operating power range. In these applications, the master or the slave dynamics have to be appropriately scaled to provide reasonable force feedback and facilitate intuitive operation.

The downside of defining haptic feedback to be interaction forces is that any unstable interaction force is directly transmitted to the operator. Therefore stable interaction between the slave system and the environment is not only essential from operation stand point, but also for the safety of the human operator at the master system. As shown in earlier works [3], interaction between passive systems is guaranteed to be stable. The environment interacting with the slave systems is generally passive, while the muscle dynamics of the human operator can be approximated to be passive [4]. If passive interconnection is established between the master and the slave systems, then the interaction between them will be stable resulting in safe tele-operation. A framework for tele-operation between multiple single-DOF actuators is reported in this chapter. In the presented framework, the tele-operator behaves as a common passive mechanical tool that interacts simultaneously with mechanical power input from the human operators and the physical environments at the master and the slave systems. In the absence of the mechanical power input at the human interaction ports and physical environment ports, the system will remain at rest.

In chapter 3, it was shown that pneumatic actuators with reversible thermodynamics (isothermal/adiabatic) can be modeled as a two-port nonlinear spring. However, due to the active input at the fluid interaction port, the pneumatic actuator will not behave as a passive device. For achieving safe operation, passive behavior has to be

imposed on the master and the slave pneumatic actuators by appropriately controlling the flow input at the fluid port of both these actuators. In chapter 5, a framework for passive operation of single DOF human power amplifier with a pneumatic actuator was presented. In the current chapter, the control framework for human power amplification is extended to a system with multiple pneumatic actuated systems for achieving multilateral tele-operation along with amplification of input human power. The multilateral tele-operation framework proposed in this chapter can also be used to achieve tele-operation between systems with different actuating devices [75].

In the following section, the inertial dynamics of the master and the slave systems are presented. Dynamics of the pneumatic actuator for both the isothermal and adiabatic process have been presented in section 5.1 of the previous chapter and are hence not repeated here for brevity. The problem statement for multilateral tele-operation between single-DOF pneumatic actuators is presented in section 6.2. The framework for achieving passive multilateral tele-operation with human power amplification is presented in section 6.3.1. In this section it is shown that the framework proposed for human power amplifier in the previous chapter can be conveniently extended to achieve multilateral tele-operation. Controller design for position and velocity co-ordination between the two pneumatic actuators is presented in section 6.3.4. For investigating the effect of the assumed thermodynamic process on the system performance, controllers for both isothermal and adiabatic actuators are independently developed and evaluated. In section 6.5, experimental results from bilateral tele-operation between a single master and a single slave system are provided for demonstrating the effectiveness of the proposed controllers. In the experimental test bench used for evaluating the controllers, the master and the slave systems are co-located. As there is no communication delay between the two systems and the computer for evaluating the controller, the passivity framework proposed in this study assumes that there is no communication delay between the master and the slave systems. If the physical separation between the master and the slave systems increases, communication delay will introduce another source of non-passive behavior. Additional measures have to be taken to mitigate its adverse effects [76].

6.1 Dynamics of system with multiple actuators

Co-ordinated movement of multiple actuators can be used to move heavy loads for limited supply pressure. Schematic of such an application is as shown in Fig. (6.1). The actuator with the interface for direct human interaction is the master system. All the other actuators are the slave systems. For ease of presentation, it is assumed that the master and the multiple slave systems, are all single-DOF systems. The position x_m of the master actuator is measured using position sensors, while the velocity $\dot{x}_m$ is estimated from the position signal. It is assumed that position sensors are also available on all the slave systems. The position vector $\boldsymbol{x}_s$ and the velocity vector $\dot{\boldsymbol{x}}_s$ of the multiple slave actuators is defined as,

$$\boldsymbol{x}_s = \begin{pmatrix} x_{s_1} \\ x_{s_2} \\ x_{s_3} \\ \vdots \\ x_{s_N} \end{pmatrix}, \quad \dot{\boldsymbol{x}}_s = \begin{pmatrix} \dot{x}_{s_1} \\ \dot{x}_{s_2} \\ \dot{x}_{s_3} \\ \vdots \\ \dot{x}_{s_N} \end{pmatrix} \tag{6.1}$$

where x_{s_i} represents the position of the i^{th} slave actuator ($i = 4$ in Fig. (6.1)). The dynamics of the inertial mass M_m of the master are influenced by the interacting human force $F_h(t)$, the actuator force F_{a_m}, external environmental forces F_{e_m} and is given by,

$$M_m \ddot{x}_m = F_h(t) + F_{a_m} + F_{e_m} \tag{6.2}$$

In this chapter it is assumed that a force sensor is available at the human interaction interface to measure the applied force $F_h(t)$. For the operation shown in Fig. (6.1), the slave systems share the inertia being moved. In a generalized setting, the slave systems can form multiple groups that each share an inertial load, with other slave actuators moving each moving an independent inertial load. For simplicity of presentation, it is assumed in this chapter that the dynamics of the individual slave systems are decoupled from each other and from the master system. Multilateral co-ordination framework presented for these decoupled systems is also applicable to a system with groups of slave actuators sharing an inertial load.

Let M_{s_i} represent the inertia of the i^{th} slave system. The consolidated inertial matrix

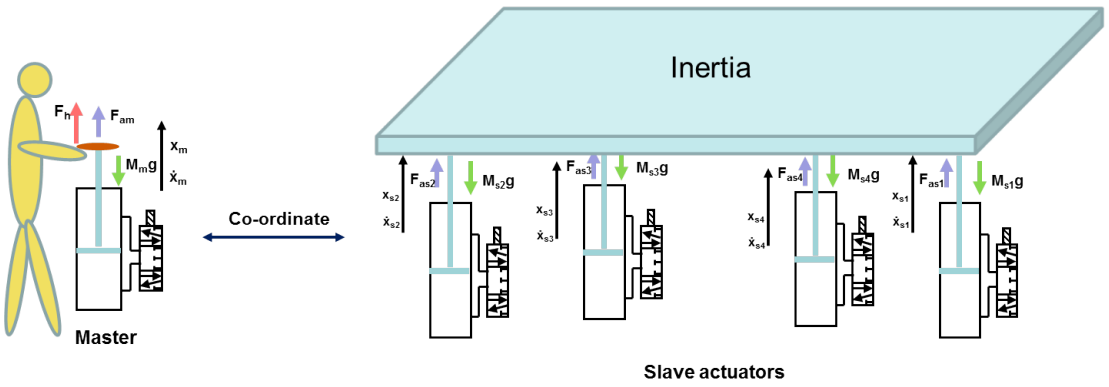

Figure 6.1: An illustration of an application where co-ordination between a master actuator and multiple ($N = 4$) slave actuators is used to move a heavy inertial load such as a sheet rock.

$\boldsymbol{M}_s$ of the slave systems is a diagonal matrix and is given by,

$$\boldsymbol{M}_s = \begin{pmatrix} M_{s_1} & 0 & 0 & \dots & 0 \\ 0 & M_{s_2} & 0 & \dots & 0 \\ 0 & 0 & M_{s_3} & \dots & 0 \\ \vdots & \vdots & \vdots & \ddots & \vdots \\ 0 & 0 & 0 & \dots & M_{s_N} \end{pmatrix} \tag{6.3}$$

The dynamics of the inertial matrix $\boldsymbol{M}_s$ are influenced by the slave actuator force vector $\boldsymbol{F}_{a_s} \in R^{N\times 1}$, the external (environmental) force vector $\boldsymbol{F}_{e_s} \in R^{N\times 1}$ and is given by,

$$\boldsymbol{M}_s \ddot{\boldsymbol{x}}_s = \boldsymbol{F}_{e_s} + \boldsymbol{F}_{a_s} \tag{6.4}$$

The external force $F_{e_{s_i}}$ on the i^{th} slave system includes gravitational force, unmodeled forces such as frictional force and other unknown external forces. The force exerted by the pneumatic actuator $(F_{a_m}, \boldsymbol{F}_{a_s})$ depends on the individual chamber pressure as shown in Eq. (5.6). The individual chamber pressure depends on the chamber air temperature, mass, and volume of chamber. In the following section, the actuator dynamics are briefly presented.

6.1.1 Actuator dynamics

The results presented in this chapter assume that the thermodynamic process in the actuator is reversible (isothermal/adiabatic). Pressure dynamics corresponding to isothermal and adiabatic actuators are as given in Eq. (5.8). By changing mass flow rate to each actuator chamber, the chamber pressure and thus the corresponding actuator force output can be varied. As shown in Eq. (5.9), mass flow rate to the actuator chamber is determined by the commanded effective flow area. As presented in section 3.1.1, the effective flow area is a function of the spool position, and is designated to be the command input to the pneumatic actuator.

Let u_m represent the commanded effective flow area in the valve connected to the master system, while $\boldsymbol{u}_s \in \boldsymbol{R}^{N\times 1}$ be the vector of commanded flow areas to the N single-DOF slave systems. In the following section, the problem statement describing the desired characteristics from co-ordination of multiple actuators is presented. In the subsequent section, appropriate command inputs to the master (u_m) and the slave systems ($\boldsymbol{u}_s$) for achieving the desired co-ordination characteristics is derived.

6.2 Problem statement

For ease of presentation, let $\boldsymbol{\mathcal{I}}_{N\times 1}$ be defined as the following vector,

$$\boldsymbol{\mathcal{I}}_{N\times 1} = \begin{pmatrix} 1 \\ 1 \\ 1 \\ \vdots \\ 1 \end{pmatrix}_{N\times 1} \tag{6.5}$$

The desired characteristics of operation of multiple actuators in the applications such as shown in Fig. (6.1) are:

1. *Position and velocity co-ordination:* To execute the defined task with multiple pneumatic (or hydraulic) actuators, position and velocity co-ordination between the actuators is required. For a system with N slave actuators, the co-ordination problem can be stated as,

$$\textbf{Position co-ordination}: \quad \bar{\boldsymbol{q}}_E = x_m \boldsymbol{\mathcal{I}}_{N\times 1} - \boldsymbol{x}_s \rightarrow \boldsymbol{0}_{N\times 1} \tag{6.6}$$

$$\textbf{Velocity co-ordination}: \quad \dot{\boldsymbol{q}}_E = \dot{x}_m \boldsymbol{\mathcal{I}}_{N\times 1} - \dot{\boldsymbol{x}}_s \rightarrow \mathbf{0}_{N\times 1} \tag{6.7}$$

where $\boldsymbol{\mathcal{I}}_{N\times 1}$ is as defined in Eq. (6.5).

2. *Multilateral-operation:* A desired characteristic of interaction between the master system and the multiple slave systems is multilateral operation, wherein the forces acting on the master or any of the slave systems will influence the dynamic response of all the systems. The resulting force feedback at the master system of the environmental force acting on any of the slave systems will allow the operator to navigate the co-ordinated system intuitively.

3. *Human power amplification and Master power scaling:* Pneumatic actuators typically have very high stiffness over the entire stroke length. While interacting with a pneumatic actuated master system, it is very strenuous for the human operator to work against the actuator stiffness and provide the required position and velocity commands. To aid the operator, the input human power at the master system is amplified by the master actuator. In some applications there is significant difference in the operating power range of the master and the slave systems. In such scenarios, it is desirable to impose power scaling on the interaction between the master and the slave systems. In this chapter it is assumed that all the slave actuators are in the same power range and that this power range is different from the master system. Let $\eta > 1$ be the amplification factor on the input human force $F_h(t)$ and $\rho \in \Re^+$ represent power scaling from the master to the slave systems that ensures that the master and the slave systems are in the same power range. The preferred supply rate to the co-ordinated system with power scaling from the master to the slave and with human power amplification is then given by,

$$s_m(F_h, F_{e_m}, \boldsymbol{F}_{e_s}, \dot{x}_m, \dot{\boldsymbol{x}}_s) := \rho((\eta+1)F_h(t) + F_{e_m})\dot{x}_m + \boldsymbol{F}_{e_s}^T \dot{\boldsymbol{x}}_s \tag{6.8}$$

If the operating power range of the master is larger than a slave system (example application: Tele-surgery), then the scaling factor ρ is selected to be smaller than 1. The assigned value to ρ would be greater than 1 if the operating power range of the master is less than the corresponding slave system (example application : under water exploration).

4. *Passive operation:* Stable multilateral operation can be achieved by imposing passive dynamics on the operation of pneumatic actuated systems. Passive co-ordinated multilateral operation is achieved if the desired supply rate in Eq. (6.8) satisfies the following condition for all time t,

$$\int_0^t s_m(F_h, F_{e_m}, \boldsymbol{F}_{e_s}, \dot{x}_m, \dot{\boldsymbol{x}}_{\boldsymbol{s}})\ d\tau > -d_o^2 \tag{6.9}$$

where $d_o^2 \in \Re^+$, and represents the maximum work that can be extracted from the co-ordinated system for no external input energy. If position and velocity co-ordination is achieved ($\dot{x}_m = \dot{x}_{s_1} = \dot{x}_{s_2} = \cdots = \dot{x}_{s_N} = \dot{x}_c$), then the desired passivity condition for the co-ordinated system is obtained from Eq. (6.9) as,

$$\int_0^T s_m(F_h, F_{e_m}, \boldsymbol{F}_{e_s}, \dot{x}_c, \dot{x}_c \boldsymbol{\mathcal{I}}_{N\times 1})\ d\tau > -d_o^2 \tag{6.10}$$

where $\dot{x}_c$ represents the velocity of a co-ordinated system and $\boldsymbol{\mathcal{I}}_{N\times 1}$ is as defined in Eq. (6.5).

A framework for designing the controller to achieve the objectives enumerated in this section is presented in the following section.

6.3 Controller design

As presented in section 3.2.4, a pneumatic actuator with reversible thermodynamics can be modeled as a two-port nonlinear spring, with one port connected to the mechanical inertia and the other port corresponding to interaction with fluid source. This representation of the pneumatic actuator was used to formulate a framework for passive operation of human power amplifier in section 5.3.2. In this section, the framework for human power amplification is extended to multilateral tele-operation with human power amplification. Within this framework, the objectives of the control input for achieving the desired characteristics of the tele-operator presented in the previous section are then formulated. Similar to the controller design presented in section 5.3.2, a two-stage back-stepping controller is then used to achieve the desired control objectives.

6.3.1 Framework for multilateral operation with human power amplification

To achieve passive operation of human power amplifier,in section 5.3.2 a virtual inertia under the influence of desired external forces was used as a passive realization of the flow input at the fluid port of the actuator. For multilateral tele-operation with human power amplification, the fluid port flow variable for the master and N slave systems is similarly realized as velocity of a virtual inertia. This is illustrated in Fig. (6.2). In this figure, F_{v_m} represents the desired external force on the virtual inertia connected to master, while $F_{v_{s_i}}$ represents the desired external force on the virtual inertia connected to the i^{th} slave actuator.

Power-scaling from master to slave system:

To achieve power scaling from the master to the slave, the dynamics of the master are scaled while designing the controller. As illustrated in Fig. (6.2), the master inertia and the effort variables on the master system are scaled by the factor ρ to achieve this power scaling.

Multi-lateral operation:

On using a common virtual inertial as illustrated in Fig. (6.3), the master and the slave systems are interconnected such that external interaction forces at either the master or the slave systems will propagate through the internal connections to effect the response of all the other systems. Therefore, a common virtual inertia ensures multilateral operation. State feedback is however required to achieve position and velocity co-ordination. Feedback inputs (u_{f_m} and $u_{f_{s_i}}$ in Fig. (6.3)) at the fluid port of the master and the slave actuators will have to be designed to achieve the desired multilateral tele-operation.

Human power amplification:

As presented in section 5.3.2, the framework for amplification of the input human power at the master requires application of amplified human force on the virtual mass. Let η represents the desired amplification of the human power at the master system. The amplified human force $\rho\eta F_h$ is then imposed on the virtual inertia as illustrated in Fig.

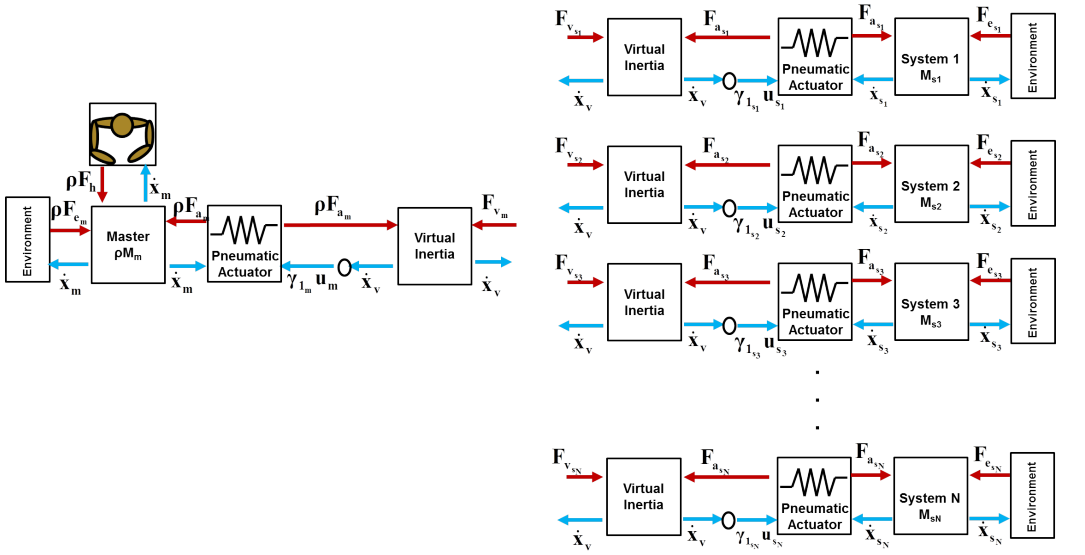

Figure 6.2: Port representation of the master and the slave pneumatic actuated systems with the flow source represented by a virtual mass. The master dynamics are scaled by ρ to achieve power scaling from the master to the slave systems.

(6.3). An additional input u_d is applied on the virtual mass to ensure passive operation of the co-ordinated system. From Fig. (6.3), dynamics of the virtual inertia are obtained as,

$$M_v \ddot{x}_v = \rho \eta F_h - u_d - \rho F_{a_m} - \boldsymbol{F}_{a_s}^T \boldsymbol{\mathcal{I}}_{N\times 1} \tag{6.11}$$

where $\boldsymbol{\mathcal{I}}_{N\times 1}$ is as defined in Eq. (6.5).

Co-ordination of multiple fluid-powered slave actuators with an electrically driven master:

The framework for human power amplification and co-ordination of multiple pneumatic actuators shown in Fig. (6.3) can also be extended to systems wherein the master is actuated by an electric motor where the motor torque cab be directly commanded. In this scenario, the virtual inertia is not required and the master inertial system connected to the motor is used in its place. The flow variable at the fluid port at all the slave pneumatic actuators is determined by the velocity of the master. Power amplification

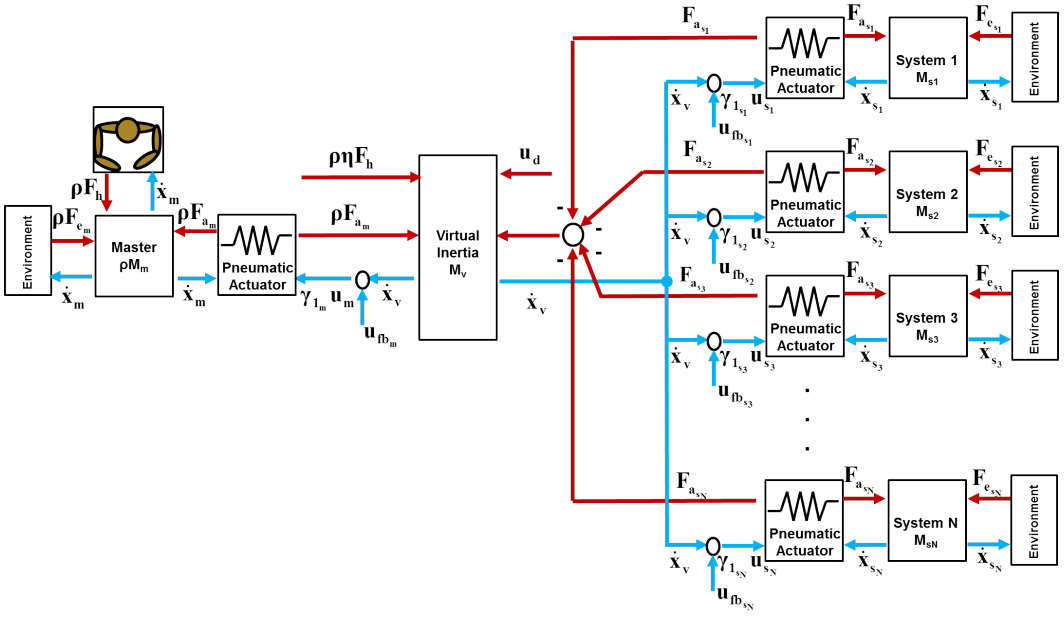

Figure 6.3: Schematic of the solution framework for achieving multilateral operation and human power amplification in systems where both the master and the slave are pneumatic actuated.

is achieved by suitably amplifying the master dynamics. For an electric motor torque of F_m and a desired power amplification of ρ from the slave to the master, the framework for multilateral operation with human power amplification is as shown in Fig. (6.4).

The focus of this chapter is on design of controllers for pneumatically actuated master and slave systems. Formulation of the control problem is presented in the following subsection. Controller design for tele-operation with electrically actuated master is presented in the next chapter.

6.3.2 Control problem formulation

Based on the interconnection presented in Fig. (6.3), the objectives of the feedback controller for achieving multilateral tele-operation with human power amplification can now be stated as, *1. Position co-ordination between master and slave systems as given*

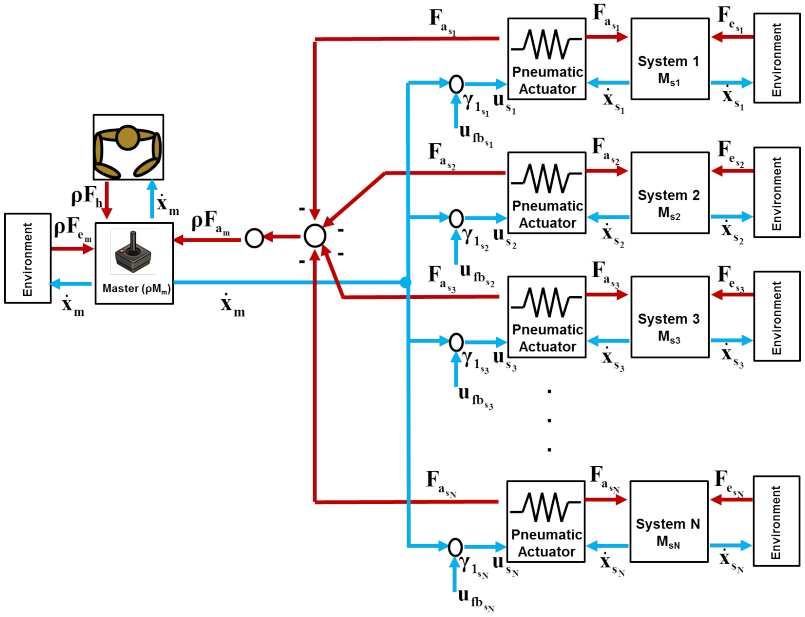

Figure 6.4: Schematic of the solution framework for achieving multilateral operation and human power amplification in systems where the master is driven by electric actuator while the slave is pneumatically actuated.

in Eq. (6.6)

$$\bar{\boldsymbol{q}}_E(x_m, \boldsymbol{x}_s) := \begin{pmatrix} x_m \\ x_m \\ x_m \\ \vdots \\ x_m \end{pmatrix}_{N\times 1} - \begin{pmatrix} x_{s_1} \\ x_{s_2} \\ x_{s_3} \\ \vdots \\ x_{s_N} \end{pmatrix} \rightarrow \mathbf{0}_{N\times 1} \tag{6.12}$$

2. Velocity co-ordination between master, slave and virtual inertial systems

$$\boldsymbol{V_E}(\dot{x}_m, \dot{x}_v, \dot{\boldsymbol{x}}_s) := \begin{pmatrix} \dot{x}_m - \dot{x}_v \\ \dot{x}_m - \dot{x}_{s_1} \\ \dot{x}_m - \dot{x}_{s_2} \\ \vdots \\ \dot{x}_m - \dot{x}_{s_N} \end{pmatrix} \rightarrow \mathbf{0}_{(N+1)\times 1} \tag{6.13}$$

while satisfying the desired passivity condition in Eq. (6.10). The velocity co-ordination error $\boldsymbol{V}_E(\dot{x}_m, \dot{x}_v, \dot{\boldsymbol{x}}_s)$ in the above equation includes all the elements of the original co-ordination error $\dot{\tilde{\boldsymbol{q}}}_E$ in Eq. (6.7). From Fig. (6.3) dynamics of the co-ordinated tele-operator can be expressed as,

$$(\rho M_m + M_v + \sum_{i=1}^{N} M_{s_i})\ddot{x}_c = \rho((\eta+1)F_h + F_{e_m}) + \boldsymbol{F}_{e_s}^T \boldsymbol{\mathcal{I}}_{N\times 1} - u_d \tag{6.14}$$

where $\dot{x}_c$ represents the velocity of the co-ordinated system and u_d is the damping input on the virtual inertia imposed to guarantee passive operation. This input is designed in section 6.4. With an inertia of $(\rho M_m + M_v + \sum_{i=1}^{N} M_{s_i})$, the co-ordinated system moves only under the influence of external forces and thus behaves as a common passive mechanical tool with multiple mechanical ports corresponding to human force and other environmental forces available for power interaction. The co-ordinated tele-operator dynamics in Eq. (6.14) are similar to the desired dynamics of a human power amplifier in Eq. (5.11), with the cumulative actuator forces after co-ordination related to the amplified human force as,

$$(\rho F_{a_m} + \boldsymbol{F}_{a_s}^T \boldsymbol{\mathcal{I}}_{N\times 1}) = \rho\eta F_h \tag{6.15}$$

where $\boldsymbol{\mathcal{I}}_{N\times 1}$ is as defined in Eq. (6.5). In the following section, transformation of the velocity state space to obtain the dynamics of the velocity co-ordination error are presented.

6.3.3 Passive velocity decomposition

As explained in section 6.3.1 (and illustrated in Fig. (6.2)), the co-ordination controller is formulated by scaling the master dynamics by a factor ρ. This is done to achieve power amplification from the master to the slave subsystem. Therefore from the inertial dynamics of the master system, the slave system and the virtual inertia in Eqs. (6.2, 6.4, and 6.11) respectively, the inertial dynamics of interest for controller design are

given by,

$$\begin{pmatrix} \rho M_m & 0 & \mathbf{0}_{1\times N} \\ 0 & M_v & \mathbf{0}_{1\times N} \\ \mathbf{0}_{N\times 1} & \mathbf{0}_{N\times 1} & \boldsymbol{M}_s \end{pmatrix} \begin{pmatrix} \ddot{x}_m \\ \ddot{x}_v \\ \ddot{\boldsymbol{x}}_s \end{pmatrix} = \underbrace{\begin{pmatrix} \rho & \mathbf{0}_{1\times N} \\ -\rho & -\boldsymbol{\mathcal{I}}_{1\times N} \\ \mathbf{0}_{N\times 1} & \boldsymbol{I}_{N\times N} \end{pmatrix}}_{\boldsymbol{B}} \underbrace{\begin{pmatrix} F_{a_m} \\ \boldsymbol{F}_{a_s} \end{pmatrix}}_{\boldsymbol{F_a}} + \underbrace{\begin{pmatrix} \rho(F_h + F_{e_m}) \\ \rho\eta F_h - u_d \\ \boldsymbol{F}_{e_s} \end{pmatrix}}_{\boldsymbol{F_{ex}}} \tag{6.16}$$

where $\boldsymbol{\mathcal{I}}_{m\times n}$ is an $m \times n$ matrix with all entries corresponding to one, $\boldsymbol{I}_{N\times N}$ represents the $(N \times N)$ identity matrix, $\boldsymbol{F_a}$ represents the actuator force vector, while $\boldsymbol{F_{ex}}$ represents the vector of all the other forces acting on the inertial system.

Transformation Matrix

By using the passive decomposition presented in section 5.3.3 for human power amplifier, the velocity space $(\dot{x}_m, \dot{x}_v, \dot{\boldsymbol{x}}_s)$ of the tele-operator is transformed to obtain dynamics of the center of mass of the tele-operator and the co-ordination error dynamics. In accordance with the terminology presented in [30], the system representing the dynamics of the center of mass system is referred to as the *Locked system*, while the system representing the co-ordination error dynamics is referred to as the *Shape system*. The velocity vector transformation for the tele-operator is defined as,

$$\begin{pmatrix} V_L \\ V_{E_1} \\ V_{E_2} \\ V_{E_3} \\ \vdots \\ V_{E_{N+1}} \end{pmatrix} = \underbrace{\begin{pmatrix} \frac{\rho M_m}{M_L} & \frac{M_v}{M_L} & \frac{M_{s_1}}{M_L} & \frac{M_{s_2}}{M_L} & \dots & \frac{M_{s_N}}{M_L} \\ 1 & -1 & 0 & 0 & \dots & 0 \\ 1 & 0 & -1 & 0 & \dots & 0 \\ 1 & 0 & 0 & -1 & \ddots & 0 \\ \vdots & \vdots & \ddots & \ddots & \ddots & 0 \\ 1 & 0 & 0 & 0 & \dots & -1 \end{pmatrix}}_{\boldsymbol{S}} \begin{pmatrix} \dot{x}_m \\ \dot{x}_v \\ \dot{\boldsymbol{x}}_s \end{pmatrix} \tag{6.17}$$

where $M_L \triangleq (\rho M_m + M_v + \sum_{i=1}^{N} M_{s_i})$ corresponds to the inertia of the Locked system, $\boldsymbol{S} \in \boldsymbol{R}^{(N+1)\times(N+1)}$ represents the transformation matrix, V_L corresponds to velocity

of the Locked system, while $V_{E_i} := (\dot{x}_m - \dot{x}_{s_i})$, $i \in (1, \ldots, N+1)$ corresponds to the velocity co-ordination error described in Eq. (6.13). The velocity co-ordination error vector $\boldsymbol{V}_E = (V_{E_1}, V_{E_2}, \ldots, V_{E_{N+1}})$ represents the state vector of the Shape system dynamics.

Inertial dynamics in transformed space

The total energy associated with the inertial dynamics has to remain the same, irrespective of the state space used to represent the velocity vector. The combined inertia matrix $\boldsymbol{M}_T$ consisting of the Locked system inertia M_L and the Shape system inertia matrix $\boldsymbol{M}_E \in \boldsymbol{R}^{(N+1)\times(N+1)}$ is obtained as,

$$\boldsymbol{M}_T = \boldsymbol{S}^{-T} \begin{pmatrix} \rho M_m & 0 & \mathbf{0}_{1\times N} \\ 0 & M_v & \mathbf{0}_{1\times N} \\ \mathbf{0}_{N\times 1} & \mathbf{0}_{N\times 1} & \boldsymbol{M}_s \end{pmatrix} \boldsymbol{S}^{-1} = \begin{pmatrix} M_L & \mathbf{0}_{1\times(N+1)} \\ \mathbf{0}_{(N+1)\times 1} & \boldsymbol{M_E} \end{pmatrix} \tag{6.18}$$

where $\mathbf{0}_{mxn}$ represents a zero matrix of m rows and n columns. The inertial matrix $\boldsymbol{M_T}$ in the above equation satisfies the conservation of kinetic energy before and after velocity transformation,

$$\frac{1}{2} \begin{pmatrix} V_L & \boldsymbol{V}_E^T \end{pmatrix} \boldsymbol{M}_T \begin{pmatrix} V_L \\ \boldsymbol{V}_E \end{pmatrix} = \frac{\rho}{2} M_m \dot{x}_m^2 + \frac{1}{2} M_v \dot{x}_v^2 + \frac{1}{2} \dot{\boldsymbol{x}}_s^T M_s \dot{\boldsymbol{x}}_s \tag{6.19}$$

Using the definition of the velocity transformation matrix $\boldsymbol{S}$ in Eq. (6.17), the inertial elements of the Locked and the Shape system are obtained in terms of the master inertia M_m, virtual inertia M_v and the inertias M_{s_i} $i \in (1, N)$ of the N slave systems as,

$$\begin{aligned} M_L &:= (\rho M_m + M_v + M_{s_1} + M_{s_2} + \cdots + M_{s_N}) \\ \boldsymbol{M_E} &:= \begin{pmatrix} \frac{M_v(\rho M_m + \sum_{i=1}^N M_{s_i})}{M_L} & -\frac{M_v M_{s_1}}{M_L} & -\frac{M_v M_{s_2}}{M_L} & \cdots & -\frac{M_v M_{s_N}}{M_L} \\ -\frac{M_{s_1} M_v}{M_L} & \frac{M_{s_1} M_{11}}{M_L} & -\frac{M_{s_1} M_{s_2}}{M_L} & \cdots & -\frac{M_{s_1} M_{s_N}}{M_L} \\ -\frac{M_{s_2} M_v}{M_L} & \frac{M_{s_2} M_{s_1}}{M_L} & \frac{M_{s_2} M_{22}}{M_L} & \cdots & -\frac{M_{s_2} M_{s_N}}{M_L} \\ \vdots & \vdots & \vdots & \ddots & \vdots \\ -\frac{M_{s_N} M_v}{M_L} & \frac{M_{s_N} M_{s_1}}{M_L} & -\frac{M_{s_N} M_{s_2}}{M_L} & \cdots & \frac{M_{s_N} M_{NN}}{M_L} \end{pmatrix} \end{aligned} \tag{6.20}$$

where for $j \in (1, N)$, $M_{jj} := (\rho M_m + M_v + \sum_{i=1}^N M_{s_i} - M_{s_j})$. From the inertial transformation in Eq. (6.18) the coefficient matrix $\boldsymbol{B}$ and the force vector $\boldsymbol{F_{ex}}$ in Eq.

(6.16) are obtained in the transformed space as,

$$\boldsymbol{B_t} = \boldsymbol{S^{-T}B} = \begin{pmatrix} \boldsymbol{B_L} \\ \boldsymbol{B_E} \end{pmatrix}, \quad \boldsymbol{F_T} = \boldsymbol{S^{-T}F_{ex}} = \begin{pmatrix} F_L \\ \boldsymbol{F_E} \end{pmatrix} \tag{6.21}$$

where $\boldsymbol{B_L} \in \boldsymbol{R^{1\times(N+1)}}$ is the coefficient matrix for the Locked system dynamics, $\boldsymbol{B_E} \in \boldsymbol{R^{(N+1)\times(N+1)}}$ is the invertible coefficient matrix for the Shape system dynamics and are obtained as,

$$\boldsymbol{B_L} = \begin{pmatrix} 0 \\ 0 \\ 0 \\ \vdots \\ 0 \end{pmatrix}^T, \quad \boldsymbol{B_E} = \begin{pmatrix} \rho & 1 & 1 & 1 & \dots & 1 \\ 0 & -1 & 0 & 0 & \dots & 0 \\ 0 & 0 & -1 & 0 & \dots & 0 \\ 0 & 0 & 0 & -1 & \dots & 0 \\ \vdots & \vdots & \vdots & \vdots & \ddots & \vdots \\ 0 & 0 & 0 & 0 & \dots & -1 \end{pmatrix} \tag{6.22}$$

while the force F_L on the Locked system and the force vector $\boldsymbol{F_E} \in \boldsymbol{R^{(N+1)\times 1}}$ on the Shape system are obtained as,

$$\begin{aligned} F_L &= \rho((\eta+1)F_h + F_{e_m}) - u_d + \boldsymbol{\mathcal{I}_{1\times N}F_{e_s}} \\ \boldsymbol{F_E} &= \begin{pmatrix} \frac{M_v}{M_L}F_L - (\rho\eta F_h - u_d) \\ \frac{M_{s_1}}{M_L}F_L - F_{e_{s_1}} \\ \frac{M_{s_2}}{M_L}F_L - F_{e_{s_2}} \\ \vdots \\ \frac{M_{s_N}}{M_L}F_L - F_{e_{s_N}} \end{pmatrix} \end{aligned} \tag{6.23}$$

Applying the inertial transformation from Eq. (6.18) and the velocity transformation from Eq. (6.17) to the dynamics in Eq. (6.16), the Locked and the Shape system inertial dynamics are obtained as,

$$\textbf{Locked system dynamics:} \quad M_L\dot{V}_L = F_L \tag{6.24}$$

$$\textbf{Shape system dynamics:} \quad \boldsymbol{M}_E\dot{\boldsymbol{V}}_E = \boldsymbol{B_E F_a} - \boldsymbol{F_E} \tag{6.25}$$

where the coefficient matrix $\boldsymbol{B_E}$ on the actuator force vector $\boldsymbol{F_a} \in \boldsymbol{R}^{(N+1)\times 1}$ given in Eq. (6.22) is an invertible matrix, and $\boldsymbol{F_E} \in \boldsymbol{R}^{(N+1)\times 1}$ given in Eq. (6.23) represents the vector of external forces acting on the Shape system. In a co-ordination problem

with a single slave system ($N = 1$), the coefficient matrix $\boldsymbol{B_E}$ and the force vector $\boldsymbol{F_E}$ are obtained as,

$$\boldsymbol{B_E} = \begin{pmatrix} \rho & 1 \\ 0 & -1 \end{pmatrix}, \quad \boldsymbol{F_E} = \begin{pmatrix} \frac{\rho M_v}{M_L}(\rho((\eta+1)F_h + F_{e_m}) + F_{e_{s_1}} - u_d) - (\rho\eta F_h - u_d) \\ \frac{M_{s_1}}{M_L}(\rho((\eta+1)F_h + F_{e_m}) + F_{e_{s_1}} - u_d) - F_{e_{s_1}} \end{pmatrix} \tag{6.26}$$

After the desired velocity co-ordination is achieved ($\dot{x}_m = \dot{x}_v = \dot{x}_{s_i} = V_L$, $\boldsymbol{V}_E = \boldsymbol{0}$), the Locked system dynamics in Eq. (6.24) represent the desired dynamics of the co-ordinated system in Eq. (6.14).

6.3.4 Shape system regulation

Controller design for regulation of the Shape system dynamics in Eq. (6.25) is presented in this subsection. The position co-ordination error vector $\boldsymbol{q_E} \in \boldsymbol{R}^{(N+1)\times 1}$ corresponding to the velocity co-ordination error vector $\boldsymbol{V_E}$ in Eq. (6.17) is given by,

$$\boldsymbol{q_E} = \begin{pmatrix} \int(\dot{x}_m - \dot{x}_v)\, dt \\ (x_m - x_{s_1}) \\ (x_m - x_{s_2}) \\ \vdots \\ (x_m - x_{s_N}) \end{pmatrix} \tag{6.27}$$

The dynamics of the position co-ordination error $\boldsymbol{q_E}$ and the velocity co-ordination error $\boldsymbol{V_E}$ are given by,

$$\begin{aligned} \dot{\boldsymbol{q}}_{\boldsymbol{E}} &= \boldsymbol{V_E} \\ \boldsymbol{M_E}\dot{\boldsymbol{V}}_{\boldsymbol{E}} &= \boldsymbol{B_E F_a} - \boldsymbol{F_E} \end{aligned} \tag{6.28}$$

Regulation of position error vector $\boldsymbol{q_E}$ will ensure that the desired position co-ordination in Eq. (6.12) is also achieved. The actuator force vector $\boldsymbol{F_a}$ is the controllable input to the Shape system inertial dynamics. For pneumatic actuators, the force output depends on the chamber pressure, which can be modulated by changing the input commands to the flow control valve. The valve command input does not directly influence the inertial dynamics of the Shape system. Due to this cascaded structure, a two-stage back-stepping controller is again used to determine the valve command input. The actuator force vector required for regulating the states of the inertial subsystem is

determined in the first stage of the controller design. In the second stage of the controller design, the required command inputs (u_m, $\boldsymbol{u}_s$) to the pneumatic actuators for providing the desired actuator forces is determined. First stage of the controller design is presented in the next section.

First stage controller design

Let $\boldsymbol{F_a^d}$ represent the actuator force vector required for regulation of Shape system dynamics. Consider the following Lyapunov function for design of this force vector in the first stage of controller design,

$$\bar{V}_1(\boldsymbol{q_E}, \boldsymbol{V_E}) = \frac{1}{2}\begin{pmatrix} \boldsymbol{V_E^T} & \boldsymbol{q_E^T} \end{pmatrix} \underbrace{\begin{pmatrix} \boldsymbol{M_E} & \boldsymbol{\varepsilon M_E} \\ \boldsymbol{\varepsilon M_E} & \boldsymbol{K_p + \varepsilon K_v} \end{pmatrix}}_{\boldsymbol{\mathcal{Q}}} \begin{pmatrix} \boldsymbol{V_E} \\ \boldsymbol{q_E} \end{pmatrix} \tag{6.29}$$

where $\boldsymbol{K_p} \in \boldsymbol{R}^{(N+1)\times(N+1)}$, $\boldsymbol{K_v} \in \boldsymbol{R}^{(N+1)\times(N+1)}$ are constant positive definite diagonal matrices, and $\boldsymbol{\varepsilon} \in \Re^+$ is a sufficiently small positive constant selected such that $\mathcal{Q}$ in Eq. (6.29) is a positive definite matrix. Therefore the Lyapunov function $\bar{V}_1(\boldsymbol{q_E}, \boldsymbol{V_E})$ in Eq. (6.29) can be bounded as,

$$\frac{1}{2}\sigma_{min}(\boldsymbol{\mathcal{Q}}) \left\| \begin{pmatrix} \boldsymbol{V_E} \\ \boldsymbol{q_E} \end{pmatrix} \right\|^2 \leq \bar{V}_1(\boldsymbol{q_E}, \boldsymbol{V_E}) \leq \frac{1}{2}\sigma_{max}(\boldsymbol{\mathcal{Q}}) \left\| \begin{pmatrix} \boldsymbol{V_E} \\ \boldsymbol{q_E} \end{pmatrix} \right\|^2 \tag{6.30}$$

where $\sigma_{min}(.)$ and $\sigma_{max}(.)$ correspond to the operators for determining the minimum and the maximum singular values. Using the Shape system dynamics from Eq. (6.28), the derivative $\dot{\bar{V}}_1(\boldsymbol{q_E}, \boldsymbol{V_E})$ of the Lyapunov function in Eq. (6.29) is obtained as,

$$\begin{aligned} \dot{\bar{V}}_1(\boldsymbol{q_E}, \boldsymbol{V_E}) = (\boldsymbol{V_E^T} + \boldsymbol{\varepsilon q_E})(\boldsymbol{B_E F_a} - \boldsymbol{F_E} + \boldsymbol{K_p q_E} + \boldsymbol{K_v V_E}) - \boldsymbol{V_E^T}(\boldsymbol{K_v} - \boldsymbol{\varepsilon M_E})\boldsymbol{V_E} \\ - \boldsymbol{q_E^T K_p q_E} \end{aligned} \tag{6.31}$$

Perfect information on $\boldsymbol{F_E}$: When information about all the external forces influencing $\boldsymbol{F_E}$ in Eq. (6.26) (for $N = 1$) and Eq. (6.28) are known, if the actuator force $\boldsymbol{F_a}$ corresponds to the following desired force vector $\boldsymbol{F_a^d}$,

$$\boldsymbol{F_a^d} = \boldsymbol{B_E^{-1}}(\boldsymbol{F_E} - \boldsymbol{K_p q_E} - \boldsymbol{K_v V_E}) \tag{6.32}$$

then the derivative $\dot{\bar{V}}_1(\boldsymbol{q_E}, \boldsymbol{V_E})$ of the Lyapunov function in Eq. (6.31) can be simplified as,

$$\begin{aligned}\dot{\bar{V}}_1(\boldsymbol{q_E}, \boldsymbol{V_E}) &= -\begin{pmatrix} \boldsymbol{V_E^T} & \boldsymbol{q_E^T} \end{pmatrix} \underbrace{\begin{pmatrix} \boldsymbol{K_v} - \varepsilon \boldsymbol{M_E} & \boldsymbol{0_{N+1}} \\ \boldsymbol{0_{N+1}} & \boldsymbol{K_p} \end{pmatrix}}_{\boldsymbol{\mathcal{P}}} \begin{pmatrix} \boldsymbol{V_E} \\ \boldsymbol{q_E} \end{pmatrix} \\ &< -\frac{2\sigma_{min}(\boldsymbol{\mathcal{P}})}{\sigma_{max}(\boldsymbol{\mathcal{Q}})}\, \bar{V}_1(\boldsymbol{q_E}, \boldsymbol{V_E})\end{aligned} \tag{6.33}$$

where $\boldsymbol{0_{N+1}} \in \boldsymbol{R}^{(N+1)\times(N+1)}$ represents a zero matrix with $(N+1)$ rows and $(N+1)$ columns. The matrix $\boldsymbol{\mathcal{P}}$ On integrating both sides of Eq. (6.33) it can be shown that for an appropriately small $\boldsymbol{\varepsilon}$, the Lyapunov function $\bar{V}_1(\boldsymbol{q_E}, \boldsymbol{V_E})$ converges exponentially to zero. As the Lyapunov function is defined to be a positive definite function in the Shape system states ($\boldsymbol{q_E}$, $\boldsymbol{V_E}$), exponential regulation of the position and velocity error is also achieved.

***F_E* not completely known:** The actuator force vector required for exponential convergence, as defined in Eq. (6.32), requires perfect information of all the external forces ($\boldsymbol{F_E}$ in Eq. (6.28) and Eq. (6.26) for $N = 1$) acting on the system. This can be achieved by integrating appropriate force sensors on the tele-operator. But the force sensors tend to be fairly expensive. In addition, forces such as friction are not easy to model for exact compensation. Therefore, it was deemed preferable to estimate the un-modeled and unknown external forces acting on the system.

Let $\hat{\boldsymbol{F}}_{\boldsymbol{E}}$ represent the estimate of the force $\boldsymbol{F_E}$ acting on the Shape system. The desired actuator force in Eq. (6.32) is defined in terms of this force estimate as,

$$\boldsymbol{F_a^d = B_E^{-1}(\hat{F}_E - K_p q_E - K_v V_E)} \tag{6.34}$$

Using the above definition of the actuator force in Eq. (6.28), the Shape system velocity dynamics are obtained as,

$$\boldsymbol{M_E \dot{V}_E = (\hat{F}_E - F_E) - K_v V_E - K_p q_E} \tag{6.35}$$

From the above equation it is can noticed that the information about the force estimation error can be extracted from steady state value of the Shape system velocity vector $\boldsymbol{V_E}$. A full state Luenberger observer with states corresponding to an estimate

of the Shape system velocity vector $\hat{\boldsymbol{V}}_{\boldsymbol{E}}$ and an estimate of the force $\hat{\boldsymbol{F}}_{\boldsymbol{E}}$ is proposed. Assuming that the external force vector $\boldsymbol{F}_{\boldsymbol{E}}$ is constant, the following observer dynamics are defined,

$$\begin{aligned} \boldsymbol{M}_{\boldsymbol{E}}\dot{\hat{\boldsymbol{V}}}_{\boldsymbol{E}} &= \boldsymbol{F}_{\boldsymbol{a}} - \hat{\boldsymbol{F}}_{\boldsymbol{E}} + \boldsymbol{L}_{\boldsymbol{1}}(\boldsymbol{V}_{\boldsymbol{E}} - \hat{\boldsymbol{V}}_{\boldsymbol{E}}) \\ \dot{\hat{\boldsymbol{F}}}_{\boldsymbol{E}} &= -\boldsymbol{L}_{\boldsymbol{2}}(\boldsymbol{V}_{\boldsymbol{E}} - \hat{\boldsymbol{V}}_{\boldsymbol{E}}) \end{aligned} \tag{6.36}$$

where $\boldsymbol{L}_{\boldsymbol{1}} \in \boldsymbol{R}^{(\boldsymbol{N}+\boldsymbol{1})\times(\boldsymbol{N}+\boldsymbol{1})}$ and $\boldsymbol{L}_{\boldsymbol{2}} \in \boldsymbol{R}^{(\boldsymbol{N}+\boldsymbol{1})\times(\boldsymbol{N}+\boldsymbol{1})}$ are constant positive definite matrices corresponding to the observer gains. Let $\tilde{\boldsymbol{V}}_{\boldsymbol{E}} \triangleq (\boldsymbol{V}_{\boldsymbol{E}} - \hat{\boldsymbol{V}}_{\boldsymbol{E}})$ be the error in estimating the Shape system velocity $\boldsymbol{V}_{\boldsymbol{E}}$, while $\tilde{\boldsymbol{F}}_{\boldsymbol{E}} \triangleq (\boldsymbol{F}_{\boldsymbol{E}} - \hat{\boldsymbol{F}}_{\boldsymbol{E}})$ be the error in estimating the force $\boldsymbol{F}_{\boldsymbol{E}}$. From the Shape system dynamics in Eq. (6.28) and the observer dynamics in Eq. (6.36) the estimation error dynamics are obtained as,

$$\begin{pmatrix} \dot{\tilde{\boldsymbol{V}}}_{\boldsymbol{E}} \\ \dot{\tilde{\boldsymbol{F}}}_{\boldsymbol{E}} \end{pmatrix} = \underbrace{\begin{pmatrix} -\boldsymbol{M}_{\boldsymbol{E}}^{-\boldsymbol{1}}\boldsymbol{L}_{\boldsymbol{1}} & -\boldsymbol{M}_{\boldsymbol{E}}^{-\boldsymbol{1}} \\ \boldsymbol{L}_{\boldsymbol{2}} & \boldsymbol{0}_{(\boldsymbol{N}+\boldsymbol{1})} \end{pmatrix}}_{\boldsymbol{A}_{\boldsymbol{o}}} \begin{pmatrix} \tilde{\boldsymbol{V}}_{\boldsymbol{E}} \\ \tilde{\boldsymbol{F}}_{\boldsymbol{E}} \end{pmatrix} \tag{6.37}$$

where $\boldsymbol{A}_{\boldsymbol{o}}$ is a Hurwitz matrix and $\boldsymbol{0}_{(\boldsymbol{N}+\boldsymbol{1})} \in \boldsymbol{R}^{(\boldsymbol{N}+\boldsymbol{1})\times(\boldsymbol{N}+\boldsymbol{1})}$ is a matrix with all elements zero. Therefore the following Lyapunov equation can be solved for a positive definite $\boldsymbol{P}_o \in \boldsymbol{R}^{(\boldsymbol{2N}+\boldsymbol{2})\times(\boldsymbol{2N}+\boldsymbol{2})}$ for a given positive definite $\boldsymbol{Q}_o \in \boldsymbol{R}^{(\boldsymbol{2N}+\boldsymbol{2})\times(\boldsymbol{2N}+\boldsymbol{2})}$,

$$\boldsymbol{P}_o\boldsymbol{A}_o + \boldsymbol{A}_o^T\boldsymbol{P}_o = -\boldsymbol{Q}_o \tag{6.38}$$

The desired force for regulation of Shape system dynamics is summarized in the following theorem.

Theorem 6.1. *If the force vector $\boldsymbol{F}_{\boldsymbol{E}}$ is completely known, then exponential regulation of Shape system dynamics in Eq. (6.28) can be achieved by defining the desired actuator force vector $\boldsymbol{F}_{\boldsymbol{a}}^{\boldsymbol{d}}$ as,*

$$\boldsymbol{F}_{\boldsymbol{a}}^{\boldsymbol{d}} = \boldsymbol{B}_{\boldsymbol{E}}^{-\boldsymbol{1}}(\boldsymbol{F}_{\boldsymbol{E}} - \boldsymbol{K}_{\boldsymbol{v}}\boldsymbol{V}_{\boldsymbol{E}} - \boldsymbol{K}_{\boldsymbol{p}}\boldsymbol{q}_{\boldsymbol{E}}) \tag{6.39}$$

For a constant but unknown external force vector $\boldsymbol{F}_{\boldsymbol{E}}$, exponential regulation of Shape system dynamics is achieved for the following actuator force vector,

$$\boldsymbol{F}_{\boldsymbol{a}}^{\boldsymbol{d}} = \boldsymbol{B}_{\boldsymbol{E}}^{-\boldsymbol{1}}(\hat{\boldsymbol{F}}_{\boldsymbol{E}} - \boldsymbol{K}_{\boldsymbol{v}}\boldsymbol{V}_{\boldsymbol{E}} - \boldsymbol{K}_{\boldsymbol{p}}\boldsymbol{q}_{\boldsymbol{E}}) \tag{6.40}$$

where $\boldsymbol{K_p} \in \boldsymbol{R}^{(N+1)\times(N+1)}$ *and* $\boldsymbol{K_v} \in \boldsymbol{R}^{(N+1)\times(N+1)}$ *are constant positive definite matrices, while* $\hat{\boldsymbol{F}}_{\boldsymbol{E}}$ *represents an estimate of external forces, and is obtained from the following observer dynamics,*

$$\begin{aligned} \boldsymbol{M_E}\dot{\hat{\boldsymbol{V}}}_{\boldsymbol{E}} &= \boldsymbol{F_a} - \hat{\boldsymbol{F}}_{\boldsymbol{E}} + \boldsymbol{L_1}(\boldsymbol{V_E} - \hat{\boldsymbol{V}}_{\boldsymbol{E}}) \\ \dot{\hat{\boldsymbol{F}}}_{\boldsymbol{E}} &= -\boldsymbol{L_2}(\boldsymbol{V_E} - \hat{\boldsymbol{V}}_{\boldsymbol{E}}) \end{aligned} \tag{6.41}$$

where $\hat{\boldsymbol{V}}_{\boldsymbol{E}}$ *corresponds to the estimate of the Shape system velocity* $\boldsymbol{V_E}$*, while* $\boldsymbol{L_1} \in \boldsymbol{R}^{(N+1)\times(N+1)}$*,* $\boldsymbol{L_2} \in \boldsymbol{R}^{(N+1)\times(N+1)}$ *are constant positive definite diagonal matrices.*

Proof. If complete information about the force vector $\boldsymbol{F_E}$ is available, then the Lyapunov function $\bar{V}_1(\boldsymbol{q_E}, \boldsymbol{V_E})$ can be defined as given in Eq. (6.29). Using the definition of the required actuator force vector $\boldsymbol{F_a^d}$ from Eq. (6.39), derivative of the Lyapunov function $\dot{\bar{V}}_1(\boldsymbol{q_E}, \boldsymbol{V_E})$ is obtained as given in Eq. (6.33). From this definition of Lyapunov function derivative, exponential convergence follows.

If $\boldsymbol{F_E}$ is a constant but unknown force vector, consider the following Lyapunov function candidate,

$$V_1(\boldsymbol{q_E}, \boldsymbol{V_E}, \tilde{\boldsymbol{V}}_{\boldsymbol{E}}, \tilde{\boldsymbol{F}}_{\boldsymbol{ex}}) = \frac{1}{2}\begin{pmatrix} \boldsymbol{V_E} \\ \boldsymbol{q_E} \\ \tilde{\boldsymbol{V}}_{\boldsymbol{E}} \\ \tilde{\boldsymbol{F}}_{\boldsymbol{E}} \end{pmatrix}^{\boldsymbol{T}} \boldsymbol{\mathcal{Q}_1} \begin{pmatrix} \boldsymbol{V_E} \\ \boldsymbol{q_E} \\ \tilde{\boldsymbol{V}}_{\boldsymbol{E}} \\ \tilde{\boldsymbol{F}}_{\boldsymbol{E}} \end{pmatrix} \tag{6.42}$$

where $\boldsymbol{\mathcal{Q}_1}$ is a positive definite matrix and is given by,

$$\boldsymbol{\mathcal{Q}_1} = \begin{pmatrix} \boldsymbol{M_E} & \varepsilon\boldsymbol{M_E} & \boldsymbol{0}_{(N+1)\times(N+1)} & \boldsymbol{0}_{(N+1)\times(N+1)} \\ \varepsilon\boldsymbol{M_E} & \boldsymbol{K_p} + \varepsilon\boldsymbol{K_v} & \boldsymbol{0}_{(N+1)\times(N+1)} & \boldsymbol{0}_{(N+1)\times(N+1)} \\ \boldsymbol{0}_{(N+1)\times(N+1)} & \boldsymbol{0}_{(N+1)\times(N+1)} & \boldsymbol{P_o^1} & \boldsymbol{P_o^2} \\ \boldsymbol{0}_{(N+1)\times(N+1)} & \boldsymbol{0}_{(N+1)\times(N+1)} & \boldsymbol{P_o^3} & \boldsymbol{P_o^4} \end{pmatrix} \tag{6.43}$$

where $\boldsymbol{P}_o := \begin{pmatrix} \boldsymbol{P}_o^1 & \boldsymbol{P}_o^2 \\ \boldsymbol{P}_o^3 & \boldsymbol{P}_o^4 \end{pmatrix} \in \boldsymbol{R}^{(2N+2)\times(2N+2)}$ satisfies the Lyapunov equation in Eq. (6.38). The Lyapunov function $V_1(\boldsymbol{q_E}, \boldsymbol{V_E}, \tilde{\boldsymbol{V}}_{\boldsymbol{E}}, \tilde{\boldsymbol{F}}_{\boldsymbol{ex}})$ is a radially unbounded positive definite function of the arguments $(\boldsymbol{q_E}, \boldsymbol{V_E}, \tilde{\boldsymbol{V}}_{\boldsymbol{E}}, \tilde{\boldsymbol{F}}_{\boldsymbol{ex}})$ for an appropriately small value

of ε and satisfies the following bounds,

$$\frac{1}{2}\sigma_{min}(\boldsymbol{\mathcal{Q}_1})\left\|\begin{pmatrix} V_E \\ q_E \\ \tilde{V}_E \\ \tilde{F}_E \end{pmatrix}\right\|_2^2 \leq V_1(\boldsymbol{q_E}, \boldsymbol{V_E}, \tilde{\boldsymbol{V}}_{\boldsymbol{E}}, \tilde{\boldsymbol{F}}_{\boldsymbol{ex}}) \leq \frac{1}{2}\sigma_{max}(\boldsymbol{\mathcal{Q}_1})\left\|\begin{pmatrix} V_E \\ q_E \\ \tilde{V}_E \\ \tilde{F}_E \end{pmatrix}\right\|_2^2 \tag{6.44}$$

From the inertia dynamics in Eq. (6.28) and the velocity estimation error dynamics in Eq. (6.37), derivative of the Lyapunov function $V_1(\boldsymbol{q_E}, \boldsymbol{V_E}, \tilde{\boldsymbol{V}}_{\boldsymbol{E}}, \tilde{\boldsymbol{F}}_{\boldsymbol{ex}})$ in Eq. (6.42) is obtained as,

$$\dot{V}_1(\boldsymbol{q_E}, \boldsymbol{V_E}, \tilde{\boldsymbol{V}}_{\boldsymbol{E}}, \tilde{\boldsymbol{F}}_{\boldsymbol{ex}}) = -\begin{pmatrix} \boldsymbol{V_E} \\ \boldsymbol{q_E} \\ \tilde{\boldsymbol{V}}_{\boldsymbol{E}} \\ \tilde{\boldsymbol{F}}_{\boldsymbol{E}} \end{pmatrix}^T \boldsymbol{\mathcal{P}_1} \begin{pmatrix} \boldsymbol{V_E} \\ \boldsymbol{q_E} \\ \tilde{\boldsymbol{V}}_{\boldsymbol{E}} \\ \tilde{\boldsymbol{F}}_{\boldsymbol{E}} \end{pmatrix} \tag{6.45}$$

where $\boldsymbol{\mathcal{P}_1}$ is a positive definite matrix and is obtained as,

$$\boldsymbol{\mathcal{P}_1} = \begin{pmatrix} \boldsymbol{K_v} - \varepsilon \boldsymbol{M_E} & \boldsymbol{0_{(N+1)\times(N+1)}} & \boldsymbol{0_{(N+1)\times(N+1)}} & 0.5\boldsymbol{I}_{N+1} \\ \boldsymbol{0_{(N+1)\times(N+1)}} & \varepsilon \boldsymbol{K_p} & \boldsymbol{0_{(N+1)\times(N+1)}} & \frac{\varepsilon}{2}\boldsymbol{I}_{N+1} \\ \boldsymbol{0_{(N+1)\times(N+1)}} & \boldsymbol{0_{(N+1)\times(N+1)}} & \boldsymbol{Q}_1 & \boldsymbol{Q}_2 \\ \frac{\varepsilon}{2}\boldsymbol{I}_{N+1} & \frac{\varepsilon}{2}\boldsymbol{I}_{N+1} & \boldsymbol{Q}_3 & \boldsymbol{Q}_4 \end{pmatrix} \tag{6.46}$$

where $\boldsymbol{I}_{N+1} \in \boldsymbol{R}^{(N+1)\times(N+1)}$ is a identity matrix, while $\boldsymbol{Q}_1 \in \boldsymbol{R}^{(N+1)\times(N+1)}$, $\boldsymbol{Q}_2 \in \boldsymbol{R}^{(N+1)\times(N+1)}$, $\boldsymbol{Q}_3 \in \boldsymbol{R}^{(N+1)\times(N+1)}$ and $\boldsymbol{Q}_4 \in \boldsymbol{R}^{(N+1)\times(N+1)}$ are elements of the positive definite matrix $\boldsymbol{Q}_o := \begin{pmatrix} \boldsymbol{Q}_1 & \boldsymbol{Q}_2 \\ \boldsymbol{Q}_3 & \boldsymbol{Q}_4 \end{pmatrix}$ in Eq. (6.38). Therefore the matrix $\boldsymbol{\mathcal{P}_1} \in \boldsymbol{R}^{(4N+4)\times(4N+4)}$ is also a positive definite matrix. From the bounds on the Lyapunov function $V_1(\boldsymbol{q_E}, \boldsymbol{V_E}, \tilde{\boldsymbol{V}}_{\boldsymbol{E}}, \tilde{\boldsymbol{F}}_{\boldsymbol{ex}})$ in Eq. (6.44), the derivative $\dot{V}_1(.)$ of the Lyapunov function in Eq. (6.45) satisfies the following inequalities,

$$\dot{V}_1(\boldsymbol{q_E}, \boldsymbol{V_E}, \tilde{\boldsymbol{V}}_{\boldsymbol{E}}, \tilde{\boldsymbol{F}}_{\boldsymbol{ex}}) \leq -\sigma_{max}(\boldsymbol{\mathcal{P}_1})\left\|\begin{pmatrix} \boldsymbol{V_E} \\ \boldsymbol{q_E} \\ \tilde{\boldsymbol{V}}_{\boldsymbol{E}} \\ \tilde{\boldsymbol{F}}_{\boldsymbol{E}} \end{pmatrix}\right\|_2^2 \leq -\frac{2\sigma_{min}(\boldsymbol{\mathcal{P}_1})}{\sigma_{max}(\boldsymbol{\mathcal{Q}_1})} V_1(\boldsymbol{q_E}, \boldsymbol{V_E}, \tilde{\boldsymbol{V}}_{\boldsymbol{E}}, \tilde{\boldsymbol{F}}_{\boldsymbol{ex}}) \tag{6.47}$$

On integrating both sides of the above inequality, exponential convergence of the Lyapunov function $V_1(\boldsymbol{q_E}, \boldsymbol{V_E}, \tilde{\boldsymbol{V}}_{\boldsymbol{E}}, \tilde{\boldsymbol{F}}_{\boldsymbol{ex}})$ follows. As $V_1(\boldsymbol{q_E}, \boldsymbol{V_E}, \tilde{\boldsymbol{V}}_{\boldsymbol{E}}, \tilde{\boldsymbol{F}}_{\boldsymbol{ex}})$ is a positive definite function, the arguments $(\boldsymbol{q_E}, \boldsymbol{V_E}, \tilde{\boldsymbol{V}}_{\boldsymbol{E}}, \tilde{\boldsymbol{F}}_{\boldsymbol{ex}})$ also converge exponentially to zero. □

Remark 6.1. *For an unknown time-varying force $\boldsymbol{F_E}(t)$, the actuator force in Eq. (6.40) can only guarantee exponential convergence of Shape system velocity $\boldsymbol{V_E}$ to a region in the neighborhood of origin. The size of this neighborhood is determined by the magnitude of $\|\dot{\boldsymbol{F}}_{\boldsymbol{E}}(t)\|_\infty$.*

If the force provided by the actuator $\boldsymbol{F_a}$ is different from the required force $\boldsymbol{F_a^d}$ in Eq. (6.40), let the error between $\boldsymbol{F_a}$ and $\boldsymbol{F_a^d}$ be represented by $\tilde{\boldsymbol{F}} \triangleq (\boldsymbol{F_a} - \boldsymbol{F_a^d})$. The effect of this force error vector $\tilde{\boldsymbol{F}}$ on the Lyapunov function derivative $\dot{V}_1(\boldsymbol{q_E}, \boldsymbol{V_E}, \tilde{\boldsymbol{V}}_{\boldsymbol{E}}, \tilde{\boldsymbol{F}}_{\boldsymbol{ex}})$ in Eq. (6.45) is obtained as,

$$\dot{V}_1(\boldsymbol{q_E}, \boldsymbol{V_E}, \tilde{\boldsymbol{V}}_{\boldsymbol{E}}, \tilde{\boldsymbol{F}}_{\boldsymbol{ex}}) = -\begin{pmatrix} \boldsymbol{V_E} \\ \boldsymbol{q_E} \\ \tilde{\boldsymbol{V}}_{\boldsymbol{E}} \\ \tilde{\boldsymbol{F}}_{\boldsymbol{E}} \end{pmatrix}^T \boldsymbol{\mathcal{P}_1} \begin{pmatrix} \boldsymbol{V_E} \\ \boldsymbol{q_E} \\ \tilde{\boldsymbol{V}}_{\boldsymbol{E}} \\ \tilde{\boldsymbol{F}}_{\boldsymbol{E}} \end{pmatrix} + (\boldsymbol{V_E^T} + \varepsilon \boldsymbol{q_E^T}) \boldsymbol{B_E} \tilde{\boldsymbol{F}} \tag{6.48}$$

In the above equation, as the term involving $\tilde{\boldsymbol{F}}$ is sign indefinite, exponential convergence of Lyapunov function is achieved only by regulating the actuator force error. The command input required for regulating the actuator force error $\tilde{\boldsymbol{F}}$ to zero is presented in the following section. For convenience of presentation, controller design for a system with a single slave actuator ($N = 1$) is derived in the next section. The controller for co-ordination between multiple actuators will have a similar structure and this is also highlighted in the following section.

Second stage of controller design for a system with single slave ($N = 1$)

The controller design for achieving the desired actuator force in Eq. (6.40) is presented in this section for a system with single slave actuator ($N = 1$). An illustration of an application with a single slave is shown in Fig. (6.5).

Let $F_{a_m}^d$ and $F_{a_s}^d$ represent the force required from the master and the slave actuators respectively. These forces are the elements of the desired actuator force vector $\boldsymbol{F_a^d}$ in

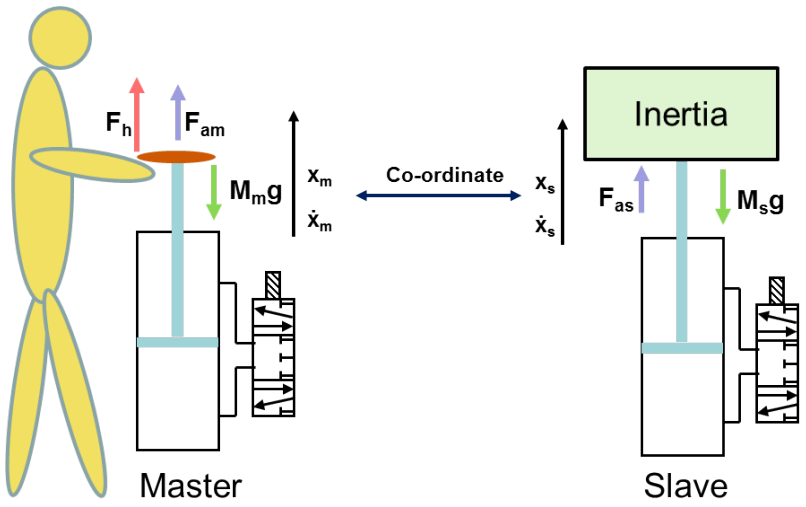

Figure 6.5: One example application of tele-operation, illustrating the human operator moving an inertial load at a remote location of the slave, while interacting with the master system

Eq.(6.40),

$$\boldsymbol{F_a^d} = \begin{pmatrix} F_{a_m}^d \\ F_{a_s}^d \end{pmatrix} \tag{6.49}$$

The elements of the actuator force error $\tilde{\boldsymbol{F}}$ corresponding to the actuator force error for the master and the slave systems are defined as,

$$\tilde{F}_m = F_{a_m} - F_{a_m}^d, \qquad \tilde{F}_s = F_{a_s} - F_{a_s}^d \tag{6.50}$$

Let $\boldsymbol{m} := (m_1, m_2)$, $\boldsymbol{P} := (P_1, P_2)$, and $\boldsymbol{T} := (T_1, T_2)$ represent the vector of air mass, pressure, and temperature in each chamber of a pneumatic actuator. The energy based Lyapunov function for the force error dynamics of a pneumatic actuator is as presented in lemma 3.3 of chapter 3 and is given by,

$$W_L^j(\boldsymbol{m}, \boldsymbol{P}, \boldsymbol{P^d}) = m_1 W_m^j(P_1, P_1^d) + m_2 W_m^j(P_2, P_2^d) \tag{6.51}$$

where $j \in (adb, iso)$ is the index for representing the thermodynamic process in the actuator and $W_m^j(.)$ represents the gravimetric energy density of the actuator and is as

defined in Eq. (3.144) and Eq. (3.145) for adiabatic and isothermal actuators respectively.

From the analysis provided in section (3.3.3) the supply rate to the energy function for the actuator force error in Eq. (6.51) is given by,

$$\dot{W}_L^j(\boldsymbol{m}, \boldsymbol{P}, \boldsymbol{P^d}) = \gamma_3^j(\boldsymbol{m}, \boldsymbol{P}, \boldsymbol{P^d}, u)\tilde{F}u - \tilde{F}\dot{x} - \dot{F}_a^d(t)\frac{\tilde{F}}{K_j^d(\boldsymbol{m}, x, x_d)} \tag{6.52}$$

where u is the command input to the valve metering the air flow to the pneumatic actuator, while the nonlinear gain function $\gamma_3^j(.)$ is as defined in Eq. (A.26), and the nonlinear function $K_j^d(.)$ is as defined in Eq. (3.142). Let u_m and u_s represent the valve command input to the master and the slave actuators. In the following theorem, the valve command input for regulating the actuator force error $\tilde{\boldsymbol{F}}$ to zero, is presented.

Theorem 6.2. *If the force $\boldsymbol{F_E}$ is completely known, then exponential convergence of Shape system dynamics in Eq. (6.25) is achieved for the following definition of desired actuator force vector $\boldsymbol{F_a^d}$,*

$$\boldsymbol{F_a^d} := \begin{pmatrix} F_{a_m}^d \\ F_{a_s}^d \end{pmatrix} = \boldsymbol{B_E^{-1}(F_E - K_p q_E - K_v V_E)} \tag{6.53}$$

where $F_{a_m}^d$ and $F_{a_s}^d$ represent the desired forces from the master and the slave actuators respectively. To output these desired forces, the valve command inputs u_m to the flow control valve on the master and u_s to the flow control valve on the slave actuators are defined as,

$$\begin{aligned} u_m &= \frac{1}{\gamma_3^j(\boldsymbol{m}_m, \boldsymbol{P}_m, \boldsymbol{P^d}_m, u_m)}\left(\dot{x}_v + \frac{\dot{F}_{a_m}^d}{K_j^d(\boldsymbol{m}_m, x_m, x_{d_m})} - \varepsilon q_{E_1} - K_{F_1}(F_{a_m} - F_{a_m}^d)\right) \\ u_s &= \frac{1}{\gamma_3^j(\boldsymbol{m}_s, \boldsymbol{P}_s, \boldsymbol{P^d}_s, u_s)}\left(\dot{x}_v + \frac{\dot{F}_{a_s}^d}{K_j^d(\boldsymbol{m}_s, x_s, x_{d_s})} - \varepsilon(q_{E_1} - q_{E_2}) - K_{F_2}(F_{a_s} - F_{a_s}^d)\right) \end{aligned} \tag{6.54}$$

where K_{F_1} and K_{F_2} are positive constants, F_{a_m} is the force provided master actuator, F_{a_s} is the force provided by the slave actuator, while q_{E_1} and q_{E_2} are elements of the position co-ordination error vector $\boldsymbol{q_E}$ in Eq. (6.28).

If accurate information about $\boldsymbol{F_E}$ is not known, then exponential convergence of Shape system dynamics in Eq. (6.25) is achieved for the following definition of the

desired actuator force,

$$\boldsymbol{F_a^d} := \begin{pmatrix} F_{a_m}^d \\ F_{a_s}^d \end{pmatrix} = \boldsymbol{B_E^{-1}}(\hat{\boldsymbol{F}}_{\boldsymbol{E}} - \boldsymbol{K_p q_E} - \boldsymbol{K_v V_E}) \tag{6.55}$$

where $\hat{\boldsymbol{F}}_{\boldsymbol{E}}$ is an estimate of force vector $\boldsymbol{F_E}$ and is obtained from the observer dynamics in Eq. (6.36). The valve command inputs u_m, u_s to the master and the slave system respectively for obtaining the desired actuator force in Eq. (6.55) are again as given in Eq. (6.54).

Proof. For ease of presentation $\boldsymbol{\chi}_m^d$ and $\boldsymbol{\chi}_s^d$ represent the states of the error dynamics of the master and the slave pneumatic actuators respectively and are defined as,

$$\boldsymbol{\chi}_m^d := (\boldsymbol{m}_m, \boldsymbol{P}_m, \boldsymbol{P}_m^d), \qquad \boldsymbol{\chi}_s^d := (\boldsymbol{m}_s, \boldsymbol{P}_s, \boldsymbol{P}_s^d) \tag{6.56}$$

where the subscript m is used to represent states corresponding to master system, and the subscript s is used to represent states corresponding to slave system. If the force $\boldsymbol{F_E}$ is completely known, then consider the following Lyapunov function,

$$\begin{aligned} V_2(\boldsymbol{q_E}, \boldsymbol{V_E}, \boldsymbol{\chi}_m^d, \boldsymbol{\chi}_s^d) = & \underbrace{\frac{1}{2}\begin{pmatrix} \boldsymbol{V_E^T} & \boldsymbol{q_E^T} \end{pmatrix}\begin{pmatrix} \boldsymbol{M_E} & \boldsymbol{\varepsilon M_E} \\ \boldsymbol{\varepsilon M_E} & \boldsymbol{K_p} + \boldsymbol{\varepsilon K_v} \end{pmatrix}\begin{pmatrix} \boldsymbol{V_E} \\ \boldsymbol{q_E} \end{pmatrix}}_{\bar{V}_1(\boldsymbol{q_E}, \boldsymbol{V_E})} \\ & + \rho W_L^j(\boldsymbol{m}_m, \boldsymbol{P}_m, \boldsymbol{P}_m^d) + W_L^j(\boldsymbol{m}_s, \boldsymbol{P}_s, \boldsymbol{P}_s^d) \end{aligned} \tag{6.57}$$

where $\rho \in \Re^+$ is the scaling factor from master to slave actuator, $\bar{V}_1(\boldsymbol{q_E}, \boldsymbol{V_E})$ is the Lyapunov function for the inertial dynamics of the Shape system, $W_L^j(.)$ is the available energy in the pneumatic actuator and is as defined in Eq. (6.51) for actuator error dynamics. From the definition of the bounds on actuator Lyapunov function $W_L^j(.)$ in

Eq. (5.47), the Lyapunov function $V_2(\boldsymbol{q_E}, \boldsymbol{V_E}, \boldsymbol{\chi}_m^d, \boldsymbol{\chi}_s^d)$ can be expressed as,

$$
\begin{aligned}
V_2(\boldsymbol{q_E}, \boldsymbol{V_E}, \boldsymbol{\chi}_m^d, \boldsymbol{\chi}_s^d) \leq \\
\frac{1}{2}\begin{pmatrix} \boldsymbol{V_E} \\ \boldsymbol{q_E} \\ \tilde{F}_m \\ \tilde{F}_s \end{pmatrix}^T \underbrace{\begin{pmatrix} \boldsymbol{M_E} & \varepsilon \boldsymbol{M_E} & 0 & 0 \\ \varepsilon \boldsymbol{M_E} & \boldsymbol{K_p} + \varepsilon \boldsymbol{K_v} & 0 & 0 \\ \boldsymbol{0_{1\times 2}} & \boldsymbol{0_{1\times 2}} & \rho Q_{max}(\boldsymbol{m}_m) & 0 \\ \boldsymbol{0_{1\times 2}} & \boldsymbol{0_{1\times 2}} & 0 & Q_{max}(\boldsymbol{m}_s) \end{pmatrix}}_{\boldsymbol{\mathcal{Q}}_t} \begin{pmatrix} \boldsymbol{V_E} \\ \boldsymbol{q_E} \\ \tilde{F}_m \\ \tilde{F}_s \end{pmatrix} \\
\leq \frac{1}{2}\sigma_{max}(\boldsymbol{\mathcal{Q}}_t) \left\| \begin{pmatrix} \boldsymbol{V_E} \\ \boldsymbol{q_E} \\ \tilde{F}_m \\ \tilde{F}_s \end{pmatrix} \right\|_2^2
\end{aligned}
\tag{6.58}
$$

where $Q_{max}(\boldsymbol{m}_m) \in \Re^+$ and $Q_{max}(\boldsymbol{m}_s) \in \Re^+$ represent the weight on the upper bound of the master and the slave actuator Lyapunov functions respectively. For a pneumatic actuator behaving as a spring, these upper bounds can be interpreted as the inverse of the minimum spring stiffness. Using the expression for the time derivative $\dot{V}_1(.)$ from Eq. (6.31), the actuator Lyapunov function derivative $\dot{W}_L^j(.)$ from Eq. (6.52) and the definition of the valve command inputs from Eq. (6.54), the derivative $\dot{V}_2(.)$ of the Lyapunov function in Eq. (6.57) is obtained as,

$$
\dot{V}_2(\boldsymbol{q_E}, \boldsymbol{V_E}, \boldsymbol{\chi}_m^d, \boldsymbol{\chi}_s^d) = -\begin{pmatrix} \boldsymbol{V_E} \\ \boldsymbol{q_E} \\ \tilde{F}_m \\ \tilde{F}_s \end{pmatrix}^T \underbrace{\begin{pmatrix} \boldsymbol{K_v} - \varepsilon \boldsymbol{M_E} & \boldsymbol{0_{2\times 1}} & 0 & 0 \\ \boldsymbol{0_2} & \varepsilon \boldsymbol{K_p} & 0 & 0 \\ \boldsymbol{0_{1\times 2}} & \boldsymbol{0_{1\times 2}} & K_{F_1} & 0 \\ \boldsymbol{0_{1\times 2}} & \boldsymbol{0_{1\times 2}} & 0 & K_{F_2} \end{pmatrix}}_{\boldsymbol{\mathcal{P}}_t} \begin{pmatrix} \boldsymbol{V_E} \\ \boldsymbol{q_E} \\ \tilde{F}_m \\ \tilde{F}_s \end{pmatrix}
\tag{6.59}
$$

From the definition of the bounds on $V_2(\boldsymbol{q_E}, \boldsymbol{V_E}, \boldsymbol{\chi}_m^d, \boldsymbol{\chi}_s^d)$ in Eq. (6.58) the derivative $\dot{V}_2(.)$ in Eq. (6.59) can be expressed as,

$$
\dot{V}_2(\boldsymbol{q_E}, \boldsymbol{V_E}, \boldsymbol{\chi}_m^d, \boldsymbol{\chi}_s^d) \leq -\frac{2\sigma_{min}(\boldsymbol{\mathcal{P}}_t)}{\sigma_{max}(\boldsymbol{\mathcal{Q}}_t)}\ V_2(\boldsymbol{q_E}, \boldsymbol{V_E}, \boldsymbol{\chi}_m^d, \boldsymbol{\chi}_s^d)
\tag{6.60}
$$

where $\sigma_{min}(.)$ and $\sigma_{max}(.)$ represent the operators for obtaining the maximum and the minimum singular values. On integrating both sides of Eq. (6.60) exponential

convergence of the Lyapunov function $V_2(\boldsymbol{q_E}, \boldsymbol{V_E}, \boldsymbol{\chi}_m^d, \boldsymbol{\chi}_s^d)$ follows. As the Lyapunov function in Eq. (6.57) is a positive definite function of states $((\boldsymbol{q_E}, \boldsymbol{V_E}, \boldsymbol{\chi}_m^d, \boldsymbol{\chi}_s^d))$, the Shape system velocity vector $\boldsymbol{V_E}$ and the actuator force error vector $(\boldsymbol{F_a} - \boldsymbol{F_a^d})$ also exponentially converges to zero.

If the force $\boldsymbol{F_E}$ is not well-known, given the inertial system Lyapunov function $V_1(\boldsymbol{q_E}, \boldsymbol{V_E}, \tilde{\boldsymbol{V}}_{\boldsymbol{E}}, \tilde{\boldsymbol{F}}_{\boldsymbol{ex}})$ in Eq. (6.42), consider the following Lyapunov function $V_2(.)$ for the second stage of controller design,

$$V_2(\boldsymbol{q_E}, \boldsymbol{V_E}, \tilde{\boldsymbol{V}}_{\boldsymbol{E}}, \tilde{\boldsymbol{F}}_{\boldsymbol{ex}}, \boldsymbol{\chi}_m^d, \boldsymbol{\chi}_s^d) = V_1(\boldsymbol{q_E}, \boldsymbol{V_E}, \tilde{\boldsymbol{V}}_{\boldsymbol{E}}, \tilde{\boldsymbol{F}}_{\boldsymbol{ex}}) + \rho W_L^j(\boldsymbol{\chi}_m^d) + W_L^j(\boldsymbol{\chi}_s^d) \quad (6.61)$$

where the actuator Lyapunov function $W_L^j(.)$ for the master and the slave systems is as defined in Eq. (5.46) and $\rho \in \Re^+$ is the amplification factor from the master to the slave system. From the definition of the bounds on the actuator Lyapunov function $W_L^j(.)$ in Eq. (5.47), the Lyapunov function $V_2(\boldsymbol{q_E}, \boldsymbol{V_E}, \tilde{\boldsymbol{V}}_{\boldsymbol{E}}, \tilde{\boldsymbol{F}}_{\boldsymbol{ex}}, \boldsymbol{\chi}_m^d, \boldsymbol{\chi}_s^d)$ in the above equation can be bounded for $N = 1$ as,

$$V_2(\boldsymbol{q_E}, \boldsymbol{V_E}, \tilde{\boldsymbol{V}}_{\boldsymbol{E}}, \tilde{\boldsymbol{F}}_{\boldsymbol{ex}}, \boldsymbol{\chi}_m^d, \boldsymbol{\chi}_s^d) \leq \frac{1}{2} \begin{pmatrix} \boldsymbol{V_E} \\ \boldsymbol{q_E} \\ \tilde{\boldsymbol{V}}_{\boldsymbol{E}} \\ \tilde{\boldsymbol{F}}_{\boldsymbol{E}} \\ \tilde{F}_m \\ \tilde{F}_s \end{pmatrix}^T \boldsymbol{\mathcal{Q}_u} \begin{pmatrix} \boldsymbol{V_E} \\ \boldsymbol{q_E} \\ \tilde{\boldsymbol{V}}_{\boldsymbol{E}} \\ \tilde{\boldsymbol{F}}_{\boldsymbol{E}} \\ \tilde{F}_m \\ \tilde{F}_s \end{pmatrix} \leq \frac{1}{2} \sigma_{max}(\boldsymbol{\mathcal{Q}_u}) \left\| \begin{pmatrix} \boldsymbol{V_E} \\ \boldsymbol{q_E} \\ \tilde{\boldsymbol{V}}_{\boldsymbol{E}} \\ \tilde{\boldsymbol{F}}_{\boldsymbol{E}} \\ \tilde{F}_m \\ \tilde{F}_s \end{pmatrix} \right\|_2^2$$

$$\text{where } \boldsymbol{\mathcal{Q}_u} = \begin{pmatrix} \boldsymbol{M_E} & \varepsilon \boldsymbol{M_E} & \boldsymbol{0}_{2\times2} & \boldsymbol{0}_{2\times2} & 0 & 0 \\ \varepsilon \boldsymbol{M_E} & \boldsymbol{K_p} + \varepsilon \boldsymbol{K_v} & \boldsymbol{0}_{2\times2} & \boldsymbol{0}_{2\times2} & 0 & 0 \\ \boldsymbol{0}_{2\times2} & \boldsymbol{0}_{2\times2} & \boldsymbol{P}_o^1 & \boldsymbol{P}_o^2 & 0 & 0 \\ \boldsymbol{0}_{2\times2} & \boldsymbol{0}_{2\times2} & \boldsymbol{P}_o^3 & \boldsymbol{P}_o^4 & 0 & 0 \\ \boldsymbol{0}_{1\times2} & \boldsymbol{0}_{1\times2} & \boldsymbol{0}_{1\times2} & \boldsymbol{0}_{1\times2} & \rho Q_{max}(\boldsymbol{m}_m) & 0 \\ \boldsymbol{0}_{1\times2} & \boldsymbol{0}_{1\times2} & \boldsymbol{0}_{1\times2} & \boldsymbol{0}_{1\times2} & 0 & Q_{max}(\boldsymbol{m}_s) \end{pmatrix} \quad (6.62)$$

where $\boldsymbol{P}_o^1 \in \boldsymbol{R^{2\times2}}$, $\boldsymbol{P}_o^2 \in \boldsymbol{R^{2\times2}}$, $\boldsymbol{P}_o^3 \in \boldsymbol{R^{2\times2}}$, $\boldsymbol{P}_o^4 \in \boldsymbol{R^{2\times2}}$ are the elements of the solution $\boldsymbol{P_o} := \begin{pmatrix} \boldsymbol{P}_o^1 & \boldsymbol{P}_o^2 \\ \boldsymbol{P}_o^3 & \boldsymbol{P}_o^4 \end{pmatrix}$ to the Lyapunov equation in Eq. (6.38). Using the expression for $\dot{V}_1(.)$ from Eq. (6.48) and the actuator Lyapunov function derivative

$\dot{W}_L^j(\boldsymbol{\chi}_{jl}^d)$ from Eq. (6.52), the derivative $\dot{V}_2(.)$ of the Lyapunov function in Eq. (6.61) is obtained for a single slave system ($N = 1$) as,

$$\begin{aligned}
&\dot{V}_2(\boldsymbol{q_E}, \boldsymbol{V_E}, \tilde{\boldsymbol{V}}_{\boldsymbol{E}}, \tilde{\boldsymbol{F}}_{\boldsymbol{ex}}, \boldsymbol{\chi}_m^d, \boldsymbol{\chi}_s^d) = \\
&-\begin{pmatrix} \boldsymbol{V_E} \\ \boldsymbol{q_E} \\ \tilde{\boldsymbol{V}}_{\boldsymbol{E}} \\ \tilde{\boldsymbol{F}}_{\boldsymbol{E}} \end{pmatrix}^T \begin{pmatrix} \boldsymbol{K_v} - \varepsilon \boldsymbol{M_E} & \boldsymbol{0_{2\times 2}} & \boldsymbol{0_{2\times 2}} & 0.5\boldsymbol{I}_{2\times 2} \\ \boldsymbol{0_{2\times 2}} & \varepsilon \boldsymbol{K_p} & \boldsymbol{0_{2\times 2}} & \frac{\varepsilon}{2}\boldsymbol{I}_{2\times 2} \\ \boldsymbol{0_{2\times 2}} & \boldsymbol{0_{2\times 2}} & \boldsymbol{Q}_1 & \boldsymbol{Q}_2 \\ \frac{\varepsilon}{2}\boldsymbol{I}_{2\times 2} & \frac{\varepsilon}{2}\boldsymbol{I}_{2\times 2} & \boldsymbol{Q}_3 & \boldsymbol{Q}_4 \end{pmatrix} \begin{pmatrix} \boldsymbol{V_E} \\ \boldsymbol{q_E} \\ \tilde{\boldsymbol{V}}_{\boldsymbol{E}} \\ \tilde{\boldsymbol{F}}_{\boldsymbol{E}} \end{pmatrix} \\
&+ (\boldsymbol{V_E^T} + \varepsilon \boldsymbol{q_E^T}) \boldsymbol{B_E} \tilde{\boldsymbol{F}} + \gamma_{3_m}^j(\boldsymbol{\chi}_m^d) u_m \tilde{F}_m - \tilde{F}_m V_{E_1} - \tilde{F}_m \dot{x}_v - \dot{F}_m^d \frac{\tilde{F}_m}{K_{j_m}^d(\boldsymbol{\chi}_m^d)} \\
&+ \gamma_3^j(\boldsymbol{\chi}_s^d) u_s \tilde{F}_s - \tilde{F}_s(V_{E_1} - V_{E_2}) - \tilde{F}_s \dot{x}_v - \dot{F}_{a_s}^d \frac{\tilde{F}_s}{K_{j_s}^d(\boldsymbol{\chi}_s^d)}
\end{aligned} \tag{6.63}$$

where $\boldsymbol{I}_{2\times 2} \in \boldsymbol{R}^{2\times 2}$ is the identity matrix, $\boldsymbol{Q}_1 \in \boldsymbol{R}^{2\times 2}$, $\boldsymbol{Q}_2 \in \boldsymbol{R}^{2\times 2}$, $\boldsymbol{Q}_3 \in \boldsymbol{R}^{2\times 2}$ and $\boldsymbol{Q}_4 \in \boldsymbol{R}^{2\times 2}$ are elements of the positive definite matrix $\boldsymbol{Q}_o := \begin{pmatrix} \boldsymbol{Q}_1 & \boldsymbol{Q}_2 \\ \boldsymbol{Q}_3 & \boldsymbol{Q}_4 \end{pmatrix}$ in Eq. (6.38), while V_{E_1}, V_{E_2} are the elements of the Shape system velocity vector and are as defined in Eq. (6.13). Using the definition of $\boldsymbol{B_E}$ from Eq. (6.26) for a system with single slave actuator, and after some algebraic manipulation, the Lyapunov function derivative $\dot{V}_2(.)$ in Eq. (6.63) is obtained as,

$$\begin{aligned}
&\dot{V}_2(\boldsymbol{q_E}, \boldsymbol{V_E}, \tilde{\boldsymbol{V}}_{\boldsymbol{E}}, \tilde{\boldsymbol{F}}_{\boldsymbol{ex}}, \boldsymbol{\chi}_m^d, \boldsymbol{\chi}_s^d) = \\
&-\begin{pmatrix} \boldsymbol{V_E} \\ \boldsymbol{q_E} \\ \tilde{\boldsymbol{V}}_{\boldsymbol{E}} \\ \tilde{\boldsymbol{F}}_{\boldsymbol{E}} \end{pmatrix}^T \begin{pmatrix} \boldsymbol{K_v} - \varepsilon \boldsymbol{M_E} & \boldsymbol{0_{2\times 2}} & \boldsymbol{0_{2\times 2}} & 0.5\boldsymbol{I}_{2\times 2} \\ \boldsymbol{0_{2\times 2}} & \varepsilon \boldsymbol{K_p} & \boldsymbol{0_{2\times 2}} & \frac{\varepsilon}{2}\boldsymbol{I}_{2\times 2} \\ \boldsymbol{0_{2\times 2}} & \boldsymbol{0_{2\times 2}} & \boldsymbol{Q}_1 & \boldsymbol{Q}_2 \\ \frac{\varepsilon}{2}\boldsymbol{I}_{2\times 2} & \frac{\varepsilon}{2}\boldsymbol{I}_{2\times 2} & \boldsymbol{Q}_3 & \boldsymbol{Q}_4 \end{pmatrix} \begin{pmatrix} \boldsymbol{V_E} \\ \boldsymbol{q_E} \\ \tilde{\boldsymbol{V}}_{\boldsymbol{E}} \\ \tilde{\boldsymbol{F}}_{\boldsymbol{E}} \end{pmatrix} \\
&\quad + \tilde{F}_m \left(\gamma_{3_m}^j(\boldsymbol{\chi}_m^d) u_m - \dot{x}_v + \varepsilon q_{E_1} - \frac{\dot{F}_m^d}{K_{j_m}^d(\boldsymbol{\chi}_m^d)} \right) \\
&\quad + \tilde{F}_s \left(\gamma_3^j(\boldsymbol{\chi}_s^d) u_s - \dot{x}_v + \varepsilon(q_{E_1} - q_{E_2}) - \frac{\dot{F}_s^d}{K_{j_s}^d(\boldsymbol{\chi}_s^d)} \right)
\end{aligned} \tag{6.64}$$

Using the definition of the valve command inputs u_m to the master actuator and u_s to the slave actuator from Eq. (6.54), the Lyapunov function derivative $\dot{V}_2(.)$ in the

above equation can be expressed as,

$$\dot{V}_2(\boldsymbol{q_E}, \boldsymbol{V_E}, \tilde{\boldsymbol{V}}_{\boldsymbol{E}}, \tilde{\boldsymbol{F}}_{\boldsymbol{E}}, \boldsymbol{\chi}_m^d, \boldsymbol{\chi}_s^d) =$$

$$-\begin{pmatrix} \boldsymbol{V_E} \\ \boldsymbol{q_E} \\ \tilde{\boldsymbol{V}}_{\boldsymbol{E}} \\ \tilde{\boldsymbol{F}}_{\boldsymbol{E}} \\ \tilde{F}_m \\ \tilde{F}_s \end{pmatrix}^T \underbrace{\begin{pmatrix} \boldsymbol{K_v} - \varepsilon \boldsymbol{M_E} & \boldsymbol{0_{2\times 2}} & \boldsymbol{0_{2\times 2}} & 0.5\boldsymbol{I}_{2\times 2} & 0 & 0 \\ \boldsymbol{0_2} & \varepsilon \boldsymbol{K_p} & \boldsymbol{0_{2\times 2}} & \frac{\varepsilon}{2}\boldsymbol{I}_{2\times 2} & 0 & 0 \\ \boldsymbol{0_{2\times 2}} & \boldsymbol{0_{2\times 2}} & \boldsymbol{Q}_1 & \boldsymbol{Q}_2 & 0 & 0 \\ \frac{\varepsilon}{2}\boldsymbol{I}_{2\times 2} & \frac{\varepsilon}{2}\boldsymbol{I}_{2\times 2} & \boldsymbol{Q}_3 & \boldsymbol{Q}_4 & 0 & 0 \\ \boldsymbol{0_{1\times 2}} & \boldsymbol{0_{1\times 2}} & \boldsymbol{0_{1\times 2}} & \boldsymbol{0_{1\times 2}} & K_{F_1} & 0 \\ \boldsymbol{0_{1\times 2}} & \boldsymbol{0_{1\times 2}} & \boldsymbol{0_{1\times 2}} & \boldsymbol{0_{1\times 2}} & 0 & K_{F_2} \end{pmatrix}}_{\boldsymbol{\mathcal{P}_u}} \begin{pmatrix} \boldsymbol{V_E} \\ \boldsymbol{q_E} \\ \tilde{\boldsymbol{V}}_{\boldsymbol{E}} \\ \tilde{\boldsymbol{F}}_{\boldsymbol{E}} \\ \tilde{F}_m \\ \tilde{F}_s \end{pmatrix} \tag{6.65}$$

$$\leq -\sigma_{min}(\boldsymbol{\mathcal{P}_u}) \left\| \begin{pmatrix} \boldsymbol{V_E} \\ \boldsymbol{q_E} \\ \tilde{\boldsymbol{V}}_{\boldsymbol{E}} \\ \tilde{\boldsymbol{F}}_{\boldsymbol{E}} \\ \tilde{F}_m \\ \tilde{F}_s \end{pmatrix} \right\|_2^2$$

Using the definition of the bounds on the Lyapunov function $V_2(.)$ from Eq. (6.62), the Lyapunov function derivative in the above equation can be simplified as,

$$\dot{V}_2(\boldsymbol{q_E}, \boldsymbol{V_E}, \tilde{\boldsymbol{V}}_{\boldsymbol{E}}, \tilde{\boldsymbol{F}}_{\boldsymbol{E}}, \boldsymbol{\chi}_m^d, \boldsymbol{\chi}_s^d) \leq -\frac{2\sigma_{min}(\boldsymbol{\mathcal{P}_u})}{\sigma_{max}(\boldsymbol{\mathcal{Q}_u})} V_2(\boldsymbol{q_E}, \boldsymbol{V_E}, \tilde{\boldsymbol{V}}_{\boldsymbol{E}}, \tilde{\boldsymbol{F}}_{\boldsymbol{E}}, \boldsymbol{\chi}_m^d, \boldsymbol{\chi}_s^d) \tag{6.66}$$

On integrating both side of the above equation, exponential convergence of $V_2(.)$ follows. As the Lyapunov function is a positive definite function of the states $\boldsymbol{q_E}$, $\boldsymbol{V_E}$, $\tilde{\boldsymbol{V}}_{\boldsymbol{E}}$, $\tilde{\boldsymbol{F}}_{\boldsymbol{E}}$, $\boldsymbol{\chi}_m^d$ and $\boldsymbol{\chi}_s^d$, exponential convergence of the Shape system states, observer states and the actuator error states to zero also follows.

□

Command input vector for a system with multiple (N) slave actuators

In this subsection the valve command input for a system with single slave actuator in Eq. (6.54) is extended to a system with multiple (N) slave actuators. Based on the structure for the valve command input u_s in Eq. (6.54) for a system with a single slave actuator, the command input to the i^{th} slave pneumatic actuator in a multiple actuator

co-ordination problem can be expressed as,

$$u_{s_i} = \frac{1}{\gamma_3^j(\boldsymbol{m}_{s_i}, \boldsymbol{P}_{s_i}, \boldsymbol{P^d}_{s_i}, u_{s_i})} \left(\dot{x}_v + \frac{\dot{F}^d_{a_{s_i}}}{K_j^d(\boldsymbol{\chi}^d_{j_{s_i}})} - \varepsilon(q_{E_1} - q_{E_i}) - K_{F_i}\tilde{F}_{s_i} \right) \tag{6.67}$$

where $q_{E_i} = (x_m - x_{s_i})$ is the position co-ordination error between the master and the i^{th} slave system, $F^d_{a_{s_i}}$ is the desired force from the i^{th} slave actuator, and K_{F_i} is a positive constant.

Consider the following matrix definitions for system with N slave actuators,

$$\begin{aligned} \boldsymbol{\Gamma}_3^j &= diag(\gamma_3^j(\boldsymbol{m}_s, \boldsymbol{P}_{s_1}, \boldsymbol{P^{d_1}}_{s_1}, u_{s_1}), \gamma_3^j(\boldsymbol{m}_{s_2}, \boldsymbol{P}_{s_2}, \boldsymbol{P^d}_{s_2}, u_{s_2}), ..., \\ &\qquad \gamma_3^j(\boldsymbol{m}_{s_N}, \boldsymbol{P}_{s_N}, \boldsymbol{P^d}_{s_N}, u_{s_N})) \\ \boldsymbol{K}_j^d &= diag(\boldsymbol{\chi}^d_{j_{s_1}}, \boldsymbol{\chi}^d_{j_{s_2}}, ..., \boldsymbol{\chi}^d_{j_{s_N}}) \\ \boldsymbol{K}_F &= diag(K_{F_1}, K_{F_2}, ...K_{F_N}) \end{aligned} \tag{6.68}$$

The command input vector $\boldsymbol{u}_s = [u_{s_1}, u_{s_2}, ..., u_{s_N}]$ to the N slave actuators can now be expressed as,

$$\boldsymbol{u}_s = \left(\boldsymbol{\Gamma}_3^j\right)^{-1} \left(\dot{x}_v \boldsymbol{\mathcal{I}}_{N\times 1} + \left(\boldsymbol{K}_j^d\right)^{-1} \boldsymbol{\dot{F}^d_{a_s}} - \varepsilon(q_{E_1}\boldsymbol{\mathcal{I}_{N\times 1}} - \boldsymbol{q_E}) - \boldsymbol{K}_F\boldsymbol{\tilde{F}_s} \right) \tag{6.69}$$

In the following section, passivity analysis of the closed loop system is presented.

6.4 Closed loop passivity analysis

In this section, closed loop passivity property of a tele-operator with a single slave actuator ($N = 1$) is presented. Passivity properties of a system with multiple slave systems will be along similar lines. For ease of presentation, the control input to the master and the slave actuators given in Eq. (6.54) is re-written as,

$$\begin{aligned} u_m &= \frac{1}{\gamma_3^j(\boldsymbol{m}_m, \boldsymbol{P}_m, \boldsymbol{P^d}_m, u_m)} \left(\dot{x}_v + \frac{\dot{F}^d_{a_m}}{K_j^d(\boldsymbol{\chi}^d_s)} + u_{f_m} \right) \\ u_s &= \frac{1}{\gamma_3^j(\boldsymbol{m}_s, \boldsymbol{P}_s, \boldsymbol{P^d}_s, u_s)} \left(\dot{x}_v + \frac{\dot{F}^d_{a_s}}{K_j^d(\boldsymbol{\chi}^d_m)} + u_{f_s} \right) \end{aligned} \tag{6.70}$$

where u_{f_m} and u_{f_s} correspond to the feedback elements of the command input and are defined as,

$$u_{f_m} = -\varepsilon q_{E_1} - K_{F_1}\tilde{F}_m, \qquad u_{f_s} = -\varepsilon(q_{E_1} - q_{E_2}) - K_{F_2}\tilde{F}_s \tag{6.71}$$

where $\varepsilon \in \Re^+$ is a small positive constant. When the combination of all the external forces on the Shape system, represented by the $\boldsymbol{F_E}$ in Eq. (6.25) is either known or is an un-known constant, then as shown in theorem 6.2 the valve command input in Eq. (6.70) provides exponential regulation of Shape system dynamics. For a co-ordinated tele-operator velocity of V_L, the dynamics of the co-ordinated system is obtained from Eq. (6.24) as,

$$M_L \dot{V}_L = \rho((\eta + 1)F_h + F_{e_m}) + F_{e_s} - u_d \tag{6.72}$$

Other than the virtual inertia input u_d, the external forces acting on the co-ordinated system in the above equation correspond to the desired supply rate in Eq. (6.8) (for $N = 1$). In the following section, the supply rate to the closed-loop tele-operator is studied and the input u_d is defined to ensure that the supply rate to the tele-operator satisfied the passivity condition stated in Eq. (6.10).

6.4.1 Supply rate to the closed loop tele-operator

The storage function for the closed loop tele-operator is defined to be the cumulative energy function of the different sub-systems in the tele-operator. Therefore the storage function of the closed loop system includes kinetic energy of the master inertia, the slave inertia and the virtual mass, and the available energy from the master ($W^j_{act}(\boldsymbol{m}_m, \boldsymbol{P}_m)$) and the slave ($W^j_{act}(\boldsymbol{m}_s, \boldsymbol{P}_s)$) pneumatic actuators. Let $\boldsymbol{\chi}_m := (\boldsymbol{m}_m, \boldsymbol{P}_m)$ be the vector of chamber air mass and pressure for the master actuator and $\boldsymbol{\chi}_s := (\boldsymbol{m}_s, \boldsymbol{P}_s)$ is the vector of chamber air mass and pressure of the slave actuator. By considering the fact that the master dynamics are scaled by $\rho \in \Re^+$ for obtaining the closed loop dynamics, the storage function for the tele-operator is defined as,

$$W_s(\dot{x}_m, \dot{x}_s, \dot{x}_v, \boldsymbol{\chi}_m, \boldsymbol{\chi}_s) = \frac{\rho}{2} M_m \dot{x}_m^2 + \rho W^j_{act}(\boldsymbol{m}_m, \boldsymbol{P}_m) + \frac{1}{2} M_v \dot{x}_v^2 + \frac{1}{2} M_s \dot{x}_s^2 + W^j_{act}(\boldsymbol{m}_s, \boldsymbol{P}_s) \tag{6.73}$$

where $j \in (iso, adb)$ is the index to represent the thermodynamic process in the actuator and the energy available from the pneumatic actuator ($W^j_{act}(.)$) for adiabatic and isothermal actuators is as defined in Eq. (3.94) and Eq. (3.100) respectively. The kinetic energy of the virtual mass represents the energy associated with the velocity feed-forward input $\dot{x}_v$ at the fluid interaction port of the actuator. Using the master and the slave inertial dynamics from Eq. (6.28), virtual inertia dynamics from Eq. (6.11) and

the time derivative $\dot{W}^j_{act}(.)$ of the isothermal and the adiabatic actuator energy function from Eq. (3.121) and Eq. (3.135) respectively, the derivative of the storage function in Eq. (6.73) is obtained as,

$$\begin{aligned}\dot{W}_s(\dot{x}_m, \dot{x}_s, \dot{x}_v, \boldsymbol{\chi}_m, \boldsymbol{\chi}_s) =& \rho((F_h(t) + F_{e_m})\dot{x}_m + \gamma^j_1(\boldsymbol{\chi}_{j_m})F_{a_m}u_m) + F_{e_s}\dot{x}_s \\ &+ (\rho\eta F_h(t) - \rho F_{a_m} - F_{a_s} - u_d)\dot{x}_v + \gamma^j_1(\boldsymbol{\chi}_{j_s})F_{a_s}u_s\end{aligned} \tag{6.74}$$

To demonstrate the desired passivity condition reported in Eq. (6.9), the above equation is re-written as,

$$\begin{aligned}\dot{W}_s(\dot{x}_m, \dot{x}_s, \dot{x}_v, \boldsymbol{\chi}_m, \boldsymbol{\chi}_s) =& (\rho(\eta+1)F_h(t) + \rho F_{e_m})\dot{x}_m + F_{e_s}\dot{x}_s - \rho\eta F_h V_{E_1} \\ &+ \rho(\gamma^j_1(\boldsymbol{\chi}_{j_m})F_{a_m}u_m - F_{a_m}\dot{x}_v) - u_d\dot{x}_v + (\gamma^j_1(\boldsymbol{\chi}_{j_s})F_{a_s}u_s - F_{a_s}\dot{x}_v)\end{aligned} \tag{6.75}$$

where $V_{E_1} \triangleq (\dot{x}_m - \dot{x}_v)$ represents the co-ordination error between the master system and the virtual inertia. From the definition of the valve command input to the master and the slave actuators in Eq. (6.70), the derivative of the storage function in the above equation can be expressed as,

$$\begin{aligned}\dot{W}_s(\dot{x}_m, \dot{x}_s, \dot{x}_v, \boldsymbol{\chi}_m, \boldsymbol{\chi}_s) =& (\rho(\eta+1)F_h(t) + \rho F_{e_m})\dot{x}_m + F_{e_s}\dot{x}_s - u_d\dot{x}_v - \rho\eta F_h V_{E_1} \\ &+ \rho\left(\left(\frac{\gamma^j_1(\boldsymbol{\chi}_m, u_m)}{\gamma^j_3(\boldsymbol{\chi}^d_m, u_m)} - 1\right)F_{a_m}\dot{x}_v + \frac{\gamma^j_1(\boldsymbol{\chi}_m, u_m)}{\gamma^j_3(\boldsymbol{\chi}^d_m, u_m)}F_{a_m}\left(u_{f_m} + \frac{\dot{F}^d_{a_m}}{K^d_j(\boldsymbol{\chi}^d_m)}\right)\right) \\ &+ \left(\frac{\gamma^j_1(\boldsymbol{\chi}_s, u_s)}{\gamma^j_3(\boldsymbol{\chi}^d_s, u_s)} - 1\right)F_{a_s}\dot{x}_v + \frac{\gamma^j_1(\boldsymbol{\chi}_s, u_s)}{\gamma^j_3(\boldsymbol{\chi}^d_s, u_s)}F_{a_s}\left(u_{f_s} + \frac{\dot{F}^d_{a_s}}{K^d_j(\boldsymbol{\chi}^d_s)}\right)\end{aligned} \tag{6.76}$$

where u_{f_m} and u_{f_s} are as defined in Eq. (6.71), $\boldsymbol{\chi}^d_{m,s} := (\boldsymbol{m}_{m,s}, \boldsymbol{P}_{m,s}, \boldsymbol{P}^d_{m,s})$ as defined in Eq. (6.56), while $\boldsymbol{\chi}_{m,s} := (\boldsymbol{m}_{m,s}, \boldsymbol{P}_{m,s})$. For ease of presentation define a function $\beta(.)$ as,

$$\beta(\boldsymbol{\chi}^d_m) = \left(\frac{\gamma^j_1(\boldsymbol{\chi}_m, u_m)}{\gamma^j_3(\boldsymbol{\chi}^d_m, u_m)} - 1\right)F_{a_m}, \qquad \beta(\boldsymbol{\chi}^d_s) = \left(\frac{\gamma^j_1(\boldsymbol{\chi}_s, u_s)}{\gamma^j_3(\boldsymbol{\chi}^d_s, u_s)} - 1\right)F_{a_s} \tag{6.77}$$

As shown in section 5.4, both $\beta(\boldsymbol{\chi}^d_m)\dot{x}_v$ and $\beta(\boldsymbol{\chi}^d_s)\dot{x}_v$ are sign indefinite and act as a power source/sink. To compensate for this active power signal, the input u_d on the

virtual inertia is therefore designed as,

$$u_d = \begin{cases} (\rho\beta(\boldsymbol{\chi}_m^d) + \beta(\boldsymbol{\chi}_s^d)), & \text{if } (\rho\beta(\boldsymbol{\chi}_m^d) + \beta(\boldsymbol{\chi}_s^d))\dot{x}_v > 0 \\ 0 & \text{if } (\rho\beta(\boldsymbol{\chi}_m^d) + \beta(\boldsymbol{\chi}_s^d))\dot{x}_v \leq 0 \end{cases} \tag{6.78}$$

As shown in the section 5.5, the nonlinear functions $\gamma_1^j(\boldsymbol{\chi}_{(m,s)})$ and $\gamma_3^j(\boldsymbol{\chi}_{(m,s)}^d)$ have the same sign and are fairly close in magnitude. Therefore the magnitude of u_d is typically very small and does not effect the feel factor of the tele-operator. Using the definition of u_d from Eq. (6.78), the time-derivative of the storage function $\dot{W}_s(.)$ in Eq. (6.76) can be expressed as,

$$\begin{aligned} \dot{W}_s(\dot{x}_m, \dot{x}_s, \dot{x}_v, \boldsymbol{\chi}_m, \boldsymbol{\chi}_s) &\leq (\rho(\eta+1)F_h(t) + \rho F_{e_m})\dot{x}_m + F_{e_s}\dot{x}_s - \rho\eta F_h V_{E_1} \\ &+ \rho\frac{\gamma_1^j(\boldsymbol{\chi}_m, u_m)}{\gamma_3^j(\boldsymbol{\chi}_m^d, u_m)}F_{a_m}\left(u_{f_m} + \frac{\dot{F}_{a_m}^d}{K_j^d(\boldsymbol{\chi}_m^d)}\right) + \frac{\gamma_1^j(\boldsymbol{\chi}_s, u_s)}{\gamma_3^j(\boldsymbol{\chi}_s^d, u_s)}F_{a_s}\left(u_{f_s} + \frac{\dot{F}_{a_s}^d}{K_j^d(\boldsymbol{\chi}_s^d)}\right) \end{aligned} \tag{6.79}$$

For a time-varying unknown force $\boldsymbol{F_E}(t)$ on the Shape system, exponential convergence of $\boldsymbol{q_E}$ and $\boldsymbol{V_E}$ is achieved to only a neighborhood around the origin. The feedback inputs u_{f_m} and u_{f_s} are non-zero and sign indefinite in this neghborhood. Also, the desired force $F_{a_m}^d$ from the master actuator and $F_{a_s}^d$ from the slave actuator depend on $\boldsymbol{F_E}(t)$ and are also time-varying. Therefore, u_{f_m}, u_{f_s} and $\dot{\boldsymbol{F}}_{\boldsymbol{a}}^{\boldsymbol{d}}$ act as energy source/sink for the tele-operator. To achieve the desired passivity condition in the presence of these active power interactions, the procedure outlined in section 5.4 is followed. A virtual flywheel is used to monitor the power demands of the controller to the tele-operator. When excess power is transferred to the tele-operator due to the controller requirements, the control input is modified to drain some energy away from the tele-operator. In the following section, dynamics of the flywheel required to achieve passive operation of the co-ordinated tele-operator is presented.

6.4.2 Augmented system with flywheel dynamics

Similar to the analysis in section 5.4 for human power amplifier, the dynamics of the flywheel are defined as

$$M_f\ddot{x}_f = T_f \tag{6.80}$$

where M_f, x_f and T_f again correspond to the flywheel inertia, position of the flywheel and the torque acting on flywheel respectively. The torque acting on the flywheel is

defined such that the power demanded by the controller for tele-operation is extracted from the flywheel. Therefore power interaction to/from the tele-operator change the kinetic energy of the flywheel. When the flywheel energy is above a threshold value, the tele-operator is said to be in normal mode of operation. If the power requirements are excessive and the kinetic energy of the flywheel falls below a pre-defined threshold value, the operation of tele-operator is switched to emergency mode. In the emergency mode of operation, energy is extracted from the tele-operator and is transferred to the flywheel. To realize this energy transfer, the input u_d on the virtual mass is augmented with a damping force and the virtual inertia dynamics in Eq. (6.11) are modified as,

$$M_v\ddot{x}_v = \rho\eta F_h - \rho F_{a_m} - F_{a_s} - (u_d + b\dot{x}_v) \tag{6.81}$$

where $b \in \Re^+$ is the damping coefficient. Energy dissipated by this damping force is transferred to the flywheel. In the following section a storage function for the augmented system of tele-operator and flywheel is defined. The supply rate to this augmented system is identified and the flywheel torque T_f is defined to ensure that the co-ordinated tele-operator satisfies the desired passivity condition in Eq. (6.10).

6.4.3 Passivity properties of the fictitious flywheel augmented system

The storage function in Eq. (6.73) is now augmented with the kinetic energy of the flywheel as,

$$\begin{aligned} W_t(\dot{x}_m, \dot{x}_s, \dot{x}_v, \boldsymbol{\chi}_m, \boldsymbol{\chi}_s, \dot{x}_f) =& \frac{\rho}{2}M_m\dot{x}_m^2 + \rho W_{act}(\boldsymbol{\chi}_{j_m}) + \frac{1}{2}M_v\dot{x}_v^2 + \frac{1}{2}M_s\dot{x}_s^2 \\ &+ W_{act}(\boldsymbol{\chi}_{j_s}) + \frac{1}{2}M_f\dot{x}_f^2 \end{aligned} \tag{6.82}$$

Note that a single flywheel is defined to monitor the active energy interaction between the controller and the actuators on both the master and the slave systems. Using the inertial dynamics for the master and the slave system from Eq. (6.28), the virtual inertia dynamics from Eq. (6.81), the supply rate for the isothermal and adiabatic actuators from Eq. (3.121) and Eq. (3.135) respectively, and the dynamics of the flywheel from Eq. (6.80), the supply rate to the new storage function in the above equation is

obtained as,

$$\dot{W}_t(\dot{x}_m, \dot{x}_s, \dot{x}_v, \boldsymbol{\chi}_m, \boldsymbol{\chi}_s, \dot{x}_f) = (F_d + \rho F_h + \rho F_{e_m})\dot{x}_m + F_{e_s}\dot{x}_s - F_d V_{E_1} - (u_d - (\rho\beta(\boldsymbol{\chi}_m^d) + \beta(\boldsymbol{\chi}_s^d)))\dot{x}_v + \rho\frac{\gamma_1^j(\boldsymbol{\chi}_{j_m})}{\gamma_3^j(\boldsymbol{\chi}_m^d)}F_{a_m}\left(u_{f_m} + \frac{\dot{F}_{a_m}^d}{K_j^d(\boldsymbol{\chi}_m^d)}\right) + \frac{\gamma_1^j(\boldsymbol{\chi}_{j_s})}{\gamma_3^j(\boldsymbol{\chi}_s^d)}F_{a_s}\left(u_{f_s} + \frac{\dot{F}_{a_s}^d}{K_j^d(\boldsymbol{\chi}_s^d)}\right) + T_f\dot{x}_f \tag{6.83}$$

The updated valve input commands u_m and u_s to the master and the slave actuators respectively, the damping coefficient b, and the torque on the flywheel inertia T_f required for passive operation are presented in the following theorem.

Theorem 6.3. *For a tele-operation system with inertial dynamics of a pneumatic actuated master system as given in Eq. (6.2), inertial dynamics of a pneumatic actuated slave system (for $N = 1$) as given in Eq. (6.4), with the pressure dynamics of the pneumatic actuator as given in Eq. (5.8) and the mass flow to each chamber of the actuator as given by Eq. (5.9), for the following definition of the valve input command,*

$$u_m = \frac{1}{\gamma_3^j(\boldsymbol{\chi}_m^d, u_m)}\left(\dot{x}_v + \frac{\dot{F}_{a_m}^d}{K_j^d(\boldsymbol{\chi}_m^d)} + \hat{u}_{f_m}\right) \tag{6.84}$$

$$u_s = \frac{1}{\gamma_3^j(\boldsymbol{\chi}_s^d, u_s)}\left(\dot{x}_v + \frac{\dot{F}_{a_s}^d}{K_j^d(\boldsymbol{\chi}_s^d)} + \hat{u}_{f_s}\right) \tag{6.85}$$

where the vector $\boldsymbol{\chi}_{m,s}^d = (\boldsymbol{m}_{m,s}, \boldsymbol{P}_{m,s}, \boldsymbol{P}_{m,s}^d)$ is as defined in Eq. (6.56), $F_{a_m}^d$ and $F_{a_s}^d$ represent the desired force from the master and the slave actuator respectively and are as defined in Eq. (6.55), while the feedback elements $\hat{u}_{f_m}$, $\hat{u}_{f_s}$ of the command input and the flywheel torque T_f are related through the following skew-symmetric matrix,

$$\begin{pmatrix} \hat{u}_{f_m} \\ \hat{u}_{f_s} \\ T_f \end{pmatrix} = \begin{pmatrix} 0 & 0 & g(\dot{x}_f)u_{f_m} \\ 0 & 0 & g(\dot{x}_f)u_{f_s} \\ -g(\dot{x}_f)u_{f_m} & -g(\dot{x}_f)u_{f_s} & 0 \end{pmatrix} \begin{pmatrix} \frac{\gamma_1^j(\boldsymbol{\chi}_m, u_m)}{\gamma_3^j(\boldsymbol{\chi}_m^d, u_m)}F_{a_m} \\ \frac{\gamma_1^j(\boldsymbol{\chi}_s, u_s)}{\gamma_3^j(\boldsymbol{\chi}_s^d, u_s)}F_{a_s} \\ \dot{x}_f \end{pmatrix} + \begin{pmatrix} 0 \\ 0 \\ \frac{1}{\dot{x}_f}\left(\rho\eta F_h V_E - \left(\rho\beta(\boldsymbol{\chi}_m^d, u_m) + \beta(\boldsymbol{\chi}_s^d, u_s) - u_d\right)\dot{x}_v + b\dot{x}_v^2 \right. \\ \left. + \frac{\gamma_1^j(\boldsymbol{\chi}_m, u_m)}{\gamma_3^j(\boldsymbol{\chi}_m^d, u_m)}\frac{\dot{F}_{a_m}^d}{K_j^d(\boldsymbol{\chi}_m^d)} + \frac{\gamma_1^j(\boldsymbol{\chi}_s, u_s)}{\gamma_3^j(\boldsymbol{\chi}_s^d, u_s)}\frac{\dot{F}_{a_s}^d}{K_j^d(\boldsymbol{\chi}_s^d)}\right) \end{pmatrix} \tag{6.86}$$

where u_d is as defined in Eq. (6.78), while the function $g(\dot{x}_f)$ and the damping coefficient b depend on the flywheel velocity and are defined as,

$$\textit{Regular mode} : \begin{pmatrix} g(\dot{x}_f) = \frac{1}{\dot{x}_f} \\ b = 0 \end{pmatrix} \quad \textit{if } \dot{x}_f \geq f_o \tag{6.87}$$

$$\textit{Emergency mode} : \begin{pmatrix} g(\dot{x}_f) = \frac{1}{f_o} \\ b \in \Re^+ \end{pmatrix} \quad \textit{if } \dot{x}_f < f_o \tag{6.88}$$

where f_o corresponds to the threshold velocity of the flywheel for switching to the emergency mode of operation, operation of the tele-operator satisfies the following passivity condition,

$$\int_0^t \rho((\eta+1)F_h(\tau) + F_{e_m}(\tau))\dot{x}_m(\tau) + F_{e_s}(\tau)\dot{x}_s(\tau)\, d\tau \geq -d_o^2 \tag{6.89}$$

Proof. The storage function for the augmented tele-operator with flywheel dynamics is as given in Eq. (6.82). From the definition of the valve command inputs for the master and the slave actuators in Eq. (6.84) and Eq. (6.85) respectively, the supply rate to the augmented system is as given in Eq. (6.83).

Defining the flywheel torque as given in Eq. (6.86), and using the definition of $g(\dot{x}_f)$ and the damping coefficient b from Eq. (6.87), the supply rate to the actuator in both the regular mode and emergency mode of operation is obtained from Eq. (6.83) as,

$$\dot{W}_t(\dot{x}_m, \dot{x}_s, \dot{x}_v, \boldsymbol{\chi}_m, \boldsymbol{\chi}_s, \dot{x}_f) = \rho((\eta+1)F_h + F_{e_m})\dot{x}_m + F_{e_s}\dot{x}_s \tag{6.90}$$

On integrating on both sides of the above equation, the passivity condition for operation of the tele-operator in Eq. (6.9) is satisfied as,

$$\int_0^t \rho((\eta+1)F_h(t) + F_{e_m})\dot{x}_m + F_{e_s}\dot{x}_s\, d\tau \geq -W_t(\dot{x}_m, \dot{x}_s, \dot{x}_v, \boldsymbol{\chi}_m, \boldsymbol{\chi}_s, \dot{x}_f)\Big|_{t=0} \tag{6.91}$$

where $W_t(\dot{x}_m, \dot{x}_s, \dot{x}_v, \boldsymbol{\chi}_m, \boldsymbol{\chi}_s, \dot{x}_f)\Big|_{t=0}$ represents the initial available energy in the augmented system. Once co-ordination is achieved, the passivity condition for the tele-operator in Eq. (6.10) is satisfied. Note that the co-ordinated tele-operator behaves like a human power amplifier.

In the emergency mode of operation when the flywheel velocity drops below the threshold value of f_o, the damping coefficient b is selected to be large enough to put energy back into the flywheel.

□

When the velocity of the flywheel increases in emergency mode, it is recommended to maintain the control input corresponding to emergency mode until velocity $\dot{x}_f$ of the flywheel is such that $\dot{x}_f > f_1 > f_o$. Here f_1 represents velocity of the flywheel required to switch back to regular mode of operation. This will prevent any high frequency switching at the boundary between the emergency mode and the normal mode of operation.

The control algorithm developed in this section is implemented on a system consisting of a single master and a single slave ($N = 1$) actuator.

6.5 Experimental results

Experimental results validating the efficacy of the proposed controller are presented in this section. The setup to investigate this bilateral tele-operation is as shown in Fig. (6.6). It consists of two vertically mounted, single DOF pneumatic actuators with integrated position feedback. Both the actuators have similar specifications of $0.0508m$ (2 inches) bore diameter, rod diameter of $0.0254m$ (1 inch) and stroke length of $0.3048m$ (12 inches). An inertial load of $3.4kgs$ is applied on the slave system. A MLP-50 force sensor from Transducer Techniques is used to measure the input human force on the master actuator and is attached as shown in Fig. (6.6). The pressure in each chamber of the actuator required for evaluating the actuator force per Eq. (5.6) is obtained by using SDET-22T-D16 pressure sensors from FESTO. A FESTO MPYE-5-LF010 proportional servo valve is used to meter the air flow to each actuator. The valve input-output characteristics are as shown in Fig. (5.4). To study interaction stability of the tele-operator, a metal obstacle used as a hard contact surface is placed in the path of the slave actuator as shown in Fig. (6.6). All the experiments are conducted at the maximum available supply pressure of $6.89e5Pa$ ($100psi$).

Virtual velocity is determined from the virtual inertia dynamics in Eq. (6.81). The velocity of each actuator is again determined by assuming constant acceleration and

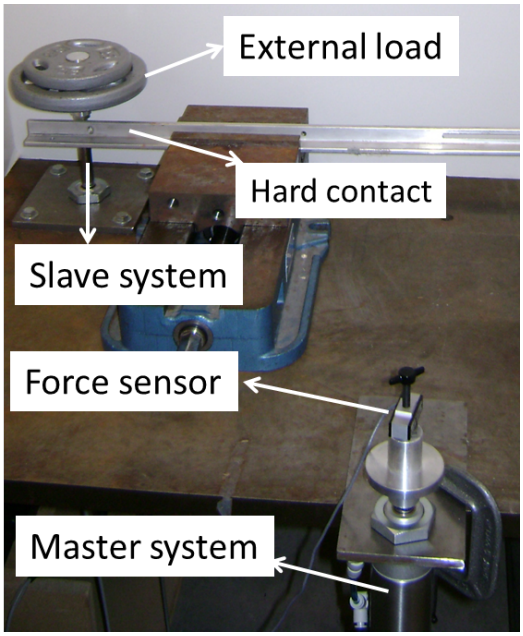

Figure 6.6: Experimental setup for passive bilateral tele-operation of two single d.o.f. pneumatic actuators

using a high gain observer. The velocity observer dynamics are as presented in Eq. (5.80) of section 5.5.

The parameters used in the controller implementation are listed in table 6.1. Again, high enough gains are used in the first stage of the controller design to achieve faster regulation of Shape system inertia dynamics ($\boldsymbol{q_E}, \boldsymbol{V_E}$) to zero. The feedback gain on the force error is not required to be very high, as the feed-forward input of virtual velocity $\dot{x}_v$ is fairly effective in moving the actuator in the desired direction with nearly the desired velocity.

As both the actuators used in this experimental study have the same dimensions and operate in the same power range, the power scaling factor ρ from the master to the slave actuator is selected to be 1. To understand the effect of assumptions on the underlying thermodynamic process in the actuator, controllers developed for both isothermal and adiabatic models has been tested in experiments.

Table 6.1: Parameters used in the implementation of tele-operation controller for the isothermal and the adiabatic models of the actuator

Parameter	Magnitude (Isothermal)	Magnitude (Adiabatic)
$\boldsymbol{K_p}$	diag(4.8e3,1.74e4)	diag(4.8e3, 1.74e4)
$\boldsymbol{K_v}$	diag(70,90)	diag(70,90)
$\boldsymbol{K_F}$	diag(0.0025,0.025)	diag(0.002,0.002)
$\boldsymbol{Q_1}$	1.8e3*diag(25.04,12.57)	1.8e3*diag(25.04,12.57)
$\boldsymbol{Q_2}$	diag(12.27,6.785)	diag(12.27,6.785)
$\boldsymbol{Q_3}$	diag(12.27,6.785)	diag(12.27,6.785)
$\boldsymbol{Q_4}$	1.8e3*diag(25.04,12.57)	1.8e3*diag(25.04,12.57)
$\boldsymbol{L_1}$	diag(1800,1800)	diag(1800,1800)
$\boldsymbol{L_2}$	diag(2.6042e4,2.6146e4)	diag(2.6042e4,2.6146e4)
ε	0.1	0.1
ρ	1	1
η	15	15
M_v	15 kgs	15 kgs

Isothermal model for controller design

Performance of the controller, designed by assuming the thermodynamic process to be isothermal is shown in Fig. (6.7). This figure illustrates tracking performance in both free space and when the tele-operator interacts with the hard surface in the path of the slave actuator. As shown in the figure, the position of the master and slave track very well while traversing an arbitrary profile in free space. When the motion of the slave actuator is impeded by a hard surface, the master actuator overshoots the slave position for a very short time due to compliance in the pneumatic tele-operator. The controller quickly compensates for this overshoot and the desired position co-ordination is restored. For the data reported in Fig. (6.7), the root mean square error in position tracking for the isothermal process is obtained as $2.1mm$ in free motion and $1.2mm$ during hard contact.

Velocity co-ordination between the master, the slave and the virtual inertia is as

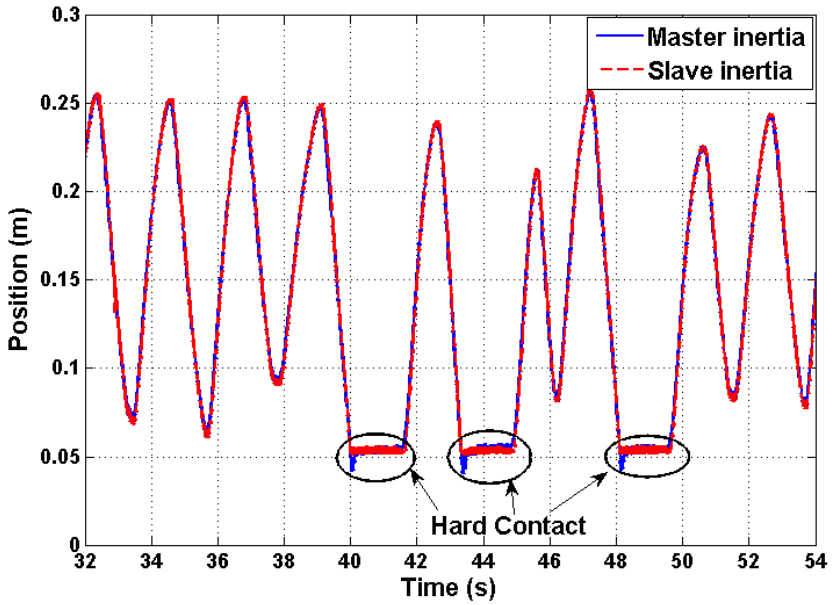

Figure 6.7: Position co-ordination achieved between the master and the slave inertia during tele-operation of the slave along an arbitrary path in free space and during interaction with a hard surface. The controller implemented to obtain the data in this figure is designed by assuming the thermodynamic process in the actuator to be isothermal.

shown in Fig. (6.8). This figure illustrates good co-ordination characteristics in free space. When the slave actuator interacts with the hard surface, the velocity of the slave immediately drops to zero. There is a small overshoot in the velocity of the master and the virtual inertias, again due to compliance in the pneumatic actuator, but their velocities also quickly drop to zero due to controller action. During the course of interaction with the hard surface, the velocities of the master, the slave and the virtual inertia are all uniformly zero, indicating that contact instabilities are not induced when the tele-operator suddenly interacts with a hard surface.

As presented in Eq. (6.14), the dynamics of the co-ordinated tele-operator are similar to that of a human power amplifier in Eq. (5.11). From Eq. (6.15), the cumulative force applied by the master and the slave actuator is related to amplified human force $\rho\eta F_h$ as

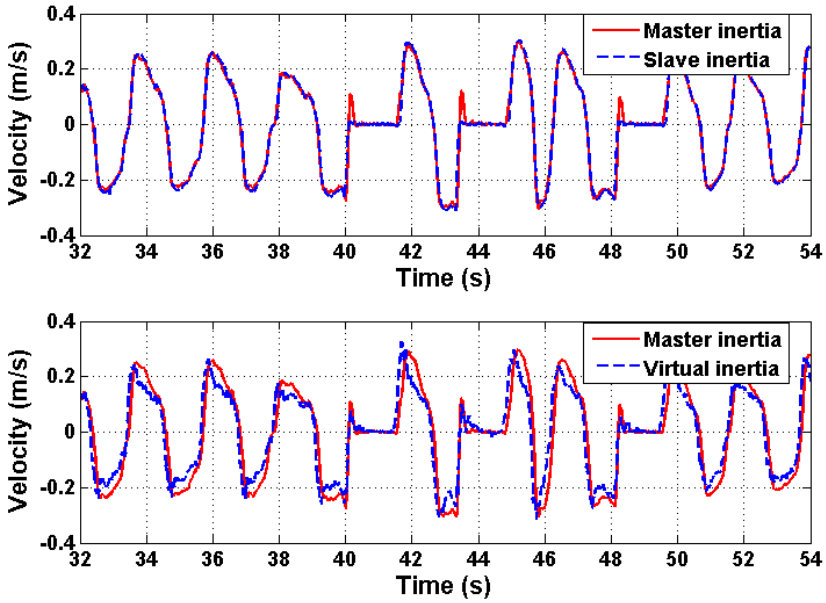

Figure 6.8: Velocity co-ordination achieved between the master and the slave inertia (top figure), and between the master and the virtual inertia (bottom figure) during tele-operation of the slave along an arbitrary path in free space and during interaction with a hard surface. The controller implemented to obtain the data in this figure is designed by assuming the thermodynamic process in the actuator to be isothermal.

$(\rho F_{a_m} + F_{a_s}) = \rho\eta F_h$. As illustrated in Fig. (6.9), the cumulative force from the master and the slave actuators as given in Eq. (6.15) corresponds well with the amplified human force. Note that when interacting with the hard surface, despite the high magnitude of the input human force, the tele-operator position does not change. The reaction force increases with the input human force to maintain position and velocity co-ordination.

Adiabatic model for controller design

Position tracking with an adiabatic model of the actuator for controller design is as shown in Fig. (6.10). Good position tracking is achieved during operation in free space for an arbitrary position profile. Similar to the isothermal actuator, when the

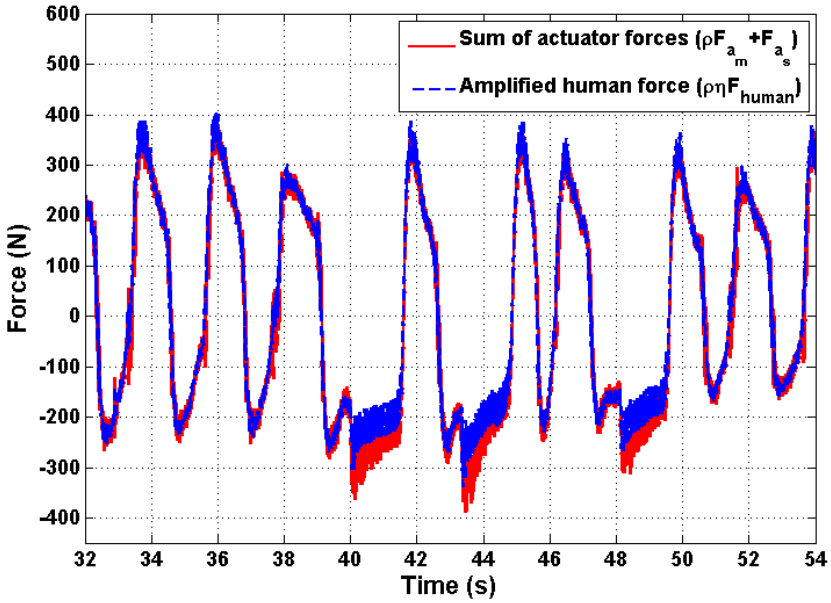

Figure 6.9: Comparison of the amplified cumulative actuator forces $\rho F_{a_m} + F_{a_s}$, with the amplified human force $\rho\eta F_h$ measured during tele-operation of the slave along an arbitrary path in free space and when interacting with a hard surface. The controller implemented to obtain the data in this figure is designed by assuming the thermodynamic process in the actuator to be isothermal.

slave suddenly interacts with a hard contact, the master position overshoots the desired position due to compliance in the pneumatic actuator. But the desired position coordination is quickly restored. For the adiabatic process, the root mean square value of the position tracking error is $1.8mm$ in free motion and $0.9mm$ during hard contact.

Velocity tracking achieved with an adiabatic model of the actuator is shown in Fig. 6.11. Desired tracking between the master, the slave and the virtual mass are achieved in free space for an arbitrary profile. When interacting with hard surface, velocities of all the inertias are uniformly zero, illustrating no contact instabilities. As shown in Fig. (6.12), the cumulative forces $(\rho F_{a_m} + F_{a_s})$ from the actuators when assuming adiabatic thermodynamic model correspond well with the amplified human force $\rho\eta F_h$ as stated in Eq. (6.15).

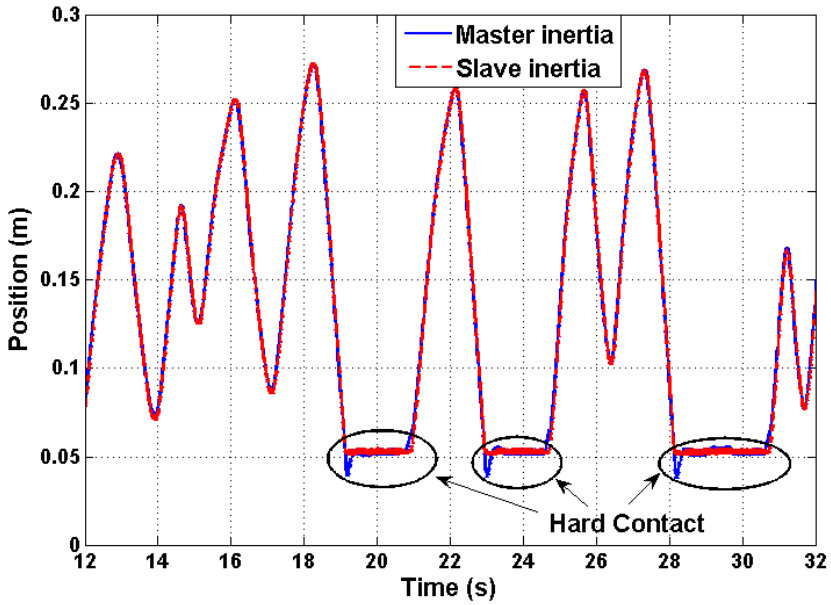

Figure 6.10: Position co-ordination achieved between the master and the slave inertia during tele-operation of the slave along an arbitrary path in free space and during interaction with a hard surface. The controller implemented to obtain the data in this figure is designed by assuming the thermodynamic process in the actuator to be adiabatic.

From the co-ordination results presented in this section, controllers designed by assuming either the isothermal or the adiabatic thermodynamic process in the actuator provide good co-ordination performance.

Input force u_d on slave actuator

As shown in Figs. (6.13 and 6.14), the magnitude of the ratio $\gamma^j_{1_{(m,s)}}(.)/\gamma^j_{3_{(m,s)}}(.)$ is very close to one during operation of the tele-operator in free space. Therefore, the effect of input u_d on the tele-operator dynamics, as determined from Eq. (6.78), is very small compared to other external forces. Thus u_d while have negligible effect on the tele-operator response, while helping in satisfying the technical requirements for passive operation. During hard contact the co-ordinated tele-operator is at rest, and

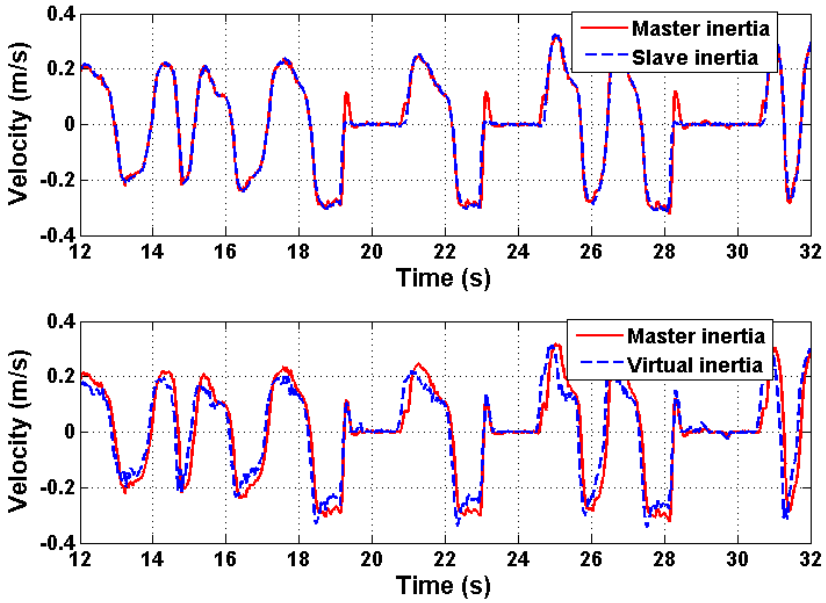

Figure 6.11: Velocity co-ordination achieved between the master and the slave inertia during tele-operation of the slave along an arbitrary path in free space and during interaction with a hard surface. The controller implemented to obtain the data in this figure is designed by assuming the thermodynamic process in the actuator to be adiabatic.

per definition in Eq. (6.78), u_d will have a value of 0 during hard contact.

6.6 Summary

In this chapter a framework for multilateral operation between multiple fluid powered actuators has been presented. It is shown that the controller framework for human power amplification can be conveniently extended to formulate multilateral tele-operation. Controllers for a system consisting of a pneumatic actuated master and a single pneumatic actuated slave have been also presented in this chapter. By assuming that the thermodynamics in the pneumatic actuator to be reversible (isothermal/adiabatic), the standard back-stepping controller is used to design the command input to the actuators

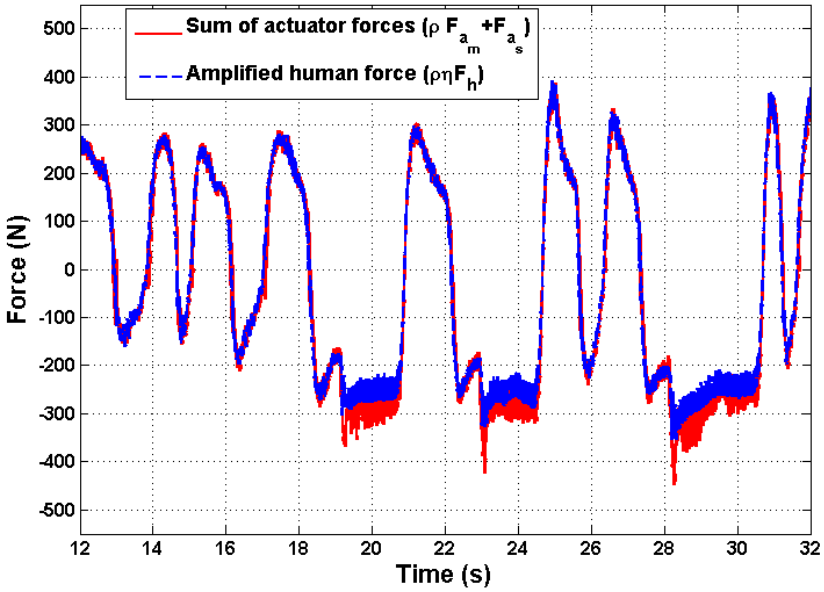

Figure 6.12: Comparison of the amplified cumulative actuator forces $\rho F_{a_m} + F_{a_s}$, with the amplified human force $\rho\eta F_h$ measured during tele-operation of the slave along an arbitrary path in free space and when interacting with a hard surface. The controller implemented to obtain the data in this figure is designed by assuming the thermodynamic process in the actuator to be adiabatic.

for achieving bilateral position and velocity co-ordination. Controllers for both isothermal and adiabatic actuators have been reported in this chapter. These controllers were implemented on an experimental setup consisting of two single DOF double ended pneumatic actuators. Experimental results demonstrate good performance both in free space and when interacting with a hard metal surface. In the following chapter the proposed framework for multilateral tele-operation and human power amplification is extended to a multiple degrees of freedom robotic system with electrically actuated master system.

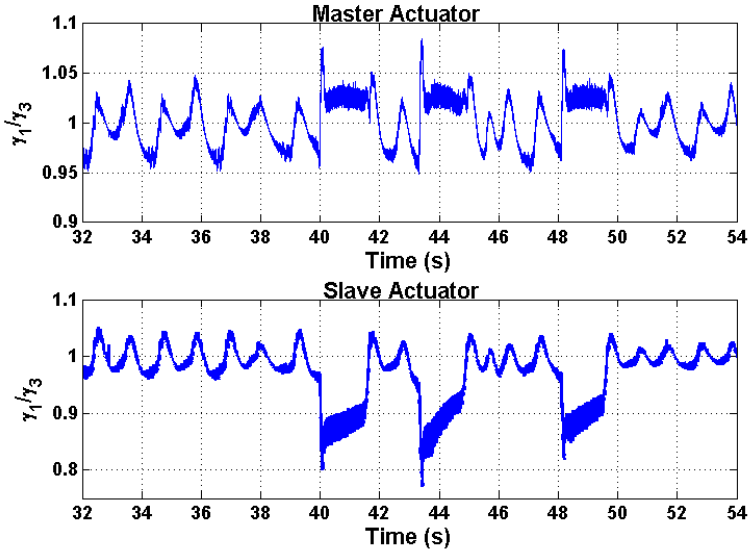

Figure 6.13: Magnitude of the ratio $\gamma^{iso}_{1_{m,s}}(.)/\gamma^{iso}_{3_{m,s}}(.)$ used in the definition of u_d in Eq. (6.78), when the thermodynamic process is assumed to be isothermal.

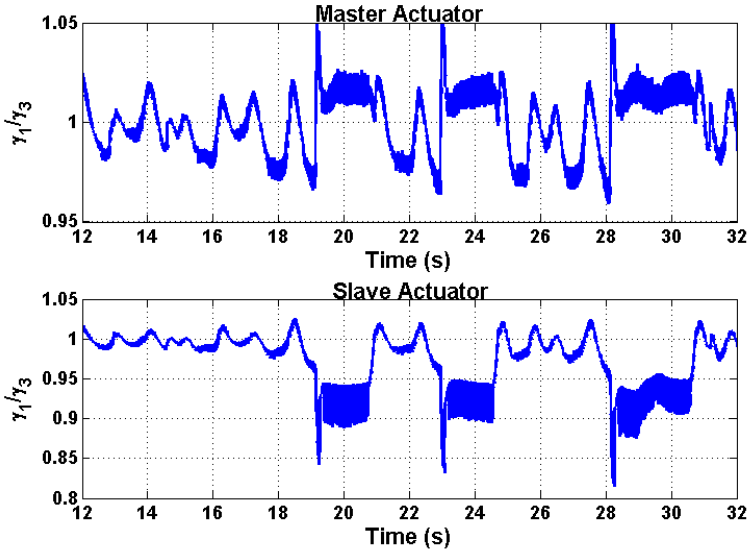

Figure 6.14: Magnitude of the ratio $\gamma^{iso}_{1_{m,s}}(.)/\gamma^{iso}_{3_{m,s}}(.)$ used in the definition of u_d in Eq. (6.78), when the thermodynamic process is assumed to be adiabatic.

Chapter 7

Passive Bilateral Tele-operation of a Pneumatic Rescue Robot with Multiple-DOF

In chapter 5, a framework for human power amplification was presented. This framework was extended to multilateral tele-operation and human power amplification with multiple actuators in chapter 6. The controller design reported in chapters 5 and 6 were for single-DOF systems. In the current chapter, the framework for human power amplification and passive tele-operation presented in earlier chapters is used to design controllers for passive bilateral tele-operation and human power amplification of a pneumatic actuated multi-DOF crawling robot.

The crawler is intended to be a four legged robot for use in rescue environments whose terrain is typically unknown. An illustration of the crawling robot, designed and built at the Intelligent Machine Dynamics Laboratory (IMDL) at Georgia Institute of Technology, is as shown in Fig. (7.1). Each leg of the crawler has three joints and each joint is actuated by a pneumatic actuator. The crawler is remotely operated by commanding a PHANToM(TM[1]) haptic device, also shown in Fig. (7.1). As the crawler and the PHANToM(TM[1]) operate at different power range, human power input at the PHANToM(TM[1]) is amplified by following the framework for bilateral

[1] PHANToM is a trademarked product of Sensable Technologies,MA

tele-operation presented in chapter 6. In addition, it is shown that this framework can easily be extended to amplify human power input on an interface on the crawler leg. This feature, which enables the crawler leg to be operated as a multi-DOF human power amplifier, can aid in on-site rescue.

In chapters 5 and 6, controllers designed for both isothermal and adiabatic thermodynamic models of the actuator were evaluated. The results demonstrated that controllers designed with either thermodynamic models are equally good in achieving the desired performance. Therefore, for ease of presentation, co-ordination controller for bilateral tele-operation and human power amplification is derived in this chapter by assuming the thermodynamic process in the actuator to be adiabatic. The controller development for an isothermal actuator will be similar to the adiabatic actuator considered in this chapter.

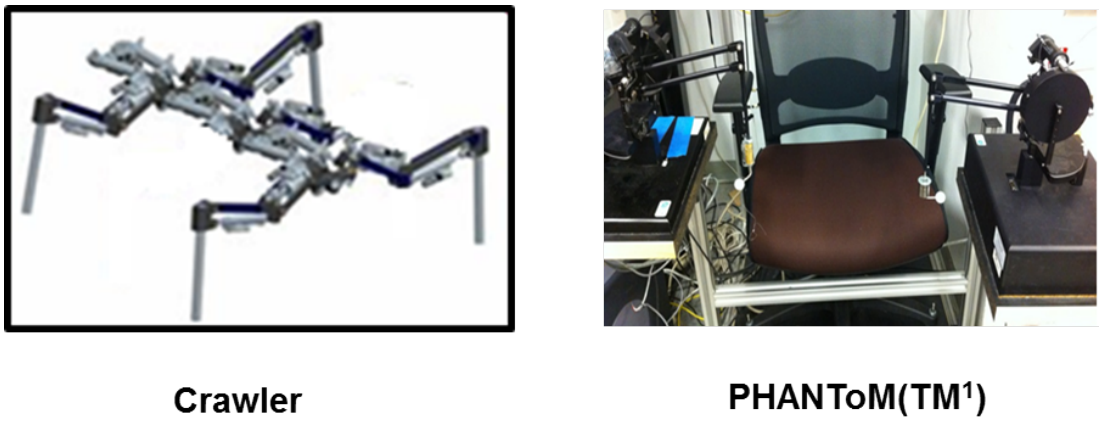

Figure 7.1: A solid model rendition of the proposed 4-legged crawler design

Current configuration and the desired operational characteristics of the crawler and the PHANToM(TM^1) systems are described in the next section. System dynamics are presented in section 7.2. Crawler inertial dynamics are presented in section 7.2.1. The dynamics of the adiabatic actuator are as presented in chapter 3 and are briefly referenced in section 7.2.2. Dynamics of the PHANToM(TM^1) haptic device are presented in section 7.2.3. The problem of bilateral tele-operation with human power amplification is formally stated in section 7.3. The framework for passive bilateral tele-operation and human power amplification of the multi-DOF systems is presented in section 7.4. The

control problem is formally stated within this framework and a two-stage back-stepping controller design is presented in section 7.5. Passivity analysis of the co-ordinated tele-operator is presented in section 7.6. Experimental results verifying efficacy of the proposed controller are presented in section 7.7.

7.1 System configuration and operational characteristics

In this section, the configuration and the operational characteristics of the crawler and the PHANToM(TM^1) haptic device are presented. A schematic of the crawler is shown in Fig. (7.1). A particular strategy for the movement of hind legs is for them to follow the trajectory generated by the front legs [77]. The desired movement of the front two legs is remotely commanded by a human operator through a pair of PHANToM(TM^1) haptic devices. Figure (7.2) illustrates the mode of human interaction with the haptic device. However, as seen in Fig. (7.2), the hind legs are yet to be fabricated for the current manifestation of the robot. Therefore, this chapter will only focus on bilateral tele-operation of the front legs of the crawler. The hind carriage of the robot (consisting of micro-processor, data acquisition and the power supply) is mounted on a pair of caster wheels and a pair of regular wheels and can easily roll along the ground.

Forward motion of the crawler is achieved by placing both the front legs forward and then pushing off the ground. Force from the actuators on the crawler's front legs is used to provide forward motion to the entire mass of the crawler, including mass of the chassis and the hind cart. This movement of the front legs of the crawler to achieve forward motion is similar to butterfly stroke in swimming. When moving the front legs forward in free space, the crawler base is at rest and the motion of the crawler legs is decoupled. Each leg will behave as a three-link manipulator with revolute joints and a fixed base. When pushing off the ground, the legs of the crawler, and the base form a closed chain. In this mode, the dynamics of the legs are coupled. In this study it is assumed that the individual leg dynamics are still decoupled, with the coupling torques assumed to be external environmental torques.

During tele-operation, haptic feedback provides the operator with a *feel* for the interaction between the crawler and its environment. This information could be very important for mapping a safe path for the crawler, especially in the absence of visual

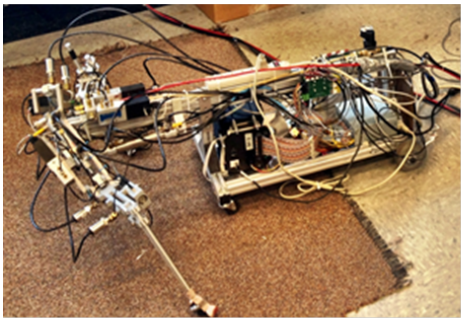

Crawler (slave system)

Human interacting with PHANToM(TM[1])
(Master system)

Figure 7.2: Current experimental configuration of the PHANToM(TM) and the crawler

or audio feedback to the operator. As shown in previous studies [[78] and the references therein], haptic feedback also helps in improving operational effectiveness of tele-operation.

In [77], a virtual linear spring was used to connect the PHANToM(TM[1]) with the crawler in the task space of the crawler leg. The spring force due to error between the position commanded at the PHANToM(TM[1]) and the actual crawler position was used to provide the haptic feedback force. Such a formulation for haptic feedback informs the operator on positional accuracy of the foot and presence of impediments in the path of the crawler. However, the spring stiffness has to be appropriately selected to provide discernible feedback for interaction with both hard and soft surfaces. As the crawler navigates its way around its working environment, the actuator forces are a good measure of the interaction forces between the crawler and its environment. Actuator force at the crawler joints are thus used to provide haptic feedback to the operator. The framework for multilateral tele-operation with an electrically actuated master, presented in

section 6.3.1, is used to achieve bilateral tele-operation in this chapter. In this framework, the tele-operator will behave as a common passive mechanical tool, with ports for mechanical power interaction with the human operator and the physical environment at both the master and the slave systems. In the absence of power interaction at these mechanical ports, the tele-operator will remain at rest.

As shown in Fig. (7.3), a 3-axis force sensor with a handle is attached to one of the front legs of the crawler as an additional interface for human power amplification. Any force applied on this interface is amplified through the actuators attached to that leg of the crawler. This feature will enable people on-site a rescue location to move heavier loads and help in the rescue operation. The crawler leg is thus operated as a multi-DOF human power amplifier. Since the interaction between the crawler and the PHANToM(TM^1) is required to be bilateral, any interaction at the force amplifier interface will be transmitted to the operator at the PHANToM(TM^1) device. Due to this configuration, shared control between the two operators is required to accomplish certain tasks. The current location of the force sensor on the crawler leg is sufficient to demonstrate human power amplification. Future redesign of the rescue robot can consider a more detailed study on more appropriate location of this interface. The PHANToM(TM^1) and the crawler communicate on a local area network connected through Ethernet cables. In this study no communication delay between the PHANToM(TM^1) and the crawler was noticed and is hence not considered in the controller design.

Inertial dynamics of the crawler and the PHANToM(TM^1), and the dynamics of the adiabatic actuator are presented in the following section.

7.2 System dynamics

In this section, inertial dynamics of an individual crawler leg are presented. Dynamics of the other leg will be exactly the same. The three revolute joints on a leg of the crawler are actuated by the three linear pneumatic actuator. Dynamics of an adiabatic actuator providing the actuation torque are briefly presented in section 7.2.2. Energy associated with the three adiabatic actuators on a crawler leg and the associated supply rate is also presented in section 7.2.2. Similar to the crawler, each PHANToM(TM^1) device also has three revolute joints. Each joint has a position sensor to determine the joint

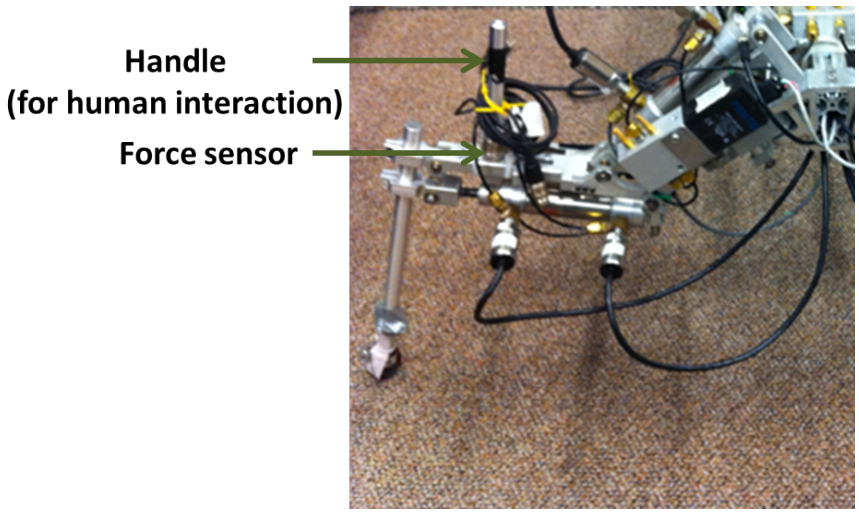

Figure 7.3: Location of the force sensor on the second joint of the right leg

angle. The actuation torque at these joints is provided by a DC servo motor. Inertial dynamics of the PHANToM(TM[1]) haptic device are presented in section 7.2.3.

7.2.1 Crawler leg dynamics

Orientation of the co-ordinate axis for the crawler foot tip workspace is as shown in Fig. (7.4). The figure also illustrates the length a_1 of link 1 (Coxa), the offset d between the joint 1 and 2, the length a_2 of link 2 (Femur) and the length a_3 of link 3 (Tibia). The position of the foot tip is determined by the angles at each joint of the crawler.

The Cartesian co-ordinate axis for measuring the joint angle is defined at each joint by using the Denavit-Hartenberg [1] convention. The co-ordinate axes and the measured orientation of the joint angles on the right leg of the crawler is as shown in Fig. (7.5). The shoulder joint angle between the base (Thorax) of the leg and link 1 (Coxa) is denoted by θ_1, the angle between link 1 (Coxa) and link 2 (Femur) is denoted by θ_2 and the joint angle between link 2 (Femur) and link 3 (Tibia) is denoted by θ_3. The allowed range of motion of the joint angles is determined by geometry of the design. With respect to the joint co-ordinate axes shown in Fig. (7.5), the allowed range of joint angles is obtained in degrees as $\theta_1 \in [-47^o, 90^o]$, $\theta_2 \in [-67^o, -1^o]$, and $\theta_3 \in [17^o, 95^o]$. Note that on the left leg, the allowable range for shoulder joint angle is $[270^o, 407^o]$.

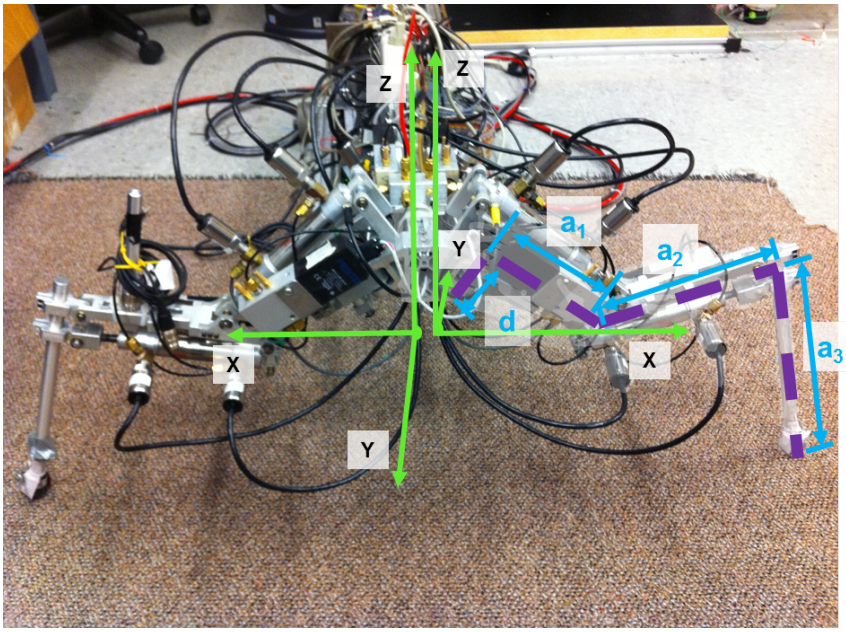

Figure 7.4: Orientation of the Cartesian co-ordinate axes of the foot tip workspace of each leg of the crawler. The geometric parameters d a_1, a_2 and a_3 corresponding to the three links is also shown in the figure.

In the joint co-ordinate axes shown in Fig. (7.5), let y_1 be the stroke position of the pneumatic actuator at shoulder joint, x_2 be the stroke of the actuator at the shank joint, and x_3 be the stroke position of the actuator at the foot joint. Let $\boldsymbol{X} := (y_1, x_2, x_3)$ be the vector of cylinder position along the three joints. There is a one-to-one mapping between the actuator stroke position at each joint and the corresponding joint angle. Using the known information on the range of the joint angles, a linear mapping is established between the position sensor output and the joint angles. This mapping is used to identify the joint angles for any measured output of the actuator position sensor.

In this study, the joint angles are designated to be the generalized co-ordinates and the dynamics of each leg of the crawler is obtained in its joint space. Let $\boldsymbol{q} := [\theta_1, \theta_2, \theta_3]$ be the vector of joint angles on a crawler leg. Let $\boldsymbol{F_{h_e}}$ be the input human force vector along the Cartesian co-ordinates of the interface shown in Fig. 7.3. This force is mapped into the torque $\boldsymbol{\tau_{h_e}}$ in the crawler joint space using the Jacobian $\boldsymbol{J_h^T(q)}$ as,

$$\boldsymbol{\tau_{h_e}} = \boldsymbol{J_h^T(\dot{q})F_{h_e}} \tag{7.1}$$

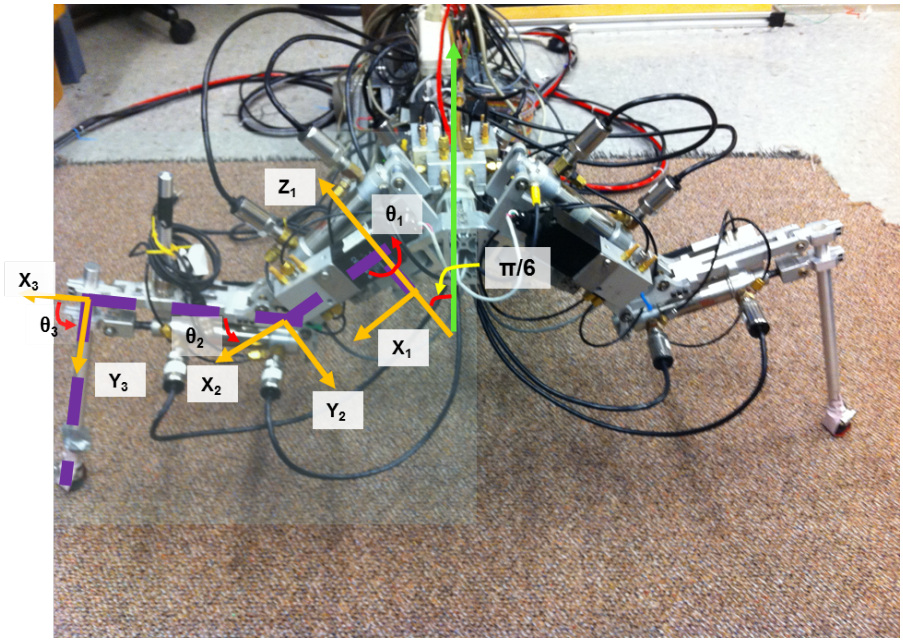

Figure 7.5: Orientation the joint angles (generalized co-ordinates) on the right leg of the crawler obtained by using Denavit-Hartenberg convention [1]

Using the Lagrangian formulation [1], the inertia dynamics of an individual crawler leg is then obtained as,

$$\boldsymbol{M_q(q)\ddot{q} + C_q(q,\dot{q})\dot{q} + g_q(q) = \tau_a + \tau_{e_c} + \tau_{h_e}} \tag{7.2}$$

where $\boldsymbol{M_q(q)} \in R^{3\times3}$ is the inertial matrix of the leg in the joint space, $\boldsymbol{C_q(q,\dot{q})} \in R^{3\times3}$ is the matrix for Coriolis acceleration, $\boldsymbol{g_q(q)} \in R^{3\times1}$ is the gravitational torque vector, $\boldsymbol{\tau_a} \in R^{3\times1}$ is the vector of torque applied by the three pneumatic actuators on the three joints, $\boldsymbol{\tau_{e_c}} \in R^{3\times1}$ is the vector of un-modeled and unknown torques (such as friction, ground reaction forces when interacting with the ground) applied on the three joints. Elements of the matrices $\boldsymbol{M_q(q)}$, $\boldsymbol{C_q(q,\dot{q})}$, and $\boldsymbol{g_q(q)}$ are provided in appendix D.1.

Remark 7.1. *The dynamics in Eq. (7.2) are obtained from Lagrangian formulation, and hence satisfy the skew-symmetry property* $\boldsymbol{A^T(\dot{M}_q(q) - 2C_q(q,\dot{q}))A} = 0$ *for any given vector* $\boldsymbol{A} \in R^{3\times1}$.

7.2.2 Actuator dynamics

The force F_a from a linear pneumatic actuator depends on the cap-side chamber pressure P_1, rod-side chamber pressure P_2, and the piston cross-sectional areas on the cap-side (A_1) and the rod side (A_2) as,

$$F_a = P_1 A_1 - P_2 A_2 - P_{atm}(A_1 - A_2) \tag{7.3}$$

where P_{atm} is the atmospheric pressure acting on the exposed rod. In this chapter, the thermodynamic process in the actuator is assumed to be adiabatic. For a chamber volume of V_i and chamber air mass of m_i, the dynamics of the chamber pressure P_i in an adiabatic actuator is obtained from Eq. (3.13) as,

$$\frac{\dot{P}_i}{P_i} = \gamma \left(\frac{\dot{m}_i}{m_i} - \frac{\dot{V}_i}{V_i} \right) \tag{7.4}$$

where γ corresponds to the ratio of specific heats, and has a magnitude of 1.4 for air. The direction of the air mass flow rate $\dot{m}$ depends on the spool position in the valve regulating the flow to/from the pneumatic actuator, while the magnitude of the air flow depends on the pressure upstream and downstream of the valve and the effective area u available for the flow rate. As given in Eq. (3.26), the air mass flow rate $\dot{m}_i$ to the $i^{th} \in (1, 2)$ chamber of a two-chambered pneumatic actuator is determined from the following equation,

$$\dot{m}_i = \Psi(P_i, T_i, u)u \tag{7.5}$$

where the nonlinear function $\Psi(P_i, T_i, u)$ is as defined in Eq. (3.27). The effective valve area u is used to vary the mass flow rate and consequently vary the chamber pressure. Further details on the actuator model are provided in chapter 3.

From the geometry of the leg, the moment arms $r_1(\theta_1)$, $r_2(\theta_2)$ and $r_3(\theta_3)$ corresponding to joints 1, 2 and 3 on the right leg are obtained as,

$$r_1(\theta_1) = 0.0508Cos(\theta_1), \quad r_2(\theta_2) = 0.0601Cos(\pi/2 + \theta_2), \quad r_3(\theta_3) = -0.0381Sin(\theta_3) \tag{7.6}$$

Let $\boldsymbol{F}_a \triangleq (F_{a_1}, F_{a_2}, F_{a_3})$ represent the vector of forces from the three actuators on a leg. The torque vector $\boldsymbol{\tau_a}$ corresponding to the actuator force vector $\boldsymbol{F_a}$ is then determined as,

$$\boldsymbol{\tau_a} = \boldsymbol{R^T(q)F}_a \tag{7.7}$$

where $\boldsymbol{R(q)} := diag(r_1(\theta_1), r_2(\theta_2), r_3(\theta_3))$ is a diagonal matrix of moment arms.

Energy function and supply rate corresponding to the actuators on each crawler leg

For the multi-DOF system (crawler leg) studied in this chapter, let $\boldsymbol{m}_1 \in \boldsymbol{R}^2$ represent the vector of air mass in chambers 1 and 2 of the pneumatic actuator connected at joint 1, while $\boldsymbol{m}_2 \in \boldsymbol{R}^2$, and $\boldsymbol{m}_3 \in \boldsymbol{R}^2$ be the vector of air mass in the two chambers of the pneumatic actuators on joints 2 and 3 respectively. Let $\boldsymbol{P}_1 \in \boldsymbol{R}^2$, $\boldsymbol{P}_2 \in \boldsymbol{R}^2$ and $\boldsymbol{P}_3 \in \boldsymbol{R}^2$ be the vector of pressures in chambers 1 and 2 of the actuators connected at joints 1, 2 and 3 respectively. As shown in chapter 3, the energy $W_{act}^{adb}(\boldsymbol{m}_i, \boldsymbol{P}_i)$ associated with the actuator on the $i^{th} \in (1, 2, 3)$ joint is defined to be the work available along the adiabatic trajectory and is as given in Eq. (3.94). The available energy $W_{act}(\boldsymbol{m}, \boldsymbol{P})$ associated with all the actuators on a crawler leg would be the cumulative energy of the three actuators and is obtained as,

$$W_{act}(\boldsymbol{m}, \boldsymbol{P}) = W_{act}^{adb}(\boldsymbol{m}_1, \boldsymbol{P}_1) + W_{act}^{adb}(\boldsymbol{m}_2, \boldsymbol{P}_2) + W_{act}^{adb}(\boldsymbol{m}_3, \boldsymbol{P}_3) \tag{7.8}$$

where $\boldsymbol{m} := (\boldsymbol{m}_1, \boldsymbol{m}_2, \boldsymbol{m}_3)$ and $\boldsymbol{P} := (\boldsymbol{P}_1, \boldsymbol{P}_2, \boldsymbol{P}_3)$. Let u_1, u_2 and u_3 be the input command to the actuators connected at joints 1, 2 and 3 respectively and let $\boldsymbol{u} \triangleq (u_1, u_2, u_3)$ be the input command vector. The time derivative $\dot{W}_{act}^{adb}(.)$ of the energy available from an adiabatic actuator, given in Eq. (3.132), shows that the actuator can be considered as a two-port system with the valve command input u_i as the flow variable at the fluid port of the actuator. From the definition of $\dot{W}_{act}^{adb}(.)$ in Eq. (3.132), the time derivative $\dot{W}_{act}(\boldsymbol{m}, \boldsymbol{P})$ of the cumulative energy function of the three actuators on the crawler leg is obtained as,

$$\dot{W}_{act}(\boldsymbol{m}, \boldsymbol{P}) = \boldsymbol{(\Gamma_1(m, P, u)u)^T F_a - \dot{X}^T F_a} \tag{7.9}$$

where $\dot{\boldsymbol{X}} \triangleq (\dot{y}_1, \dot{x}_2, \dot{x}_3)$ is the vector of linear speeds of the cylinder pistons and the matrix $\boldsymbol{\Gamma_1}(\boldsymbol{m}, \boldsymbol{P}, \boldsymbol{u})$ is defined as,

$$\boldsymbol{\Gamma_1}(\boldsymbol{m}, \boldsymbol{P}, \boldsymbol{u}) = \begin{pmatrix} \gamma_1^{adb}(\boldsymbol{m}_1, \boldsymbol{P}_1, u_1) & 0 & 0 \\ 0 & \gamma_1^{adb}(\boldsymbol{m}_2, \boldsymbol{P}_2, u_2) & 0 \\ 0 & 0 & \gamma_1^{adb}(\boldsymbol{m}_3, \boldsymbol{P}_3, u_3) \end{pmatrix} \tag{7.10}$$

where $\gamma_1^{adb}(\boldsymbol{m}_1, \boldsymbol{P}_1, u_1)$ is as defined in Eq. (3.134). The power transmitted at the mechanical port of the pneumatic actuators ($\dot{\boldsymbol{X}}^{\boldsymbol{T}}\boldsymbol{F_a}$) is independent of the co-ordinate frame and satisfies the following equation from power continuity,

$$\dot{\boldsymbol{X}}^{\boldsymbol{T}}\boldsymbol{F_a} = \dot{\boldsymbol{q}}^{\boldsymbol{T}}\boldsymbol{\tau_a} \tag{7.11}$$

Using the expression for the actuator torque vector $\boldsymbol{\tau_a}$ from Eq. (7.7) in the above equation, the linear speed vector $\dot{\boldsymbol{X}}$ of the actuator pistons is related to the joint angle velocity vector $\dot{\boldsymbol{q}}$ as,

$$\dot{\boldsymbol{q}} = \boldsymbol{R}^{-1}(\boldsymbol{q})\dot{\boldsymbol{X}} \tag{7.12}$$

Using Eq. (7.11) to express the power transferred at the mechanical port in terms of the actuator torque $\boldsymbol{\tau_a}$, and using the expression for $\boldsymbol{\tau_a}$ from Eq. (7.7), the time derivative $\dot{W}_{act}(.)$ of the actuator energy function in Eq. (7.9) can be expressed in terms of the actuator torque $\boldsymbol{\tau_a}$ as,

$$\dot{W}_{act}(\boldsymbol{m}, \boldsymbol{P}) = (\boldsymbol{R}^{-1}(\boldsymbol{q})\boldsymbol{\Gamma_1}(\boldsymbol{m}, \boldsymbol{P}, \boldsymbol{u})\boldsymbol{u})^{\boldsymbol{T}}\boldsymbol{\tau_a} - \dot{\boldsymbol{q}}^{\boldsymbol{T}}\boldsymbol{\tau_a} \tag{7.13}$$

The rate of change of actuator energy presented in the above equation will be used in studying the passivity properties of the co-ordinated tele-operator in section 7.6. In the following subsection dynamics of the PHANToM(TM^1) haptic device are presented.

7.2.3 PHANToM(TM) dynamics

The PHANToM(TM^1) is a haptic device with three degrees of freedom. In this study, a pair of PHANToM(TM^1) devices are used to remotely operate the front two legs of the crawler. The orientation of the co-ordinate axes in the workspace of the PHANToM(TM^1) device are as shown in the Fig. (7.6). Each joint of the PHANToM(TM^1) device is actuated with an electric motor. When acting autonomously (no human interaction), the torque $\boldsymbol{\tau_{a_{ph}}} \in \boldsymbol{R^{3\times 1}}$ applied by the electric motors are used to move the joint angles of the PHANToM(TM^1) along a desired trajectory. When used as a *master* system in tele-operation, the actuator force from the motors is used to provide haptic feedback force to the interacting human operator. The operating power range of these motors is not very high and their torque $\boldsymbol{\tau_{a_{ph}}}$ can be easily overcome by torque $\boldsymbol{\tau_h} \in \boldsymbol{R^{3\times 1}}$ imposed by a human operator.

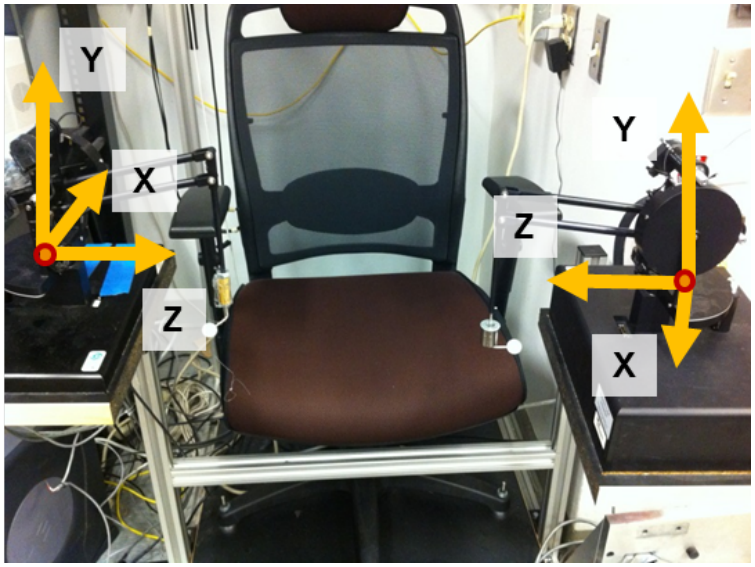

Figure 7.6: Orientation of the co-ordinate axes on the two PHANToM(TM) devices when viewed from the front

A detailed model of the PHANToM(TM^1) inertia dynamics in its joint space has been presented in [79]. Further modifications and simplifications have been reported in [80] and [81] respectively. The dynamics presented in [79] are used for controller design in this study. Let $\boldsymbol{q_{ph}} \in R^{3\times1}$ represent the vector of joint angles in the joint space of a PHANToM(TM^1) haptic device. For an external torque $\boldsymbol{\tau_{p_{ex}}} \in R^{3\times1}$ representing any un-modeled external forces on the device, actuator torque of $\boldsymbol{\tau_{a_{ph}}}$ and a torque $\boldsymbol{\tau_h}$ from human operator, the inertia dynamics are obtained in the PHANToM(TM^1) joint space by using Lagrangian formulation [79] as,

$$\boldsymbol{M_{qh}(q_{ph})\ddot{q}_{ph} + C_{qh}(q_{ph}, \dot{q}_{ph})\dot{q}_{ph} + g(q_{ph}) = \tau_h + \tau_{p_{ex}} + \tau_{a_{ph}}} \tag{7.14}$$

where $\boldsymbol{M_{qh}(q_{ph})} \in \boldsymbol{R^{3\times3}}$ is the inertia matrix, $\boldsymbol{C_{qh}(q_{ph}, \dot{q}_{ph})} \in \boldsymbol{R^{3\times3}}$ is the Coriolis matrix, $\boldsymbol{g(q_{ph})} \in \boldsymbol{R^{3\times1}}$ is the vector of gravitational torque. Elements of $\boldsymbol{M_{qh}(q_{ph})}$, $\boldsymbol{C_{qh}(q_{ph}, \dot{q}_{ph})}$ and $\boldsymbol{g(q_{ph})}$ matrices are as reported in appendix D.2.

Remark 7.2. *The PHANToM(TM^1) dynamics in Eq. (7.14) are obtained from Lagrangian formulation [79] and hence satisfy the following skew-symmetry property*

$$\boldsymbol{A^T(\dot{M}_{qh}(q_{ph}) - 2C_{qh}(q_{ph}, \dot{q}_{ph}))A} = 0 \tag{7.15}$$

for any given vector $\boldsymbol{A} \in \boldsymbol{R}^{3\times 1}$.

For co-ordination controller design, the PHANToM(TM^1) dynamics in Eq. (7.14) have to be transformed from the PHANToM(TM^1) joint space to the crawler joint space. This transformation is presented in the following subsections.

PHANToM(TM) dynamics in crawler joint space

As shown in Fig. (7.4) and Fig. (7.6), co-ordinate axes for the crawler and the PHANToM(TM^1) do not have the same orientation. To define an appropriate co-ordination problem, the dynamics of the crawler and the PHANToM(TM^1) have to defined in the same co-ordination axes. In this section, PHANToM(TM^1) dynamics are transformed and expressed in the crawler joint space. Let $\boldsymbol{X_o}$ be the position vector of the origin of the Cartesian co-ordinates of the PHANToM(TM^1) tip task space expressed in the crawler foot tip task space. As shown in Fig. (7.6), the origin of PHANToM(TM^1) tip task space is fixed. The origin of the crawler foot tip task space is attached to the body of the crawler and moves with the crawler. The mapping of the PHANToM(TM^1) origin in the crawler task space, moves with the crawler body to maintain a constant offset of $\boldsymbol{X_o}$ from the origin of the crawler task space co-ordinate axis.

The PHANToM(TM^1) device is equipped with position sensors to measure the position of the tip of the device in its task space. Let $\boldsymbol{X_{ph}}$ represent the measured Cartesian position vector of the tip of the PHANToM(TM^1) haptic device in its task space. The joint angular velocity vector $\dot{\boldsymbol{q}}_{\boldsymbol{ph}}$ in the PHANToM(TM^1) joint space is related to the foot tip velocity vector of the foot tip velocity vector $\dot{\boldsymbol{X}}_{\boldsymbol{ph}}$ through the Jacobian $\boldsymbol{J_{ph}(q_{ph})}$ as,

$$\dot{\boldsymbol{X}}_{\boldsymbol{ph}} = \boldsymbol{J_{ph}(q_{ph})}\dot{\boldsymbol{q}}_{\boldsymbol{ph}} \tag{7.16}$$

PHANToM(TM^1) task space to crawler task space: Let $\boldsymbol{X}_{ph2c}$ be the position of the PHANToM(TM^1) tip in the crawler task space. For a kinematic scaling of α, transformation from the PHANToM(TM^1) task space to the crawler task space is then

given by,

$$\boldsymbol{X_{ph2c}} = \underbrace{\alpha \begin{bmatrix} 0 & 0 & -1 \\ 1 & 0 & 0 \\ 0 & -1 & 0 \end{bmatrix}}_{\boldsymbol{J_{ph2cr}}} \boldsymbol{X_{ph}} + \boldsymbol{X_o} \tag{7.17}$$

where $\boldsymbol{J_{ph2cr}}$ is the transformation matrix representing rotation of the co-ordinate axes from the PHANToM(TM^1) space to the crawler space.

Crawler task space to joint space: The position of the PHANToM(TM^1) tip $\boldsymbol{X_{ph2c}}$ in the crawler task space, evaluated from $\boldsymbol{X_{ph}}$ as shown in Eq. (7.17), is used to determine the desired crawler joint angles as commanded at the PHANToM(TM^1). As shown in Fig. (7.5), Denavit-Hartenberg [1] convention is used to define the co-ordinate axes at each joint on the crawler leg. Let $\boldsymbol{q_p}$ be the vector of joint angles corresponding to the commanded PHANToM(TM^1) position vector $\boldsymbol{X_{ph2c}}$ in the crawler task space. The kinematic mapping from the crawler task space to the crawler joint space is as shown in [82] and is repeated in appendix D.3. The velocity vector $\dot{\boldsymbol{X}}_{\boldsymbol{ph2c}}$ in the crawler task space is related to the angular velocity vector $\dot{\boldsymbol{q}}_{\boldsymbol{p}}$ in the crawler joint space through the Jacobian $\boldsymbol{J_{cr}(q_p)}$ as,

$$\dot{\boldsymbol{X}}_{\boldsymbol{ph2c}} = \boldsymbol{J_{cr}(q_p)}\dot{\boldsymbol{q}}_{\boldsymbol{p}} \tag{7.18}$$

Let $\boldsymbol{J_T(q_p)} := (\boldsymbol{J_{ph}(q_{ph})J_{ph2cr}})^{-1}\boldsymbol{J_{cr}(q_p)}$ be the Jacobian between the PHANToM(TM^1) joint space and the crawler joint space. The angular velocity vector $\dot{\boldsymbol{q}}_{\boldsymbol{ph}}$ commanded in the PHANToM(TM^1) joint space and its corresponding velocity vector $\dot{\boldsymbol{q}}_{\boldsymbol{p}}$ in the crawler joint space are related through the Jacobian $\boldsymbol{J_T(q_p)}$ as,

$$\dot{\boldsymbol{q}}_{\boldsymbol{p}} = \boldsymbol{J_T^{-1}(q_p)}\dot{\boldsymbol{q}}_{\boldsymbol{ph}} \tag{7.19}$$

From power continuity, the input human torque vector $\boldsymbol{\tau_h}$, the external torque vector $\boldsymbol{\tau_{p_{ex}}}$ and the actuator torque vector $\boldsymbol{\tau_{a_{ph}}}$ in the PHANToM(TM^1) joint space are obtained in the crawler joint space as,

$$\boldsymbol{\tau_{h_p}} = \boldsymbol{J_T^T(q_p)\tau_h}, \quad \boldsymbol{\tau_{e_p}} = \boldsymbol{J_T^T(q_p)\tau_{p_{ex}}}, \quad \boldsymbol{\tau_{a_p}} = \boldsymbol{J_T^T(q_p)\tau_{a_{ph}}} \tag{7.20}$$

where $\boldsymbol{\tau_{h_p}}$ represents the input human torque in the crawler joint space, $\boldsymbol{\tau_{e_p}}$ represents the vector of un-modeled external torques acting on the PHANToM(TM^1) in the crawler

joint space, and $\boldsymbol{\tau_{a_p}}$ corresponds to the actuator joint torque vector expressed in the crawler joint space.

Using the velocity transformation from Eq. (7.19) and the torque transformations from Eq. (7.20), the PHANToM(TM^1) dynamics in Eq. (7.14) are obtained in the crawler joint space as,

$$\boldsymbol{M_p(q_p)\ddot{q}_p + C_p(q_p,\dot{q}_p)\dot{q}_p + g_p(q_p) = \tau_{h_p} + \tau_{e_p} + \tau_{a_p}} \tag{7.21}$$

where the inertial matrix $\boldsymbol{M_p(q_p)}$, the Coriolis acceleration matrix $\boldsymbol{C_p(q_p,\dot{q}_p)}$ and the gravitational torque vector $\boldsymbol{g_p(q_p)}$ in the crawler joint space are obtained as,

$$\begin{aligned} \boldsymbol{M_p(q_p) = J_T^T(q_p)M_{ph}(q_{ph})J_T(q_p),} \quad \boldsymbol{g_p(q_p) = J_T^T(q_p)g(q_{ph})} \\ \boldsymbol{C_p(q_p,\dot{q}_p) = J_T^T(q_p)(C_{ph}(q_{ph},\dot{q}_{ph})J_T(q_p) + M_{ph}(q_{ph})\dot{J}_T(q_p))J_T(q_p)} \end{aligned} \tag{7.22}$$

Remark 7.3. *The PHANToM(TM^1) dynamics in Eq. (7.21) satisfies the skew-symmetry property,* $\boldsymbol{A^T(\dot{M}_p - 2C_p)A} = 0$*, for any vector* $\boldsymbol{A} \in R^{3\times 1}$*.*

Desired characteristics of the tele-operator in the crawler joint space are now presented in the following section.

7.3 Problem statement

It is desired that tele-operation of the crawler with the PHANToM(TM^1) haptic device have the following characteristics to behave as a passive mechanical tool,

1. *Co-ordinated tele-operation* : An essential objective of tele-operation is position and velocity co-ordination between the crawler and the PHANToM(TM^1) haptic device. This is required to remotely move the crawler along a desired path. For a crawler joint angle vector of $\boldsymbol{q}$ and PHANToM(TM^1) joint angle vector of $\boldsymbol{q_p}$ in the crawler joint space, the co-ordination requirements can be stated as,

$$\boldsymbol{q_E := q - q_p \to 0}, \qquad \boldsymbol{\dot{q}_E := \dot{q} - \dot{q}_p \to 0} \tag{7.23}$$

   where $\boldsymbol{q_E}$ and $\boldsymbol{\dot{q}_E}$ represent errors in the position and the velocity co-ordination respectively.

2. *PHANToM(TM^1) Power scaling and on-site human power amplification* : The operating power range of the actuators on the crawler is significantly higher than the PHANToM(TM^1) actuators. To achieve tele-operation of the crawler by using allowable human power input at the PHANToM(TM^1), the power interaction at the PHANToM(TM^1) has to be scaled.

   A desired feature on the crawler is a haptic interface for amplifying the input human power. This feature allows the crawler legs to be used as a multi-DOF human power amplifier which can be used by humans in a rescue environment to move heavier loads and aid with on-site rescue operation. Figure 7.3 illustrates such a haptic interface on the leg of a crawler.

   Therefore, the desired supply rate to a co-ordinated tele-operator with master power amplification and on-site human power amplification is given by,

$$s_h(\boldsymbol{\tau_{e_c}}, \boldsymbol{\tau_{e_p}}, \boldsymbol{\tau_{h_e}}, \boldsymbol{\tau_{h_p}}, \dot{\boldsymbol{q}}, \dot{\boldsymbol{q}}_{\boldsymbol{p}}) := \dot{\boldsymbol{q}}_{\boldsymbol{p}}^{\boldsymbol{T}}(\rho(\boldsymbol{\tau_{h_p}} + \boldsymbol{\tau_{e_p}})) + \dot{\boldsymbol{q}}^{\boldsymbol{T}}(\boldsymbol{\tau_{e_c}} + (\eta + 1)\boldsymbol{\tau_{h_e}}) \quad (7.24)$$

   where $\rho \in \Re^+$ is the desired scaling of the external power input at the PHANToM(TM^1), $\boldsymbol{\tau_{h_e}}$ represents the torque in the crawler joint space due to input human force at the interface and is as defined in Eq. (7.1), and $\eta \in \Re^+$ is the desired amplification of the input human power at the crawler interface.

3. *Passive operation* : The crawler deployed in rescue operations will have to interact with unfamiliar and/or un-modeled environments. As the forces due this interaction are used to provide haptic feedback to the operator, safe interaction between the crawler and the environment is essential. Safe interaction is guaranteed if the external supply rate to the tele-operator as given in Eq. (7.24) satisfies the following condition for energetic passivity,

$$\int_0^t s_h(\boldsymbol{\tau_{e_c}}, \boldsymbol{\tau_{e_p}}, \boldsymbol{\tau_{h_p}}, \boldsymbol{\tau_{h_e}}, \dot{\boldsymbol{q}}, \dot{\boldsymbol{q}}_{\boldsymbol{p}})\ dt \geq -c_o^2 \quad (7.25)$$

   where c_o^2 corresponds to the energy that can be extracted from the co-ordinated tele-operator in the absence of any external energy input. After velocity co-ordination ($\dot{\boldsymbol{q}} = \dot{\boldsymbol{q}}_{\boldsymbol{p}} = \dot{\boldsymbol{q}}_{\boldsymbol{c}}$), the desired passivity condition is obtained from the above equation as,

$$\int_0^t s_h(\boldsymbol{\tau_{e_c}}, \boldsymbol{\tau_{e_p}}, \boldsymbol{\tau_{h_p}}, \boldsymbol{\tau_{h_e}}, \dot{\boldsymbol{q}}_{\boldsymbol{c}}, \dot{\boldsymbol{q}}_{\boldsymbol{c}})\ dt \geq -c_o^2 \quad (7.26)$$

In the following section, framework for achieving the above listed operational characteristics of the tele-operator as a common passive mechanical tool is presented.

7.4 Formulation of the control problem

The desired characteristics of the multi-DOF tele-operator with an electric motor driven master, as enumerated in the previous section, are similar to those listed in section 6.2 for a single-DOF tele-operator. The framework for the design of co-ordination controller for single-DOF systems presented in section 6.3.1 is generic in nature. In the following subsection, the framework from section 6.3.1 is used to formulate the framework for bilateral tele-operation between multi-DOF nonlinear systems. The control problem is then formally stated within this framework.

7.4.1 Frame work for energetic bilateral tele-operation and on-site human power amplification

Figure (7.7) illustrates the power flow variables corresponding to various elements of the tele-operator. The framework for appropriate interconnection between these subsystems for achieving the desired operational characteristics is presented in this sub-section.

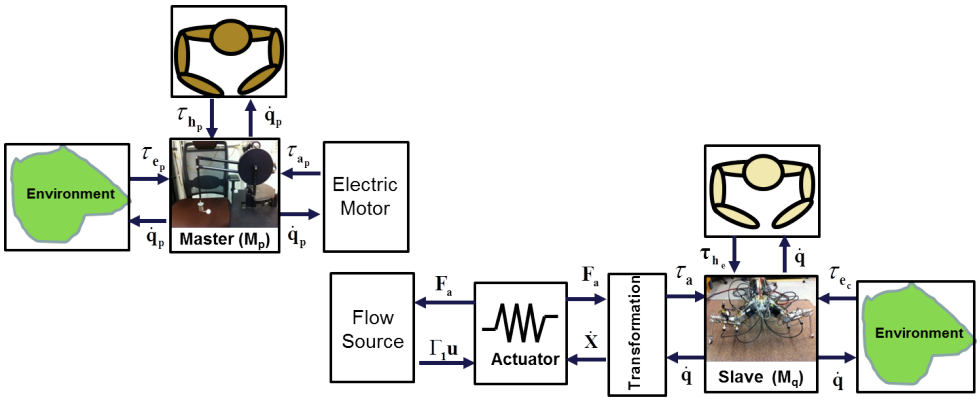

Figure 7.7: Port power variables of the crawler and the PHANToM(TM) expressed in the crawler joint space.

Scaling of the power input at PHANToM(TM)

To achieve power amplification from the PHANToM(TM^1) haptic device to the crawler, the dynamics of the PHANToM(TM^1) are scaled by the desired amplification factor $\rho > 1$. The PHANToM(TM^1) dynamics used in the controller design are therefore obtained from Eq. (7.21) as,

$$\rho\left(\boldsymbol{M_p}(\boldsymbol{q_p})\ddot{\boldsymbol{q}}_{\boldsymbol{p}} + \boldsymbol{C_p}(\boldsymbol{q_p}, \dot{\boldsymbol{q}}_{\boldsymbol{p}})\dot{\boldsymbol{q}}_{\boldsymbol{p}} + \boldsymbol{g_p}(\boldsymbol{q_p}) = \boldsymbol{\tau}_{\boldsymbol{h_p}} + \boldsymbol{\tau}_{\boldsymbol{e_p}} + \boldsymbol{\tau}_{\boldsymbol{a_p}}\right) \tag{7.27}$$

The scaling is done such that the inertia and the external torques corresponding to the amplified dynamics of the PHANToM(TM^1) in the above equation are of the same order of magnitude as those of the crawler.

Bilateral tele-operation and on-site human power amplification

To achieve bilateral operation between a pneumatically actuated slave (crawler) and an electrically actuated master (PHANToM(TM^1)), velocity of the master is used as the flow input at the fluid port of the pneumatic actuator. To achieve human power amplification the approach proposed in section 5.3.2 is adapted by using the PHANToM(TM^1) inertia in a fashion analogous to the virtual inertia. The electro-mechanical actuators on the PHANToM(TM^1) joints are used to apply the desired amplified human torque ($\eta\boldsymbol{\tau}_{\boldsymbol{h_e}}$) on the PHANToM(TM^1) dynamics.

To achieve bilateral tele-operation and with human power amplification through position and velocity co-ordination, additional feedback input is required. The feedback input $\boldsymbol{u_{fb}}$ is injected at the fluid port of the pneumatic actuator as shown in Fig. (7.8) to achieve co-ordinated operation. The interconnection for achieving human power amplification with bilateral tele-operation is as shown in Fig. (7.8).

7.4.2 Passive state transformation

It is convenient to design co-ordination controllers in the co-ordination error space. In this subsection, state transformation to obtain the relative error dynamics is presented. The PHANToM(TM^1) and the crawler inertial dynamics used in the controller design

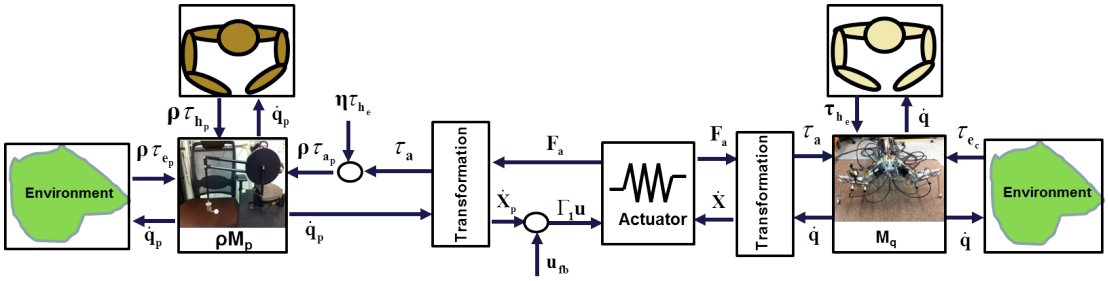

Figure 7.8: Interconnection of the crawler and the PHANToM(TM) power variables to achieve bilateral tele-operation and human power amplification. The feedback input $\boldsymbol{u_{fb}}$ is injected at the fluid port flow input to achieve co-ordinated motion.

can be expressed as,

$$\begin{pmatrix} \rho \boldsymbol{M_p(q_p)} & \boldsymbol{0} \\ \boldsymbol{0} & \boldsymbol{M_q(q)} \end{pmatrix} \begin{pmatrix} \ddot{\boldsymbol{q}}_{\boldsymbol{p}} \\ \ddot{\boldsymbol{q}} \end{pmatrix} + \begin{pmatrix} \rho \boldsymbol{C_p(q_p, \dot{q}_p)} & \boldsymbol{0} \\ \boldsymbol{0} & \boldsymbol{C_q(q, \dot{q})} \end{pmatrix} \begin{pmatrix} \dot{\boldsymbol{q}}_{\boldsymbol{p}} \\ \dot{\boldsymbol{q}} \end{pmatrix} + \begin{pmatrix} \rho \boldsymbol{g_p(q_p)} \\ \boldsymbol{g_q(q)} \end{pmatrix} = \begin{pmatrix} \rho(\boldsymbol{\tau_{h_p}} + \boldsymbol{\tau_{e_p}} + \boldsymbol{\tau_{a_p}}) \\ \boldsymbol{\tau_a} + \boldsymbol{\tau_{e_c}} + \boldsymbol{\tau_{h_e}} \end{pmatrix} \tag{7.28}$$

Passive decomposition

As tele-operation entails regulation of co-ordination error, the crawler and the PHANToM(TM[1]) dynamics in the above equation are transformed to obtain co-ordination error dynamics. The velocity transformation reported in [30] and presented in section 5.3.3 is again employed. Let $\boldsymbol{V_L}$ be the velocity vector of the Locked system corresponding to the center of mass of the crawler and the PHANToM(TM[1]) systems. The system whose velocity corresponds to the co-ordination velocity error $\dot{\boldsymbol{q}}_{\boldsymbol{E}} := (\boldsymbol{q} - \boldsymbol{q_p})$ is referred to as Shape system. The transformation from the original velocity space $(\dot{\boldsymbol{q}}, \dot{\boldsymbol{q}}_{\boldsymbol{p}})$ to the Locked and Shape system velocity space $(\boldsymbol{V_L}, \dot{\boldsymbol{q}}_{\boldsymbol{E}})$ is defined as,

$$\begin{pmatrix} \boldsymbol{V_L} \\ \dot{\boldsymbol{q}}_{\boldsymbol{E}} \end{pmatrix} = \underbrace{\begin{pmatrix} \boldsymbol{I} - \boldsymbol{\phi(q, q_p)} & \boldsymbol{\phi(q, q_p)} \\ \boldsymbol{I} & -\boldsymbol{I} \end{pmatrix}}_{\boldsymbol{S(q, q_p)}} \begin{pmatrix} \dot{\boldsymbol{q}} \\ \dot{\boldsymbol{q}}_{\boldsymbol{p}} \end{pmatrix} \tag{7.29}$$

where $\boldsymbol{S(q, q_p)} \in \boldsymbol{R^{6\times 6}}$ is the transformation matrix, $\boldsymbol{I} \in \boldsymbol{R}^{3\times 3}$ is the identity matrix and the matrix $\boldsymbol{\phi(q, q_p)} \in \boldsymbol{R}^{3\times 3}$ is defined as,

$$\boldsymbol{\phi(q, q_p)} \triangleq (\boldsymbol{M_q(q)} + \rho \boldsymbol{M_p(q_p)})^{-1} \rho \boldsymbol{M_p} \tag{7.30}$$

Let $\boldsymbol{M_T(q, q_p)}$ correspond to the inertia matrix in the transformed velocity space. As kinetic energy in the original velocity space and the transformed velocity space should be the same, the inertia matrices before and after the velocity transformation in Eq. (7.29) are related as,

$$\begin{pmatrix} \boldsymbol{V_L^T} & \boldsymbol{\dot{q}_E^T} \end{pmatrix} \boldsymbol{M_T(q, q_p)} \begin{pmatrix} \boldsymbol{V_L} \\ \boldsymbol{\dot{q}_E} \end{pmatrix} = \frac{\rho}{2} \boldsymbol{\dot{q}_p^T M_p(q_p) \dot{q}_p} + \frac{1}{2} \boldsymbol{\dot{q}^T M_q(q) \dot{q}} \tag{7.31}$$

Using the velocity transformation defined in Eq. (7.29), the inertia matrix $\boldsymbol{M_T}(q, q_p)$ in the transformed state space is obtained as,

$$\begin{aligned} \boldsymbol{M_T}(q, q_p) =& \boldsymbol{S^{-T}(q, q_p)} \begin{pmatrix} \rho \boldsymbol{M_p(q_p)} & \boldsymbol{0}_{2\times 2} \\ \boldsymbol{0}_{2\times 2} & \boldsymbol{M_q(q)} \end{pmatrix} \boldsymbol{S^{-1}(q, q_p)} \\ =& \begin{pmatrix} \boldsymbol{M_L(q, q_p)} & \boldsymbol{0}_{2\times 2} \\ \boldsymbol{0}_{2\times 2} & \boldsymbol{M_E(q, q_p)} \end{pmatrix} \end{aligned} \tag{7.32}$$

where $\boldsymbol{M_L(q, q_p)}$ and $\boldsymbol{M_E(q, q_p)}$ correspond to the inertia of the Locked system and the Shape system respectively and are obtained as,

$$\begin{aligned} \boldsymbol{M_L(q, q_p)} &= (\boldsymbol{M_q(q)} + \rho \boldsymbol{M_p(q_p)}) \\ \boldsymbol{M_E(q, q_p)} &= \boldsymbol{\phi^T(q, q_p) M_q(q) \phi} + \boldsymbol{(I - \phi(q, q_p))^T} \rho \boldsymbol{M_p(q_p)(I - \phi(q, q_p))} \end{aligned} \tag{7.33}$$

Again, there is no inertial coupling between the Locked and the Shape system dynamics due to the definition of the $\boldsymbol{\phi(q, q_p)}$ matrix in Eq. (7.30). Let $\boldsymbol{\tau_L}$ and $\boldsymbol{\tau_E}$ be the actuator torques acting on the Locked and the Shape system respectively. Using the inertia transformation from Eq. (7.32) and the velocity transformation from Eq. (7.29) on the PHANToM(TM[1]) and the crawler dynamics in Eq. (7.28), the Locked and Shape system dynamics are obtained as,

$$\begin{aligned} \boldsymbol{M_L(q, q_p)\dot{V}_L + C_L(q, q_p, \dot{q}, \dot{q}_p)V_L + C_{LE}(q, q_p, \dot{q}, \dot{q}_p)\dot{q}_E + g_L(q, q_p)} = \\ \rho(\boldsymbol{\tau_{h_p}} + \boldsymbol{\tau_{e_p}}) + \boldsymbol{\tau_{e_c}} + \boldsymbol{\tau_{h_e}} + \boldsymbol{\tau_L} \end{aligned} \tag{7.34}$$

$$\begin{aligned} \boldsymbol{M_E(q, q_p)\ddot{q}_E + C_E(q, q_p, \dot{q}, \dot{q}_p)\dot{q}_E + C_{EL}(q, q_p, \dot{q}, \dot{q}_p)V_L + g_E(q, q_p)} = \\ \boldsymbol{\phi^T(q, q_p)}(\boldsymbol{\tau_{e_c}} + \boldsymbol{\tau_{h_e}}) - (\boldsymbol{I} - \boldsymbol{\phi^T(q, q_p)})\, \rho(\boldsymbol{\tau_{h_p}} + \boldsymbol{\tau_{e_p}}) + \boldsymbol{\tau_E} \end{aligned} \tag{7.35}$$

The Coriolis matrices $\boldsymbol{C_L(q, q_p, \dot{q}, \dot{q}_p)}$, $\boldsymbol{C_{LE}(q, q_p, \dot{q}, \dot{q}_p)}$, $\boldsymbol{C_{EL}(q, q_p, \dot{q}, \dot{q}_p)}$ and $\boldsymbol{C_E(q, q_p, \dot{q}, \dot{q}_p)}$ in the transformed space are obtained as,

$$\boldsymbol{C_L(q, q_p, \dot{q}, \dot{q}_p)} = \boldsymbol{C_q(q, \dot{q})} + \rho \boldsymbol{C_p(q_p, \dot{q}_p)} \tag{7.36}$$

$$\boldsymbol{C_{LE}(q, q_p, \dot{q}, \dot{q}_p)} = \boldsymbol{C_q(q, \dot{q})\phi(q, q_p)} - \rho \boldsymbol{C_p(q_p, \dot{q}_p)(I - \phi(q, q_p))} + (\boldsymbol{M_q(q)} + \rho \boldsymbol{M_p(q_p)})\dot{\boldsymbol{\phi}}\boldsymbol{(q, q_p)} \tag{7.37}$$

$$\boldsymbol{C_E(q, q_p, \dot{q}, \dot{q}_p)} = \boldsymbol{\phi^T(q, q_p)C_q(q, \dot{q})\phi(q, q_p)} + \boldsymbol{(I - \phi(q, q_p))^T} \rho \boldsymbol{C_p(q_p, \dot{q}_p)(I - \phi(q, q_p))} \tag{7.38}$$

$$\boldsymbol{C_{EL}(q, q_p, \dot{q}, \dot{q}_p)} = \boldsymbol{\phi^T(q, q_p)C_q(q, \dot{q})} - \boldsymbol{(I - \phi(q, q_p))^T} \rho \boldsymbol{C_p(q_p, \dot{q}_p)} \tag{7.39}$$

The gravitational vectors $\boldsymbol{g_L(q, q_p)}$, $\boldsymbol{g_E(q, q_p)}$, and the actuator torques $\boldsymbol{\tau_L}$, $\boldsymbol{\tau_E}$ acting on the Locked and the Shape system dynamics respectively are obtained as,

$$\begin{aligned} \boldsymbol{g_L(q, q_p)} &= (\boldsymbol{g_q(q)} + \rho \boldsymbol{g_p(q_p)}) \\ \boldsymbol{g_E(q, q_p)} &= (\boldsymbol{\phi^T(q, q_p)g_q(q)} - \boldsymbol{(I - \phi^T(q, q_p))}\rho \boldsymbol{g_p(q_p)}) \\ \boldsymbol{\tau_L} &= \rho \boldsymbol{\tau_{a_p}} + \boldsymbol{\tau_a}, \;\; \boldsymbol{\tau_E} = \boldsymbol{\phi^T(q, q_p)\tau_a} - \boldsymbol{(I - \phi^T(q, q_p))}\rho \boldsymbol{\tau_{a_p}} \end{aligned} \tag{7.40}$$

Passive controllers take advantage of the properties of the system that facilitate design of controllers with simpler structure. In the following remark it is shown that the Shape system dynamics in Eq. (7.49) satisfy a skew-symmetric property. This property will be used in later part of the section to design co-ordination controllers.

Remark 7.4. *Inertial dynamics of the Shape system in Eq. (7.49) satisfy the following skew-symmetry condition,*

$$\boldsymbol{A^T}(\dot{\boldsymbol{M}}_{\boldsymbol{E}}\boldsymbol{(q, q_p)} - 2\boldsymbol{C_E(q, q_p, \dot{q}, \dot{q}_p)})\boldsymbol{A} = \boldsymbol{0} \tag{7.41}$$

for any vector $\boldsymbol{A} \in \boldsymbol{R^{3\times 1}}$.

Proof. Proof as shown in appendix D.4.1 □

Decoupling torque for the Locked and the Shape system dynamics

The Locked and the Shape system dynamics in Eq. (7.34) and Eq. (7.35) respectively, are coupled through the Coriolis terms $\boldsymbol{C_{LE}(q, q_p, \dot{q}, \dot{q}_p)\dot{q}_E}$ and $\boldsymbol{C_{EL}(q, q_p, \dot{q}, \dot{q}_p)V_L}$ respectively. In proposition 2 of [30] it is shown that the coupling Coriolis matrices are

related as $\boldsymbol{C_{LE}(q, q_p, \dot{q}, \dot{q}_p) = -C_{EL}^T(q, q_p, \dot{q}, \dot{q}_p)}$. As shown in corollary 1 of [30], the supply rate corresponding to the decoupling torques $\boldsymbol{\tau_L^d := C_{LE}(q, q_p, \dot{q}, \dot{q}_p)\dot{q}_E}$ and $\boldsymbol{\tau_E^d := C_{EL}(q, q_p, \dot{q}, \dot{q}_p)V_L}$ on the Locked and Shape systems respectively is zero as,

$$\boldsymbol{V_L^T \tau_L^d + \dot{q}_E^T \tau_E^d = 0} \tag{7.42}$$

To achieve tele-operation with human power amplification, the actuator torques $\boldsymbol{\tau_L}$ and $\boldsymbol{\tau_E}$ are therefore defined as,

$$\begin{pmatrix} \boldsymbol{\tau_L} \\ \boldsymbol{\tau_E} \end{pmatrix} = \begin{pmatrix} \boldsymbol{C_{LE}(q, q_p, \dot{q}, \dot{q}_p)\dot{q}_E} \\ \boldsymbol{C_{EL}(q, q_p, \dot{q}, \dot{q}_p)V_L} \end{pmatrix} + \begin{pmatrix} \eta\boldsymbol{\tau_{h_e}} \\ \boldsymbol{\tau_E^c} \end{pmatrix} \tag{7.43}$$

where $\boldsymbol{\tau_E^c}$ is part of the co-ordination controller that will be designed in section 7.5 for regulating the Shape system dynamics. With the torque $\boldsymbol{\tau_L}$ as defined in Eq. (7.43), the Locked system dynamics are obtained as,

$$\boldsymbol{M_L(q, q_p)\dot{V}_L + C_L(q, q_p, \dot{q}, \dot{q}_p)V_L + g_L(q, q_p) = \rho(\tau_{h_p} + \tau_{e_p}) + \tau_{e_c} + (\eta + 1)\tau_{h_e}} \tag{7.44}$$

where the net external torque on the $r.h.s$ of the above equation corresponds to the desired supply rate $s_h(.)$ in Eq. (7.24) for tele-operation with human power amplification. The Locked system dynamics in Eq. (7.44) corresponds to inertia dynamics that is influenced by external input torques at multiple ports such as the input human torques $\boldsymbol{\tau_{h_p}}$ and $\boldsymbol{\tau_{h_e}}$, external torques $\boldsymbol{\tau_{e_p}}$ and $\boldsymbol{\tau_{e_c}}$, and the gravitational torque vector $\boldsymbol{g_L(q, q_p)}$. The Locked system thus behaves as a common passive mechanical tool that feels like an extension of the human limb, providing work output only under the influence of input human torque and other external environmental torques (such as gravity). The desired supply rate in Eq. (7.25) is satisfied by using the kinetic energy of the Locked system for a co-ordinated tele-operator ($\boldsymbol{\dot{q}_E = 0}$) as the storage function.

Using the definition of the Locked system torque $\boldsymbol{\tau_L := \rho\tau_{a_p} + \tau_a}$ from Eq. (7.40) in Eq. (7.43), the PHANToM(TM[1]) actuator torque is obtained as,

$$\boldsymbol{\tau_{a_p} = -\frac{1}{\rho}(\tau_a - C_{LE}(q, q_p, \dot{q}, \dot{q}_p)\dot{q}_E) + \frac{\eta}{\rho}\tau_{h_e}} \tag{7.45}$$

The actuator torque on the PHANToM(TM[1]) device is used to achieve multiple objectives including providing haptic feedback to the human operator, decoupling of

the Locked and the Shape system dynamics, and to facilitate amplification of human power input on the interface on the crawler leg. When operating the crawler legs as a human power amplifier, the PHANToM(TM[1]) thus behaves in a fashion analogous to the virtual inertia defined in the controller design for a human power amplifier as described in section 5.3.2.

The actuator torque $\boldsymbol{\tau_a}$ on the crawler is designed to regulate the Shape system dynamics in Eq. (7.35). Using the definition of $\boldsymbol{\tau_E}$ from Eq. (7.40), and from the definition of $\boldsymbol{\tau_{a_p}}$ in Eq. (7.45), the Shape system dynamics in Eq. (7.35) are expressed in terms of $\boldsymbol{\tau_a}$. For ease of presentation let $\boldsymbol{\tau_k(q, q_p)}$ represent the net torque acting on the Shape system due to coupling in the Coriolis terms of the Locked and Shape system dynamics, and $\boldsymbol{\tau_{ex}(q, q_p)}$ consist of the external torque vectors acting on the PHANToM(TM[1]) and the crawler. These vectors are defined as,

$$\boldsymbol{\tau_k(q, q_p)} = \boldsymbol{(I - \phi^T(q, q_p))C_{LE}(q, q_p, \dot{q}, \dot{q}_p)\dot{q}_E + C_{EL}(q, q_p, \dot{q}, \dot{q}_p)V_L} \tag{7.46}$$

$$\boldsymbol{\tau_{ex}(q, q_p)} = \boldsymbol{(I - \phi^T(q, q_p))}\rho(\boldsymbol{\tau_{h_p} + \tau_{e_p}}) + \eta\boldsymbol{\tau_{h_e}} - \boldsymbol{\phi^T(q, q_p)}(\boldsymbol{\tau_{e_c}} + (\eta + 1)\boldsymbol{\tau_{h_e}}) \tag{7.47}$$

Using the inverse of the torque transformation in Eq. (7.40), and from the definition of $\boldsymbol{\tau_k(q, q_p)}$ in the above equation, the energy conservative relationship between the decoupling torque on the Locked and the Shape system dynamics in Eq. (7.42) can be expressed as,

$$\begin{gathered}\boldsymbol{\dot{q}_p^T(\phi^T(q, q_p)C_{LE}(q, q_p, \dot{q}, \dot{q}_p)\dot{q}_E - C_{EL}(q, q_p, \dot{q}, \dot{q}_p)V_L) + \dot{q}^T\tau_k(q, q_p)} = \\ \boldsymbol{\dot{q}_p^T C_{LE}(q, q_p, \dot{q}, \dot{q}_p)\dot{q}_E + \dot{q}_E^T\tau_k(q, q_p)} = 0\end{gathered} \tag{7.48}$$

Controller design for regulation of Shape system dynamics in the above equation is presented in the following section.

7.5 Co-ordination controller design

The Shape system dynamics in Eq. (7.35) are influenced by the valve input command vector $\boldsymbol{u}$ only through the actuator torque vector $\boldsymbol{\tau_a}$. Due to this structure, the controller can be designed in a two step back-stepping process [2]. The desired actuator torque $\boldsymbol{\tau_a^d}$ required for regulation of the inertia dynamics in Eq. (7.35) is designed in the first step.

The valve command input vector $\boldsymbol{u}$ to provide the desired torque $\boldsymbol{\tau_a^d}$ is then designed in the second step of the control design process. The required torque input in the first stage of controller design is derived in the following subsection.

7.5.1 First stage controller design to determine desired actuator torque output

From the definition of the haptic feedback torque $\boldsymbol{\tau_{a_p}}$ in Eq. (7.45), the Shape system dynamics in Eq. (7.35) can be expressed as,

$$\begin{aligned} \dot{\boldsymbol{q}}_{\boldsymbol{E}} &= \boldsymbol{V_E} \\ \boldsymbol{M_E}(\boldsymbol{q},\boldsymbol{q_p})\dot{\boldsymbol{V}}_{\boldsymbol{E}} + \boldsymbol{C_E}(\boldsymbol{q},\boldsymbol{q_p},\dot{\boldsymbol{q}},\dot{\boldsymbol{q}}_{\boldsymbol{p}})\boldsymbol{V_E} + \boldsymbol{g_E}(\boldsymbol{q},\boldsymbol{q_p}) &= \boldsymbol{\tau_a} - \boldsymbol{\tau_k}(\boldsymbol{q},\boldsymbol{q_p}) - \boldsymbol{\tau_{ex}}(\boldsymbol{q},\boldsymbol{q_p}) \end{aligned} \tag{7.49}$$

The desired torque input $\boldsymbol{\tau_a^d}$ for regulation of inertial dynamics in Eq. (7.49) is determined in this section by using Exact Compensation Control Law (ECCL) [83]. The actuator torque is first designed for the case when the external torque $\boldsymbol{\tau_{ex}}$ is well-known. The design is then extended to the scenario when $\boldsymbol{\tau_{ex}}$ is not well known and must be estimated.

As is required for ECCL, the following reference velocity error vector $\boldsymbol{e_v}$ is defined,

$$\boldsymbol{e_v} = \boldsymbol{V_E} + \boldsymbol{\Lambda_1}\boldsymbol{q_E} \tag{7.50}$$

where $\boldsymbol{\Lambda_1} \in \boldsymbol{R}^{3\times 3}$ is a positive definite diagonal matrix. The definition of $\boldsymbol{e_v}$ is similar to a sliding surface employed in sliding mode control [2]. Regulation of $\boldsymbol{e_v}$ to zero will lead to exponential convergence of position error $\boldsymbol{q_E}$. By extension, the velocity error $\boldsymbol{V_E}$ also converges exponentially to zero. Dynamics of $\boldsymbol{e_v}$ is obtained from the Shape system dynamics in Eq. (7.49) as,

$$\begin{aligned} \boldsymbol{M_E}(\boldsymbol{q},\boldsymbol{q_p})\dot{\boldsymbol{e}}_{\boldsymbol{v}} + \boldsymbol{C_E}(\boldsymbol{q},\boldsymbol{q_p},\dot{\boldsymbol{q}},\dot{\boldsymbol{q}}_{\boldsymbol{p}})\boldsymbol{e_v} + \boldsymbol{g_E}(\boldsymbol{q},\boldsymbol{q_p}) &= \boldsymbol{\tau_a} - \boldsymbol{\tau_k}(\boldsymbol{q},\boldsymbol{q_p}) - \boldsymbol{\tau_{ex}}(\boldsymbol{q},\boldsymbol{q_p}) + \\ & \boldsymbol{M_E}(\boldsymbol{q},\boldsymbol{q_p})\boldsymbol{\Lambda_1}\boldsymbol{V_E} + \boldsymbol{C_E}(\boldsymbol{q},\boldsymbol{q_p},\dot{\boldsymbol{q}},\dot{\boldsymbol{q}}_{\boldsymbol{p}})\boldsymbol{\Lambda_1}\boldsymbol{q_E} \end{aligned} \tag{7.51}$$

Desired actuator torque when $\boldsymbol{\tau_{ex}}$ is completely known

For designing the actuator torque $\boldsymbol{\tau_a}$ to regulate reference velocity $\boldsymbol{e_v}$ to zero, consider the following positive definite function of the reference velocity error $\boldsymbol{e_v}$ and the position

co-ordination error $\boldsymbol{q_E}$ as a Lyapunov function,

$$\bar{V}_1(\boldsymbol{e_v}, \boldsymbol{q_E}) = \frac{1}{2} \begin{pmatrix} \boldsymbol{e_v^T} & \boldsymbol{q_E^T} \end{pmatrix} \underbrace{\begin{pmatrix} \boldsymbol{M_E} & \boldsymbol{0_3} \\ \boldsymbol{0_3} & \boldsymbol{K_p} \end{pmatrix}}_{\boldsymbol{\mathcal{P}_c}} \begin{pmatrix} \boldsymbol{e_v} \\ \boldsymbol{q_E} \end{pmatrix} \tag{7.52}$$

where $\boldsymbol{K_p} \in \boldsymbol{R}^{3\times3}$ is a constant positive definite diagonal matrix. As the above Lyapunov function is quadratic, it can bounded from above and below as,

$$\frac{1}{2}\sigma_{min}(\boldsymbol{\mathcal{P}}_c) \left\| \begin{matrix} \boldsymbol{e_v} \\ \boldsymbol{q_E} \end{matrix} \right\|_2^2 \leq \bar{V}_1(\boldsymbol{e_v}, \boldsymbol{q_E}) \leq \frac{1}{2}\sigma_{max}(\boldsymbol{\mathcal{P}}_c) \left\| \begin{matrix} \boldsymbol{e_v} \\ \boldsymbol{q_E} \end{matrix} \right\|_2^2 \tag{7.53}$$

where $\sigma_{min}(.)$ and $\sigma_{max}(.)$ correspond to the operator for finding the minimum and the maximum singular values of input matrix. By regulating the Lyapunov function $\bar{V}_1(\boldsymbol{e_v}, \boldsymbol{q_E})$ in Eq. (7.52) to zero, the Shape system states $(\boldsymbol{q_E}, \boldsymbol{V_E})$ are also regulated to zero. Using the dynamics of $\boldsymbol{e_v}$ from Eq. (7.51), and assuming the actuator is providing the desired torque $\boldsymbol{\tau_a^d}$ $(\boldsymbol{\tau_a = \tau_a^d})$, the time derivative of Lyapunov function $\bar{V}_1(\boldsymbol{e_v}, \boldsymbol{q_E})$ in Eq. (7.52) is obtained as,

$$\begin{aligned} \dot{\bar{V}}_1(\boldsymbol{e_v}, \boldsymbol{q_E}) = \boldsymbol{e_v^T}(\boldsymbol{\tau_a^d} - \boldsymbol{\tau_k}(\boldsymbol{q}, \boldsymbol{q_p}) - \boldsymbol{\tau_{ex}}(\boldsymbol{q}, \boldsymbol{q_p}) - \boldsymbol{C_E}(\boldsymbol{q}, \boldsymbol{q_p}, \dot{\boldsymbol{q}}, \dot{\boldsymbol{q}}_{\boldsymbol{p}})\boldsymbol{e_v} - \boldsymbol{g_E}(\boldsymbol{q}, \boldsymbol{q_p}) + \\ \boldsymbol{M_E}(\boldsymbol{q}, \boldsymbol{q_p})\boldsymbol{\Lambda_1}\boldsymbol{V_E} + \boldsymbol{C_E}(\boldsymbol{q}, \boldsymbol{q_p}, \dot{\boldsymbol{q}}, \dot{\boldsymbol{q}}_{\boldsymbol{p}})\boldsymbol{\Lambda_1}\boldsymbol{q_E}) + \boldsymbol{e_v^T}\frac{\dot{\boldsymbol{M}}_{\boldsymbol{E}}(\boldsymbol{q}, \boldsymbol{q_p})}{2}\boldsymbol{e_v} + \boldsymbol{V_E^T}\boldsymbol{K_p}\boldsymbol{q_E} \end{aligned} \tag{7.54}$$

Using the skew-symmetry property of the Shape system inertia from Eq. (7.41), and if the desired actuator torque $\boldsymbol{\tau_a^d}$ is defined as,

$$\begin{aligned} \boldsymbol{\tau_a^d} = \boldsymbol{\tau_k}(\boldsymbol{q}, \boldsymbol{q_p}) + \boldsymbol{\tau_{ex}}(\boldsymbol{q}, \boldsymbol{q_p}) - \boldsymbol{g_E}(\boldsymbol{q}, \boldsymbol{q_p}) - \boldsymbol{K_d}\boldsymbol{e_v} - \boldsymbol{K_p}\boldsymbol{q_E} - \boldsymbol{M_E}(\boldsymbol{q}, \boldsymbol{q_p})\boldsymbol{\Lambda_1}\boldsymbol{V_E} \\ - \boldsymbol{C_E}(\boldsymbol{q}, \boldsymbol{q_p}, \dot{\boldsymbol{q}}, \dot{\boldsymbol{q}}_{\boldsymbol{p}})\boldsymbol{\Lambda_1}\boldsymbol{q_E} \end{aligned} \tag{7.55}$$

where $\boldsymbol{K_d} \in \boldsymbol{R}^{3\times3}$ is a constant positive definite diagonal matrix, the Lyapunov function derivative $\dot{\bar{V}}_1(\boldsymbol{e_v}, \boldsymbol{q_E})$ in Eq. (7.63) can be simplified as,

$$\dot{\bar{V}}_1(\boldsymbol{e_v}, \boldsymbol{q_E}) = -\begin{pmatrix} \boldsymbol{e_v^T} & \boldsymbol{q_E^T} \end{pmatrix} \underbrace{\begin{pmatrix} \boldsymbol{K_d} & \boldsymbol{0_3} \\ \boldsymbol{0_3} & \boldsymbol{\Lambda_1}\boldsymbol{K_p} \end{pmatrix}}_{\boldsymbol{\mathcal{Q}_c}} \begin{pmatrix} \boldsymbol{e_v} \\ \boldsymbol{q_E} \end{pmatrix} \leq -\sigma_{min}(\boldsymbol{\mathcal{Q}}_c) \left\| \begin{matrix} \boldsymbol{e_v} \\ \boldsymbol{q_E} \end{matrix} \right\|_2^2 \tag{7.56}$$

Using the bounds on the Lyapunov function $\bar{V}_1(\boldsymbol{e_v}, \boldsymbol{q_E})$ from Eq. (7.53), the Lyapunov function derivative $\dot{\bar{V}}_1(\boldsymbol{e_v}, \boldsymbol{q_E})$ in Eq. (7.56) can be expressed as,

$$\dot{\bar{V}}_1(\boldsymbol{e_v}, \boldsymbol{q_E}) \leq -\frac{2\sigma_{min}(\boldsymbol{\mathcal{Q}}_c)}{\sigma_{max}(\boldsymbol{\mathcal{P}}_c)} \bar{V}_1(\boldsymbol{e_v}, \boldsymbol{q_E}) \tag{7.57}$$

On integrating both sides of the above equation, exponential convergence of Lyapunov function $\bar{V}_1(\boldsymbol{e_v}, \boldsymbol{q_E})$ to zero follows. As $\bar{V}_1(\boldsymbol{e_v}, \boldsymbol{q_E})$ is a positive definite function of $\boldsymbol{q_E}$ and $\boldsymbol{V_E}$, they also exponentially converge to zero.

The desired actuator torque vector in Eq. (7.55) requires perfect information of the external torque $\boldsymbol{\tau_{ex}(q, q_p)}$ for feed forward compensation. The PHANToM(TM[1]) haptic device used in this study is not equipped with a force sensor for measuring the input human torque $\boldsymbol{\tau_{h_p}}$. In addition, it is difficult to model all the external forces such as friction in the actuating cylinders, interaction forces between the crawler and its operating environment. Therefore $\boldsymbol{\tau_{ex}(q, q_p)}$ has to be estimated for determining the desired actuator torque $\boldsymbol{\tau_a^d}$ required for regulation of Shape system dynamics. The estimator dynamics, and the corresponding design of $\boldsymbol{\tau_a^d}$ is presented in the following subsection.

Desired actuator torque when $\boldsymbol{\tau_{ex}}$ is not well-known

In this section, $\boldsymbol{\tau_{ex}}$ estimated by assuming it to be a constant (or slowly varying) but unknown parameter. Due to nonlinear dynamics of the reference velocity error e_v in Eq. (7.51), it is not possible to use a linear Luenberger observer to estimate $\boldsymbol{\tau_{ex}}$. In this section, the estimate of $\boldsymbol{\tau_{ex}}$ is obtained by using direct adaptive control. Let $\boldsymbol{\hat{\tau}_{ex}}$ represent an estimate of the external torque vector on the Shape system. The desired actuator torque in Eq. (7.55) is redefined in terms of $\boldsymbol{\hat{\tau}_{ex}}$ as,

$$\begin{aligned}\boldsymbol{\tau_a^d} = \boldsymbol{\tau_k(q, q_p)} + \boldsymbol{\hat{\tau}_{ex}} - \boldsymbol{g_E(q, q_p)} - \boldsymbol{K_d e_v} - \boldsymbol{K_p q_E} \\ - \boldsymbol{M_E(q, q_p)\Lambda_1 V_E} - \boldsymbol{C_E(q, q_p, \dot{q}, \dot{q}_d)\Lambda_1 q_E}\end{aligned} \tag{7.58}$$

Let $\boldsymbol{\tilde{\tau}_{ex} := \tau_{ex}(q, q_p) - \hat{\tau}_{ex}}$ be the error in estimating the torque vector $\boldsymbol{\tau_{ex}(q, q_p)}$. From the expression for desired torque in Eq. (7.58), the Shape system dynamics in Eq.

(7.49) are obtained as,

$$\begin{aligned}\boldsymbol{M_E(q,q_p)\dot{V}_E + C_E(q,q_p,\dot{q},\dot{q}_p)V_E} = &- \boldsymbol{\tilde{\tau}_{ex} - K_d e_v - K_p q_E} \\ &- \boldsymbol{M_E(q,q_p)\Lambda_1 V_E - C_E(q,q_p,\dot{q},\dot{q}_p)\Lambda_1 q_E}\end{aligned} \tag{7.59}$$

From the above equation it can be noticed that the information on error in estimating $\boldsymbol{\tau_{ex}(q,q_p)}$ is available in the Shape system dynamics. Let $\boldsymbol{\hat{V}_E}$ be an estimate of the Shape system velocity. From the Shape system dynamics in Eq. (7.49) the dynamics of $\boldsymbol{\hat{V}_E}$ are obtained as,

$$\begin{aligned}\boldsymbol{M_E(q,q_p)\dot{\hat{V}}_E + C_E(q,q_p,\dot{q},\dot{q}_p)\hat{V}_E + g_E(q,q_p)} =&\boldsymbol{\tau_a - \tau_k(q,q_p)} \\ &\boldsymbol{- \hat{\tau}_{ex} + L_1(V_E - \hat{V}_E)}\end{aligned} \tag{7.60}$$

where $\boldsymbol{L_1} \in \boldsymbol{R}^{3\times3}$ is a positive definite diagonal matrix corresponding to observer gain.

Let $\boldsymbol{\tilde{V}_E := V_E - \hat{V}_E}$ be the error in estimating the Shape system velocity. From the velocity estimation dynamics in Eq. (7.60), and the Shape system dynamics in Eq. (7.49), the dynamics of estimation error $\boldsymbol{\tilde{V}_E}$ are obtained as,

$$\boldsymbol{M_E(q,q_p)\dot{\tilde{V}}_E + C_E(q,q_p,\dot{q},\dot{q}_p)\tilde{V}_E = -\tilde{\tau}_{ex} - L_1\tilde{V}_E} \tag{7.61}$$

Consider the following Lyapunov function $V_1(\boldsymbol{e_v, q_E, \hat{V}_E, \hat{\tau}_{ex}})$,

$$\begin{aligned}V_1(\boldsymbol{e_v,q_E,\hat{V}_E,\hat{\tau}_{ex}}) = \frac{1}{2}\boldsymbol{e_v^T M_E(q,q_p)e_v} + \frac{1}{2}\boldsymbol{q_E^T K_p q_E} + &\frac{1}{2}\boldsymbol{\tilde{V}_E^T \Lambda_3^{0.5} M_E(q,q_p)\Lambda_3^{0.5}\tilde{V}_E} \\ &+ \frac{1}{2}\boldsymbol{\tilde{\tau}_{ex}^T \Lambda_2^{-1}\tilde{\tau}_{ex}}\end{aligned} \tag{7.62}$$

where $\boldsymbol{\Lambda_2} \in \boldsymbol{R}^{3\times3}$ and $\boldsymbol{\Lambda_3} \in \boldsymbol{R}^{3\times3}$ are positive definite constant diagonal matrices. Using the dynamics of the reference velocity $\boldsymbol{e_v}$ from Eq. (7.51), the observer error dynamics for Shape system velocity $\boldsymbol{\hat{V}_E}$ from Eq. (7.61) and the skew-symmetry property of the Shape system inertia from Eq. (7.41), the derivative $\dot{V}_1(\boldsymbol{e_v, q_E, \hat{V}_E, \hat{\tau}_{ex}})$ of the Lyapunov function in Eq. (7.62) is obtained as,

$$\begin{aligned}\dot{V}_1(\boldsymbol{e_v,q_E,\hat{V}_E,\hat{\tau}_{ex}}) =&\boldsymbol{e_v^T(\tau_a - \tau_k(q,q_p) - \tau_{ex}(q,q_p) - g_E(q,q_p) + M_E(q,q_p)\Lambda_1 V_E} \\ &\boldsymbol{+ C_E(q,q_p,\dot{q},\dot{q}_p)\Lambda_1 q_E) + V_E^T K_p q_E - \tilde{V}_E^T \Lambda_3 L_1 \tilde{V}_E} \\ &\boldsymbol{- (\tilde{V}_E^T \Lambda_3 - \dot{\tilde{\tau}}_{ex}^T \Lambda_2^{-1})\tilde{\tau}_{ex}}\end{aligned} \tag{7.63}$$

The dynamics of torque estimate $\hat{\boldsymbol{\tau}}_{\boldsymbol{ex}}$ and desired actuator torque $\boldsymbol{\tau}_{\boldsymbol{a}}^{\boldsymbol{d}}$ required for regulation of the Lyapunov function $V_1(\boldsymbol{e_v}, \boldsymbol{q_E}, \hat{\boldsymbol{V}}_{\boldsymbol{E}}, \hat{\boldsymbol{\tau}}_{\boldsymbol{ex}})$ and the reference velocity error $\boldsymbol{e_v}$ is presented in the following theorem.

Theorem 7.1. *If the external torque $\boldsymbol{\tau_{ex}}$ is well known, the desired torque $\boldsymbol{\tau}_{\boldsymbol{a}}^{\boldsymbol{d}}$ from the actuator for achieving exponential convergence of the reference velocity $\boldsymbol{e_v}$ dynamics in Eq. (7.51) and the position error vector $\boldsymbol{q_E}$ is given by,*

$$\begin{aligned}\boldsymbol{\tau}_{\boldsymbol{a}}^{\boldsymbol{d}} = \boldsymbol{\tau_k}(\boldsymbol{q}, \boldsymbol{q_p}) + \boldsymbol{\tau_{ex}}(\boldsymbol{q}, \boldsymbol{q_p}) - \boldsymbol{g_E}(\boldsymbol{q}, \boldsymbol{q_p}) - \boldsymbol{K_d e_v} - \boldsymbol{K_p q_E} - \boldsymbol{M_E}(\boldsymbol{q}, \boldsymbol{q_p})\boldsymbol{\Lambda_1 V_E} \\ - \boldsymbol{C_E}(\boldsymbol{q}, \boldsymbol{q_p}, \dot{\boldsymbol{q}}, \dot{\boldsymbol{q}}_{\boldsymbol{p}})\boldsymbol{\Lambda_1 q_E}\end{aligned} \tag{7.64}$$

where $\boldsymbol{K_d} \in \boldsymbol{R}^{3\times3}$, $\boldsymbol{K_p} \in \boldsymbol{R}^{3\times3}$, $\boldsymbol{\Lambda_1} \in \boldsymbol{R}^{3\times3}$ are constant positive definite diagonal matrices.

For a constant but unknown external torque $\boldsymbol{\tau_{ex}}$, asymptotic regulation of the reference velocity $\boldsymbol{e_v}$ dynamics in Eq. (7.51), position error vector $\boldsymbol{q_E}$, and the velocity estimation error $\tilde{\boldsymbol{V}}_{\boldsymbol{E}}$ is achieved if the actuator is able to provide the following desired torque $\boldsymbol{\tau}_{\boldsymbol{a}}^{\boldsymbol{d}}$,

$$\begin{aligned}\boldsymbol{\tau}_{\boldsymbol{a}}^{\boldsymbol{d}} = \boldsymbol{\tau_k}(\boldsymbol{q}, \boldsymbol{q_p}) + \hat{\boldsymbol{\tau}}_{\boldsymbol{ex}} - \boldsymbol{g_E}(\boldsymbol{q}, \boldsymbol{q_p}) - \boldsymbol{K_d e_v} - \boldsymbol{K_p q_E} \\ - \boldsymbol{M_E}(\boldsymbol{q}, \boldsymbol{q_p})\boldsymbol{\Lambda_1 V_E} - \boldsymbol{C_E}(\boldsymbol{q}, \boldsymbol{q_p}, \dot{\boldsymbol{q}}, \dot{\boldsymbol{q}}_{\boldsymbol{p}})\boldsymbol{\Lambda_1 q_E}\end{aligned} \tag{7.65}$$

where $\hat{\boldsymbol{\tau}}_{\boldsymbol{ex}}$ is the estimate of the external torques on the Shape system and is obtained from the following observer dynamics,

$$\begin{aligned}\boldsymbol{M_E}(\boldsymbol{q}, \boldsymbol{q_p})\dot{\hat{\boldsymbol{V}}}_{\boldsymbol{E}} + \boldsymbol{C_E}(\boldsymbol{q}, \boldsymbol{q_p}, \dot{\boldsymbol{q}}, \dot{\boldsymbol{q}}_{\boldsymbol{p}})\hat{\boldsymbol{V}}_{\boldsymbol{E}} + \boldsymbol{g_E}(\boldsymbol{q}, \boldsymbol{q_p}) = \boldsymbol{\tau_a} - \boldsymbol{\tau_k}(\boldsymbol{q}, \boldsymbol{q_p}) - \hat{\boldsymbol{\tau}}_{\boldsymbol{ex}} \\ + \boldsymbol{L_1}(\boldsymbol{V_E} - \hat{\boldsymbol{V}}_{\boldsymbol{E}})\end{aligned} \tag{7.66}$$

$$\dot{\hat{\boldsymbol{\tau}}}_{\boldsymbol{ex}} = -\boldsymbol{\Lambda_2}(\boldsymbol{e_v} + \boldsymbol{\Lambda_3}(\boldsymbol{V_E} - \hat{\boldsymbol{V}}_{\boldsymbol{E}})) \tag{7.67}$$

where $\hat{\boldsymbol{V}}_{\boldsymbol{E}}$ corresponds to the estimate of the Shape system velocity, while $\boldsymbol{L_1} \in \boldsymbol{R}^{3\times3}$, $\boldsymbol{\Lambda_2} \in \boldsymbol{R}^{3\times3}$ and $\boldsymbol{\Lambda_3} \in \boldsymbol{R}^{3\times3}$ are constant positive definite diagonal matrices.

Proof. If the actuator torque $\boldsymbol{\tau_{ex}}$ is well known, let $V_1(\boldsymbol{e}_v, \boldsymbol{q}_E)$ in Eq. (7.52) be the Lyapunov function . The time derivative of this Lyapunov function is as given in Eq. (7.63). Assuming that the actuator torque $\boldsymbol{\tau}_a$ corresponds to the desired torque $\boldsymbol{\tau}_a^d$ in

Eq. (7.64), the time derivative $\dot{V}_1(\boldsymbol{e}_v, \boldsymbol{q}_E)$ of the Lyapunov function can be expressed as given in Eq. (7.56). Using the bounds on $V_1(\boldsymbol{e}_v, \boldsymbol{q}_E)$ from Eq. (7.53), the time derivative $\dot{V}_1(\boldsymbol{e}_v, \boldsymbol{q}_E)$ is obtained as given in Eq. (7.57). On integrating both sides of Eq. (7.57) exponential convergence follows.

If the external torque $\boldsymbol{\tau_{ex}}$ is an unknown constant, consider the following Lyapunov function $V_1(\boldsymbol{e_v}, \boldsymbol{q_E}, \hat{\boldsymbol{V}}_{\boldsymbol{E}}, \hat{\boldsymbol{\tau}}_{\boldsymbol{ex}})$ as defined in Eq. (7.62). For a constant external torque vector $\boldsymbol{\tau_{ex}}$, dynamics of the estimate $\hat{\boldsymbol{\tau}}_{\boldsymbol{ex}}$ and the estimation error $\tilde{\boldsymbol{\tau}}_{\boldsymbol{ex}}$ are related as,

$$\dot{\tilde{\boldsymbol{\tau}}}_{\boldsymbol{ex}} = -\dot{\hat{\boldsymbol{\tau}}}_{\boldsymbol{ex}} \tag{7.68}$$

From the above relationship, and assuming that the actuator is able to provide the desired torque in Eq. (7.65) ($\boldsymbol{\tau_a} = \boldsymbol{\tau_a^d}$), the derivative $\dot{V}_1(\boldsymbol{e_v}, \boldsymbol{q_E}, \hat{\boldsymbol{V}}_{\boldsymbol{E}}, \hat{\boldsymbol{\tau}}_{\boldsymbol{ex}})$ of the Lyapunov function in Eq. (7.63) can be expressed as,

$$\begin{aligned}\dot{V}_1(\boldsymbol{e_v}, \boldsymbol{q_E}, \hat{\boldsymbol{V}}_{\boldsymbol{E}}, \hat{\boldsymbol{\tau}}_{\boldsymbol{ex}}) = &-\boldsymbol{e_v^T K_d e_v} - \boldsymbol{e_v^T}\tilde{\boldsymbol{\tau}}_{\boldsymbol{ex}} - \boldsymbol{e_v^T K_p q_E} + \boldsymbol{V_E^T K_p q_E} \\ &- \tilde{\boldsymbol{V}}_{\boldsymbol{E}}^{\boldsymbol{T}} \boldsymbol{\Lambda_3 L_1} \tilde{\boldsymbol{V}}_{\boldsymbol{E}} - (\tilde{\boldsymbol{V}}_{\boldsymbol{E}}^{\boldsymbol{T}} \boldsymbol{\Lambda_3} - \dot{\tilde{\boldsymbol{\tau}}}_{\boldsymbol{ex}}^{\boldsymbol{T}} \boldsymbol{\Lambda_2^{-1}}) \tilde{\boldsymbol{\tau}}_{\boldsymbol{ex}}\end{aligned} \tag{7.69}$$

Using the definition $\boldsymbol{e_v} := \boldsymbol{V_E} + \boldsymbol{\Lambda_1 q_E}$ from Eq. (7.50) in the above equation, and also using the definition of $\dot{\tilde{\boldsymbol{\tau}}}_{\boldsymbol{ex}}$ from Eq. (7.68) and Eq. (7.67), the Lyapunov function derivative $\dot{V}_1(.)$ in the above equation can be written as,

$$\dot{V}_1(\boldsymbol{e_v}, \boldsymbol{q_E}, \hat{\boldsymbol{V}}_{\boldsymbol{E}}, \hat{\boldsymbol{\tau}}_{\boldsymbol{ex}}) = -\begin{pmatrix} \boldsymbol{e_v} \\ \boldsymbol{q_E} \\ \tilde{\boldsymbol{V}}_{\boldsymbol{E}} \end{pmatrix}^T \begin{pmatrix} \boldsymbol{K_d} & \boldsymbol{0_3} & \boldsymbol{0_3} \\ \boldsymbol{0_3} & \boldsymbol{\Lambda_1 K_p} & \boldsymbol{0_3} \\ \boldsymbol{0_3} & \boldsymbol{0_3} & \boldsymbol{\Lambda_3 L_1} \end{pmatrix} \begin{pmatrix} \boldsymbol{e_v} \\ \boldsymbol{q_E} \\ \tilde{\boldsymbol{V}}_{\boldsymbol{E}} \end{pmatrix} \tag{7.70}$$

The Lyapunov function derivative in the above equation is negative semi-definite. As all the external signals are smooth and bounded, $\ddot{V}_1(\boldsymbol{e_v}, \boldsymbol{q_E}, \hat{\boldsymbol{V}}_{\boldsymbol{E}}, \hat{\boldsymbol{\tau}}_{\boldsymbol{ex}})$ can be shown to be bounded. From Barbalat's lemma [2], asymptotic convergence of the Lyapunov function $\dot{V}_1(\boldsymbol{e_v}, \boldsymbol{q_E}, \hat{\boldsymbol{V}}_{\boldsymbol{E}}, \hat{\boldsymbol{\tau}}_{\boldsymbol{ex}})$ to zero follows. As $\dot{V}_1(\boldsymbol{e_v}, \boldsymbol{q_E}, \hat{\boldsymbol{V}}_{\boldsymbol{E}}, \hat{\boldsymbol{\tau}}_{\boldsymbol{ex}})$ is a negative semi-definite function of $\boldsymbol{e_v}$, $\boldsymbol{q_E}$, $\hat{\boldsymbol{V}}_{\boldsymbol{E}}$, and $\hat{\boldsymbol{\tau}}_{\boldsymbol{ex}}$, these vectors also converge asymptotically to zero.

□

7.5.2 Actuator torque error

As actuator torque $\boldsymbol{\tau_a}$ cannot be directly controlled and must be controlled *via* the air pressure dynamics, when $\boldsymbol{\tau_a}$ is the not the same as the desired actuator torque vector

$\boldsymbol{\tau_a^d}$ given in Eq. (7.65), let the torque error $\tilde{\boldsymbol{\tau}}$ be defined as,

$$\tilde{\boldsymbol{\tau}} = \boldsymbol{\tau_a} - \boldsymbol{\tau_a^d} \tag{7.71}$$

Due to the error $\tilde{\boldsymbol{\tau}}$ in providing the desired actuator torque, the derivative $\dot{V}_1(.)$ of the Lyapunov function in Eq. (7.70) is obtained as,

$$\dot{V}_1(\boldsymbol{e_v}, \boldsymbol{q_E}, \hat{\boldsymbol{V}}_{\boldsymbol{E}}, \hat{\boldsymbol{\tau}}_{\boldsymbol{ex}}) = -\begin{pmatrix} \boldsymbol{e_v} \\ \boldsymbol{q_E} \\ \tilde{\boldsymbol{V}}_{\boldsymbol{E}} \end{pmatrix}^T \begin{pmatrix} \boldsymbol{K_d} & \boldsymbol{0_3} & \boldsymbol{0_3} \\ \boldsymbol{0_3} & \boldsymbol{\Lambda_1 K_p} & \boldsymbol{0_3} \\ \boldsymbol{0_3} & \boldsymbol{0_3} & \boldsymbol{\Lambda_3 L_1} \end{pmatrix} \begin{pmatrix} \boldsymbol{e_v} \\ \boldsymbol{q_E} \\ \tilde{\boldsymbol{V}}_{\boldsymbol{E}} \end{pmatrix} + \boldsymbol{e_v^T \tilde{\tau}} \tag{7.72}$$

As $\boldsymbol{e_v^T \tilde{\tau}}$ is sign indefinite, regulation of the Lyapunov function $V_1(\boldsymbol{e_v}, \boldsymbol{q_E}, \hat{\boldsymbol{V}}_{\boldsymbol{E}}, \hat{\boldsymbol{\tau}}_{\boldsymbol{ex}})$ to zero is only achieved if the actuator torque error $\tilde{\boldsymbol{\tau}}$ is also identically zero. Input command vector $\boldsymbol{u}$ to the actuator valves required for regulating the torque error vector $\tilde{\boldsymbol{\tau}}$ to zero is derived in the second stage of control design.

As the command input vector $\boldsymbol{u}$ effects the force output from the actuator, the torque error $\tilde{\boldsymbol{\tau}}$ is expressed in terms of an equivalent actuator force error vector $\tilde{\boldsymbol{F}}$. Using the torque-force relationship in Eq. (7.7), the actuator force error $\tilde{\boldsymbol{F}}$ corresponding to the torque error vector $\tilde{\boldsymbol{\tau}}$ in Eq. (7.71) is obtained as,

$$\tilde{\boldsymbol{F}} = \boldsymbol{R^{-1}(q)}(\boldsymbol{\tau_a} - \boldsymbol{\tau_a^d}) = \boldsymbol{F_a} - \boldsymbol{F_a^d} \tag{7.73}$$

where $\boldsymbol{F_a^d} \triangleq (F_{a_1}^d, F_{a_2}^d, F_{a_3}^d)$ corresponds to the vector of desired forces from the three actuators on the crawler leg and is obtained from the desired actuator torque $\boldsymbol{\tau_a^d}$ as,

$$\boldsymbol{F_a^d} = \boldsymbol{R^{-1}(q)\tau_a^d} \tag{7.74}$$

From the relationship $\dot{\boldsymbol{q}} = \boldsymbol{R^{-1}(q)\dot{X}}$ between the piston linear velocity vector $\dot{\boldsymbol{X}}$ and the joint angular velocity $\dot{\boldsymbol{q}}$ in Eq. (7.12), the product $\boldsymbol{e_v^T \tilde{\tau}}$ of $\tilde{\boldsymbol{F}}$ as,

$$\boldsymbol{e_v^T \tilde{\tau}} = (\boldsymbol{V_E} + \boldsymbol{\Lambda_1 q_E})^T \tilde{\boldsymbol{\tau}} = (\dot{\boldsymbol{X}}^T - \dot{\boldsymbol{q}}_{\boldsymbol{p}}^T \boldsymbol{R(q)})\tilde{\boldsymbol{F}} + \boldsymbol{q_E^T \Lambda_1^T R(q)}\tilde{\boldsymbol{F}} \tag{7.75}$$

where $\boldsymbol{F_a}$ is the actuator force vector and $\dot{\boldsymbol{X}}$ is the piston velocity vector.

7.5.3 Second stage controller design

In this subsection, the energy function for the actuator error dynamics and its corresponding supply rate derived in section 3.3 are expressed in a form suitable for design of

controllers to a multi-DOF system. The valve command input vector $\boldsymbol{u}$ is then designed to regulate the actuator torque error $\tilde{\boldsymbol{\tau}}$ to zero. In the following subsection, a Lyapunov function for the multi-DOF crawler leg is presented and some of its properties required for the control design are highlighted.

Actuator error energy function : definition and properties

In this chapter, the command inputs to the pneumatic actuator valve are designed by assuming that the thermodynamic process in the actuator is adiabatic. For an air mass vector of $\boldsymbol{m}_i$, air pressure vector of $\boldsymbol{P}_i$ and a desired pressure vector of $\boldsymbol{P_i^d} := (\boldsymbol{P_{1_i}^d}, \boldsymbol{P_{2_i}^d})$ in the i^{th} actuator, the Lyapunov function $V_{act}(\boldsymbol{m}, \boldsymbol{P}, \boldsymbol{P^d})$ for the actuator subsystem on a leg of the crawler is defined in terms the error energy function $W_L^{adb}(\boldsymbol{m}_i, \boldsymbol{P}_i, \boldsymbol{P_i^d})$ of a single actuator as,

$$V_{act}(\boldsymbol{m}, \boldsymbol{P}, \boldsymbol{P^d}) = \sum_{i=1}^{3} W_L^{adb}(\boldsymbol{m}_i, \boldsymbol{P}_i, \boldsymbol{P_i^d}) \tag{7.76}$$

where the error energy function $W_L^{adb}(\boldsymbol{m}_i, \boldsymbol{P}_i, \boldsymbol{P_i^d})$ is as defined in Eq. (3.143).

As shown in Eq. (5.47), the Lyapunov function $W_L^{adb}(\boldsymbol{m}_i, \boldsymbol{P}_i, \boldsymbol{P_i^d})$ for a single actuator can be bounded from above and below by a quadratic function of the actuator force error $\tilde{F}$. Let $Q_{min_i}(\boldsymbol{m}_i) \in \Re^+$ be the weight on the lower bound, while $Q_{max_i}(\boldsymbol{m}_i) \in \Re^+$ be the weight on the upper bound of the error function $W_L^{adb}(\boldsymbol{m}_i, \boldsymbol{P}_i, \boldsymbol{P_i^d})$ corresponding to the i^{th} actuator. These weights are as defined in Eq. (C.4). Using these bounds, the Lyapunov function candidate $V_{act}(\boldsymbol{m}, \boldsymbol{P}, \boldsymbol{P^d})$ for the actuator subsystem on a single leg can be bounded as,

$$\frac{1}{2} Q_{min}(\boldsymbol{m}) \|\tilde{\boldsymbol{F}}\|_2^2 \leq V_{act}(\boldsymbol{m}, \boldsymbol{P}, \boldsymbol{P^d}) \leq \frac{1}{2} Q_{max}(\boldsymbol{m}) \|\tilde{\boldsymbol{F}}\|_2^2 \tag{7.77}$$

where $Q_{min}(\boldsymbol{m}) := min(Q_{min}(\boldsymbol{m}_1), Q_{min}(\boldsymbol{m}_2), Q_{min}(\boldsymbol{m}_3))$ is the weight on the lower bound, while $Q_{max}(\boldsymbol{m}) := max(Q_{max}(\boldsymbol{m}_1), Q_{max}(\boldsymbol{m}_2), Q_{max}(\boldsymbol{m}_3))$ is the weight on the upper bound. In the following subsection, the time derivative of the actuator Lyapunov function in Eq. (7.76) is presented in a compact form convenient for controller design.

Time derivative of the actuator Lyapunov function

The time derivative $\dot{W}_L^{adb}(.)$ of the error energy function of an individual actuator on the crawler leg is as given in Eq. (3.151). This expression is used to define the time derivative

of the actuator error energy function $V_{act}(\boldsymbol{m}, \boldsymbol{P}, \boldsymbol{P^d})$. As shown in Eq. (3.150), the effort variable at the fluid port of the supply rate to the error energy function of i^{th} actuator is transformed by using a nonlinear function $\gamma_{3_i}^{adb}(\boldsymbol{m}_i, \boldsymbol{P}_i, \boldsymbol{P^d}_i, u_i)$. For a multi-DOF system, such as the crawler leg, the nonlinear function at the fluid port of each actuator can be consolidated and conveniently expressed in the form of a matrix $\Gamma_3(\boldsymbol{m}, \boldsymbol{P}, \boldsymbol{P^d}, \boldsymbol{u})$ as,

$$\Gamma_3(\boldsymbol{m}, \boldsymbol{P}, \boldsymbol{P^d}, \boldsymbol{u}) = \begin{pmatrix} \gamma_{3_1}^{adb}(\boldsymbol{m}_1, \boldsymbol{P}_1, \boldsymbol{P^d}_1, u_1) & 0 & 0 \\ 0 & \gamma_{3_2}^{adb}(\boldsymbol{m}_2, \boldsymbol{P}_2, \boldsymbol{P^d}_2, u_2) & 0 \\ 0 & 0 & \gamma_{3_3}^{adb}(\boldsymbol{m}_3, \boldsymbol{P}_3, \boldsymbol{P^d}_3, u_3) \end{pmatrix} \tag{7.78}$$

For a desired force $F_{a_i}^d$ from the i^{th} actuator, let the position of the actuator providing that force for a fixed mass of air $\boldsymbol{m}_i$ be x_{d_i}. For known temperature in the actuator chambers, given by the elements of the temperature vector $\boldsymbol{T}_i$, the effective spring stiffness $K_{adb}^d(\boldsymbol{m}_i, \boldsymbol{T}_i, x_i, x_{d_i}) \in \Re^+$ of the adiabatic actuator between the current position of the actuator x_i and the desired position x_{d_i} is as defined in Eq. (3.142). Define a vector $\dot{\boldsymbol{\Delta}}_{\boldsymbol{p}}$ as,

$$\dot{\boldsymbol{\Delta}}_{\boldsymbol{p}} = \begin{pmatrix} \frac{\dot{F}_{a_1}^d}{K_{adb}^d(\boldsymbol{m}_1, \boldsymbol{T}_1, x_1, x_{d_1})}, & \frac{\dot{F}_{a_2}^d}{K_{adb}^d(\boldsymbol{m}_2, \boldsymbol{T}_2, x_2, x_{d_2})}, & \frac{\dot{F}_{a_3}^d}{K_{adb}^d(\boldsymbol{m}_3, \boldsymbol{T}_3, x_3, x_{d_3})} \end{pmatrix}^T \tag{7.79}$$

The time derivative of the error energy function $V_{act}(\boldsymbol{m}, \boldsymbol{P}, \boldsymbol{P^d})$ is then obtained from the time derivative of individual actuator Lyapunov function in Eq. (3.151) as,

$$\dot{V}_{act}(\boldsymbol{m}, \boldsymbol{P}, \boldsymbol{P^d}) = (\boldsymbol{\Gamma}_3(\boldsymbol{m}, \boldsymbol{P}, \boldsymbol{P^d}, \boldsymbol{u})\boldsymbol{u})^T \tilde{\boldsymbol{F}} - \dot{\boldsymbol{X}}^{\boldsymbol{T}} \tilde{\boldsymbol{F}} - \dot{\boldsymbol{\Delta}}_{\boldsymbol{p}}^{\boldsymbol{T}} \tilde{\boldsymbol{F}} \tag{7.80}$$

Design of the valve input command $\boldsymbol{u}$ for regulation of actuator force error $\tilde{\boldsymbol{F}}$ to zero is now presented in the following subsection.

Design of the valve command input u

Consider the following Lyapunov function for the combined system of the Shape system inertia and the pneumatic actuator,

$$V_2(\boldsymbol{e_v}, \boldsymbol{q_E}, \tilde{\boldsymbol{V}}_{\boldsymbol{E}}, \tilde{\boldsymbol{\tau}}_{\boldsymbol{ex}}, \boldsymbol{m}, \boldsymbol{P}, \boldsymbol{P^d}) = V_{act}(\boldsymbol{m}, \boldsymbol{P}, \boldsymbol{P^d}) + \underbrace{\frac{1}{2}\begin{pmatrix} \boldsymbol{e_v} \\ \boldsymbol{q_E} \\ \tilde{\boldsymbol{V}}_{\boldsymbol{E}} \\ \tilde{\boldsymbol{\tau}}_{\boldsymbol{ex}} \end{pmatrix}^T \begin{pmatrix} \boldsymbol{M_E(q, q_p)} & \boldsymbol{0_3} & \boldsymbol{0_3} & \boldsymbol{0_3} \\ \boldsymbol{0_3} & \boldsymbol{K_p} & \boldsymbol{0_3} & \boldsymbol{0_3} \\ \boldsymbol{0_3} & \boldsymbol{0_3} & \boldsymbol{\Lambda_3 M_E(q, q_p)} & \boldsymbol{0_3} \\ \boldsymbol{0_3} & \boldsymbol{0_3} & \boldsymbol{0_3} & \boldsymbol{\Lambda_2^{-1}} \end{pmatrix} \begin{pmatrix} \boldsymbol{e_v} \\ \boldsymbol{q_E} \\ \tilde{\boldsymbol{V}}_{\boldsymbol{E}} \\ \tilde{\boldsymbol{\tau}}_{\boldsymbol{ex}} \end{pmatrix}}_{V_1(\boldsymbol{e_v}, \boldsymbol{q_E}, \hat{\boldsymbol{V}}_{\boldsymbol{E}}, \hat{\boldsymbol{\tau}}_{\boldsymbol{ex}})} \tag{7.81}$$

where the actuator Lyapunov function $V_{act}(.)$ is defined in Eq. (7.76), while the Lyapunov function $V_1(.)$ for the first stage is given in Eq. (7.62). From the derivative $\dot{V}_{act}(.)$ of the actuator Lyapunov function in Eq. (7.80), and using the Lyapunov function derivative $\dot{V}_1(.)$ from the first stage of controller design in Eq. (7.72), the derivative $\dot{V}_2(.)$ of the second stage Lyapunov function in Eq. (7.81) is obtained as,

$$\begin{aligned} \dot{V}_2(\boldsymbol{e_v}, \boldsymbol{q_E}, \tilde{\boldsymbol{V}}_{\boldsymbol{E}}, \tilde{\boldsymbol{\tau}}_{\boldsymbol{ex}}, \boldsymbol{m}, \boldsymbol{P}, \boldsymbol{P^d}) = &- \begin{pmatrix} \boldsymbol{e_v} \\ \boldsymbol{q_E} \\ \tilde{\boldsymbol{V}}_{\boldsymbol{E}} \end{pmatrix}^T \begin{pmatrix} \boldsymbol{K_d} & \boldsymbol{0_3} & \boldsymbol{0_3} \\ \boldsymbol{0_3} & \boldsymbol{\Lambda_1 K_p} & \boldsymbol{0_3} \\ \boldsymbol{0_3} & \boldsymbol{0_3} & \boldsymbol{\Lambda_3 L_1} \end{pmatrix} \begin{pmatrix} \boldsymbol{e_v} \\ \boldsymbol{q_E} \\ \tilde{\boldsymbol{V}}_{\boldsymbol{E}} \end{pmatrix} \\ &+ \boldsymbol{e_v^T \tilde{\tau}} + \boldsymbol{(\Gamma_3 u)^T \tilde{F}} - \boldsymbol{\dot{X}^T \tilde{F}} - \boldsymbol{\dot{\Delta}_p^T \tilde{F}} \end{aligned} \tag{7.82}$$

Using expression for $\boldsymbol{e_v^T \tilde{\tau}}$ from Eq. (7.75) in the above equation, $\dot{V}_2(.)$ can be simplified as,

$$\begin{aligned} \dot{V}_2(\boldsymbol{e_v}, \boldsymbol{q_E}, \tilde{\boldsymbol{V}}_{\boldsymbol{E}}, \tilde{\boldsymbol{\tau}}_{\boldsymbol{ex}}, \boldsymbol{m}, \boldsymbol{P}, \boldsymbol{P^d}) = &- \begin{pmatrix} \boldsymbol{e_v} \\ \boldsymbol{q_E} \\ \tilde{\boldsymbol{V}}_{\boldsymbol{E}} \end{pmatrix}^T \begin{pmatrix} \boldsymbol{K_d} & \boldsymbol{0_3} & \boldsymbol{0_3} \\ \boldsymbol{0_3} & \boldsymbol{\Lambda_1 K_p} & \boldsymbol{0_3} \\ \boldsymbol{0_3} & \boldsymbol{0_3} & \boldsymbol{\Lambda_3 L_1} \end{pmatrix} \begin{pmatrix} \boldsymbol{e_v} \\ \boldsymbol{q_E} \\ \tilde{\boldsymbol{V}}_{\boldsymbol{E}} \end{pmatrix} \\ &+ \boldsymbol{((\Gamma_3 u)^T - \dot{q}_p^T R(q) + q_E^T \Lambda_1^T R(q) - \dot{\Delta}_p^T) \tilde{F}} \end{aligned} \tag{7.83}$$

The controller for regulation of the actuator force error $\tilde{\boldsymbol{F}}$ (and consequently the Shape system dynamics $\boldsymbol{q_E}$, $\boldsymbol{V_E}$) and is presented in the following theorem.

Theorem 7.2. *If the external torque $\boldsymbol{\tau_{ex}}$ on the Shape system dynamics in Eq. (7.49) is accurately known, then actuator force error $\tilde{\boldsymbol{F}} := (\boldsymbol{F_a} - \boldsymbol{F_a^d})$, for the desired actuator force $\boldsymbol{F_a^d} = \boldsymbol{R^{-1}(q)\tau_a^d}$ in Eq. (7.74) determined from the desired actuator torque $\boldsymbol{\tau_a^d}$ in Eq. (7.64), exponentially converges to zero for the following definition of the valve input command vector $\boldsymbol{u}$,*

$$\boldsymbol{u} = \boldsymbol{\Gamma_3^{-1}}(\boldsymbol{m}, \boldsymbol{P}, \boldsymbol{P^d}, \boldsymbol{u})(\boldsymbol{R^T(q)\dot{q}_p} + \boldsymbol{\dot{\Delta}_p} - \boldsymbol{\Lambda_1 R^T(q) q_E} - \boldsymbol{K_f}\tilde{\boldsymbol{F}}) \tag{7.84}$$

where $\boldsymbol{K_f} \in \boldsymbol{R}^{3\times3}$ is positive definite diagonal matrix, the matrix of nonlinear functions $\boldsymbol{\Gamma_3}(\boldsymbol{m}, \boldsymbol{P}, \boldsymbol{P^d}, \boldsymbol{u}) \in \boldsymbol{R}^{3\times3}$ is as defined in Eq. (7.78), while $\boldsymbol{\dot{\Delta}_p} \in \boldsymbol{R^{3\times1}}$ is as defined in Eq. (7.79).

If the torque vector $\boldsymbol{\tau_{ex}}$ on tele-operator is an unknown constant, then, for the desired actuator force $\boldsymbol{F_a^d} = \boldsymbol{R^{-1}(q)\tau_a^d}$ in Eq. (7.74) determined from the desired actuator torque $\boldsymbol{\tau_a^d}$ in Eq. (7.65), asymptotic convergence of the actuator force error $\tilde{\boldsymbol{F}}$, and the Shape system states $\boldsymbol{q_E}$, $\boldsymbol{V_E}$ is achieved with the input command vector $\boldsymbol{u}$ defined in Eq. (7.84).

Proof. If the external torque $\boldsymbol{\tau_{ex}}$ is well known, then the Lyapunov function for regulation of Shape system dynamics is defined in terms of the first stage Lyapunov function $\bar{V}_1(\boldsymbol{e_v}, \boldsymbol{q_E})$ in Eq. (7.52) and the actuator energy function $V_{act}(\boldsymbol{m}, \boldsymbol{P}, \boldsymbol{P^d})$ in Eq. (7.76) as,

$$\bar{V}_2(\boldsymbol{e_v}, \boldsymbol{q_E}, \boldsymbol{m}, \boldsymbol{P}, \boldsymbol{P^d}) = \underbrace{\frac{1}{2}\boldsymbol{e_v^T M_E(q, q_p) e_v} + \frac{1}{2}\boldsymbol{q_E^T K_p q_E}}_{\bar{V}_1(\boldsymbol{e_v}, \boldsymbol{q_E})} + V_{act}(\boldsymbol{m}, \boldsymbol{P}, \boldsymbol{P^d}) \tag{7.85}$$

From the definition of the bounds on the actuator Lyapunov function $V_{act}(\boldsymbol{m}, \boldsymbol{P}, \boldsymbol{P^d})$ in Eq. (7.77), the Lyapunov function $\bar{V}_2(.)$ in Eq. (7.85) can be expressed as,

$$\bar{V}_2(\boldsymbol{e_v}, \boldsymbol{q_E}, \boldsymbol{m}, \boldsymbol{P}, \boldsymbol{P^d}) \leq \frac{1}{2}\begin{pmatrix} \boldsymbol{e_v} \\ \boldsymbol{q_E} \\ \tilde{\boldsymbol{F}} \end{pmatrix}^T \underbrace{\begin{pmatrix} \boldsymbol{M_E(q, q_p)} & \boldsymbol{0_3} & \boldsymbol{0_3} \\ \boldsymbol{0_3} & \boldsymbol{K_p} & \boldsymbol{0_3} \\ \boldsymbol{0_3} & \boldsymbol{0_3} & Q_{max}(\boldsymbol{m})\boldsymbol{I_3} \end{pmatrix}}_{\boldsymbol{\mathcal{P}_d}} \begin{pmatrix} \boldsymbol{e_v} \\ \boldsymbol{q_E} \\ \tilde{\boldsymbol{F}} \end{pmatrix} \tag{7.86}$$

where $\boldsymbol{I_3} \in \boldsymbol{R^{3\times3}}$ is the identity matrix. For known external torque $\boldsymbol{\tau_{ex}}$, the desired actuator torque $\boldsymbol{\tau_a^d}$ is as given in Eq. (7.55). From the definition of the desired actuator

force vector $\boldsymbol{F_a^d} := \boldsymbol{R^{-1}(q)\tau_a^d}$ in Eq. (7.74), using time derivative $\dot{\bar{V}}_1(\boldsymbol{e_v}, \boldsymbol{q_E})$ of the first stage Lyapunov function from Eq. (7.56) for desired actuator torque $\boldsymbol{\tau_a^d}$, and using the relationship in Eq. (7.75) to express $\boldsymbol{e_v\tilde{\tau}}$ in terms of the actuator force error $\boldsymbol{\tilde{F}}$, the time derivative $\dot{\bar{V}}_2(.)$ of the Lyapunov function in Eq. (7.85) is obtained as,

$$\begin{aligned}\dot{\bar{V}}_2(\boldsymbol{e_v, q_E, m, P, P^d}) = &- \begin{pmatrix} \boldsymbol{e_v} \\ \boldsymbol{q_E} \end{pmatrix}^T \begin{pmatrix} \boldsymbol{K_d} & \boldsymbol{0_3} \\ \boldsymbol{0_3} & \boldsymbol{\Lambda_1 K_p} \end{pmatrix} \begin{pmatrix} \boldsymbol{e_v} \\ \boldsymbol{q_E} \end{pmatrix} \\ &+ (\boldsymbol{\dot{X}^T - \dot{q}_p^T R(q)})\boldsymbol{\tilde{F}} + \boldsymbol{q_E^T \Lambda_1^T R(q)\tilde{F}} + \dot{V}_{act}(\boldsymbol{m, P, P^d})\end{aligned} \tag{7.87}$$

Using the definition of the time derivative of the actuator Lyapunov function $\dot{V}_{act}(.)$ from Eq. (7.80) and the definition of the valve command input vector $\boldsymbol{u}$ from Eq. (7.84), the derivative $\dot{\bar{V}}_2(.)$ of the actuator Lyapunov function in Eq. (7.87) is obtained as,

$$\begin{aligned}\dot{\bar{V}}_2(\boldsymbol{e_v, q_E, m, P, P^d}) &= - \begin{pmatrix} \boldsymbol{e_v} \\ \boldsymbol{q_E} \\ \boldsymbol{\tilde{F}} \end{pmatrix}^T \underbrace{\begin{pmatrix} \boldsymbol{K_p} & \boldsymbol{0_3} & \boldsymbol{0_3} \\ \boldsymbol{0_3} & \boldsymbol{\Lambda_1 K_p} & \boldsymbol{0_3} \\ \boldsymbol{0_3} & \boldsymbol{0_3} & \boldsymbol{K_f} \end{pmatrix}}_{\boldsymbol{\mathcal{Q}_d}} \begin{pmatrix} \boldsymbol{e_v} \\ \boldsymbol{q_E} \\ \boldsymbol{\tilde{F}} \end{pmatrix} \\ &\leq -\sigma_{min}(\boldsymbol{\mathcal{Q}_d}) \left\| \begin{matrix} \boldsymbol{e_v} \\ \boldsymbol{q_E} \\ \boldsymbol{\tilde{F}} \end{matrix} \right\|_2^2\end{aligned} \tag{7.88}$$

where $\sigma_{min}(.)$ represents the operator to obtain the minimum singular value of the input matrix. Using the bounds on the Lyapunov function $\bar{V}_2(\boldsymbol{e_v, q_E, m, P, P^d})$ from Eq. (7.86), the Lyapunov function derivative $\dot{\bar{V}}_2(.)$ in the above equation can be expressed as,

$$\dot{\bar{V}}_2(\boldsymbol{e_v, q_E, m, P, P^d}) \leq - \left(\frac{2\sigma_{min}(\boldsymbol{\mathcal{Q}_d})}{\sigma_{max}(\boldsymbol{\mathcal{P}_d})} \right) \bar{V}_2(\boldsymbol{e_v, q_E, m, P, P^d}) \tag{7.89}$$

where $\sigma_{max}(.)$ represents the operator to obtain the maximum singular value of the input matrix. On integrating both sides of Eq. (7.89) exponential convergence follows. As the Lyapunov function in Eq. (7.85) is a positive definite function of $\boldsymbol{e_v}$, $\boldsymbol{q_E}$ and $\tilde{F}$, they also converge exponentially to zero.

If the torque $\boldsymbol{\tau_{ex}}$ is an unknown constant, consider the Lyapunov function $V_2(.)$ as given in Eq. (7.81). For a desired actuator force vector $\boldsymbol{F_a^d}$ in Eq. (7.74), the time

derivative $\dot{V}_2(.)$ of this Lyapunov function is as given in Eq. (7.83). Using the definition of the input command $\boldsymbol{u}$ from Eq. (7.84), the Lyapunov function derivative $\dot{V}_2(.)$ in Eq. (7.83) can be simplified as,

$$\dot{V}_2(\boldsymbol{e_v}, \boldsymbol{q_E}, \tilde{\boldsymbol{V}}_{\boldsymbol{E}}, \boldsymbol{m}, \boldsymbol{P}, \boldsymbol{P^d}) = -\begin{pmatrix} \boldsymbol{e_v} \\ \boldsymbol{q_E} \\ \tilde{\boldsymbol{V}}_{\boldsymbol{E}} \\ \tilde{\boldsymbol{F}} \end{pmatrix}^T \underbrace{\begin{pmatrix} \boldsymbol{K_d} & \boldsymbol{0_3} & \boldsymbol{0_3} & \boldsymbol{0_3} \\ \boldsymbol{0_3} & \boldsymbol{\Lambda_1 K_p} & \boldsymbol{0_3} & \boldsymbol{0_3} \\ \boldsymbol{0_3} & \boldsymbol{0_3} & \boldsymbol{\Lambda_3 L_1} & \boldsymbol{0_3} \\ \boldsymbol{0_3} & \boldsymbol{0_3} & \boldsymbol{0_3} & \boldsymbol{K}_f \end{pmatrix}}_{\boldsymbol{\mathcal{Q}_p}} \begin{pmatrix} \boldsymbol{e_v} \\ \boldsymbol{q_E} \\ \tilde{\boldsymbol{V}}_{\boldsymbol{E}} \\ \tilde{\boldsymbol{F}} \end{pmatrix} \tag{7.90}$$

The Lyapunov function derivative $\dot{V}_2(.)$ in the above equation is only negative semi-definite. However, as all the external signals are bounded, $\ddot{V}_2(.)$ can be shown to be bounded. From Barbalat's lemma [2], $\dot{V}_2(.)$ converges asymptotically to zero, thus the reference velocity error vector $\boldsymbol{e_v}$, the position error vector $\boldsymbol{q_E}$ and the velocity error vector $\boldsymbol{V_E}$ converge asymptotically to zero.

□

In the following section, passivity properties of the tele-operator are investigated.

7.6 Closed loop passivity analysis

In this section, passivity properties of the tele-operator for the control input designed in the previous section are investigated. The control input u is modified to provide the required co-ordination properties in Eq.(7.23) while satisfying the passivity properties in Eq. (7.25). For brevity of presentation, the control input in Eq. (7.84) is expressed as,

$$\boldsymbol{u} = \boldsymbol{\Gamma_3^{-1}}(\boldsymbol{R^T}(\boldsymbol{q})\dot{\boldsymbol{q}}_{\boldsymbol{p}} + \dot{\boldsymbol{\Delta}}_{\boldsymbol{p}} + \boldsymbol{u_{fb}}) \tag{7.91}$$

where $\boldsymbol{u_{fb}}$ consists of the feedback components of the control input and is given by,

$$\boldsymbol{u_{fb}} = -\boldsymbol{\Lambda_1 R^T}(\boldsymbol{q})\boldsymbol{q_E} - \boldsymbol{K}_f\tilde{\boldsymbol{F}} \tag{7.92}$$

The dynamics of the tele-operator after co-ordination ($\boldsymbol{q} = \boldsymbol{q_p}$ and $\boldsymbol{V_L} = \dot{\boldsymbol{q}} = \dot{\boldsymbol{q}}_{\boldsymbol{p}}$) are obtained from the Locked system dynamics in Eq. (7.44) as,

$$\boldsymbol{M_L}(\boldsymbol{q}, \boldsymbol{q})\ddot{\boldsymbol{q}} + \boldsymbol{C_L}(\boldsymbol{q}, \boldsymbol{q}, \dot{\boldsymbol{q}}, \dot{\boldsymbol{q}})\dot{\boldsymbol{q}} + \boldsymbol{g_L}(\boldsymbol{q}, \boldsymbol{q}) = \rho(\boldsymbol{\tau_{h_p}} + \boldsymbol{\tau_{e_p}}) + \boldsymbol{\tau_{e_c}} + (\eta + 1)\boldsymbol{\tau_{h_e}} \tag{7.93}$$

The external torques acting on the co-ordinated system dynamics in the above equation correspond to the desired supply rate $s_h(.)$ in Eq. (7.24). In the following subsection, storage function for the tele-operator is defined and the effect of the input vector $\boldsymbol{u}$ on the the supply rate to the tele-operator is investigated.

7.6.1 Storage function for the tele-operator

The storage function for the tele-operator is defined as the sum of the amplified available energy in the PHANToM(TM^1), available energy from the crawler leg, and the available energy in the pneumatic actuator. The available energy in the mechanical systems is the sum of their kinetic energy and their potential energy. Let $W_p(\boldsymbol{q_p})$ represents the potential energy of PHANToM(TM^1) in the crawler joint space, while $W_q(\boldsymbol{q})$ be the potential energy of the crawler in its joint space. The inertial dynamics of the crawler and the PHANToM(TM^1) are obtained from Lagrangian formulation. For the gravitational torque $\boldsymbol{g_q^T(q)}$ on the crawler leg, and the gravitational torque $\boldsymbol{g_p^T(q_p)}$ on the PHANToM(TM^1) leg in the crawler joint space, the potential energies $W_q(\boldsymbol{q})$ and $W_p(\boldsymbol{q_p})$ respectively satisfy the following conditions,

$$\dot{W}_q(\boldsymbol{q}) = \boldsymbol{g_q^T(q)\dot{q}}, \qquad \dot{W}_p(\boldsymbol{q_p}) = \boldsymbol{g_p^T(q_p)\dot{q}_p} \tag{7.94}$$

Using the definition of the available energy $W_{act}(\boldsymbol{m}, \boldsymbol{P})$ in the system of adiabatic actuators on the the crawler leg from Eq. (7.8), the storage function $W_s(\boldsymbol{q}, \boldsymbol{q_p}, \boldsymbol{m}, \boldsymbol{P})$ is defined as,

$$\begin{aligned} W_s(\boldsymbol{q}, \dot{\boldsymbol{q}}, \boldsymbol{q_p}, \dot{\boldsymbol{q}}_{\boldsymbol{p}}, \boldsymbol{m}, \boldsymbol{P}) = \frac{\rho}{2}\boldsymbol{\dot{q}_p^T M_p(q_p)\dot{q}_p} + \rho W_p(\boldsymbol{q_p}) + \frac{1}{2}\boldsymbol{\dot{q}^T M_q(q)\dot{q}} + W_q(\boldsymbol{q}) \\ + W_{act}(\boldsymbol{m}, \boldsymbol{P}) \end{aligned} \tag{7.95}$$

where ρ is the amplification factor on the PHANToM(TM^1) dynamics. Using the definition of the rate of change of gravitational potential energy in Eq. (7.94), the derivative $\dot{W}_s(.)$ of the storage function in the above equation is obtained as,

$$\begin{aligned} \dot{W}_s(\boldsymbol{q}, \dot{\boldsymbol{q}}, \boldsymbol{q_p}, \dot{\boldsymbol{q}}_{\boldsymbol{p}}, \boldsymbol{m}, \boldsymbol{P}) = \rho(\boldsymbol{\dot{q}_p^T M_p(q_p)\ddot{q}_p} + \boldsymbol{\dot{q}_p^T}\frac{\boldsymbol{\dot{M}_p(q_p)}}{\boldsymbol{2}}\boldsymbol{\dot{q}_p} + \boldsymbol{g_p^T(q_p)\dot{q}_p}) \\ + \boldsymbol{\dot{q}^T M_q(q)\ddot{q}} + \boldsymbol{\dot{q}^T}\frac{\boldsymbol{\dot{M}_q(q)}}{\boldsymbol{2}}\boldsymbol{\dot{q}} + \boldsymbol{g_q^T(q)\dot{q}} + \dot{W}_{act}(\boldsymbol{m}, \boldsymbol{P}) \end{aligned} \tag{7.96}$$

Using the dynamics of the crawler and the PHANToM(TM[1]) device from Eq. (7.28), and from the skew-symmetric property of their inertia matrices $\boldsymbol{M_q(q)}$, $\boldsymbol{M_p(q_p)}$ shown in remarks 7.1 and 7.3 respectively, the derivative of the storage function $\dot{W}_s(.)$ in Eq. (7.96) can be simplified as,

$$\dot{W}_s(\boldsymbol{q}, \dot{\boldsymbol{q}}, \boldsymbol{q_p}, \dot{\boldsymbol{q}}_{\boldsymbol{p}}, \boldsymbol{m}, \boldsymbol{P}) = \rho \dot{\boldsymbol{q}}_{\boldsymbol{p}}^{\boldsymbol{T}} (\boldsymbol{\tau_{h_p}} + \boldsymbol{\tau_{a_p}} + \boldsymbol{\tau_{e_p}}) + \dot{\boldsymbol{q}}^{\boldsymbol{T}} (\boldsymbol{\tau_a} + \boldsymbol{\tau_{e_c}} + \boldsymbol{\tau_{h_e}}) + \dot{W}_{act}(\boldsymbol{m}, \boldsymbol{P}) \tag{7.97}$$

From the definition of the input torque $\boldsymbol{\tau_{a_p}}$ on the PHANToM(TM[1]) device from Eq. (7.45), the rate of change of actuator energy function $\dot{W}_{act}(\boldsymbol{m}, \boldsymbol{P})$ from Eq. (7.13), and using the definition of the input vector $\boldsymbol{u}$ from Eq. (7.91), the supply rate $\dot{W}_s(.)$ in Eq. (7.97) can be expressed as,

$$\begin{aligned} \dot{W}_s(\boldsymbol{q}, \dot{\boldsymbol{q}}, \boldsymbol{q_p}, \dot{\boldsymbol{q}}_{\boldsymbol{p}}, \boldsymbol{m}, \boldsymbol{P}) =& \dot{\boldsymbol{q}}^{\boldsymbol{T}} (\boldsymbol{\tau_{e_c}} + (\eta + 1)\boldsymbol{\tau_{h_e}}) + \rho \dot{\boldsymbol{q}}_{\boldsymbol{p}}^{\boldsymbol{T}} (\boldsymbol{\tau_{h_p}} + \boldsymbol{\tau_{e_p}}) - \eta \dot{\boldsymbol{q}}_{\boldsymbol{E}}^{\boldsymbol{T}} \boldsymbol{\tau_{h_e}} \\ &+ \dot{\boldsymbol{q}}_{\boldsymbol{p}}^{\boldsymbol{T}} \boldsymbol{C_{LE}} \dot{\boldsymbol{q}}_{\boldsymbol{E}} + (\boldsymbol{\Gamma_3^{-T}} \boldsymbol{\Gamma_1^T} - \boldsymbol{I_3}) \dot{\boldsymbol{q}}_{\boldsymbol{p}}^{\boldsymbol{T}} \boldsymbol{\tau_a} \\ &+ (\boldsymbol{R^{-1}(q)} \boldsymbol{\Gamma_3^{-1}} \boldsymbol{\Gamma_1} \boldsymbol{u_{fb}})^{\boldsymbol{T}} \boldsymbol{\tau_a} + \dot{\boldsymbol{\Delta}}_{\boldsymbol{p}}^{\boldsymbol{T}} \boldsymbol{\Gamma_3^{-T}} \boldsymbol{\Gamma_1^T} \boldsymbol{R^{-T}(q)} \boldsymbol{\tau_a} \end{aligned} \tag{7.98}$$

where $\boldsymbol{I_3} \in \boldsymbol{R}^{3\times3}$ is an identity matrix. The first two terms on the *r.h.s* of the above equation correspond to the desired supply rate $s_h(.)$ of the uncoordinated tele-operator as presented in Eq. (7.24). As shown in section 5.5 for human power amplification, and section 6.5 for tele-operation with single-DOF systems, the magnitude of $\Gamma_3^{-1}\Gamma_1$ for adiabatic actuators is very close to the identity matrix $\boldsymbol{I_3}$. The other terms in the *r.h.s* of Eq. (7.98) are however nonzero and influence the supply rate to the tele-operator. The desired actuator force vector $\boldsymbol{F_a^d}$ typically varies with time in such a way that the vector $\dot{\boldsymbol{\Delta}}_{\boldsymbol{p}}$ is sign indefinite. The power input $\dot{\boldsymbol{q}}_{\boldsymbol{p}}^{\boldsymbol{T}} \boldsymbol{C_{LE}} \dot{\boldsymbol{q}}$ required due to the decoupling torque $\boldsymbol{C_{LE}} \dot{\boldsymbol{q}}$ is also sign indefinite. Therefore the command input $\boldsymbol{u}$ can act as an energy source or a sink. To guarantee passive operation, the proposed method in section 6.4 for monitoring the power interaction between the tele-operator and the controller by using a flywheel is adopted. In the following section, dynamics of the flywheel required for passive operation of the tele-operator are presented.

7.6.2 Augmented system with flywheel dynamics

The flywheel is assumed to be an inertial system with a mass M_f. The dynamics of the flywheel are determined by torque T_f and are given by,

$$M_f \ddot{x}_f = T_f \tag{7.99}$$

where x_f is the position of the inertia M_f. A virtual skew-symmetric interconnection between the flywheel and the tele-operator is established such that any power input to the tele-operator, as required by the controller, results in loss of same amount of power from the flywheel. By keeping track of the change in the kinetic energy of the flywheel, the energy change in the tele-operator due to controller requirements can be monitored. When the kinetic energy of the flywheel is above a threshold value ($\dot{x}_f \geq f_o$), then the available energy with the tele-operator is within acceptable value and the tele-operator is said to be operating in normal mode. If the kinetic energy of the flywheel falls below a threshold value ($\dot{x}_f < f_o$) due to excessive energy transfer to the tele-operator, then the operation of tele-operator is said to be in emergency mode. In emergency mode additional damping is applied on the tele-operator. The energy dissipated by the tele-operator in emergency mode is transmitted to the flywheel through the virtual interconnection. When the kinetic energy of the flywheel increases above a reasonable value ($\dot{x}_f > f_1 > f_o$), then the operation of tele-operator is switched back to normal mode by resetting the additional damping to zero. By regulating the power available from the tele-operator to be within a reasonable value, passive operation is guaranteed.

Additional damping on the tele-operator dynamics is realized by designing the actuator torque on the PHANToM(TM^1) device in Eq. (7.45) (in the crawler joint space) to include damping torque $\boldsymbol{B\dot{q}_p}$ as,

$$\boldsymbol{\tau_{a_p}} = -\frac{1}{\rho}(\boldsymbol{\tau_a - C_{LE}\dot{q}_E} + \eta\boldsymbol{\tau_{h_e}} + \boldsymbol{B\dot{q}_p}) \tag{7.100}$$

where $\boldsymbol{B} \in \boldsymbol{R}^{3\times3}$ is a positive definite diagonal matrix. With the above torque on the PHANToM(TM^1), the supply rate to the tele-operator in Eq. (7.98) is modified as,

$$\begin{aligned}\dot{W}_s(\boldsymbol{q}, \dot{\boldsymbol{q}}, \boldsymbol{q_p}, \dot{\boldsymbol{q}}_{\boldsymbol{p}}, \boldsymbol{m}, \boldsymbol{P}) =& \boldsymbol{\dot{q}^T}(\boldsymbol{\tau_{e_c}} + (\eta+1)\boldsymbol{\tau_{h_e}}) + \rho\boldsymbol{\dot{q}_p^T}(\boldsymbol{\tau_{h_p}} + \boldsymbol{\tau_{e_p}}) - \eta\boldsymbol{\dot{q}_E^T\tau_{h_e}} \\ &+ \boldsymbol{\dot{q}_p^T C_{LE}\dot{q}_E} - \boldsymbol{\dot{q}_p^T B\dot{q}_p} + (\boldsymbol{\Gamma_3^{-T}\Gamma_1^T - I_3})\boldsymbol{\dot{q}_p^T\tau_a} \\ &+ \boldsymbol{\dot{\Delta}_p^T\Gamma_3^{-T}\Gamma_1^T R^{-T}(q)\tau_a} + (\boldsymbol{R^{-1}(q)\Gamma_3^{-1}\Gamma_1 u_{fb}})^{\boldsymbol{T}}\boldsymbol{\tau_a}\end{aligned} \tag{7.101}$$

In the following section, the supply rate to the augmented system consisting of the tele-operator and the flywheel is studied, and the flywheel torque required to establish the desired virtual connection between them is defined.

7.6.3 Passivity properties of the flywheel augmented system

The storage function $W_t(\boldsymbol{q}, \dot{\boldsymbol{q}}, \boldsymbol{q_p}, \dot{\boldsymbol{q}}_{\boldsymbol{p}}, \boldsymbol{m}, \boldsymbol{P}, \dot{x}_f)$ for the augmented system with flywheel is obtained by including the kinetic energy of the flywheel in the definition of the storage function $W_s(.)$ in Eq. (7.95) as,

$$W_t(\boldsymbol{q}, \dot{\boldsymbol{q}}, \boldsymbol{q_p}, \dot{\boldsymbol{q}}_{\boldsymbol{p}}, \boldsymbol{m}, \boldsymbol{P}, \dot{x}_f) = W_s(\boldsymbol{q}, \dot{\boldsymbol{q}}, \boldsymbol{q_p}, \dot{\boldsymbol{q}}_{\boldsymbol{p}}, \boldsymbol{m}, \boldsymbol{P}) + \frac{1}{2} M_f \dot{x}_f^2 \tag{7.102}$$

The time derivative $\dot{W}_t(.)$ of the storage function in the above equation is obtained from $\dot{W}_s(.)$ in Eq. (7.101) and the flywheel dynamics in Eq. (7.99) as,

$$\begin{aligned} \dot{W}_t(\boldsymbol{q}, \dot{\boldsymbol{q}}, \boldsymbol{q_p}, \dot{\boldsymbol{q}}_{\boldsymbol{p}}, \boldsymbol{m}, \boldsymbol{P}, \dot{x}_f) = {} & \dot{\boldsymbol{q}}^{\boldsymbol{T}}(\boldsymbol{\tau_{e_c}} + (\eta+1)\boldsymbol{\tau_{h_e}}) + \rho \dot{\boldsymbol{q}}_{\boldsymbol{p}}^{\boldsymbol{T}}(\boldsymbol{\tau_{h_p}} + \boldsymbol{\tau_{e_p}}) - \eta \dot{\boldsymbol{q}}_{\boldsymbol{E}}^{\boldsymbol{T}} \boldsymbol{\tau_{h_e}} \\ & + \dot{\boldsymbol{q}}_{\boldsymbol{p}}^{\boldsymbol{T}} \boldsymbol{C_{LE}} \dot{\boldsymbol{q}}_{\boldsymbol{E}} - \dot{\boldsymbol{q}}_{\boldsymbol{p}}^{\boldsymbol{T}} \boldsymbol{B} \dot{\boldsymbol{q}}_{\boldsymbol{p}} + (\boldsymbol{R^{-1}(q)\Gamma_3^{-1}\Gamma_1 u_{fb}})^{\boldsymbol{T}} \boldsymbol{\tau_a} \\ & + (\boldsymbol{\Gamma_3^{-T}\Gamma_1^T - I_3}) \dot{\boldsymbol{q}}_{\boldsymbol{p}}^{\boldsymbol{T}} \boldsymbol{\tau_a} + \dot{\boldsymbol{\Delta}}_{\boldsymbol{p}}^{\boldsymbol{T}} \boldsymbol{\Gamma_3^{-T}\Gamma_1^T R^{-T}(q)} \boldsymbol{\tau_a} + T_f \dot{x}_f \end{aligned} \tag{7.103}$$

The flywheel torque T_f and the updated valve command input $\boldsymbol{u}$ for establishing the virtual skew-symmetric interconnection between the flywheel and the tele-operator is presented in the following theorem.

Theorem 7.3. *For the dynamics of the crawler leg as given in Eq. (7.2), the PHANToM(TM[1]) dynamics in the crawler joint space as given in Eq. (7.21) and the adiabatic actuator dynamics as described in section 7.2.2, with the following command input,*

$$\boldsymbol{u} = \boldsymbol{\Gamma_3^{-1} R^T(q)} \dot{\boldsymbol{q}}_{\boldsymbol{p}} + \dot{\boldsymbol{\Delta}}_{\boldsymbol{p}} + \hat{\boldsymbol{u}}_{\boldsymbol{fb}} \tag{7.104}$$

where $\dot{\boldsymbol{\Delta}}_{\boldsymbol{p}}$ as defined in Eq. (7.79) depends on the desired actuator force vector $\boldsymbol{F_a^d} := \boldsymbol{R^{-1}(q)\tau_a^d}$, with the desired actuator torque $\boldsymbol{\tau_a^d}$ as defined in Eq. (7.65), and the feedback input vector $\hat{\boldsymbol{u}}_{\boldsymbol{fb}}$ is related to the flywheel torque T_f through the following skew-symmetric

matrix,

$$\begin{pmatrix} \hat{\boldsymbol{u}}_{\boldsymbol{fb}} \\ T_f \end{pmatrix} = \begin{pmatrix} \mathbf{0_3} & g(\dot{x}_f)\boldsymbol{u_{fb}} \\ -g(\dot{x}_f)\boldsymbol{u_{fb}^T} & 0 \end{pmatrix} \begin{pmatrix} (\boldsymbol{\Gamma_1^T\Gamma_3^{-T}R^{-T}(q)})\boldsymbol{\tau_a} \\ \dot{x}_f \end{pmatrix} + \begin{pmatrix} \mathbf{0_{3\times 1}} \\ \frac{1}{\dot{x}_f}\Big(-\dot{\boldsymbol{q}}_{\boldsymbol{p}}^{\boldsymbol{T}}\boldsymbol{C_{LE}}\dot{\boldsymbol{q}}_{\boldsymbol{E}} + \eta\dot{\boldsymbol{q}}_{\boldsymbol{E}}^{\boldsymbol{T}}\boldsymbol{\tau_{h_e}} + (\boldsymbol{\Gamma_3^{-T}\Gamma_1^T - I_3})\dot{\boldsymbol{q}}_{\boldsymbol{p}}^{\boldsymbol{T}}\boldsymbol{\tau_a} \\ +\dot{\boldsymbol{q}}_{\boldsymbol{p}}^{\boldsymbol{T}}\boldsymbol{B}\dot{\boldsymbol{q}}_{\boldsymbol{p}} + (\boldsymbol{R^{-1}(q)\Gamma_3^{-1}\dot{\Delta}_p})^{\boldsymbol{T}}\boldsymbol{\tau_a}\Big) \end{pmatrix} \tag{7.105}$$

where $\boldsymbol{u_{fb}}$ *is as defined in Eq. (7.92), while the function* $g(\dot{x}_f)$ *and the damping coefficient* $\boldsymbol{B}$ *depend on flywheel velocity* $\dot{x}_f$ *as,*

$$\textit{Normal mode}: \begin{pmatrix} g(\dot{x}_f) = \frac{1}{\dot{x}_f} \\ \boldsymbol{B} = \mathbf{0_{3\times 3}} \end{pmatrix} \quad \textit{if } \dot{x}_f \geq f_o \tag{7.106}$$

$$\textit{Emergency mode}: \begin{pmatrix} g(\dot{x}_f) = \frac{1}{f_o} \\ \boldsymbol{B} \in (\boldsymbol{R}^+)^{3\times 3} \end{pmatrix} \quad \textit{if } \dot{x}_f < f_o \tag{7.107}$$

where f_o *corresponds to the threshold velocity of the flywheel for switching to the emergency mode of operation, the external supply rate to the tele-operator* $s_h(.)$ *with human power amplification given in Eq. (7.24), robustly satisfies the following passivity condition,*

$$\int_0^t s_h(\boldsymbol{\tau_{e_c}}, \boldsymbol{\tau_{e_p}}, \boldsymbol{\tau_{h_e}}, \boldsymbol{\tau_{h_p}}, \dot{\boldsymbol{q}}, \dot{\boldsymbol{q}}_{\boldsymbol{p}}) \geq -c_o^2 \tag{7.108}$$

Proof. Define the storage function $W_t(\boldsymbol{q}, \dot{\boldsymbol{q}}, \boldsymbol{q_p}, \dot{\boldsymbol{q}}_{\boldsymbol{p}}, \boldsymbol{m}, \boldsymbol{P}, \dot{x}_f)$ for the augmented system of the tele-operator and the virtual flywheel system as presented in Eq. (7.102). The time-derivative $\dot{W}_t(.)$ of the storage function is as presented in Eq. (7.103).

Using the definition of the valve command input vector $\boldsymbol{u}$ from Eq. (7.104) and the feedback component $\hat{\boldsymbol{u}}_{\boldsymbol{fb}}$ of $\boldsymbol{u}$ from Eq. (7.105) in Eq. (7.103), the time derivative $\dot{W}_t(.)$ is related to the desired supply rate $s_h(\boldsymbol{\tau_{e_c}}, \boldsymbol{\tau_{e_p}}, \boldsymbol{\tau_{h_p}}, \boldsymbol{q}, \dot{\boldsymbol{q}}_{\boldsymbol{p}})$ as,

$$\begin{aligned} \dot{W}_t(\boldsymbol{q}, \dot{\boldsymbol{q}}, \boldsymbol{q_p}, \dot{\boldsymbol{q}}_{\boldsymbol{p}}, \boldsymbol{m}, \boldsymbol{P}, \dot{x}_f) &= \dot{\boldsymbol{q}}^{\boldsymbol{T}}(\boldsymbol{\tau_{e_c}} + (\eta+1)\boldsymbol{\tau_{h_e}}) + \rho\dot{\boldsymbol{q}}_{\boldsymbol{p}}^{\boldsymbol{T}}(\boldsymbol{\tau_{h_p}} + \boldsymbol{\tau_{e_p}}) \\ &= s_h(\boldsymbol{\tau_{e_c}}, \boldsymbol{\tau_{e_p}}, \boldsymbol{\tau_{h_p}}, \boldsymbol{\tau_{h_e}}, \dot{\boldsymbol{q}}, \dot{\boldsymbol{q}}_{\boldsymbol{p}}) \end{aligned} \tag{7.109}$$

On integrating the above equation, the desired external supply rate $s_h(.)$ satisfies the following passivity condition,

$$\int_0^t s_h(\boldsymbol{\tau_{e_c}}, \boldsymbol{\tau_{e_p}}, \boldsymbol{\tau_{h_p}}, \boldsymbol{\tau_{h_e}}, \dot{\boldsymbol{q}}, \dot{\boldsymbol{q}}_{\boldsymbol{p}})\ d\tau \geq -W_t(\boldsymbol{q}, \dot{\boldsymbol{q}}, \boldsymbol{q_p}, \boldsymbol{m}, \boldsymbol{P}, \dot{x}_f)|_{t=0} \tag{7.110}$$

where $W_t(\boldsymbol{q}, \dot{\boldsymbol{q}}, \boldsymbol{q_p}, \dot{\boldsymbol{q}}_{\boldsymbol{p}}, \boldsymbol{m}, \boldsymbol{P}, \dot{x}_f)|_{t=0} \geq 0$ corresponds to the initial energy (at $t = 0$) in the augmented system.

Note that during the emergency mode of operation, the damping coefficient $\boldsymbol{B}$ must be selected large enough to put energy back into the flywheel.

□

As mentioned in section 6.4, the tele-operator is maintained in the emergency mode of operation until the velocity of the flywheel increase to $f_1 > f_o$. This is to prevent chattering of the control input at the boundary of regular mode and emergency mode of operation.

7.7 Experimental results

Results from implementation of the controller designed in the previous section on the multi-DOF test bed in Fig. (7.2) are presented in this section. Before walking the crawler remotely with the PHANToM(TM[1]) device, some preliminary experiments were conducted to test the controller performance in achieving bilateral tele-operation and stable interaction with a hard surface. With no external human torque on the crawler ($\boldsymbol{\tau_{h_e}} = \boldsymbol{0}$), the controller derived in the previous section is evaluated in different modes of operation such as, tele-operation of the individual crawler leg in free space, interaction with a hard surface, and bilateral operation before walking the crawler remotely with commands at the PHANToM(TM[1]) interface. The controller performance was then evaluated by walking the crawler along a level ground. As only the front two legs of the crawler are functional, the front two legs of the crawler are moved in a fashion similar to *butterfly stroke* in swimming. Amplification of the input human power ($\boldsymbol{\tau_{h_e}}\dot{\boldsymbol{q}}$) by the actuators on a crawler leg is evaluated with the crawler stationary. The right leg of the crawler was operated as a multi-DOF human power amplifier and was used to move a $2.27kgs$ ($5lbs$) load.

The bore and the stroke length of the linear pneumatic actuators on different joints of the crawler are presented in table 7.1.

The MPYE-3-LF010 proportional valves from FESTO are being currently used to meter the air flow to/from the actuators. The input command to these valves is a voltage signal in the range of 0 to 10 volts, with $5V$ corresponding to the closed center

Table 7.1: Specifications of the actuator on each joint on a crawler leg

Joint number	Stroke length(m)	Bore diameter(m)	Rod diameter (m)
1	0.0889	0.027	0.0097
2	0.0444	0.027	0.0097
3	0.0444	0.027	0.0097

position. A polynomial relationship between the voltage command input V_o to the valve and the effective valve open area u is determined from open loop experiments described in section 5.5 as,

$$V_o = \begin{cases} a_0 + a_1 u + a_2 u^2 + a_3 u^3 & \text{if } u \geq 0 \\ b_0 + b_1 u + b_2 u^2 + b_3 u^3 & \text{if } u < 0 \end{cases} \tag{7.111}$$

where the polynomial coefficients a_i and b_i with $i \in (0, 1, 2, 3)$ for all the six valves are as given in tables 7.2 and 7.3 for the right and the left leg respectively.

Table 7.2: Coefficients in the regression model of the servo valves used on the right leg

Parameter	Joint 1	Joint 2	Joint 3
a_0	4.9	4.82	5.46
a_1	5.265e6	3.9291e6	3.531e6
a_2	6.686e12	5.5811e12	2.668e12
a_3	4.6176e18	7.8581e18	1.8195e18
b_0	5.1	5.05	5.85
b_1	5.054e6	5.473e6	3.4548e6
b_2	-5.928e12	-1.489e13	-1.8264e12
b_3	6.744e18	2.1829e19	1.6756e18

Velocities of both the crawler and the PHANToM(TM[1]) are estimated by assuming constant acceleration and by using a high gain observer on the position measurement of the actuator on each joint. The observer dynamics and the observer gains are as described in section 5.5.

The controller gains are selected by using an approach similar to the one presented in section 5.5 for single-DOF system. The gains $\mathbf{\Lambda_2}$ and $\mathbf{\Lambda_3}$ on the torque observer

Table 7.3: Coefficients in the regression model of the servo valves used on the left leg

Parameter	Joint 1	Joint 2	Joint 3
a_0	4.863	5.25	4.9
a_1	3.823e6	6.889e6	4.26381e6
a_2	3.1738e12	2.0289e13	3.9525e12
a_3	1.8464e18	3.075e19	2.6115e18
b_0	5.1	5.05	5.28
b_1	5.4503e6	8.3498e6	8.11174e6
b_2	-1.008e13	-3.1645e13	-3.351e13
b_3	1.289e19	5.622e19	6.3876e19

in Eq. (7.67) are selected to be high enough to achieve quick estimation of the torque $\boldsymbol{\tau_{ex}}$. The gain $\boldsymbol{K_p}$ on position error $\boldsymbol{q_E}$ and the gain $\boldsymbol{K_d}$ on reference velocity $\boldsymbol{e_v}$ in Eq. (7.65) are respectively selected to be high enough to achieve quick regulation of position error $\boldsymbol{q_E}$ and the reference velocity error $\boldsymbol{e_v}$ to zero. The feed-forward command input corresponding to the velocity of the haptic device ($\boldsymbol{\Gamma_3^{-1} R^T(q)\dot{q}_p}$) ensures that the actuator force vector $\boldsymbol{F_a}$ has the correct direction. As a result, the crawler and the PHANToM(TM[1]) move in the same direction. The feedback gain $\boldsymbol{K_f}$ on the actuator force error $\tilde{\boldsymbol{F}}$ is thus not required to be high for regulating $\tilde{\boldsymbol{F}}$ to zero. The magnitude of the observer and the controller gains is listed in table 7.4.

Experimental results from tele-operation operation of the crawler legs are presented in the following subsections.

Tele-operation and interaction with a hard surface

For the experiment reported in this subsection, the crawler legs are remotely commanded to move in its task space, and then hit a metal wall at arbitrary intervals. A hard metal surface as shown in Fig. (7.9) is placed in the path of the crawler leg to evaluate interaction with a hard surface. In the interest of brevity, experimental results from operation of the left front leg of the crawler are only reported in this section. Similar results were obtained from operation of the front right leg. The experimental results reported in this section were conducted at an air pressure of $6.894e5 N/m^2$ ($100 psi$).

Table 7.4: Parameters used in the implementation of the controller

Parameter	Magnitude
$\boldsymbol{K_p}$	2.5425*diag(1,1,1)
$\boldsymbol{K_p}$	0.14*diag(2,0.5,0.5)
$\boldsymbol{K_f}$	0.0003*diag(3.5,2.5,3.3)
$\boldsymbol{L_1}$	40*diag(2,20,0.5)
$\boldsymbol{\Lambda_1}$	diag(4.1425,3.7425,2.9425)
$\boldsymbol{\Lambda_2}$	0.8*diag(33,140,30)
$\boldsymbol{\Lambda_3}$	diag(1,1,1)
ε	0.1
ρ	150
η	3.5

For the position commands provided by the human operator at the PHANToM(TM^1) device, Fig. (7.10) illustrates the co-ordination achieved between the PHANToM(TM^1) and the crawler joint angles expressed in the crawler joint space. The figure shows good co-ordination between the commanded joint angles at the PHANToM(TM^1) and the crawler joint angles, both during motion in free space and when interacting with a hard surface. The position data shows that no oscillations are induced in the crawler position due to the sudden interaction with a hard surface and the interaction is stable. For the experimental data shown in Fig. (7.10), the root mean square value of the error in the position of the tip of the crawler leg is about $5mm$, which is well within the foot tip diameter of $25.4mm$.

From the velocity data in Fig. (7.11) it can be noticed that the shoulder joint of both the PHANToM(TM^1) and the crawler comes to rest ($\dot{\theta}_1 = 0$) immediately after hitting the hard surface ($184.2s \leq t \leq 186.1s$, $187.2s \leq t \leq 189s$ and $195.3s \leq t \leq 197.3s$). This corroborates the earlier conclusion that sudden interaction with hard surface is stable.

The torque vector $\boldsymbol{\tau_a}$ applied at the joints of the crawler and the desired actuator torque vector $\boldsymbol{\tau_a^d}$ are as shown in Fig. (7.12). The magnitude of $\boldsymbol{\tau_a^d}$ is fairly low during

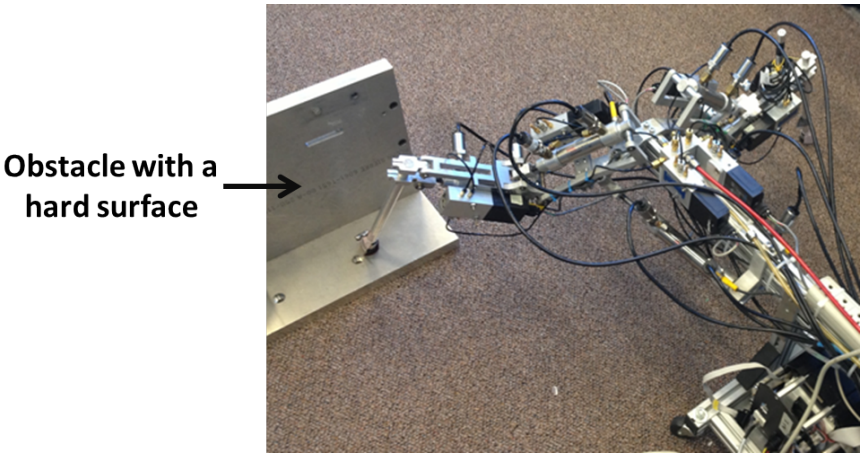

Figure 7.9: The experimental set-up used to verify stability when the crawler interacts with hard surfaces

operation in free space. As the obstacle is along the shoulder joint, the torque τ_1 on this joint increases substantially when interacting with hard surface. During motion in free space, and when interacting with hard surface, the actuator torque vector $\boldsymbol{\tau_a}$ tracks the desired actuator torque vector $\boldsymbol{\tau_a^d}$ fairly well. The lack of oscillation in the actuator torque when interacting with hard surface again confirms stability of interaction. Since the tele-operator is at rest when interacting with the metal surface, the high actuator torque corresponds to the reaction torque due to increase in the input human torque $\boldsymbol{\tau_h}$ ($\boldsymbol{\tau_{h_p}}$ in the crawler joint space) on the PHANToM(TM^1) dynamics in Eq. (7.14). The magnitude of increase in the reaction torque provide haptic information to human operator about the nature of interaction with the obstacle thus facilitating suitable response.

Bilateral operation

To investigate bilateral operation, position commands to the tele-operator were provided by moving the crawler leg, with no human interaction at the PHANToM(TM^1) device ($\boldsymbol{\tau_h} = \mathbf{0}$ in Eq. (7.14)). In this experiment, the input human torque on the crawler legs with be part of the external un-modeled torque $\boldsymbol{\tau_{e_c}}$ on the crawler leg dynamics in Eq. (7.2) and there is no interaction with the interface for human power amplification

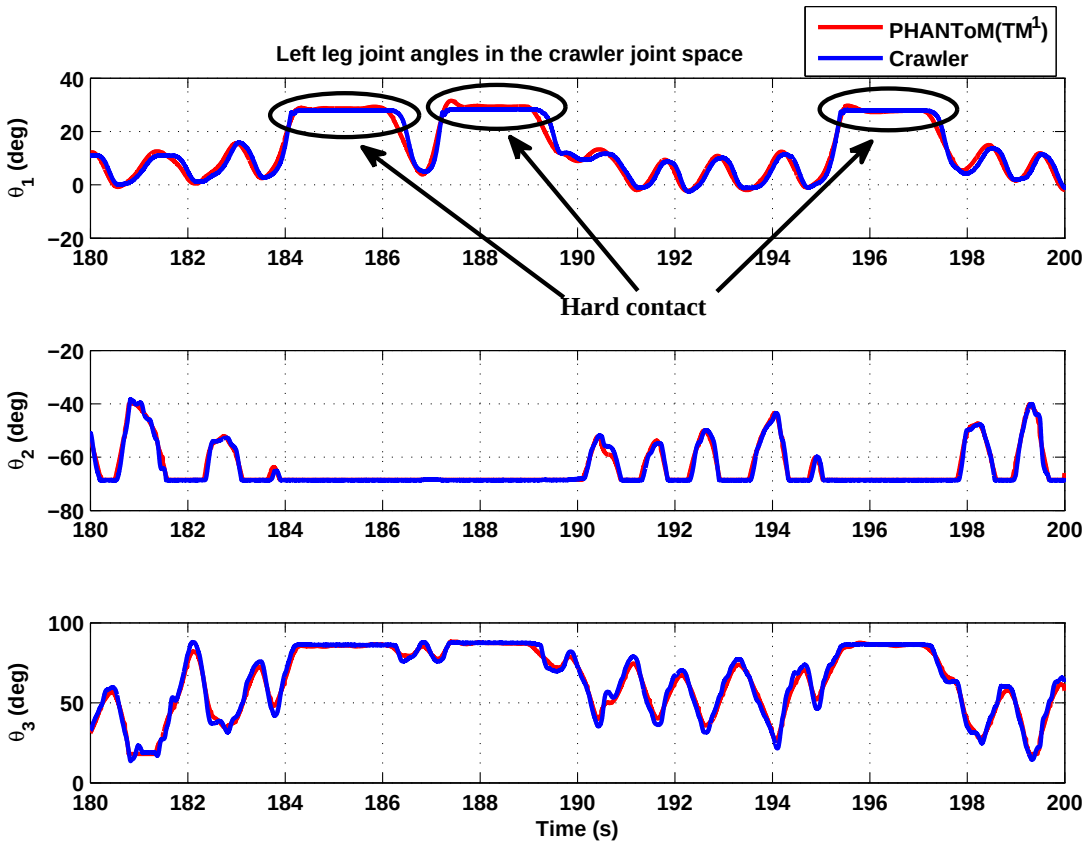

Figure 7.10: Co-ordination between the joint angles of the left leg of the crawler with the commanded angles at the PHANToM(TM), when moving in free space and then suddenly interacting with a hard surface

i.e $\boldsymbol{\tau_{h_e}} = \mathbf{0}$. Under bilateral operation, the PHANToM(TM^1) is expected to follow the position commands at the crawler leg. Note that in this case the role of the master and the slave systems are reversed. Good tracking in this mode of operation confirms that suitable haptic feedback force is provided at the PHANToM(TM^1) for the human operator. Again, for brevity of presentation, results from experiments on the left leg of the crawler are only provided. Similar results were obtained for experiments with the right leg. All the experiments to test bilateral operation were conducted at an air pressure of $6.894e5 N/m^2$ $(100 psi)$.

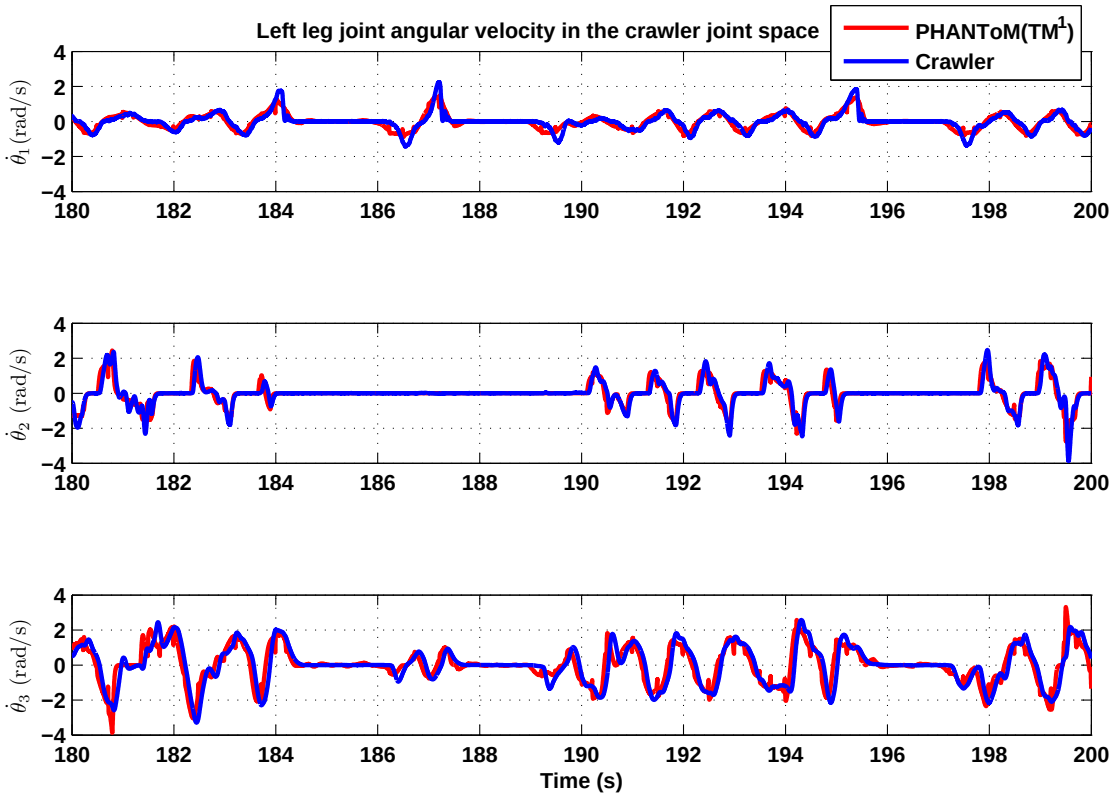

Figure 7.11: Co-ordination between the angular velocity of the left leg joints of the crawler with the commanded angular velocity at the PHANToM(TM), when moving in free space and then suddenly interacting with a hard surface

During the experiment, the crawler leg is arbitrarily moved in its task space by a human operator. The resulting crawler leg joint angle vector $\boldsymbol{q}$, and the PHANToM(TM^1) joint angle vector $\boldsymbol{q_p}$ expressed in the crawler joint space, are shown in Fig. (7.13). The $r.m.s$ valve of the error in the foot tip position corresponding to these joint angles is calculated to be about $7mm$. This error is again significantly lower than $25.4mm$, which corresponds to the diameter of the foot tip. The velocity tracking results from this experiment are as shown in Fig. (7.14). These results demonstrate good co-ordination confirming the ability to achieve bilateral tele-operation.

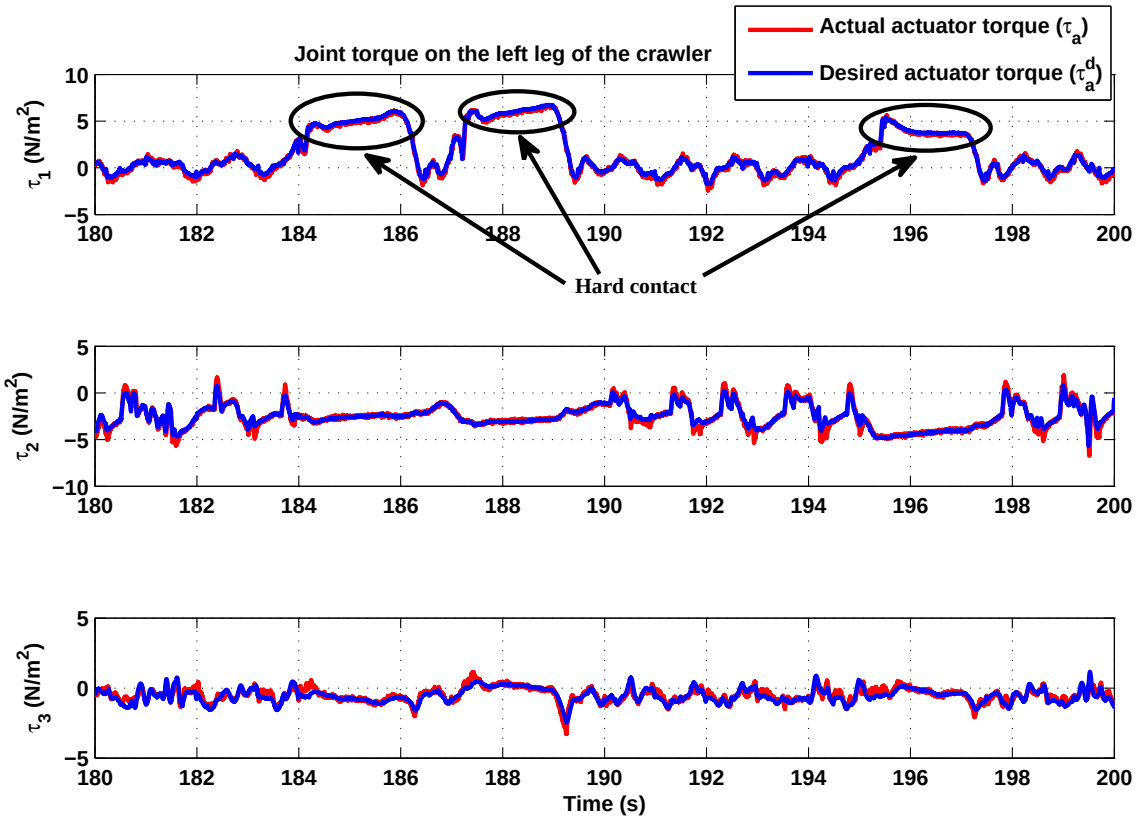

Figure 7.12: Comparison of the applied actuator torque $\boldsymbol{\tau_a}$ tracking with the desired actuator torque $\boldsymbol{\tau_a^d}$, when moving in free space and then suddenly interacting with hard surface

During this experiment, the generated actuator torque vector $\boldsymbol{\tau_a}$ tries to oppose the input torque from the human operator used to provide the input position commands. This can be noticed from the actuator torque information provided in Fig. (7.15). Consider the motion of the shoulder joint angle represented by θ_1 in Fig. (7.13). It can be noticed from this figure that between the time of $88s$ and $90s$, the joint angle θ_1 begins to increase due to input from the human operator. From the actuator torque information in Fig. (7.15) it can be seen that during this time ($88s < t < 90s$), as the joint angle θ_1 continues to increase, the applied actuator torque τ_1 attains a negative

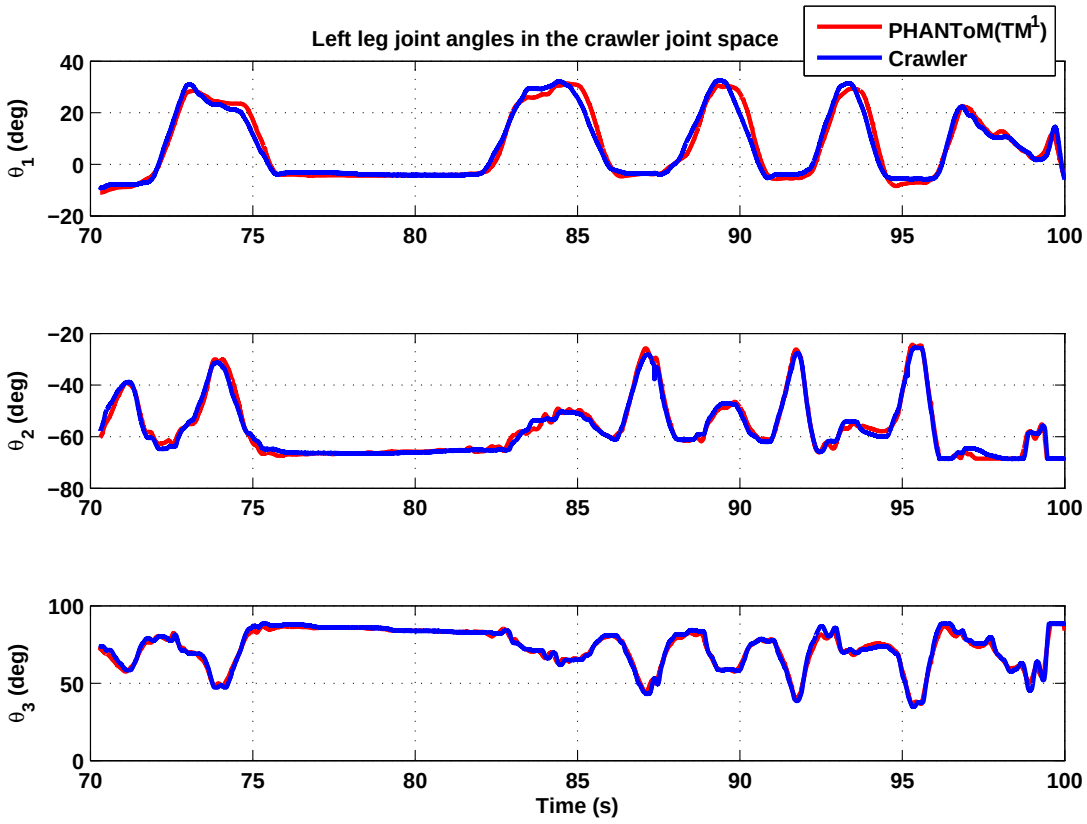

Figure 7.13: Co-ordination between the joint angles on the left leg of the crawler and the PHANToM(TM) in the crawler joint space, when the position commands to the tele-operator are provided by moving the crawler leg

value, opposing the torque applied by the human operator. As shown in Eq. (7.45), the feedback torque $\boldsymbol{\tau_{a_p}}$ on the PHANToM(TM^1) is designed to be negative of the scaled actuator torque ($-\frac{\tau_a}{\rho}$), it experiences a positive torque and thus moves in the direction of position commands provided by the human operator on the crawler leg.

Walking the crawler on level ground

In the current configuration, only the front two legs of the crawler are functional. A cart carrying the processors and power supply for the valves and the sensors is attached

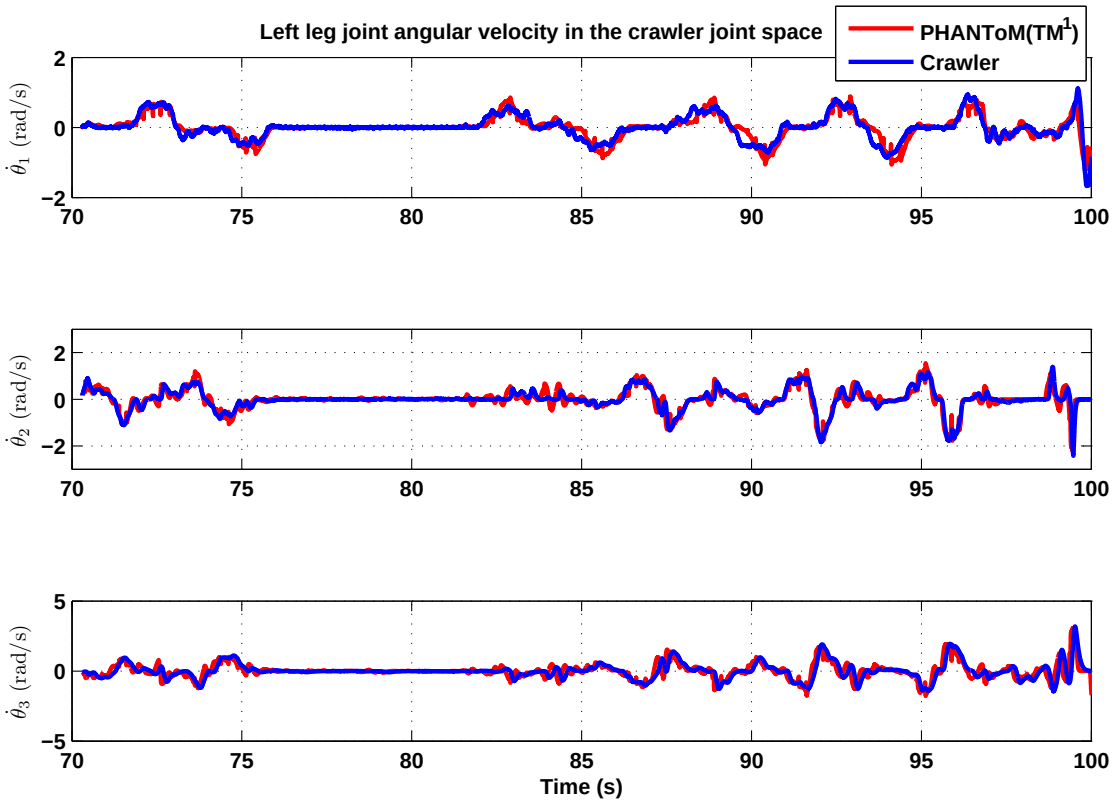

Figure 7.14: Co-ordination between joint angular velocities of joints on the left leg of the crawler and the PHANToM(TM), expressed in the crawler joint space, when input position commands are provided by moving the crawler leg

at the rear end of the crawler chassis. The cart is mounted on a pair of wheels, with the front pair being caster wheels. Due to this construction, it was very difficult to move the crawler forward along a straight line by using one leg at a time. Therefore the gait pattern used to tested the controller involved moving both the legs of the crawler forward at the same time, much like the *butterfly stroke* in swimming.

A key issue in the implementation of the controller is lack of sensors to measure contact forces when the crawler leg pushes against the ground. During this phase of walking, the inertia of crawler as seen by the actuators increases considerably, as the

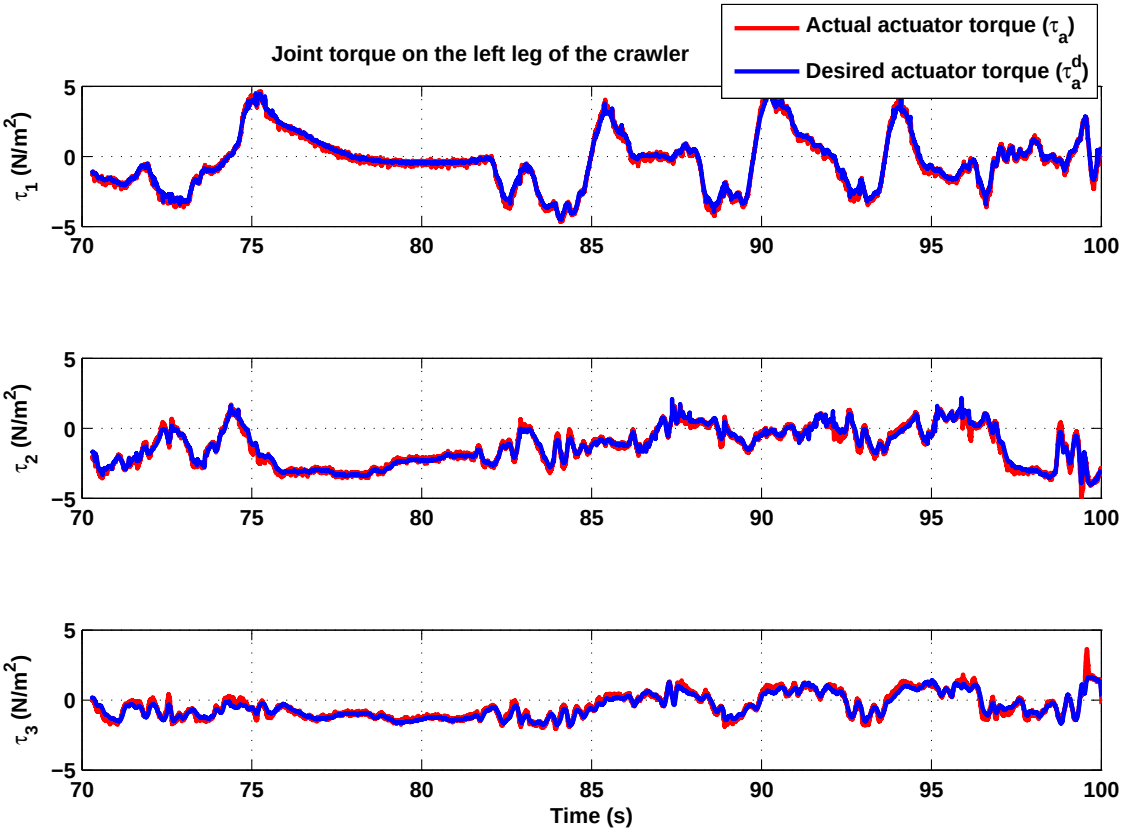

Figure 7.15: Comparison of the desired actuator torque vector $\boldsymbol{\tau_a^d}$ and the actuator torque $\boldsymbol{\tau_a}$ applied at the crawler joints while responding to the input position commands provided on the crawler leg

actuators have to move the mass corresponding to the entire cart. In the section 7.5 on controller design, it was stated that the unknown vector $\boldsymbol{\tau_{ex}}$ consisting of external interaction torques is estimated using direct adaptive control. However, due to the difference in inertia between the crawler legs and the entire cart, the magnitude of observer gains $\boldsymbol{\Lambda_2}$ and $\boldsymbol{\Lambda_3}$ presented in table 7.4, selected for control of the leg dynamics only, are not sufficiently high for properly estimating ground reaction forces during push-off required for forward motion. Poor estimation of contact forces resulted in significant co-ordination error. To improve the tracking performance of the observer, the estimation

gains $\mathbf{\Lambda_2}$ and $\mathbf{\Lambda_3}$ are scheduled to be significantly higher when the crawler is pushing off the ground. These gains are used only when the position of the foot tip is at or below the ground level. In this experiment, the supply pressure to the pneumatic actuators was also increased to $20.68e5N/m^2$ $(300psi)$ for generating sufficient force required to move the weight of the entire cart.

The implementation results from walking the crawler are shown in Fig. (7.16) to Fig. (7.21). Co-ordination of the crawler and the PHANToM(TM^1) joint angles on the left and the right leg are shown in Fig. (7.16) and Fig. (7.19) respectively. These results show good co-ordination between the commanded angles at the PHANToM(TM^1), and the resulting crawler joint angles. The $r.m.s$ value of the foot tip position error for each leg is about $7mm$, which again is quite small compared to the foot diameter of $25.4mm$. The corresponding angular velocity co-ordination achieved on the left leg and the right leg of the crawler are shown in Fig. (7.17) and Fig. (7.20) respectively. The velocity plots show some oscillations when pushing off the ground. This could be due to high estimation gains used for estimating the interaction forces with the ground. A force sensor at the foot of the crawler to provide an accurate measure of interaction forces will improve the interaction stability. Comparison between the actuator torque $\boldsymbol{\tau_a}$ and the desired actuator torque $\boldsymbol{\tau_a^d}$ is as shown in Fig. (7.18) and Fig. (7.21) for the left leg and the right leg respectively. These results show fairly good tracking between $\boldsymbol{\tau_a}$ and $\boldsymbol{\tau_a^d}$.

On-site human power amplification

In this set of experiments, the crawler leg is operated as a multi-DOF human power amplifier and is used to move an inertial load. Human force vector $\boldsymbol{F_{h_e}}$, corresponding to torque vector $\boldsymbol{\tau_{h_e}}$ in the crawler joint space in Eq. (7.2), is applied on an interface with a force sensor. As shown in Fig. (7.3), this interface is placed on the second joint of the right leg of the crawler. For the experiments reported in this section, the human torque $\boldsymbol{\tau_h}$ on the PHANToM(TM^1) dynamics in Eq. (7.14) is zero. A $2.27kg$ $(5lbs)$ lead block attached to an aluminum metal rod is used as the inertial load. A metal wire wrapped around the rod is used to engage the inertial load with an L-bracket attached on the crawler right leg for this experiments. By exerting suitable forces on the interface, the load is picked-up at a location, moved some distance in the crawler

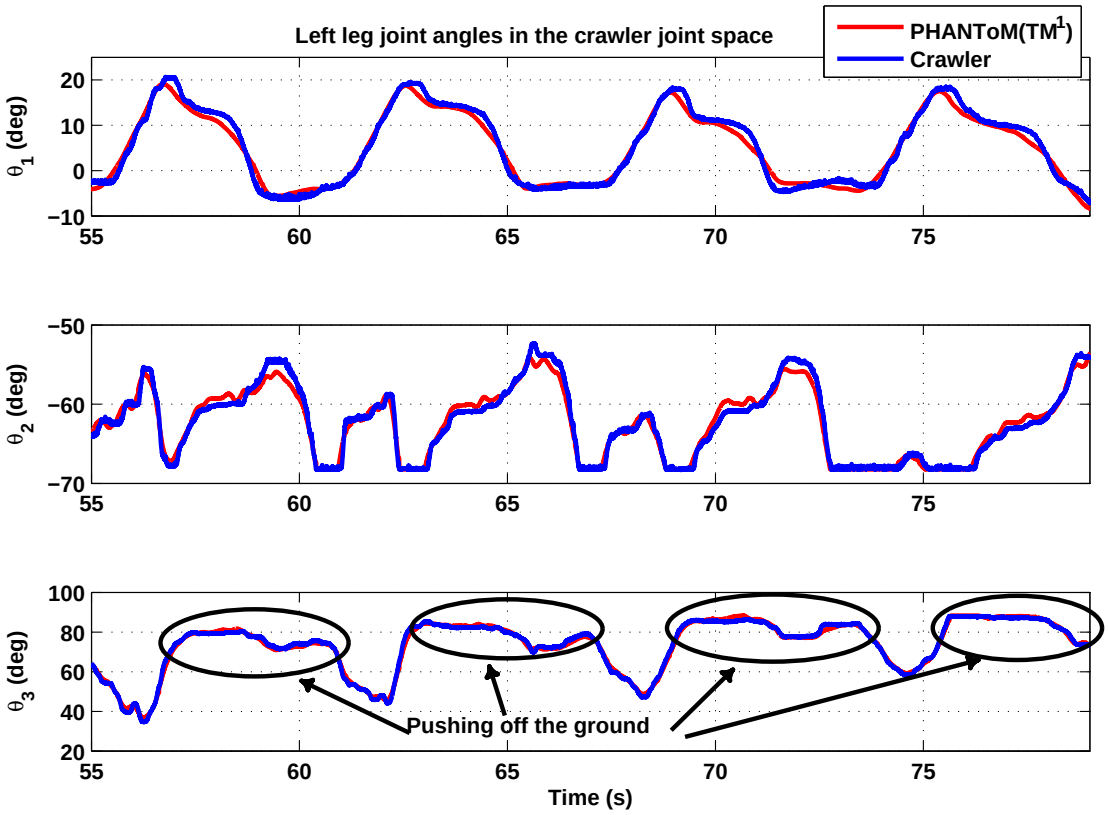

Figure 7.16: Co-ordination between the crawler joint angles and the PHANToM(TM) joint angles in the crawler joint space on the left leg of the crawler when walking the crawler by providing command inputs at the PHANToM(TM)

task space and then dropped off. For the experimental results reported in this section, the amplification factor η on the input human torque is set to be 3.5.

Comparison of the desired actuator torque vector $\boldsymbol{\tau_a^d}$ required for amplifying the input human power and the applied actuator torque vector $\boldsymbol{\tau_a}$ is as shown in Fig. (7.22). From this figure it can be seen that the torque $\boldsymbol{\tau_a}$ provided by the actuator is very close in magnitude to the desired torque $\boldsymbol{\tau_a^d}$ required for human power amplification. Due to bilateral nature of operation, the movement of crawler leg will induce corresponding motion in the PHANToM(TM^1) device. Co-ordination between the crawler joint angles

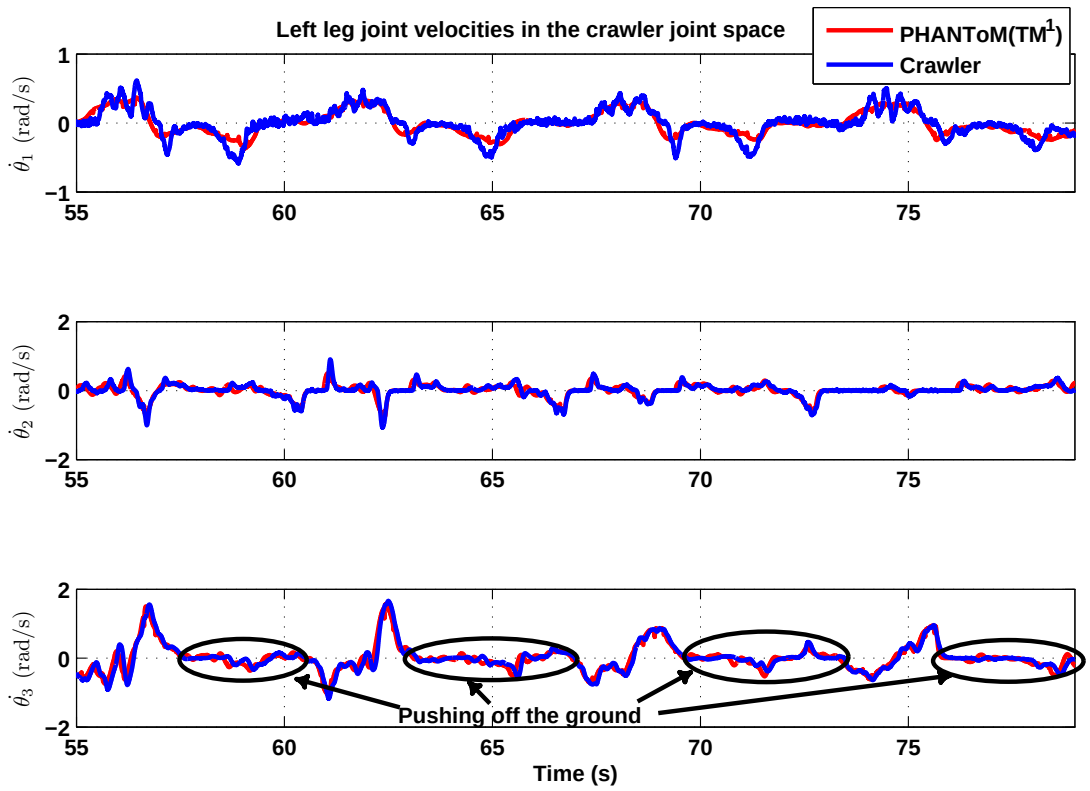

Figure 7.17: Co-ordination between the crawler joint angular velocity and the PHANToM(TM) joint angular velocity in the crawler joint space on the left leg of the crawler when walking the crawler by providing command inputs at the PHANToM(TM)

and the PHANToM(TM^1) joint angles, expressed in the crawler joint space, is shown in Fig. (7.23). The *r.m.s* value of position error in the foot tip is $15mm$, again well within the foot tip diameter of $25.4mm$. Joint angular velocity co-ordination between the PHANToM(TM^1) device and the crawler leg is as shown in Fig. (7.24). As seen in this figure, the achieved velocity co-ordination is not as good as the data reported in earlier experiments, especially along the third joint angle, wherein the PHANToM(TM^1) velocity has some high frequency oscillations. Structural oscillations in the crawler leg (and consequently the interface located on the second link of the crawler) result in an

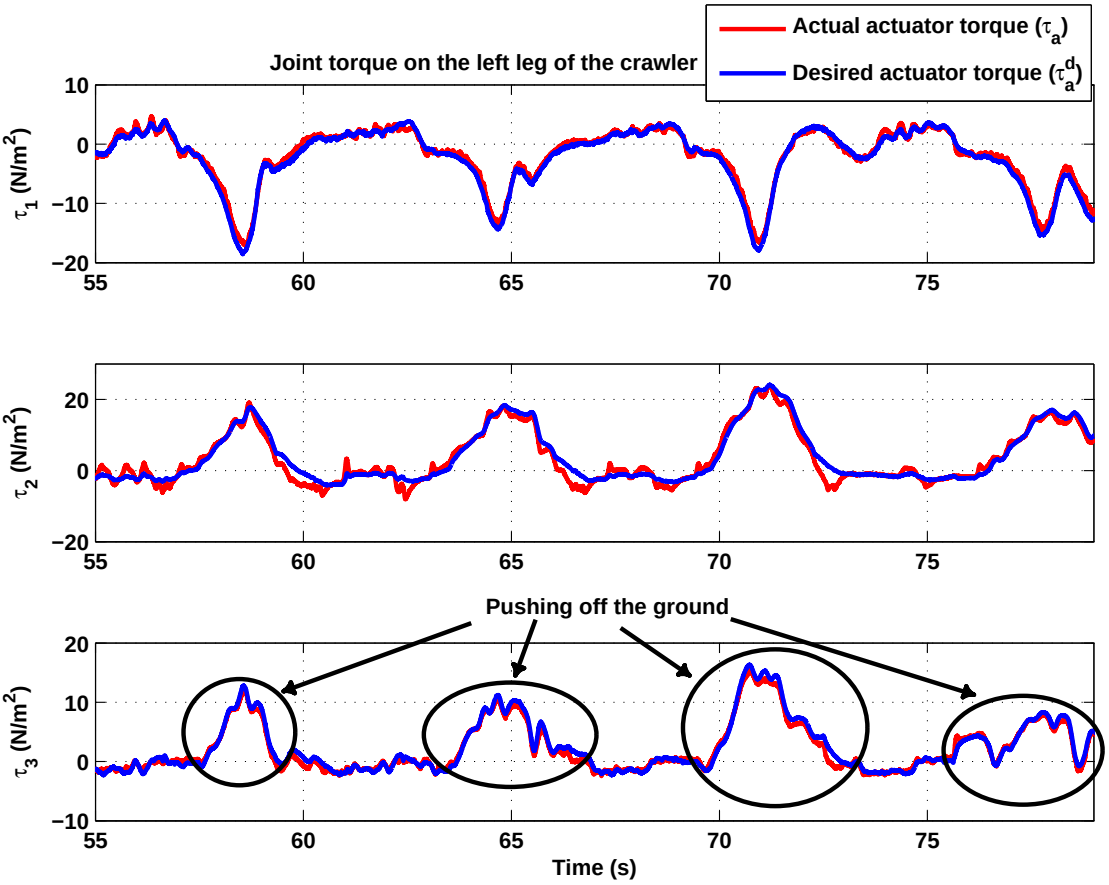

Figure 7.18: Comparison of the desired actuator torque $\boldsymbol{\tau_a^d}$ and the actuator torque $\boldsymbol{\tau_a}$ applied at the joints of the left leg of the crawler when walking the crawler by providing command inputs at the PHANToM(TM)

oscillatory input torque ($\boldsymbol{\tau_{h_e}}$) from the interacting human operator. As this input is amplified and applied on the PHANToM(TM^1), oscillations with higher amplitude are caused in the PHANToM(TM^1) velocity $\boldsymbol{\dot{q}_p}$. These oscillations in the PHANToM(TM^1) velocity form a positive feedback loop with the crawler leg dynamics, resulting in less satisfactory tracking performance. This issue will have to be addressed in future research efforts through effective design of interface, or through active compensation of these oscillations (either at the PAHNToM(TM^1) or the crawler).

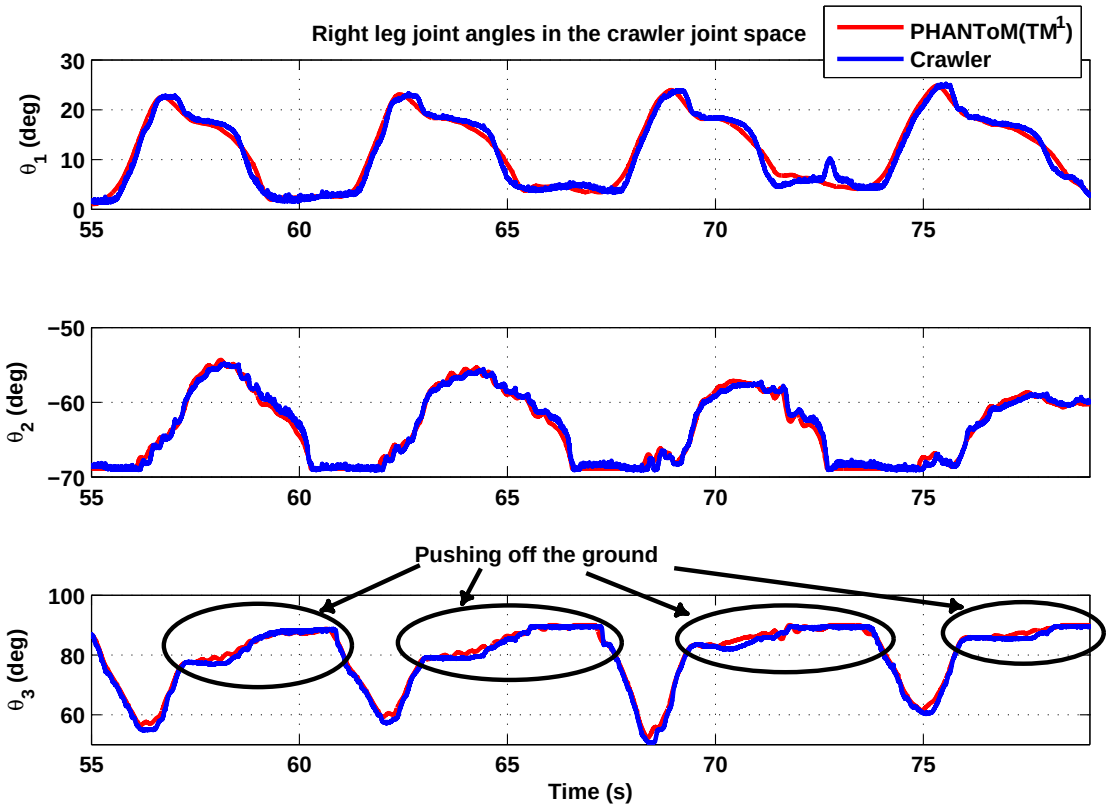

Figure 7.19: Co-ordination between the crawler joint angles and the PHANToM(TM) joint angles in the crawler joint space on the right leg of the crawler when walking the crawler by providing command inputs at the PHANToM(TM)

7.8 Summary

In this chapter, a framework for tele-operation between single-DOF systems presented in chapter 6 is applied to achieve bilateral tele-operation between two multi-DOF systems. The master system is a 3-DOF PHANToM(TM[1]) haptic device with electro-mechanical actuators. The slave system is a pneumatic actuated crawling robot, with 3-DOF on each leg. As only the front two legs of the crawler were functional, bilateral

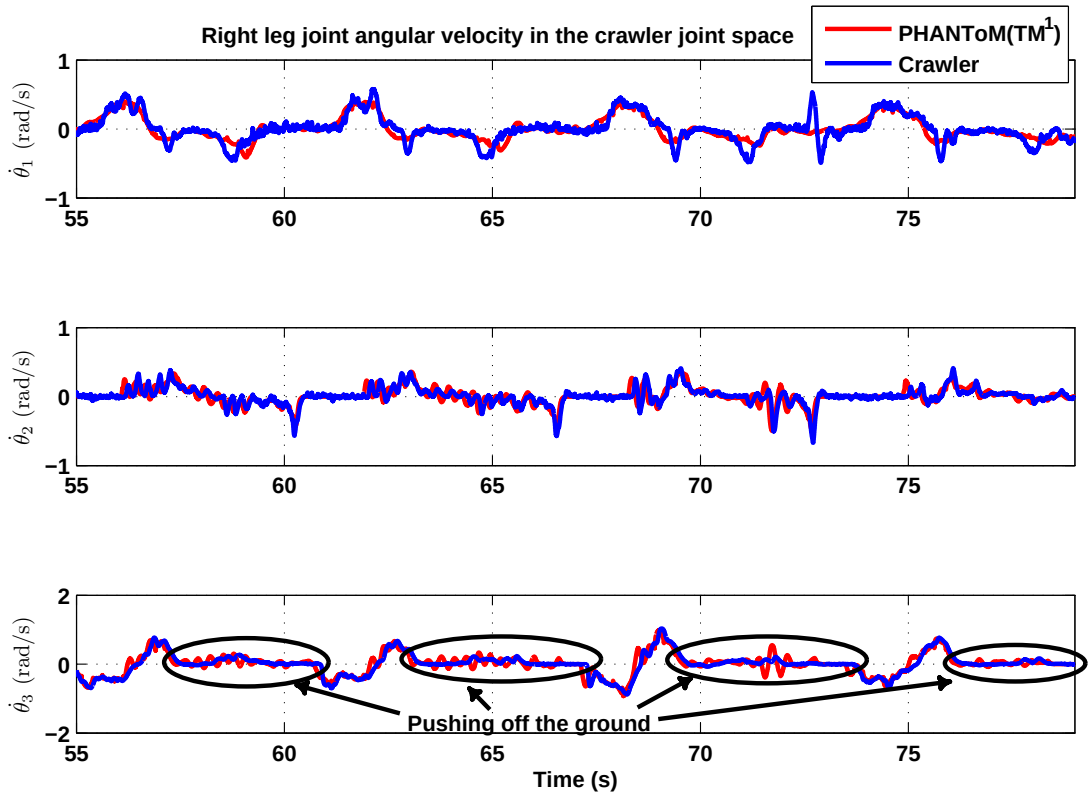

Figure 7.20: Co-ordination between the crawler joint angular velocity and the PHANToM(TM) joint angular velocity in the crawler joint space on the right leg of the crawler when walking the crawler by providing command inputs at the PHANToM(TM)

tele-operation of these legs with a pair of PHANToM(TM^1) haptic devices has been reported in this chapter. The tele-operation problem was formulated to provide amplified energetic passivity. Direct adaptive control is used to estimate the external un-modeled torques acting on the tele-operator. Controller for tele-operation of the front legs was developed by assuming that the thermodynamics in the pneumatic actuator are adiabatic in nature.

The controllers were evaluated in different modes of operation including, bilateral tele-operation, interaction with hard surface and on-site human power amplification.

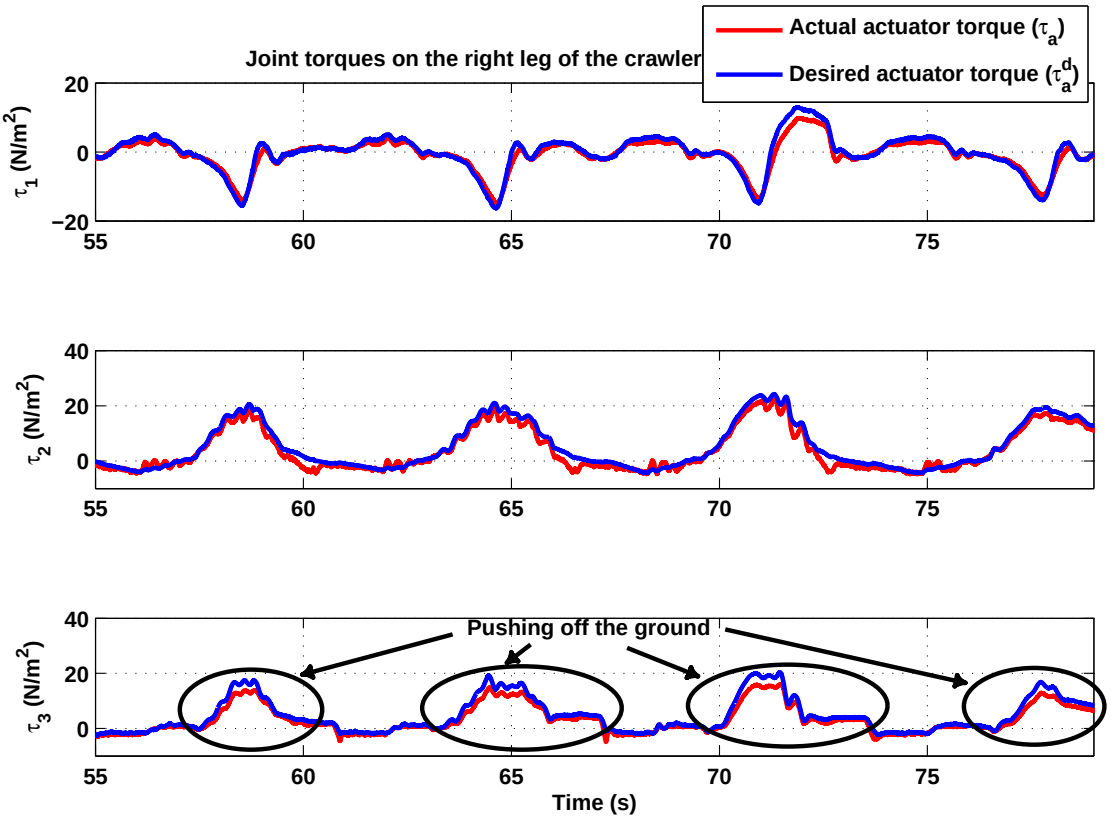

Figure 7.21: Comparison of the desired actuator torque $\boldsymbol{\tau_a^d}$ and the actuator torque $\boldsymbol{\tau_a}$ applied at the joints of the right leg of the crawler when walking the crawler by providing command inputs at the PHANToM(TM)

The experimental results can be summarized as follows,

1. The proposed controller was very effective in achieving desired bilateral tele-operation of the crawler legs in free space. The $r.m.s$ value of the position error was less than $7mm$, which is very reasonable considering the diameter of the foot tip of the crawler leg is about $25.4mm$.

2. The tele-operator demonstrated stable interaction when suddenly interacting with a hard metal wall.

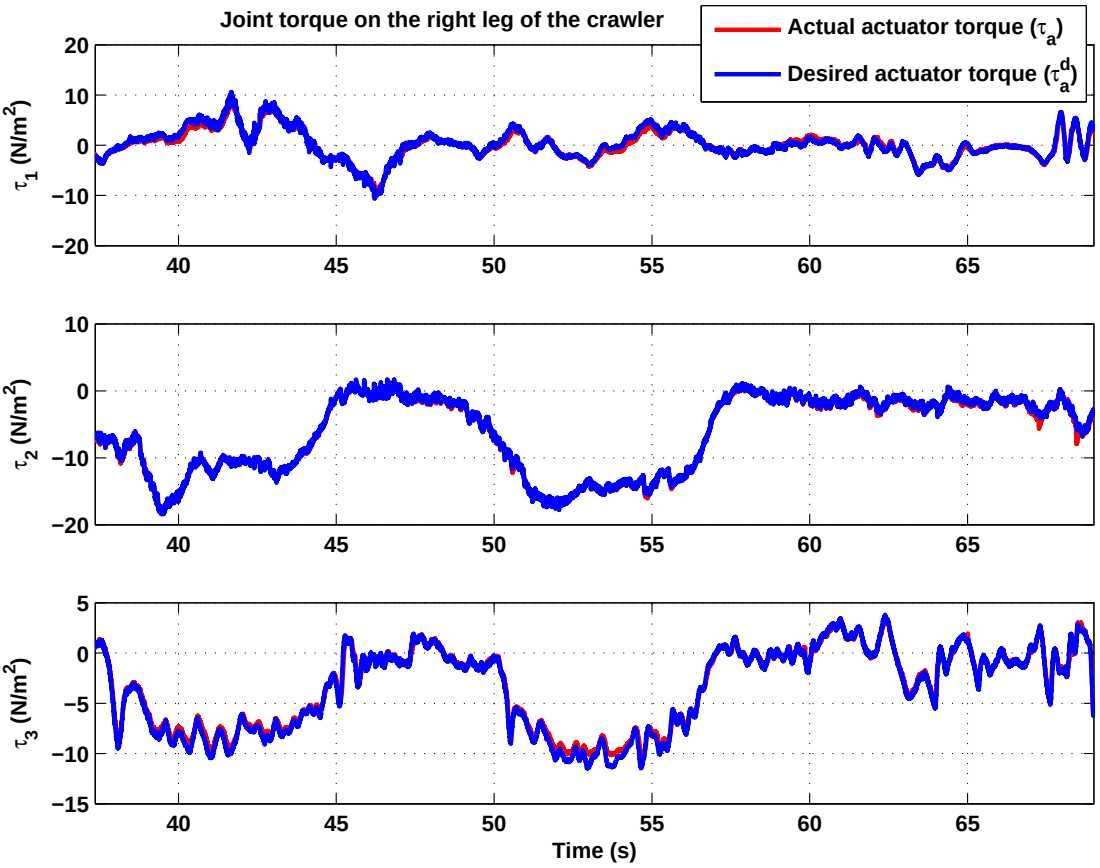

Figure 7.22: A comparison of the desired actuator torque with the applied actuator torque when a human operator applies torque on the power amplification interface on the crawler leg for moving a load of $5kgs$

3. When operated in the walking mode, the $r.m.s$ value of the position error was around $7mm$, again a reasonable number compared to the crawler leg foot tip diameter of $25.4mm$. However, the joint angular velocities were oscillatory when the crawler legs pushed off the ground. This could be due to inadequate estimation of the ground reaction forces induced by the entire weight of the cart.

4. When operated as a multi-DOF human power amplifier, the torque vector $\boldsymbol{\tau_a}$ provided by the actuator corresponds well with the desired actuator torque $\boldsymbol{\tau_a^d}$.

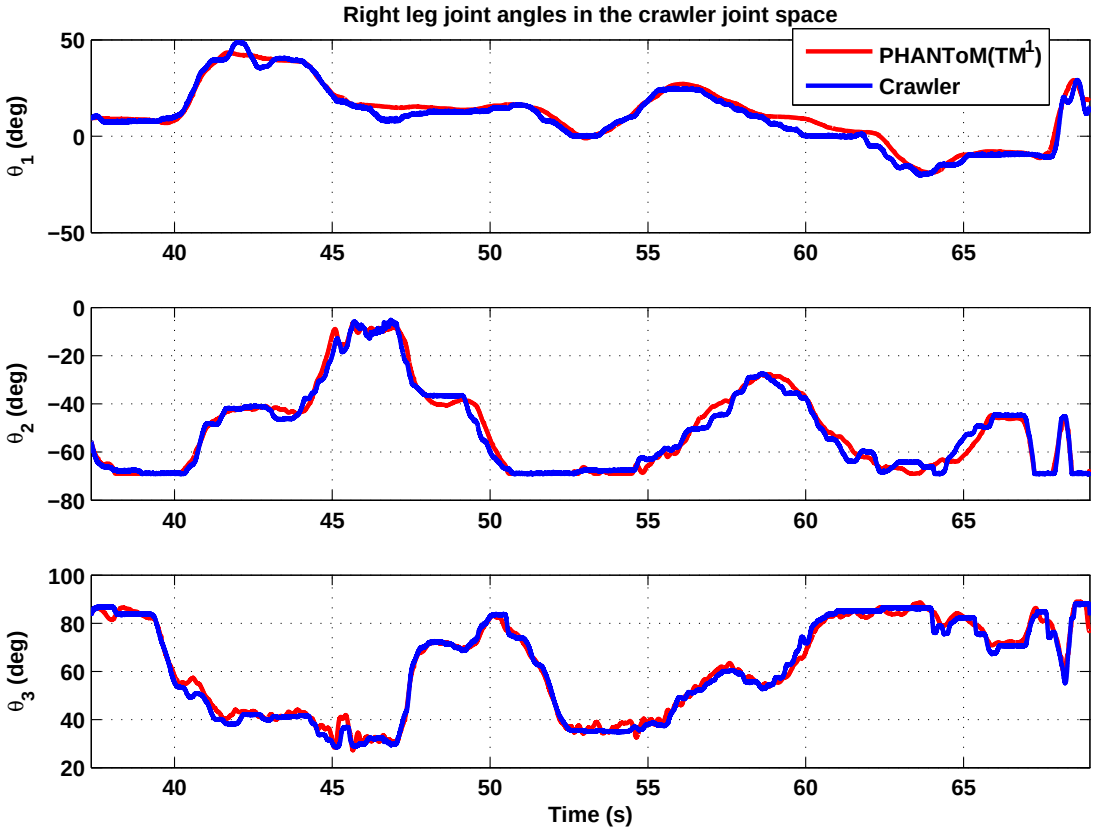

Figure 7.23: Co-ordination achieved between the crawler joint angles and the PHANToM(TM) joint angles in the crawler joint space while using the crawler leg to amplify input human power to move a load of $5kgs$

Therefore the experimental results demonstrate efficacy of the proposed controller in the various modes of operation. The results presented in this chapter also demonstrate that the framework presented in chapter 5 for single-DOF systems can be conveniently extended to achieve bilateral tele-operation of systems with multiple degrees of freedom, dissimilar kinematics and different actuating mechanisms. In the next chapter, independent metering of air flow to the two chambers of a pneumatic actuator is investigated for improving efficiency of operation of pneumatic actuators.

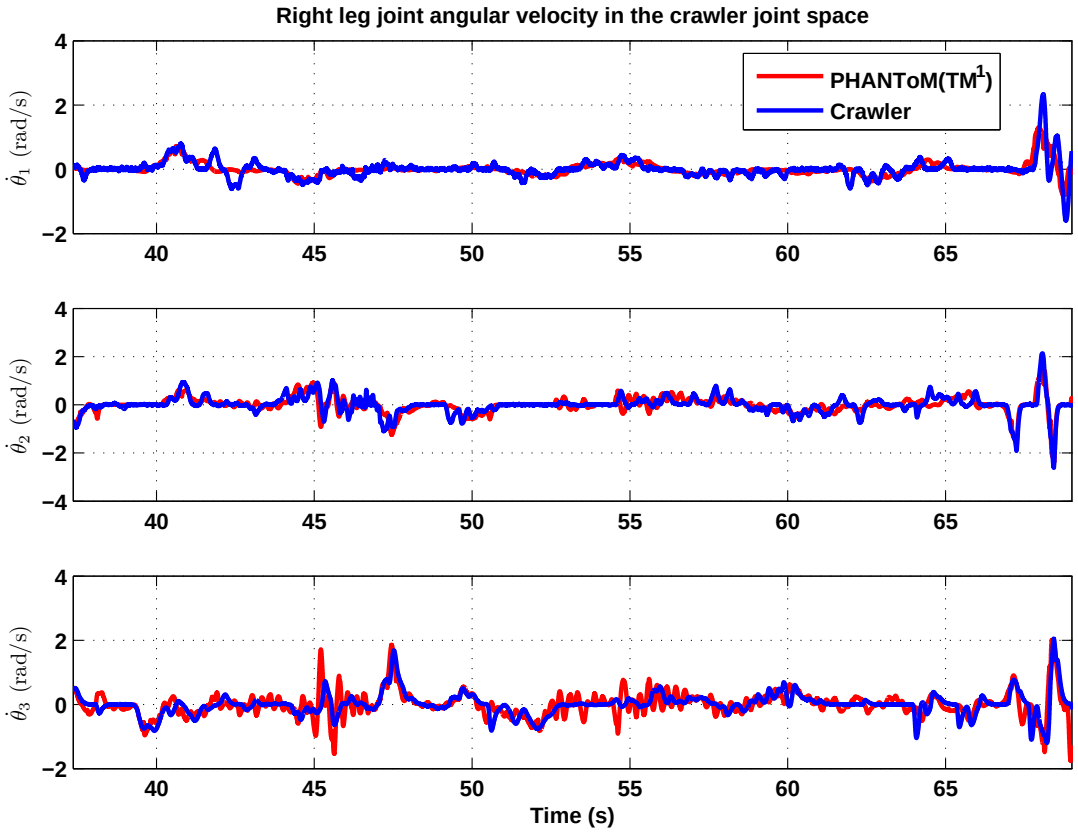

Figure 7.24: Co-ordination achieved between the crawler joint angles and the PHANToM(TM) joint angular velocity in the crawler joint space while using the crawler leg to amplify input human power to move a load of $5kgs$

Chapter 8

Efficiency improvement through independent metering of pneumatic actuator chambers

The high power density of fluid powered actuators can enable the design of compact human interactive systems amenable for mobile operation. In such applications with limited supply of pressurized air, the time of operation can be increased by improving the efficiency of operation. In typical pneumatic applications, a single valve is used to meter the air flow to the actuator. A source of energy loss in such a configuration is the discharge of high pressure air to the atmosphere. Efficiency of operation can be improved by mitigating this loss. As presented in chapter 2, previous work on efficiency improvement by mitigating loss of high pressure air includes reuse of high pressure air through an accumulator [62] and using two-way valves to achieve cross-flow from the high pressure side to the low pressure side [63].

In a proportional servo-valve, the flow areas metering the flow in and out of the actuator are mechanically coupled. As a result, it is impossible to control the pressure in both chambers of the actuator independently. By using two separate valves, air pressure in individual actuator chambers can be controlled independently. This approach is referred to as independent metering. An illustration of a two-chambered actuator with independently metered chambers is as shown in Fig. (8.1). The force F_a from

the actuator shown in Eq. (3.1) depends on the differential pressure between the two chambers. With independent metering, the required actuator force F_a can be achieved, by reducing the pressures P_1 and P_2, while maintaining the same area weighted pressure differential. The pressures P_1 and P_2 required to output a certain force F_a can therefore be kept low by regulating the pressure in the chamber connected to the ambient to a low target pressure. As the air pressure discharged to the ambient is kept low, energy lost in this process is mitigated, thus improving efficiency of operation. The valve metering the air flow to the chamber connected to the supply pressure is controlled to perform the desired actuator task.

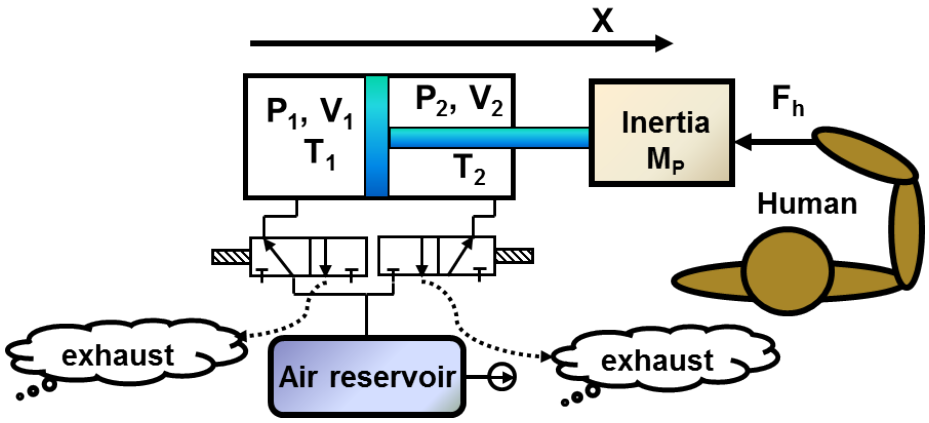

Figure 8.1: Operation of pneumatic actuator with two independent, 3-port 2-way proportional valves

In [11], independently metered pneumatic actuator is controlled to move along a desired trajectory, while maintaining the average pressure in both chambers to be around atmospheric pressure P_{atm}. In the current chapter, efficient operation of pneumatic actuator as a human power amplifier (presented in chapter 5) thorough independent metering is investigated. Human power amplification coupled with minimum operating pressure provides the two objectives that determine the command inputs to the two valves in Fig. (8.1). A function in terms of the error between the current pressure and a desired pressure is defined for the actuator chamber connected to the ambient pressure. The command input to the valve connecting the actuator chamber to the

ambient is designed so as to regulate this pressure error function to zero. When the direction of desired actuator force changes, the valves connecting the actuator chambers to supply pressure P_s and ambient pressure P_{atm} are swapped. Similar work involving force control with independently metered hydraulic actuator had been presented in [64]. The novelty of the approach proposed in this chapter is that the desired pressure in both chambers of the actuator, when connected to the ambient pressure, are defined such that the irrespective of the chamber connected to ambient pressure, the pressure error function exponentially converges to zero, whereas in the previous works [64], the desired pressure is arbitrarily defined, resulting in an error function dynamics that is not non-increasing. The valve connecting the actuator chamber to supply pressure can be controlled to meet the performance objective of the pneumatic actuator such as position tracking or force tracking. In this chapter, the input to the valve connecting the actuator chamber to air supply is designed to provide human power amplification.

The results presented in chapter 5 show that controllers designed by assuming either the adiabatic or the isothermal thermodynamic process have similar performance. Therefore, for the sake of simplicity, the controllers for both the pneumatic valves are designed in this chapter by assuming that the thermodynamic process in the actuator is isothermal.

In the following section, the experimental setup and the system dynamics are briefly presented. The control objectives for the two pneumatic valves used to independently meter the air flow rate are formally presented in section 8.2. The control input design for the two valves is presented in section 8.3. Experimental results comparing the performance of a single valve with that of independent metering are presented in section 8.4. The experimental results reveal that operation time can be substantially improved by independently metering the air flow rate to the actuator. Some concluding remarks are provided in section 8.5.

8.1 System model

The experimental setup used in this study is as shown in Fig. (8.2). It consists of a two-chambered pneumatic actuator with a force sensor mounted on top for measuring the input human force $F_h(t)$. A pair of pressure sensors are used to calculate the chamber

pressures P_1 and P_2. The actuator force F_a is determined from the chamber 1 air pressure P_1, the chamber 2 air pressure P_2 and the corresponding piston cross-sectional areas A_1 and A_2 as,

$$F_a = P_1 A_1 - P_2 A_2 - P_{atm} A_p = (P_1 - P_{atm}) A_1 - (P_2 - P_{atm}) A_2 \tag{8.1}$$

where P_{atm} is the atmospheric pressure and A_p is the rod cross sectional area exposed to atmospheric pressure. A portable air compressor is used as the reservoir of pressurized air for the experiment. Once fully charged, the compressor is turned off to avoid recharging during an experiment. Two, 3-position 2-way pneumatic servo valves are used to meter the air flow independently to the actuator chambers. The human force $F_h(t)$ in combination with the actuator force F_a moves the actuator piston in the vertical plane. During the experiment, the actuator is moved in the vertical plane until the reservoir is discharged to a pressure insufficient for providing the desired actuation force. For the purpose of comparing single valve metering with independent valve metering, the piston velocity $\dot{x}$ was kept very similar in both the experimental runs. The dynamics of the inertia being moved by the actuator is given by,

$$M_p \ddot{x} = F_h(t) + F_e(t) + F_a \tag{8.2}$$

where, x is the piston position, M_p is the piston inertia and $F_e(t)$ includes environment force such as gravity and un-modeled forces such as friction.

For air mass of m_1 and m_2 in chamber 1 and 2 respectively, and an air temperature of T_o, the pressure dynamics for the isothermal actuator are obtained from Eq. (3.81) in chapter 3 as,

$$\dot{P}_1 = \frac{\dot{m}_1 R T_o A_1}{V_1(x)} - \frac{P_1 \dot{V}_1(x)}{V_1(x)} \tag{8.3}$$

$$\dot{P}_2 = \frac{\dot{m}_2 R T_o A_2}{V_2(x)} - \frac{P_2 \dot{V}_2(x)}{V_2(x)} \tag{8.4}$$

For a pneumatic actuator with independently metered chambers, the air flow rate to the $i^{th} \in (1, 2)$ chamber of the isothermal actuator (chamber temperature $= T_o$) depends on the chamber pressure P_i and the effective valve area u_i open for air flow as defined in Eq. (3.26) and is given by,

$$\dot{m}_i = \Psi_i(P_i, u_i) u_i \tag{8.5}$$

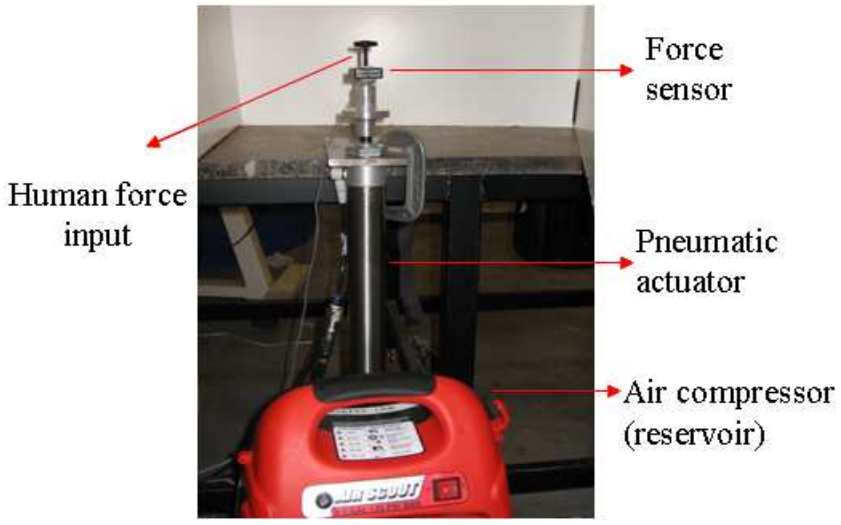

Figure 8.2: The experimental setup with an air compressor as a source of compressed air supply

where the nonlinear function $\Psi_i(P_i, u_i)$ is as defined in Eq. (3.27). The control objective for designing the appropriate valve input command u_i is presented in the following section.

8.2 Controller formulation

As each pneumatic actuator chamber is independently metered, there are two degrees of freedom in the controller design :

1. Command input to the valve connecting the actuator chamber to the ambient pressure P_{atm}
2. Command input to the valve connecting the actuator chamber to the supply pressure P_s

8.2.1 Framework for controller design

Ambient port valve command input: The force F_a exerted by the two-chambered actuator in Fig. (8.1) is as given in Eq. (8.1). To obtain positive actuator force,

chamber 1 is connected to the supply pressure P_s, while chamber 2 is connected to the ambient pressure P_{atm}. From Eq. (8.1) it can be seen that a desired positive force can be obtained for a smaller value of P_1 by maintaining P_2 at a low target pressure. When the direction of force changes, chamber 1 is now connected to the ambient pressure P_{atm}, while chamber 2 is connected to the supply pressure P_s. As the pressure P_1 in chamber 1 was not very high before the change in the direction of force F_a, the pressure P_2 in chamber 2 does not have to be very high to provide the desired negative force. By extending this analysis to further cycles of operation, it can be inferred that the maximum required pressure in both the actuator chambers can be lowered by maintaining a lower pressure in the chamber connected to the ambient pressure P_{atm}. Therefore the control objective for the valve connecting the pneumatic actuator chamber to ambient pressure is to maintain the chamber pressure at a target low pressure.

The initial pressure in the chamber connected to ambient pressure P_{atm} depends on the magnitude and direction of the desired force output from the pneumatic actuator. To prevent discrete change in the value of the error function at the point of switching the target pressure in the low pressure chamber has to be appropriately defined.

Supply port valve command input: The valve connected to the compressed air supply P_s is commanded to provide the air flow rate $\dot{m}_i$ required for achieving the desired human power amplification. As presented in section 5.1, the desired inertial dynamics of the power amplifier with an amplification factor of ρ is given by,

$$M_p\ddot{x} = (\rho + 1)F_h(t) + F_e(t) \tag{8.6}$$

with the desired external supply rate $s(F_h(t), F_e(t), \dot{x})$ defined as,

$$s(F_h(t), F_e(t), \dot{x}) := ((\rho + 1)F_h(t) + F_e(t))\dot{x} \tag{8.7}$$

satisfying the following passivity condition,

$$\int_0^t s(F_h(\tau), F_e(\tau), \dot{x})\ d\tau \geq -c_o^2 \tag{8.8}$$

In the above passivity condition c_o^2 represents the maximum energy that can be extracted from the system in the absence of any external inputs.

As presented in section 5.3.2, the controller design for achieving the supply rate corresponding to human power amplification is formulated as a velocity co-ordination

problem. The flow source at the fluid port of the chamber connected to the supply pressure is defined to be the sum of the velocity $\dot{x}_v$ of a virtual inertia and an active feedback signal u_{fb}. For an inertial mass of M_v, by defining the dynamics of the virtual inertia as,

$$M_v \ddot{x}_v = \rho F_h(t) - u_d - F_a \tag{8.9}$$

where u_d is included to guarantee passive operation, and on designing the feedback input u_{fb} to achieve velocity co-ordination between the dynamics of inertia M_p Eq. (8.2) and the virtual inertia M_v in Eq. (8.9) ($\dot{x} = \dot{x}_v$), the co-ordinated system dynamics are obtained as,

$$(M_p + M_v)\ddot{x} = (\rho + 1)F_h(t) + F_e(t) - u_d \tag{8.10}$$

For a very small magnitude of input signal u_d, the coordinated system dynamics in the above equation are similar to the desired power amplifier dynamics in Eq. (8.6). By designing the input u_d to be dissipative, the system with dynamics shown in Eq. (8.10) can be shown to satisfy the passivity condition in Eq. (8.8). Design of u_d is presented in section 8.3.3. The control objective for the valve connected to the supply pressure is therefore to achieve velocity co-ordination between the virtual mass M_v and the inertia M_p being moved.

8.2.2 Control objectives

The control objectives for the two valves can therefore be summarized as,

1. *Ambient side control objective* : Maintain a low pressure in the chamber ported to the ambient pressure

2. *Supply side control objective* : Co-ordination between the velocity $\dot{x}$ of the actual mass M_p, and the velocity $\dot{x}_v$ of the virtual inertia M_v

$$V_E \triangleq (\dot{x} - \dot{x}_v \to 0) \tag{8.11}$$

   while satisfying the passivity condition in Eq. (8.8).

Controller design to achieve the listed objectives are presented in the following section.

8.3 Controller design

8.3.1 Ambient port valve input design

To achieve positive actuator force ($F_a > 0$), chamber 2 is typically connected to ambient pressure. Chamber 1 is connected to the ambient pressure when the actuator force is negative ($F_a < 0$). In this chapter, a continuous error function $J_p(P_1, P_2, F_a)$ is defined for each actuator chamber when the corresponding valve is ported to the ambient pressure P_{atm} as,

$$J_p(P_1, P_2, F_a) = \begin{cases} (P_2 - (1+\epsilon_2)P_{atm})A_2 & \text{if } F_a \geq 0 \\ (P_1 - (1+\epsilon_1)P_{atm})A_1 & \text{if } F_a < 0 \end{cases} \tag{8.12}$$

where $\epsilon_i > 0$ is a positive constant, and $(1+\epsilon_i)P_{atm}$ is the target operating pressure for the i^{th} chamber. Continuity of the error function $J_p(P_1, P_2, F_a)$ is achieved at $F_a := 0$ in Eq. (8.1) for the following relationship between ϵ_1 and ϵ_2,

$$\frac{\epsilon_2}{\epsilon_1} = \frac{A_1}{A_2} \tag{8.13}$$

The valve command input u_i to valve connecting the actuator chamber with the ambient pressure is determined by regulating $J_p(P_1, P_2, F_a)$ to zero. Consider the dynamics of the pressure error function $J_p(P_1, P_2, F_a)$ in Eq. (8.12),

$$\dot{J}_p(P_1, P_2, F_a) = \begin{cases} \dot{P}_2 A_2 & \text{if } F_a \geq 0 \\ \dot{P}_1 A_1 & F_a < 0 \end{cases} \tag{8.14}$$

Using the expression for $\dot{P}_1$ from Eq. (8.3) and the expression for $\dot{P}_2$ from Eq. (8.4), along with the expression for mass flow rate $\dot{m}_i$ from Eq. (8.5), the derivative of $J_p(P_1, P_2, F_a)$ in the above equation can be expressed as,

$$\dot{J}_p(P_1, P_2, F_a) = \begin{cases} \frac{\Psi(P_2, T_o, u_2) R T_o A_2}{V_2(x)} u_2 - \frac{P_2 \dot{V}_2(x)}{V_2(x)} & \text{if } F_a \geq 0 \\ \frac{\Psi(P_1, T_o, u_1) R T_o A_1}{V_1(x)} u_1 - \frac{P_1 \dot{V}_1(x)}{V_1(x)} & \text{if } F_a < 0 \end{cases} \tag{8.15}$$

Design of these input commands u_1 and u_2 to achieve a continuous exponential convergence of the pressure error function $J_p(P_1, P_2, F_a)$ in Eq. (8.12) is presented in the following theorem.

Theorem 8.1. *The pressure error function $J_p(P_1, P_2, F_a)$ in Eq. (8.12) continuously and exponentially converges to zero if the command input u_L to the valve connecting the $L^{th} \in (1, 2)$ actuator chamber to the ambient pressure P_{atm} is defined as,*

$$u_L = \begin{cases} u_2 & \text{if } F_a \geq 0 \\ u_1 & \text{if } F_a < 0 \end{cases} \tag{8.16}$$

where u_i for $i \in (1, 2)$ is defined as,

$$u_i = \frac{V_i(x)}{\Psi(P_i, T_o, u_i) R T_o} \left(\frac{P_1 \dot{V}_2(x)}{V_2(x)} + \eta((1 + \epsilon_i) P_{atm} - P_i) \right) \tag{8.17}$$

where η is a positive constant that determines the rate of convergence, while ϵ_1 and ϵ_2 are small positive constants that are related to the area A_1 on the cap side and the area A_2 on the piston side of the actuator respectively as given in Eq. (8.13)

Proof. When the actuator force F_a is positive, chamber 2 in Fig. (8.1) is the connected to the ambient pressure P_{atm}. The dynamics of pressure P_2 in chamber 2 are as given in Eq. (8.4). Using definition of the mass flow rate $\dot{m}_2$ from Eq. (8.5) and using the input command u_2 to the valve from Eq. (8.16), the dynamics of P_2 in Eq. (8.4) can be expressed as,

$$\dot{P}_2 = -\eta(P_2 - (1 + \epsilon_2) P_{atm}) \tag{8.18}$$

Using the above equation for $\dot{P}_2$ in Eq, (8.14), the pressure error dynamics is obtained as,

$$\dot{J}_p(P_1, P_2, F_a) = -\eta J_p(P_1, P_2, F_a) \tag{8.19}$$

Integrating both sides of the above equation, exponential convergence of the error function $J_p(P_1, P_2, F_a)$ follows.

When the actuator force F_a is negative, chamber 1 is connected to the ambient pressure. Using the definition for the valve command input u_1 from Eq. (8.16) and the air mass flow rate $\dot{m}_1$ from Eq. (8.5), the dynamics of pressure P_1 in Eq. (8.3) can be expressed as,

$$\dot{P}_1 = -\eta(P_1 - (1 + \epsilon_1) P_{atm}) \tag{8.20}$$

From the above expression for $\dot{P}_1$ when chamber 1 is connected to ambient pressure, the corresponding dynamics of the error function $J_p(P_1, P_2, F_a)$ is again obtained as,

$$\dot{J}_p(P_1, P_2, F_a) = -\eta J_p(P_1, P_2, F_a) \tag{8.21}$$

Again, integrating both sides of the above equation, exponential convergence follows.

For both the positive actuator force ($F_a > 0$) and the negative actuator force ($F_a < 0$), the error function $J_p(P_1, P_2, F_a)$ in Eq. (8.19) and Eq. (8.21) respectively, has the same exponential convergence characteristics. When the direction of force changes at $F_a = 0$, the following condition is satisfied,

$$P_1 A_1 - P_{atm} A_1 = P_2 A_2 - P_{atm} A_2 \tag{8.22}$$

Adding $\epsilon_1 P_{atm} A_1$ to both sides of the above equation and using the relationship between ϵ_1 and ϵ_2 from Eq. (8.13) in the above equation, the following condition is obtained,

$$(P_1 - (1 + \epsilon_1) P_{atm}) A_1 = (P_2 - (1 + \epsilon_2) P_{atm}) A_2 \tag{8.23}$$

The above equation implies that the following condition is satisfied,

$$J_p(P_1, P_2, F_a)\|_{F_a = 0^+} = J_p(P_1, P_2, F_a)\|_{F_a = 0^-} \tag{8.24}$$

Thus, the dynamics of the error function as defined by Eq. (8.19) and Eq. (8.21) are continuous. Therefore, the control input u_L as defined in Eq. (8.16) for the L^{th} chamber connected to the ambient pressure, coupled with the condition on ϵ_1 and ϵ_2 as defined in Eq. (8.13) results in exponentially convergence of the error function $J_p(P_1, P_2, F_a)$ to zero, irrespective of the valve switching.

□

Note that the controller design for the valve connecting the actuator chamber to the ambient is independent of the control objective on the high pressure side. The minimum possible target pressure for a pneumatic system is the atmospheric pressure P_{atm}. However, from Eq. (3.27) it can be noticed that this value for operating pressure will lead to a singularity ($\Psi(P_i, u_i) = 0$, if, $P_i = P_{atm}$). In our experiments, a value of 0.5 was arbitrarily assigned to ϵ_1. From the specifications of A_1 and A_2 for the actuator used in our experiments, and using Eq. (8.13), ϵ_2 is evaluated to be 0.45. The controller design for the valve connected to the compressed air supply is presented in the following section.

8.3.2 Supply port valve input design

In this chapter, the input command to the valve connecting the actuator chamber with the source of compressed air is designed to achieve the desired human power amplification. The prescribed approach for controller design is as outlined in section 5.3. As mentioned in section 8.2, the desired supply rate $s_h(F_h, F_e, \dot{x})$ corresponding to amplified human power is supplied to the inertial mass M_p when its velocity $\dot{x}$ and the velocity $\dot{x}_v$ of the virtual inertia M_v are co-ordinated. As presented in section 5.3, the velocity state space $[\dot{x}, \dot{x}_v]$ is transformed to a space consisting of the velocity V_L of the center is mass of M_p and M_v (*a.k.a* Locked system velocity), and the co-ordination velocity error $V_E := (\dot{x} - \dot{x}_v)$ (*a.k.a* Shape system velocity).

A two-stage back-stepping controller as presented in section 5.3 is used to regulate the Shape system velocity V_E to zero. In the first stage of controller design, the desired actuator force F_a^d is the pseudo-control input for the inertial dynamics and is designed as presented in Theorem 5.1. If the actuator is unable to provide the desired force F_a^d in Eq. (5.27), the force error $\tilde{F}$ between the applied actuator force F_a and the desired actuator force F_a^d is defined as,

$$\tilde{F} = F_a - F_a^d \tag{8.25}$$

When independently metering the air flow to the two chambers of the pneumatic actuator, the desired actuator force F_a^d in Eq. (5.27) can be obtained by providing appropriate input commands u_i to the valve connecting the actuator chamber to the supply pressure P_s. The actuator Lyapunov function for the second stage of the controller design, and its relevant properties when using independent valves to meter air flow to the actuator are presented in the following section.

Actuator Lyapunov function: definition and properties

Let P_1^d and P_2^d be the pressures in chambers 1 and 2 respectively corresponding to the desired actuator force F_a^d. These pressures are related to F_a^d from Eq. (5.27) as,

$$F_a^d(t) = P_1^d A_1 - P_2^d A_2 - P_{atm} A_p \tag{8.26}$$

For a given mass of air m_1 and m_2 in chambers 1 and 2 of the actuator respectively, let $\boldsymbol{m} := (m_1, m_2)$ be the vector of air mass in both actuator chambers, $\boldsymbol{P} := (P_1, P_2)$ be

the vector of air pressure in the actuator chambers, while $\boldsymbol{P^d} := (P_1^d, P_2^d)$ be the vector of desired pressure from each actuator chamber. As mentioned in the earlier sections, the valve input command is designed by assuming the thermodynamic process in the actuator to be isothermal. By using the definition of the specific energy of an actuator chamber from Eq. (3.145), the Lyapunov function $V^{iso}(\boldsymbol{m}, \boldsymbol{P}, \boldsymbol{P^d})$ for the isothermal actuator is obtained from Eq. (3.143) as,

$$\begin{aligned} V^{iso}(\boldsymbol{m}, \boldsymbol{P}, \boldsymbol{P^d}) = m_1 R T_o \left(\left(\frac{P_1^d}{P_1} - 1 \right) - \log \left(\frac{P_1^d}{P_1} \right) \right) \\ + m_2 R T_o \left(\left(\frac{P_2^d}{P_2} - 1 \right) - \log \left(\frac{P_2^d}{P_2} \right) \right) \end{aligned} \tag{8.27}$$

From the definition of mass flow rate $\dot{m}_i$ in Eq. (8.5), the time derivative $\dot{V}^{iso}(.)$ of the actuator Lyapunov function in Eq. (8.27) is obtained from Eq. (3.146) as,

$$\begin{aligned} \dot{V}^{iso}(\boldsymbol{m}, \boldsymbol{P}, \boldsymbol{P^d}) = \Psi(P_1, T_o, u_1) R T_o \log \left(\frac{P_1}{P_1^d} \right) u_1 + \Psi(P_2, T_o, u_2) R T_o \log \left(\frac{P_2}{P_2^d} \right) u_2 \\ - \tilde{F} \dot{x} - \dot{F}_a^d (x_d - x) \end{aligned} \tag{8.28}$$

where x_d is the position of the actuator when providing the desired force F_a^d. When using a single valve for metering air flow, the fluid port power variable for the both the actuator chambers in Eq. (8.28) are combined and analyzed as a single port connection to the source of compressed air. With independent metering, the valve being controlled to provide the desired actuator force F_a^d varies with the direction of the force F_a. As a result, the port variables for connecting the fluid port of the actuator to the virtual inertia vary with direction of the force. The flow variable at the actuator port connected to the supply pressure P_s is given by the valve command input (u_1 or u_2). The effort variable $Z_\gamma^s(P_i, P_i^d, u_i)$ at the fluid port of $i^{th} \in (1, 2)$ chamber of the actuator connected to the supply pressure is obtained from Eq. (8.28) as,

$$Z_\gamma^s(P_i, P_i^d, u_i) = \begin{cases} \Psi(P_1, T_o, u_1) R T_o \log \left(\frac{P_1}{P_1^d} \right) & \text{if } F_a \geq 0 \\ \Psi(P_2, T_o, u_2) R T_o \log \left(\frac{P_2}{P_2^d} \right) & F_a < 0 \end{cases} \tag{8.29}$$

In the following subsection, the transformation of the effort variable $Z_\gamma^s(P_i, P_i^d, u_i)$ in the above equation and the corresponding power variables the actuator fluid port are presented.

Transformation of the supply port power variables when independent metering

From the remark 3.5, the force error $\tilde{F}$ is monotonically related to the position error $(x_d - x)$ through a nonlinear function $K^d_{iso}(\boldsymbol{m}, x, x_d)$ as,

$$\tilde{F} = K^d_{iso}(\boldsymbol{m}, x, x_d)(x_d - x) \tag{8.30}$$

where $K^d_{iso}(\boldsymbol{m}, x, x_d) \in \Re^+$ is defined in Eq. (3.142) and can be interpreted as the stiffness of a nonlinear spring between the current position x and the desired position x_d. The actuator force error $\tilde{F}$ as defined in Eq. (8.30) varies monotonically with $(x_d - x)$. Along the lines of remark 3.6 for system with single valve metering, the following remark can be stated for pneumatic system with independent metering.

Remark 8.1. *The effort variable $Z^s_\gamma(P_i, P^d_i, u_i)$ at the fluid port of the $i^th \in (1, 2)$ chamber connected to the supply pressure P_s, as shown in Eq. (8.29), varies monotonically with actuator force error $\tilde{F}$ as defined in Eq. (8.30), and is identically zero only if the force error $\tilde{F}$ is also zero. In addition, the nonlinear gain $\gamma^s_3(P_i, P^d_i, u_i)$ from the force error $\tilde{F}$ to the effort variable $Z^s_\gamma(P_i, P^d_i, u_i)$ defined as,*

$$\gamma^s_3(P_i, P^d_i, u_i) = \frac{Z^s_\gamma(P_i, P^d_i, u_i)}{\tilde{F}} \tag{8.31}$$

is well defined.

Proof. Proof is as shown in appendix E.1 □

The command input u_i $(i \in (1, 2))$ to the valve connected to the supply pressure for regulating the actuator force error $\tilde{F}$ to zero is presented in the following section.

Design of valve command input

If the external force $F_{ex}(t)$ is unknown, the Lyapunov function $V_2(.)$ for the second stage of the controller design is defined to be function of the velocity estimation error $\tilde{V}_E$ and

the force estimation error $\tilde{F}_E$ as shown in Eq. (5.48) and is given by,

$$V_2(V_E, \tilde{V}_E, \tilde{F}_{ex}, \boldsymbol{m}, \boldsymbol{P}, \boldsymbol{P^d}) = \frac{1}{2} \begin{pmatrix} V_E \\ \tilde{V}_E \\ \tilde{F}_E \end{pmatrix}^T \underbrace{\begin{pmatrix} M_E & \mathbf{0}_{1\times 2} \\ \mathbf{0}_{2\times 1} & \boldsymbol{P}_o \end{pmatrix}}_{\boldsymbol{\mathcal{Q}}_1} \begin{pmatrix} V_E \\ \tilde{V}_E \\ \tilde{F}_{ex} \end{pmatrix} + V^{iso}(\boldsymbol{m}, \boldsymbol{P}, \boldsymbol{P^d}) \tag{8.32}$$

where $\boldsymbol{P}_o \in \boldsymbol{R}^{2\times 2}$ satisfies the Lyapunov equation presented in Eq. (5.31). As the above Lyapunov function is positive definite, by regulating it to zero, the Shape system velocity V_E, and the estimation errors $\tilde{V}_E$ and $\tilde{F}_E$ are also regulated to zero.

From the Shape system dynamics in Eq. (5.20), the defintion of the desired actuator force F_a^d from Eq. (5.27), the actuator force error $\tilde{F}$ definition from Eq. (8.25), the observer error dynamics from Eq. (5.36) and Eq. (5.37), and from the derivative $\dot{V}^{iso}(\boldsymbol{m}, \boldsymbol{P}, \boldsymbol{P^d})$ of the isothermal Lyapunov function in Eq. (8.28), the derivative $\dot{V}_2(.)$ of the Lyapunov function in Eq. (8.32) is obtained as,

$$\begin{aligned} \dot{V}_2(V_E, \tilde{V}_E, \tilde{F}_{ex}, \boldsymbol{m}, \boldsymbol{P}, \boldsymbol{P^d}) = &- \begin{pmatrix} V_E \\ \tilde{V}_E \\ \tilde{F}_{ex} \end{pmatrix}^T \begin{pmatrix} K_v & \mathbf{0}_{1\times 2} \\ \mathbf{0}_{2\times 1} & \boldsymbol{Q}_o \end{pmatrix} \begin{pmatrix} V_E \\ \tilde{V}_E \\ \tilde{F}_{ex} \end{pmatrix} \\ &+ \Psi(P_1, T_o, u_1) R T_o \log\left(\frac{P_1}{P_1^d}\right) u_1 + \Psi(P_2, T_o, u_2) R T_o \log\left(\frac{P_2}{P_2^d}\right) u_2 \\ &- \tilde{F}\dot{x}_v + \dot{F}_a^d \frac{\tilde{F}}{K_{iso}^d(\boldsymbol{m}, x, x_d)} \end{aligned} \tag{8.33}$$

where $\boldsymbol{Q}_o \in \boldsymbol{R}^{2\times 2}$ is a positive definite matrix defined to obtain the solution of the Lyapunov equation in Eq. (5.31).

Design of the valve command inputs (u_1, u_2), for regulation of the Shape system velocity V_E and actuator force error $\tilde{F}$ to zero is presented in the following theorem.

Theorem 8.2. *For a given external force $F_{ex}(t)$, exponential regulation of the Shape system dynamics in Eq. (5.20) is achieved if the actuator is able to provide the desired force F_a^d as defined in Eq. (5.25), which can be provided for the following command input $u_H \in (u_1, u_2)$ to the valve connecting the $H \in (1, 2)$ chamber to the supply pressure,*

$$u_H = \frac{1}{\gamma_3^s(P_H, P_H^d, u_H)} \left(\dot{x}_v - K_f \tilde{F} + \frac{\dot{F}_a^d}{K_{iso}^d(\boldsymbol{m}, x, x_d)} \right) - \zeta_H(\boldsymbol{P}, \boldsymbol{P}^d, u_L) \tag{8.34}$$

where the nonlinear function $\gamma_3^s(\boldsymbol{P}, \boldsymbol{P}^d, \boldsymbol{u})$ *is as defined in Eq. (8.31), the nonlinear function* $K_{iso}^d(\boldsymbol{m}, x, x_d) \in \Re^+$ *is as defined in Eq. (3.142),* K_f *is a positive constant, while* $\zeta_H(\boldsymbol{P}, \boldsymbol{P}^d, u_L)$ *is a function of the control input* (u_L) *to the valve connecting the pneumatic actuator to ambient pressure and is defined as,*

Chamber 1 connected to supply:

$$\zeta_1(\boldsymbol{P}, \boldsymbol{P}^d, u_2) = \Psi(P_2, T_o, u_2) \log\left(\frac{P_2}{P_2^d}\right) u_2 / \left(\Psi(P_1, T_o, u_1) \log\left(\frac{P_1}{P_1^d}\right)\right)$$

Chamber 2 connected to supply: (8.35)

$$\zeta_2(\boldsymbol{P}, \boldsymbol{P}^d, u_1) = -\Psi(P_1, T_o, u_1) \log\left(\frac{P_1}{P_1^d}\right) u_1 / \left(\Psi(P_2, T_o, u_2) \log\left(\frac{P_2}{P_2^d}\right)\right)$$

If the force F_{ex} *is an unknown constant, exponential convergence can still be achieved for the desired actuator force* F_a^d *as defined in Eq. (5.27) and the valve command input* u_H *as defined in Eq. (8.34).*

Proof. If the force F_{ex} is well known, consider the Lyapunov function $\bar{V}_2(V_E, \boldsymbol{m}, \boldsymbol{P}, \boldsymbol{P^d})$ as defined in Eq. (5.52) which is given by,

$$\bar{V}_2(V_E, \boldsymbol{m}, \boldsymbol{P}, \boldsymbol{P^d}) = \frac{1}{2} M_E V_E^2 + V^{iso}(\boldsymbol{m}, \boldsymbol{P}, \boldsymbol{P^d}) \tag{8.36}$$

As shown in Eq. (5.53), the Lyapunov function $\bar{V}_2(V_E, \boldsymbol{m}, \boldsymbol{P}, \boldsymbol{P^d})$ is bounded from above. Using the Shape system dynamics from Eq. (5.20), the definition of the desired actuator force F_a^d from Eq. (5.25) and the derivative $\dot{V}^{iso}(\boldsymbol{m}, \boldsymbol{P}, \boldsymbol{P^d})$ of the actuator Lyapunov function from Eq. (8.28), the time derivative $\dot{\bar{V}}_2(.)$ of the Lyapunov function in Eq. (8.36) is obtained as,

$$\begin{aligned}\dot{\bar{V}}_2(V_E, \boldsymbol{m}, \boldsymbol{P}, \boldsymbol{P^d}) = -K_v V_E^2 - \tilde{F}\dot{x}_v + \Psi(P_1, T_o, u_1) R T_o \log\left(\frac{P_1}{P_1^d}\right) u_1 \\ + \Psi(P_2, T_o, u_2) R T_o \log\left(\frac{P_2}{P_2^d}\right) u_2 - \dot{F}_a^d \frac{\tilde{F}}{K_{iso}^d(\boldsymbol{m}, x, x_d)}\end{aligned} \tag{8.37}$$

If chamber 1 is connected to the compressed air supply, then using Eq. (8.31) to obtain the effort variable $Z_\gamma^s(P_1, P_1^d, u_1)$, the Lyapunov function derivative in Eq. (8.37)

can be expressed as,

$$\dot{\tilde{V}}_2(V_E, \boldsymbol{m}, \boldsymbol{P}, \boldsymbol{P^d}) = -K_v V_E^2 + \gamma_3^s(P_1, P_1^d, u_1) u_1 \tilde{F} + \dot{m}_2 R T_o \log\left(\frac{P_2}{P_2^d}\right) - \tilde{F}\dot{x}_v - \dot{F}_a^d \frac{\tilde{F}}{K_{iso}^d(\boldsymbol{m}, x, x_d)} \tag{8.38}$$

where $\gamma_3^s(P_1, P_1^d, u_1)$ is as defined in Eq. (8.31). If chamber 2 is connected to the compressed air supply, the Lyapunov function derivative $\dot{\tilde{V}}_2(.)$ in Eq. (8.37) is obtained as,

$$\dot{\tilde{V}}_2(V_E, \boldsymbol{m}, \boldsymbol{P}, \boldsymbol{P^d}) = -K_v V_E^2 + \dot{m}_1 R T_o \log\left(\frac{P_1}{P_1^d}\right) + \gamma_3^s(P_2, P_2^d, u_2) u_2 \tilde{F} - \tilde{F}\dot{x}_v - \dot{F}_a^d \frac{\tilde{F}}{K_{iso}^d(\boldsymbol{m}, x, x_d)} \tag{8.39}$$

From the definition of the valve input $u_H \in (u_1, u_2)$ given in Eq. (8.34), the derivative $\dot{\tilde{V}}_2(.)$ of the Lyapunov function in Eq. (8.38) and Eq. (8.39) can be simplified as,

$$\dot{\tilde{V}}_2(V_E, \boldsymbol{m}, \boldsymbol{P}, \boldsymbol{P^d}) = -\begin{pmatrix} V_E & \tilde{F} \end{pmatrix} \underbrace{\begin{pmatrix} K_v & 0 \\ 0 & K_f \end{pmatrix}}_{\boldsymbol{\mathcal{Q}}} \begin{pmatrix} V_E \\ \tilde{F} \end{pmatrix} \leq -\sigma_{min}(\boldsymbol{\mathcal{Q}}) \left\| \begin{pmatrix} V_E \\ \tilde{F} \end{pmatrix} \right\|_2^2 \tag{8.40}$$

From the definition of the upper bound on the Lyapunov function $\bar{V}_2(V_E, \boldsymbol{m}, \boldsymbol{P}, \boldsymbol{P^d})$ in Eq. (5.53), the Lyapunov function derivative $\dot{\tilde{V}}_2(.)$ in the above equation can be expressed as,

$$\dot{\tilde{V}}_2(V_E, \boldsymbol{m}, \boldsymbol{P}, \boldsymbol{P^d}) \leq -\frac{2\sigma_{min}(\boldsymbol{\mathcal{Q}})}{\sigma_{max}(\boldsymbol{\mathcal{P}})} \bar{V}_2(V_E, \boldsymbol{m}, \boldsymbol{P}, \boldsymbol{P^d}) \tag{8.41}$$

On integrating both sides of the above equation, exponential convergence follows.

If the force F_{ex} is an unknown constant, consider the Lyapunov function $V_2(.)$ as defined in Eq. (8.32). The Lyapunov function $V_2(.)$ is bounded as shown in Eq. (5.49). The time derivative $\dot{V}_2(.)$ of the Lyapunov function is obtained as given in Eq. (8.33). Using the definition of the valve command input $u_H \in (u_1, u_2)$ as provided in Eq. (8.34) for the appropriate chamber connected to the supply pressure, the time derivative $\dot{V}_2(.)$

of the Lyapunov function in Eq. (8.33) can be simplified as,

$$\begin{aligned}\dot{V}_2(V_E,\tilde{V}_E,\tilde{F}_{ex},\boldsymbol{m},\boldsymbol{P},\boldsymbol{P^d}) &= -\begin{pmatrix} V_E \\ \tilde{V}_E \\ \tilde{F}_{ex} \\ \tilde{F} \end{pmatrix}^T \underbrace{\begin{pmatrix} K_v & \mathbf{0}_{1\times 2} & 0 \\ \mathbf{0}_{2\times 1} & \boldsymbol{Q}_o & \mathbf{0}_{2\times 1} \\ 0 & \mathbf{0}_{1\times 2} & K_f \end{pmatrix}}_{\boldsymbol{\mathcal{Q}}_3} \begin{pmatrix} V_E \\ \tilde{V}_E \\ \tilde{F}_{ex} \\ \tilde{F} \end{pmatrix} \\ &\leq -\sigma_{min}(\boldsymbol{\mathcal{Q}}_3) \left\| \begin{pmatrix} V_E \\ \tilde{V}_E \\ \tilde{F}_{ex} \\ \tilde{F} \end{pmatrix} \right\|_2^2 \end{aligned} \tag{8.42}$$

From the definition of the upper bound on the Lyapunov function $V_2(.)$ in Eq. (5.49), the Lyapunov function derivative in Eq. (8.42) can be expressed as,

$$\dot{V}_2(V_E,\tilde{V}_E,\tilde{F}_{ex},\boldsymbol{m},\boldsymbol{P},\boldsymbol{P^d}) \leq -\frac{2\sigma_{min}(\boldsymbol{\mathcal{Q}}_3)}{\sigma_{max}(\boldsymbol{\mathcal{P}}_3)} V_2(V_E,\tilde{V}_E,\tilde{F}_{ex},\boldsymbol{m},\boldsymbol{P},\boldsymbol{P^d}) \tag{8.43}$$

Exponential convergence follows on integrating both sides of the above equation.

□

As stated in remark 5.1, for a time varying external force $F_{ex}(t)$, exponential convergence is guaranteed only to a region in the neighborhood of the origin. The size of this region is determined by the maximum magnitude of the rate of the rate of change of $F_{ex}(t)$, *i.e.* $\|\dot{F}_{ex}(t)\|_\infty$.

Note that the control input to the high pressure side depends on the input to the low pressure through the term $\zeta_i(\boldsymbol{P},\boldsymbol{P}^d,u_L)$. Passivity analysis of the proposed controller is presented in the following section.

8.3.3 Closed loop passivity

In this section, a storage function for the independently metered pneumatic human power amplifier is defined, and the proposed controller in the previous section is modified to provide the required human power amplification at low operating pressure, while satisfying the desired passivity condition in Eq. (8.8). For convenience of passivity

analysis, the command input u_H to the valve connecting the supply pressure P_s to an actuator chamber, presented in Eq. (8.34) is expressed as,

$$u_H = \frac{1}{\gamma_3^s(P_H, P_H^d, u_H)} \left(\dot{x}_v + \frac{\dot{F}_a^d}{K_{iso}^d(\boldsymbol{m}, x_d, x)} + u_{H_f} \right) - \zeta_H(\boldsymbol{P}, \boldsymbol{P}^d, u_L) \tag{8.44}$$

where u_{H_f} consists of the feedback elements of the input and is given by,

$$u_{H_f} = -K_f \tilde{F} \tag{8.45}$$

To study passivity properties of the human power amplifier, the sum of the kinetic energy in the inertia, kinetic energy of the virtual mass and the energy available in the pneumatic actuator is defined to be the storage function. For a given vector $\boldsymbol{m} := (m_1, m_2)$ of air mass in chamber 1 and 2 of the actuator, and for a given vector of pressures $\boldsymbol{P} := (P_1, P_2)$, the available energy $W_{act}^{iso}(\boldsymbol{m}, \boldsymbol{P})$ in a two-chambered isothermal actuator is as presented in Eq. (3.102). The storage function $W_s(\dot{x}, \dot{x}_v, \boldsymbol{m}, \boldsymbol{P})$ for the human power amplifier is therefore given by,

$$W_s(\dot{x}, \dot{x}_v, \boldsymbol{m}, \boldsymbol{P}) = \frac{1}{2} M_p \dot{x}^2 + \frac{1}{2} M_v \dot{x}_v^2 + W_{act}^{iso}(\boldsymbol{m}, \boldsymbol{P}) \tag{8.46}$$

From the dynamics of inertia M_p in Eq. (8.2), the dynamics of inertia M_v in Eq. (8.9) and using the supply rate to the isothermal actuator from Eq. (3.115), the time derivative $\dot{W}_s(.)$ of the storage function in Eq. (8.46) is obtained as,

$$\begin{aligned} \dot{W}_s(\dot{x}, \dot{x}_v, \boldsymbol{m}, \boldsymbol{P}) &= ((\rho + 1)F_h(t) + F_e(t))\dot{x} - \rho F_h(t) V_E - (F_a + u_d)\dot{x}_v \\ &+ \Psi(P_1, T_o, u_1) R T_o \log\left(\frac{P_1}{\bar{P}_1(\boldsymbol{m})} \right) u_1 + \Psi(P_2, T_o, u_2) R T_o \log\left(\frac{P_2}{\bar{P}_2(\boldsymbol{m})} \right) u_2 \end{aligned} \tag{8.47}$$

where $\bar{P}_1(\boldsymbol{m})$ and $\bar{P}_2(\boldsymbol{m})$ correspond to the pressure in chambers 1 and 2 respectively of the actuator at the equilibrium position $\bar{x}(\boldsymbol{m})$. With independent metering, each chamber of the actuator can be treated as a single-chambered actuator. The effort variables $Z_\gamma^s(\boldsymbol{m}, P_1, u_1)$ and $Z_\gamma^s(P_2, \bar{P}_2, u_2)$ for chambers 1 and 2 of the actuator respectively are defined as,

$$\begin{aligned} Z_\gamma^s(P_1, \bar{P}_1, u_1) &= \Psi(P_1, T_o, u_1) R T_o \log\left(\frac{P_1}{\bar{P}_1(\boldsymbol{m})} \right) = \Psi(P_1, T_o, u_1) R T_o \log\left(\frac{L_{1o} + \bar{x}(\boldsymbol{m})}{L_{1o} + x} \right) \\ Z_\gamma^s(P_2, \bar{P}_2, u_2) &= \Psi(P_2, T_o, u_2) R T_o \log\left(\frac{P_2}{\bar{P}_2(\boldsymbol{m})} \right) = \Psi(P_2, T_o, u_2) R T_o \log\left(\frac{L_{2o} - \bar{x}(\boldsymbol{m})}{L_{2o} - x} \right) \end{aligned} \tag{8.48}$$

Remark 8.2. *The fluid port effort variable $Z^s_\gamma(P_i, \bar{P}_i, u_i)$ at the $i^{th} \in (1,2)$ chamber, as defined in Eq. (8.48), varies monotonically with the actuator force F_a. The non-linear mapping $\gamma^s_1(P_i, \bar{P}_i, u_i)$ from the actuator force F_a to the fluid port effort variable $Z^s_\gamma(\boldsymbol{m}, P_i, u_i)$ is given by,*

$$\gamma^s_1(P_i, \bar{P}_i, u_i) = \frac{Z^s_\gamma(P_i, \bar{P}_i, u_i)}{F_a} \tag{8.49}$$

is well defined for all F_a

Proof. In the proof for remark 8.1 presented in appendix E, replace the the desired actuator chamber pressures P^d_1, P^d_2 in chambers 1 and 2 respectively with the equilibrium pressures $\bar{P}_1$ and $\bar{P}_2$. The proof for this remark then follows. □

The supply rate to the actuator depends on which chamber is connected to the supply pressure P_s and which chamber is connected to the ambient pressure P_{atm}. When chamber 1 is connected to the supply port, using the definition of the valve command inputs, u_1 from Eq. (8.34) and u_2 from Eq. (8.16) respectively, the supply rate $\dot{W}_s(.)$ in Eq. (8.47) can be expressed as,

$$\begin{aligned}\dot{W}_s(\dot{x}, \dot{x}_v, \boldsymbol{m}, \boldsymbol{P}) &= ((\rho+1)F_h(t) + F_e(t))\dot{x} - \rho F_h(t) V_E - (F_a + u_d)\dot{x}_v \\ &+ \frac{\gamma^s_1(P_1, \bar{P}_1, u_1)}{\gamma^s_3(P_1, \bar{P}_1, u_1)} F_a \dot{x}_v + \frac{\gamma^s_1(P_1, \bar{P}_1, u_1)}{\gamma^s_3(P_1, \bar{P}_1, u_1) K_s(\boldsymbol{m}, x, x_d)} F_a \dot{F}^d_a - \frac{\gamma^s_1(P_1, \bar{P}_1, u_1)}{\gamma^s_3(P_1, \bar{P}_1, u_1)} F_a K_f \tilde{F} \\ &- \left(\frac{\log\left(\frac{P_1}{\bar{P}_1}\right)}{\log\left(\frac{P_1}{P^d_1}\right)} - \frac{\log\left(\frac{P_2}{\bar{P}_2}\right)}{\log\left(\frac{P_2}{P^d_2}\right)} \right) \dot{m}_2 R T_o \log\left(\frac{P_2}{\bar{P}_2(\boldsymbol{m})}\right)\end{aligned} \tag{8.50}$$

The desired supply rate to the human power amplifier corresponds to the first term on the *r.h.s* of the above equation. All the other terms on the *r.h.s* of the above equation are sign indefinite. In passivity analysis of human power amplifier with single valve for metering the air flow presented in section 5.4, it is shown that the input u_d on the virtual inertia is defined to compensate for some of the sign indefinite terms to guarantee passive operation. Along the lines of Eq. (5.65), when chamber 1 is connected to supply pressure, the input u_d on the virtual inertia is defined as,

$$u_d = \begin{cases} \left(\frac{\gamma^s_1(P_1, \bar{P}_1, u_1)}{\gamma^s_3(\boldsymbol{m}, P_1, P^d_1, u_1)} - 1\right) F_a, \text{ if } \left(\frac{\gamma^s_1(P_1, \bar{P}_1, u_1)}{\gamma^s_3(\boldsymbol{m}, P_1, P^d_1, u_1)} - 1\right) F_a \dot{x}_v > 0 \\ 0 \text{ if } \left(\frac{\gamma^s_1(P_1, \bar{P}_1, u_1)}{\gamma^s_3(\boldsymbol{m}, P_1, P^d_1, u_1)} - 1\right) F_a \dot{x}_v \leq 0 \end{cases} \tag{8.51}$$

The time derivative of the supply rate in Eq. (8.50) can then be expressed as,

$$\begin{aligned}\dot{W}_s(\dot{x},\dot{x}_v,\boldsymbol{m},\boldsymbol{P}) \leq ((\rho+1)F_h(t)+F_e(t))\dot{x} - \rho F_h(t)V_E - \\ F_a\dot{x}_v + \frac{\gamma_1^s(P_1,\bar{P}_1,u_1)}{\gamma_3^s(P_1,\bar{P}_1,u_1)K_s(\boldsymbol{m},x,x_d)}F_a\dot{F}_a^d - \frac{\gamma_1^s(P_1,\bar{P}_1,u_1)}{\gamma_3^s(P_1,\bar{P}_1,u_1)}F_aK_f\tilde{F} \\ - \left(\frac{\log\left(\frac{P_1}{\bar{P}_1}\right)}{\log\left(\frac{P_1}{P_1^d}\right)} - \frac{\log\left(\frac{P_2}{\bar{P}_2}\right)}{\log\left(\frac{P_2}{P_2^d}\right)}\right)\dot{m}_2RT_o\log\left(\frac{P_2}{\bar{P}_2(\boldsymbol{m})}\right)\end{aligned} \tag{8.52}$$

If chamber 2 is connected to the supply pressure P_s and chamber 1 is connected to the ambient pressure P_{atm}, then the supply rate in Eq. (8.47) can be expressed as,

$$\begin{aligned}\dot{W}_s(\dot{x},\dot{x}_v,\boldsymbol{m},\boldsymbol{P}) = ((\rho+1)F_h(t)+F_e(t))\dot{x} - \rho F_h(t)V_E - (F_a+u_d)\dot{x}_v \\ + \frac{\gamma_1^s(P_2,\bar{P}_2,u_2)}{\gamma_3^s(P_2,\bar{P}_2,u_2)}F_a\dot{x}_v + \frac{\gamma_1^s(P_2,\bar{P}_2,u_2)}{\gamma_3^s(P_2,\bar{P}_2,u_2)K_s(\boldsymbol{m},x,x_d)}F_a\dot{F}_a^d - \frac{\gamma_1^s(P_2,\bar{P}_2,u_2)}{\gamma_3^s(P_2,\bar{P}_2,u_2)}F_aK_f\tilde{F} \\ - \left(\frac{\log\left(\frac{P_1}{\bar{P}_1}\right)}{\log\left(\frac{P_1}{P_1^d}\right)} - \frac{\log\left(\frac{P_2}{\bar{P}_2}\right)}{\log\left(\frac{P_2}{P_2^d}\right)}\right)\dot{m}_1RT_o\log\left(\frac{P_1}{\bar{P}_1(\boldsymbol{m})}\right)\end{aligned} \tag{8.53}$$

The input u_d on the virtual inertia, when chamber 2 is connected to supply pressure, is then defined as,

$$u_d = \begin{cases}\left(\frac{\gamma_1^s(P_2,\bar{P}_2,u_2)}{\gamma_3^s(\boldsymbol{m},P_1,P_2^d,u_2)}-1\right)F_a, \text{ if } \left(\frac{\gamma_1^s(P_2,\bar{P}_2,u_2)}{\gamma_3^s(\boldsymbol{m},P_1,P_2^d,u_2)}-1\right)F_a\dot{x}_v > 0 \\ 0 \text{ if } \left(\frac{\gamma_1^s(P_2,\bar{P}_2,u_2)}{\gamma_3^s(\boldsymbol{m},P_1,P_2^d,u_2)}-1\right)F_a\dot{x}_v \leq 0\end{cases} \tag{8.54}$$

The time derivative of the supply rate in Eq. (8.53) can then be expressed as,

$$\begin{aligned}\dot{W}_s(\dot{x},\dot{x}_v,\boldsymbol{m},\boldsymbol{P}) \leq ((\rho+1)F_h(t)+F_e(t))\dot{x} - \rho F_h(t)V_E - F_a\dot{x}_v \\ + \frac{\gamma_1^s(P_2,\bar{P}_2,u_2)}{\gamma_3^s(P_2,\bar{P}_2,u_2)K_s(\boldsymbol{m},x,x_d)}F_a\dot{F}_a^d - \frac{\gamma_1^s(P_2,\bar{P}_2,u_2)}{\gamma_3^s(P_2,\bar{P}_2,u_2)}F_aK_f\tilde{F} \\ - \left(\frac{\log\left(\frac{P_1}{\bar{P}_1}\right)}{\log\left(\frac{P_1}{P_1^d}\right)} - \frac{\log\left(\frac{P_2}{\bar{P}_2}\right)}{\log\left(\frac{P_2}{P_2^d}\right)}\right)\dot{m}_1RT_o\log\left(\frac{P_1}{\bar{P}_1(\boldsymbol{m})}\right)\end{aligned} \tag{8.55}$$

For ease of subsequent analysis, the power interaction at the valve connected to the

low pressure port is defined as,

$$\beta_1(\boldsymbol{m}, \boldsymbol{P}, \boldsymbol{P^d}) = \left(\frac{\log\left(\frac{P_1}{\bar{P}_1}\right)}{\log\left(\frac{P_1}{P_1^d}\right)} - \frac{\log\left(\frac{P_2}{\bar{P}_2}\right)}{\log\left(\frac{P_2}{P_2^d}\right)} \right) \dot{m}_2 R T_o \log\left(\frac{P_2}{\bar{P}_2(\boldsymbol{m})}\right) \tag{8.56}$$

$$\beta_2(\boldsymbol{m}, \boldsymbol{P}, \boldsymbol{P^d}) = \left(\frac{\log\left(\frac{P_1}{\bar{P}_1}\right)}{\log\left(\frac{P_1}{P_1^d}\right)} - \frac{\log\left(\frac{P_2}{\bar{P}_2}\right)}{\log\left(\frac{P_2}{P_2^d}\right)} \right) \dot{m}_1 R T_o \log\left(\frac{P_1}{\bar{P}_1(\boldsymbol{m})}\right) \tag{8.57}$$

To monitor the supply rate due to other sign indefinite terms on the *r.h.s* of Eq. (8.52) and Eq. (8.55) a fictitious flywheel as presented in the section 5.4 is utilized. The augmented system with the flywheel dynamics is analyzed in the following section.

Augmented system with a virtual flywheel

For an inertia of M_f and an external torque T_f, the dynamics of the flywheel position x_f are as given in Eq. (5.68). The objective again is establish a skew-symmetric relationship between the flywheel and the human power amplifier by appropriately defining the flywheel torque T_f. The change in the kinetic energy of the flywheel then reflects the energy transferred to/from the human power amplifier. If the flywheel energy falls below a threshold value f_o, additional damping is introduced in the controller design to extract energy from the human power amplifier and transfer it to the flywheel. This additional damping is applied on the virtual inertia dynamics by modifying the virtual inertia dynamics as,

$$M_v \ddot{x}_v = \rho F_h(t) - F_a - u_d - b\dot{x}_v \tag{8.58}$$

where $b \in \Re^+$ is the damping coefficient.

The flywheel torque T_f and the damping coefficient b required for passive operation of the human power amplifier are provided in the next section.

Passivity property of the virtual flywheel augmented system

The storage function $W_{tot}(\dot{x}, \dot{x}_v, \boldsymbol{m}, \boldsymbol{P}, \dot{x}_f)$ for the augmented system is obtained as given in Eq. (5.70) by augmenting the storage function $W_s(\dot{x}, \dot{x}_v, \boldsymbol{m}, \boldsymbol{P})$ with the kinetic energy $\frac{1}{2} M_f \dot{x}_f^2$ of the flywheel. Unlike the human power amplifier with single valve metering presented in section 5.4, with independent metering, the supply rate to the

pneumatic actuator varies with the connections at the two fluid ports of the actuator. In this section, the supply rate for each of the two scenarios is considered in defining the torque to the flywheel.

Consider the case when chamber 1 is connected to the supply pressure P_s and chamber 2 is connected to ambient pressure P_{atm}. Using the expression for $\dot{W}_s(.)$ from Eq. (8.50), along with the modified dynamics of the virtual inertia from Eq. (8.58) and the definition of $\beta_1(\boldsymbol{m}, \boldsymbol{P}, \boldsymbol{P^d})$ from Eq. (8.56), the time derivative $\dot{W}_{tot}(.)$ of the storage function in the above equation is obtained as,

$$\begin{aligned}\dot{W}_{tot}(\dot{x}, \dot{x}_v, \boldsymbol{m}, \boldsymbol{P}, \dot{x}_f) = &((\rho+1)F_h(t) + F_e(t))\dot{x} - \rho F_h(t) V_E - (F_a + u_d)\dot{x}_v - b\dot{x}_v^2 \\ &+ \frac{\gamma_1^s(P_2, \bar{P}_2, u_2)}{\gamma_3^s(P_2, \bar{P}_2, u_2)} F_a \dot{x}_v + \frac{\gamma_1^s(P_2, \bar{P}_2, u_2)}{\gamma_3^s(P_2, \bar{P}_2, u_2) K_s(\boldsymbol{m}, x, x_d)} F_a \dot{F}_a^d \\ &- \frac{\gamma_1^s(P_2, \bar{P}_2, u_2)}{\gamma_3^s(P_2, \bar{P}_2, u_2)} F_a K_f \tilde{F} - \beta_1(\boldsymbol{m}, \boldsymbol{P}, \boldsymbol{P^d}) + T_f \dot{x}_f\end{aligned} \tag{8.59}$$

If chamber 2 is connected to the supply pressure P_s, and chamber 1 is connected to the ambient pressure, then, using the expression for $\dot{W}_s(.)$ from Eq. (8.53) along with the modified dynamics of the virtual inertia in Eq. (8.58) and the definition of $\beta_2(\boldsymbol{m}, \boldsymbol{P}, \boldsymbol{P^d})$ from Eq. (8.56), the time derivative $\dot{W}_{tot}(.)$ is then obtained as,

$$\begin{aligned}\dot{W}_{tot}(\dot{x}, \dot{x}_v, \boldsymbol{m}, \boldsymbol{P}, \dot{x}_f) = &((\rho+1)F_h(t) + F_e(t))\dot{x} - \rho F_h(t) V_E - (F_a + u_d)\dot{x}_v - b\dot{x}_v^2 \\ &+ \frac{\gamma_1^s(P_2, \bar{P}_2, u_2)}{\gamma_3^s(P_2, \bar{P}_2, u_2)} F_a \dot{x}_v + \frac{\gamma_1^s(P_2, \bar{P}_2, u_2)}{\gamma_3^s(P_2, \bar{P}_2, u_2) K_s(\boldsymbol{m}, x, x_d)} F_a \dot{F}_a^d \\ &- \frac{\gamma_1^s(P_2, \bar{P}_2, u_2)}{\gamma_3^s(P_2, \bar{P}_2, u_2)} F_a K_f \tilde{F} - \beta_2(\boldsymbol{m}, \boldsymbol{P}, \boldsymbol{P^d}) + T_f \dot{x}_f\end{aligned} \tag{8.60}$$

Design of the flywheel torque T_f required for passive operation is presented in the following theorem.

Theorem 8.3. *The inertia dynamics of a pneumatically actuated human power amplifier in Eq. (8.2), with the pressure dynamics in the pneumatic actuator given in Eqs. (8.3, 8.4) varied with air mass flow rate $\dot{m}_i$ in Eq. (8.5) for providing the actuator force F_a^d as defined in Eq. (5.27) (and in Eq. (5.25) for known F_{ex}), the command input u_L to the valve connecting the actuator chamber to ambient pressure P_{atm} as presented in*

Eq. (8.16) and the command input u_H to the valve connecting the actuator chamber to supply pressure given by,

$$u_H = \frac{1}{\gamma_3^s(P_H, P_H^d, u_H)} \left(\dot{x}_v + \left(\frac{\dot{F}_a^d}{K_{iso}^d(\boldsymbol{m}, x_d, x)} \right) \right) - \zeta_H(\boldsymbol{P}, \boldsymbol{P^d}, u_L) + \frac{\hat{u}_{H_f}}{\gamma_3^s(P_H, P_H^d, u_H)} \tag{8.61}$$

where the feedback component $\hat{u}_{H_f}$ is used to establish a skew-symmetric relationship with the flywheel torque T_f and is defined as,

$$\begin{aligned} \begin{pmatrix} \hat{u}_{H_f} \\ T_f \end{pmatrix} &= \begin{pmatrix} 0 & g(\dot{x}_f) u_{H_f} \\ -g(\dot{x}_f) u_{fb} & 0 \end{pmatrix} \begin{pmatrix} \frac{\gamma_i^s(\boldsymbol{m}, P_i, u_i)}{\gamma_3^s(\boldsymbol{m}, P_i, P^{d_i}, u_i)} F_a \\ \dot{x}_f \end{pmatrix} \\ &+ \begin{pmatrix} 0 \\ \rho F_h V_E - \left(\left(\frac{\gamma_i^s(\boldsymbol{m}, P_i, u_i)}{\gamma_3^s(\boldsymbol{m}, P_i, P^{d_i}, u_i)} - 1 \right) F_a - u_d \right) \dot{x}_v + b \dot{x}_v^2 \\ + \frac{\gamma_i^s(\boldsymbol{m}, P_i, u_i)}{\gamma_3^s(\boldsymbol{m}, P_i, P^{d_i}, u_i)} \frac{\dot{F}_a^d}{K_i^d(\boldsymbol{m}, x, x_d)} + \beta_i(\boldsymbol{m}, \boldsymbol{P}, \boldsymbol{P^d}) \end{pmatrix} \end{aligned} \tag{8.62}$$

where $i \in (1, 2)$ is the index to represent the chamber connected to the supply pressure, $\beta_{1,2}(.)$ is as defined in Eqs. (8.56 and 8.57), while the function $g(\dot{x}_f)$ and the damping coefficient b depend on the flywheel velocity $\dot{x}_f$ and are defined as,

$$\textit{Normal mode} : \begin{pmatrix} g(\dot{x}_f) = \frac{1}{\dot{x}_f} \\ b = 0 \end{pmatrix} \quad \textit{if } \dot{x}_f \geq f_o \tag{8.63}$$

$$\textit{Emergency mode} : \begin{pmatrix} g(\dot{x}_f) = \frac{1}{f_o} \\ b \in \Re^+ \end{pmatrix} \quad \textit{if } \dot{x}_f < f_o \tag{8.64}$$

where f_o represents the velocity threshold to switch to emergency mode of operation, will satisfy the following passivity condition,

$$\int_0^t ((\rho + 1) F_h(t) + F_e(t)) \dot{x} \; d\tau \geq -c_o^2 \tag{8.65}$$

Proof. Proof is along the lines of the proof presented for Theorem 5.3 in section 5.4 □

Experimental results to validate the controller performance are provided in the following section.

8.4 Experimental results

In this section, experimental results for evaluating efficacy of independent metering for improving efficiency of operation by implementing the controller designed in the previous section on a single-DOF pneumatic actuator are presented. The experimental setup is as described in section 8.1. The cap side area A_1 and the rod side area A_2 of the pneumatic actuator used in this study are, $0.002m^2$ and $0.0018m^2$ respectively. The area ratio $\frac{A_2}{A_1}$ is given by 0.9.

The amplification factor ρ for the input human force is set to be 7. The compressor shown in Fig. (8.2) is charged to an initial pressure of $105psi$. For the purpose of comparison, both the single valve metering and independent metering control schemes are taken through similar velocity profile. The velocity of the inertia is estimated from the position measurement using the observer dynamics presented in Eq. (5.80). The controller gain K_f on the actuator force error $\tilde{F}$, and the observer gains L_1 and L_2 in the Shape system velocity estimate $\hat{V}_E$ and the external force estimate $\hat{F}_{ex}$ are as presented in table 5.1. The constant η that determines the rate of convergence of the pressure error in the chamber connected to the ambient pressure is selected to be 22.

8.4.1 Single valve metering

A MPYE-5-LF010, 5 port-3 way proportional valve from FESTO is used to meter the limited air flow from the compressor to the two-chambered actuator. The range of the input command voltage command to the valve is between 0 to 10 volts. At 5 volts input, the valve spool is at center position with no air flow sent to either chamber. The relationship between input voltage and the available orifice area in the valve is as shown in Fig. (5.4).

Co-ordination between the inertial velocity $\dot{x}$ and the velocity of virtual inertia $\dot{x}_v$ is as shown in Fig.(8.3). The voltage command input to the valve, shown in Fig. (8.4), begins to saturate at the limit (10 volts and 0 volts) after $t = 37s$, indicating that the valve is fully open. However, the supply pressure available in the reservoir after $37s$ is too low for the actuator to provide the required force. The velocity co-ordination degrades after $37s$ due to the lack of sufficient pressure to provide the actuator force required to maintain velocity co-ordination.

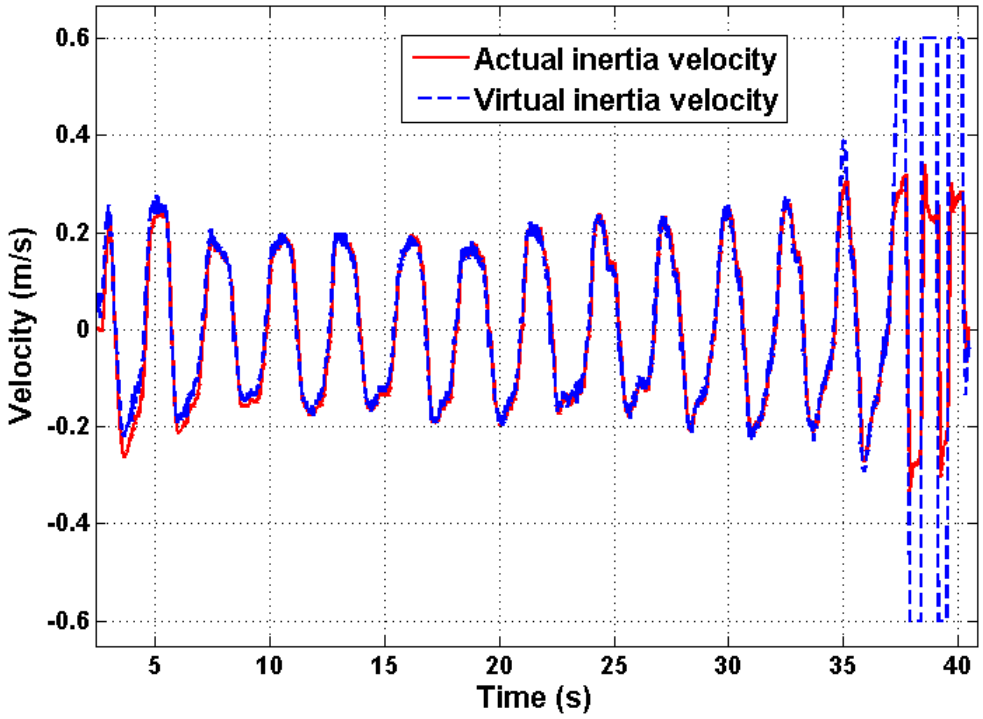

Figure 8.3: Velocity co-ordination between the actual inertia and the virtual inertia obtained with single valve metering

Comparison of the actuator force F_a with the desired actuator force F_a^d is as presented in Fig. (8.5). The actuator force tracks the desired actuator force well. Note that as the operating pressure decreases due to depletion of pressurized air from the reservoir, the force magnitude in Fig. (8.5) required to achieve the desired velocity, shown in Fig. (8.3), also decreases. This was experimentally determined to be due to reduction in resistance to motion at lower operating pressure.

8.4.2 Independent metering

To implement independent metering, two MPYE-5-LF010, 5 port-3 way proportional valves from FESTO are modified by plugging an outlet port to behave as 4 port-3 way

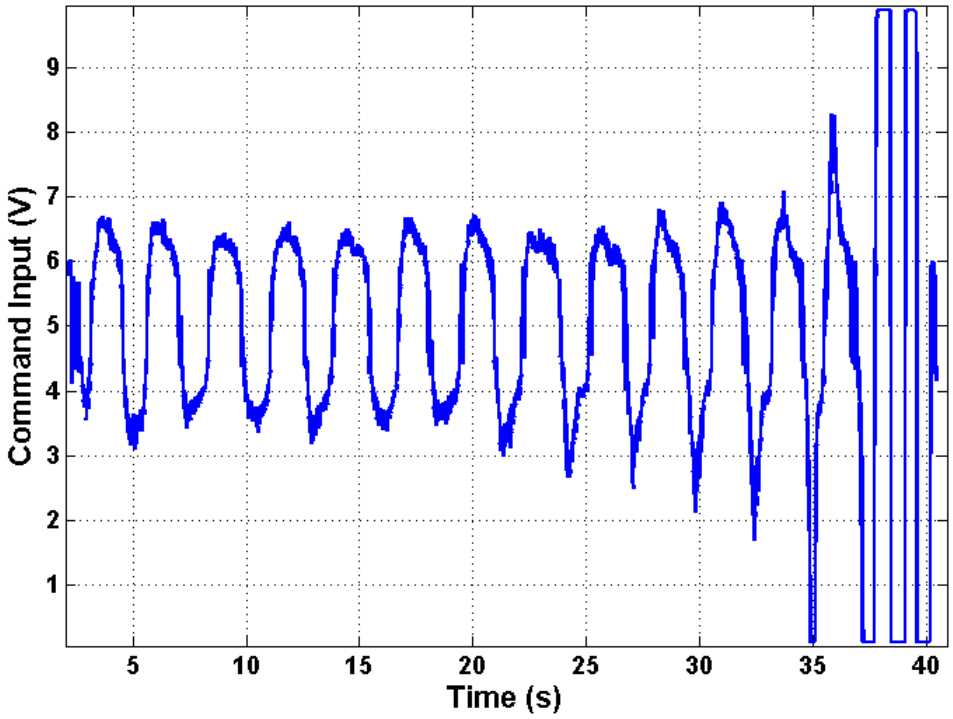

Figure 8.4: Command input to the single valve metering the air flow rate to the actuator

proportional valves. With independent metering, velocity and force tracking performance are shown in Fig. (8.6) and Fig. (8.7) respectively. Both velocity co-ordination and force tracking are good and are comparable to that achieved with single valve metering. The actuator velocity profile with independent metering, shown in Fig. (8.6), is kept similar to the velocity profile with single valve metering shown in Fig. (8.3) for equitable comparison. The magnitude of force required to move the actuator with independent metering, shown in Fig. (8.7), is smaller than the force required with single valve metering shown in Fig. (8.5). This is again due to the reduced friction force in the actuator at the lower operating pressures achieved with independent metering.

The variation in pressure error function $J_p(P_1, P_2, F_a)$ defined for the chamber connected to the ambient pressure P_{atm} defined in Eq. (8.12) is as shown in Fig. (8.8). This error quickly decreases to a neighborhood around origin. The high frequency oscillations

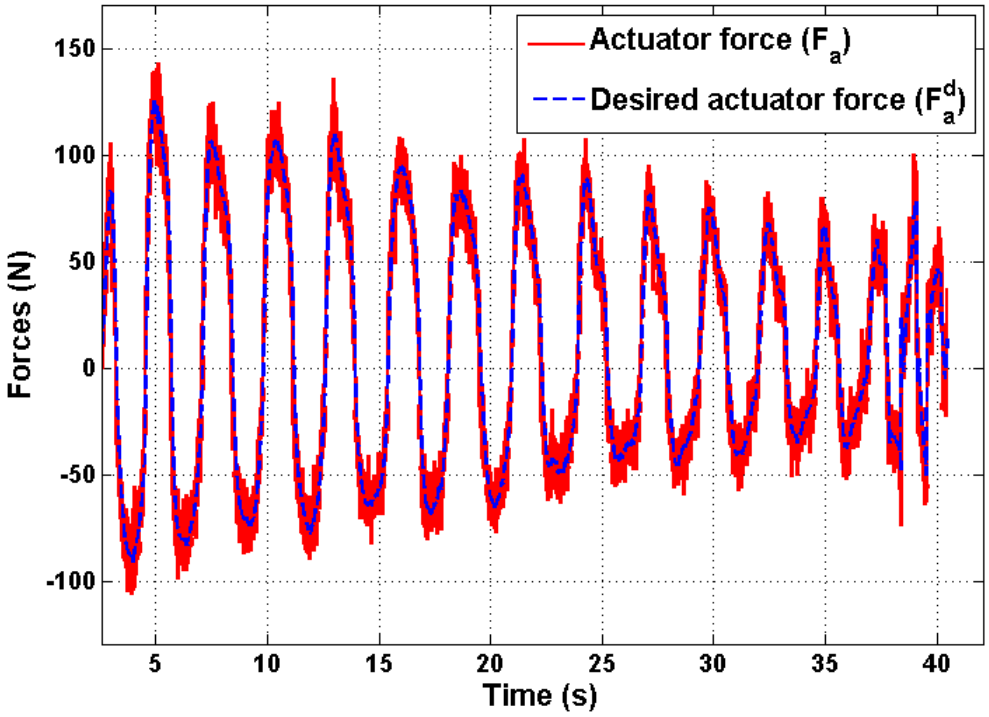

Figure 8.5: Comparison of the applied actuator force with the desired actuator force with single valve metering

around origin are due to noise in the pressure signal.

A comparison of variation in the supply pressure P_s when using a single valve for metering the flow and when using independent valve to meter the flow is as shown in Fig. (8.9). After the same duration, the pressure loss in the compressor, when independent metering, is lower than the pressure loss when using a single valve to meter air flow to the actuator. The performance of the actuator degrades considerably when the supply pressure falls below $2.1e5(N/m^2)$. As observed in Fig. (8.3), this happens at around $37s$ when using a single valve to meter air flow. When independently metering the air flow to the actuator chambers, the compressor pressure falls below the threshold of $2.1e5(N/m^2)$ at around 62s. This corresponds to nearly 70% increase in operational duration, thus confirming the efficacy of independent metering.

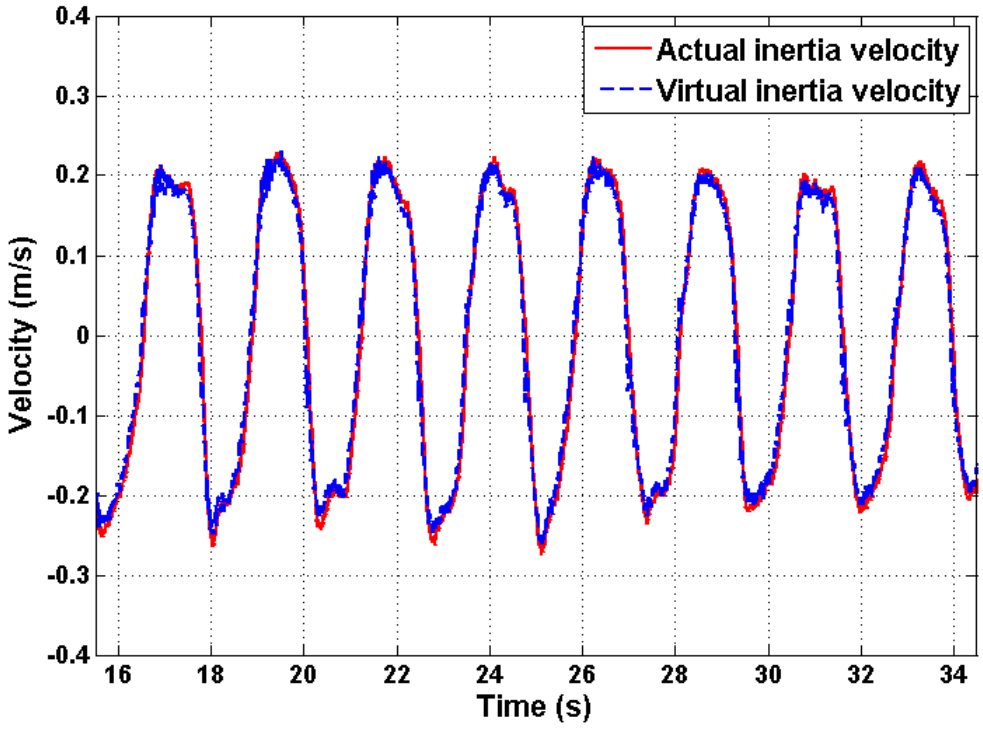

Figure 8.6: Velocity co-ordination between the actual inertia and virtual inertia obtained with independent valve metering

8.5 Summary

In this chapter, independent metering of each chamber of a two-chambered pneumatic actuator, for improving efficiency of operation of the actuator is presented. Two servo-valves are used to independently control the pressure in each actuator chamber. The additional degree of freedom offered by the second valve is used to maintain low operating pressure. The novelty of the approach presented in this chapter is the definition of a pressure error function for the chamber connected to the ambient pressure that remains continuous even as the chamber connected to ambient pressure varies depending on the actuator force. The command input to the valve connecting the chamber pressure to ambient pressure is designed such that the pressure error function continuously and exponentially decreases to zero. The valve connecting the chamber pressure

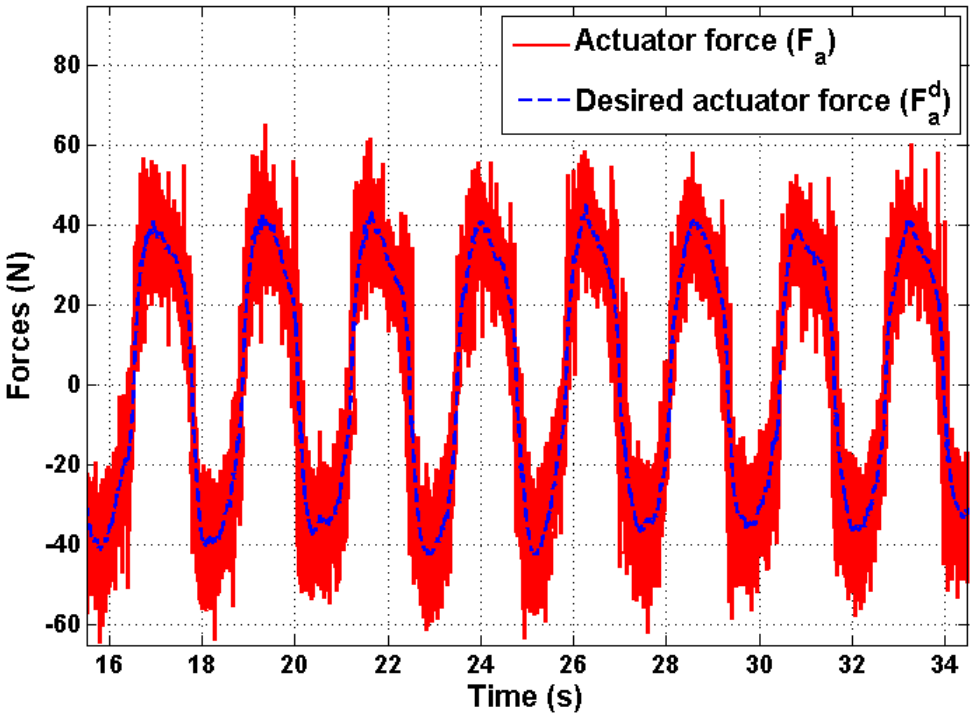

Figure 8.7: Comparison of the applied actuator force with the desired actuator force with independent valve metering

to supply pressure can be controlled to perform a desired task. In this chapter, the valve connected to supply pressure is used to provide human power amplification. Efficacy of the proposed approach is investigated on a pneumatic human power amplifier. An external compressor, with the recharge disabled, is used as a source of compressed air. Experimental results show that significant improvement in operation time can be achieved with independent metering. The reported improvement is however specific to the experiment. It will vary depending on the initial supply pressure and the expected work from the actuator. Since the study was performed with servo-valves, the throttling losses in the valve are not mitigated. Previous studies on hydraulic systems has shown that throttling losses are a significant contributor to inefficiency of operation. This can be be mitigated by using on-off solenoid valves (digital valves). Digital valves are also

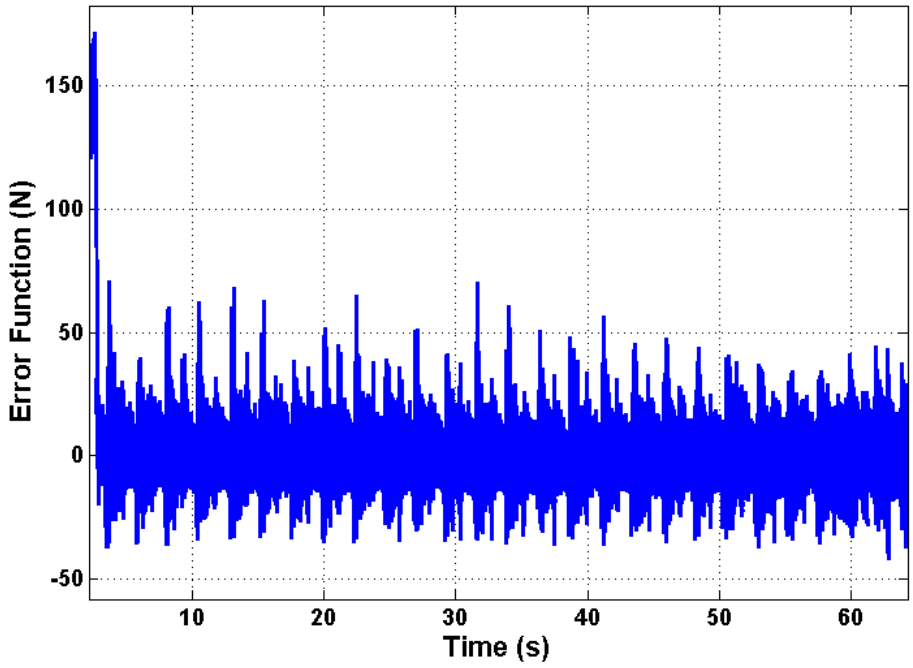

Figure 8.8: Trajectory of the error function $J_p(P_1, P_2, F_a)$ defined for the low pressure chamber in Eq. (8.12)

cheaper to procure than servo-valves. Passivity based control with digital valves is not investigated in this study. However, given their benefits and their general acceptance in industry, passive operation with digital valves should be investigated in the future.

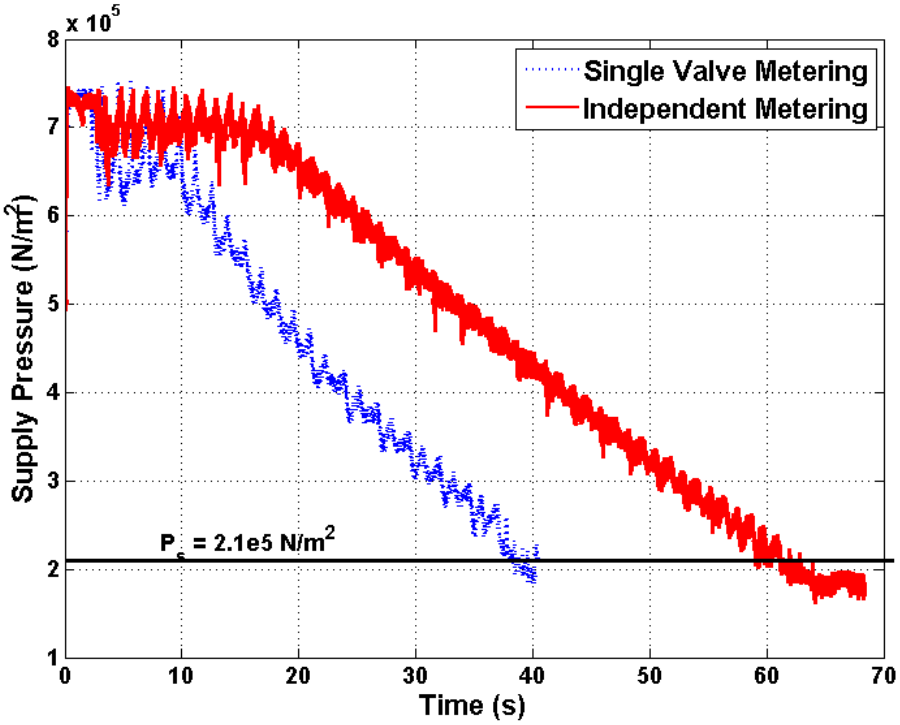

Figure 8.9: Comparison of reservoir pressure variation between single valve metering and independent valve metering

Chapter 9

Conclusion and Future Work

9.1 Conclusions

In this thesis, a framework for energetic passivity analysis of pneumatic actuated systems has been presented. Specifically, pneumatic actuators with three different heat transfer models *viz* adiabatic, isothermal and finite heat transfer were studied. In accordance with the requirements of energetic passivity analysis, an energy function is derived for each of the three thermodynamic models. For pneumatic actuators with reversible thermodynamic process (adiabatic/isothermal), the energy function is defined as the available work from the actuator. For the pneumatic actuator with finite heat transfer, the energy function is defined as the maximum available work from the actuator for a given thermodynamic state. It is shown that while the process for obtaining maximum work output from a pneumatic actuator with finite heat transfer is non-unique, the maximum available work along all these process trajectories is the same, and has a form similar to sum of exergy of air in each chamber of the pneumatic actuator.

Using the energy function as a storage function, the external energetic supply rate to the pneumatic actuator for the three heat transfer models is identified. For both the adiabatic and isothermal models the supply rate to the pneumatic actuator is similar to that of a two-port nonlinear spring, with one port corresponding to mechanical power interaction and the other port corresponding to interaction at the fluid port. Each chamber of the two-chambered actuator with finite heat transfer model has an additional port for external power interaction due to heat transfer between the chamber air and the

ambient. From the power interaction at this thermal port it is observed that irrespective of the chamber air temperature, heat transfer reduces the actuator's potential to do work. Thus heat transfer aids in passive behavior. The flow variable at the fluid port of the pneumatic actuator (for all thermodynamics models) is however an active input as it is connected to the source of compressed air.

To achieve passive operation of pneumatic actuated devices in human interactive applications, a framework for appropriately designing the control input at the fluid port of the actuator has been presented in this dissertation. For both the adiabatic and the isothermal actuators, the fluid port power variables are transformed such that the effort variable corresponds to the actuator force $F_a(\boldsymbol{P})$ and flow variable corresponds to an input dependent pseudo-velocity variable. By defining the pseudo-velocity variable as a combination of the velocity of a suitably defined virtual inertia dynamics, and an appropriate feedback signal, passive operation of the pneumatic actuator is achieved. In the current document, this proposed framework for control of pneumatic actuators has been used to develop the controller for a pneumatic human power amplifier. Experimental results that demonstrate the efficacy of the proposed controller have also been reported in this thesis. Controllers designed for both the adiabatic and the isothermal models of heat transfer demonstrated similar performance in experiments.

In this thesis, it is shown that the control design framework presented for human power amplification with a single actuator can be extended to achieve human power amplification and co-ordinated tele-operation of multiple pneumatic and/or hydraulic actuators with reversible (adiabatic/isothermal) thermodynamics. Modifications in the proposed framework for multilateral operation between multiple fluid-powered actuators to facilitate co-ordinated tele-operation of multiple fluid-powered (hydraulic/pneumatic) actuators with a single electro-mechanically actuated device has also been presented. The control objective of multilateral tele-operation within the proposed framework is achieved by using a two-stage controller designed through back-stepping. The controller was implemented on an experimental setup consisting of two single-DOF systems. Results demonstrating efficacy of the proposed controllers have also been presented in this dissertation. In the reported experimental results, no difference in performance was noticed between controllers designed by using adiabatic or isothermal model in the pneumatic actuator.

The controller developed for tele-operation between two single-DOF pneumatic actuators was then adapted for bilateral tele-operation between a multi-DOF PHANToM(TM[1]) haptic device actuated by a DC servomotor, and a multi-DOF pneumatic actuated crawling robotic system. The framework for bilateral tele-operation was modified to also amplify input human power on an interface on the crawler leg. By assuming the heat transfer model in the actuator to be adiabatic, a two-stage back-stepping controller was designed to achieve the desired control objective. Experimental results demonstrating good tracking performance in operations such as, bilateral motion in free-space, interaction with a hard surface, amplification of the input human power at the interface on the crawler leg, and walking the crawler by commanding the PHANToM(TM[1]), have been presented. Force sensors for measuring the ground reaction force when walking the crawler by commanding the PHANToM(TM[1]) haptic device are currently not available in the experimental setup. The ground reaction forces on the crawler were therefore estimated by using direct adaptive control. Controller performance when walking the crawler can be further improved by using a force sensor at the tip of the foot.

Independent metering as a means for improving operational efficiency of pneumatic actuators has also been investigated in this thesis. By assuming the heat transfer model in the actuator to be isothermal, controllers were developed for achieving human power amplification, while maintaining a low operating pressure. The novelty of the approach for independent metering proposed in this thesis is the definition of a pressure error function for the low pressure side of the actuator which remains continuous even as the chamber connected to the ambient pressure varies with the actuator force. The control input to the valve connecting the actuator chamber to ambient pressure is designed to achieve continuous exponential convergence of the pressure error function. The control input to the valve connecting the actuator chamber to supply pressure is designed to achieve human power amplification. When using a source of limited compressed air, experimental results show that with independent metering, the human power amplifier can be operated for 70% longer than when using a single valve for metering the air flow.

[1] PHANToM is a trademarked product of Sensable Technologies,MA

9.2 Future work

The pneumatic actuator controller design presented in this thesis is for adiabatic and isothermal actuators only. Unlike these actuators, the fluid port power variables of the actuator with finite heat transfer cannot be transformed to have the actuator force as an effort variable. As a result, the control techniques presented in this thesis for achieving human power amplification and co-ordination of multiple actuators cannot be directly adopted for a pneumatic actuator with finite heat transfer. Further work is required to identify a suitable framework for designing passive controllers for pneumatic actuator with finite heat transfer.

The controllers for bilateral tele-operation between the PHANToM(TM[1]) haptic device and the crawling rescue robot were developed by assuming that the front two legs of the crawler are decoupled. This is because the gait pattern used in this study was similar to butterfly stroke in swimming. In a crawler with four legs however, their motion would be coupled through the motion of the crawler chassis. An accurate model of the robot should include the motion of the chassis in the overall dynamics. Such a dynamic model can be developed by assuming the chassis to be a floating platform [84].

In this thesis, independent metering was implemented with two independent servo-valves. As a result, the throttling losses associated with servo-valves has not been mitigated. This can be addressed by using digital on/off valves. Since these valves are either completely open or closed, throttling losses can be avoided. Independent metering with on/off valves has been investigated for hydraulic systems. However, passivity based controllers are yet to be developed for fluid-powered systems with digital inputs. A potential extension of the work presented in this thesis is the development of passivity based controllers for fluid-powered systems with digital inputs.

The energy density of pneumatic actuators is fairly poor in comparison to batteries. Research in chemo-fluidic actuators [85], miniature HCCI engines [15], free-piston engines [14] and carbon-dioxide powered actuators [13], highlight some of the efforts towards improving energy density of pneumatic actuators. The actuating medium in these new actuators is a gas produced through some chemical processes. Therefore, the reaction dynamics have to be considered in the passivity analysis for investigating interaction stability. This would entail formulation of an appropriate energy function

to characterize the energy of the reaction process. While there is some body of work on passivity analysis of chemical reactions [86], these ideas have not yet been successfully pursued for a system with combination of chemical and mechanical processes. As the technologies for these new breed of actuators mature, the ideas presented in this thesis can be extended to define a framework for energetically passive operation of devices that use chemical reaction to produce gas.

References

[1] M.W. Spong, S. Hutchinson, and M. Vidyasagar. *Robot Modeling and Control*. Wiley New Jersey, 2006.

[2] H.Khalil. *Nonlinear Systems*. Prentice Hall, 1995.

[3] J.C.Willems. Dissipative Dynamical Systems, Part 1: General theory. *Archive Rational Mechanical Analysis*, 45(22):321–351, 1972.

[4] N.Hogan. Controlling Impedance at the Man/Machine Interface. *Proceedings, IEEE International Conference on Robotics and Automation, 1989*, pages 1626–1631, 1989.

[5] Y. Minamiyama, T. Kiyota, T. Sasaki, and N. Sugimoto. Application of Passive Dynamic Control to Pneumatic Cylinders. In *IEEE International Conference on Robotics and Automation*, pages 4497–4502. IEEE, 2007.

[6] P.Y.Li and K.Krishnaswamy. Passive Bilateral Teleoperation of a Hydraulic Actuator Using an Electrohydraulic Passive Valve. *International Journal of Fluid Power*, 5(2):43–56, 2004.

[7] Y. Zhu and E.J. Barth. Passivity-Based Impact and Force Control of a Pneumatic Actuator. *Journal of Dynamic Systems, Measurement, and Control*, 130:024501, 2008.

[8] N. Hogan. On the Stability of Manipulators Performing Contact Tasks. *IEEE Journal of Robotics and Automation*, 4(6):677–686, 1988.

[9] A.J. van der Schaft. Port-Hamiltonian Systems: Network Modeling and Control of Nonlinear Physical Systems. *Advanced Dynamics and Control of Structures and Machines CISM Courses and lectures*, (444):15–19, 2004.

[10] S. Stramigioli. *Modeling and IPC Control of Interactive Mechanical Systems: A Coordinate-Free Approach*, volume 266. Springer, 2001.

[11] K.A. Al-Dakkan, E.J. Barth, and M. Goldfarb. Dynamic Constraint-Based Energy-Saving Control of Pneumatic Servo Systems. *Journal of Dynamic Systems, Measurement, and Control*, 128:655, 2006.

[12] B.L. Shields, K.B. Fite, and M. Goldfarb. Design, Control, and Energetic Characterization of a Solenoid-Injected Monopropellant-Powered Actuator. *IEEE/ASME Transactions on Mechatronics*, 11(4):477–487, 2006.

[13] A. Kitagawa, H. Wu, H. Tsukagoshi, and S.H. Park. Development of a Portable Pneumatic Power Source using Phase Transition at the Triple Point. *Transactions of the Japan Fluid Power System Society*, 36(6):158–164, 2005.

[14] J.A. Riofrio and E.J. Barth. Design of a Free Piston Pneumatic Compressor as a Mobile Robot Power Supply. *IEEE Conference on Robotics and Automation*, pages 235–240, 2005.

[15] L. Tian, D.B. Kittelson, and W.K. Durfee. Miniature HCCI Free-Piston Engine Compressor For Orthosis Application. *SAE papers*, 2009.

[16] C.R. Burrows and C.R. Webb. Use of Root Loci in Design of Pneumatic Servo-Motors (Pneumatic Servomotor Synthesis by Root Loci Technique Providing Direct Insight into Effects of Parameter Changes on System Response). *Control*, 10:423–427, 1966.

[17] S. Liu and J.E. Bobrow. An Analysis of a Pneumatic Servo System and its Application to a Computer-Controlled Robot. *Journal of Dynamic Systems, Measurement, and Control*, 110:228, 1988.

[18] C. Kunt and R. Singh. A Linear Time Varying Model for On-Off Valve Controlled Pneumatic Actuators. *Journal of Dynamic Systems, Measurement, and Control*, 112:740, 1990.

[19] J.E. Bobrow and F. Jabbari. Adaptive Pneumatic Force Actuation and Position Control. *Journal of Dynamic Systems, Measurement, and Control*, 113:267, 1991.

[20] B.W. McDonell and J.E. Bobrow. Adaptive Tracking Control of an Air Powered Robot Actuator. *Journal of Dynamic Systems, Measurement, and Control*, 115:427, 1993.

[21] E.Richer and Y.Hurmuzlu. A High Performance Pneumatic Force Actuator System: Part I-Nonlinear Mathematical Model. *Journal Dynamic Systems Measurement and Control*, 4(122):416–425, September 2000.

[22] E.Richer and Y.Hurmuzlu. A High Performance Pneumatic Force Actuator System: Part II-Nonlinear Controller Design. *Journal Dynamic Systems Measurement and Control*, 4(122):426–434, September 2000.

[23] E.T. Wolbrecht, J. Leavitt, D.J. Reinkensmeyer, and J.E. Bobrow. Control of a Pneumatic Orthosis for Upper Extremity Stroke Rehabilitation. In *Engineering in Medicine and Biology Society*, pages 2687–2693. IEEE, 2006.

[24] R.J. Sanchez Jr, E. Wolbrecht, R. Smith, J. Liu, S. Rao, S. Cramer, T. Rahman, J.E. Bobrow, and D.J. Reinkensmeyer. A Pneumatic Robot for Re-training Arm Movement After Stroke: Rationale and Mechanical Design. *9th International Conference on Rehabilitation Robotics*, pages 500–504, 2005.

[25] P.V. Kokotovic, M. Krstic, and I. Kanellakopoulos. Backstepping to Passivity: Recursive Design of Adaptive Systems. In *Proceedings of the 31st IEEE Conference on Decision and Control*, pages 3276–3280. IEEE, 1992.

[26] D.J. Hill and P.J. Moylan. Stability Results for Nonlinear Feedback Systems. *Automatica*, 13(4):377–382, 1977.

[27] W. Book, R. Charles, H. Davis, and M. Gomes. The Concept and Implementation of a Passive Trajectory Enhancing Robot. In *Proc. ASME Dynamic Systems and Control Division*, volume 58, page 633, 1996.

[28] M.A. Peshkin, J.E. Colgate, W. Wannasuphoprasit, C.A. Moore, R.B. Gillespie, and P. Akella. Cobot Architecture. *IEEE Transactions on Robotics and Automation*, 17(4):377–390, 2001.

[29] D. Gao and W.J. Book. Steerability for Planar Dissipative Passive Haptic Interfaces. *IEEE/ASME Transactions on Mechatronics*, 11(2):179, 2006.

[30] D.Lee and P.Y.Li. Passive Bilateral Control and Tool Dynamics Rendering for Nonlinear Mechanical Teleoperators. *IEEE Transactions on Robotics*, 21(5):936–951, October 2005.

[31] R. Ortega, A. Loria, P.J. Nicklasson, and H.J. Sira-Ramirez. *Passivity-Based Control of Euler-Lagrange Systems: Mechanical, Electrical and Electromechanical Applications*. Springer, 1998.

[32] R. Ortega, A. Van Der Schaft, B. Maschke, and G. Escobar. Interconnection and Damping Assignment Passivity-Based Control of Port-Controlled Hamiltonian Systems. *Automatica*, 38(4):585–596, 2002.

[33] K. Fujimoto, K. Sakurama, and T. Sugie. Trajectory Tracking Control of Port-Controlled Hamiltonian Systems via Generalized Canonical Transformations. *Automatica*, 39(12):2059–2069, 2003.

[34] P.Y. Li and R. Horowitz. Passive Velocity Field Control of Mechanical Manipulators. *IEEE Transactions on Robotics and Automation*, 15(4):751–763, 1999.

[35] B. Hannaford and J.H. Ryu. Time-Domain Passivity Control of Haptic Interfaces. *IEEE Transactions on Robotics*, 18(1):1–10, February 2002.

[36] P.Y.Li. Towards Safe and Human Friendly Hydraulics: The Passive Valve. *ASME Journal Dynamic Systems Measurement and Control*, 122:402–409, 2000.

[37] F. Mazenc and E. Richard. Stabilization of Hydraulic Systems using a Passivity Property. *Systems & Control Letters*, 44(2):111–117, 2001.

[38] A. Kugi and W. Kemmetmüller. New Energy-Based Nonlinear Controller for Hydraulic Piston Actuators. *European journal of control*, 10(2):163–173, 2004.

[39] G. Grabmair and K. Schlacher. Energy-Based Nonlinear Control of Hydraulically Actuated Mechanical Systems. In *44th IEEE Conference on Decision and Control and European Control Conference. (CDC-ECC'05)*, pages 7520–7525. IEEE, 2005.

[40] S. Sakai and S. Stramigioli. Passivity Based Control of Hydraulic Robot Arms Using Natural Casimir Functions: Theory and Experiments. In *IEEE/RSJ International Conference on Intelligent Robots and Systems*, pages 538–544. IEEE, 2008.

[41] P. Y. Li and M. Wang. Natural Storage Function for Passivity-Based Trajectory Control of Hydraulic Actuators. *IEEE/ASME Transactions on Mechatronics*, 19(3):1057–1068, 2014.

[42] Y. Zhu and E.J. Barth. An Energetic Control Methodology for Exploiting the Passive Dynamics of Pneumatically Actuated Hopping. *Journal of Dynamic Systems, Measurement, and Control*, 130:041004, 2008.

[43] M. Goldfarb. On the Enhanced Passivity of Pneumatically Actuated Impedance-Type Haptic Interfaces. *IEEE Transactions on Robotics*, 22(3):470–480, 2006.

[44] T. Kagawa, M. Cai, and K. Kawashima. Energy Assessment in Pneumatic Systems and Air Power Meter. In *BATH Workshop on Power Transmission and Motion Control*, pages 377–388. Professional Engineering Publishing, 2002.

[45] R.D. Robinett III and D.G. Wilson. Exergy and Irreversible Entropy Production Thermodynamic Concepts for Nonlinear Control Design. *International Journal of Exergy*, 6(3):357–387, 2009.

[46] H. Kazerooni and J. Guo. Human Extenders. *Journal of Dynamic Systems, Measurement, and Control*, 115:281, 1993.

[47] H Kazerooni. Exoskeletons for Human Power Augmentation. In *IEEE/RSJ International Conference on Intelligent Robots and Systems*, pages 3459–3464. IEEE, 2005.

[48] P.Y. Li and R. Horowitz. Control of Smart Exercise Machines- Part I: Problem Formulation and Nonadaptive Control. *IEEE/ASME Transactions on Mechatronics*, 2(4):237–246, 1997.

[49] P.Y. Li and R. Horowitz. Passive Velocity Field Control (PVFC). Part I. Geometry and Robustness. *IEEE Transactions on Automatic Control*, 46(9):1346–1359, 2001.

[50] P.Y. Li and R. Horowitz. Passive Velocity Field Control (PVFC). Part II. Application to Contour Following. *IEEE Transactions on Automatic Control*, 46(9):1360–1371, 2001.

[51] J.A. Doubler and D.S. Childress. An Analysis of Extended Physiological Proprioception as a Prosthesis-Control Technique. *Journal of Rehabilitation Research and Development*, 21(1):5, 1984.

[52] J.A. Doubler and D.S. Childress. Design and Evaluation of a Prosthesis Control System Based on the Concept of Extended Physiological Proprioception. *Journal of Rehabilitation Research and Development*, 21(1):19, 1984.

[53] K.Kosuge T.Itoh and T.Fukuda. Human-Machine Cooperative Telemanipulation with Motion and Force Scaling Using Task-Oriented Virtual Tool Dynamics. *IEEE Transactions on Robotics and Automation*, 16(5):505–516, October 2000.

[54] K. Krishnaswamy. *Passive Teleoperation of Hydraulic Systems*. PhD thesis, University of Minnesota, 2004.

[55] K.Krishnaswamy and P.Y.Li. Bond Graph Based Approach to Passive Teleoperation of a Hydraulic Backhoe. *Journal of Dynamic Systems, Measurement, and Control*, 128(1):176–185, 2006.

[56] K. Tadano and K. Kawashima. Development of a Master Slave System with Force Sensing using Pneumatic Servo System for Laparoscopic Surgery. In *IEEE International Conference on Robotics and Automation*, pages 947–952. IEEE, 2007.

[57] M.Q. Le, M.T. Pham, M. Tavakoli, R. Moreau, J.P. Simon, and T. Redarce. Bilateral Control of a Nonlinear Pneumatic Teleoperation System with Solenoid Valves. *IEEE Transactions on Control Systems Technology*, 2012.

[58] B. Guerriero and W. Book. Haptic Feedback Applied to Pneumatic Walking. In *ASME Dynamic Systems and Controls Conference*, 2008.

[59] P.Y. Li. A New Passive Controller for a Hydraulic Human Power Amplifier. In *IMECE*, pages 1–11, Chicago, November 2006. ASME.

[60] P.Y.Li and V.Durbha. Passive Control of Fluid Powered Human Power Amplifiers. In *Japan Fluid Power Symp.*, pages –, Toyama, Japan, September 2008. Int. Fluid Power Symp.

[61] F. Eskilsson. Passive Control for a Human Power Amplifier, providing Force Amplification, Guidance and Obstacle Avoidance. Master's thesis, Linköping, 2011.

[62] F.E. Sanville. Two-level Compressed Air Systems for Energy Saving. In *The 7 th International Fluid Control Symposium*, pages 375–383, 1986.

[63] X. Shen and M. Goldfarb. Energy Saving in Pneumatic Servo Control Utilizing Interchamber Cross-Flow. *Journal of Dynamic Systems, Measurement, and Control*, 129:303, 2007.

[64] B. Yao and S. Liu. Energy-Saving Control of Hydraulic Systems with Novel Programmable Valves. In *Proceedings of the 4th World Congress on Intelligent Control and Automation (WCICA)*, volume 4, 2002.

[65] Y. A. Cengel, M. A. Boles, and M. Kanoğlu. *Thermodynamics: An Engineering Approach*, volume 5. McGraw-Hill New York, 2011.

[66] P.Y. Li and M. Wang. Passivity Based Nonlinear Control of Hydraulic Actuators Based on Euler-Lagrange Formulation. *ASME Proc. Dynamic Systems and Control Conference*, 2011.

[67] H.M. Paynter, M. Cambridge, E.P. Fahrenthold, and T. Austin. On the Nonexistence of Simple Polytropes and Other Thermodynamic Consequences of the Dispersion Relation. *Network Thermodynamics, Heat and Mass Transfer in Biotechnology: Presented at the Winter Annual Meeting of the American Society of Mechanical Engineers, Boston, Massachusetts, December 13-18, 1987*, page 37, 1987.

[68] W.A. Day. A Theory of Thermodynamics for Materials with Memory. *Archive for Rational Mechanics and Analysis*, 34(2):85–96, 1969.

[69] J.Falco Carneiro and F.Gomes de Almeida. Reduced-order thermodynamic models for servo-pneumatic actuator chambers. In *IMECE Journal Systems Control Engineering.*, pages 301–314. ASME, March 2006.

[70] J. Wyatt, L. Chua, J. Gannett, I. Goknar, and D. Green. Energy Concepts in the State-Space Theory of Nonlinear n-ports: Part i-Passivity. *IEEE Transactions on Circuits and Systems*, 28(1):48–61, 1981.

[71] A.E. Bryson and Yu-Chi Ho. *Applied Optimal Control*. Blaisdell, Waltham, Mass, 1969.

[72] P.Y. Li. Design and Control of a Hydraulic Human Power Amplifier. In *IMECE*, pages 1–11, Chicago, November 2004. ASME.

[73] D Lee and P. Y. Li. Passive Decomposition of Mechanical Systems with Coordination Requirement. *IEEE Transactions on Automatic Control*, 58(1):230–235, 2013.

[74] A. Astolfi, R. Ortega, and A. Venkatraman. A Globally Exponentially Convergent Immersion and Invariance Speed Observer for n Degrees Of Freedom Mechanical Systems. In *Proceedings of the 48th IEEE Conference on Decision and Control, held jointly with the 28th Chinese Control Conference (CDC/CCC 2009)*, pages 6508–6513. IEEE, 2009.

[75] V. Durbha and P. Li. A Nonlinear Spring Model of Hydraulic Actuator for Passive Controller Design in Bilateral Tele-Operation. In *American Control Conference*, pages 3471–3476. IEEE, 2012.

[76] D Lee and M. W. Spong. Passive Bilateral Teleoperation with Constant Time Delay. *IEEE Transactions on Robotics*, 22(2):269–281, 2006.

[77] B.A. Guerriero. Haptic Control and Operator-Guided Gait Coordination of a Pneumatic Hexapedal Rescue Robot. Master's thesis, Georgia Institute of Technology, 2008.

[78] M.D. Elton. Operator Efficiency Improvements from Novel Human-Machine Interfaces. Master's thesis, Georgia Institute of Technology, 2010.

[79] M.C. Cavusoglu and D. Feygin. Kinematics and Dynamics of PHANToM (TM) model 1.5 Haptic Interface. *University of California at Berkeley, Electronics Research Laboratory memo M*, 1, 2001.

[80] A.M. Tahmasebi, B. Taati, F. Mobasser, and K. Hashtrudi-Zaad. Dynamic Parameter Identification and Analysis of a PHANToM Haptic Device. In *Proceedings of IEEE Conference on Control Applications*, pages 1251–1256. IEEE, 2005.

[81] C. Cruz-Valverde, O.A. Dominguez-Ramirez, E.R. Ponce-de León-Sánchez, I. Trejo-Mota, and G. Sepúlveda-Cervantes. Kinematic and Dynamic Modeling of the PHANToM Premium 1.0 Haptic Device: Experimental Validation. In *Electronics, Robotics and Automotive Mechanics Conference (CERMA)*, pages 494–501. IEEE, 2010.

[82] T.Y. Kim. Simulation and Control of a Four Legged Rescue Robot. Master's thesis, Georgia Institute of Technology, 2009.

[83] N. Sadegh and R. Horowitz. Stability and Robustness Analysis of a Class of Adaptive Controllers for Robotic Manipulators. *The International Journal of Robotics Research*, 9(3):74–92, 1990.

[84] R. Featherstone. *Rigid Body Dynamics Algorithms*, volume 49. Springer, 2008.

[85] K.B. Fite, J.E. Mitchell, E.J. Barth, and M. Goldfarb. A Unified Force Controller for a Proportional-Injector Direct-Injection Monopropellant-Powered Actuator. *Journal of Dynamic Systems, Measurement, and Control*, 128:159, 2006.

[86] J. Bao and P.L. Lee. *Process Control: The Passive Systems Approach*. Springer-Verlag, 2007.

Appendix A

Proofs from Chapter 3

In this appendix proof for some of statements in chapter 3, regarding the properties of adiabatic and isothermal actuators are provided. Some preliminary relationships between chamber pressure, temperature and volume along the adiabatic and the isothermal trajectories is first presented. These relationships are then used to establish the properties of the adiabatic and isothermal actuators.

A.1 Isothermal actuator

For given mass of air m_1 and m_2 be the mass of air in chamber 1 and 2 respectively, using the definition of the chamber volumes $V_1(x) = A_1(L_{1o} + x)$, $V_2(x) = A_2(L_{2o} - x)$ from Eq. (3.73) in Eq. (3.82), the pressures P_1 and P_2 in chambers 1 and 2 of the isothermal chamber can be written in terms of the actuator position x as,

$$P_1(A_1(L_{1o} + x)) = k_{c_1}(m_1) = m_1 R T_o, \qquad P_2(A_2(L_{2o} - x)) = k_{c_2}(m_2) = m_2 R T_o \quad \text{(A.1)}$$

Using the above relationship between chamber pressures P_1, P_2 and the actuator position x in the expression for actuator force $F_a(\boldsymbol{P})$ in Eq. (3.1), the force from a two-chambered isothermal actuator can be expressed as,

$$\begin{aligned} F_a(\boldsymbol{P}) &= P_1 A_1 - P_2 A_2 - P_o A_p \\ &= \frac{m_1 R T_o}{L_{1o} + x} - \frac{m_2 R T_o}{L_{2o} - x} - P_o A_p \end{aligned} \quad \text{(A.2)}$$

The equilibrium position $\bar{x}(\boldsymbol{m})$ of the isothermal actuator corresponding to zero actuator force ($F_a(\bar{\boldsymbol{P}}) = 0$) is obtained as the solution of Eq. (3.98). Using Eq. (3.98), the actuator force $F_a(\boldsymbol{P})$ in Eq. (A.2) can be expressed as the product of the nonlinear spring stiffness $K_{iso}(\boldsymbol{m}, x)$ and the position deviation from equilibrium state $(\bar{x}(\boldsymbol{m}) - x)$ as,

$$\begin{aligned} F_a(\boldsymbol{P}) &= \left(\frac{m_1 RT_o}{L_{1o} + x} - \frac{m_2 RT_o}{L_{2o} - x}\right) - \left(\frac{m_1 RT_o}{L_{1o} + \bar{x}(\boldsymbol{m})} - \frac{m_2 RT_o}{L_{2o} - \bar{x}(\boldsymbol{m})}\right) \\ &= K_{iso}(\boldsymbol{m}, x)(\bar{x}(\boldsymbol{m}) - x) \end{aligned} \tag{A.3}$$

where the nonlinear spring stiffness $K_{iso}(\boldsymbol{m}, x) \in \Re^+$ is given by,

$$K_{iso}(\boldsymbol{m}, x) = \left(\frac{m_1 RT_o}{(L_{1o} + x)(L_{1o} + \bar{x}(\boldsymbol{m}))} + \frac{m_2 RT_o}{(L_{2o} - x)(L_{2o} - \bar{x}(\boldsymbol{m}))}\right) \tag{A.4}$$

Lemma A.1. *For a given mass of air m_1 and m_2 in chambers 1 and 2 of the actuator, the force $F_a(\boldsymbol{P})$ from an isothermal actuator in Eq. (A.3) is a strict monotonic function of the position deviation $(\bar{x}(\boldsymbol{m}) - x)$.*

Proof. For ease of analysis, the actuator force $F_a(\boldsymbol{P})$ in Eq. (A.3) is written as,

$$F_a(\boldsymbol{P}) = \frac{m_1 RT_o}{L_{1o} + \bar{x}(\boldsymbol{m})}\left(\frac{L_{1o} + \bar{x}(\boldsymbol{m})}{L_{1o} + x} - 1\right) + \frac{m_2 RT_o}{L_{2o} - \bar{x}(\boldsymbol{m})}\left(1 - \frac{L_{2o} - \bar{x}(\boldsymbol{m})}{L_{2o} - x}\right) \tag{A.5}$$

In the above equation, for an increasing $(\bar{x}(\boldsymbol{m}) - x)$, $(L_{1o} + \bar{x}(\boldsymbol{m}))/(L_{1o} + x) - 1$ increases monotonically, while $1 - (L_{2o} - \bar{x}(\boldsymbol{m}))/(L_{2o} - x)$ decreases monotonically. On the other hand, if $(\bar{x}(\boldsymbol{m}) - x)$ is decreasing, $(L_{1o} + \bar{x}(\boldsymbol{m}))/(L_{1o} + x) - 1$ decreases monotonically, while $1 - (L_{2o} - \bar{x}(\boldsymbol{m}))/(L_{2o} - x)$ increases monotonically. In addition, as $(\bar{x}(\boldsymbol{m}) - x)$, $((L_{1o} + \bar{x}(\boldsymbol{m}))/(L_{1o} + x) - 1)$ and $(1 - (L_{2o} - \bar{x}(\boldsymbol{m}))/(L_{2o} - x))$ have the same sign, the actuator force $F_a(\boldsymbol{P})$ in Eq. (A.5) is zero only when $x = \bar{x}(\boldsymbol{m})$ and is non-zero everywhere else. Therefore, the actuator force $F_a(\boldsymbol{P})$ varies strictly monotonically with position deviation $(\bar{x}(\boldsymbol{m}) - x)$.

□

A.1.1 Proof of proposition 3.3

Proof. In this proof the monotonic relationship between the fluid port effort variable $Z_\gamma^{iso}(\boldsymbol{m}, \boldsymbol{P}, u)$ and the actuator force $F_a(\boldsymbol{P})$ is first established. The nonlinear function

$\gamma_1^{iso}(\boldsymbol{m}, \boldsymbol{P}, u)$ mapping the actuator force $F_a(\boldsymbol{P})$ to the effort variable $Z_\gamma^{iso}(\boldsymbol{m}, \boldsymbol{P}, u)$ is then shown to be well-defined.

From the pressure-volume $(P - V)$ relationship for an isothermal actuator in Eq. (3.82), the effort variable $Z_\gamma^{iso}(\boldsymbol{m}, \boldsymbol{P}, u)$ at the fluid port in Eq. (3.118) can be expressed in terms of the actuator position x as,

$$\begin{aligned} Z_\gamma^{iso}(\boldsymbol{m}, \boldsymbol{P}, u) &= \Psi(P_1, T_1, u) R T_o \log\left(\frac{P_1}{\bar{P}_1(\boldsymbol{m})}\right) - \Psi(P_2, T_2, -u) R T_o \log\left(\frac{P_2}{\bar{P}_2(\boldsymbol{m})}\right) \\ &= \Psi(P_1, T_1, u) R T_o \log\left(\frac{L_{1o} + \bar{x}(\boldsymbol{m})}{L_{1o} + x}\right) - \Psi(P_2, T_2, -u) R T_o \log\left(\frac{L_{2o} - \bar{x}(\boldsymbol{m})}{L_{2o} - x}\right) \end{aligned} \quad \text{(A.6)}$$

where the nonlinear function $\Psi(.) \in \Re^+$ is as defined in Eq. (3.27). In the above equation, for a known $\bar{x}(\boldsymbol{m})$, the term $\log\left((L_{1o} + \bar{x}(\boldsymbol{m}))/(L_{1o} + x)\right)$ is a strictly monotonically increasing function of $(\bar{x}(\boldsymbol{m}) - x)$, while $\log\left((L_{2o} - \bar{x}(\boldsymbol{m}))/(L_{2o} - x)\right)$ is a strictly monotonically decreasing functions of $(\bar{x}(\boldsymbol{m}) - x)$. As $\log\left((L_{1o} + \bar{x}(\boldsymbol{m}))/(L_{1o} + x)\right)$ and $\log\left((L_{2o} - \bar{x}(\boldsymbol{m}))/(L_{2o} - x)\right)$ have opposite sign, the effort variable $Z_\gamma^{iso}(\boldsymbol{m}, \boldsymbol{P}, u)$ at the fluid port is identically zero only when the actuator position x corresponds to the equilibrium position $\bar{x}(\boldsymbol{m})$. Thus, $Z_\gamma^{iso}(\boldsymbol{m}, \boldsymbol{P}, u)$ as defined in Eq. (A.6) is also a strict monotonic function of position deviation $(\bar{x}(\boldsymbol{m}) - x)$. As shown in lemma A.1, the actuator force $F_a(\boldsymbol{P})$ is also has a strict monotonic variation with $(\bar{x}(\boldsymbol{m}) - x)$. Therefore, from transitive property, $Z_\gamma^{iso}(\boldsymbol{m}, \boldsymbol{P}, u)$ increases strictly monotonically with the actuator force $F_a(\boldsymbol{P})$.

The nonlinear function $\gamma_1^{iso}(\boldsymbol{m}, \boldsymbol{P}, u)$ be to map from the actuator force $F_a(\boldsymbol{P})$ to the effort variable $Z_\gamma^{iso}(\boldsymbol{m}, \boldsymbol{P}, u)$ is defined as,

$$\gamma_1^{iso}(\boldsymbol{m}, \boldsymbol{P}, u) = \frac{Z_\gamma^{iso}(\boldsymbol{m}, \boldsymbol{P}, u)}{F_a(\boldsymbol{P})} \quad \text{(A.7)}$$

As $Z_\gamma^{iso}(\boldsymbol{m}, \boldsymbol{P}, u)$ varies monotonically with actuator force $F_a(\boldsymbol{P})$, by definition, $\gamma_1^{iso}(\boldsymbol{m}, \boldsymbol{P}, u)$ is positive function for all $(\boldsymbol{m}, \boldsymbol{P}, u)$ when $x \neq \bar{x}(\boldsymbol{m})$ *i.e* $F_a(\boldsymbol{P}) \neq 0$. Using the definition of $F_a(\boldsymbol{P})$ from Eq. (A.5), the nonlinear map $\gamma_1^{iso}(\boldsymbol{m}, \boldsymbol{P}, u)$ is obtained at

the equilibrium state ($x = \bar{x}(\boldsymbol{m})$) as,

$$\begin{aligned}\gamma_1^{iso}(\boldsymbol{m},\boldsymbol{P},u)|_{x=\bar{x}(\boldsymbol{m})} &= \lim_{(\bar{x}(\boldsymbol{m})-x)\to 0} \frac{\Psi(P_1,T_1,u)RT_o}{K_{iso}(\boldsymbol{m},x)(\bar{x}(\boldsymbol{m})-x)} \log\left(1+\frac{\bar{x}(\boldsymbol{m})-x}{L_{1o}+x}\right) \\ &\quad + \lim_{(\bar{x}(\boldsymbol{m})-x)\to 0} \frac{\Psi(P_2,T_2,-u)RT_o}{K_{iso}(\boldsymbol{m},x)(\bar{x}(\boldsymbol{m})-x)} \log\left(1-\frac{\bar{x}(\boldsymbol{m})-x}{L_{2o}-x}\right) \\ &= \frac{RT_o}{K_{iso}(\boldsymbol{m},x)}\left(\frac{\Psi(P_1,T_1,u)}{L_{1o}+x}+\frac{\Psi(P_2,T_2,-u)}{L_{2o}-x}\right) \end{aligned} \tag{A.8}$$

where the nonlinear function $K_{iso}(\boldsymbol{m},x) \in \Re^+$ is as defined in Eq. (A.4). As the nonlinear function $\gamma_1^{iso}(\boldsymbol{m},\boldsymbol{P},u)$ has a finite positive value at equilibrium state ($x = \bar{x}(\boldsymbol{m})$) also, it is therefore positive and bounded for all bounded $(\boldsymbol{m},\boldsymbol{P},u)$. □

A.2 Adiabatic actuator

Let m_1 and m_2 be the mass of air in chamber 1 and 2 respectively. Using the expression for the chamber volumes $V_1(x) = A_1(L_{1o}+x)$ and $V_2(x) = A_2(L_{2o}-x)$ from Eq. (3.73) in Eq. (3.78), the pressures P_1 and P_2 in chambers 1 and 2 of the adiabatic chamber can be written in terms of the actuator position x as,

$$P_1(A_1(L_{1o}+x))^\gamma = k_{p_1}(m_1), \qquad P_2(A_2(L_{2o}-x))^\gamma = k_{p_2}(m_2) \tag{A.9}$$

where $k_{p_1}(m) \in \Re^+$ and $k_{p_2}(m) \in \Re^+$ are parameters that determine the trajectory of the adiabatic actuator, and are as determined from initial conditions as shown in Eq. (3.78). Using the expression for chamber pressures P_1 and P_2 from Eq. (A.9), the actuator force $F_a(\boldsymbol{P})$ in Eq. (3.1) can be written as,

$$\begin{aligned} F_a(\boldsymbol{P}) &= P_1A_1 - P_2A_2 - P_oA_p \\ &= \frac{k_{p_1}(m_1)}{A_1^{\gamma-1}(L_{1o}+x)^\gamma} - \frac{k_{p_2}(m_2)}{A_2^{\gamma-1}(L_{2o}-x)^\gamma} - P_oA_p \end{aligned} \tag{A.10}$$

where $A_p = (A_1 - A_2)$ is the piston rod area exposed to atmospheric pressure. For a fixed mass of air $\boldsymbol{m} := (m_1, m_2)$, the equilibrium position $\bar{x}(\boldsymbol{m})$ of the adiabatic actuator corresponding to $F_a(\bar{\boldsymbol{P}}) = 0$ is obtained from solution of Eq. (3.91). From the definition of the actuator equilibrium force in Eq. (3.91), the actuator force in Eq.

(A.10) can be expressed as,

$$F_a(\boldsymbol{P}) = \frac{k_{p_1}(m_1)}{A_1^{\gamma-1}(L_{1o}+x)^{\gamma}}\left(1-\left(\frac{L_{1o}+x}{L_{1o}+\bar{x}(\boldsymbol{m})}\right)^{\gamma}\right) - \frac{k_{p_2}(m_2)}{A_2^{\gamma-1}(L_{2o}-x)^{\gamma}}\left(1-\left(\frac{L_{2o}-x}{L_{2o}-\bar{x}(\boldsymbol{m})}\right)^{\gamma}\right) \tag{A.11}$$

Lemma A.2. *For a given mass of air m_1 and m_2 in the chambers 1 and 2 of the adiabatic actuator, the actuator force $F_a(\boldsymbol{P})$ in Eq. (A.11) is a strict monotonic function of $(\bar{x}(\boldsymbol{m})-x)$.*

Proof. When $(\bar{x}(\boldsymbol{m})-x)$ is increasing, $(1-(L_{1o}+x/L_{1o}+\bar{x}(\boldsymbol{m}))^{\gamma})$ increases strictly monotonically, while $(1-(L_{2o}-x/L_{2o}-\bar{x}(\boldsymbol{m}))^{\gamma})$ decreases strictly monotonically. On the other hand, when $(\bar{x}(\boldsymbol{m})-x)$ is decreasing, $(1-(L_{1o}+x/L_{1o}+\bar{x}(\boldsymbol{m}))^{\gamma})$ decreases strictly monotonically, while $(1-(L_{2o}-x/L_{2o}-\bar{x}(\boldsymbol{m}))^{\gamma})$ increases strictly monotonically. As $(1-(L_{1o}+x/L_{1o}+\bar{x}(\boldsymbol{m}))^{\gamma})$ and $(1-(L_{2o}-x/L_{2o}-\bar{x}(\boldsymbol{m}))^{\gamma})$ always have the opposite sign, the actuator force $F_a(\boldsymbol{P})$ in Eq. (A.11) is identically zero only if $\bar{x}(\boldsymbol{m})=x$. Therefore, the actuator force is a strict monotonic function of $(\bar{x}(\boldsymbol{m})-x)$. The nonlinear function $K_{adb}(\boldsymbol{m},x)$ mapping the position deviation $(\bar{x}(\boldsymbol{m})-x)$ to the actuator force $F_a(\boldsymbol{P})$ is analogous to nonlinear spring stiffness and is defined as,

$$K_{adb}(\boldsymbol{m},x) = \frac{F_a(\boldsymbol{P})}{(\bar{x}(\boldsymbol{m})-x)} \tag{A.12}$$

When the actuator position approaches the equilibrium position $((\bar{x}(\boldsymbol{m})-x)\to 0)$, the nonlinear function $K_{adb}(\boldsymbol{m},x)$ in the above equation is obtained as,

$$\begin{aligned} K_{adb}(\boldsymbol{m},x) &= \lim_{(\bar{x}(\boldsymbol{m})-x)\to 0}\frac{F_a(\boldsymbol{P})}{(\bar{x}(\boldsymbol{m})-x)} \\ &= \gamma\left(\frac{m_1RT_1}{(L_{1o}+x)(L_{1o}+\bar{x}(\boldsymbol{m}))}+\frac{m_2RT_2}{(L_{2o}-x)(L_{2o}-\bar{x}(\boldsymbol{m}))}\right) \end{aligned} \tag{A.13}$$

Thus, the nonlinear function $K_{adb}(\boldsymbol{m},x)$ is positive for all values of $\boldsymbol{m}$ and x. The actuator force $F_a(\boldsymbol{P})$ in Eq. (A.11) can then be expressed like a spring-force,

$$F_a(\boldsymbol{P}) = -K_{adb}(\boldsymbol{m},x)(x-\bar{x}(\boldsymbol{m})) \tag{A.14}$$

□

A.2.1 Proof of proposition 3.4

Proof. In this proof the monotonic relationship between the fluid port effort variable $Z_{\gamma}^{adb}(\boldsymbol{m}, \boldsymbol{P}, u)$ and the actuator force $F_a(\boldsymbol{P})$ is first established. The nonlinear function $\gamma_1^{adb}(\boldsymbol{m}, \boldsymbol{P}, u)$ mapping the actuator force $F_a(\boldsymbol{P})$ to the effort variable $Z_{\gamma}^{adb}(\boldsymbol{m}, \boldsymbol{P}, u)$ is then shown to be well-defined.

Using the temperature-volume $(T - V)$ relationship for an adiabatic actuator from Eq. (3.78), the fluid port effort variable $Z_{\gamma}^{adb}(\boldsymbol{m}, \boldsymbol{P}, u)$ in Eq. (3.133) can be expressed as,

$$Z_{\gamma}^{adb}(\boldsymbol{m}, \boldsymbol{P}, u) = \Psi(P_1, T_1, u) C_p T_1 \left(1 - \left(\frac{L_{1o} + x}{L_{1o} + \bar{x}(\boldsymbol{m})}\right)^{\gamma - 1}\right) - \Psi(P_2, T_2, -u) C_p T_2 \left(1 - \left(\frac{L_{2o} - x}{L_{2o} - \bar{x}(\boldsymbol{m})}\right)^{\gamma - 1}\right) \tag{A.15}$$

where the function $\Psi(.)$ is positive definite and is as defined in Eq. (3.27). In the above equation, $(1-((L_{1o}+x)/(L_{1o}+\bar{x}(\boldsymbol{m})))^{\gamma-1})$ decreases strictly monotonically with $(\bar{x}(\boldsymbol{m}) - x)$, while $(1 - ((L_{2o} - x)/(L_{2o} - \bar{x}(\boldsymbol{m})))^{\gamma-1})$ increases strictly monotonically with $(\bar{x}(\boldsymbol{m}) - x)$. As $(1 - ((L_{1o} + x)/(L_{1o} + \bar{x}(\boldsymbol{m})))^{\gamma-1})$ and $(1 - ((L_{2o} - x)/(L_{2o} - \bar{x}(\boldsymbol{m})))^{\gamma-1})$ always have opposite sign, the fluid port effort variable $Z_{\gamma}^{adb}(\boldsymbol{m}, \boldsymbol{P}, u)$ in Eq. (A.15) is identically zero only when the actuator position x corresponds to the equilibrium position $\bar{x}(\boldsymbol{m})$. Therefore $Z_{\gamma}^{adb}(\boldsymbol{m}, \boldsymbol{P}, u)$ varies strictly monotonically with $(\bar{x}(\boldsymbol{m}) - x)$. As shown in lemma A.2, there is a similar strict monotonic relationship between actuator force $F_a(\boldsymbol{P})$ and $(\bar{x}(\boldsymbol{m}) - x)$. Therefore, from transitive property, the adiabatic actuator force $F_a(\boldsymbol{P})$, and the effort variable $Z_{\gamma}^{adb}(\boldsymbol{m}, \boldsymbol{P}, u)$ also have a strict monotonically increasing relationship. Therefore, the nonlinear mapping $\gamma_1^{adb}(\boldsymbol{m}, \boldsymbol{P}, u)$ from the actuator force $F_a(\boldsymbol{P})$ to the effort variable $Z_{\gamma}^{adb}(\boldsymbol{m}, \boldsymbol{P}, u)$ is positive for all $x \neq \bar{x}(\boldsymbol{m})$ and is defined as,

$$\gamma_1^{adb}(\boldsymbol{m}, \boldsymbol{P}, u) = \frac{Z_{\gamma}^{adb}(\boldsymbol{m}, \boldsymbol{P}, u)}{F_a(\boldsymbol{P})} \tag{A.16}$$

Using the expression for actuator force $F_a(\boldsymbol{P})$ from Eq. (A.14), the nonlinear gain $\gamma_1^{adb}(\boldsymbol{m}, \boldsymbol{P}, u)$ is obtained at the equilibrium position $x = \bar{x}(\boldsymbol{m})$ as,

$$\lim_{(\bar{x}(\boldsymbol{m}) - x) \to 0} \gamma_1^{adb}(\boldsymbol{m}, \boldsymbol{P}, u) = \frac{\gamma R}{K_{adb}(\boldsymbol{m}, \boldsymbol{P})} \left(\frac{\Psi(P_1, T_1, u) T_1}{L_{1o} + x} + \frac{\Psi(P_2, T_2, -u) T_2}{L_{2o} - x}\right) \tag{A.17}$$

where the nonlinear gain $K_{adb}(\boldsymbol{m}, x)$ is as defined in Eq. (A.12). Therefore $\gamma_1^{adb}(\boldsymbol{m}, \boldsymbol{P}, u)$ has a finite positive value at equilibrium state ($x = \bar{x}(\boldsymbol{m})$). Therefore $\gamma_1^{adb}(\boldsymbol{m}, \boldsymbol{P}, u)$ is positive and well defined for all feasible values of air mass vector $\boldsymbol{m}$, chamber pressure vector $\boldsymbol{P}$ and valve input command u. □

A.2.2 Proof of remark 3.5

Proof. 1. Using the definition of desired chamber pressures in isothermal actuator from Eq. (3.140) in the expression for desired actuator force F_a^d in Eq. (3.138), and using the definition of isothermal actuator force $F_a(\boldsymbol{P})$ from Eq. (A.2), the force tracking error ($tildeF := (F_a - F_a^d)$) can be expressed in terms of the position error $(x_d - x)$ as,

$$\tilde{F} = F_a - F_a^d = \frac{m_1 R T_o}{L_{1o} + x_d}\left(\frac{L_{1o} + x_d}{L_{1o} + x} - 1\right) + \frac{m_2 R T_o}{L_{2o} - x_d}\left(1 - \frac{L_{2o} - x_d}{L_{2o} - x}\right) \quad \text{(A.18)}$$

The expression for $\tilde{F}$ in the above equation is similar to the expression for actuator force $F_a(\boldsymbol{P})$ in Eq. (A.5). By replacing the equilibrium position $\bar{x}(\boldsymbol{m})$ with the desired position x_d of the actuator, strict monotonic relationship between force error $\tilde{F}$ and the position error $(x_d - x)$ follows from the proof of lemma A.1.

Using the definition of desired chamber pressures for adiabatic actuator from Eq. (3.140) in the expression for desired actuator force F_a^d in Eq. (3.138), and using the definition of adiabatic actuator force $F_a(\boldsymbol{P})$ from Eq. (A.10), the force tracking error ($tildeF := (F_a - F_a^d)$) for the adiabatic actuator can be expressed as,

$$\tilde{F} = \frac{k_{p_1}(m_1)}{A_1^{\gamma-1}(L_{1o} + x)^\gamma}\left(1 - \left(\frac{L_{1o} + x}{L_{1o} + x_d}\right)^\gamma\right) + \frac{k_{p_2}(m_2)}{A_2^{\gamma-1}(L_{2o} - x)^\gamma}\left(\left(\frac{L_{2o} - x}{L_{2o} - x_d}\right)^\gamma - 1\right) \quad \text{(A.19)}$$

The above expression for force error $\tilde{F}$ is similar to the expression for force $F_a(\boldsymbol{P})$ from adiabatic actuator in Eq. (A.11). By replacing the equilibrium position $\bar{x}(\boldsymbol{m})$ in Eq. (A.11) with the desired position x_d, proof follows from lemma A.2.

2. *Isothermal actuator:* The force error $\tilde{F}$ for the isothermal actuator from Eq.

(A.18) can be expressed as,

$$\tilde{F} = \underbrace{\left(\frac{m_1 R T_o}{(L_{1o} + x)(L_{1o} + x_d)} + \frac{m_2 R T_o}{(L_{2o} - x)(L_{2o} - x_d)} \right)}_{K^d_{iso}(\boldsymbol{m}, x, x_d)} (x_d - x) \tag{A.20}$$

where $K^d_{iso}(\boldsymbol{m}, x, x_d)$ is analogous to the effective stiffness of the pneumatic actuator between the current position x and the desired position x_d. Using the ideal gas $PV = mRT_o$ for the isothermal chamber, $K^d_{iso}(\boldsymbol{m}, x, x_d)$ can be expressed in a form similar to $K_{iso}(\boldsymbol{m}, x)$ in Eq. (A.4) as,

$$K^d_{iso}(\boldsymbol{m}, x, x_d) = \frac{P_1 A_1}{(L_{1o} + x_d)} + \frac{P_2 A_2}{(L_{2o} - x_d)} \tag{A.21}$$

Therefore, $K^d_{iso}(\boldsymbol{m}, x, x_d)$ is positive for all feasible values of $(\boldsymbol{m}, x, x_d)$.

Adiabatic actuator: The nonlinear function $K^d_{adb}(\boldsymbol{m}, x, x_d)$ mapping the position error $(x_d - x)$ to the actuator force error $\tilde{F}$ of an adiabatic actuator be defined as,

$$K^d_{adb}(\boldsymbol{m}, x, x_d) = \frac{F_a - F^d_a}{x_d - x} \tag{A.22}$$

Due to the strictly monotonic relationship between $\tilde{F}$ and $(x_d - x)$, the nonlinear gain $K^d_{adb}(\boldsymbol{m}, x, x_d)$ is positive for all $x_d \neq x$. When the actuator position x, corresponds to the desired position x_d, then $K^d_{adb}(\boldsymbol{m}, x, x_d)$ is obtained as,

$$\begin{aligned} K^d_{adb}(\boldsymbol{m}, x, x_d)|_{x=x_d} &= \lim_{x \to x_d} \frac{F_a - F^d_a}{x_d - x} \\ &= \gamma \left(\frac{m_1 R T_1}{(L_{1o} + x_d)^2} + \frac{m_2 R T_2}{(L_{2o} - x_d)^2} \right) \end{aligned} \tag{A.23}$$

Therefore, the nonlinear gain $K^d_{adb}(\boldsymbol{m}, x, x_d)$ is well defined and positive for all feasible values of mass vector ($\boldsymbol{m}$, position x, and the desired actuator position x_d).

□

A.2.3 Proof of remark 3.6

Proof. Using the relationship between the chamber pressure and the chamber volume from Eq. (A.1) for the isothermal actuator and Eq. (A.9) for the adiabatic actuator

respectively, the effort variable for the isothermal actuator in Eq. (3.148) and the adiabatic actuator in Eq.(3.149) can be expressed as,

$$\begin{aligned} Z_\gamma^{iso}(\boldsymbol{m}, \boldsymbol{P}, \boldsymbol{P^d}, u) = \Psi(P_1, T_o, u) R T_o \log\left(\frac{L_{1o} + x_d}{L_{1o} + x}\right) \\ - \Psi(P_2, T_o, -u) R T_o \log\left(\frac{L_{2o} - x_d}{L_{2o} - x}\end{aligned} \right) \tag{A.24}$$

$$\begin{aligned} Z_\gamma^{adb}(\boldsymbol{m}, \boldsymbol{P}, \boldsymbol{P^d}, u) = \Psi(P_1, T_1, u) C_p T_1 \left(1 - \left(\frac{L_{1o} + x}{L_{1o} + x_d}\right)^{\gamma - 1}\right) \\ - \Psi(P_2, T_2, -u) C_p T_2 \left(1 - \left(\frac{L_{2o} - x}{L_{2o} - x_d}\right)^{\gamma - 1}\right)\end{aligned} \tag{A.25}$$

As expression for $Z_\gamma^{iso}(\boldsymbol{m}, \boldsymbol{P}, \boldsymbol{P^d}, u)$ in Eq. (A.24) is similar to the expression for $Z_\gamma^{iso}(\boldsymbol{m}, \boldsymbol{P}, u)$ in Eq. (A.6). The expression for $Z_\gamma^{adb}(\boldsymbol{m}, \boldsymbol{P}, \boldsymbol{P^d}, u)$ in Eq. (A.25) is also similar to the effort variable $Z_\gamma^{adb}(\boldsymbol{m}, \boldsymbol{P}, u)$ at the adiabatic actuator fluid port presented in Eq. (A.15). Let $j = (iso, adb)$ be the index to represent the thermodynamic process. By replacing the equilibrium position $\bar{x}(\boldsymbol{m})$ with the desired position x_d in Eq. (A.6) and Eq. (A.15) respectively, strictly monotonic relationship between $Z_\gamma^j(\boldsymbol{m}, \boldsymbol{P}, \boldsymbol{P^d}, u)$ and the position error $(x_d - x)$ is obtained from the proof for proposition 3.3. As shown in the remark 3.5, the actuator force error $\tilde{F}$ also has a strictly monotonic relationship with position error $(x_d - x)$. By using transitive property, the effort variables $Z_\gamma^j(\boldsymbol{m}, \boldsymbol{P}, \boldsymbol{P^d}, u)$ varies strictly monotonically with the actuator force error $\tilde{F}$. Therefore, the nonlinear function $\gamma_3^j(\boldsymbol{m}, \boldsymbol{P}, \boldsymbol{P^d}, u)$ mapping the actuator force error $\tilde{F}$ to the effort variable $Z_\gamma^j(\boldsymbol{m}, \boldsymbol{P}, \boldsymbol{P^d}, u)$ is positive for all $\boldsymbol{m}$, $\boldsymbol{P}$, $\boldsymbol{P^d}$, u and $\tilde{F} \neq 0$.

To determine the expression for $\gamma_3^j(\boldsymbol{m}, \boldsymbol{P}, \boldsymbol{P^d}, u)$ when $\tilde{F} = 0$, consider the following definition for $\gamma_3^j(\boldsymbol{m}, \boldsymbol{P}, \boldsymbol{P^d}, u)$,

$$\gamma_3^j(\boldsymbol{m}, \boldsymbol{P}, \boldsymbol{P^d}, u) = \frac{Z_\gamma^j(\boldsymbol{m}, \boldsymbol{P}, \boldsymbol{P^d}, u)}{K_j^d(\boldsymbol{m}, x, x_d)(x_d - x)} \tag{A.26}$$

where the expression $\tilde{F} = K_j^d(\boldsymbol{m}, x, x_d)(x_d - x)$ from Eq. (5.42) is used to represent the actuator force error. In the above equation, $K_j^d(\boldsymbol{m}, x, x_d)$ represents the equivalent spring stiffness for the isothermal or the adiabatic actuators and is as defined in Eq. (A.21) and Eq. (A.22) respectively. As the actuator force error is zero only when $x_d = x$,

at this condition $\gamma_3^j(\boldsymbol{m}, \boldsymbol{P}, \boldsymbol{P^d}, u)$ is obtained as,

$$\gamma_3^j(\boldsymbol{m}, \boldsymbol{P}, \boldsymbol{P^d}, u)\Big|_{x=x_d} = \lim_{x \to x_d} \frac{Z_\gamma^j(\boldsymbol{m}, \boldsymbol{P}, \boldsymbol{P^d}, u)}{K_j^d(\boldsymbol{m}, x, x_d)(x_d - x)} \tag{A.27}$$

In the limiting case when $x = x_d$, the nonlinear gain for isothermal and adiabatic actuators is obtained as,

$$\begin{aligned}
\gamma_3^{iso}(\boldsymbol{m}, \boldsymbol{P}, \boldsymbol{P^d}, u)\Big|_{x=x_d} &= \frac{RT_o}{K_{iso}^d(\boldsymbol{m}, x, x_d)} \left(\frac{\Psi(P_1, T_o, u)}{L_{1o} + x_d} + \frac{\Psi(P_2, T_o, -u)}{L_{2o} - x_d} \right) \\
\gamma_3^{adb}(\boldsymbol{m}, \boldsymbol{P}, \boldsymbol{P^d}, u)\Big|_{x=x_d} &= \frac{1}{K_{adb}^d(\boldsymbol{m}, x, x_d)} \left(\frac{\Psi(P_1, T_1, u) RT_1}{L_{1o} + x_d} + \frac{\Psi(P_2, T_2, -u) RT_2}{L_{2o} - x_d} \right)
\end{aligned} \tag{A.28}$$

As $\gamma_3^j(\boldsymbol{m}, \boldsymbol{P}, \boldsymbol{P^d}, u)$ is positive and bounded at also $\tilde{F} = 0$ ($i.e$ at $x = x_d$), it is well defined for all feasible values of $\boldsymbol{m}, \boldsymbol{P}, \boldsymbol{P^d}, u$.

□

Appendix B

Proofs from Chapter 4

B.1 Proof of remark 4.4

Proof. From Eq. (4.30), the gravimetric energy density of the actuator is defined as,

$$\begin{aligned} W_m(P,T,P_o) &= \frac{W_{act}(m,P,T,P_o)}{m} \\ &= C_v(T-T_o) - T_o\left(C_p\log\left(\frac{T}{T_o}\right) - R\log\left(\frac{P}{P_o}\right)\right) - P_o\left(\frac{\bar{V}}{m} - \frac{V}{m}\right) \end{aligned} \tag{B.1}$$

Using the definition of air density from Eq. (3.38), the gravimetric energy density in the above equation can be expressed as,

$$\begin{aligned} W_m(P,T,P_o) = C_v(T-T_o) - T_o\left(C_p\log\left(\frac{T}{T_o}\right) - R\log\left(\frac{P}{P_o}\right)\right) \\ - P_o\left(\frac{1}{\rho(P_o,T_o)} - \frac{1}{\rho(P,T)}\right) \end{aligned} \tag{B.2}$$

Using the relationship between the specific heat capacities, $(C_p - C_v) = R$, the gravimetric energy density in the above equation can be expressed as,

$$\begin{aligned} W_m(P,T,P_o) = C_vT_o\left(\left(\frac{T}{T_o}-1\right) - \log\left(\frac{T}{T_o}\right)\right) \\ + RT_o\left(\left(\frac{P_oT}{PT_o}-1\right) - \log\left(\frac{P_oT}{PT_o}\right)\right) \end{aligned} \tag{B.3}$$

As the following relationship holds for all $\alpha \in R$,

$$(\alpha - 1) - \log(\alpha) = \begin{cases} > 0 & \text{if } \alpha > 0 \\ = 0 & \text{if } \alpha = 0 \end{cases} \tag{B.4}$$

proof follows from using the above condition in Eq.(B.3). □

Appendix C

Proofs from Chapter 5

C.1 Proof of lemma 5.1

Proof. As the Lyapunov function candidate in Eq. (5.46) is defined as the sum of energetic functions for the two actuator chambers, suitability of the Lyapunov function is determined by analyzing the individual chamber Lyapunov functions.

Let $j \in iso, adb$ represent the index for the thermodynamic process. From theorems 3.1 and 3.2, the gravimetric energy density $W_m^j(P_i, P_i^d)$ for adiabatic and isothermal actuator chambers respectively, is known to be positive for all P, P_i^d and is identically zero only if $P_i = P_i^d$. With an increasing $(|P_i^d - P_i|)$, the gravimetric energy densities, $W_m^{adb}(P_i, P_i^d)$ for the adiabatic actuator in Eq. (3.37) and $W_m^{iso}(P_i, P_i^d)$ for the isothermal actuator in Eq. (3.48), increase monotonically and are thus radially unbounded in the pressure error $(|P_i^d - P_i|)$. As the actuator Lyapunov function is a linear combination of the individual chamber Lyapunov functions, it satisfies all the properties enumerated in the lemma statement to be a suitable Lyapunov function candidate. □

C.2 Proof of remark 5.2

Proof. As the actuator Lyapunov function candidate $W_L^j(\boldsymbol{m}, \boldsymbol{P}, \boldsymbol{P^d})$ $(j \in (adb, iso))$ in Eq. (5.46) is radially unbounded, it can be bounded from above and below by quadratic

functions as,

$$\begin{pmatrix} \tilde{P}_1 & \tilde{P}_2 \end{pmatrix} \frac{\boldsymbol{K}_{min}}{2} \begin{pmatrix} \tilde{P}_1 \\ \tilde{P}_2 \end{pmatrix} \leq W_L^j(\boldsymbol{m}, \boldsymbol{P}, \boldsymbol{P^d}) \leq \begin{pmatrix} \tilde{P}_1 & \tilde{P}_2 \end{pmatrix} \frac{\boldsymbol{K}_{max}}{2} \begin{pmatrix} \tilde{P}_1 \\ \tilde{P}_2 \end{pmatrix} \quad \text{(C.1)}$$

where $\tilde{P}_i \triangleq (P_i - P_i^d)$ is the error between the current pressure and the desired pressure for each chamber, while $\boldsymbol{K}_{min} \in \boldsymbol{R}^{2\times 2}$ and $\boldsymbol{K}_{max} \in \boldsymbol{R}^{2\times 2}$ are positive definite matrices. For controller design through Lyapunov analysis it is more convenient to express the error in pressure tracking in terms of error in force tracking. The force error $\tilde{F}$ is defined in terms of the pressure errors $\tilde{P}_1 := (P_1 - P_1^d)$ and $\tilde{P}_2 := (P_2 - P_2^d)$ as,

$$\tilde{F} = \tilde{P}_1 A_1 - \tilde{P}_2 A_2 = \begin{pmatrix} A_1 & -A_2 \end{pmatrix} \begin{pmatrix} \tilde{P}_1 \\ \tilde{P}_2 \end{pmatrix} \quad \text{(C.2)}$$

Using the above equation in Eq. (C.1), the following condition on the actuator Lyapunov function $W_L^j(\boldsymbol{m}, \boldsymbol{P}, \boldsymbol{P^d})$ is achieved,

$$\frac{1}{2} Q_{min} \tilde{F}^2 \leq W_L^j(\boldsymbol{m}, \boldsymbol{P}, \boldsymbol{P^d}) \leq \frac{1}{2} Q_{max} \tilde{F}^2 \quad \text{(C.3)}$$

where Q_{min} and Q_{max} are the following positive constants,

$$Q_{min} = \begin{pmatrix} A_1 \\ -A_2 \end{pmatrix}^T \boldsymbol{K}_{min} \begin{pmatrix} A_1 \\ -A_2 \end{pmatrix}, \quad Q_{max} = \begin{pmatrix} A_1 \\ -A_2 \end{pmatrix}^T \boldsymbol{K}_{max} \begin{pmatrix} A_1 \\ -A_2 \end{pmatrix} \quad \text{(C.4)}$$

□

Appendix D

Kinematics and Dynamics of the Crawler and the PHANToM(TM) systems

D.1 Crawler dynamics

Each leg on the crawler is made up of three links. Let m_1, m_2 and m_3 represent the mass of each link, while a_1, a_2 and a_3 be the length of each link. The inertia and length of individual links is listed in table D.1.

Table D.1: Magnitude of individual link inertia and link lengths

Parameter	Magnitude
m_1	4kgs
m_2	2kgs
m_3	0.5kgs
a_1	0.1460m
a_2	0.2286m
a_3	0.3048m

The inertia matrix $\boldsymbol{M_q(q)}$ of a crawler leg in Eq. (7.2) is given by,

$$\boldsymbol{M_q(q)} := \begin{pmatrix} m_{11} & m_{12} & m_{13} \\ m_{12} & m_{22} & m_{23} \\ m_{13} & m_{23} & m_{33} \end{pmatrix} \tag{D.1}$$

where the elements of $\boldsymbol{M_q(q)}$ are obtained in terms the individual link inertias m_1, m_2, m_3, and the link lengths a_1, a_2, a_3 as,

$$\begin{aligned} m_{11} &= m_1\frac{a_1^2}{4} + m_2 l_2^2 + m_3 l_3^2 + I_1 + I_2 + I_3, \quad m_{12} = m_{13} = 0 \\ m_{22} &= m_2\frac{a_2^2}{4} + m_3(a_2^2 + \frac{a_3^2}{4} + a_2 a_3 cos(\theta_3)) + I_2 + I_3 \\ m_{23} &= m_3 l_4 \frac{a_3}{2} + I_3, \quad m_{33} = m_3\frac{a_3^2}{4} + I_3 \\ I_1 &= \frac{m_1 a_1^2}{4}, \;\; I_2 = \frac{m_2 a_2^2}{4}, \;\; I_3 = \frac{m_3 a_3^2}{4} \end{aligned} \tag{D.2}$$

Let the quantities b_2, b_3, D_2 and D_3 be defined as,

$$\begin{aligned} b_2 &= a_1 + a_2 cos(\theta_2) + 0.5 a_3 cos(\theta_2 + \theta_3) \\ b_3 &= (a_2 sin(\theta_2) + 0.5 a_3 sin(\theta_2 + \theta_3)) \\ D_2 &= -(m_2 a_2 (a_1 + 0.5 a_2 cos(\theta_2)) sin(\theta_2) - 2 m_3 b_2 b_3) \\ D_3 &= m_3 a_3 b_2 sin(\theta_2 + \theta_3) \end{aligned} \tag{D.3}$$

The vector $\boldsymbol{q} := (\theta_1, \theta_2, \theta_3)$ represents the joint angle vector of a crawler leg. The Coriolis matrix $\boldsymbol{C_q(q, \dot{q})}$ in Eq. (7.2) is given by,

$$\boldsymbol{C_q(q, \dot{q})} = \begin{pmatrix} C_{11} & C_{12} & C_{13} \\ C_{12} & C_{22} & C_{23} \\ C_{13} & C_{23} & C_{33} \end{pmatrix} \tag{D.4}$$

where the elements of the Coriolis matrix $\boldsymbol{C_q(q, \dot{q})}$ are obtained as,

$$\begin{aligned} &C_{11} = 0.5(D_2\dot{\theta}_2 + D_3\dot{\theta}_3), \;\; C_{21} = -0.5(D_2\dot{\theta}_1), \;\; C_{31} = -0.5 D q_3 \dot{\theta}_1 \\ &C_{12} = 0.5 D q_2 \dot{\theta}_1, \;\; C_{22} = -0.5 m_3 a_2 a_3 sin(\theta_3)\dot{\theta}_3, \;\; C_{32} = 0.5 m_3 a_3 a_2 sin(\theta_3)\dot{\theta}_2 \\ &C_{13} = -0.5 m_3 a_3 b_2 sin(\theta_2 + \theta_3), \; C_{23} = m_3\frac{a_3}{2} a_2 sin(\theta_3)(\dot{\theta}_2 - \dot{\theta}_3), \; C_{33} = 0 \end{aligned} \tag{D.5}$$

where the parameters b_2, b_3, D_2 and D_3 are as defined in Eq. (D.3). Let g represent acceleration due to gravity. The elements of the gravitational torque vector $\boldsymbol{g(q)} := (g_1(\boldsymbol{q}), g_2(\boldsymbol{q}), g_3(\boldsymbol{q}))^T$ on a crawler dynamics in Eq. (7.2) are given by,

$$\begin{aligned} g_1(\boldsymbol{q}) &= ((m_1\frac{a_1}{2} + m_2(a_1 + \frac{a_2}{2}cos(\theta_2)) + m_3(a_1 + a_2cos(\theta_2)) \\ &\quad + \frac{a_3}{2}cos(\theta_2+\theta_3)))gsin(\theta_1)sin(\alpha) \\ g_2(\boldsymbol{q}) &= -(\frac{m_2}{2} + m_3)ga_2(cos(\theta_2)cos(\alpha) - sin(\theta_2)sin(\alpha)cos(\theta_1)) \\ &\quad - m_3g\frac{a_3}{2}(cos(\alpha)cos(\theta_2+\theta_3) - sin(\alpha)sin(\theta_2+\theta_3)cos(\theta_1)) \end{aligned} \tag{D.6}$$

$$g_3(\boldsymbol{q}) = -m_3\frac{a_3}{2}(cos(\alpha)cos(\theta_2+\theta_3) - sin(\alpha)sin(\theta_2+\theta_3cos(\theta_1))g \tag{D.7}$$

D.2 PHANToM(TM) dynamics

Dynamics of the PHANToM(TM[1]) haptic manipulator as given in [79] are used in this study and are presented below for ease of reference. Let $\boldsymbol{q_{ph}} \triangleq [\varphi_1, \varphi_2, \varphi_3]$ represent the vector of haptic manipulator joint angles. Dynamics of the manipulator in its joint space is given by,

$$\boldsymbol{M_{qh}(q_{ph})\ddot{q}_{ph} + C_{qh}(q_{ph}, \dot{q}_{ph})\dot{q}_{ph} + g(q_{ph}) = \tau_h + \tau_{p_{ex}} + \tau_{a_{ph}}} \tag{D.8}$$

where the inertial matrix $\boldsymbol{M_{qh}(q_{ph})}$, the Coriolis matrix $\boldsymbol{C_{qh}(q_{ph}, \dot{q}_{ph})}$ and the gravitational vector $\boldsymbol{g(q_{ph})}$ are obtained from Lagrangian formulation to have the following structure,

$$\boldsymbol{M_{qh}(q_{ph})} = \begin{pmatrix} M_{11} & 0 & 0 \\ 0 & M_{22} & M_{23} \\ 0 & M_{23} & M_{33} \end{pmatrix} \tag{D.9}$$

$$\boldsymbol{C_{qh}(q_{ph}, \dot{q}_{ph})} = \begin{pmatrix} C_{11} & C_{12} & C_{13} \\ C_{21} & 0 & C_{23} \\ C_{31} & C_{32} & 0 \end{pmatrix} \tag{D.10}$$

$$\boldsymbol{g_{qh}(q_{ph})} = \begin{pmatrix} 0 \\ g_2 \\ g_3 \end{pmatrix} \tag{D.11}$$

[1] PHANToM is a trademarked product of Sensable Technologies,MA

The elements of the inertial matrix $\boldsymbol{M_{qh}(q_{ph})}$ in Eq. (D.9) are obtained from [79] as,

$$\begin{aligned}
M_{11} =& \frac{1}{8}\left(4m_a l_1^2 + m_a l_2^2 + m_c(l_1^2 + 4l_3^2) + I_1 + I_2 cos(2\varphi_2)\right. \\
&\left. + I_3 cos(2\varphi_3)\right) + I_s cos(\varphi_2) sin(\varphi_3) \\
M_{22} =& \frac{m_c l_1^2}{4} + I_{be_{xx}} + I_{c_{xx}} + m_a l_1^2 \\
M_{23} =& -\frac{1}{2} I_s sin(\varphi_2 - \varphi_3) \\
M_{33} =& m_c l_3^2 + m_a \frac{l_2^2}{4} + I_{axx} + I_{df_{xx}}
\end{aligned} \tag{D.12}$$

where I_1, I_2, I_3 and I_s are defined as,

$$\begin{aligned}
I_1 &= 4I_{ayy} + 4I_{azz} + 8I_{base_{yy}} + 4I_{be_{yy}} + 4I_{be_{zz}} + 4I_{cyy} + 4I_{czz} + 4I_{df_{yy}} + 4I_{df_{zz}} \\
I_2 &= 4I_{be_{yy}} - 4I_{be_{zz}} + 4I_{cyy} - 4I_{czz} + l_1^2(4m_a + m_c) \\
I_3 &= 4I_{ayy} - 4I_{azz} + 4I_{df_{yy}} - 4I_{df_{zz}} - m_a l_2^2 - 4m_c l_3^2 \\
I_s &= (m_a l_2 + m_c l_3) l_1
\end{aligned} \tag{D.13}$$

The values of the individual link inertias and link lengths used in defining the elements of $\boldsymbol{M(q_{ph})}$ in the above equation are obtained from [79] as,

Elements of the Coriolis matrix $\boldsymbol{C_{qh}(q_{ph}, \dot{q}_{ph})}$ in Eq. (D.10) are obtained as,

$$\begin{aligned}
C_{11} =& -\frac{1}{4} sin(\varphi_2)\left(I_2 cos(\varphi_2) + I_s sin(\varphi_3)\right)\dot{\varphi}_2 + \frac{1}{4} cos(\varphi_3)\left(2I_s cos(\varphi_2) - I_3 sin(\varphi_3)\right)\dot{\varphi}_3 \\
C_{12} =& -\frac{1}{8}\left(I_2 sin(2\varphi_2) + 4I_s sin(\varphi_2) sin(\varphi_3)\right)\dot{\varphi}_1 \\
C_{13} =& \frac{1}{8}(4I_s cos(\varphi_2) cos(\varphi_3)) - I_3 sin(2\varphi_3)\dot{\varphi}_1 \\
C_{21} =& -C_{12}, \quad C_{23} = \frac{1}{2} I_s cos(\varphi_2 - \varphi_3)\dot{\varphi}_3 \\
C_{31} =& -C_{13}, \quad C_{32} = \frac{1}{2} I_s cos(\varphi_2 - \varphi_3)\dot{\varphi}_2
\end{aligned} \tag{D.14}$$

Let g is the acceleration due to gravity. Elements of the gravitational force vector $\boldsymbol{g_{qh}(q_{ph})}$ in Eq. (D.11) are then obtained as,

$$\begin{aligned}
g_2(\boldsymbol{q_{ph}}) =& \frac{g}{2}(2m_a l_1 + 2m_{be} l_5 + m_c l_1) cos(\varphi_2) \\
g_3(\boldsymbol{q_{ph}}) =& \frac{g}{2}(m_a l_2 + 2m_c l_3 - 2m_{df} l_6) sin(\varphi_3)
\end{aligned} \tag{D.15}$$

Table D.2: Magnitude of individual link inertia and link lengths of the PHANToM(TM) haptic device

Parameter	Magnitude
m_a	0.0202kgs
m_c	0.0249kgs
m_{be}	0.2359kgs
m_{df}	0.1906kgs
I_{axx}	0.4864e-4 $kg - m^2$
I_{ayy}	0.00184e-4 $kg - m^2$
I_{azz}	0.4864e-4 $kg - m^2$
I_{cxx}	0.959e-4 $kg - m^2$
I_{cyy}	0.959e-4 $kg - m^2$
I_{czz}	0.0051e-4 $kg - m^2$
I_{bexx}	11.09e-4 $kg - m^2$
I_{beyy}	10.06e-4 $kg - m^2$
I_{bezz}	0.591e-4 $kg - m^2$
I_{dfxx}	7.11e-4 $kg - m^2$
I_{dfyy}	0.629e-4 $kg - m^2$
I_{dfzz}	6.246e-4 $kg - m^2$
I_{baseyy}	11.87e-4 $kg - m^2$
a_2	0.2286m
l_1	0.215m
l_2	0.17m
l_3	0.0325m
l_5	0.0368m
l_6	0.0527m

D.3 Kinematic mapping from crawler task space to crawler joint space

The tip of PHANToM(TM[1]) haptic device is mapped into the crawler task space. The desired joint angles in the crawler joint space are determined from the commanded foot tip position as shown in [82]. In this section, the mapping presented in [82] is repeated for convenience of the readers.

```
function jt_angles   = inv_kin_right(roboXYZ, jt_limits)

% CONSTANTS
d1 = 1.608;
a1 = 5.750;
a2 = 9.00; % 6.828
a3 = 12.00;
thetas = 30;

feet_pos = roboXYZ;

% Find Joint Angle 1
% (1) project the vector pointing from the shoulder to the end effector
%     on the plane normal to the z coordinate of the shoulder.
% (2) project this projection on the plane to the z and x coordinate of
%     the shoulder.
% (3) when the vector in the z coordinate is positive, joint angle 1 is
%     positive and when it is negative, the joint angle 1 is negative

B0 = [cosd(thetas), 0, sind(thetas), 0;
      0, 1, 0, 0;
      -sind(thetas), 0, cosd(thetas), 0;
      0, 0, 0, 1];

pt_s2ee = feet_pos - B0(1:3,4);
```

```
proj_s2ee=cross(B0(1:3,3),cross(pt_s2ee,B0(1:3,3)))...
                /(norm(B0(1:3, 3)))^2;
proj_s2ee_y=dot(proj_s2ee, B0(1:3, 2))*B0(1:3,2)...
                 /(norm(B0(1:3,2)))^2;
temp_shift_jt1=(dot(proj_s2ee,B0(1:3, 1))...
                /(norm(proj_s2ee)*norm(B0(1:3,1))));

if temp_shift_jt1 > 1
    temp_shift_jt1 = 1;
end

if proj_s2ee_y(2) >=0;
    jt1 = acosd(temp_shift_jt1);
else
    jt1 = -acosd(temp_shift_jt1);
end

% Joint 1 Limits
if jt1 > jt_limits(2);
    jt1 = jt_limits(2);
elseif jt1 < jt_limits(1);
    jt1 = jt_limits(1);
end

% from shoulder to joint 1
Bg4 = B0*[cosd(jt1), -sind(jt1), 0, 0;
          sind(jt1), cosd(jt1), 0, 0;
          0, 0, 1, d1;
          0, 0, 0, 1];

B45 = [1, 0, 0, a1; 0, 1, 0, 0; 0, 0, 1, 0; 0, 0, 0, 1];
Bg5 = Bg4*B45;
```

```
% using shoulder position and feet position find the angle of joint 3
% c^2 = a^2 + b^2 - 2*a*b*cos(theta)

a = norm(feet_pos - Bg5(1:3, 4));

if abs(-(a2^2 + a3^2 - a^2)/(2*a2*a3)) > 1
    jt3 = acosd(1);
else
    jt3 = (acosd(-(a2^2 + a3^2 - a^2)/(2*a2*a3)));
end

% Joint 3 Limits
if jt3 > jt_limits(6);
    jt3 = jt_limits(6);
    a = sqrt(a2^2+a3^2-2*a2*a3*cosd(180-jt3));
elseif jt3 < jt_limits(5);
    jt3 = jt_limits(5);
    a = sqrt(a2^2+a3^2-2*a2*a3*cosd(180-jt3));
end

% using the shoulder orientation figure out the angle of joint 2
if abs((a2^2 + a^2 - a3^2)/(2*a2*a)) > 1
    theta2temp = acosd(1);
else
    theta2temp = acosd((a2^2 + a^2 - a3^2)/(2*a2*a));
end

del_theta2=acosd(dot(Bg4(1:3,1),feet_pos-Bg5(1:3,4))...
             /(norm(Bg4(1:3,1))*norm(feet_pos-Bg5(1:3,4))));

% Defining Joint 2 Angle
% (1) project the vector pointing from the shoulder to the end effector
```

```
%     normal to the z coordinate of the shoulder.
% (2) when the vector in the z coordinate is positive, joint angle 3 is
%     positive is the sum of the two and when it is negative, the joint
%     angle 3 is negative is the difference of the two

norm_s2ee = [cosd(-thetas), 0, sind(-thetas);
             0, 1, 0;
             -sind(-thetas), 0, cosd(-thetas)]*(feet_pos-Bg5(1:3,4));

if norm_s2ee(3) >= 0
    jt2 = -(theta2temp + del_theta2);
else
    jt2 = -theta2temp + del_theta2;
end



% joint 2 limits
if jt2 > jt_limits(4);
    jt2 = jt_limits(4);
elseif jt2 < jt_limits(3);
    jt2 = jt_limits(3);
end

jt_angles = [jt1; jt2; jt3];
```

D.4 Proof on skew-symmetry property of Shape system

D.4.1 Proof of remark 7.4

Proof. The time derivative of the Shape system inertia matrix $\boldsymbol{M_E(q, q_p)}$ in Eq. (7.35) is obtained as,

$$\begin{aligned}\dot{\boldsymbol{M}}_{\boldsymbol{E}}(\boldsymbol{q}, \boldsymbol{q_p}) =& \boldsymbol{\phi^T(q, q_p)}\dot{\boldsymbol{M}}_{\boldsymbol{q}}(\boldsymbol{q})\boldsymbol{\phi(q, q_p)} + \boldsymbol{(I - \phi^T(q, q_p))}\rho\dot{\boldsymbol{M}}_{\boldsymbol{p}}(\boldsymbol{q_p})\boldsymbol{(I - \phi(q, q_p))} \\ &+ \dot{\boldsymbol{\phi}}^{\boldsymbol{T}}(\boldsymbol{q}, \boldsymbol{q_p})(\boldsymbol{M_q(q)\phi(q, q_p)} - \rho\boldsymbol{M_p(q_p)(I - \phi(q, q_p))}) \\ &+ (\boldsymbol{\phi^T(q, q_p)M_q(q)} - \boldsymbol{(I - \phi^T(q, q_p))}\rho\boldsymbol{M_p(q_p)})\dot{\phi}^T(q, q_p)\end{aligned} \tag{D.16}$$

From the definition of $\boldsymbol{\phi(q, q_p)}$ in Eq. (7.30) the time derivative $\dot{\boldsymbol{\phi}}^{\boldsymbol{T}}\boldsymbol{(q, q_p)}$ is obtained as,

$$\dot{\boldsymbol{\phi}}^{\boldsymbol{T}}(\boldsymbol{q}, \boldsymbol{q_p}) = -\boldsymbol{M_L^{-1}(q, q_p)}\dot{\boldsymbol{M}}_{\boldsymbol{L}}^{-1}(\boldsymbol{q}, \boldsymbol{q_p})\boldsymbol{M_L^{-1}(q, q_p)}\rho\boldsymbol{M_p(q_p)} + \boldsymbol{M_L^{-1}(q, q_p)}\rho\dot{\boldsymbol{M}}_{\boldsymbol{p}}(\boldsymbol{q_p}) \tag{D.17}$$

where $\boldsymbol{M_L(q, q_p) := (M_q(q) + M_p(q_p))}$ is the Locked system inertia. Using the fact that the inertia matrices $\boldsymbol{M_q(q)}$ and $\boldsymbol{M_p(q_p)}$ are symmetric, and from the expression for $\dot{\boldsymbol{\phi}}^{\boldsymbol{T}}\boldsymbol{(q, q_p)}$ from Eq. (D.17), the derivative of the Shape system inertia $\dot{\boldsymbol{M}}_{\boldsymbol{E}}\boldsymbol{(q, q_p)}$ can be expressed as,

$$\dot{\boldsymbol{M}}_{\boldsymbol{E}}(\boldsymbol{q}, \boldsymbol{q_p}) = \boldsymbol{\phi^T(q, q_p)}\dot{\boldsymbol{M}}_{\boldsymbol{q}}(\boldsymbol{q})\boldsymbol{\phi(q, q_p)} + \boldsymbol{(I - \phi^T(q, q_p))}\rho\dot{\boldsymbol{M}}_{\boldsymbol{p}}(\boldsymbol{q_p})\boldsymbol{(I - \phi(q, q_p))} \tag{D.18}$$

Using the above definition for $\dot{\boldsymbol{M}}_{\boldsymbol{E}}\boldsymbol{(q, q_p)}$ and the definition for the Coriolis matrix $\boldsymbol{C_E(q, q_p, \dot{q}, \dot{q}_p)}$ from Eq. (7.38), the skew-symmetry condition in Eq. (7.41) can be restated as,

$$\begin{aligned}\boldsymbol{A}^T(\dot{\boldsymbol{M}}_{\boldsymbol{E}}(\boldsymbol{q}, \boldsymbol{q_p}) - 2\boldsymbol{C_E(q, q_p, \dot{q}, \dot{q}_p)})\boldsymbol{A} = \boldsymbol{A}^T \Big(& \boldsymbol{\phi^T(q, q_p)}(\dot{\boldsymbol{M}}_{\boldsymbol{q}}(\boldsymbol{q}) - 2\boldsymbol{C_q(q, \dot{q})})\boldsymbol{\phi(q, q_p)} \\ & + \boldsymbol{(I - \phi^T(q, q_p))}\rho(\dot{\boldsymbol{M}}_{\boldsymbol{p}}(\boldsymbol{q_p}) - 2\boldsymbol{C_p(q_p, \dot{q}_p)})\boldsymbol{(I - \phi(q, q_p))}\Big)\,\boldsymbol{A}\end{aligned} \tag{D.19}$$

Define the vector $\boldsymbol{A_2 := \phi(q, q_p)A}$. Then the above equation can be simplified as,

$$\boldsymbol{A}^{\boldsymbol{T}}(\dot{\boldsymbol{M}}_{\boldsymbol{E}} - 2\boldsymbol{C_E})\boldsymbol{A} = \boldsymbol{A_2^T}(\dot{\boldsymbol{M}}_{\boldsymbol{q}} - 2\boldsymbol{C_q})\boldsymbol{A_2} + \boldsymbol{(A - A_2)}^{\boldsymbol{T}}\rho(\dot{\boldsymbol{M}}_{\boldsymbol{p}} - 2\boldsymbol{C_p})\boldsymbol{(A - A_2)} \tag{D.20}$$

Using the skew-symmetry properties of the crawler inertia dynamics stated in remark 7.1 and the PHANToM(TM^1) inertia dynamics in remark 7.3 the proof follows. □

Appendix E

Proofs from Chapter 8

E.1 Proof of proposition 8.1

Proof. Using the characteristic equation for isothermal process ($P_1V_1(x) = P_1^dV_1(x_d)$), the effort variable $Z_\gamma^s(\boldsymbol{P}, \boldsymbol{P}^d, \boldsymbol{u})$ at the fluid port of the actuator in Eq. (8.29) can be expressed as,

$$Z_\gamma^s(\boldsymbol{P}, \boldsymbol{P}^d, \boldsymbol{u}) = \begin{cases} \Psi(P_1, T_o, u_1)RT_o \log\left(\frac{L_{1o}+x_d}{L_{1o}+x}\right) & \text{if } F_a \geq 0 \\ \Psi(P_2, T_o, u_2)RT_o \log\left(\frac{L_{2o}-x_d}{L_{2o}-x}\right) & F_a < 0 \end{cases} \tag{E.1}$$

where $\Psi(.) \in \Re^+$ is as defined in Eq. (3.27). When the actuator force F_a is positive, the effort variable $Z_\gamma^s(\boldsymbol{P}, \boldsymbol{P}^d, \boldsymbol{u})$ monotonically increases with the position error $(x_d - x)$, and if the actuator force F_a is negative, the effort variable $Z_\gamma^s(\boldsymbol{P}, \boldsymbol{P}^d, \boldsymbol{u})$ will monotonically decrease with the position error $(x_d - x)$. Also, $Z_\gamma^s(\boldsymbol{P}, \boldsymbol{P}^d, \boldsymbol{u})$ is identically zero only if the actuator position x corresponds to the desired actuator position x_d.

From the remark 3.5, the force error $\tilde{F}$ for an isothermal actuator is a strictly monotonically increasing function of the position error $(x_d - x)$. Using transitivity property, the effort variable $Z_\gamma^s(\boldsymbol{P}, \boldsymbol{P}^d, \boldsymbol{u})$, and the force error $\tilde{F}$ increase strictly monotonically with each other if the actuator force F_a is positive. If the actuator force F_a is negative, the effort variable $Z_\gamma^s(\boldsymbol{P}, \boldsymbol{P}^d, \boldsymbol{u})$ decreases strictly monotonically with increasing $\tilde{F}$.

Due to the monotonic relationship between $Z_\gamma^s(\boldsymbol{P}, \boldsymbol{P}^d, \boldsymbol{u})$ and the actuator force error $\tilde{F}$, a nonlinear gain $\gamma_3(\boldsymbol{P}, \boldsymbol{P}^d, \boldsymbol{u})$ can be defined as,

$$Z_\gamma^s(\boldsymbol{P}, \boldsymbol{P}^d, \boldsymbol{u}) = \gamma_3^s(\boldsymbol{P}, \boldsymbol{P}^d, \boldsymbol{u})\tilde{F} \tag{E.2}$$

Using the expression for the effort variable $Z^s_\gamma(\boldsymbol{P}, \boldsymbol{P}^d, \boldsymbol{u})$ from Eq. (8.29), and the definition of $\tilde{F}$ from Eq. (8.30), the nonlinear gain $\gamma^s_3(\boldsymbol{P}, \boldsymbol{P}^d, \boldsymbol{u})$ can be expressed as,

$$\gamma^s_3(\boldsymbol{P}, \boldsymbol{P}^d, \boldsymbol{u}) = \begin{cases} \frac{\Psi_1(P_1,T_o,u_1)RT_o}{K^d_{iso}(\boldsymbol{m},x,x_d)(x_d-x)} \log\left(1+\frac{x_d-x}{L_{1o}+x}\right) & \text{if } F_a \geq 0 \\ \frac{\Psi_2(P_2,T_o,u_2)RT_o}{K^d_{iso}(\boldsymbol{m},x,x_d)(x_d-x)} \log\left(1-\frac{x_d-x}{L_{2o}-x}\right) & F_a < 0 \end{cases} \tag{E.3}$$

In the limiting case when the actuator position x corresponds to the desired position x_d, the nonlinear gain $\gamma^s_3(\boldsymbol{P}, \boldsymbol{P}^d, \boldsymbol{u})$ is obtained as,

$$\lim_{x\to x_d} \gamma^s_3(\boldsymbol{P}, \boldsymbol{P}^d, \boldsymbol{u}) = \begin{cases} \frac{\Psi_1(P_1,u_1)RT_o}{K^d_{iso}(\boldsymbol{m},x,x_d)(L_{1o}+x)} & \text{if } F_a \geq 0 \\ -\frac{\Psi_2(P_2,u_2)RT_o}{K^d_{iso}(\boldsymbol{m},x,x_d)(L_{2o}-x)} & F_a < 0 \end{cases} \tag{E.4}$$

Therefore, the nonlinear gain $\gamma^s_3(\boldsymbol{P}, \boldsymbol{P}^d, \boldsymbol{u})$ as presented in Eq. (8.31) is well defined for all possible values of actuator force error $\tilde{F}$, including at $\tilde{F} = 0$ ($x = x_d$).

□